Passive Noise Control in Industrial Fans

Edited by Geoff Sheard

Sigel Press

Sigel Press
51A Victoria Road
Cambridge CB4 3BW
England

4403 Belmont Court
Medina, Ohio 44256
USA

Visit us on the World Wide Web at: www.sigelpress.com

Internal Design: Professional Book Compositors, Lorain, Ohio, USA
Cover Design: Harp Mando
Cover Images: Alessandro Corsini, *Sapienza* University of Rome

ISBN 10: 1-905941-19-6
ISBN 13: 978-1-90541-19-13

A catalogue record for this book is available from the British Library.
Typeset in Times Roman

The publisher's policy is to use paper manufactured from sustainable forests.

Permissions Acknowledgements

Chapter 1, *A Critical Review of Passive Noise Control Techniques in Industrial Fans*, was originally published in the Proceedings of the 58th American Society of Mechanical Engineers Gas Turbine and Aeroengine Congress, paper number GT2013-94803 and subsequently in the transactions of the American Society of Mechanical Engineers Journal of Engineering for Gas Turbines and Power, Volume 136. Reprinted with the permission of The American Society of Mechanical Engineers. Permission to publish received September 4, 2013.

Chapter 2, *Experimental Development of a Measurement Technique to Resolve the Radial Distribution of Fan Aeroacoustic Emissions*, was originally published in the Proceedings of the 3rd International Symposium on Fan Noise and subsequently in the Institute of Noise Control Engineering Noise Control Engineering Journal, Volume 57. Reprinted with the permission of the Institute of Noise Control Engineering. Permission to publish received October 10, 2013.

Chapter 3, *Detection of Aerodynamic Noise Sources in Low-speed Axial Fans with Tip End-plates*, was published in the Proceedings of the Institute of Mechanical Engineering Part C, Journal of Mechanical Engineering Science, Volume 223. Reprinted with the permission of the Institute of Mechanical Engineering. Permission to publish received September 12, 2013.

Chapter 4, *Experimental Aeroacoustic Studies on Improved Tip Configurations for Passive Control of Noise Signatures in Low-Speed Axial Fans*, was originally published in the proceedings of the 53rd American Society of Mechanical Engineers Turbine and Aeroengine Congress, paper number GT2008-51057 and subsequently in the transactions of the American Society of Mechanical Engineers Journal of Vibration & Acoustics, Volume 131. Reprinted with the permission of The American Society of Mechanical Engineers. Permission to publish received September 4, 2013.

Chapter 5, *Far-field Radiation of Tip Aerodynamic Sound Sources in Axial Fans Fitted with Passive Noise Control Features*, was originally published in the proceedings of the 54th American Society of Mechanical Engineers Turbine and Aeroengine Congress, paper number GT2009-59980 and subsequently in the transactions of the American Society of Mechanical Engineers Journal of Vibration & Acoustics, Volume 123. Reprinted with the permission of The American Society of Mechanical Engineers. Permission to publish received September 4, 2013.

Chapter 6, *Experimental Study on the Self-noise of a Turbulent Round Jet Investing a Cambered Aerofoil*, was originally published in the Budapest University of Technology and Economics Periodica Polytechnica Mechanical Engineering, Volume 57, an

Chapter 13, *Installed Acoustic Performance of Cooling Axial Fans Fitted with Endplates*, was originally published in the Institute of Noise Control Engineering Journal, Volume 60. Reprinted with the permission of the Institute of Noise Control Engineering. Permission to publish received October 10, 2013.

Appendix 1, *A Meridional Fan*, was originally published as Patent Number GB 2 452 104 B. Reprinted in accordance with the requirements of the Copyright, Designs and Patents Act, Section 30 (1) and Section 47 (1).

Contents

List of Figures

List of Tables

Foreword

Research and development. Within engineering organisations engineers typically talk about the two together as if it they are one and the same. In fact, research and development are not the same at all. They are two separate and very different endeavours.

We may define research as the systematic investigation into and study of materials and sources in order to establish facts and reach new conclusions. In the broadest sense, a researcher investigates the nature, causes and principles underpinning knowledge. Although researchers invariably do use empirical methods, the choices they make are based on logical reasoning. Consequently, researchers are also philosophers, making explicit the nature and significance of scientific beliefs.

In contrast, we may define development as determining the best techniques for applying to a new device or process for the production of goods. In the broadest sense, development encompasses any activity that a product needs to maintain its competitiveness. Consequently, development includes redesigning a product to reduce its manufacturing cost, or certifying a product to demonstrate compliance with a new regulation. Development engineers have a matter-of-fact way of approaching and assessing situations and of solving problems. They are not philosophers; they are pragmatists.

Given the different perspectives of the individuals involved in research and those involved in development, is it really so surprising that usually they do not communicate well? From the development engineer's perspective researchers seem to move so slowly they stand still. They are perpetually concerned with exploring the unexplored and never take the time to explain what it is they have done, let alone what they are doing.

Despite the difficulty of linking research to product development, these links are necessary if research is to be relevant. Those involved in research must explain what they are doing and why. They must document their work, and perhaps most importantly, must find a way to bridge the gap from their research environment into the world of development.

The collection of papers in this volume illustrates how a developmental need can inform research, and how the resulting research creates new knowledge that is then harnessed to develop a new product. In collecting and editing these papers, Geoff Sheard has provided an important record which is an essential source of information to those who wish to really understand the link between research and development. This story will also appeal to those who wish to understand the processes involved in product design and development. All readers will be interested to follow the path described in this volume and will learn much in the process.

Alain Guedel
Centre Technique des Industries Aérauliques et Thermiques (CTIAT)
21 November 2014

Acknowledgements

Many individuals have helped in writing the academic papers upon which this volume is based and it is my pleasure to acknowledge this. Foremost among these are the authors, Stefano Bianchi, Alessandro Corsini, Iain Kinghorn and Franco Rispoli.

I also wish to thank Thomas Sigel, first for his tremendous contribution in turning around extensive scripts into succinct and easily readable text, and second for his assistance with the process of converting the final text into this published volume.

I would like to acknowledge the contribution of Kirsten Greenzweig, who converted the original academic papers upon which this volume is based into electronic files that could then be edited and typeset. Kirsten also recreated the original figures in electronic form, an undertaking that proved to be far more time consuming then either of us imagined.

I would also like to acknowledge the contribution of the Institution of Mechanical Engineers (IMechE) library staff. They helped ensure that the references for the academic papers upon which this volume is based are both complete and technically correct. The resulting edited volume is a better reference text as a consequence.

Last, I also wish to thank Cecilia Tortora who assisted during the process of converting the separate papers upon which this edited volume is based into a self-consistent set of manuscripts that could be used as the basis of the chapters of this edited volume.

Geoff Sheard
Fläkt Woods Group

About the Editor

Wearing many hats, Geoff Sheard is the Fläkt Woods Group Vice President of Fan Technology, a leading global supplier of energy-efficient solutions operating in both the air climate for buildings and air movement for the infrastructure and industry markets. He is a director of Fläkt Woods Limited, Solyvent Fläkt Woods Limited and Fläkt Woods Fans (Australia) Pty Limited.

Geoff is an Honorary Professor at the Aston University Department of Engineering and Applied Science, a Visiting Professor at *Sapienza* University of Rome *Dipartimento di Ingegneria Meccanica e Aerospaziale* and a Visiting Professor at the University of Northampton Business School.

Geoff is President of the Air Movement & Control Association (AMCA), member of the AMCA Executive Board and Chairman of the European Air Movement & Control Association Board of Directors. He is also a member of the International Gas Turbine Institute (IGTI) Board of Directors and Vice Chairman of the Institution of Mechanical Engineers (IMechE) Fluid Machinery Group.

Geoff has doctorate degrees from the University of Oxford in turbomachinery aerodynamics and from the University of Northampton in leadership and team development. He also holds a master's degree in business administration from Cranfield University and a bachelor's degree in mechanical engineering from Liverpool University.

A chartered engineer, a Liveryman of the Worshipful Company of Engineers, a fellow of the Institution of Mechanical Engineers, a fellow of the Royal Aeronautical Society, a fellow of the American Society of Mechanical Engineers, and a fellow of the Chartered Institute of Building Service Engineers, Geoff has published widely in both technical and management areas. His publication list extends to 236 publications including 10 books, two monographs plus over 60 journal articles and patents. Geoff is editor of the *Journal of Management Development*, a member of the *Journal of Power & Energy* and *African Journal of Engineering* editorial boards, and the *Leadership and Organisational Development Journal* editorial review board.

Introduction: Passive Noise Control

Geoff Sheard

> '*Philosophy is a hypothetical interpretation of the unknown …, or of the inexactly known …; it is the front trench in the siege of truth. Science is the captured territory; and behind it are those secure regions in which knowledge and art build our imperfect marvelous world. Philosophy seems to sand still, perplexed; but only because she leaves fruits of victory to her daughters the sciences, and herself passes on, divinely discontent, to the uncertain and unexplored.*'
>
> Will Duran (1926), *The Story of Philosophy*

This volume of collected papers documents research undertaken in response to a need — yesterday's product is no longer competitive today. The volume arises from discussions around thirteen papers and one patent that collectively comprise the chapters and appendix. Each marks a milestone in the development of technology that underpins a new generation of low-noise induced draft fans. This new generation has proven itself competitive in today's uncertain world.

The chapters relate to one of three separate, but complementary developmental phases that collectively comprised a single research and development effort:

- Experimental methodology development for dissecting aeroacoustic fan noise
- Computationally aided development of passive noise control technologies
- Design and assessment of a new passive noise control technology

During the early 2000s, the compact cooling unit market expanded as air conditioning systems became a standard feature in new commercial buildings. As that market grew, it also became more demanding. People were no longer willing to tolerate noisy air conditioning when working in their office or staying in a hotel. The fans fitted to air conditioning system compact cooling units were responsible for the majority of the cooling units' acoustic emissions. Therefore, design engineers found themselves under increasing pressure to design lower noise fans. At the time design engineers within the air movement and control community were still developing new products using empirical techniques dating back to the 1950s. However, these empirical techniques had reached the limit of their potential. Before they could design a new generation of low noise fans, a new generation of experimental methodologies for dissecting aeroacoustic noise sources was necessary.

The developed experimental methodologies facilitated insight into both the blade-span and chord-wise aerodynamic flow features that constitute noise sources. Most significant was the role of the blade-tip leakage vortex which, as a dominant noise source, has a primary impact on tonal and broadband fan far-field noise. In an effort to better understand the linkage between flow features in the blade tip-to-casing region and fan far-field noise, a computational analysis of the flow-field was necessary. The computational analysis constituted a numerical laboratory, providing insight into flow-field structures and thus complemented the previously developed experimental methodologies.

In combination, the developed experimental methodologies and computational analysis provided insight into the flow-field physics. This insight facilitated elucidation of the role of the blade-tip leakage vortex and other organised vortical structures in generating fan far-field noise. The authors concluded that the vortex's intensity required minimisation, without reducing the intensity so far that the vortex would break down or promote the creation of other organised vortical structures. Blade-tip leakage vortex breakdown was a highly productive acoustic feature of the flow-field. In response, the authors developed a design procedure with the objective of creating a new blade-tip treatment that would minimise vortex intensity and avoid both vortex breakdown and the creation of additional acoustically productive vortical structures. The authors designated the resultant blade-tip end-plate Multiple Vortex Breakdown (MVB). When experimentally assessed, the studied fan fitted with the MVB blade-tip end-plate improved the fan pressure developing capability, maintained aerodynamic efficiency and reduced fan far-field noise. Compact cooling units that had previously struggled to meet the market requirement were now the quietest in their class.

Chapter 1: Literature Review

The adopted research philosophy, first developing experimental methodologies and then complementing them with computational analysis had provided the necessary insight into the flow-field physics. It was this insight that researchers needed before developing a low noise fan using the new passive noise control technology. However, researchers did not create and develop the experimental methodologies and complementary computational analysis techniques in a vacuum. The work of other researchers working in both the aerospace and air movement and control fan communities informed their development.

Chapter 1 presents a review of passive noise control techniques. The authors wrote this paper to place the work undertaken and reported in the other papers that form the body of the edited volume into context. The review identifies the key challenges those within the aerospace fan, aerospace compressor and air movement and control fan communities are addressing. The review's specific focus is on identifying those aspects of aerospace technology that one can most likely apply successfully into fans intended for air movement applications. Thus, the review provides a road

map for researchers who are both developing noise control technology and attempting to apply that technology into air movement fans.

Chapters 2, 3, 4, 5 and 6: Experimental Methodologies

The work of other scholars and engineers within the aerospace fan community informed the process of developing experimental methodologies for dissecting aeroacoustic noise sources. However, the experimental methodologies reported in the extant literature were not directly applicable to the study of an air movement fan. In practice, the process of developing new experimental methodologies was organic in nature. Consequently, the five chapters that follow do not constitute a linear progression from inception to delivery of a single experimental methodology. The five chapters document milestones in the process of developing experimental methods and analysis techniques for dissecting aeroacoustic noise sources. Each provides a different insight into either span- or chord-wise flow features that constitute a noise source. Thus, each chapter provides a complementary perspective on the near-field aerodynamic origin of fan far-field noise. Collectively they provide the necessary quantitative data to move on to the development of a new passive noise technology.

Chapter 2 presents an experimental methodology that assesses the studied fan's effectiveness with and without blade-tip end-plates. Previously, development engineers had applied a constant thickness blade-tip end-plate to the studied fan in an early attempt to reduce fan noise. The fan blades are manufactured from injection moulded plastic, with the blade-tip end-plate thickness as the largest possible within the available manufacturing technology limits. The constant thickness blade-tip end-plate constituted the limit for 1950s empirical design techniques, and was a starting point for developing new passive noise technologies. The developed experimental methodology involved varying a near-field microphone's blade span-wise position. The researchers correlated the resulting data with the data from a far-field microphone. The near- and far-field correlation technique provides a method for resolving aeroacoustic noise sources along the blade span.

Chapter 3 applies the near- and far-field correlation technique presented in Chapter 2. The authors correlated near-and far-field measurements for the studied fan, both with and without a fitted blade-tip end-plate. This facilitated the identification of flow-field features in the blade tip-to-casing region. Thus, it is possible to clarify the role of specific end-plate design features in the generation of tonal and broadband fan far-field noise. The authors went on to analyse the role of coherent vortical structures and blade tip-to-casing leakage flow features as noise sources using a novel symmetrised dot pattern visualisation of fan far-field noise. The symmetrised dot pattern visualisation technique facilitated a study of the way in which human perception of fan noise changes as the blade-tip treatment changed. The correlation technique and subsequent symmetrised dot pattern analysis identified that the blade-tip treatment has an effect on blade-tip leakage vortex formation by altering the near-wall fluid path on blade surfaces.

Chapter 4 once again applies the near- and far-field correlation technique presented in Chapter 2, with an analysis focused on tonal noise span-wise variation. Far-field spectra were dominated by the blade passing frequency's first, second, third and fourth harmonics. Although the fifth and sixth harmonics were evident in the data, they had reduced in magnitude to the point where they effectively merged with the broadband noise. The developed analysis technique presented span-wise distributions of coherence values between the near- and far-field microphones. Because the coherence function involves a signal normalisation that highlights highly coherent events, irrespective of energy content, it was effective in establishing the acoustic relationship between the near- and far-field. The analysis identified six distinct coherent regions, each associated with a different combination of span-wise location and frequency. Therefore, the analysis provided insight into the acoustic far-field consequences of aerodynamic near-field flow features.

Chapter 5 presents an extension of the experimental methodology presented in Chapter 2. This included one far-field noise measurement 30 degrees off the fan centre line. The authors extended the experimental methodology to include far-field noise measurements on the fan centre line and 30, 45, 60, 75 and 90 degrees off the fan centre line. The authors processed data at each azimuthal position to provide a broadband noise measurement. They also processed it to provide spectra at each azimuthal position. The resulting directivity analysis confirmed that fan far-field noise was anisotropic, both tonally and in the broadband. The primary contribution of the analysis was to quantify the change in directivity that occurs with a change in blade-tip end-plate geometry. Thus, the analysis complemented the span-wise coherence analysis presented in Chapter 4.

Chapter 6 presents an experimental methodology that the authors developed for making acoustic measurements along the blade chord. This 'frozen rotor' methodology involved mounting an isolated fan blade in an anechoic chamber and then measuring the interaction noise from a jet impacting on the fan blade. Although the blade did not move, the authors reproduced the Mach number, Reynolds number and blade incidence angle in the static frame of reference. They then correlated the near-field unsteady pressure measurements at ten blade-tip chord-wise locations with a far-field acoustic measurement at 30 degrees from the fan axis. They analysed the chord-wise acoustic measurements using the analysis techniques presented in Chapters 4 and 5. An analysis result identified a causal relationship between aerodynamic flow features in the blade-tip region and far-field noise emissions. Thus, the frozen rotor experimental methodology provided a method for identifying the role of blade-tip geometry in producing blade self-noise when interacting with a turbulent inflow.

Chapters 7, 8, 9 and 10: Computational Analysis

The experimental methodologies and analytical techniques that the authors present in Chapters 2, 3, 4, 5 and 6 provide a basis for identifying near-field aerodynamic flow features that resulted in fan far-field noise. Chapters 7, 8, 9 and 10

present blade-to-blade flow-field computational analysis techniques that complement this experimental work. The authors used fan blade-to-blade flow-field computational predictions as a 'numerical laboratory' to provide a detailed prediction of flow-field features induced in the blade tip-to-casing region by different blade-tip end-plate designs.

The computational analysis' objective was to facilitate development of new blade-tip end-plate concepts that would reduce fan far-field noise. The four chapters present the developed computational analysis techniques as a linear progression. In practice their development overlapped, whilst establishing simultaneously the relative merits of different blade-tip end-plate designs. Collectively, Chapters 7, 8, 9 and 10 provide insight into the linkage between blade-tip end-plate geometry, flow-field features in the blade-tip region and fan far-field noise. This insight facilitated the development of a new approach to passive noise control in fans intended for air movement application.

Chapter 7 presents an initial computational analysis of the blade-to-blade flow-field for the studied fan both with and without a fitted blade-tip end-plate. Previously, development engineers applied a constant thickness blade-tip end-plate to the studied fan in an early attempt to reduce fan noise. It did reduce fan far-field noise, and therefore, the authors undertook the initial computational analysis in an effort to clarify why. Previous experimental work reported in Chapters 3, 4, 5 and 6 had established the importance of the blade-tip leakage vortex, and therefore the computational analysis focused on the flow-field in the blade-tip region. The computational analysis indicated that at the fan's design point the presence of the constant thickness blade-tip end-plate reduced the overall blade-tip leakage flow and therefore the intensity of the blade-tip leakage vortex. The authors concluded that the reduced intensity was responsible for the reduced fan far-field noise. However, the reduced intensity resulted in the blade-tip leakage vortex bursting, a flow-field feature that is acoustically productive. The chapter goes on to present a design methodology that enhances vortex swirl using a variable thickness blade-tip end-plate intended to prevent the vortex bursting. By avoiding vortex bursting, the acoustic emissions associated with vortex bursting would be eliminated. Therefore the authors speculated fan far-field noise reduce would be reduced.

Chapter 8 presents and analyses the blade-to-blade flow-field for the studied fan without blade-tip treatment, with a constant thickness blade-tip end-plate and with a variable thickness blade-tip end-plate. The authors used computational analysis to calculate the blade-tip leakage flow's helicity. In studying the helicity contours, the authors found that the variable thickness blade-tip end-plate increased blade-tip leakage vortex swirl level sufficiently to avoid blade-tip leakage vortex bursting. Assessing the aerodynamic performance demonstrated an improved pressure developing capability and efficiency that one may attribute to the blade-tip leakage vortex not bursting. However, noise measurements indicated that the variable thickness blade-tip end-plate resulted in an overall noise level approximately 0.5 dB higher than that associated with the constant thickness blade-tip end-plate. When the authors studied the computational analysis, they found that the end-plate's variable

thickness induced the creation of multiple organised vortical structures. These vortical structures did break down, and were acoustically productive enough to result in increased overall fan far-field broad band noise. This increase in broadband noise was in spite of the blade-tip leakage vortex not bursting. Therefore, the blade tip end-plate design methodology was effective, in that the authors avoided bursting the blade-tip leakage vortex, but the methodology was not effective at reducing overall fan far-field noise.

Chapter 9 builds on the computational analysis from Chapter 8. The variable thickness blade-tip end-plate design had been successful in that there was no blade-tip leakage vortex breakdown. Additionally, fan pressure developing capability and efficiency had improved. However, overall fan far-field noise increased slightly due to the presence of multiple organised vortical structures. The authors used computational analysis to calculate total pressure loss coefficient distributions. When they studied the total pressure loss coefficient distributions, the highest loss regions for the studied fan, both with and without a fitted blade-tip end-plate, always coincided with the blade-tip leakage vortex core. When the authors studied the total pressure loss coefficient distributions for the variable thickness blade-tip end-plate, they found the multiple organised vortical structures weak and therefore aerodynamically insignificant compared to the blade-tip leakage vortex. Despite the low loss associated with the multiple organised vortical structures, they proved to be disproportionately acoustically productive. The authors realised that the variable thickness blade-tip end-plate required redesigning to minimise the blade-tip leakage vortex's intensity whilst both ensuring that it does not burst and that the blade-tip end-plate design avoids generating organised vortical structures.

Chapter 10 presents a development of the constant and variable thickness blade-tip end-plate designs, incorporating a step along the blade chord at the blade-tip and end-plate's intersection. The objective of incorporating the stepped blade-tip features was to provide an additional mechanism to weaken the multiple organised vortical structures' intensity. It was these multiple organised vortical structures' that had resulted in the studied fan's relatively poor far-field acoustic performance when fitted with the variable thickness end-plate. The authors hoped that the benefit of the blade-tip leakage vortex not bursting would be retained, but the negative effect of having created multiple organised vortical structures in the process would be negated. The authors used computational analysis to calculate Powell's sound-source distributions of blade-tip leakage flow, as Powell's sound-source distributions characterises the vortical motion that is responsible for acoustic emissions. When the authors studied Powell's sound-source distributions for the variable thickness blade-tip end-plate, they indicated the presence of a highly skewed blade-tip leading-edge vortex interacting with the blade-tip leakage vortex. This interaction resulted in the creation of the multiple organised vortical structures. Studying Powell's sound-source distributions for both constant and variable thickness, blade-tip end-plates with the step feature added indicated that it weakened the near-field acoustic emissions' intensity from the organised vortical structures, reduced blade tip leakage flow, but actually increased fan far-field noise.

Chapters 11, 12 and 13: Technologies Readiness

The computational analysis presented in Chapters 7, 8, 9 and 10 provided an insight into the studied fan's flow-field physics, and constituted the creation of a new passive noise control philosophy. In Chapter 11, this new philosophy is transformed into a design methodology. The authors used this methodology to design a new blade-tip end-plate, named the Multiple Vortex Breakdown (MVB) end-plate. Chapter 12 presents the studied fan's aerodynamic and acoustic performance when fitted with the MVB end plate. Chapter 13 then verifies the aerodynamic and acoustic performance with the studied fan installed over a tube bank as it is in practical application.

Chapter 11 presents the design procedure for an anti-vortex blade tip end-plate. The design process exploits the link between aerodynamic flow features in the blade-tip region and fan far-field noise. The design procedure configures the end-plate design in accordance with a multiple vortex breakdown criterion. Reversing the computational analysis techniques from Chapters 7, 8, 9 and 10 specifies the end-plate geometry. Instead of using the computational analysis to predict the flow-field induced by existing end-plate geometry, the authors use it to define the necessary geometry to minimise blade-tip leakage vortex mass flow rate whilst maintaining the vortex vorticity above a required critical threshold to ensure it does not burst. Additionally, the end-plate geometry's definition focused on inhibiting the formation of other organised vortical structures in the blade-tip region. Thus, the design process eliminates any acoustic emissions that one would have associated with the presence of these flow-field structures.

Chapter 12 presents an experimental investigation of the studied fan when fitted with the MVB end-plate. The authors used the near- and far-field correlation technique from Chapter 2 in combination with the span-wise analysis of coherence values from Chapter 4 and the directivity analysis from Chapter 5. When fitted with the MVB end-plate, the studied fan's measured pressure developing capability improved in comparison to the fan without an end-plate or any other studied end-plate configurations. The authors achieved this improvement in pressure developing capability without an efficiency penalty. Fan efficiency with the MVB end-plate remained similar to that of the studied fan with no end plate fitted or with any of the other studied end-plate configurations despite an increase in blade loading. Directivity measurements confirmed that overall fan far-field noise reduced by 10 dB(A) on the fan centre line and 8 dB(A) overall at its peak pressure operating point. At its high flow operating point, overall fan far-field noise reduced by 4 dB(A). The experimental results confirmed that the design procedure from Chapter 11 was an effective method for defining the geometry in a blade-tip end-plate, improving both fan aerodynamic and acoustic performance.

Chapter 13 extends the experimental investigation from Chapter 12 from assessing aerodynamic and acoustic performance in a laboratory environment to assessing an installed fan's performance. In practice, the studied fan draws air across a compact cooling unit's tube bank. The tube bank presence distorts the in-flow velocity

profile and increases the in-flow turbulence level. The experimental methodology from Chapter 6 had established that fan performance was sensitive to in-flow conditions and consequently, it was necessary to verify installed performance. At the fan's design operating point, installation effects degraded to a 2.5 dB(A) reduction the 5.8 dB(A) reduction in overall fan far-field noise. Although an apparently modest improvement, in combination with the reduced tonal noise peaks, the resultant compact cooling unit acoustic performance when fitted with the studied fan fitted with the MVB end-plate was the best in its class. The authors achieved this improvement without increasing the fan's manufacturing cost, or changing any of the compact cooling unit mechanical or electrical interfaces.

Summary of Chapters

Geoff Sheard

This chapter-by-chapter summary of technical contribution provides the reader with a detailed description of the work in each chapter. It clarifies each chapter's content and summarises its contribution to knowledge. This summary augments the description of the work itself with discussion as to why the authors undertook the work. It also lays out the rationale for undertaking the research, and the logic underpinning the move from one reported research programme to the next. Therefore, this summary links each chapter and makes explicit their collective contribution to knowledge.

The papers comprising each chapter constitute selected publications from the published scholarly work relating to the development of passive noise control technology. The Editor selected them for inclusion based on the degree to which the content contributed towards the creation of a coherent body of knowledge.

Chapter 1 A Critical Review of Passive Noise Control Techniques in Industrial Fans

The review paper that forms the basis of Chapter 1 was written specifically to be the first chapter of this edited volume. The developed experimental and computational methodologies reported in the research papers that form the remaining chapters of this edited volume were not created in a vacuum. Their development was informed by the work of other researchers working in both the aerospace and air movement fan community. Before considering the developed experimental methodologies, computational methodologies and the resulting new noise control technology, it is first helpful to consider the context within which they were developed.

The chapter systematically reviews the extant literature on passive noise control techniques, with a particular focus on experimental rather than theoretical research. The review examines the interaction between aerodynamic cause and acoustic effect that current control technologies have inspired. The review reflects an emphasis on low-speed air movement fans. The chapter considers high-speed turbomachinery fan and compressor noise control technology, but with the objective of illustrating the linkage between aerospace and air movement technologies. This identifies aspects of aerospace technology that one can most likely apply successfully to air movement fans.

Engineers broadly categorise noise control technology as either passive or active. Passive noise control technology focuses on aerodynamic flow control, with the

review identifying eleven different approaches to passive noise control. The chapter reviews active noise control technologies within the context of their applicability to air movement fans. However, the cost of active noise control technologies is high by air movement fan standards and therefore the review primarily focuses on aerospace research regarding passive noise control technologies.

The most promising noise control technology for air movement fan application is technology with a synergy between flow and noise control. Such technology offers the potential to both reduce fan far-field noise and improve fan efficiency. Improving fan efficiency is critical as air movement fan designers have historically focused on mechanical integrity first and aerodynamic efficiency second. However, this historic focus is not consistent with the emerging regulatory environment within Europe. The Energy using Product (EuP) Directive, European Commission Directive 327, became legally binding within Europe on 1 January, 2013, setting minimum standards for fan efficiency. These standards will rise on 1 January, 2015.

Research into flow and noise control technology could be more effective if industrialists and academics focus their research on elucidating the physics underpinning the link between fluid flow and acoustics. Computational modelling of the fan flow-field has the potential to provide insight into the aerodynamic cause of experimentally measured acoustic effect. This insight is necessary to inform the development of new design methodologies that can both reduce fan far-field noise and improve fan efficiency.

New design methodologies require validation, and then integration into air movement fan design procedures. The development, validation and integration of new design methodologies are a substantive undertaking requiring skills and expertise that generally do not exist within the air movement fan community. A pragmatic response to the reality that air movement fan manufacturers do not have all the skills required to develop the needed design methodologies is to work collaboratively with a university partner. A collaborative approach between academic researchers and air movement development engineers has the potential to both originate new flow and noise control technology and bridge the gap between academic research and air movement fan development.

Chapter 2 Experimental Development of a Measurement Technique to Resolve the Radial Distribution of Fan Aeroacoustic Emissions

In many cases, the experimental methodologies that researchers reported in the extant literature were not developed for application with rotating machinery. Consequently, there was a need to adapt and develop the reported techniques to create an air movement fan specific experimental methodology that would facilitate the dissection of aeroacoustic noise sources. It was the dissection of aeroacoustic noise sources that was the developed experimental methodology's primary focus. It is this dissection that constitutes elucidating the physical flow mechanisms in the near-field.

Chapter 2 presents an experimental methodology developed to facilitate assessment of fan acoustic performance. The authors developed the methodology to pro-

vide insight into the far-field acoustic consequences of near-field flow features induced in the flow by blade-tip end-plates. Air movement fan engineers originally developed the studied fan for application in compact cooling units. During the early 2000s, the market for compact cooling units was expanding as air conditioning systems became a standard feature in new commercial buildings. The fans fitted to air conditioning system compact cooling units were responsible for the majority of the cooling units' acoustic emissions and hence, engineers were under pressure to reduce fan far-field noise.

At the time, engineers within the air movement fan community were still developing new products using empirical techniques dating back to the 1950s. In an attempt to reduce fan far-field noise, they fitted a constant thickness blade-tip end-plate. The fan blades are manufactured from injection moulded plastic, with the blade-tip end-plate's thickness simply the largest possible within the available manufacturing technology limits. This constant thickness blade-tip end-plate constituted the limit of 1950s empirical design techniques.

The developed experimental technique involved placing a microphone ten per cent blade chord down-stream of the studied fan blade's trailing edge. The authors then varied the microphone's span-wise location in steps of two per cent from blade hub to blade-tip. They made acoustic measurements simultaneously with a far-field microphone. Thus, the experimental technique was able to provide data sets of fan near- and far-field noise that the authors could then correlate to establish the far-field acoustic consequences of near-field noise sources. It was this near- and far-field correlation technique that provides the required method for resolving aeroacoustic noise sources along the blade span.

A limitation of the developed near- and far-field correlation technique is that it relies on fan far-field noise measurements taken when the near-field microphone is present. One can measure fan far-field noise without the near-field microphone. The authors use a measurement of fan far-field noise without the near-field microphone as part of the technique to correct for the near-field microphone's acoustic influence.

The experimental methodology and associated near- and far-field correlation technique proved effective. The span-wide correlation of near- and far-field noise was distinctly different for the studied fan without a fitted blade-tip end-plate and when fitted with an end-plate. Therefore, the experimental technique facilitated identifying near-field noise sources unique to each of the tested fan geometries and their far-field acoustic consequences.

Chapter 3 Detection of Aerodynamic Noise Sources in Low-speed Axial Fans with Tip End-plates

Chapter 3 applies the developed experimental methodology and near- and far-field correlation technique. The research's focus was the association of flow-field features in the blade tip-to-casing region with blade-tip end-plate design features. Thus, the objective was to clarify the role of specific blade-tip end-plate design features in generating tonal and broadband fan far-field noise.

One could reasonably expect that a blade-tip end-plate will influence the flow-field in the blade-tip region only, but this was not the case. The presence of blade-tip end-plates influenced the blade-to-blade flow-field over the entire blade span. The authors measured the flow coefficient's span-wise distributions 1.2 blade chords down-stream of the studied fan. When they analysed the flow coefficient's span-wise distributions, the results indicated that the presence of a blade-tip end-plate resulted in a boundary layer at the blade root that was less likely to separate.

A consequence of hub boundary layers that are less likely to separate is a reduction in the volume of fluid centrifuged up the blade pressure surface towards the blade-tip. A reduction in the tendency of the hub boundary layers to separate also resulted in the suppression of a hub separation bubble, eliminating a possible near-field flow-field feature that had negative far-field acoustic consequences.

The authors analysed the role of coherent vortical structures and blade tip-to-casing leakage flow features as noise sources using a novel Symmetrised Dot Pattern (SDP) visualisation of fan far-field noise. The SDP visualisation technique facilitated a study of the way in which human perception of fan far-field noise changes as the authors changed the blade-tip treatment.

The authors produced the SDPs using an algorithm that maps a normalised time waveform derived from a fan far-field noise measurement onto a radial component with the adjacent point mapping onto an angular component. The resulting SDP shapes provided a qualitative assessment of human acceptability of fan far-field noise associated with the studied fan both with and without fitted blade-tip end-plates.

Previous researchers who have applied the SPD technique have concluded that the human ear finds noise more acceptable if the noise is correlated with the smallest area of dots in the associated SDP. Consequently, one may use the area of SDPs as a proxy for the human ears' perception of the acceptability of a fan's far-field noise. Although somewhat subjective, the applications into which the studied fan is fitted are invariably within close proximity to people. As such, the acceptability of the fan far-field noise, as well as its overall level, is important. The authors found that the studied fan with a fitted blade-tip end-plate occurred with a smaller SDP area than when no end-plate was fitted.

The presence of blade-tip end-plates reduces the absolute level of fan far-field noise as a consequence of both reducing the blade-tip leakage flow rate and influencing the development of boundary layers and secondary flow features in the blade hub region. Additionally, the acceptability of fan far-field noise improves with adding a blade-tip end-plate which constitutes a secondary benefit associated with applying blade-tip end-plates.

Chapter 4 Experimental Aeroacoustic Studies on Improved Tip Configurations for Passive Control of Noise Signatures in Low-Speed Axial Fans

Chapter 4 once again applies the near- and far-field correlation technique, focusing on the tonal noise's span-wise variation. This focus on tonal noise was a consequence of the blade passing frequency and its second, third and fourth harmonics dominating the fan far-field noise spectra. The fifth and sixth harmonics were evident

in the data, but were tonally less important as they had reduced in magnitude to the point where they effectively merged with the broadband noise.

The authors used a coherence function that involves normalising the signal, highlighting highly coherent events, irrespective of energy content. Highlighting highly coherent events made the technique effective at isolating coherent regions in the coherence maps. The authors created coherence maps by plotting coherence against blade span and frequency. The coherence analysis identified six distinct coherent regions, each associated with a different combination of span-wise location and frequency.

We may regard the first three coherent regions as generally occurring with the studied fan, with or without a blade-tip end-plate fitted. The first occurred with noise which the electric motor driving the fan generated. The authors mounted the fan impeller directly on the motor shaft, and consequently, acoustic measurements included the motor's contribution. The second occurred with ingested noise from the fan inlet plenum. The inlet plenum boundary layer's interaction with the blade-to-blade flow-field in the blade-tip region was acoustically productive. The third occurred with rotor only noise. The rotor only noise is primarily a single tone at the blade passing frequency.

The fourth coherent region provides an insight into the likely in-service effectiveness of blade-tip end-plate designs as it is generated by turbulence in the in-flow. In practice, engineers install the studied fan over a tube-bank with flow drawing across the tube bank and into the fan inlet. Consequently, they associated the in-service installation with significantly higher inlet turbulence levels than those that occur with a laboratory test. The relative susceptibility of different blade-tip end-plate designs to turbulence induced noise provides a measure of their likely effectiveness in-service.

The fifth and sixth coherent regions occur with specific flow features in the blade-to-blade flow-field that blade-tip end-plate presence induces. The fifth occurred with secondary flow noise. The blade-hub secondary flow vortex presence is responsible for this noise source. The sixth occurred as a consequence of the blade-tip leakage vortex's bursting. The blade-tip leakage vortex may either pass out of the blade-to-blade passage without bursting, or burst in the blade-to-blade passage. Bursting in the blade-to-blade passage is acoustically productive.

The difference between coherence maps for the studied fan with and without blade-tip end-plates then enabled the authors to associate end-plate geometry with features on the coherence maps. Changes in blade-tip end-plate geometry had a significant effect on the flow features induced in the blade-to-blade flow-field. Therefore, analysing the coherence maps provided an insight into the acoustic far-field consequences of aerodynamic near-field flow-field features and thus facilitated an insight into the physical mechanisms responsible for fan far-field noise.

Chapter 5 Far-field Radiation of Tip Aerodynamic Sound Sources in Axial Fans Fitted with Passive Noise Control Features

The experimental methodology reported in Chapter 2 had proven effective, facilitating the dissection of aeroacoustic noise sources. This dissection constitutes

elucidation of the near-field physical flow mechanisms that the authors then correlate with fan far-field noise. In Chapter 5 the authors extend the experimental methodology reported in Chapter 2 to include fan far-field acoustic measurements at different azimuthal positions. Thus, the original correlation technique extends to a directivity analysis.

The authors placed a microphone ten per cent blade chord down-stream of the studied fan blade's trailing edge. The authors then varied the microphone's span-wise location in steps of two per cent from blade hub to blade-tip. At each span-wise location the authors measured far-field noise on the fan centre line and 30, 45, 60, 75 and 90 degrees off the fan centre line. They made near- and far-field acoustic measurements simultaneously. This enabled the experimental technique to provide data sets of near- and far-field noise over a range of far-field azimuthal positions that the authors could correlate to establish the near-field noise sources' far-field directivity.

The authors used the directivity analysis to characterise the fan far-field broadband noise's directivity with and without fitted blade-tip end-plates. By filtering fan far-field noise measurements, the authors established the directivity of the blade passing frequency, the second, third and fourth harmonics of blade passing frequency and high frequency noise above 1 kHz.

The broadband directivity analysis confirmed that fan far-field noise was anisotropic. The studied fan without a fitted blade-tip end-plate behaved as a dipolar broadband noise source. Including a blade-tip end-plate resulted in the fan continuing to behave as a dipolar noise source, or to become a more anisotropic noise source with the difference occurring with specific features of the blade-tip end-plate geometry. The authors correlated the broadband noise with the degree of swirl in the exhaust flow. Further they concluded that large-scale coherent structures superimposed a dipolar noise source and smaller random turbulent structures superimposed a lateral quadra-pole noise source.

The directivity analysis complemented the span-wise coherence analysis presented in Chapter 4, providing additional insight into the impact of end-plate geometry on fan far-field noise. It clarifies the acoustic effect of blade-tip end-plate geometry and thus, the analysis facilitates insight into the blade-tip end-plate geometry's impact on fan far-field noise. A comparative consideration of the directivity analysis of the studied fan both with and without a fitted blade-tip end-plate provided a basis for identifying near-field physical flow-field mechanisms responsible for fan far-field noise.

Chapter 6 Experimental Study on the Self-noise of a Turbulent Round Jet Investing a Cambered Aerofoil

The experimental methodology developed in Chapter 2 and extended in Chapter 5 provided the acoustic data that the authors needed. They were able to use the data to associate blade-tip end-plate design features with span-wise flow-field features in the near-field and their far-field acoustic consequences. Chapter 6 complements this span-wise experimental methodology with an experimental methodology for making acoustic measurements along the blade chord. This chord-wise method-

ology involved mounting an isolated fan blade in an anechoic chamber and then measuring the interaction noise from a jet impacting on the fan blade.

The authors placed ten microphones, equally spaced from leading to trailing edge at the blade-tip of a single fan blade. They mounted the instrumented blade in an anechoic chamber and measured the interaction noise with a jet impacting the blade. Although the blade did not move, the authors reproduced the Mach number, Reynolds number and blade incidence angel in the static frame of reference. This 'frozen rotor' technique enabled the authors to correlate ten chord-wise near-field acoustic measurements with far-field acoustic measurements 30 degrees off the fan axis.

The authors made the near- and far-field measurements simultaneously. This enabled the experimental methodology to provide data sets of chord-wide distributions of near-field unsteady pressure and fan far-field noise. The authors then correlated the data sets using the analysis technique presented in Chapter 5. This correlation enabled them to establish the far-field effect of chord-wise distributions of noise sources, with and without fitted blade-tip end-plates.

This chord-wise correlation of near-field unsteady pressure and fan far-field noise was distinctly different for the studied fan without a fitted blade-tip end-plate and when fitted with an end-plate. For the fan without a fitted blade-tip end-plate the predominant noise source occurred with the blade-tip leakage flow towards the blade trailing edge. The blade-tip leakage flow's intensity as a noise source is directly related to the fan casing boundary layer's thickness, with a thicker boundary layer resulting in increased fan far-field broadband noise.

When fitted with a blade-tip end-plate, the chord-wise near-field unsteady pressure measurements indicated that the blade surface in the blade-tip region acted as a mixing enhancer. This mixing enhancer resulted in the absorption of near-field noise as a consequence of vortex shedding through the blade tip-to-casing gap. This vortex shedding resulted in an increase in the local turbulence level that transformed harmonic tonal noise into broadband high frequency noise. The correlation between near-field unsteady pressure and fan far-field noise indicated that this broadband high frequency noise was more easily attenuated than the original harmonic noise sources. Consequently, the broadband high frequency noise did not transmit to the far-field as efficiently as the original harmonic noise sources. The result was that when fitted with a blade-tip end-plate, fan far-field noise reduced.

The developed frozen rotor experimental technique has proven effective, enabling the authors to identify a mechanism by which blade-tip end-plates modify the blade tip-to-casing flow that results in a change from harmonic to broadband noise. The correlation technique was also effective as it facilitated identifying the far-field acoustic consequences of changes in fan near-field flow-field.

Chapter 7 Tip End-plate Concept Based on LeakageVortex Rotation Number Control

Computational predictions can complement experimental measured data by creating a 'numerical laboratory' providing insight into the blade-to-blade flow-field. By predicting the blade-to-blade flow-field for the studied fan without a fitted blade-

tip end-plate and with fitted blade-tip end-plates, one may establish the impact of end-plate geometry on flow-field features.

Chapter 7 presents an initial computational analysis of the blade-to-blade flow-field for the studied fan both without a blade-tip end-plate, coded fan *datum* AC90/6, and with a constant thickness blade-tip end-plate, coded fan AC90/6/TF. The authors undertook the computational analysis using a Reynolds-averaged Navier–Stokes (RANS) simulation with a non-linear k-ε turbulence model in low-Reynolds number formulation.

The accuracy of Large Eddy Simulations (LESs) is largely independent of the choice of sub-grid scale closure. Consequently, researchers are increasingly favouring LESs when modelling turbomachinery flow. However, the computational effort required to undertake a LES is one to two orders of magnitude greater than that needed for a RANS simulation. Consequently, researchers still widely use RANS simulations, particularly within the air movement fan community, as they do not have access to the computational resources available within the aerospace fan community.

A limitation of RANS simulations is that they are not able to model unsteady effects and therefore model only part of the flow-field physics. The authors considered this acceptable in analysing the studied fan geometries because the RANS model was the subject of extensive application specific development. The authors adapted choice and formulation of the eddy-viscosity closure model to maximise accuracy when predicting the blade-tip leakage vortex's roll up under the influence of a pressure gradient. Additionally, the RANS model utilised an anisotropy-resolving turbulence model with a numerical diffusivity scheme previously proven to model the dominant large-scale flow features' non-isotropy.

The experimental results reported in Chapters 2, 3, 4, 5 and 6 had established the importance of the blade-tip leakage vortex, and therefore the computational analysis focused on the flow-field in the blade-tip region. The computational analysis indicated that at the fan's design point, the presence of the constant thickness blade-tip end-plate reduced the over-tip blade leakage flow and therefore the blade-tip leakage vortex's intensity. The authors concluded that this reduction in intensity was responsible for reducing fan far-field noise. However, the reduction in intensity resulted in the blade-tip leakage vortex bursting. This is a flow-field feature that researchers know is acoustically productive.

The authors used computational analysis to characterise the chord-wise distribution of blade-tip leakage vortex Rossby number. The Rossby number quantifies vortex rotation. There is a threshold value of the Rossby number below which vortex rotation cannot reduce if the vortex is to remain stable. The computational analysis indicated that for the fan *datum* AC90/6, the blade-tip leakage vortex Rossby number remained above the threshold value and did not burst. However, the fan AC/90/6/TF blade-tip leakage Rossby number fell below the threshold value at approximately 90 per cent chord and did burst.

A realisation that the blade-tip end-plate resulted in the fan AC90/6/TF blade-tip leakage vortex bursting was the insight needed to refine the blade-tip end-plate design. By reducing the blade-tip end-plate's chord-wise thickness towards the

blade's trailing edge, the blade-tip leakage vortex's vorticity could increase. Increasing blade-tip leakage vortex vorticity would ensure its Rossby number remained above the threshold value needed to avoid vortex bursting. Avoiding vortex bursting would eliminate the acoustic emissions that occurred with it and therefore should reduce fan far-field noise.

Thus, the blade-tip end-plate design methodology utilises the computational analysis to establish blade-tip leakage vortex swirl level and then varies end-plate geometry to enhance swirl level. Therefore, the design methodology produces a blade-tip end-plate design that ensures the blade-tip leakage vortex does not burst, minimising acoustic emissions from the vortex. When the authors fitted the studied fan with the new variable thickness blade-tip end-plate, they coded it fan AC90/6/TF$_{VTE}$.

Chapter 8 Development of Improved Blade Tip Endplate Concepts for Low-noise Operation in Industrial Fans

Chapter 8 examines the performance of the fan AC90/6/TF$_{VTE}$ designed using the new design methodology. The authors facilitated analysis of the predicted blade-to-blade flow-field for the fan AC90/6/TF$_{VTE}$ through comparison with the predicted blade-to-blade flow-field of fan *datum* AC90/6 and fan AC90/6/TF.

The computational analysis indicated that the variable thickness blade-tip end-plate design successfully avoided blade-tip leakage vortex bursting. Assessing aerodynamic performance demonstrated an improved pressure developing capability and fan efficiency that we may attribute to the blade-tip leakage vortex not bursting. However, noise measurements indicated that the variable thickness blade-tip end-plate resulted in an overall broadband noise level approximately 0.5 dB higher than that occurring with the constant thickness end-plate.

The authors used computational analysis to calculate the blade-tip leakage flow's helicity. In this context, the authors define helicity as the projection of vorticity along the local relative velocity vector. Helicity is a useful parameter as it provides an insight into the criteria needed for vortex bursting. When the authors studied the helicity contours, they found that the variable thickness end-plate induced the presence of multiple organised vortical structures. These vortical structures did burst, with the breakdown acoustically productive enough to result in the increase in overall fan far-field noise.

Despite the variable thickness end-plate successfully preventing the blade-tip leakage vortex bursting, the authors concluded that the breakdown of other organised vortical structures was responsible for the increased broadband noise. This increase occurred in spite of the blade-tip leakage vortex not bursting, a result that supports the existence of a strong linkage between bursting coherent swirling structures and fan far-field noise. Therefore, the blade-tip end-plate design methodology was effective, in that the authors avoided bursting the blade-tip leakage vortex, but was not effective at reducing overall fan far-field noise.

Chapter 9 Shaping of Tip End-plate to Control Leakage Vortex Swirl in Axial Flow Fans

Chapter 9 builds on the computational analysis presented in Chapter 8. The variable thickness blade-tip end-plate design had been successful in that the authors avoided blade-tip leakage vortex breakdown. Additionally, fan pressure developing capability and efficiency had improved. However, overall fan far-field noise increased due to the presence of multiple organised vortical structures.

The authors used the computational analysis to calculate the distribution of total pressure loss coefficients in the blade-to-blade passage of the fan *datum* AC90/6, fan AC90/6/TF and fan AC90/6/TF$_{VTE}$. Distributions of total pressure loss coefficients are useful because they characterise the evolution of blade boundary layers. Thus, they facilitate identifying the three-dimensional swirling cores that are a feature of the flow-fields acoustically productive organised vortical structures.

Analysis of total pressure loss coefficient distributions confirmed that the highest loss regions always coincided with the blade-tip leakage vortex core. The multiple organised vortical structures were weak in comparison and therefore aerodynamically insignificant compared to the blade-tip leakage vortex. Despite the low loss that occurred with the multiple organised vortical structures, they proved to be disproportionately acoustically productive.

Chapter 10 Aerodynamic Performance of Blade Tip End-plates Designed for Low-noise Operation in Axial Flow Fans

A realisation that the multiple organised vortical structures induced in the blade-tip region by the variable thickness end-plate were disproportionately acoustically productive resulted in a break-through in conceptual thinking. The blade-tip end-plate requires redesign to minimise the swirling intensity and size of vortices in the blade-tip region. Whilst minimising intensity and size of vortical structures, the end-plate design must ensure that neither the blade-tip leakage vortex nor those organised vortical structures that are created burst.

Chapter 10 presents a development of the fan AC90/6/TF$_{VTE}$ and fan AC90/6/TF designs, incorporating a step along the blade chord at the intersection of the blade-tip and the end-plate. The objective of incorporating these stepped blade-tip features was to provide a mechanism to weaken the intensity of the multiple organised vortical structures that had resulted in the relatively poor performance of the fan AC90/6/TF$_{VTE}$. Thus, the authors hoped that they would retain the benefit that occurred with the blade-tip leakage vortex not bursting, but would negate the negative effect with having created multiple organised vortical structures in the process.

The authors used the computational analysis to calculate Powell's sound-source distributions of blade-tip leakage flow. Powell's sound-source distributions are useful as the Powell's sound-source parameter characterises the vortical motion that is responsible for acoustic emissions. Consequently, one may use an analysis of Powell's sound-source distributions to identify the most productive sound sources in a low-speed flow.

When the authors studied Powell's sound-source distributions, they facilitated a qualitative comparison of the fan near-field noise's origin for the studied fan with and without a fitted blade-tip end-plate. The Powell's sound-source distribution for the variable thickness end-plate indicated that a highly skewed blade leading-edge vortex interacting with the blade-tip leakage vortex. It was this interaction that resulted in the creation of the multiple organised vortical structures.

The authors studied the Powell's sound-source distributions for both constant and variable thickness blade-tip end-plates with the added step feature. They found that the step constituted an end-plate feature that weakened the intensity of near-field acoustic emissions from the organised vortical structures. This weakening occurred as a consequence of stretching the length of blade chord over which the blade-tip leakage vortex developed. This reduced the blade tip-to-casing leakage flow rate. Researchers generally consider fan far-field acoustic emissions to be a function of overall blade tip-to-casing leakage flow rate. However, noise measurements indicated that when fitted with the step feature, the studied fan with variable thickness blade-tip end-plate overall broadband noise level was approximately 1.0 dB higher than that occurring with the constant thickness end-plate and no step feature.

Chapter 11 End-plate for Noise-by-flow Control in Axial Fans

The computational analysis reported in Chapters 7, 8, 9 and 10 provided an insight into the studied fan's flow-field physics. The analysis identified the impact of the blade-tip leakage vortex bursting. It is vortical structure breakdown in the blade-tip region that results in fan far-field noise. A design process that controls the blade-tip flow with the specific objective of eliminating those near-field flow features primarily responsible for fan far-field noise is needed. Such a design process is able to exploit the link between near-field aerodynamic flow features and fan far-field noise.

In Chapter 11, the authors present a design process that aims to control the blade-tip leakage flow by exploiting the link between aerodynamic flow features in the blade-tip region and fan far-field noise. The authors used the design process to design a new blade-tip end-plate, named the Multiple Vortex Breakdown (MVB) end-plate. When they fitted the studied fan with the MVB blade-tip end-plate, they coded the fan AC90/6/TF$_{MVB}$.

The authors refined the computational analysis that they first used to predict the blade-to-blade flow-field induced by existing end-plate geometry. They used the refined computational analysis to define the geometry they needed to minimise blade-tip leakage vortex mass flow rate. Specifically the blade-tip leakage vortex mass flow rate was minimised whilst maintaining the blade-tip leakage vortex vorticity above a critical threshold needed to ensure it does not burst. Additionally, the definition of end-plate geometry focused on inhibiting the formation of other organised vortical structures in the blade-tip region.

The design procedure configures the end-plate design in accordance with a multiple vortex breakdown criterion by linking blade-tip end-plate design with flow control. The authors achieved this noise-by-flow control by designing the blade-tip end-plate to control the blade-tip leakage vortex rotation number's chord-wise

evolution. The resulting blade-tip end-plate design induces augmented and then diminution sequences of momentum transfer to the blade-tip leakage vortex, up to a near-critical breakdown condition.

The design process exploits a correlation between the blade-tip end-plate thickness, the blade-tip leakage vortex kinematics, the local blade loading and the magnitude of the blade-tip leakage flow. The authors derived the resultant end-plate thickness from the tip leakage vortex swirling level, with the objective of maintaining a stable blade-tip leakage vortex that does not burst, minimising both blade-tip leakage vortex intensity and the creation of other organised vortical structures.

Chapter 12 Experimental Characterisation of the Far-field Noise in Axial Fans Fitted with Shaped Tip End-plates

Chapter 12 presents an experimental investigation of the fan *datum* AC90/6, the fan AC90/6/TF and the fan AC90/6/TF$_{MVB}$. The authors used the near- and far-field correlation technique reported in Chapter 2 in combination with the span-wise analysis of coherence values reported in Chapter 4 and the directivity analysis reported in Chapter 5.

The fan AC90/6/TF$_{MVB}$ measured pressure developing capability improved in comparison to the fan *datum* AC90/6 and fan AC90/6/TF. The authors achieved the improvement in pressure developing capability without an efficiency penalty. Efficiency of the fan AC90/6/TF$_{MVB}$ remained similar to that of the studied fan without a fitted end-plate or with any of the other studied end-plate configurations despite an increase in blade loading.

Studying directivity patterns and using a coherence analysis characterises the impact of blade-tip end-plate design. The authors were able to establish that the fan AC90/6/TF$_{MVB}$ incorporating the newly conceived end-plate results in both a reduced tonal and overall far-field fan noise. The authors found the near-axis overall far-field noise level for the fan AC90/6/TF$_{MVB}$ 10 dB(A) lower than the fan *datum* AC90/6 and 4 dB(A) lower that the fan AC90/6/TF. This reduction of near-axis noise correlates with the presence of coherent swirling structures which the blade-tip end-plate induced.

The reported research verifies the technical merit of the fan AC90/6/TF$_{MVB}$ incorporating the newly conceived end-plate. The research provides an insight into the flow-field physics underpinning the reduced fan far-field noise. The newly conceived end-plate effectively minimises blade-tip leakage vortex intensity, avoids vortex breakdown and additionally induces a blade-tip flow-field feature that reduces far-field near-axis fan noise. It is this combination that is responsible for the low noise of the fan AC90/6/TF$_{MVB}$.

Chapter 13 Installed Acoustic Performance of Cooling Axial Fans Fitted with End-plates

Chapter 13 extends the experimental investigation reported in Chapter 12 from an assessment of aerodynamic and acoustic performance in a laboratory environ-

ment to an assessment of installed fan performance. Engineers use the studied fan to draw air across a compact cooling unit's tube bank. A tube bank presence distorts the in-flow velocity profile and increases the in-flow turbulence level. The experimental methodology presented in Chapter 6 had established that fan performance was sensitive to in-flow conditions and consequently, it was necessary to verify installed performance.

At the fan's design operating point, the 5.8 dB(A) reduction in overall fan far-field noise reported in Chapter 12 when the authors tested the fan in a laboratory environment, was degraded to a 2.5 dB(A) reduction when fitted over a cooling unit's tube bank. Although a 2.5 dB(A) reduction is an apparently modest improvement, in combination with the reduced tonal noise peaks, the resultant compact cooling unit acoustic performance was the best in its class. The authors achieved this improvement without increasing the fan's manufacturing cost, or changing any of the mechanical or electrical interfaces with the compact cooling unit.

Although installation effects degraded the performance of the fan AC90/6/TF$_{MVB}$, it still outperforms the fan AC90/6/TF with the constant thickness blade-tip end-plate. Although the authors associated the fan AC90/6/TF with lower noise levels than fan *datum* AC90/6 in a laboratory test, fan far-field noise level was almost identical when installed. In contrast, the fan AC90/6/TF$_{MVB}$ was able to deliver a 'real world' noise reduction when installed.

The reported research illustrates the importance of installation effects on fan performance with the newly conceived blade-tip end-plate design reduced fan far-field acoustic emission by less when installed in a standardised airway. Nevertheless, the achieved 2.5 dB(A) reduction results in the compact cooling unit when fitted with the fan AC90/6/TF$_{MVB}$ having the lowest noise in its class.

Appendix 1 A Meridional Fan

The appendix in this volume is a developed form of a patent. Patents are written in a formal style that is difficult for those unfamiliar to penetrate. As such, we tend not to read or reference patents. To overlook patents, however, is to overlook a significant source of intellectual property. The patent included in this volume documents MVB blade-tip end-plate design features that result in reduced fan far-field noise. We have edited the patent into a more readable form, in an effort to make its content more accessible to the reader.

The research reported in the papers that constitute the chapters of this edited volume documents a passive noise control technology development effort. It was the developed passive noise control technology that resulted in the novel blade-tip end-plate design features that moderated near-field flow features that, in turn, reduced fan far-field noise. The patent that forms the basis of this appendix does not describe in detail the design process that resulted in the novel blade-tip end-plate features. Rather, the patent simply lists the novel features, stating that they result in reduced fan far-field noise.

As such, the patent does not present the MVB blade-tip end-plate design process. The research papers that form the chapters of this edited volume present the

process by which the authors achieved the necessary insight into the flow-field physics. However, the authors do not describe the MVB blade-tip end-plate design process in either the research papers or the patent. The design process is iterative in nature, with a researcher computationally assessing the impact of minor changes in blade-tip end-plate geometry. This enabled a researcher to optimise blade-tip end-plate geometry, incorporating features described in the patent that form the basis of the appendix.

The patent is effective in that it protects the use of the blade-tip end-plate features that the authors used in creating the MVB end-plate design. However, it does not present a single air movement fan design procedure with a clearly defined blade-tip end-plate design process. Experience using the end-plate features protected by the patent indicates that each developed noise-by-flow control technology application requires a different approach as a consequence of the uniqueness of each new blade. As such, the research papers that comprise the chapters of this edited volume and the patent that comprises the appendix constitute a contribution to passive noise control technology, but not a single new air movement fan design procedure that one can apply to any blade design.

The chapters and appendix collectively comprise a methodology that one can apply to blade-tip end-plate design for different blades, with each application requiring the development of an application specific method. As such, the MVB design methodology shares a similarity with the RANS based computational method that is an integral part of the blade-tip end-plate design methodology. The RANS based computational method was the subject of extensive application specific development before it was able to accurately predict the blade-tip flow-field. Similarly, the MVB blade-tip end-plate design methodology requires extensive application specific development before one uses it to produce an MVB blade-tip end-plate design for a new blade.

A realisation that the MVB blade-tip end-plate design methodology requires application specific development to create a design method suitable for a new blade illustrates both a strength and weakness of computational based design methodologies. Computational based design methodologies are capable of providing both lower noise and more efficient fan designs. They also require a high level of expertise on the part of the design engineer applying them. Consequently, academic researchers and air movement development engineers should collaborate, with academic researchers developing each application specific blade-tip end-plate design procedure in order to bridge the gap between academic research and air movement fan development.

Chapter 1

A Critical Review of Passive Noise Control Techniques in Industrial Fans

S. Bianchi, A. Corsini and A.G. Sheard

ABSTRACT

This chapter presents a review of noise control techniques used within the air movement and control community. It aims to assist design engineers understand and apply passive solutions when designing low-noise air movement fans. We systematically review the extant literature on passive noise control techniques, with a particular focus on experimental rather than theoretical research. The review provides an assessment of the current state-of-the-art techniques in air movement fan flow and noise control, offering a vision for potential improvements in noise reduction via novel application of flow and noise control technologies. We examine the interaction between aerodynamic cause and acoustic effect and the application of control technologies that current cause-and-effect theories have inspired. The purpose is twofold. First, it provides a vision for aerodynamics research over the next decade; and second, it provides air movement fan designers with an insight into the technology now available that they may apply in an on-going effort to reduce fan noise. Therefore, the review offers a pragmatic and practical assessment of available technology, and the readiness of that technology for application into air movement fan design methodologies. The review reflects an emphasis on low speed air movement fans. We consider high speed turbomachinery noise control only to illustrate the links between the two technologies. Thus, the review provides an insight into the turbomachinery technology that manufacturers today can apply practically into air movement fans. The review then summarises the opportunities for future research and the potential for design engineers to further refine flow and noise control in air movement fan design.

This chapter is a revised and extended version of Bianchi, S., Corsini, A. and Sheard, A.G. (2014), 'A Critical Review of Passive Noise Control Techniques in Industrial Fans', *Transactions of the ASME, Journal of Engineering for Gas Turbines & Power*, vol. 136(4), paper no. 044001, pp. 1–10.

INTRODUCTION

The 1990s witnessed a 'changing of the guard' in aeromechanic research, with an increased emphasis on harnessing the potential of flow control in a fully integrated, multidisciplinary framework to control noise emissions. Consequently, technologies for developing new air movement fans that combine significant improvements in cost and performance have appeared. Transitioning these technologies from the research laboratory and into practical application requires coupling further aerodynamics advances with an exploitation of non-traditional and interdisciplinary technologies; specifically, smart, distributed aerodynamic controls, passive actuators and novel mechanical systems.

Synergy between flow and noise control is a focus within the air movement and control community. More broadly, there is a realisation that there is a need to pursue a concurrent approach to research integrating fluid mechanics, structural mechanics, material science, acoustics and control theory. It is only through a concurrent approach that air movement fan designers can transition from empirical fan to industrial turbomachinery technology.

Over the last ten years, air movement fan technology has systematically evolved through the adaption and adoption of turbomachinery design tools. The trend towards turbomachinery design tool application is continuing. Pioneering research, combined with newly emerging enabling technologies, are transforming air movement fan technology. This transformation is facilitating both the practical application of novel concepts and refining and optimising those already in use. Many of the current applications in air movement fans have a history of successful application in aerospace turbomachinery. However, it is not possible to transfer directly technology from aerospace to air movement fan applications. It requires innovation. The air movement and control community must focus on innovatively applying aerospace technology for the foreseeable future.

Researchers in the 1970s, particularly Wright (1976) and Cumpsty (1977), have studied the link between the fan rotors' aerodynamic features and their acoustic emissions. Their findings have enhanced general understanding of axial turbomachinery aeroacoustics. Cumpsty (1977) concluded that, with the exception of the low-frequency range of high-speed machines, the mechanism that determines broadband noise in subsonic fans is the same as that in supersonic tip-speed fans and compressors. According to Wright (1976), this is because of the prominence of rotor noise that originates from turbulent boundary layers.

Other researchers have identified a variety of mechanisms as causing fan noise. Lighthill (1952, 1954) studied fan rotor aerodynamic noise and Blake (1986) dedicated one volume of his book on noise sources to rotor and airflow interaction. These researchers have independently concluded that the dominant sources are the rotor blades, which generate noise as a result of turbulent wake shedding from the interaction between the end-wall boundary layer and the rotor tip. In view of the aerodynamic effect that tip-leakage flow exerts on wake and secondary flows, researchers widely recognise this mechanism as one of the most significant noise sources (Fukano *et al.*, 1986; Holste and Neise, 1997).

The advent of stringent environmental regulations with respect to noise emission has stimulated academics and practitioners to pursue the development of concepts and technologies that are likely to reduce fan noise, either by attenuating noise propagation or by controlling the noise at source. In this regard, researchers have not focused attention to the rotor-tip flow-field which influences noise control and reduction. A deficient understanding of the complex flow phenomena involved is responsible for this lack of focus. Despite the complexity of the flow phenomena involved, Marcinowski (1953), the first researcher to study noise associated with tip dynamics, demonstrated that increases in broadband noise levels occur with increasing tip clearance. The largest changes in noise level were apparent at frequencies greater than the blade-passing frequency.

Mugridge and Morfey (1972) argued that an optimum tip clearance exists when broadband noise is at a minimum due to the countervailing effects of the tip clearance flow and the blade-passage vortex. However, Longhouse (1978) did not confirm this result. He searched for a practical solution to the cooling fans' tip clearance noise and concluded that the unstable blade-tip vortex impacted the adjacent blade pressure side. He obtained the lowest noise levels with the smallest possible tip clearance. Fukano and Jang (2004) reported similar findings; whereas, Kameier and Neise's (1977) experiments demonstrated that, with the smallest possible tip clearance, noise reduced over a limited frequency range, close to the blade passage frequency. However, random noise actually increased.

During the past decade, several researchers have proposed technical concepts to assess air movement fan aeroacoustic properties. Researchers based the experimental techniques, to varying degrees, on previous fan (Leggat and Siddon, 1978; Bianchi *et al.*, 2009a, 2009b, 2011), radial pump rotor (Mongeau *et al.*, 1995) and turbofan engine (Kameier and Neise, 1977; Miles, 2006) studies. These studies and experiments have facilitated the design of effective passive noise control techniques.

This chapter presents the results of a survey on the passive noise reduction possibilities that are currently available to the air movement and control community. First, we present a review of the strictly passive noise control techniques. We then dedicate a section to screens and resonators, which are useful for passively controlling the fan noise. In the last section, we present the use of actuators. The chapter concludes by commenting on the most appropriate strategy that design engineers working within the air movement and control community should employ when designing low noise air movement fans.

FLOW AND NOISE CONTROL TECHNOLOGY

The feasibility and readiness of a flow control technology changes with the choice of application. The governing flow physics and operating environment change with each application, and render each flow control technology more or less applicable. This section will explore some of the environmental factors that impact different flow control technologies for air movement fan applications.

Air movement fans are classically incompressible machines, with sub-sonic flow over the fan blades and no supersonic patches. The air movement fan blade-to-blade flow field's subsonic and incompressible nature plays a significant role in defining the environment within which the flow control technology must operate. Also, insects, dust, all forms of precipitation and pollutants are environmental factors that one must consider when assessing a technology's readiness. Researchers require experience to understand the impact or lack of impact of these environmental factors on a flow control technology. Simply understanding environmental influences requires research. Glick (1939) and Coleman's (1961) studies are an example of the detailed research that we require to understand such influences. They found that the density of insects one would expect to encounter is a function of humidity, temperature (seasons), pressure, altitude, wind velocity and insect size for fans in aero-engine application. Others have studied and documented when and where contamination may be an issue for a technology. Few flow control technologies are mature enough to enable researchers to consider undertaking research focused on environmental impact.

The value or usefulness of any new technology is not only a technical matter. Political considerations drive technological development. The 'green' lobby has become progressively more powerful over the last decade, with the result that any technology that reduces carbon emissions is progressively favoured. Economic considerations are also increasingly relevant in an increasingly competitive marketplace. When we consider the cost of electricity relative to operating costs over a 24-year period (Brinckerhoff, 2011), it is apparent that a 3 per cent increase in fan efficiency will reduce operating costs by more than the fan's initial capital cost over a 24-year period. Granted, it may be inappropriate to draw this conclusion from one data plot; however, this analysis illustrated that capital cost is a relatively small fraction of an air movement fan's overall operating cost.

The political motivation to introduce new technologies that reduce power consumption may encounter some resistance from the manufacturers in spite of the legislative aims. Economic motivations to introduce new technologies that reduce power consumption require consumers to behave rationally, something that previously never occurred. Therefore, there is no reason to expect it to happen in the near future. The above political and economic considerations are compounded by the fact that electricity is a commodity and subject to dramatic changes in price.

Despite this, the long-term trend is in only one direction – up. The development of any new technology requires a significant lead-time and also requires a long-term perspective. Unfortunately, short-term chaos in the price of electricity results in a short term rather than a long-term perspective on the part of those who must fund the development of new energy efficient technology. This point is significant as invariably, long-term research into improved fan efficiency is also research into fan acoustic emission reduction.

Focusing now on noise suppression technologies, the matrix in Table 1.1 presents the application of noise suppression technologies to the noise sources from axial fan installations, within the context of their applicability to forthcoming legislation. The Table 1.1 survey did not provide insight into the relative associated costs

Table 1.1. *Matrix of the noise control technologies and an assessment of the practicality of their application during the air movement fan design process.*

	Feasibility	Readiness	Cost	Effectiveness	Impact on efficiency
Blade count	10	10	1	9	+/-
Scarf inlet	10	9	2	3	-
Forward swept rotor	8	8	5	7	+++
Leaned stator	7	8	5	7	+++
Chevron nozzles	7	8	6	6	-/+
Crenulated trailing edge	6	8	7	6	+
Leading edge bumps	5	5	7	6	+
Blade-tip end-plates	6	7	7	8	++
Tuneable resonators	5	5	8	8	-
Turbulence screens	4	5	?	8	--
Vortex generators	3	6	?	6	--

with bringing the different technologies to market, but nevertheless, offers a qualitative comparison of their potential.

PASSIVE FLOW CONTROL FOR NOISE REDUCTION

The early work on steady aerodynamic flow control was essentially unidisciplinary, focused on the aerodynamic benefits that occur with flow control. In contrast, the later unsteady technology development has originated within a multidisciplinary, cooperative environment involving a collaborative approach between researchers working in fluid mechanics, structural mechanics, material science, acoustics and control theory. More recently, researchers have developed innovative actuators and control strategies for flow control applications. Here, Joslin *et al.*'s (2000) recent discussion of flow control technology readiness for aerodynamics and hydrodynamics expands on the traditional focus on aerodynamic flow control. Other flow control reviews include Gad-el-Hak *et al.* (1998) and Fiedler and Fernholz (1990).

Blade Count

The discrete-frequency noise is a consequence of the unsteady interactions between the blade rows in industrial turbomachinery. Design approaches that address the attenuation of tonal signatures rely on the appropriate rotor-stator relative spacing, clocking and blade count to mix out the rotor wake and reduce the stator response to incoming flow disturbances. The least complex way to reduce rotor-stator tone noise is to cut-off the lower order harmonics through reducing the rotor blade count or increasing the number of outlet guide vanes (Tyler and Sofrin, 1962). Classically, one selects the number of rotor blades and stator vanes such that one cuts off the dominant propagating mode for the first blade harmonic. An alternative approach,

which Sawyer and Fleeter proposed (1998), uses an aerodynamically detuned stator by increasing the equivalent blade count by incorporating reduced chord splitters. Whilst engineers universally use this approach for cutting off the first blade passing frequency, an investigation in the 1980s into high-speed fan acoustic performance indicated a noise reduction at the second harmonic tone when redesigning the stator (Fleeter, 1980). Further, with rotor-stator broadband noise proportional to the number of outlet guide vanes, a current research aim is to control tone noise through outlet guide vane sweep and lean, thus allowing blade count reduction and broadband noise reduction whilst cutting on the first blade passing frequency (Woodward *et al.*, 2001).

Blade Loading Versus Blade Speed

With both tone and broadband noise scaling at about the fifth power of blade speed, a way to reduce noise is to reduce the blade speed. For the same fan pressure ratio, this results in an increased blade loading. Fan manufacturers have attempted to reduce fan speed and increase blade loading with mixed success. A common theme to emerge from their experience is the need for more accurate aerodynamic design techniques. Researchers have achieved significant tonal noise reductions at speeds above 80 per cent of design relative to the *datum*, but have not observed broadband noise reductions. They attribute tonal noise reduction to the rotor alone, with the lower speed reducing the noise.

Whilst noise may scale with tip speed up to the power of five, this is not the case when loading increases to maintain pressure rise. Increases in noise due to increased loading can negate, or in some instances, dominate the total noise emission that occurs with the tip flow effect.

Bends

Practitioners have demonstrated that a reflection process attenuates a plain untreated bend in a fan duct system. For frequencies where the wavelength is higher or lower than twice the duct width, the energy passes through the bend relatively more efficiently. This is because of the ‘corner wave diffraction’ effect. It is possible to accelerate the wave’s outgoing decay; however, the only way to do this is to line the outgoing acoustic wave with a suitably absorbing material.

Scarf Inlet and Riblets

Walsh (1980) conducted pioneering research using two different riblets. He reported an eight per cent drag reduction for a turbulent flat plate with a zero pressure gradient. His inspiration came from Liu *et al.*’s (1966) experimental studies where they aligned rectangular fins with the flow direction and spaced and sized them according to inner wall variables. This led to a three to four per cent net drag reduction with those first riblets.

The scarf inlet is one in which the inlet lip protrudes more at the keel than at the crown. This design has the potential to reduce inlet radiated fan noise by redirecting a part of the acoustic energy up and away from observers. Ffowcs Williams and Hall (1970) studied the effect of a scarf inlet in reducing the noise due to the ingested turbulent eddies. The scarf inlet has a beneficial effect, reducing blade stall and speed variation. Two acoustic benefits quantify this: reduction both of the tone noise variability and of the low frequency wideband noise due to the inflow distortion. A compromise in manufacturing the control hardware probably contributed to the control system's inability to perform as expected in Ffowcs Williams and Hall's (1970) analysis.

Subaschandar *et al.* (1999) reported up to a 10 per cent drag reduction using riblets on a general aviation aerofoil in a wind tunnel. They applied a riblet film from 12 to 96 per cent of the aerofoil chord. The amount of drag reduction increased with the angle of attack up to six degrees and reduced up to 12 degrees.

Blade Sweeping

Analysis of potential tone-noise reduction techniques has indicated that both positive sweep (tip further downstream than hub) and positive lean (tip moved circumferentially in the direction of rotor rotation) would reduce noise with greater sweep angle and lean. Corsini and Rispoli (2004) report that positive sweep and lean results in greater noise reduction. This is because positive sweep and lean maximises the number of wake interactions per vane. However, tone noise is particularly reduced. Corsini and Rispoli (2004) observed a small reduction in broadband noise only at lower fan speeds.

In large and high-speed fans, the outlet guide vane sweep reduces broadband noise by reducing the Mach number's chord-wise component, Figure 1.1. Some researchers have suggested that the forward sweep at the tip also reduces broadband noise, as it is also created in the tip region. Researchers have used forward outlet guide vane rotor sweep to reduce multiple pure tones. Leaning the stator blades also reduces turbulent broadband noise.

Schulten (1982) concluded that lean is not effective; whereas, Envia and Nallassamy (1999) presented results that indicate that lean is effective, if one applies it in the opposite direction to the rotor rotation. Bryanston-Cross (2010) presented similar findings. In addition, Schulten (1997) predicted that vane sweep is effective for large sweep angles; whereas, Envia and Nallassamy (1999) concluded that any sweep angle will be effective.

The inconclusive nature of the work reported in the extant literature indicates that design engineers must take care when specifying guide vane lean angle. As a general rule, negative lean may be more beneficial than positive lean. However, there is no general consensus on the acoustic pay-off that occurs with a blade row stacking line modification. The acoustic pay-off that occurs with blade row stacking line modification appears to be dependent upon the individual test-bed. Consequently, it is crucial to validate any low noise blade design with both numerical and experimental campaigns.

FIGURE 1.1. A base-line fan (top), with vane sweep (middle) and vane sweep and lean (bottom) (Woodward *et al.*, 2001). Swept vanes reduced the blade passing frequency tone amplitude and broadband noise. Stator lean reduced rotor-stator interaction resulting in a further reduction in fan broadband noise.

The work reported in the extant literature indicates that guide vane sweep is efficient for large positive sweep angles. Negative sweep angles, although unconventional, show promise and may feature in future low noise fan configurations. We may make the general observation that both lean and sweep effectiveness depends on the number of propagating modes. For a single frequency (tonal noise), design engineers can optimise guide vane lean and sweep to reduce the sound power propagating to the far-field. However, for a frequency spectrum (broadband noise), the number of propagating modes is large, and therefore varying guide vane lean or sweep may not be beneficial.

Chevron Nozzles

The intent of the asymmetric fan chevron nozzle was to improve noise reduction by creating a favourable aeroacoustic interaction effect between the fan struts and the chevron on the nozzle (or casing) which interacted with the discharge flow, Figure 1.2. We observed this favourable interaction and improved noise reduction in model scale tests. Past studies (Amiet, 1976; Howe, 1991) have reported the favourable interaction. The aim of the reported research was to identify the fundamental flow and noise source mechanisms. The flow studies (Bhat, 2001; Massey *et al.*, 2003) show that longer fan chevrons' asymmetry near the struts work to reduce the strength of secondary flow structures which the strut itself induces. The effect of reducing the strength of secondary flows is to significantly delay merging the fan's

FIGURE 1.2. A Rolls-Royce Trent 800 gas turbine with serrated nozzle to reduce engine noise. The serrated nozzle reduces gas turbine noise on take-off and landing by 20 per cent (Bryanston-Cross, 2010).

asymmetric core shear layers. This reduces the peak turbulence kinetic energy and shifts it downstream, reducing overall noise production.

Crenulated Edge

In 1982, Wennerstrom (1982) suggested that crenulated trailing edges on aerofoils would increase the wake dissipation rate and thus reduce the noise emission, Figure 1.3. Trailing edge crenulations are intended to generate counter rotating vortices, which pressure difference between the aerofoil's suction and pressure surfaces drive. These vortices actively mix the wake into the free-stream flow. There is also the possibility that the crenulations' effects are due, in part, to interaction with secondary flows in the passage, especially the corner vortices which form where blade suction surfaces intersect the cascade sidewall.

Recently, Corsini *et al.* (2013) presented a particular fan blade crenulation which they associated with humpback whales' ability to execute very sharp rolls and loops under water. The crenulations were in the form of bumps on the leading edge of the whale's flukes. These bumps functioned as a stall-control system, Figure 1.4. The reported research focused on the modified leading edge's effects on lift-to-drag performance. The primary focus on the research was the elucidation of the fluid flow mechanisms that the bumps induced and the impact of those mechanisms on aerofoil performance.

The bumps resulted in a sinusoidal-shaped leading edge, with the resultant blade geometry having an implication for fan blade lift and drag. An assessment of the modified geometry on a cambered aerofoil entailed the comparison of aerodynamic performance against the same geometry without a sinusoidal-shaped leading,

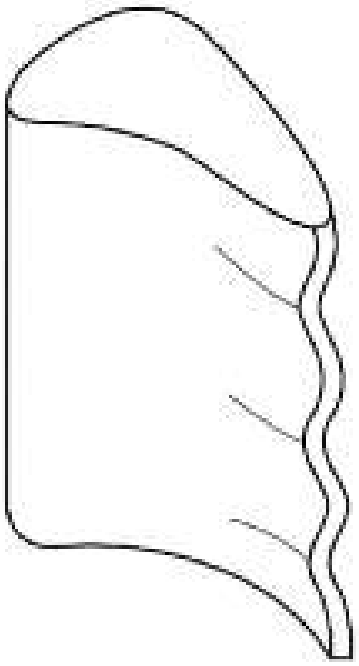

FIGURE 1.3. A crenulated blade trailing edge that increases the blade wake dissipation rate and thus reduces the blade wake generated noise emissions (Wennerstrom, 1982).

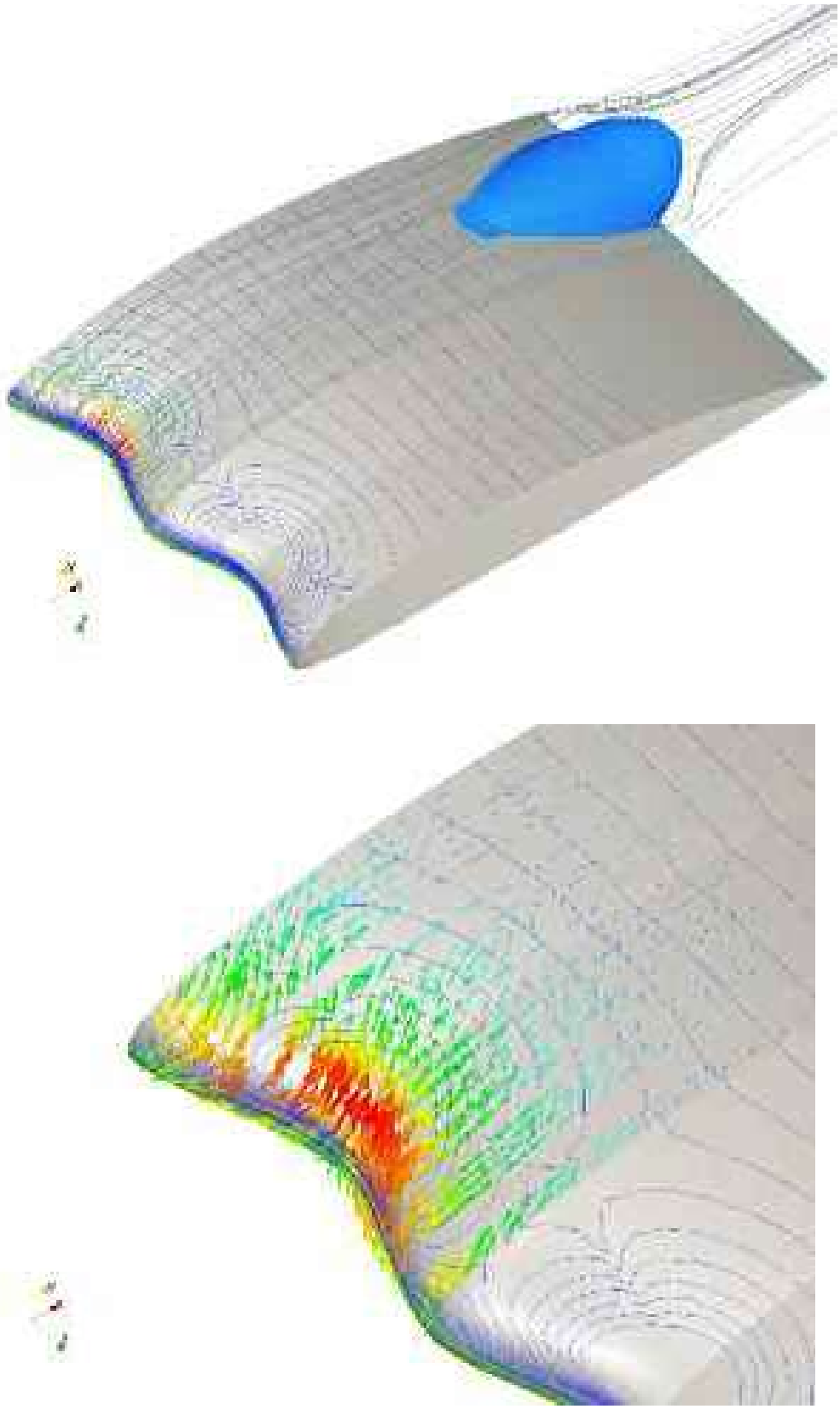

FIGURE 1.4. A trailing edge recirculation zone (top), shown in blue. The sinusoidal blade leading edge contains the recirculation zone to the sinusoid's trough at high blade angles of attack, reducing the blade's propensity to stall. The leading edge velocity field (bottom) generates a pair of counter-rotating vortex that contain the trailing edge recirculation zone (Corsini *et al.*, 2013).

as well as an uncambered aerofoil. The sinusoidal-shaped leading edge modified the aerofoil lift coefficient during stall, with an early recovery of the aerofoil's aerodynamic work capability and a 30 per cent gain in lift after stall for the WHALE4415 aerofoil (Corsini *et al.*, 2013).

The leading edge's geometry directly impacts the aerofoil's velocity and vorticity fields. The improvement in fan performance that occurs as a consequence of velocity and vorticity modifications infers that the bumps have a stabilising effect on the blade's suction side flow. The leading edge troughs between bumps appear to suppress the separation on the suction side trailing edge. Although conceived to improve the fan's stall characteristics, the technique may provide a method for controlling the origin of flow induced noise.

Blade-tip End-plates

The blade-tip end-plate technique is based on modifications to the blade tip by means of anti-vortex appendages. Quinlan and Bent (1998) have proposed blade-tip end-plates, and others have proposed various solutions in patents for air movement fans (Jensen, 1986; Longet, 2003; Mimura, 2003; Uselton *et al.*, 2005). Because of the role that organised structures in turbulent flow play in the noise generation process, controlling these structures may be a key to noise suppression (Ffowcs Williams and Hall, 1970). Experimental and numerical studies have identified that significant improvement can result from the adoption of tip leakage flow control technologies (Bianchi *et al.*, 2009a, 2009b; Corsini *et al.*, 2010). The scholars who have studied the impact of tip leakage flow technologies have each speculated on the role of leakage vortex bursting on air movement fans' aerodynamic and aeroacoustic performance. The vortex breakdown is an intriguing and practically important phenomenon that occurs in swirling flows, and depending on the application, may be either a productive or counter-productive flow feature.

Reconfiguring the end-plate at the blade-tip constitutes the optimisation of a direct noise-by-flow control mechanism. This mechanism influences the momentum transfer from leakage flow and forces some waviness into the leakage vortex trajectory in much the same way as a delta-wing (Srigrarom and Kurosaka, 2000). Researchers have purposefully varied blade-tip end-plate thickness to control the blade tip-to-casing leakage vortex rotation number's chord-wise evolution. The leakage vortex rotation number serves as a metric for the vortex swirl level. The design criteria researchers have studied (Carpenter, 1993; Corsini and Sheard, 2007; Sheard *et al.*, 2009; Corsini *et al.*, 2013) are intended to control the leaked flow and to induce a subtraction and addition of near-axis momentum to the leakage vortex as it develops along the blade chord. As such, the new end-plate design concepts passively control the leakage vortex swirl level and the new blade-tip end-plate designs enhance the mixing of coherent tip vortical structures. This mixing of coherent tip vortical structures results in a favourable change in fan far-field noise (Carpenter, 1993; Sheard *et al.*, 2009; Corsini *et al.*, 2010; Corsini and Sheard, 2013).

Corsini and Sheard (2007) and Corsini *et al.* (2007a, 2007b, 2010) have assessed the performance gains associated with blade-tip end-plate technology. They

conducted their reported research on a family of commercially available cooling fans. The studied fan configuration, coded AC90/6, incorporates a six-blade unswept rotor, with modified ARA-D profile aerofoils blades. In its original embodiment the studied fan did not include a blade tip end-plate, therefore the researchers used it as a *datum* against which to assess the performance of the fan's variants with blade tip end-plates. Corsini and Sheard named the fan without blade tip end-plates *datum* AC90/6.

In addition to the fan *datum* AC90/6, Bianchi *et al.* (2012) studied two variants of the fan. The first fan they fitted with a constant thickness blade-tip end-plate and the second with a three-dimensional blade-tip end-plate, Figure 1.5. When fitted with a constant thickness blade-tip end-plate, they named the fan AC90/6/TF. When fitted with the three-dimensional blade-tip end-plate, they named the fan AC90/6/TF$_{MVB}$. The effect of both the constant and three-dimensional blade-tip end-plate is to reduce the fan far-field noise, Table 1.2. Bianchi *et al.* achieved the reduction in fan far-field noise by managing the blade tip-to-casing leakage vortex

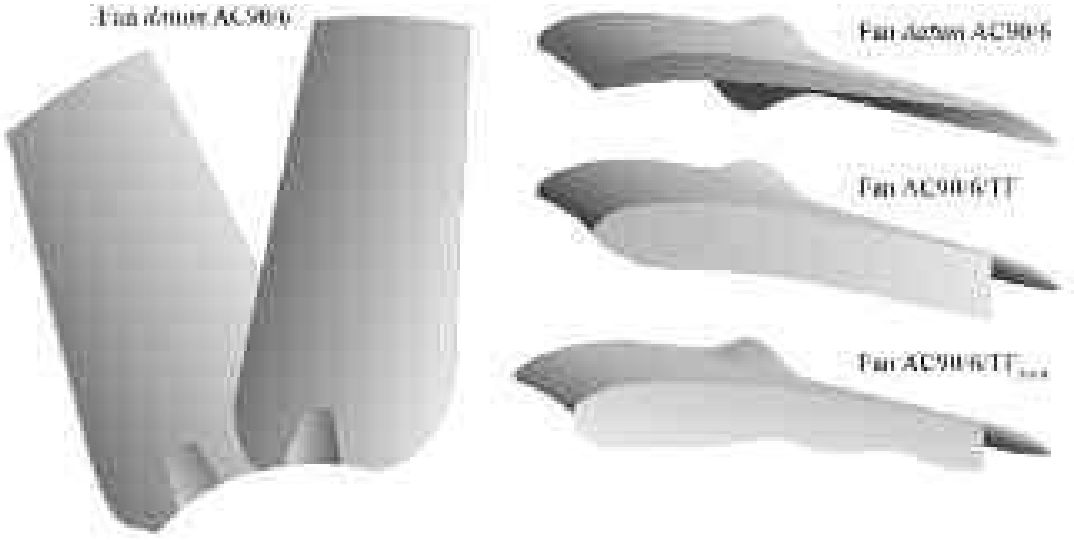

FIGURE 1.5. A *datum* fan without a fitted blade-tip end-plate and two variants with fitted blade-tip end-plates. When Bianchi *et al.* (2012) fitted Corsini and Sheard's (2013) 'multiple vortex breakdown' blade-tip end-plate to the *datum* fan, they named the resulting fan AC90/6/TF$_{MVB}$. When they tested it installed over a compact cooling unit's tube bank, the multiple vortex breakdown blade-tip end-plate reduced fan AC90/6/TF$_{MVB}$ noise to the lowest in its class of air movement fans.

Table 1.2. *A comparison of far-field fan noise for a fan with and without fitted blade-tip end-plates (Bianchi* et al.*, 2012).*

	datum AC90/6		AC90/6/TF		AC90/6/TF$_{MVB}$	
	Unweighted Overall L_W	A-weighted Overall L_W	Unweighted Overall L_W	A-weighted Overall L_W	Unweighted Overall L_W	A-weighted Overall L_W
Operating Point	dB	dB(A)	dB	dB(A)	dB	dB(A)
Maximum flow	100.1	92.5	96.7	89.3	98.6	88.1
Design	96.8	92.5	96.6	87.9	94.7	86.7
Peak pressure	95.4	93.2	92.2	87.1	89.9	85.0

vorticity to prevent bursting whilst avoiding generating acoustically productive flow-field features.

Stub Vanes

There is a radial variation of fan acoustic energy, with the majority of fan noise generating in the fan annulus' outer region. Therefore, having a vane-to-blade ratio of two only in the outer annulus would seem logical. Such an approach has the potential to reduce vane weight. It is particularly convenient as it also avoids the aerodynamic performance degradation that occurs with an increase in the number of outlet guide vanes. The short vanes extend over only the fan annulus' outer one-third. We may only estimate the benefit of this concept as there is no test data to support the assumption of noise reduction with high vane-to-blade ratios only in the outer fan annulus.

SCREENS AND RESONATORS

Gerard (2006), Gerard *et al.* (2007) and Goth *et al.* (2012) have proposed and demonstrated the use of calibrated obstructions or gaps to cancel fan noise at the blade passing frequency. An example of this technique is implementing cavities in the fan casing over the blade tips that suppress tip vortex induced noise.

Absorption and scattering from resonators in a free-field, as well as in the walls, is another technique for air movement fan noise reduction (Ingard, 1953). Neise and Koopmann (1980), Gorny *et al.* (2007) and Gorny and Koopman (2009) proved the effectiveness of resonators in reducing the noise generated by axial and centrifugal fans. Turbulence screen use, based on Howe's theory (1984), also has the potential to reduce fan noise.

Tuneable Screens

This application of turbulence screens involves placing calibrated obstructions in the airflow upstream or downstream of the fan. When placed at the optimal distance and angle, the obstruction generates pressure pulsations that interact with the fan pressure fluctuations in a destructive way. This interaction results in noise cancellation at the blade passing frequency, and in some cases at its first harmonic. The size and shape of obstacles set up or downstream from the fan blades, (typically heat exchangers, motors and motor support struts) influence the interaction with the flow. The obstacles' interaction can affect strongly the amplitude of any noise cancelling effect. Gerard *et al.* (2007) have shown that obstacles, when appropriately chosen and placed, are able to produce a significant reduction in noise at the blade passing frequency.

One can achieve acoustic attenuation with an automatic control system that is able to change an obstruction's position. Although theoretically possible, the cost of

such control systems limits the spread of the technology. When developing an automatic control system one must systematically investigate the influence of the obstruction type and position on the broadband and blade passing frequency sound pressure level. The primary aim is to define the 'tolerance zone' around the parameters' nominal value. The tolerance zone's size influences this technology's usability in real-world applications.

Goth *et al.* (2012) have tested two different obstruction sets. The first comprises periodic indentations disposed at the fan disk's periphery, with a smooth sinusoidal shape (M type) or a sharp dissymmetrical shape (D type). The number of indentations ranges from N–1 to N+1, where N is the number of fan blades. The second set comprises a unique obstacle with the shape of a portion of disk (C type).

Goth *et al.*'s results (2012) show that obstacles can be in more than one angular position whilst still leading to a significant reduction in noise at the blade passing frequency. At the optimal location, the noise reduction is sensitive to the angular (+/–1 degree) and to the axial position (+/– 2 mm). However, this type of obstruction's influence on the airflow is very low and consequently, we can achieve any noise reduction with only minimal degradation in fan efficiency.

When applied to a compact fan cooling system, the use of various types of obstruction upstream of the fan has shown an achievable 10 to 15 dB reduction in the sound power level at blade passing frequency (Goth *et al.*, 2012). As only the blade passing frequency is strongly affected by the obstructions, the maximum reduction in overall noise sound level is modest: 2 dB (A) for the axial fan, and up to 4 dB (A) for the centrifugal fan.

Turbulence Screens

Following Lighthill's pioneering work (1952), researchers have studied noise generation by turbulence and vortical flows. In heat exchanger applications there is a need to suppress mechanical resonances that are driven by acoustic coupling. In this context, acoustic coupling refers to a phenomenon analogous to flutter, where the sound emitted from a shed vortex drives heat exchanger tube vibration. Thin perforated plate deployment can break the acoustic coupling to generate vorticity from the acoustic energy.

Vorticity generation from the acoustic energy results in a net attenuation of acoustic energy, as Howe reports (1984). Alternatively, sound absorption could take place when an acoustic wave traverses a vortical or turbulent flow region as a consequence of the local mixing enhancement (Amiet, 1978). We can attribute the acoustic energy loss to the following:

- If the turbulence characteristic time scale is significantly different from that of the sound scattering from the turbulence to higher frequencies, we can implicitly assume that the sound passage does not influence the turbulence and accordingly, that acoustic energy diverted from the incident wave reappears in the medium elsewhere.

- If the turbulence characteristic time scale is of the same order of magnitude of the sound time scale, the aerodynamic sound origin dampens when it traverses or propagates through the turbulent flow region that has produced it (Ross, 1998; Guedel, 1999).

Taking a spectral component perspective, turbulence is responsible for the incident sound wave attenuation of identical frequency since only zero-sum or different frequencies can lead to a net energy transfer in wave-turbulence interactions. We found a spectral component perspective facilitated the identification of two noise reduction mechanisms:

- the effect of the vorticity's local straining by the sound and;
- the incompressible perturbation pressure's longer range tendency to restore the turbulence to its original undisturbed state.

It is then possible to decompose the acoustic pressure and perturbation velocity as the sum of coherent and fluctuating components. These components are statistically independent of the incident sound wave. This independence implies that the sound scattered out of incident acoustic waves of greater wavelength distribute isotropically. Consequently, it is possible to consider the coherent wave as the propagating incident wave whose amplitude and phase are modified by the scattering and absorbed by turbulence.

We can link the role of turbulence in noise reduction to other fan aerodynamic features including blade-tip end-plates and chevrons. In general, every turbulence promoter can act as a turbulence screen builder, but quantifying this effect demands an accurate aerodynamic survey. As a consequence of its dependence on the fan operation environment, currently it is not practical to undertake a direct design of an appropriate turbulent noise screen. However, developing a pre-existing aerodynamic design, for example, Corsini and Sheard's (2013) blade-tip end-plate is worthy of further study.

Actuators

We may classify actuator or effector technologies as passive in the sense that there is no energy input for their operation. In contrast, active systems require energy input to function. For a technology readiness assessment, we are interested in both passive and active actuators. In most cases, the passive actuators will be at a higher state of readiness than active systems.

Compliant Walls

Compliant coating research began with the postulation that dolphins achieved very high speeds through a natural drag reduction mechanism brought about as a

consequence of their compliant skins. The adoption of ideas and concepts that we observe in nature has the objective of linking them with engineering design practice. In the late 1990s, researchers started using the term 'biomimetic' as a means to classify scientific reasoning based upon a study of nature.

The link between the dolphin and compliant coatings arose from 'Gray's Paradox'. Gray (1936) compared the resistance of a towed rigid body and the observed dolphin speeds to suggest that their muscles must generate energy at a rate seven times greater than any other mammal to attain the recorded speeds. Gray then proposed laminar flow and its corresponding drag reduction as a means to explain the paradox.

Research involving flow over flexible walls exploded in the late 1950s when researchers first attempted drag reduction by using rubber coatings over rigid bodies in water. Researchers in the 1960s focused on experimentally duplicating and theoretically explaining Kramer's results (1957). The majority of these studies failed to produce any comparable results. Despite the limitations of the reported studies, theoretical developments at the time laid the foundation for future studies involving flexible walls.

Interest once again turned toward the use of compliant walls for turbulent drag reduction in the late 1970s and 1980s. NASA (Bushnell, 1984) and the Office of Naval Research (Reischman, 1984) sponsored investigations into the use of compliant walls. Although most of the results from this era were either inconclusive or unsatisfactory, the contributions, together with earlier results, have acted as stepping-stones towards an understanding of the physically complex fluid and wall interaction.

Carpenter and Morris (1989) used an energy analysis to illustrate how the presence of a compliant wall influences the many competing energy transfer mechanisms. Joslin *et al.* (1991) predicted that transition delays of 4 to 10 times the rigid wall transition Reynolds number were achievable with a compliant coating. Joslin and Morris (1992) used a secondary instability analysis with compliant coatings to demonstrate that secondary modes could be suppressed simply because the primary modes were suppressed. Sample results in Joslin *et al.* (1991) show the amplification of primary and secondary instabilities for a compliant wall case compared with a rigid wall case and the effect of the compliant wall on noise attenuation.

Carpenter (1993) suggested that the use of compliant coatings in air applications is impractical because the pressure fluctuations are insufficient to initiate a coupling of the fluid-coating combination. As such, the coating would have to be very thin to be useful in air. Carpenter's (1993) results suggest that Tollmien-Schlichting wave amplification in air is possible with very thin casing duct coatings. The use of very thin coatings may be relevant in future research into noise reduction when one uses them in conjunction with a Helmholtz resonator (Brooks *et al.*, 1989).

Trailing Edge Blowing

Trailing edge blowing is an example of noise control from flow control, Figure 1.6. The aerospace community originally developed the concept to directly alter blade

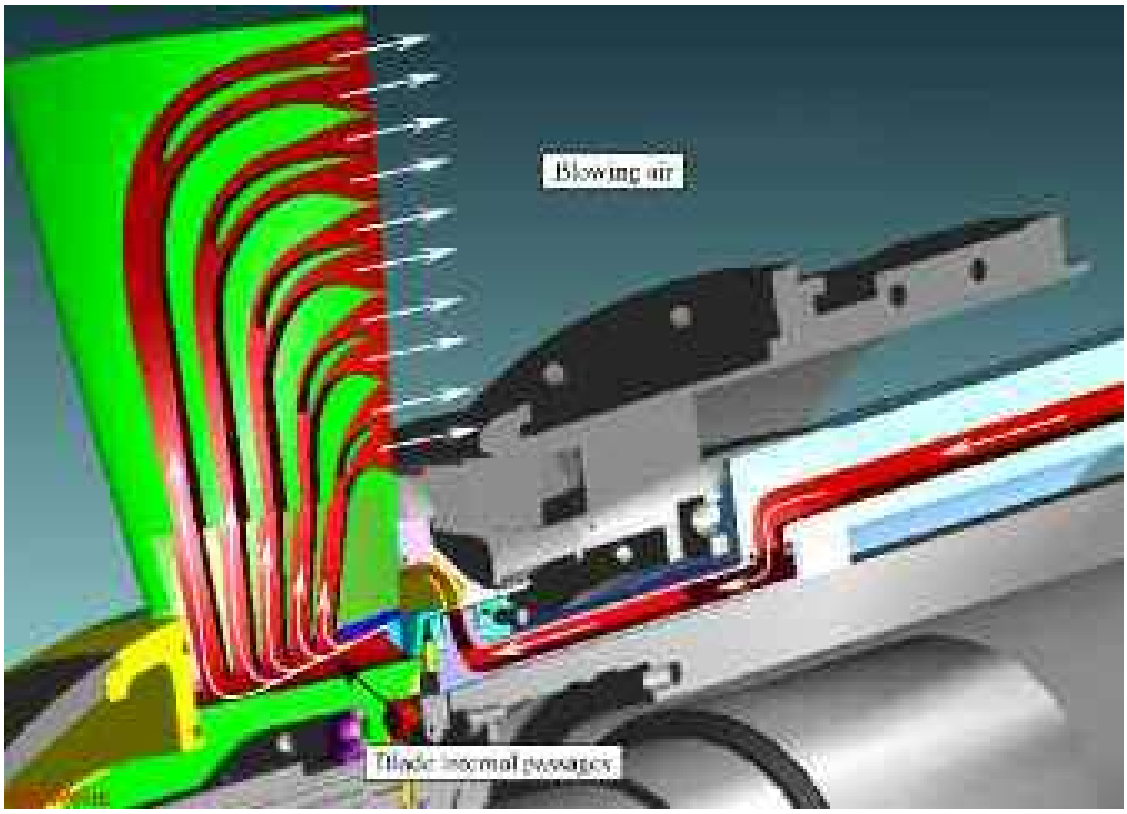

FIGURE 1.6. Trailing edge blowing 'fills in' the blade wake and thus reduces wake generated tonal noise (Sutliff *et al.*, 2002).

wake characteristics. Air is channelled to the trailing edge through passages in the fan blade. The air injected into the blade wake reduces the wake's strength by compensating for the pressure deficit that characterises all blade wakes. Consequently, unsteady pressure fluctuations are reduced, and therefore the pressure fluctuations impinging on downstream stators are also reduced. The result is reduced fan noise.

Trailing edge blowing reduces the fan tonal noise associated with pressure fluctuations impinging on downstream stators by up to 4 dB (Brookfield and Waitz, 2000). In a typical high bypass ratio gas turbine fan, the injection mass flow rate ranges from half to two per cent of the overall mass flow rate through the fan (Sutliff *et al.*, 2002). A well optimised trailing edge blowing system can minimise the performance penalty that one associates with the injection mass flow rate. However, even if we assume that the performance penalty is acceptable, which it may not be, a trailing edge blowing system still requires a secondary air system. That secondary air system will, in turn, have its own associated maintenance requirements. Consequently, the trailing edge blowing concept requires further study to establish if it has the potential for practical application in air movement fans.

Vortex Generators

A vortex generator is a passive device that induces a vortex. We generally associate the need for this vortex with preventing an otherwise separated flow condition

that causes severe aerodynamic or hydrodynamic performance reduction. Any technology that avoids an aerodynamic or hydrodynamic performance reduction has the potential to also reduce fan acoustic emissions.

Micro vortex generators constitute a mature technology for passive flow and noise control (Lin, 1999). However, their application still requires significant experimental effort to determine where the vortex generators are positioned and what size and shape is optimal in a specific application. No correlation exists in the extant literature for the design and application of vortex generators for noise attenuation. However, researchers have developed a numerical method for computationally modelling the induced effects of vortex generators on a given flow (Bender *et al.*, 1999).

Despite the numerical methods value, a good experimental database is necessary if one is to model the effect of micro-vortex generators on fan noise. Detailed measurements of the flow downstream of vortex generators for turbulent flat plate boundary layers would provide a good starting point for an experimental campaign, followed by measurements in a separated flow with associated noise measurements. Such measurements have the potential to facilitate the development of noise correlations that design engineers may then subsequently apply during the air movement fan design process.

DESIGN STRATEGIES

Air movement fan design has historically focused on mechanical integrity first, aerodynamic efficiency second, with acoustic considerations a distant third. However, this historic approach is not consistent with the emerging regulatory environment within Europe. The Energy using Product (EuP) Directive became legally binding within Europe on 1 January 2013, setting legal minimum standards for fan efficiency. The air movement fan market is also shifting towards specifications requiring lower fan noise, in part because of increasingly stringent health and safety legislation.

The air movement and control community, and the markets into which it sells its products, must define acceptable fan noise against some requirement based on detectability at a specified distance. Setting a detection criterion at a specific distance from the fan could result in the required maximum source noise level being a non-monotonic function of frequency. Fan noise is typically a non-monotonic function of frequency, and therefore air movement fan specifications are increasingly specifying not just an overall noise level, but also allowable noise levels in each octave band. This presents the fan designer with the duel challenge of both designing the fan to meet an overall noise level and spectrum.

A review of the available technology for reducing fan noise identified eleven technologies that the air movement fan designer may apply in an effort to reduce fan tonal and broadband noise, Table 1.1. In assessing the different noise reduction technologies' feasibility, readiness, cost, effectiveness and impact on efficiency we have ignored all constraints except for acoustic constraints. In practice, both cost and mechanical considerations constrain fan designers. Despite the observation that air

movement fan designers must optimise their designs around multiple constraints, assessing noise reduction technologies in isolation provides an insight into the available technology.

Air movement fan designers have historically resisted applying technology that other industries have successfully applied. Wall coating is a noise reduction technology that air movement fan designers could utilise. Wall coatings are low cost and can have a significant impact on fan noise. However, the air movement and control community is intrinsically conservative, characterising unfamiliar technology as 'expensive' and therefore unacceptable. The new regulations within Europe mandating minimum fan efficiencies are driving a change in attitude towards the use of computational methods. Applying computational methods is becoming increasingly unavoidable if designers are to design air movement fans that meet the minimum allowable efficiencies. As more efficient fans classically emit less noise, air movement fan designers adopting computational methods may result in a more open attitude towards utilising other noise reduction technologies.

Attitudes within the air movement and control community to new noise reduction technology may become more accepting. If the community embraces new technology, designers are still likely to favour using or adapting already proven techniques. Proving aerospace developed noise reduction technology in air movement and control applications will require design engineers to assess the technology's effectiveness in a range of applications. It is likely that this generic characterisation of noise reduction technology will require resources beyond those available to even the largest air movement fan manufacturers. Some may regard this technology as 'pre-competitive' research. Therefore, at least in theory, air movement fan manufacturers could choose to collaborate, jointly funding a research programme that none could fund alone.

CONCLUSIONS

This chapter has outlined some applications of flow and noise control technology in the air movement fan design process. A collaborative approach between air movement and control practitioners and academics will facilitate applying techniques proven by the aerospace community into the air movement and control community. In this review, we outlined a vision of how air movement fan technology must change in response to changing legislation. We then reviewed critical flow and noise control technologies, with an emphasis on the future direction in which design engineers are likely to develop these technologies. We discussed the practicality of synergy between flow and noise control technologies. The development of these synergies will need to accelerate if the air movements and control community is to apply aerospace developed noise control technology to meet forthcoming legislative demands.

We recommend that research into flow and noise control could be more effective if industrialists and academics focus their research on the elucidation of the physics underpinning the link between features in the fan flow-field and fan far-field noise. First, researchers must focus on developing both air movement fan fluid-flow

and acoustic modelling techniques using the computational methods that are embedded within aerospace fan design processes.

Second, researchers should develop design tools that model the fundamental fluid-flow and acoustic physics. Recent research in flow control, and to a lesser extent noise control, has emphasised the importance of application specific development. However, researchers have generally failed to identify the unique elements that one must characterise when developing a design capability for a specific application. As a result, a necessary component of any future research effort should be the validation of design tools which one can apply to air movement fans.

Third, researchers should focus on integrating flow and noise control technologies into the preliminary air movement fan design process. This should be in combination with applying computational methods into existing design methods. It is only the combination of noise control technology, computational methods and existing design methods that will facilitate the development of new flow and noise control devices.

Fourth, researchers should focus on creating a comprehensive road map that defines the required fundamental research needed to underpin developing new noise control design tools. This road map would facilitate establishing an international association of air movement fan manufacturers and universities that would collaborate on 'pre-competitive' research.

Fifth, new facilities will be necessary to provide the capabilities required to undertake the pre-competitive research. This requires a collaborative approach between universities with existing acoustic facilities developed for the aerospace community. Researchers will need to adapt these facilities for use with air movement fans if noise control technology developed within the aerospace community is to transition into the air movement and control community.

Sixth, air movement fan manufacturers must maintain and be willing to add new experimental facilities that they can then use for low cost proof-of-concept evaluation of noise control technologies. The empirical assessment of a noise control technology in a specific air movement application is a way to mitigate risk. By verifying the potential of a noise control technology in a specific application, the community may establish potential benefits of a research programme to elucidate the fundamental fluid-flow physics. It is only though understanding the fundamental fluid-flow physics that researchers may develop robust design techniques.

REFERENCES

Amiet, R.K. (1976), 'Noise Due to Turbulent Flow Past a Trailing Edge', *Journal of Sound and Vibration*, vol. 47(3), pp. 387–393.

Amiet, R.K. (1978), 'Refraction of Sound by a Shear Layer', *Journal of Sound and Vibration*, vol. 58(4), pp. 467–482.

Bender, E.E., Anderson, B.H. and Yagle, P.J. (1999), 'Vortex Generator Modeling for Navier-Stokes Codes', *Proceedings of the 3rd ASME/JSME Joint Fluids Engineering Conference*, New York, NY, USA, 15 July, paper no. FEDSM99-6919.

Bhat, T.R.S. (2001), 'Experimental Study of Acoustic Characteristics of Jets from Dual Flow Nozzles', *Proceedings of the 7th AIAA/CEAS Aeroacoustics Conference*, Maastricht, The Netherlands, 28–30 May, paper no. AIAA-2001-2183.

Bianchi, S., Corsini, A., Rispoli, F. and Sheard, A.G. (2009a), 'Detection of Aerodynamic Noise Sources in Low-speed Axial Fans with Tip End-plates', *Proceedings of the IMechE Part C, Journal of Mechanical Engineering Science*, vol. 223, pp. 1379–1392.

Bianchi, S., Sheard, A.G., Kinghorn, I.R., Corsini, A. and Rispoli, F. (2009b), 'Experimental Development of a Measurement Technique to Resolve the Radial Distribution of Fan Aero-acoustic Emissions', *Noise Control Engineering Journal*, vol. 57, pp. 360–369.

Bianchi, S., Corsini, A., Rispoli, F. and Sheard, A.G. (2011), 'Far-field Radiation of Tip Aerodynamic Sound Sources in Axial Fans Fitted with Passive Noise Control Features', *Transactions of the ASME, Journal of Vibration & Acoustics*, vol. 133, paper 051001, pp. 1–11.

Bianchi, S., Corsini, A. and Sheard, A.G. (2012), 'Experimental Characterisation of the Far-field Noise in Axial Fans Fitted with Shaped Tip End-plates', *International Scholarly Research Network, Mechanical Engineering*, vol. 2012, paper no. 212358, pp. 1–9.

Blake, W.K. (1986), *Mechanics of Flow-induced Sound and Vibration, Vols I & II*, Academic Press, Orlando, FL, USA.

Brinckerhoff, P. (2011), *Electricity Generation Cost Model – 2011 Update, Revision 1*, Department for Energy and Climate Change, London, UK, August.

Brookfield, J.M. and Waitz, I.A. (2000), 'Trailing Edge Blowing for Reduction of Turbomachinery Fan Noise', *AIAA Journal of Propulsion and Power*, vol. 16, pp. 57–64.

Brooks, T.F., Pope, D.S. and Marcolini, M.A. (1989), 'Airfoil Self-noise and Prediction', NASA Reference Publication 1218.

Bryanston-Cross, P. (2010), 'Particle Image Velocimetry (PVI) Principle of Operation', *Remote Sensing and Global Modelling Lecture Series*, University of Warwick, Warwickshire, UK.

Bushnell, D.M. (1984), 'NASA Research on Viscous Drag Reduction II', in *Laminar-Turbulent Boundary Layers, Vol. 11*, E.M. Uram and H.E. Weber (Eds), ASME, New York, NY, pp. 93–98.

Carpenter, P.W. (1993), 'The Optimization of Multiple-panel Compliant Walls for Delay of Laminar-turbulent Transition', *AIAA Journal*, vol. 31, p. 1187.

Carpenter, P.W. and Morris, P.J. (1989), 'Growth of 3-D Instabilities in Flow over Compliant Walls', *Proceedings of the 4th Asian Congress of Fluid Mechanics*, Hong Kong, China, 21–25 August.

Coleman, W.S. (1961), 'Roughness Due to Insects', in *Boundary Layer and Flow Control, Vol. 2*, G.V. Lachmann (Ed.), Pergamon Press, Oxford, UK, pp. 682–747.

Corsini, A. and Rispoli, F. (2004), 'Using Sweep to Extend Stallfree Operational Range in Sub-sonic Axial Fan Rotors', *Proceedings of the IMechE Part A, Journal of Power and Energy*, vol. 218, pp. 129–139.

Corsini, A. and Sheard A.G. (2007), 'Tip End-plate Concept Based on Leakage Vortex Rotation Number Control', *Journal of Computational and Applied Mechanics*, vol. 8, pp. 21–37.

Corsini, A. and Sheard, A.G. (2013), 'End-plate for Noise-by-Flow Control in Axial Fans', *Periodica Polytechnique, Mechanical Engineering*, vol. 57(2) pp. 3–16.

Corsini, A., Perugini, B., Rispoli, F., Sheard, A.G. and Kinghorn, I.R. (2007a), 'Aerodynamic Workings of Blade-tip End-plates Designed for Low-noise Operation in Axial-flow Fans', *Proceedings of the 52nd American Society of Mechanical Engineers Gas Turbine and Aeroengine Congress*, Montreal, Canada, 14–17 May, paper no. GT2007-27465.

Corsini, A., Rispoli, F. and Sheard A.G. (2007b), 'Development of Improved Blade-tip End-plate Concepts for Low-noise Operation in Industrial Fans', *Proceedings of the IMechE Part A, Journal of Power and Energy*, vol. 221(5), pp. 669–681.

Corsini, A., Rispoli, F. and Sheard, A.G. (2010), 'Shaping of Tip End-plate to Control Leakage Vortex Swirl in Axial Flow Fans', *Transactions of the ASME, Journal of Turbomachinery*, vol. 132, paper no. 031005, pp. 1–9.

Corsini, A., Delibra, G. and Sheard, A.G. (2013), 'On the Role of Leading-edge Bumps in the Control of Stall Onset in Axial Fan Blades', *Transactions of the ASME, Journal of Fluids Engineering*, vol. 135, paper no. 081104, pp. 1–9.

Cumpsty, N.A. (1977), 'A Critical Review of Turbomachinery Noise', *Transactions of the ASME, Journal of Fluids Engineering*, vol. 99, pp. 278–293.

Envia, E. and Nallasamy, M. (1999), 'Design Selection and Analysis of a Swept and Leaned Stator Concept', *Journal of Sound and Vibration*, vol. 228, pp. 793–836.

Ffowcs Williams, J.E. and Hall, L.H. (1970), 'Aerodynamic Sound Generation by Turbulent Flow in the Vicinity of a Scattering Half Plane', *Journal of Fluid Mechanics*, vol. 40(4), pp. 657–670.

Fiedler, H.E. and Fernholz, H.H. (1990), 'On Management and Control of Turbulent Boundary Layers', *Progress in Aerospace Sciences*, vol. 27, pp. 305–387.

Fleeter, S. (1980), 'Discrete Frequency Noise Reduction Modeling for Application to Fanjet Engines', *Journal of the Acoustical Society of America*, vol. 68(3), pp. 957–965.

Fukano, T. and Jang, C. (2004), 'Tip Clearance Noise of Axial Flow Fans Operating at Design and Off-design Condition', *Journal of Sound and Vibration*, vol. 275, pp. 1027–1050.

Fukano, T., Takamatsu, Y. and Kodama, Y. (1986), 'The Effects of Tip Clearance on the Noise of Low-pressure Axial and Mixed Flow Fans', *Journal of Sound and Vibration*, vol. 105, pp. 291–308.

Gad-el-Hak, M., Pollard, A. and Bonnet, J.-P. (Eds) (1998), *Flow Control: Fundamentals and Practices*, Springer-Verlag, Paris, France.

Gerard, A. (2006), 'Bruit de Raie des Ventilateurs Axiaux: Estimation des Sources par Modèles Aéroacoustiques Inverses et Nouvelles Méthodes de Controle', Thèse de doctorat, Université de Sherbrooke.

Gerard, A., Berry, M., Masson, P. and Gervais, Y. (2007), 'Passive Adaptive Control of Tonal Noise from Subsonic Axial Fans using Flow Control Obstructions', *Proceedings of the 3rd International Symposium of Fan Noise*, Lyon, France, 17–19 September.

Glick, P.A. (1939), 'The Distribution of Insects, Spiders, and Mites in the Air', Technical Bulletin No. 673, US Department of Agriculture.

Gorny, L.J., Koopmann, G.H., Neise, W. and Lemke, O. (2007), 'Attenuation of Ducted Axial Propulsors' Blade Tone Noise using Adaptively Tunable Resonators', *Proceedings of the 13th AIAA/CEAS Aeroacoustics Conference (28th AIAA Aeroacoustics Conference)*, Rome, Italy, 21–23 May, paper no. AIAA 2007-3529.

Gorny, W. and Koopmann, G.H. (2009), 'Axial Fan Blade Tone Cancellation using Optimally Tuned Quarter Wavelength Resonators', *Transactions of the ASME, Journal of Vibration and Acoustics*, vol. 131(2), paper no. 021002, pp. 1–13.

Goth, Y., Besombes, M., Chassaignon, C. and Gerard, A. (2012), 'Fan Tonal Noise Reduction using Calibrated Obstructions in the Flow: an Experimental Approach', *Proceedings of the Fan 2012 Conference*, Senlis, France, 18–20 April.

Gray, J. (1936), 'Studies in Animal Locomotion: the Propulsive Power of the Dolphin', *Journal of Experimental Biology*, vol. 13, pp. 192–199.

Guedel, A. (1999), *Acoustique des Ventilateurs Génération du Bruit et Moyens de Reduction*, Editions PYC Livres.

Holste, F. and Neise, W. (1997), 'Noise Source Identification in a Prop Fan Model by Means of Acoustical Near Field Measurements', *Journal of Sound and Vibration*, vol. 203, pp. 641–665.

Howe, M.S. (1984), 'On the Absorption of Sound by Turbulence', *Journal of Applied Mathematics*, vol. 32(1–3), pp. 187–209.

Howe, M.S. (1991), 'Noise Produced by a Saw-tooth Trailing Edge', *Journal of the Acoustical Society of America*, vol. 90, pp. 482–487.

Ingard, U. (1953), 'On the Theory and Design of Acoustic Resonators', *Journal of the Acoustical Society of America*, vol. 25(6), pp. 1037–1061.

Jensen, C.E. (1986), 'Axial-flow Fan', Patent No. US 4,630,993, 23 December.

Joslin, R.D. and Morris, P.J. (1992), 'The Effect of Compliant Walls on Secondary Instabilities in Boundary-layer Transition', *AIAA Journal*, vol. 30(2), pp. 332–339.

Joslin, R.D., Morris, P.J. and Carpenter, P.W. (1991), 'The Role of Three-dimensional Instabilities in Compliant Wall Boundary-layer Transition', *AIAA Journal*, vol. 29(10), pp. 1603–1610.

Joslin, R.D., Kunz, R.K. and Stinebring, D.R. (2000), 'Flow Control Technology Readiness: Aerodynamic Versus Hydrodynamic', *Proceedings of the 18th Applied Aerodynamics Conference and Exhibit*, Denver, CO, USA, 14–17 August, paper no. AIAA 2000-4412.

Kameier, F. and Neise, W. (1977), 'Rotating Blade Flow Instability as a Source of Noise in Axial Turbomachines', *Journal of Sound and Vibration*, vol. 203, pp. 833–853.

Kramer, M.O. (1957), 'Boundary Layer Stabilization by Distributed Damping', *Journal of the Aeronautical Sciences*, vol. 24(6), pp. 459–460.

Leggat, L.J. and Siddon, T.E. (1978), 'Experimental Study of Aeroacoustic Mechanism of Rotor-vortex Interactions', *Journal of the Acoustical Society of America*, vol. 64, pp. 1070–1077.

Lighthill, M.J. (1952), 'On Sound Generated Aerodynamically. I: General Theory', *Proceedings of the Royal Society*, vol. A221, pp. 564–587.

Lighthill, M.J. (1954), 'On Sound Generated Aerodynamically. II: Turbulence as a Source of Sound', *Proceedings of the Royal Society*, vol. A222, pp. 1–32.

Lin, J.C. (1999), 'Control of Turbulent Boundary-layer Separation using Micro-vortex Generators', *Proceedings of the 30th AIAA Fluid Dynamics Conference*, Norfolk, VA, USA, 28 June–1 July, paper no. AIAA 99-3404.

Liu, C.K., Kline, S.J. and Johnston, J.P. (1966), 'An Experimental Study of Turbulent Boundary Layer on Rough Walls', Report MD-15, Stanford University.

Longet, C.M.L. (2003), 'Axial Flow Fan with Noise Reducing Means', Patent No. US 2003/0123987 A1, 3 July.

Longhouse, R.E. (1978), 'Control Tip-vortex Noise of Axial Flow Fans by Rotating Shrouds', *Journal of Sound and Vibration*, vol. 58, pp. 201–214.

Marcinowski, H. (1953), 'Einfluss des Laufradspalts und der Luftfuehrung bei einem Kuehlgeblaese axialer Bauart', *Motortechnische Zeitschrift*, vol. 14, pp. 259–262.

Massey, S.J., Thomas, R.H., Abdol-Hamid, K.S. and Elmilgui, A.A. (2003), 'Computational and Experimental Flow Field Analysis of Separate Flow Chevron Nozzles and Pylon Interaction', *Proceedings of the 9th AIAA/CEAS Aeroacoustics Conference and Exhibit*, Hilton Head, SC, USA, 12–14 May, paper no. AIAA 2003–3212.

Miles, J.H. (2006), 'Procedure for Separating Noise Sources in Measurements of Turbofan Engine Core Noise', *Proceedings of the 12th AIAA/CEAS Aeroacoustics Conference (27th AIAA Aeroacoustics Conference)*, Cambridge, MA, USA, 8–10 May, paper no. AIAA 2006-2580.

Mimura, M. (2003), 'Axial Flow Fan', US Patent No. 6,648,598 B2, 18 November.

Mongeau, L., Thompson, D.E. and McLaughlin, D.K. (1995), 'A Method for Characterizing Aerodynamic Sound Sources in Turbomachines', *Journal of Sound and Vibration*, vol. 181, pp. 369–389.

Mugridge, B.D. and Morfey, C.L. (1972), 'Sources of Noise in Axial Flow Fan', *Journal of the Acoustical Society of America*, vol. 51, pp. 1411–1426.

Neise, W. and Koopmann, G.H. (1980), 'Reduction of Centrifugal Fan Noise by Use of Resonators', *Journal of Sound and Vibration*, vol. 73(2), pp. 297–308.

Quinlan, D.A. and Bent, P.H. (1998), 'High Frequency Noise Generation in Small Axial Flow Fans', *Journal of Sound and Vibration*, vol. 218, pp. 177–204.

Reischman, M.M. (1984), 'A Review of Compliant Coating Drag Reduction Research at ONR', in *Laminar-Turbulent Boundary Layers, Vol. 11*, E.M. Uram and H.E. Weber (Eds), ASME, New York, NY, pp. 99–105.

Ross, T. (1998), 'Sound Scattering from Oceanic Turbulence', PhD thesis, University of Victoria, Australia.

Sawyer, S. and Fleeter, S. (1998), 'Passive Control of Turbomachine Noise', *Proceedings of the International Compressor Engineering Conference*, West Lafayette, IN, USA, 14–17 July, pp. 779–784.

Schulten, J. (1982), 'Sound Generated by Rotor Wakes Interacting with a Leaned Vane Stator', *AIAA Journal*, vol. 20, pp. 1352–1358.

Schulten, J. (1997), 'Vane Sweep Effects on Rotor/stator Interaction Noise', *AIAA Journal*, vol. 35, pp. 945–951.

Sheard, A.G., Corsini, A. and Rispoli, F. (2009), 'A Meridional Fan', Patent No. GB 2,452,104 B, 22 July.

Srigrarom, S. and Kurosaka, M. (2000), 'Shaping of Delta-wing Platform to Suppress Vortex Breakdown', *AIAA Journal*, vol. 38, pp. 183–186.

Subaschandar, N., Kumar, R. and Sundaram, S. (1999), 'Drag Reduction due to Riblets on a GAW(2) Airfoil', *Journal of Aircraft*, vol. 36(5), pp. 890–892.

Sutliff, D.L., Tweedt, D.L., Fite, E.B. and Envia, E. (2002), 'Low-speed Fan Noise Reduction with Trailing Edge Blowing', *International Journal of Aeroacoustics*, vol. 1(3), pp. 275–305.

Tyler, J. and Sofrin, T. (1962), 'Axial Flow Compressor Noise Studies', *SAE Transactions*, vol. 70, pp. 309–332.

Uselton, R.B., Cook, L.J. and Wright, T. (2005), 'Fan with Reduced Noise Generation', US Patent No. 6,872,048 B2, 29 March.

Walsh, M.J. (1980), 'Drag Characteristics of V-groove and Transverse Curvature Riblets', in *Viscous Flow Drag Reduction, Progress in Astronautics and Aeronautics, Vol. 72,* G.R. Hough (Ed.), AIAA, Reston, VA, USA, pp. 169–184.

Wennerstrom, A.J. (1982), 'Vane Configuration for Fluid Wake Re-energization', US Patent No. 4,318,669, 9 March.

Woodward, R.P., Elliott, D.M., Hughes, C.E. and Berton, J.J. (2001), 'Benefits of Swept-and-leaned Stators for Fan Noise Reduction', *Journal of Aircraft*, vol. 38(6), pp. 1130–1138.

Wright, S.E. (1976), 'The Acoustic Spectrum of Axial Flow Machines', *Journal of Sound and Vibration*, vol. 45(2), pp. 165–223.

Chapter 2

Experimental Development of a Measurement Technique to Resolve the Radial Distribution of Fan Aeroacoustic Emissions

S. Bianchi, A.G. Sheard,
I.R. Kinghorn, A. Corsini and F. Rispoli

ABSTRACT

The chapter presents an experimental technique that we developed to facilitate assessing a fan's acoustic performance intended for application in compact cooling units. We developed the experimental technique to provide insight into the far-field acoustic consequences of near-field flow features induced in the flow by blade-tip end-plates. We placed a microphone ten per cent blade chord down-stream of the studied fan blades trailing edge. We then varied the microphone's span-wise location in steps of two per cent from blade hub to blade tip. We made acoustic measurements simultaneously with a far-field microphone. Thus, this experimental technique was able to provide data sets of near- and far-field fan noise that we then could correlate to establish the far-field consequences of near-field noise sources. The span-wise correlation of near- and far-field noise was distinctly different for the studied fan without a fitted blade tip end-plate and when fitted with one of the studied end-plates. Therefore, the experimental technique was effective as it facilitated the identification of near-field noise sources unique to each of the tested fan geometries. The correlation technique was also effective as it facilitated identification of the far-field acoustic consequences of the identified near-field noise sources. The developed correlation technique relies on a fan far-field noise measurement taken when the near-field microphone is not present to later correct measurements taken when the near-field microphone is present. In this way the technique corrects for the near-field microphone's acoustic influence. The developed experimental technique and near- and far-field correlation technique have proven to constitute an effective experimental methodology for identifying the far-field acoustic consequences of near-field span-wise flow features.

This chapter is a revised and extended version of Bianchi, S., Sheard, A.G., Kinghorn, I.R., Corsini, A. and Rispoli, F. (2009), 'Experimental Development of a Measurement Technique to Resolve the Radial Distribution of Fan Aeroacoustic Emissions', *Noise Control Engineering Journal*, vol. 57, pp. 360–369.

NOMENCLATURE

Latin letters

BPF	blade-passing frequency [Hz]
Co	numerical value of the coherence function
G_{xx}	spectra in the near-field
G_{yy}	spectra in the far-field
G_{xy}	cross-spectrum
H	blade span
ℓ	blade chord
P	static pressure [Pa]
R	non-dimensional span
T	blade pitch
S	near-field microphone distance from the root of the blade
SPL	sound pressure level [dB]

Greek letters

η_{tot}	total efficiency
σ_h	hub-to-casing diameter ratio
τ	rotor tip clearance

INTRODUCTION

Air movement fans are a source of noise pollution in heating, ventilation and air conditioning systems. They generate both tonal and broadband noise that typically constitutes the dominant noise source of any system within which they are installed. Researchers in the 1970s, particularly Wright (1976) and Cumpsty (1977), have studied the link between the fan rotors' aerodynamic features and their acoustic emissions. Their findings have enhanced general understanding of axial turbomachinery aeroacoustics. Cumpsty (1977) concluded that, with the exception of the low-frequency range of high-speed machines, the mechanism that determines broadband noise in subsonic fans is the same as that in supersonic tip-speed fans and compressors. Therefore, the design variables that impact tonal and broadband noise are similar both for fans designed for aerospace and air movement application (Ganz *et al.*, 1998). According to Wright (1976), this is because of the prominence of rotor noise that originates from turbulent boundary layers.

When studying fan and compressor acoustic performance, both Cumpsty (1977) and Holste and Neise (1997) observed that the radiated acoustic energy was small compared with the energy transferred from blades to working fluid. The human ear is highly sensitive, able to perceive very low levels of acoustic energy that if transferred into useful work would result in an immeasurable increased aerodynamic efficiency. Consequently, it is challenging to characterise the far-field acoustic effect of near-field aerodynamic cause. Those scholars who have studied the link between near-field aerodynamic cause and far-field acoustic effect have identified sig-

nificant unsteady or periodic forces, volume displacements and non-linear flow-features as dominant noise sources. These arise as a consequence of inflow-turbulence, impeller induced flow-features and features within the blade tip-to-casing flow-field (Sharland, 1964; Fukano *et al.*, 1977a, 1977b).

Inflow-turbulence generates far-field noise as a consequence of the turbulent fluctuations in the ingested air. Inflow-turbulence can result in a dominant far-field noise source over a distinct range of frequencies in both low-speed fans (Wright, 1976) and high-speed turbomachinery (Cumpsty, 1977). Wright (1976) and Cumpsty's (1977) analyses focused on the low-frequency spectrum's 'humped' nature. In this context they defined low-frequency as frequencies below the blade-passing frequency. They attributed the 'humped' nature to the large-scale features within the incoming turbulence. These large-scale features produce periodic disturbances as they sweep through the blade-to-blade passage.

Impeller induced flow-features generate far-field noise as a consequence of the pressure fluctuations generated by turbulent boundary layers over the blade and by vortex shedding from the blade trailing edge. Wright (1976) first identified the significance of impeller induced flow-features as far-field noise sources. His primary conclusions (1976) were self-consistent with Sharland's earlier observations (1964). He postulated that the random fluctuation of a moving flow over a surface might act as a noise source. When studying the acoustic consequences of impeller induced flow-features, Cumpsty (1977) argued that the interaction of shear layers with the rotating blades represents another potential noise source. The same lifting forces as those that create the shear layer also produce a dipole-like vortex structure that rotates with the blade. The repetitive pattern of the fluctuating pressure passing a stationary strut or other fixed object then produces the narrowband tone known as the blade-passing frequency (BPF). This tone and its harmonics are the hallmark of the acoustic spectrum of fans developed for both aerospace and air movement application.

Features within the blade tip-to-casing flow-field generate far-field noise as a consequence of the interaction of those features with casing boundary layers and blade-to-blade passage secondary flow features. Researchers who have studied fan and compressor acoustic performance have concluded that the features within the blade tip-to-casing flow-field constitute the most significant far-field noise sources (Longhouse, 1978; Fukano and Jang, 2004). Marcinowski (1953), the first researcher to study noise associated with tip dynamics, demonstrated that increases in broadband noise levels occur with increasing tip clearance. The largest changes in noise level were apparent at frequencies greater than the blade-passing frequency.

In contrast to Marcinowski (1953), Mugridge and Morfey (1972) argued that an optimum tip clearance exists when broadband noise is at a minimum due to the countervailing effects of the tip clearance flow and the blade-passage vortex. However, Longhouse (1978) did not confirm this result. He searched for a practical solution to a cooling fans' tip clearance noise and concluded that the unstable blade-tip vortex impacted the adjacent blade pressure side. He obtained the lowest noise levels with the smallest possible tip clearance. Fukano and Jang (2004) reported similar findings; whereas, Kameier and Neise's (1997) experiments demonstrated that, with

the smallest possible tip clearance, noise reduced over a limited frequency range, close to the blade passage frequency. However, random noise actually increased.

This chapter presents the results of a research programme to develop an experimental technique and near- and far-field correlation technique that together enable us to identify the far-field acoustic consequences of near-field span-wise flow features. The research was inspired by Longhouse (1978) and Fukano and Jang's (2004) conclusions regarding the acoustic significance of features within the blade tip-to-casing flow-field. The purpose of the developed experimental technique and near- and far-field correlation technique is to facilitate elucidation of the far-field acoustic consequences of the blade tip-to-casing flow-field features. Our research objective is to facilitate insight into the flow-field physics that will in turn aid in developing new noise control concepts and technologies. These new concepts and technologies will enable more effective control of the blade tip-to-casing flow-field, minimising the far-field acoustic consequences of near-field flow-features. The developed experimental technique help identify near-field noise sources unique to each of the tested fan geometries. The correlation technique enables one to identify the far-field acoustic consequences of the near-field noise sources. In combination, the experimental technique and near- and far-field correlation technique helped us identify the far-field acoustic consequences of near-field aerodynamic flow-field features.

CONCEPTUAL FRAMEWORK

The experimental technique and near- and far-field correlation technique enabled us to compensate for the acoustic effects induced by the presence of the near-field microphone using far-field data when processing near-field data. We base the technique on previously reported measurement techniques for use with fans (Leggat and Siddon, 1978), turbo-fan engines (Kameier and Neise, 1997; Miles, 2006) and radial pump rotors (Mongeau *et al.*, 1995).

We use the developed measurement technique to identify noise sources and their distribution along the fan blade's radial span both with and without a fitted blade-tip end-plate. Comparing the span-wise measurement sets facilitated an insight into the flow-field physics in the blade-tip region. We established measurement technique reliability by correlating the flow-field's identified features with Holste and Neise's (1997) qualitative results.

Family of Fans

We conducted the reported research on a family of commercially available cooling fans configured for application over a compact cooling unit's tube bank, Figure 2.1. The studied fan configuration, coded AC90/6, incorporates a six-blade unswept rotor, with a modified ARA-D profile aerofoil blade, Table 2.1. One may set the blade-pitch angle during final assembly to customise the fan to a desired duty point. We used a direct coupled-induction 400-volt (AC), 3-phase motor to drive the

Table 2.1. *The fan* datum *AC90/6 blade geometry and rotor specification.*

	Fan *datum* AC90/6		
Blade geometry	Hub	Mid-span	Tip
Pitch angle (°)	36	58.8	28
Camber angle (°)	46	44	41
Solidity	1.24	0.86	0.30
Fan rotor			
Blade number		6	
Blade tip pitch angle (°)		16–28	
Blade tip stagger angle (°)		74–62	
Hub-to-casing diameter ratio σ		0.22	
Tip diameter (mm)		900.0	
Rotor tip clearance τ (% span)		1.0	
Rated rotational frequency (r/min)		935–950	

rotor at a constant speed of 950 rpm, resulting in a 44.7 m/s blade tip speed and a 95 Hz blade-passing frequency (BPF). In its original embodiment the studied fan did not include a blade tip end-plate. Therefore, we used it as a *datum* against which to assess the fan's performance variants with blade tip end-plates. In the reported research we refer to the fan without blade-tip end-plates as the fan *datum* AC90/6.

In addition to the fan *datum* AC90/6, we studied two fan variants. The first fitted with a constant thickness blade-tip end-plate (named AC90/6/TF) and the second with a variable thickness blade-tip end-plate (named AC90/6/TF$_{VTE}$), Figure 2.2.

Designs developed for tip-vortex control and drag reduction in aircraft wings and catamaran hulls inspired the constant thickness blade-tip end-plate design. The constant thickness blade-tip end-plate ran along the blade pressure surface, ending at the blade trailing edge with a square tail. The addition of this constant thickness blade-tip end-plate resulted in the thickness of the fan AC90/6/TF blade tip increasing by a factor of three compared to the fan *datum* AC90/6. We considered the blade-tip end-plate's size for axial compressor blades by referring to Inoue *et al.* (1986) who estimated that the optimum blade-tip end-plate size was between 10 and 20 per cent blade span. In practice, we were able to manufacture blades with a blade-tip end-plate size five per cent of blade span. The fan blades were manufactured from injection moulded plastic, with the blade-tip end-plate's size as the largest the blade manufacturing technique could produce.

Corsini and Sheard (2007) studied both the fan *datum* AC90/6 and AC90/6/TF using a blade-tip vortex 'breakdown criteria' based on Rossby number (Spall *et al.*, 1987). Following Ito *et al.*'s method (1985), they concluded that there is a threshold value of Rossby number below which the vortex rotation cannot reduce if the vortex is to remain stable. Uchida *et al.* (1985) and Garg and Leibovich (1979) defined this critical Rossby number range. Uchida *et al.* (1985) defined a critical Rossby number associated with the breakdown of an axi-symmetric vortex in a swirling flow. Garg

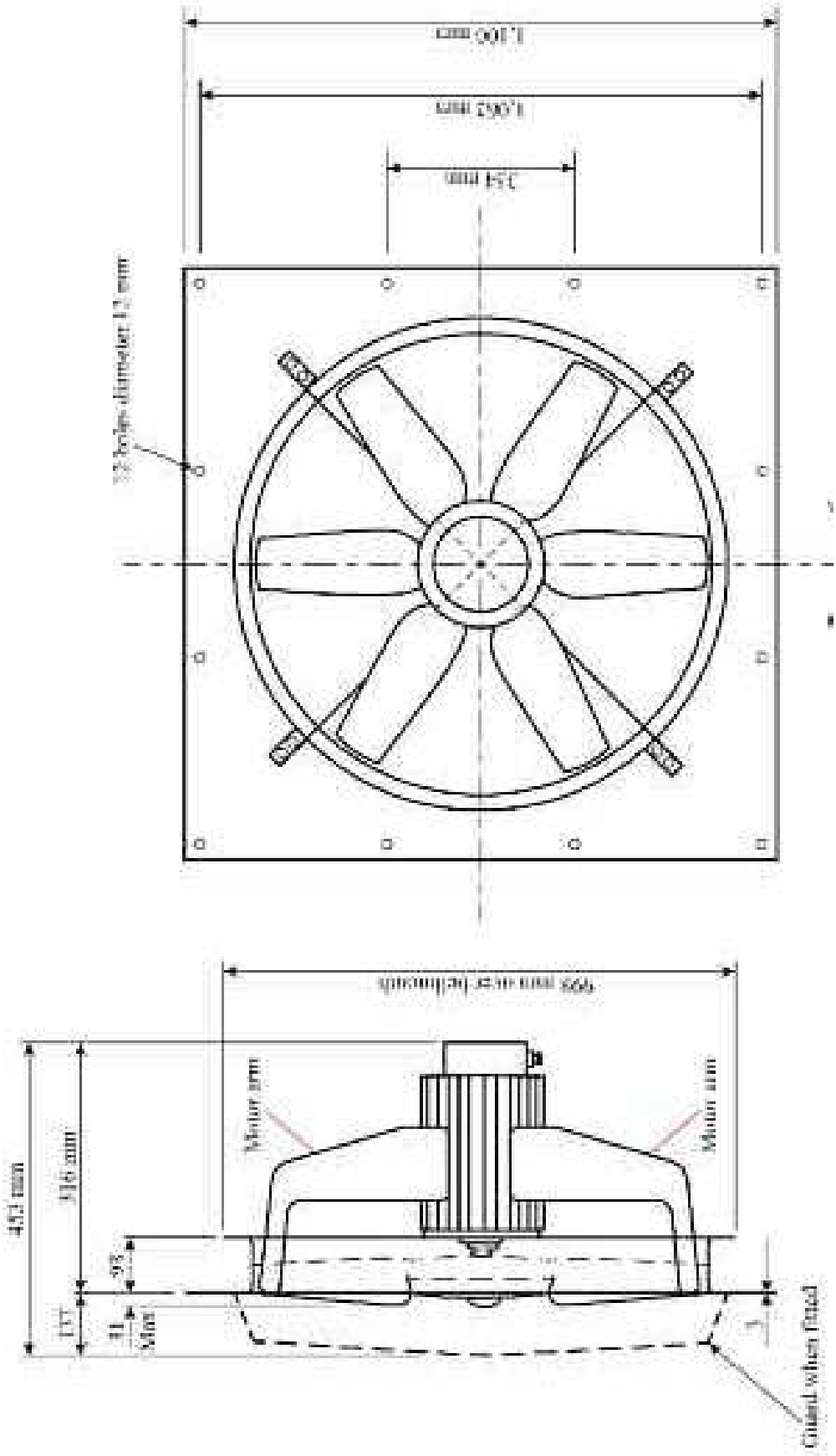

FIGURE 2.1. The studied fan is a 'plate mounted' fan, intended for application over a compact cooling unit's tube bank.

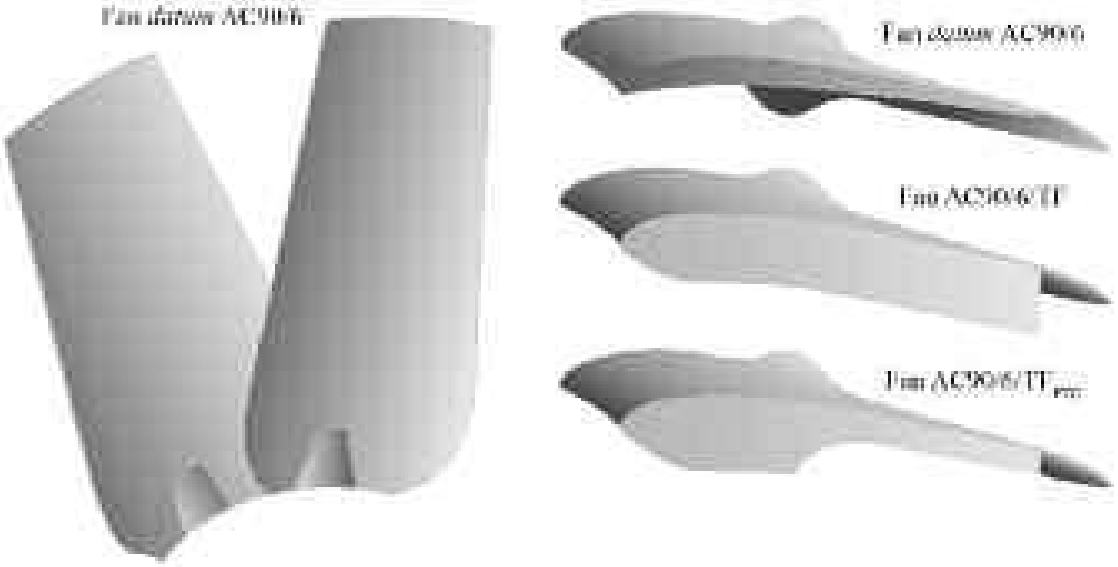

FIGURE 2.2. The studied fan *datum* AC90/6 without a fitted blade-tip end-plate, with a constant thickness blade-tip end-plate, AC90/6/TF and with a variable thickness blade-tip end-plate, AC/6/TF$_{VTE}$.

and Leibovich (1979) also defined a critical Rossby number associated with an aircraft wing tip vortices' breakdown.

Corsini *et al.* (2006) studied the aerodynamic and acoustic performance of the fan *datum* AC90/6 and fan AC90/6/TF, identifying a breakdown of the fan AC90/6/TF blade tip-to-casing leakage vortex. Vortex breakdown is acoustically productive, therefore Corsini *et al.* (2006) concluded that a revised blade-tip end-plate design that avoided leakage vortex breakdown was desirable. Corsini and Sheard (2007) developed a blade-tip end-plate design methodology that successfully eliminated the leakage vortex breakdown by adding a variable thickness blade-tip end-plate. When they appended it to the fan *datum* AC90/6 blades, they named the fan AC90/6/TF$_{VTE}$.

Fan Operating Point

The studied fan blade tip pitch angle is adjustable with settings between 16 and 28 degrees. In practical application, one typically sets the blade tip pitch angle to 28 degrees as this maximises flow rate for a given system pressure. In the research reported in this chapter we set the fan blade tip pitch angle to 28 degrees because it is typical of the angle one uses in practical application and because it results in the highest blade loading. This then results in the blade tip-to-casing vortex having the most significant effect on both fan aerodynamic and acoustic performance (Holste and Neise, 1997).

The impact of the blade tip-to-casing vortex on both fan aerodynamic and acoustic performance results in applying blade-tip end-plates changing not only the fan's acoustic performance, but also the aerodynamic performance. Consequently,

the fan *datum* AC90/6 generates a different pressure at a constant flow rate when fitted with each of the studied blade-tip end-plates. To facilitate the comparison of fan performance data when fitted with different blade-tip end-plates, we chose to define three operating points, and their respective volume flow rates, Table 2.2. The design operating point volume flow rate is typical of that required when one installs the fan over a cooling unit's tube bank. The peak pressure flow rate is typical of that required when the tube bank has become partially blocked following a period of in-service operation. The maximum flow operating point volume flow rate is typical of the flow rate associated with the lowest loss tube bank currently operating in service.

We measured the studied fan's performance characteristics in accordance with ISO 5801:2007 requirements (2007). The performance characteristics illustrate the impact of blade-tip end-plate geometry on fan pressure rise, Figure 2.3. The addition of both the constant and variable thickness blade-tip end-plates results in an increase in blade loading. We would expect blade-tip noise sources to become more acoustically productive with increasing blade loading. An increase in blade loading will therefore partially offset any reduction in fan far-field noise attributed to adding a blade-tip end-plate. Consequently an assessment of acoustic performance is inherently conservative if it neglects the increase in fan far-field noise associated with an increase in blade loading. Despite fan far-field noise being a blade loading function, we chose to neglect the change in pressure rise with the change in blade-tip treatment.

EXPERIMENTAL METHODS

We conducted the experimental measurements in an anechoic chamber in accordance with ISO 10302:1996 requirements (1996). We placed the fan centre line two metres from the floor. We made acoustic measurements using microphones at the fan inlet and the outlet, recording the near- and far-field signals on two channels of a data acquisition system. An aerofoil louver in the top of the anechoic chamber inlet section facilitated fan flow rate variation. We aerodynamically optimised the fan inlet bell mouth profile to provide uniform and unseparated flow into the fan. The fan was connected to the outside environment via up- and down-stream plenums. We

Table 2.2. *The operating points used when characterising the studied fan's performance with and without fitted blade-tip end-plates. The authors measured the performance characteristics in a Type D standardised airway (ducted inlet, ducted outlet) in accordance with ISO 5801:2007 requirements (2007).*

Operating point	Volume flow rate (m^3/s)	Studied blade tip pitch angle (°)
Maximum flow	7.0	28
Design	6.5	28
Peak pressure	5.6	28

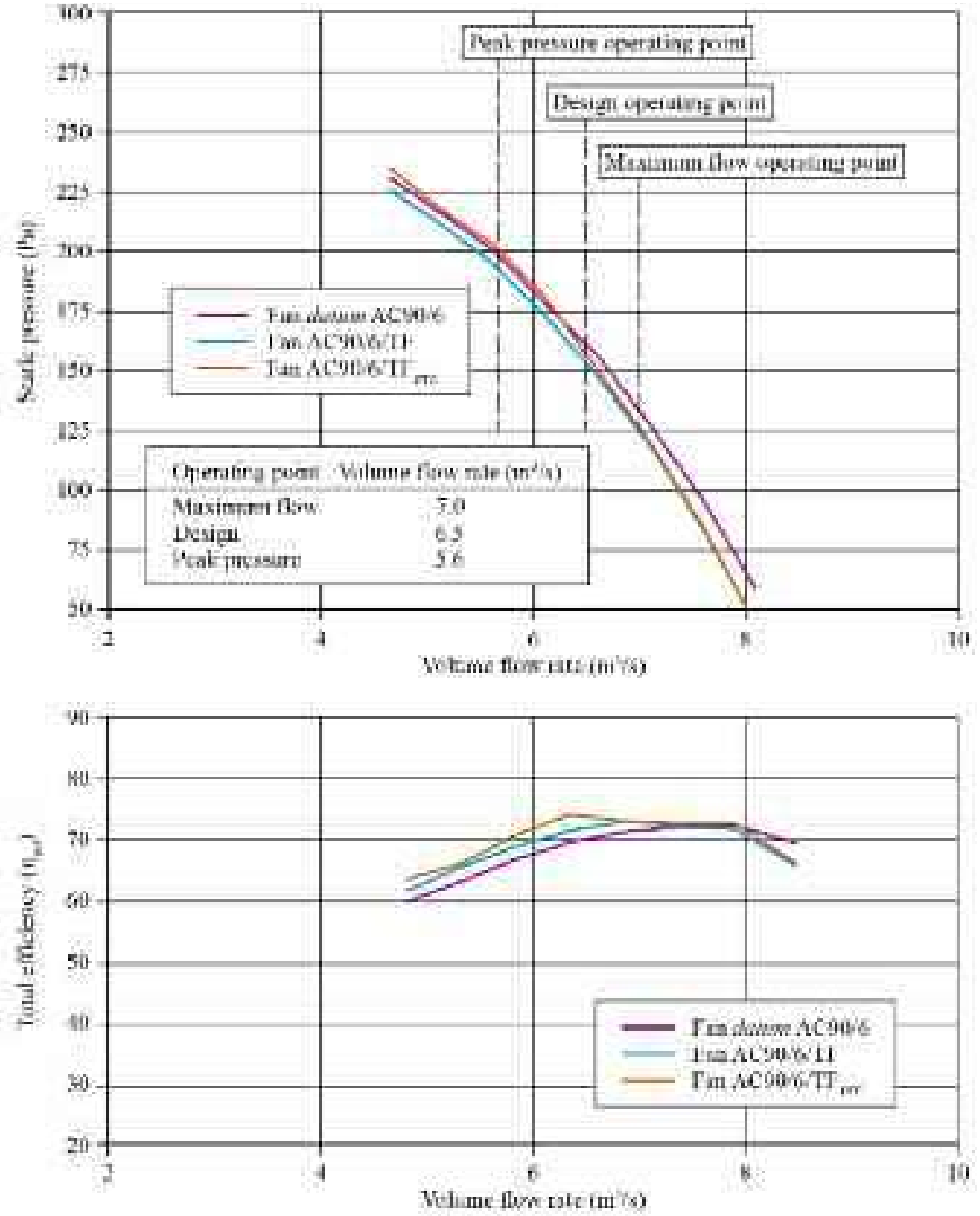

FIGURE 2.3. The performance characteristics of the studied fan *datum* AC90/6 without a fitted blade-tip end-plate, with a constant thickness blade-tip end-plate, AC90/6/TF and with a variable thickness blade-tip end-plate, AC/6/TF$_{VTE}$. The authors measured the performance characteristics with the blade tip pitch angle set to 28 degrees in a Type D standardised airway (ducted inlet, ducted outlet) in accordance with ISO 5801:2007 requirements (2007).

designed these plenums to minimise in-flow non-uniformities and acoustically treated them to both minimise noise transmission from the external environment and its reflection inside the plenum ductwork. We also covered the anechoic chamber walls with foam panels to further reduce noise transmission from the external environment.

Cross-correlating the near- and far-field measurements to differentiate near-field noise sources from the far-field noise enabled us to avoid pseudo sound, which degrades measurement accuracy. Pseudo sound is turbulence-generated noise that one records in the near-field, but it decays so quickly that it does not contribute to the far-field noise. Mugridge and Morfey (1972), Holste and Neise (1997), Miles (2006) and Laurendeau *et al.* (2007) have successfully used the cross-correlation technique we adopted in the present study to correct pseudo sound in exhaust flows.

Near-field Acoustic Measurement Technique

We made near-field measurement at the fan outlet by mounting a microphone on a 10 mm diameter radial traversing mechanism 10 per cent blade chord downstream of the blade trailing edge, Figure 2.4. We then used the traversing mechanism to move the near-field microphone from the blade hub to tip, in radial steps corresponding to two per cent of blade span. Thus, the traversing microphone facilitated the span-wise measurement of near-field fan noise.

By choosing to locate the microphone 10 per cent blade chord downstream of the blade trailing edge, we located it upstream of the motor arms, Figure 2.1. This placement effectively prevented the microphone from measuring any tonal noise sources associated with the motor arms. Despite this limitation, we selected the microphone location to ensure that we captured the acoustic emissions from the vortical flow-field structures present in the exhaust flow. This was because of our interest in the acoustic emissions from flow-field structures, and not overall impeller noise.

We made near-field measurements at the fan inlet by placing a microphone one fan diameter upstream of the fan inlet. We covered the microphone diaphragm with a standard shield to minimise the self-induced noise generated by the flow past the microphone. We conducted hot-wire anemometer measurements to determine the flow velocity at the microphone location. Using the known velocity at the inlet microphone location, we were able to calculate a correction factor to compensate for the self-induced noise generated by the flow past the microphone.

We also conducted hot-wire anemometer measurements to determine the flow velocity at each of the exhaust span wise microphone locations. As the exhaust microphone was located immediately downstream of the blade trailing edge, we chose to calibrate the traversing microphone in a dedicated test rig. We measured the background noise in the test rig with no flow, and then induced the airflow corresponding to each of the microphones' span-wise locations. This facilitated calculation of self-induced noise correction factors for the traversing microphone.

FIGURE 2.4. Microphone arrangement for the fan noise's inlet near-field measurements (left) and outlet near-field measurements (middle). The microphone that the authors used for outlet near-field measurements could be traversed from the blade hub to tip (right).

Far-field Acoustic Measurements Technique

We measured far-field noise six fan diameters from the fan exhaust, as recommended by Leggat and Siddon (1978), when measuring a fan's far-field noise without any downstream obstructions. Leggat and Siddon (1978) studied fan noise directivity in a semi-reverberant environment and concluded that the maximum noise levels were coincident with the fan axis, immediately downstream of the exhaust. In the research reported in this chapter, we chose to place the far-field microphone at an angle 30 degrees from the fan axis, Figure 2.5. This was to avoid the possibility of the fan exhaust flow impacting directly on the far-field microphone. Our logic was that the anechoic chamber within which we made our measurements was not infinitely large. Consequently, there was a possibility that the fan would induce flow-field features within the anechoic chamber itself that may have acoustic consequences.

By placing the microphone at an angle 30 degrees from the fan axis, we placed it in a location with the lowest flow-field velocity within the anechoic chamber. We considered that low flow-field velocities would result in any flow-field features within the anechoic chamber also having a low impact on measured far-field noise. We selected the far-field microphone's location after measuring flow-field velocity at different locations within the anechoic chamber. The chosen location's flow-field velocity was less than 0.1 m/s which we considered negligible.

Leggat and Siddon's (1978) recommendations apply when measuring a fan's far-field noise without any obstructions downstream of the fan. We may regard the traversing near-field microphone as an obstruction downstream of the fan. To account for the near-field microphone's acoustic impact on the measured far-field noise, we measured the fan far-field noise with the near-field traversing mechanism removed. We then made far-field noise measurements with the near-field microphone in each of the span-wise locations where we made near-field measurements.

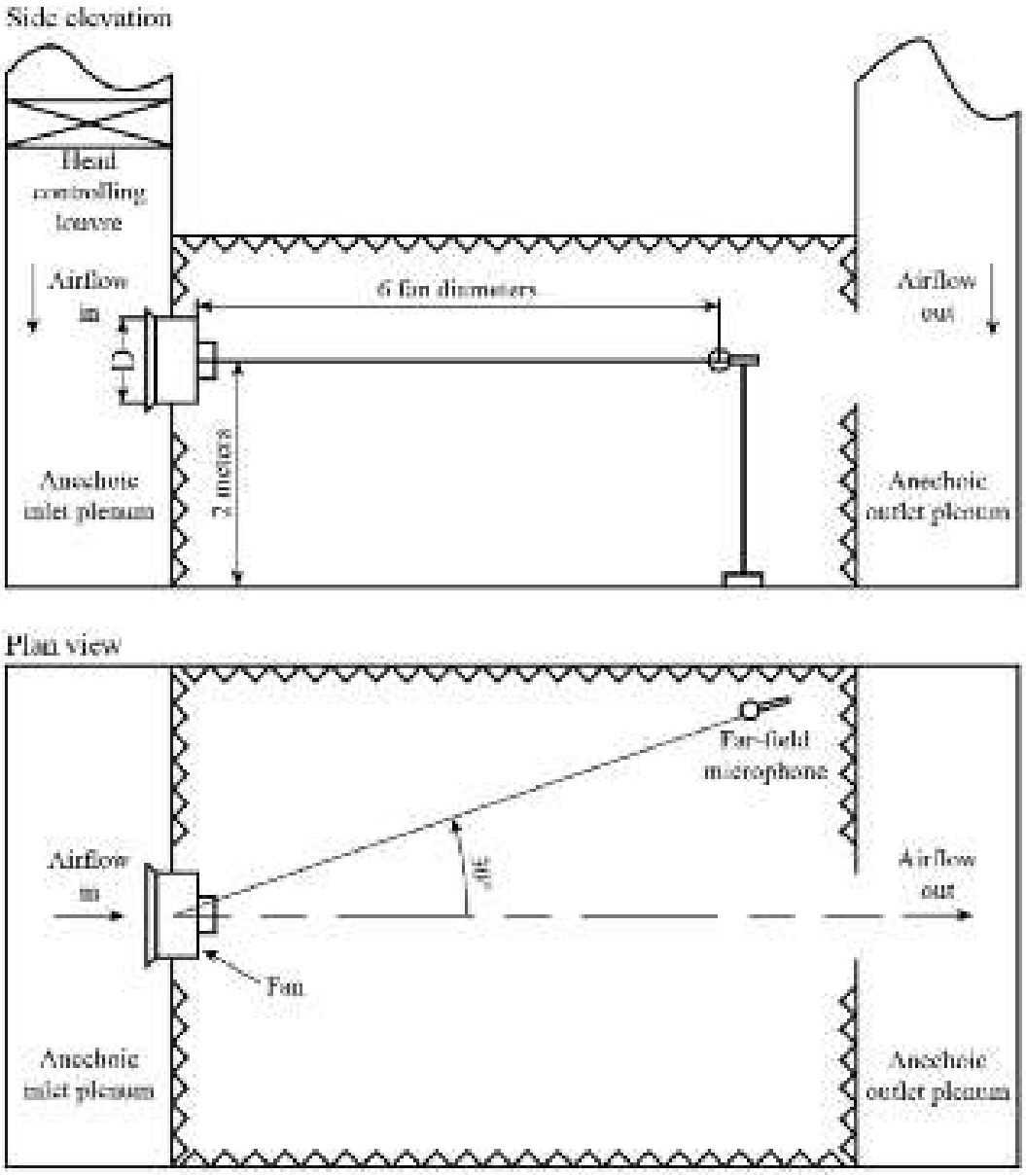

FIGURE 2.5. Microphone arrangement for the fan noise's outlet far-field measurements in the anechoic chamber that the authors used for outlet near- and far-field fan noise measurements.

We then calculated a cross-spectrum and coherence function for each near-field span-wise measurement location. These facilitated the correction of far-field measurements, enabling us to account for the near-field microphone's far-field acoustic impact.

EXPERIMENTAL RESULTS

We measured fan near-field outlet noise using the traversing microphone, and far-field noise using the microphone located six fan diameters from the fan exhaust.

For each near- and far-field measurement we computed the narrowband spectra from 50 to 10 kHz using a constant bandwidth of 3.15 Hz. We used these narrowband spectra as input to a correlation analysis which enabled us to identify causal relationships between individual vortical flow-field structures present in the near-field exhaust flow and the fan far-field noise. The coherence analysis facilitated a quantitative assessment of the near-field noise source locations, their spectra and the extent of their coherence with fan far-field noise.

We undertook the coherence analysis using a coherence function that used as input the near- and far-field spectra, *Gxx* and *Gyy* respectively, and the cross-spectrum between the two, *Gxy*. We defined coherence as:

$$Co^2 = \frac{|Gxy|^2}{|Gxx| \cdot |Gyy|} \tag{1}$$

We used a calibrated noise source to characterise the anechoic chamber's acoustic properties, establishing the coherence between the near- and far-field microphones, Welch (1967). Following Miles' method (2006), we set the threshold for coherence at 95 per cent of the calibrated noise's coherence. This approach ensured that we only used coherent noise sources when calculating the cross-spectra.

Near-field Narrowband Spectral Analysis

We may establish the coherence analysis validity within the context of the reported research by considering the inlet and outlet coherence spectra, Figure 2.6. We derived the outlet coherence spectra from measurements that we made with the traversing microphone located at the blade tip. The blade tip region is associated with the most pronounced tonal peaks in coherence.

Tones at the first and third blade passing frequency dominate the outlet coherence. In contrast, tones at the second and third blade passing frequency dominate the inlet coherence. The difference between the inlet and outlet coherence is self-consistent with both Cumpsty (1977) and Leggat and Siddon's (1978) conclusions. Studying high-speed axial compressors, they concluded that the tone associated with the first blade passing frequency in the outlet coherence occurred as a consequence of unsteady flow-field features in the blade tip region. These unsteady flow-field features migrated into the exhaust flow and thus dominated the outlet coherence.

Self-consistency of the coherence analysis results with the conclusions of Cumpsty (1977) and Leggat and Siddon (1978) gives confidence in the validity of the approach. Having established validity, the subsequent analysis will focus on outlet measurements that we made with the traversing microphone. This is a consequence of the application for this class of fan. These fans draw air over compact cooling unit heat exchangers' tube banks, and consequently exhaust to the atmosphere. Therefore, outlet rather than inlet noise is of most interest to the fan designer.

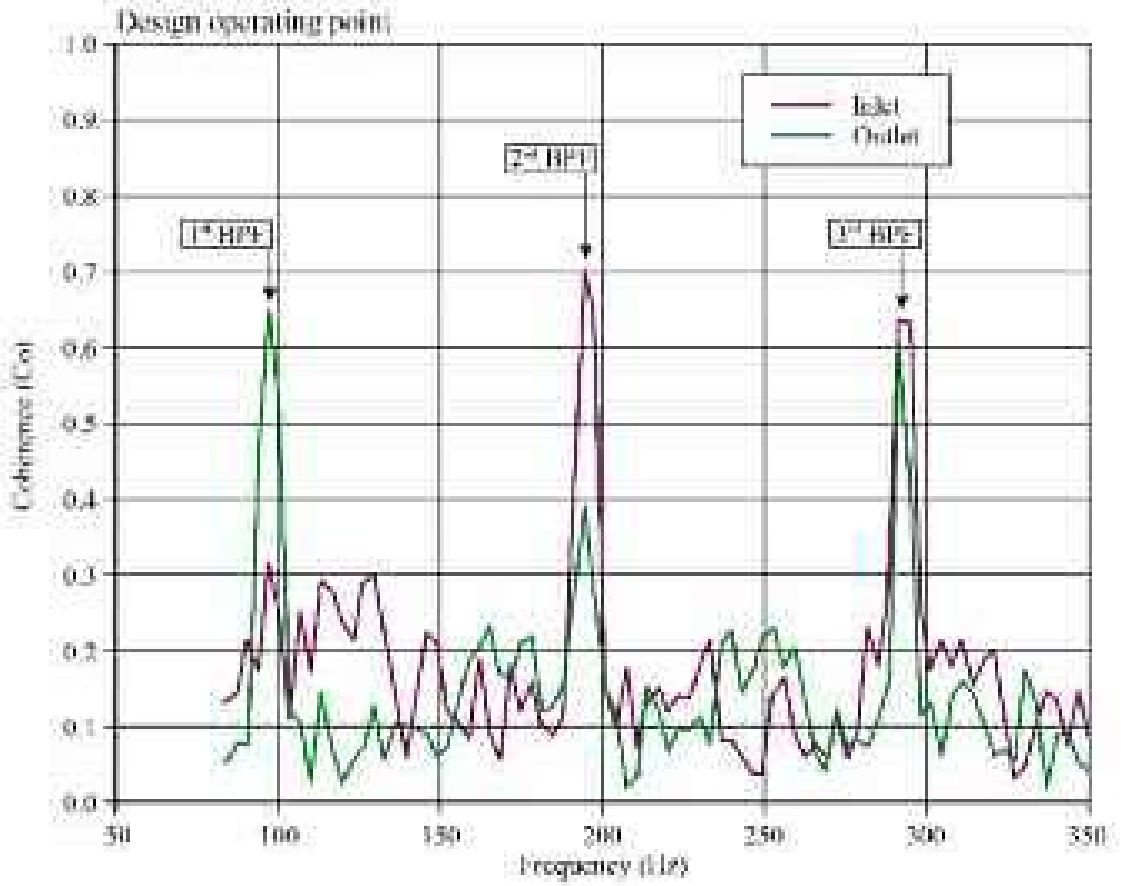

FIGURE 2.6. A comparison of the fan *datum* AC90/6 coherence between near- and far-field fan noise at the fan inlet and outlet at the fan design operating point. The authors made near-field measurements at the blade tip.

Span-wise Distribution of Aeroacoustic Noise Sources

The research presented in this chapter focused on the development of an experimental technique to facilitate assessment of fan acoustic performance. This provides insight into the far-field acoustic consequences of near-field flow features induced in the flow by blade-tip end-plates. However, before considering the impact of blade-tip end-plates on fan far-field noise, we must first analyse the performance of the fan *datum* AC90/6 with no blade-tip end-plates. Insight into the fan *datum* AC90/6 performance then facilitates comparison with the performance when blade-tip end-plates are fitted.

Our analysis of the fan *datum* AC90/6 performance starts with a review of the span-wise distribution of outlet near-field sound pressure level (L_P), Figure 2.7. We generated the span-wise distributions at the three studied operation points, peak pressure, design and maximum flow. The sound pressure level was lowest at the maximum flow operating point, Figure 2.7. There is a peak in sound pressure level in the blade tip region, as we would expect given that the blade tip-to-casing leakage vortex presence dominates the flow-field. There is also an unexpected peak in sound

pressure level at around 25 per cent blade span. This peak in the blade root region is probably associated with the local flow incidence angle in the blade root. At the maximum flow operating point the blade root incidence angle will have departed significantly from its design value. Consequently, the boundary layer has probably separated at the hub with this separated flow region responsible for the peak in sound pressure level. Between approximately 30 and 80 per cent blade span the sound pressure level remained low compared to that at both the tip and hub.

Throttling the fan from its maximum flow to design operating point resulted in a 5 dB increase in sound pressure level in the blade tip region, Figure 2.7. This increase in sound pressure level at the blade tip increased again as we throttled the fan from its design to peak pressure operating point with a further 3 dB increase in sound pressure level. However, the most dramatic change was in the sound pressure level at the hub. The shift from maximum flow to design operating point did not result in a significant change in the hub sound pressure level. In contrast, the shift from design to peak pressure operating point resulted in the peak moving from approximately 25 per cent to 40 per cent blade span and increasing by 8 dB. This shift in location and increase in sound pressure level indicates that as the fan approaches stall the hub separation becomes a more significant flow-field feature.

We may gain further insight into the outlet flow-field physics by studying the coherence spectra at different span-wise locations, Figure 2.8. The outlet coherence is at the fan's design operating point at the blade hub, 35 and 70 per cent blade span and at the blade tip. The first blade passing frequency is associated with a tone at the blade tip that is dominant compared to that at the other span-wise locations. In contrast, the second blade passing frequency outlet coherence is dominant at 35 and 70 per cent blade span.

The span-wise outlet coherence spectra indicate that the first blade passing frequency increases from hub to tip. The hub is associated with the lowest coherence, the 35 and 70 per cent are approximately the same and the tip is the highest. As previously noted, the second blade passing frequency outlet coherence is dominant at 35 and 70 per cent blade span. Magliozzi *et al.* (1973) and Cumpsty (1974, 1977) have studied the significance of the second blade passing frequency. They suggest that interaction between inflow disturbances from the inlet plenum influence the second blade passing frequency. These disturbances were capable of affecting end-wall boundary layers over 15 per cent of the blade span that went on to interact with the blade wake in both the hub and tip region. Therefore, we may speculate that the low outlet coherence in the blade hub and tip region may result because of disturbances in the inflow to the fan.

Studying inlet and outlet coherence spectra in the blade root region may establish the significance of inflow disturbances, Figure 2.9. At the blade root both the inlet and outlet coherence spectra exhibit a tone at 62.5 Hz. Cumpsty (1977) concludes that this noise source originates from the rotor alone and is directly attributable to distortions in the inlet flow induced by the rotor alone. When we study the inlet and outlet coherence spectra, we see that the rotor 62.5 Hz tone is significantly more coherent in the inlet rather than the outlet coherence spectra.

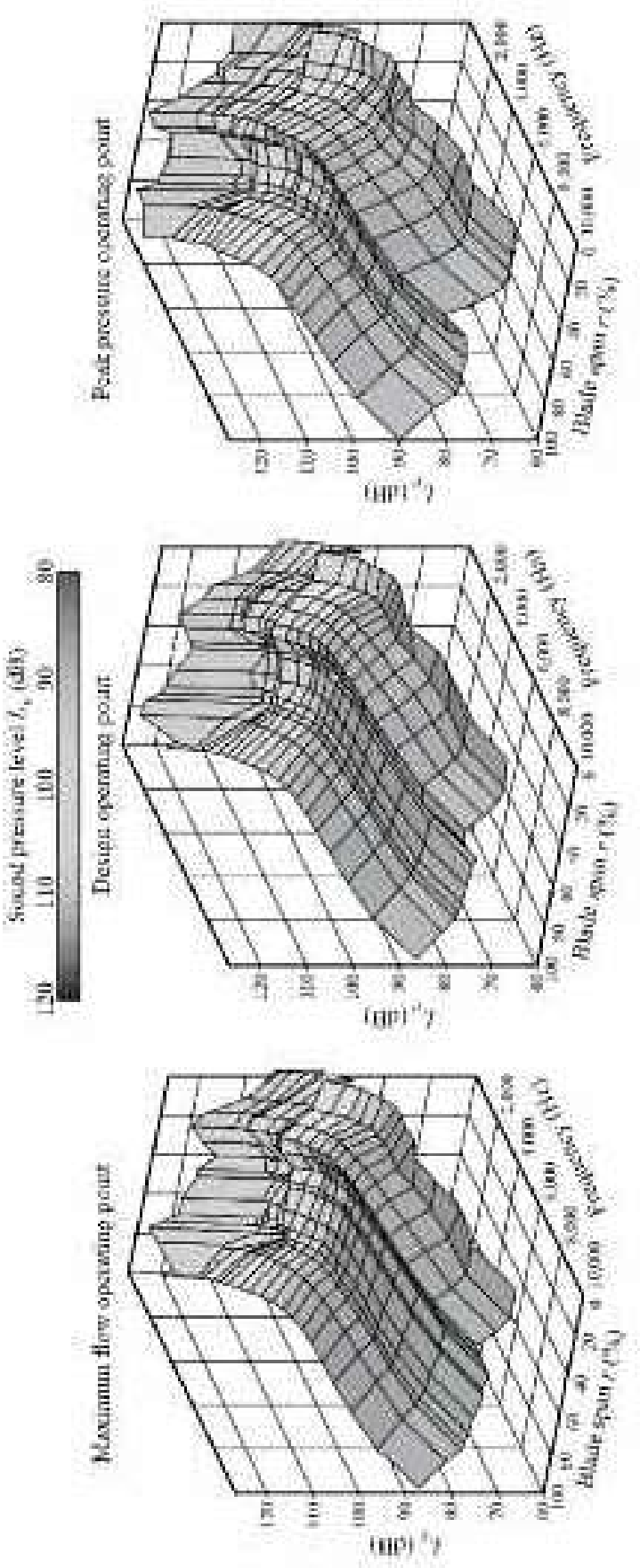

FIGURE 2.7. Span-wise distribution of the fan *datum* AC90/6 outlet near-field sound pressure level L_p that the authors measured at the maximum flow, design and peak pressure operating points. The span-wise distributions illustrate the change in spectrum with changing fan operating point.

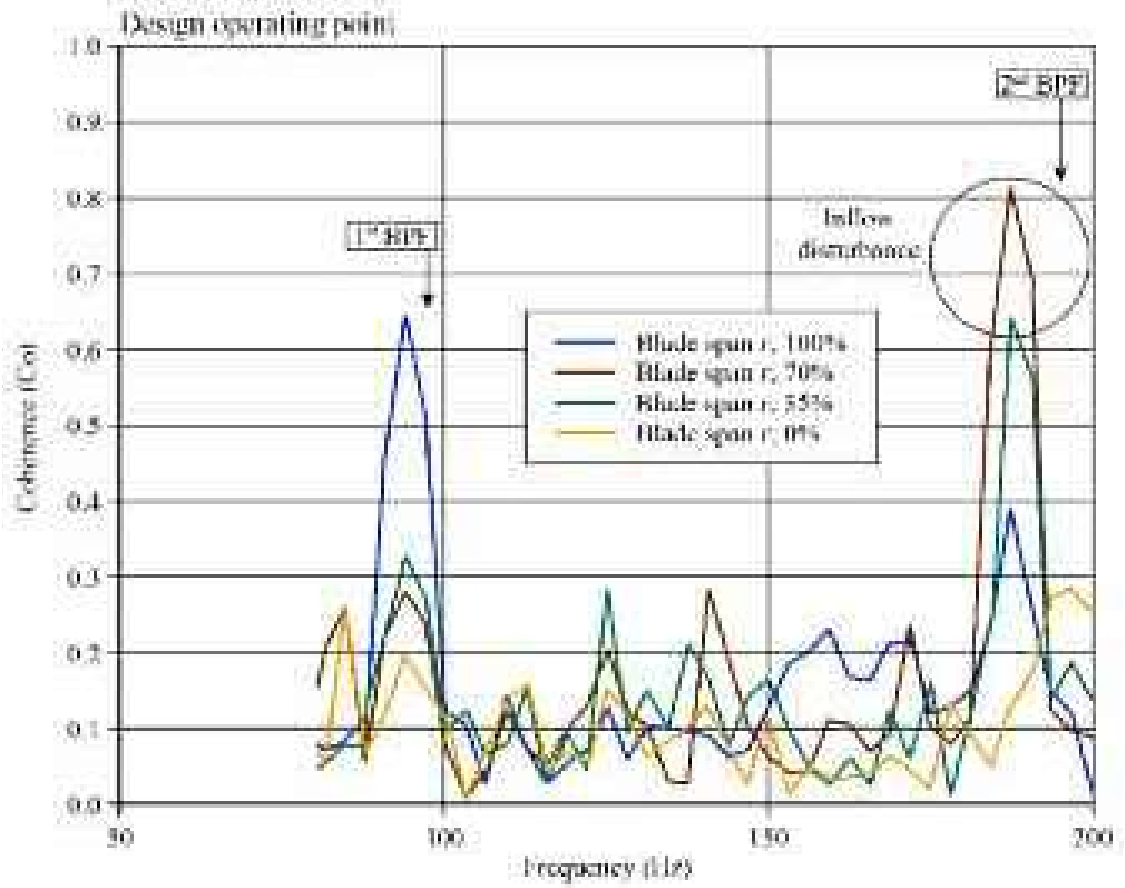

FIGURE 2.8. Fan *datum* AC90/6 outlet coherence spectrum that the authors measured at four span-wise locations from blade hub to tip at the fan design operating point. The outlet coherence spectrum illustrates the change in spectrum with span-wise location.

We may further characterise the fan *datum* AC90/6 by considering the design operating point outlet sound pressure level cross spectra and coherence at the blade tip, Figure 2.10. Both the outlet sound pressure level cross spectra and coherence illustrate the significance of the first, second and third blade passing frequencies. Although the fourth blade passing frequency is discernable, it has all but merged with the broadband noise and therefore may be an insignificant tonal component of the far-field noise.

Comparison of Blade-tip End-plate Performance

Having characterised the fan *datum* AC90/6 without a fitted blade-tip end-plate, we now study the performance of the fan AC90/6/TF incorporating a constant thickness end-plate and AC90/6/TF$_{VTE}$ incorporating a variable thickness end-plate. We characterise end-plate performance by considering the design operating point outlet sound pressure level cross spectra and coherence at the blade tip, Figure 2.11.

Both of the blade-tip end-plates resulted in reducing both tonal and broadband noise in comparison with the fan *datum* AC90/6. Cumpsty (1974) concluded that the

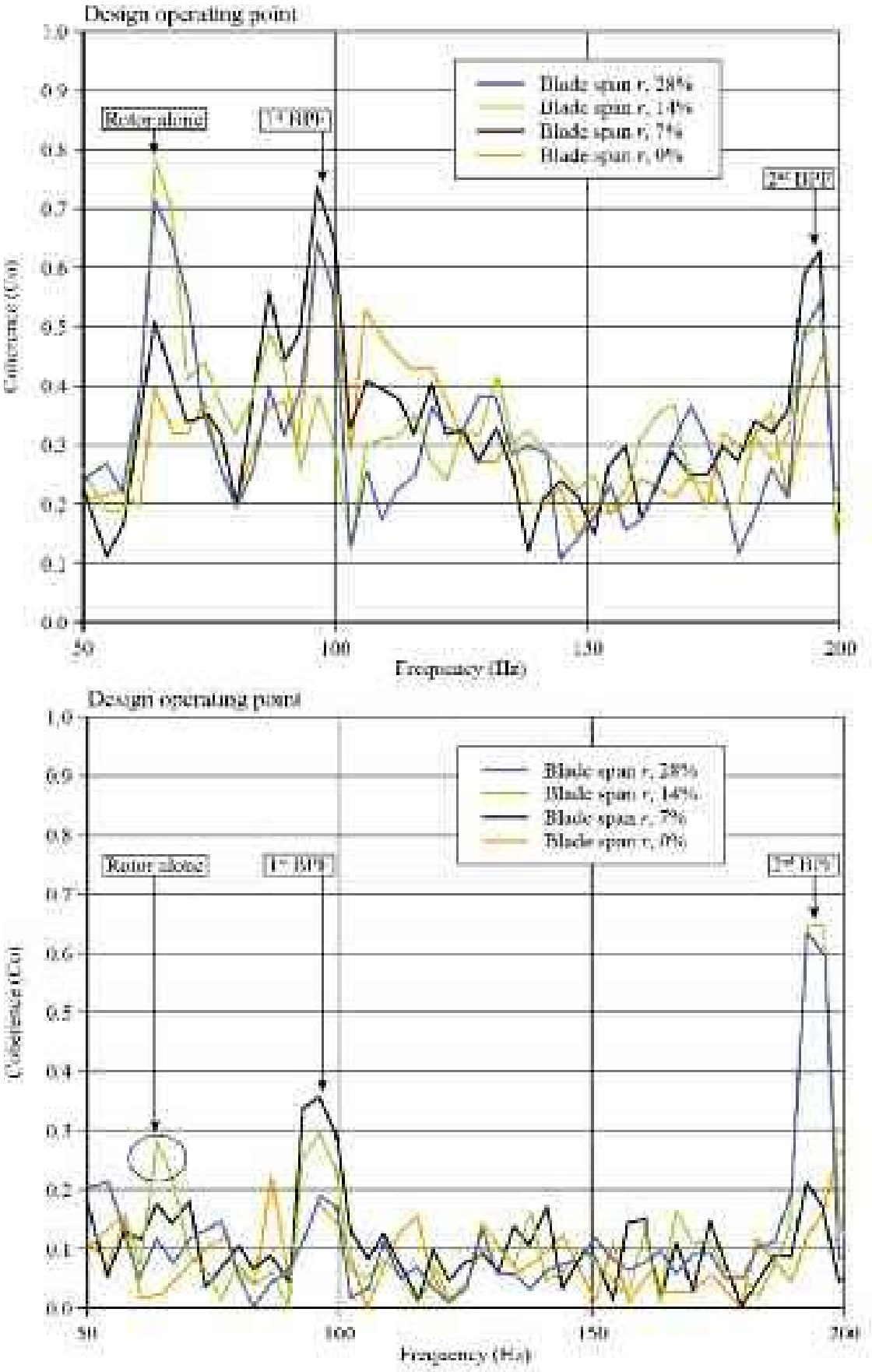

FIGURE 2.9. Fan *datum* AC90/6 inlet (top) and outlet (bottom) coherence spectrum that the authors measured at four span-wise locations in the blade hub region at the fan design operating point. The outlet coherence spectrum illustrates the blade hub flow-field features' impact on near-field fan noise.

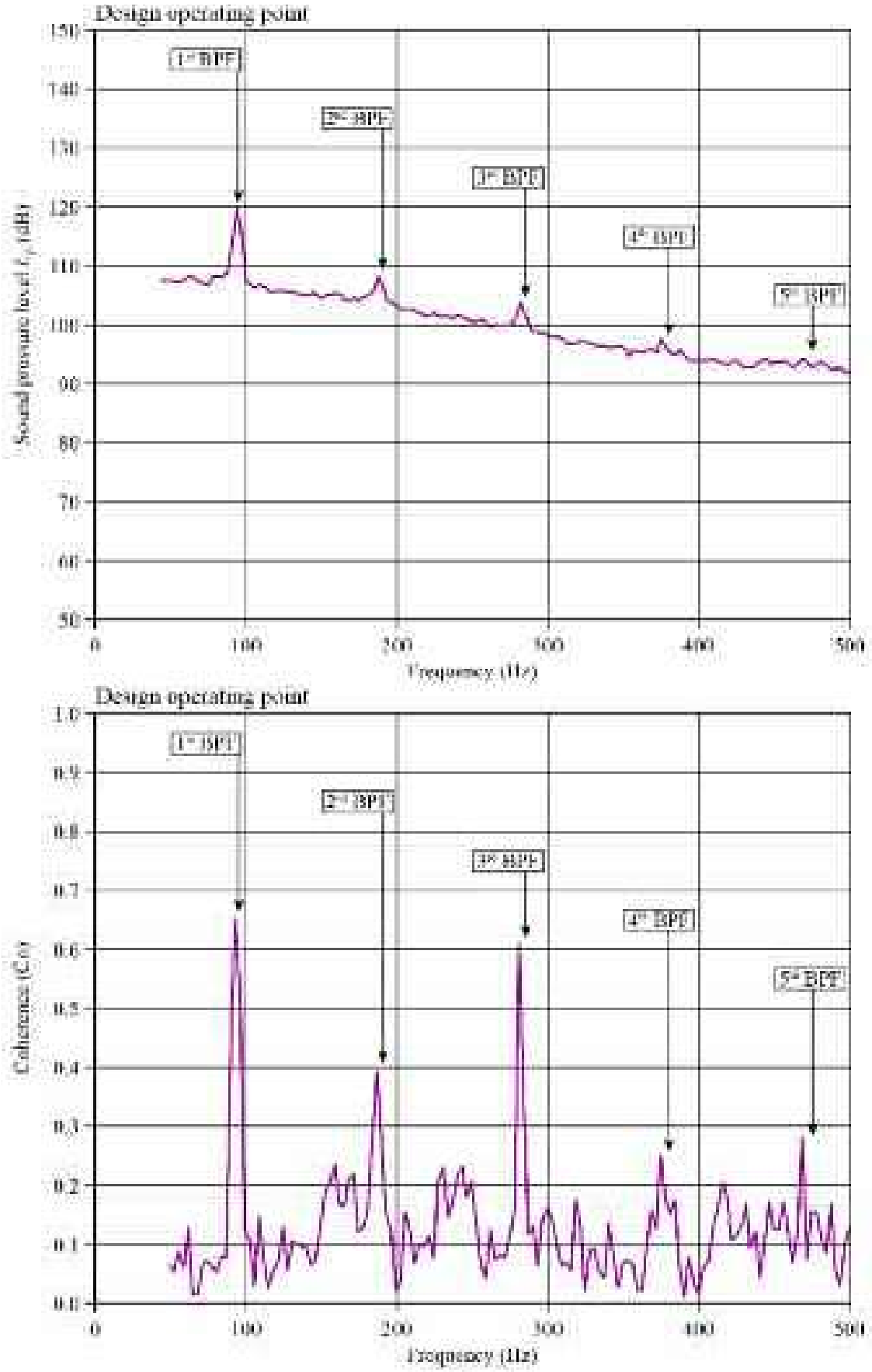

FIGURE 2.10. Fan *datum* AC90/6 outlet cross spectrum (top) and coherence spectrum (bottom) that the authors measured at the blade tip at the fan design operating point. The cross and coherence spectrum illustrates how the blade passing frequency and its second and third harmonics transmit from the near-to far-field.

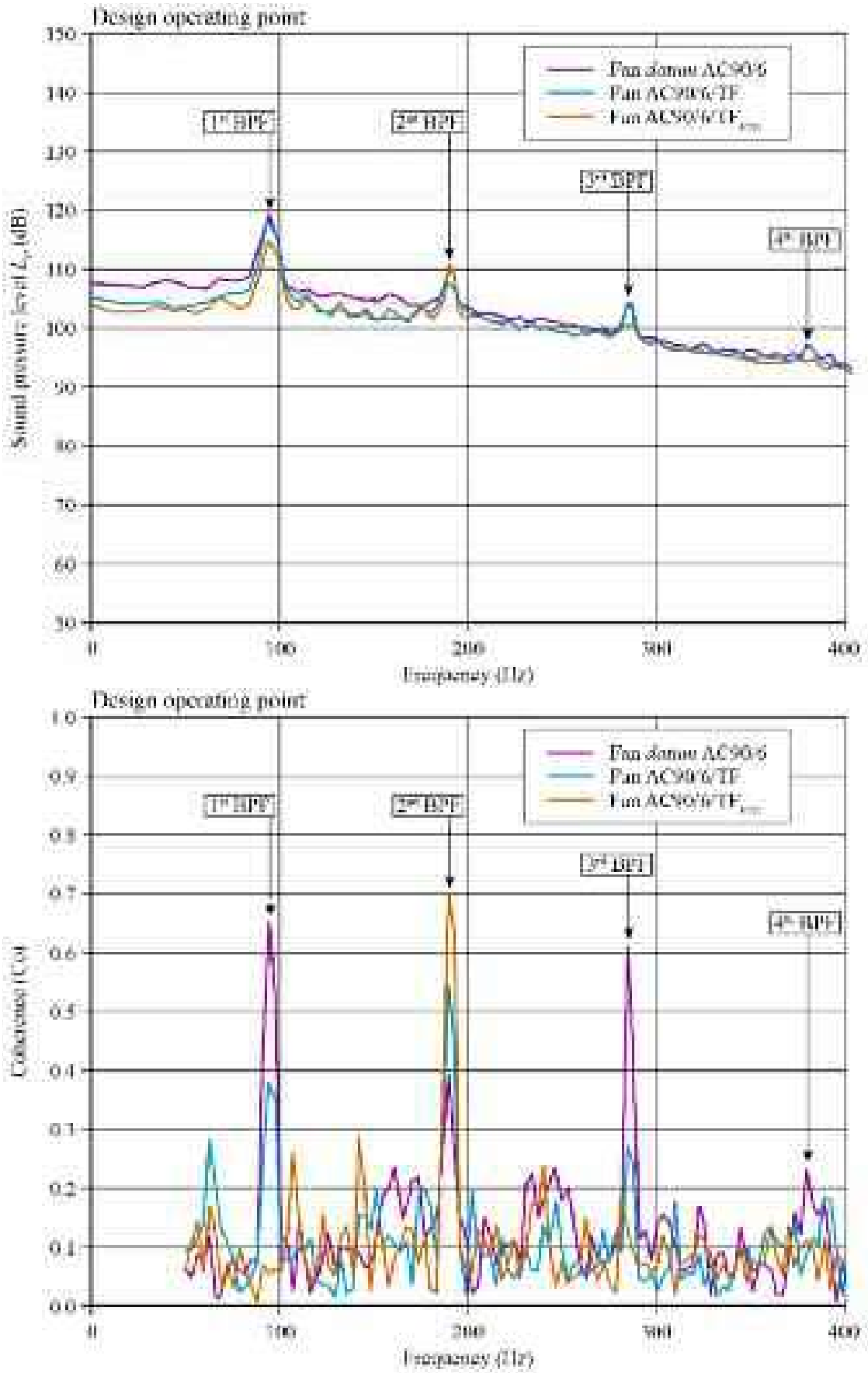

FIGURE 2.11. Fan *datum* AC90/6, AC90/6/TF and AC90/TF$_{VTE}$ outlet cross spectrum (top) and coherence spectrum (bottom) that the authors measured at the blade tip at the fan design operating point. The cross and coherence spectrum illustrates the impact of blade-tip end-plate design on the transmission of fan noise from the near-to far-field.

interaction of the blade tip-to-casing leakage vortex with downstream struts is responsible for primarily tonal noise. In contrast, Cumpsty (1974) concluded that the inherent unsteady nature of the blade tip-to-casing leakage vortex was responsible for primarily broadband noise. When we study the outlet sound pressure level cross spectra and coherence at the blade tip, it is apparent that both blade-tip end-plates have a significant impact on the tonal noise. We associate this impact with the first, second and third blade passing frequencies that coincide with the centre frequency of Wright's (1976) spectrum for self-generated noise. Reductions in broadband noise are most apparent above 400 Hz and we may associate them with reducing the blade tip-to-casing leakage vortex's instability that occurs with both of the blade-tip end-plates.

When we consider the second blade passing frequency, both blade-tip end-plates resulted in an increase in outlet coherence which we may consider a consequence of the interaction between boundary layer flow and blade-tip end-plates. Although the end-plates did not have a beneficial effect on the second blade passing frequency, they did on both the first and third. The fan AC90/6/TF's first blade passing frequency is significantly reduced compared with that of fan *datum* AC90/6. For the fan AC90/6/TF$_{VTE}$, the first and third blade passing frequencies have reduced so far that they have merged with the broadband noise. This reduction in tonal noise at the first and third blade passing frequencies combines with the reduction in broadband noise above 400 Hz to result in lower fan far-field noise. We may conclude that this reduction in far-field noise may be primarily a consequence of the blade tip-to-casing leakage vortex's reduced energy that occurs with both of the studied blade-tip end-plates. Additionally, we may speculate that the vortex shedding from the blade trailing edge is weaker with a fitted blade-tip end-plate. The interaction is probably weaker as a consequence of reduced radial migration of blade boundary layers towards the blade tip. Consequently, there is less interaction between the boundary layer flow and blade-tip end-plates.

CONCLUSIONS

In this chapter we reported an experimental methodology that we developed to facilitate assessing fan acoustic performance. We developed the methodology to provide insight into the far-field acoustic consequences of near-field flow features induced in the flow by blade-tip end-plates. The technique involved placing a microphone ten per cent blade chord down-stream of the studied fan blade's trailing edge. We then varied the microphone's span-wise location in steps of two per cent from blade hub to blade-tip whilst making acoustic measurements simultaneously with a far-field microphone. Thus, the experimental technique provides data sets of fan near- and far-field noise that we were able to correlate to establish the far-field acoustic consequences of near-field noise sources. It was this near- and far-field correlation technique that provides the required method for resolving aeroacoustic noise sources along the blade span.

A limitation of the developed near- and far-field correlation technique is that it relies on fan far-field noise measurements taken when the near-field microphone is

present. We addressed this limitation by measuring fan far-field noise without the near-field microphone. We then used the measurement of fan far-field noise without the near-field microphone as a part of the technique to correct for the near-field microphone's acoustic influence. Despite the limitations of the measurement technique, we were able to use the technique to study the span-wise distribution of noise source. We clarified the importance of blade-tip noise sources in generating far-field tonal harmonics generally, and the second blade passing frequency tonal harmonic specifically. Although blade-tip end-plate geometry did impact the fan far-field noise, the change from the maximum flow to design and then peak pressure operating point resulted in a larger change. From this we conclude that the studied fan acoustic emissions are sensitive to blade loading.

Despite the reservation that the studied fan acoustic emissions are sensitive to blade loading, we concluded that the experimental methodology and associated near- and far-field correlation technique was effective. The span-wide correlation of near- and far-field noise was distinctly different for the studied fan without a fitted blade-tip end-plate and when fitted with an end-plate. Therefore, the experimental technique facilitated identifying near-field noise sources unique to each of the tested fan geometries and their far-field acoustic consequences.

REFERENCES

ISO 5801:2007 (2007), *Industrial Fans: Performance Testing Using Standardised Airways.*

ISO 10302:1996 (1996), *Fans for General Purposes. Methods of Noise Testing.*

Corsini, A., Rispoli, F., Sheard, A.G. and Kinghorn, I.R. (2006), 'Investigation of Improved Blade-tip Concept for Axial Flow Fan', *Proceedings of the 51st American Society of Mechanical Engineers Gas Turbine and Aeroengine Congress*, Barcelona, Spain, 8–11 May, paper no. GT2006-90592.

Corsini, A. and Sheard, A.G. (2007), 'Tip End-plate Concept Based on Leakage Vortex Rotation Number Control', *Journal of Computational and Applied Mechanics*, vol. 8, pp. 21–37.

Cumpsty, N.A. (1974), 'Sum and Difference Tones from Turbomachines', *Journal of Sound and Vibration*, vol. 32, pp. 383–386.

Cumpsty, N.A. (1977), 'A Critical Review of Turbomachinery Noise', *Transactions of the ASME, Journal of Fluid Engineering*, vol. 99, pp. 278–293.

Fukano, T. and Jang, C. (2004), 'Tip Clearance Noise of Axial Flow Fans Operating at Design and Off-design Condition', *Journal of Sound and Vibration*, vol. 275, pp. 1027–1050.

Fukano, T., Kodama, Y. and Takamatsu, Y. (1977a), 'Noise Generated by Low Pressure Axial Flow Fans. I – Modeling of the Turbulent Noise', *Journal of Sound and Vibration*, vol. 50, pp. 63–74.

Fukano, T., Kodama, Y. and Takamatsu, Y. (1977b), 'Noise Generated by Low Pressure Axial Flow Fans. II – Effects of Number of Blades, Chord Length and Camber of Blade', *Journal of Sound and Vibration*, vol. 50, pp. 75–88.

Ganz, U.W., Joppa, P.D. and Scharpf, D.F. (1998), *Boeing 18-inch Fan Rig Broadband Noise Test*, Report NASA CR-1998-208704.

Garg, A.K. and Leibovich, S. (1979), 'Spectral Characteristics of Vortex Breakdown Flowfields', *Physics of Fluids*, vol. 22(11), pp. 2053–2064.

Holste, F. and Neise, W. (1997), 'Noise Source Identification in a Prop Fan Model by Means of Acoustical Near Field Measurements', *Journal of Sound and Vibration*, vol. 203, pp. 641–665.

Ito, T., Suematsu, Y. and Hayase, T. (1985), 'On the Vortex Breakdown Phenomena in a Swirling Pipe-flow', *Memoirs of the Faculty of Engineering, Nagoya University*, vol. 37, pp. 117–172.

Kameier, F. and Neise, W. (1997), 'Rotating Blade Flow Instability as a Source of Noise in Axial Turbomachines', *Journal of Sound and Vibration*, vol. 203, pp. 833–853.

Laurendeau, E., Jordan, P., Delville, J. and Bonnet, J. (2007), 'Nearfield-farfield Correlations in Subsonic Jets: What Can They Tell Us?', *Proceedings of the 13th AIAA / CEAS Aeroacoustics Conference (28th AIAA Aeroacoustics Conference)*, Rome, Italy, 21–23 May, paper no. AIAA 2007-3614.

Leggat, L.J. and Siddon, T.E. (1978), 'Experimental Study of Aeroacoustic Mechanism of Rotor-vortex Interactions', *Journal of the Acoustical Society of America*, vol. 64, pp. 1070–1077.

Longhouse, R.E. (1978), 'Control Tip-vortex Noise of Axial Flow Fans by Rotating Shrouds', *Journal of Sound and Vibration*, vol. 58, pp. 201–214.

Magliozzi, B., Johnson, B.V., Hanson, D.B. and Metzger, F.B. (1973), 'Noise and Wake Structure Measurements in a Subsonic Tip Speed Fan – Tabulation and Plots of Test Data', NASA Technical Report CR-132259, 23 July.

Marcinowski, H. (1953),'Einfluss des Laufradspalts und der Luftfuehrung bei einem Kuehlgeblaese Axialer Bauart', *Motortechnische Zeitschrift*, vol. 14, pp. 259–262.

Miles, J.H. (2006), 'Procedure for Separating Noise Sources in Measurements of Turbofan Engine Core Noise', Published as Report NASA/TM-2006-214352 and in *Proceedings of the 12th Aerospace Conference, cosponsored by the American Institute of Aeronautics and Astronautics and Confederation of European Aerospace Societies*, Cambridge, MA, USA, 8–10 May, paper no. AIAA-2006-2580.

Mongeau, L., Thompson, D.E. and McLaughlin, D.K. (1995), 'A Method for Characterizing Aerodynamic Sound Sources in Turbomachines', *Journal of Sound and Vibration*, vol. 181, pp. 369–389.

Mugridge, B.D. and Morfey, C.L. (1972), 'Sources of Noise in Axial Flow Fan', *Journal of the Acoustical Society of America*, vol. 51, pp. 1411–1426.

Sharland, I.J. (1964), 'Sources of Noise in Axial Flow Fans', *Journal of Sound and Vibration*, vol. 1, pp. 302–322.

Spall, R.E., Gatski, T.B. and Grosch, C.E. (1987), 'A Criterion for Vortex Breakdown', *Physics of Fluids*, vol. 30, pp. 3434–3440.

Uchida, S., Nakamura, Y. and Ohsawa, M. (1985), 'Experiments on the Axisymmetric Vortex Breakdown in a Swirling Air Flow', *Transactions of the Japan Society for Aeronautical Space Sciences*, vol. 27, pp. 206–216.

Welch, P.D. (1967), 'The use of Fast Fourier Transform for the Estimation of Power Spectra: a Method Based on Time Averaging Over Short, Modified Periodograms', *IEEE Transactions on Audio and Electroacoustics*, vol. 15(2), pp. 70–73.

Wright, S.E. (1976), 'The Acoustic Spectrum of Axial Flow Machines', *Journal of Sound and Vibration*, vol. 45, pp. 165–223.

Chapter 3

Detection of Aerodynamic Noise Sources in Low-speed Axial Fans with Tip End-plates

S. Bianchi, A. Corsini, F. Rispoli and A.G. Sheard

ABSTRACT

The chapter presents a symmetrised dot pattern (SDP) analysis technique developed to enable us to assess a fan's acoustic performance for application in compact cooling units. The symmetrised dot pattern analysis technique provided insight into how the human perception of fan far-field noise changed as we switched blade-tip end-plate geometry. We produced the symmetrised dot patterns using an algorithm that maps a normalised time waveform derived from a fan far-field noise measurement onto a radial component. We then mapped the adjacent point onto an angular component. The resulting symmetrised dot pattern shapes provided a qualitative assessment of human acceptability of fan far-field noise associated with the studied fan both with and without fitted blade-tip end-plates. Using the experimental technique and the near- and far-field correlation technique presented in Chapter 2, we were able to generate span-wise distributions of coherence values for the studied fan with and without fitted blade-tip end-plates. By plotting coherence value on a map of blade span against frequency, we identified map features associated with the studied fan both with and without a fitted blade-tip end-plate. The fitted blade-tip end-plates reduced the far-field noise in the studied fan. The coherence maps facilitated dissecting the span-wise noise sources, thus enabling us to associate specific blade-tip end-plate geometries with specific features on each coherence map. We then used the symmetrised dot pattern analysis technique to qualitatively assess the human impact of the change in fan far-field noise. The developed symmetrised dot pattern analysis technique complements the previously developed experimental technique and the near- and far-field correlation technique. The analysis identified that blade-tip end-plates have an effect on the blade tip-to-casing leakage vortex formation by altering the near-wall fluid path on blade surfaces. The change in blade tip-to-casing leakage vortex has an identifiable impact on the fan far-field noise, with the analysis providing a characterisation of the associated span-wise noise sources.

This chapter is a revised and extended version of Bianchi, S., Corsini, A., Rispoli, F. and Sheard, A.G. (2009), 'Detection of Aerodynamic Noise Sources in Low-speed Axial Fans with Tip End-plates', *Proceedings of the IMechE Part C, Journal of Mechanical Engineering Science*, vol. 223, pp. 1379–1392.

NOMENCLATURE

Latin letters

BPF	blade-passing frequency
Co	numerical value of the coherence function
F_j	waveform amplitude [Pa]
G_{xx}	spectra in the near-field
G_{yy}	spectra in the far-field
G_{xy}	cross-spectrum
h	blade span
H_n	normalised helicity
HM	number of hearing models
IN	inflow ingested noise
ℓ	blade chord
m	number of mirror planes
Δp_{stat}	static pressure [Pa]
r	non-dimensional span
$\bar{r}$	non-dimensional radius
r_j	dot pattern radial vector
R_c	casing radius
RN	rotor alone noise
SDP	symmetrised dot pattern
Sf	normalised frequency (f/1BPF)
SFN	secondary flow noise
SPL	sound pressure level [dB]
t	blade pitch
TIN	turbulence-induced noise
TLV	tip leakage vortex
U_c	casing relative peripheral velocity
VBN	noise-source region

Greek letters

Θ_{ij}	dot pattern phase angle
σ_h	hub-to-casing diameter ratio
ϕ_a	local axial flow coefficient (axial velocity divided by bulk velocity)
Φ	global flow coefficient (annulus area-averaged axial velocity normalised by U_c)
Φ_{ij}	dot pattern symmetric phase angle
τ	rotor tip clearance

INTRODUCTION

One of the key aspects of any axial flow fan's specification is its acoustic performance. Large axial flow air movement fans are classically used in applications in close proximity to populated areas, and are the main contributor to both tonal and broadband system noise. Researchers in the 1970s, particularly Wright (1976) and Cumpsty (1977), have studied the link between fan rotor aerodynamic features and its acoustic emissions. Cumpsty (1977) concluded that, with the exception of the low-frequency range of high-speed machines, the mechanism that determines broadband noise in subsonic fans is the same as that in supersonic tip-speed fans and compressors. Therefore, the design variables that impact tonal and broadband noise are similar both for fans designed for aerospace and air movement application (Ganz *et al.*, 1998). According to Wright (1976), this is because of the prominence of rotor noise that originates from turbulent boundary layers.

Researchers regard a fan's blade tip-to-casing flow as particularly important as it interacts with both wakes and blade-to-blade passage secondary flows. Therefore, the industry recognises blade tip-to-casing flow as one of the most significant sources of fan noise (Cumpsty, 1977; Nelson and Cooper, 1999). Several studies have attempted to resolve the causal aerodynamics relationship between fan blade-to-blade flow-field structures and fan far-field noise. Marcinowski (1953), the first researcher to study noise associated with tip dynamics, demonstrated that increases in broadband noise levels occur with increasing tip clearance. The largest changes in noise level were apparent at frequencies greater than the blade-passing frequency.

In contrast to Marcinowski (1953), Mugridge and Morfey (1972) argued that an optimum tip clearance exists when broadband noise is at a minimum due to the countervailing effects of the tip clearance flow and the blade-passage vortex. However, Longhouse (1978) did not confirm this result. He searched for a practical solution to the cooling fans' tip clearance noise and concluded that the unstable blade-tip vortex impacted the adjacent blade pressure side. He obtained the lowest noise levels with the smallest possible tip clearance. Fukano and Jang (2004) reported similar findings. In contrast, Kameier and Neise's (1997) experiments demonstrated that, with the smallest possible tip clearance, noise reduced over a limited frequency range, close to the blade passage frequency. However, random noise actually increased.

During the past decade, several researchers have proposed technical concepts to facilitate the assessment of air movement fan aeroacoustic properties. Researchers based their experimental techniques, to varying degrees, on previous fan (Leggat and Siddon, 1978; Bianchi *et al.*, 2009), radial pump rotor (Mongeau *et al.*, 1995) and turbofan engine (Kameier and Neise, 1977; Miles, 2006) studies. These researchers share a common goal, to isolate and identify the aerodynamic flow features responsible for the fan or compressor's aeroacoustic signature. By isolating the individual noise sources, researchers aim to identify their acoustic signature, their spectral distribution along the blade span and ultimately their contribution to overall fan or compressor far-field noise.

Isolating and characterising individual noise sources is challenging; however, some scholars have successfully elucidated aspects of the flow-field physics. Leggat and Siddon (1978) studied the interaction between a naturally occurring vortex and axial fan noise. They used a cross-correlation between a near-field pressure probe located in the blade tip region and the noise recorded by a far-field microphone. Mongeau *et al.* (1995) investigated the noise emitted by a ducted centrifugal pump. They used a 'noise-to-noise' cross-correlation between the pump casing and the far-field. Kameier and Neise (1997) measured the blade tip-to-casing clearance flow generated noise for a ducted low-speed axial fan. They used a 'noise-to-noise' cross-correlation as a detection tool for rotating flow instabilities. Miles (2006) developed a test rig at the NASA Glenn Research Centre that he used for measuring the core-noise of a turbofan engine. He used an array of four far-field microphones and arranged them around the turbofan inlet. He then correlated the measured noise with turbofan near-field pressure perturbations.

This chapter presents the results of a research programme that complements the experimental technique and near- and far-field correlation technique presented in Chapter 2. We used the experimental technique and near- and far-field correlation technique to generate span-wise distributions of coherence values for the studied fan with and without fitted blade-tip end-plates. The coherence maps facilitate dissecting span-wise noise sources that enabled us to associate specific blade-tip end-plate geometries with specific features on each coherence map. A symmetrised dot pattern (SDP) analysis technique complements the experimental and correlation technique. This technique enables us to study the way in which human perception of fan far-field noise transformed with changing blade-tip end-plate geometry.

Using the symmetrised dot pattern analysis technique, we were able to establish that blade-tip end-plate geometry has an effect on the blade tip-to-casing leakage vortex formation by altering the near-wall fluid path on blade surfaces. Change in the blade tip-to-casing leakage vortex has an identifiable impact on the fan far-field noise. In combination, the experimental technique and near- and far-field correlation technique presented in Chapter 2 and the symmetrised dot pattern analysis technique presented in this chapter facilitated the characterisation of span-wise noise sources.

FAMILY OF FANS UNDER INVESTIGATION

We conducted the reported research on a family of commercially available cooling fans configured for application over a compact cooling unit's tube bank. The studied fan configuration, coded AC90/6, incorporates a six-blade un-swept rotor, with modified ARA-D profile aerofoils blade, Table 3.1. One may set the blade-pitch angle during final assembly to customise the fan to a desired duty point. We used a direct coupled-induction 400-volt (AC), 3-phase motor to drive the rotor at a constant speed of 950 rpm, resulting in a 44.7 m/s blade tip speed and a 95 Hz blade-passing frequency (BPF). In its original embodiment the studied fan did not include a blade tip end-plate, therefore, we used it as a *datum* against which to assess the per-

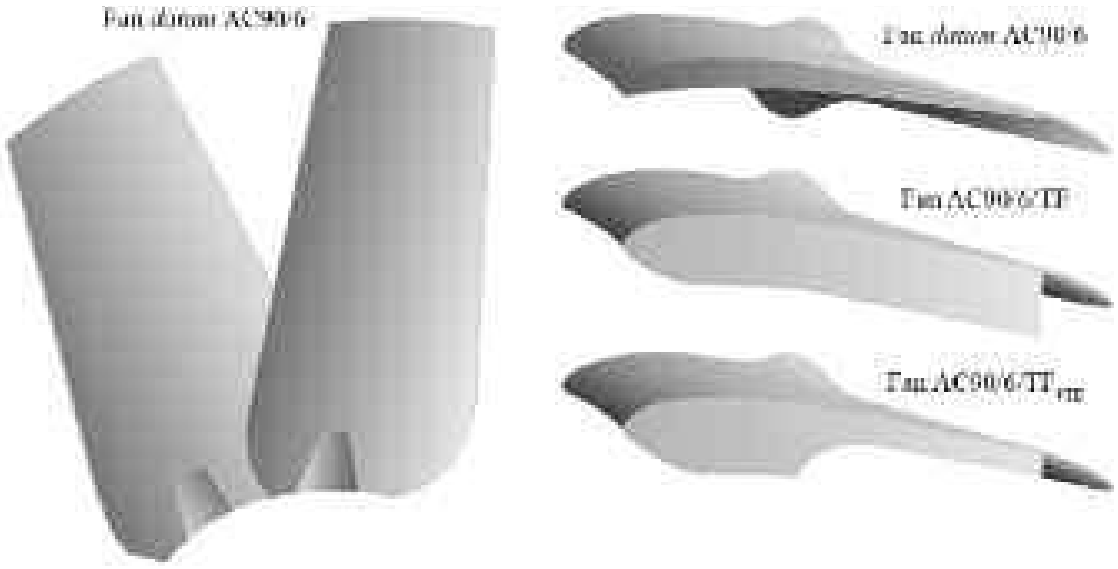

FIGURE 3.1. The studied fan *datum* AC90/6 without a fitted blade-tip end-plate, with a constant thickness blade-tip end-plate, AC90/6/TF and with a variable thickness blade-tip end-plate, AC/6/TF$_{VTE}$.

Table 3.1. *The fan* datum *AC90/6 blade geometry and rotor specification.*

	Fan *datum* AC90/6		
Blade geometry	Hub	Mid-span	Tip
Pitch angle (°)	36	58.8	28
Camber angle (°)	46	44	41
Solidity	1.24	0.86	0.30
Fan rotor			
Blade number		6	
Blade tip pitch angle (°)		16–28	
Blade tip stagger angle (°)		74–62	
Hub-to-casing diameter ratio σ		0.22	
Tip diameter (mm)		900.0	
Rotor tip clearance τ (% span)		1.0	
Rated rotational frequency (r/min)		935–950	

formance of fan variants with blade tip end-plates. In the reported research we refer to the fan without blade tip end-plates as the fan *datum* AC90/6.

In addition to the fan *datum* AC90/6, we studied two fan variants. The first was fitted with a constant thickness blade-tip end-plate and the second with a variable thickness blade-tip end-plate, Figure 3.1. We named the fan fitted with a constant thickness blade-tip end-plate AC90/6/TF and the fan fitted with the variable thickness blade-tip end-plate AC90/6/TF$_{VTE}$.

Designs developed for tip-vortex control and drag reduction in aircraft wings and catamaran hulls inspired the constant thickness blade-tip end-plate design. The

constant thickness blade-tip end-plate ran along the blade pressure surface, ending at the blade trailing edge with a square tail. The addition of this constant thickness blade-tip end-plate resulted in the thickness of the fan AC90/6/TF blade tip increasing by a factor of three compared to the fan *datum* AC90/6. We considered Inoue *et al.*'s (1986) blade-tip end-plate's size for axial compressor blades. They estimated that the optimum blade-tip end-plate size was between 10 and 20 per cent blade span. In practice we were able to manufacture blades with a blade-tip end-plate size five per cent of blade span. The fan blades were manufactured from injection moulded plastic, with the blade-tip end-plate size as the largest the blade manufacturing technique could produce.

Corsini and Sheard (2007) studied both the fan *datum* AC90/6 and AC90/6/TF using a blade-tip vortex 'breakdown criteria' based on Rossby number (Spall *et al.*, 1987). Following Ito *et al.*'s method (1985), they concluded that there is a threshold value of Rossby number below which the vortex rotation cannot be reduced if the vortex is to remain stable. We defined this critical Rossby number range using the critical Rossby numbers defined by Uchida *et al.* (1985) and Garg and Leibovich (1979). Uchida *et al.* (1985) defined a critical Rossby number associated with the breakdown of an axi-symmetric vortex in a swirling flow. Garg and Leibovich (1979) also defined a critical Rossby number associated with an aircraft wing tip vortices' breakdown.

Corsini *et al.* (2006) studied the aerodynamic and acoustic performance of the fan *datum* AC90/6 and fan AC90/6/TF, identifying a breakdown of the fan AC90/6/TF blade tip-to-casing leakage vortex. Vortex breakdown is known to be acoustically productive, and therefore Corsini *et al.* (2006) concluded that a revised blade-tip end-plate design was desirable that avoided leakage vortex breakdown. Corsini and Sheard (2007) developed a blade-tip end-plate design methodology that successfully eliminated the leakage vortex breakdown. They eliminated vortex breakdown by adding a variable thickness blade-tip end-plate, which they named AC90/6/TF$_{VTE}$ when they appended it to the fan *datum* AC90/6 blades.

Fan Operating Point

The studied fan blade tip pitch angle is adjustable and may be set to a pitch angle between 16 and 28 degrees. In practical application the blade tip pitch angle is typically set to 28 degrees as this maximises flow rate for a given system pressure. In the research reported in this chapter, we set the fan blade tip pitch angle to 28 degrees both because it is typical of the angle used in practical application and because it results in the highest blade loading. A highly loaded blade results in the blade tip-to-casing vortex having the most significant effect on both fan aerodynamic and acoustic performance (Holste and Neise, 1997).

The impact of the blade tip-to-casing vortex on both fan aerodynamic and acoustic performance results in applying blade-tip end-plates changing not only the fan's acoustic performance, but also the aerodynamic performance. Consequently, the fan *datum* AC90/6 generates a different pressure at a constant flow rate when

fitted with each of the studied blade-tip end-plates. To facilitate comparing fan performance data when fitted with different blade-tip end-plates we chose to define three operating points, and their respective volume flow rates, Table 3.2. The design operating point volume flow rate is typical of that required when one installs the fan over the cooling unit's tube bank. The peak pressure flow rate is typical of that required when the tube bank has become partially blocked following a period of in-service operation. The maximum flow operating point volume flow rate is typical of the flow rate associated with the lowest pressure loss tube banks currently operating in service.

Bianchi *et al.* (2009) measured the performance characteristics of the studied fan in accordance with ISO 5801:2007 requirements (2007). The studied fan's performance characteristics illustrate the impact on blade-tip end-plate geometry on fan pressure rise, Figure 3.2. Adding both the constant and variable thickness blade-tip end-plates result in an increase in blade loading. We would expect blade-tip noise sources to become more acoustically productive with increasing blade loading. Therefore an increase in blade loading will partially offset any reduction in fan far-field noise attributed to adding a blade-tip end-plate. To ensure a conservative assessment of blade-tip end-plate performance we chose to neglect the change in pressure rise with the change in blade-tip treatment.

We may assess the validity of our assumption that we may neglect change in pressure rise with change in blade-tip treatment by considering fan specific noise level (K_S), Figure 3.3. Both the fans AC90/6/TF and AC90/6/TF$_{VTE}$ demonstrate lower specific fan noise than the fan *datum* AC90/6. As pressure rise increased towards the fan's peak pressure operating point, both fan AC90/6/TF and AC90/6/TF$_{VTE}$ specific noise levels increased from a minimum that occurs with a pressure rise close to the fan's design operating point. Axial fans classically exhibit increased amplitude of discrete frequency tones as they approach stall (Fukano *et al.*, 1986). Therefore, we expected the increase in specific noise level as the fans AC90/6/TF and AC90/6/TF$_{VTE}$ moved from their design to peak pressure operating point. However, specific noise levels remained lower than that of fan *datum* AC90/6 over the entire fan operating range despite the increased blade loading that occurred when we fitted a blade-tip end-plate. This reduction gives confidence in the blade-tip end-plates' effectiveness.

Table 3.2. *The operating points used when characterising the studied fan's performance with and without fitted blade-tip end-plates. The authors measured performance characteristics in a Type D standardised airway (ducted inlet, ducted outlet) in accordance with ISO 5801:2007 requirements (2007).*

Operating point	Volume flow rate (m^3/s)	Studied blade tip pitch angle (°)
Maximum flow	7.0	28
Design	6.5	28
Peak pressure	5.6	28

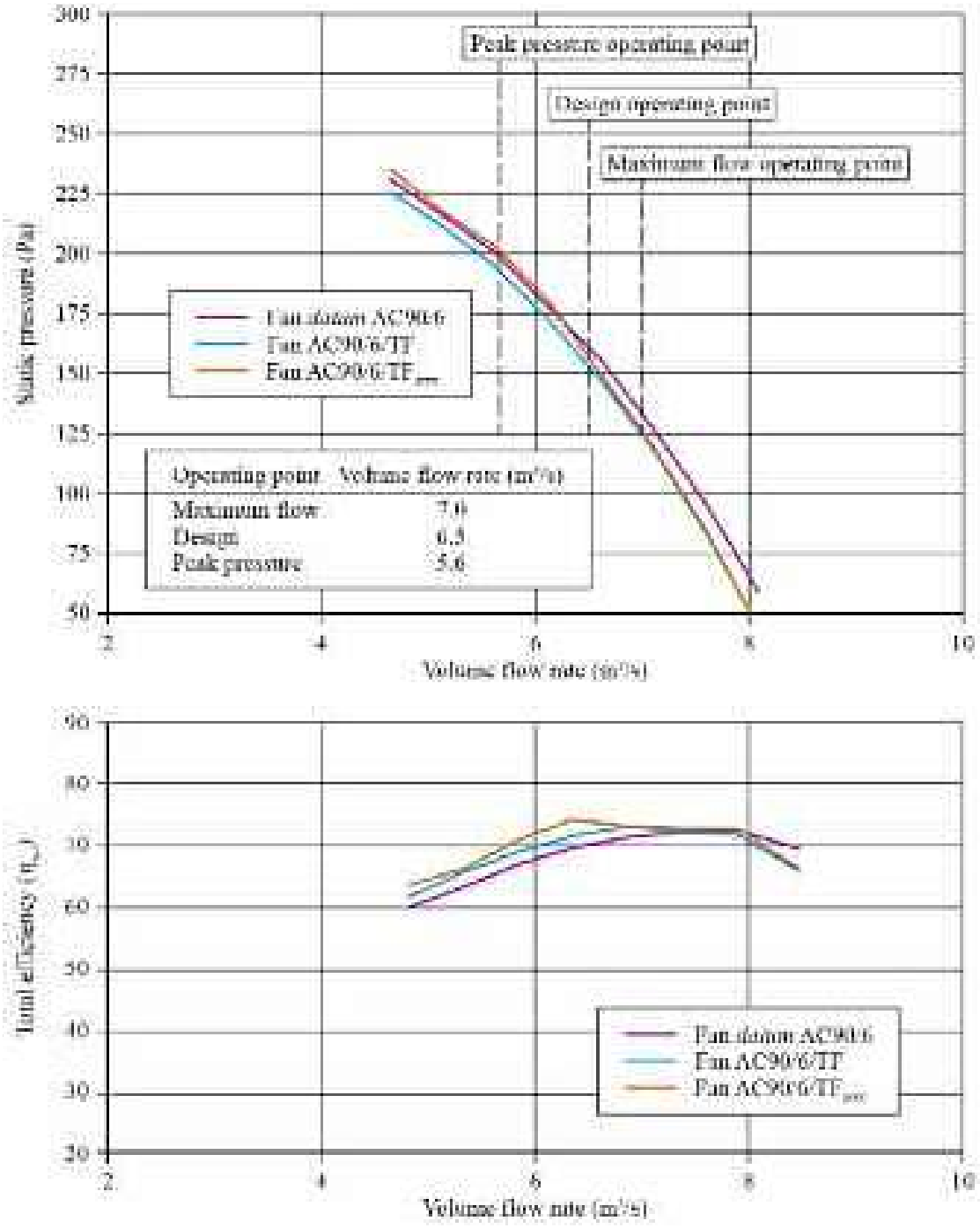

FIGURE 3.2. The performance characteristics of the studied fan *datum* AC90/6 without a fitted blade-tip end-plate, with a constant thickness blade-tip end-plate, AC90/6/TF and with a variable thickness blade-tip end-plate, AC/6/TF$_{VTE}$. Bianchi *et al.* (2009) measured performance characteristics with the blade tip pitch angle set to 28 degrees in a Type D standardised airway (ducted inlet, ducted outlet) in accordance with ISO 5801:2007 requirements (2007).

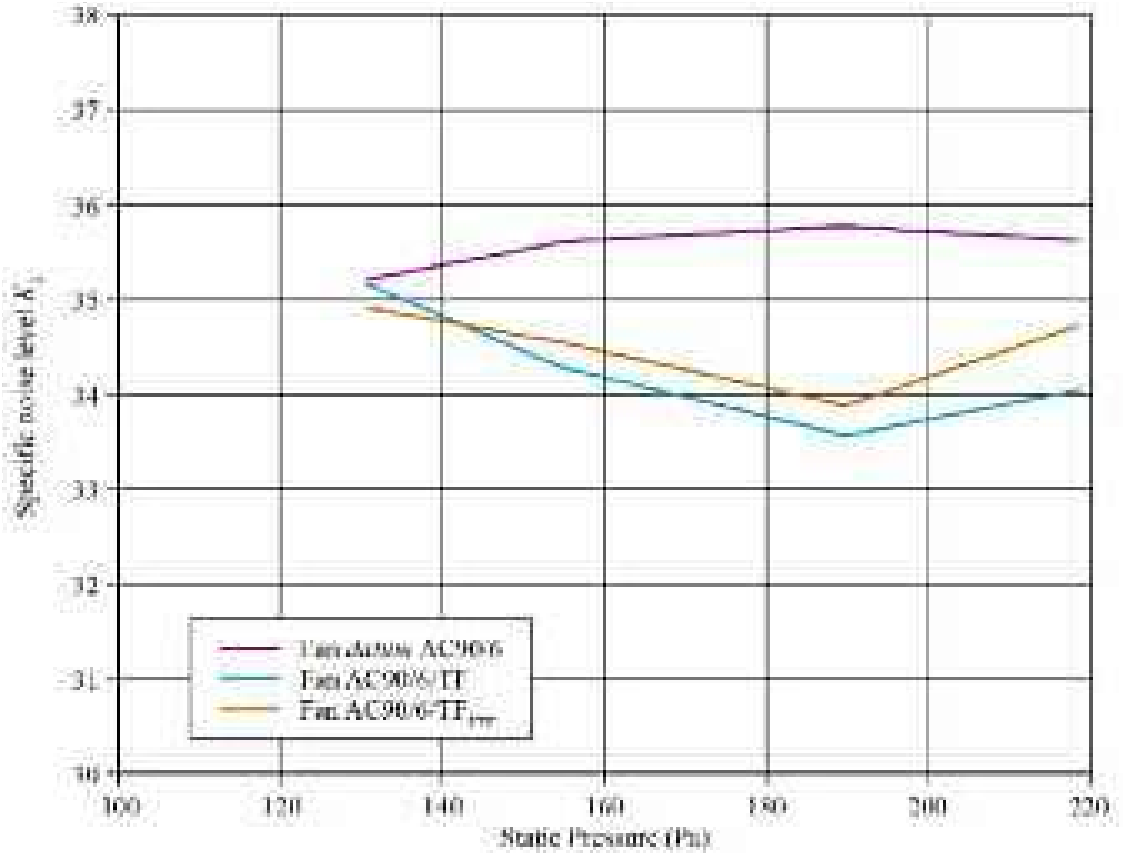

FIGURE 3.3. Specific noise level (K_S) illustrating that fan AC90/6/TF with a constant thickness blade-tip end-plate and fan AC/6/TF$_{VTE}$ with a variable thickness blade-tip end-plate both have lower specific noise levels over the fan operating range.

METHODOLOGY

We conducted the experimental measurements in an anechoic chamber in accordance with ISO 10302:1996 requirements (1996) following Bianchi *et al.*'s method (2009). We made acoustic measurements using microphones at the fan inlet and outlet, recording the near- and far-field signals on two channels of a data acquisition system. An aerofoil louver in the top of the anechoic chamber inlet section facilitated the fan flow rate variation. We aerodynamically optimised the fan inlet bell mouth profile to provide uniform and unseparated flow into the fan. The fan was connected to the outside environment via up- and down-stream plenums. We designed these plenums to minimise in-flow non-uniformities and acoustically treated them to both minimise noise transmission from the external environment and its reflection inside the plenum ductwork. We also covered the anechoic chamber walls with foam panels to further reduce noise transmission from the external environment.

Near-field Acoustic Measurement Technique

We made near-field measurement at the fan outlet by mounting a microphone on a 10 mm radial traversing mechanism 10 per cent blade chord downstream of the blade trailing edge, Figure 3.4. We then used the traversing mechanism to move the near-field microphone from the blade hub to tip, in radial steps corresponding to two per cent of blade span. Thus, the traversing microphone facilitated the span-wise measurement of near-field fan noise.

By locating the microphone 10 per cent blade chord downstream of the blade trailing edge, we located it upstream of the motor arms. This placement effectively prevented the microphone from measuring any tonal noise sources associated with the motor arms. Despite this limitation, we selected the microphone location to ensure that we captured the acoustic emissions from the vortical flow-field structures present in the exhaust flow. This was because we were interested in the acoustic emissions from flow-field structures, not overall impeller noise.

We made near-field measurements at the fan inlet by placing a microphone one fan diameter upstream of the fan inlet. We covered the microphone diaphragm with a standard shield to minimise the self-induced noise generated by the flow past the microphone. We conducted hot-wire anemometer measurements to determine the flow velocity at the microphone location. Using the known velocity at the inlet microphone location, we were able to calculate a correction factor to compensate for the self-induced noise generated by the flow past the microphone.

We also conducted hot-wire anemometer measurements to determine the flow velocity at each of the exhaust span-wise microphone locations. As the exhaust microphone was located immediately downstream of the blade trailing edge, we chose to calibrate the traversing microphone in a dedicated test rig. We measured the background noise in the test rig with no flow, and then induced the airflow corresponding to each microphone's span-wise locations. This facilitated calculation of self-induced noise correction factors for the traversing microphone.

FIGURE 3.4. Microphone arrangement for inlet near-field measurements (left) and outlet near-field measurements (middle) of fan noise (Bianchi *et al.*, 2009). The microphone used for outlet near-field measurements could be traversed from the blade hub to tip, right.

Far-field Acoustic Measurements Technique

We measured far-field noise six fan diameters from the fan exhaust, as recommended by Leggat and Siddon (1978), when measuring a fan's far-field noise without any obstructions downstream of the fan. Leggat and Siddon (1978) studied fan noise directivity in a semi-reverberant environment. They concluded that the maximum noise levels were coincident with the fan axis, immediately downstream of the exhaust. In the research reported in this chapter we chose to place the far-field microphone at an angle 30 degrees from the fan axis, Figure 3.5. This was to avoid the possibility of the fan exhaust flow impacting directly on the far-field microphone.

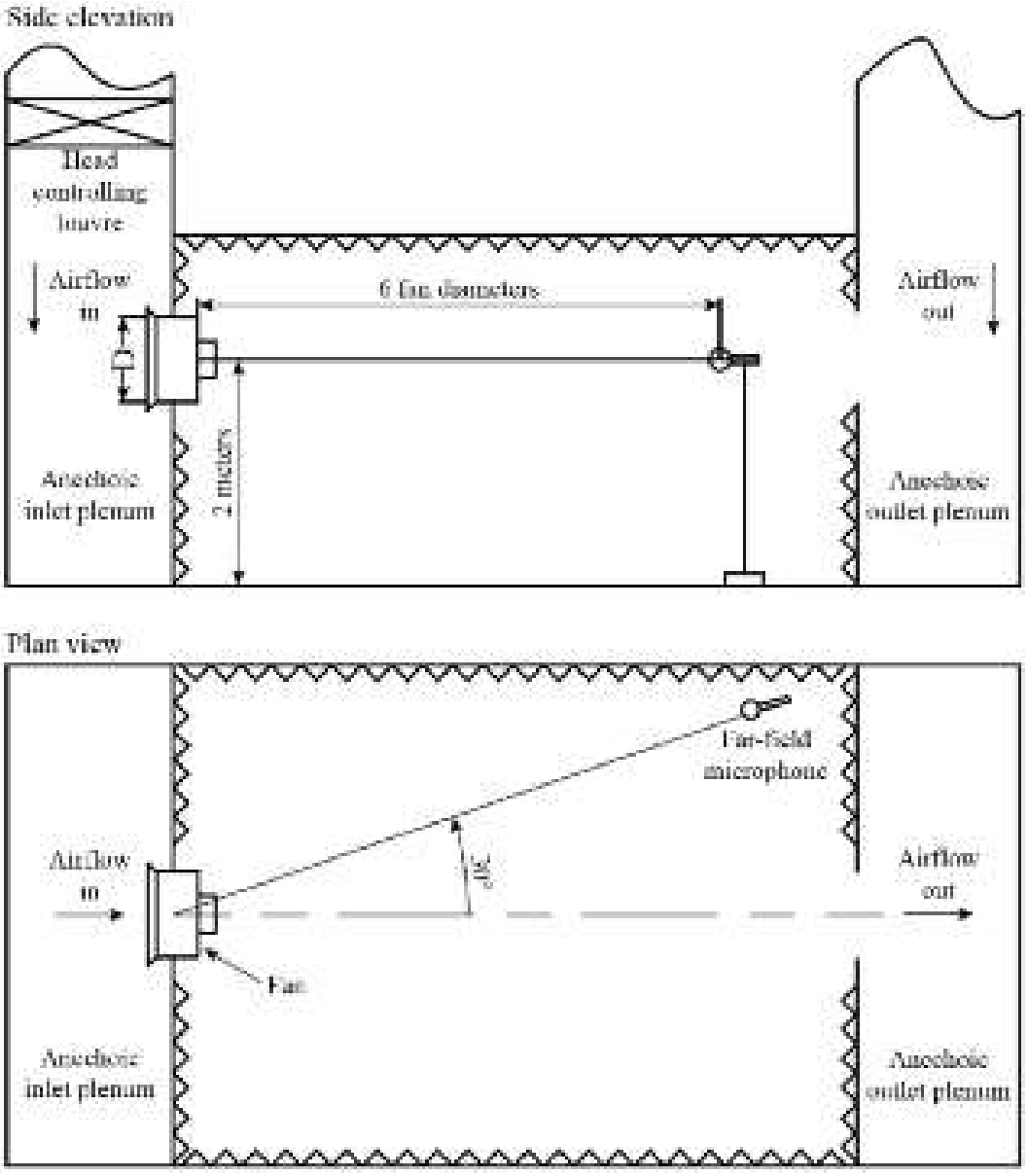

FIGURE 3.5. Microphone arrangement for outlet far-field measurements of fan noise in the anechoic chamber used for near- and far-field outlet fan noise measurements (Bianchi *et al.*, 2009).

Our logic was that the anechoic chamber within which we made our measurements was not infinitely large. Consequently, there was a possibility that the fan would induce flow-field features within the anechoic chamber itself that may have acoustic consequences.

By placing the microphone at an angle 30 degrees from the fan axis, we placed it in a location with the lowest flow-field velocity within the anechoic chamber. We considered that low flow-field velocities would result in any flow-field features within the anechoic chamber also having a low impact on measured far-field noise. We selected the far-field microphone's location after measuring flow-field velocity at different locations within the anechoic chamber. The chosen location flow-field velocity was less than 0.1 m/s which we considered negligible.

Rationale for Analysis

We measured fan near-field outlet noise using the traversing microphone, and far-field noise using the microphone located six fan diameters from the fan exhaust. For each near- and far-field measurement we computed the narrowband spectra from 50 to 10 kHz using a constant bandwidth of 3.15 Hz. We used these narrowband spectra as input to a correlation analysis. This enabled us to identify causal relationships between individual vortical flow-field structures present in the near-field exhaust flow and the fan far-field noise. Therefore, the coherence analysis facilitated a quantitative assessment of the near-field noise source locations, their spectra and the extent of their coherence with fan far-field noise.

Effectiveness of the coherence analysis is dependent on the accuracy of near-field measurements. Laurendeau *et al.* (2007) studied subsonic jet noise, making near-field pressure measurements under similar velocity gradients to those in the outflow from a fan rotor. Ribner (1969) studied the relationship between the near-field pressure and noise-source dynamics. Ribner (1969) observed that the first-order approximation of the Lighthill source term is formally related to the pressure Laplacian in incompressible flows. Laurendeau *et al.* (2007) concluded that the same pressure in the near field senses both aerodynamic cause and acoustic effect in different frequency ranges. When far-field filtering is applied, this provides insights into the source-noise emission coupling mechanisms.

We undertook the coherence analysis using a coherence function to input the near- and far-field spectra, *Gxx* and *Gyy* respectively, and the cross-spectrum between the two, *Gxy*. We defined coherence as:

$$Co^2 = \frac{|Gxy|^2}{|Gxx| \cdot |Gyy|} \tag{1}$$

We used a calibrated noise source to characterise the anechoic chamber's acoustic properties, establishing the coherence between the near- and far-field microphones, Welch (1967). Following Miles' method (2006), we set the threshold for

coherence at 95 per cent of the calibrated noise's coherence. This approach ensured that we only used coherent noise sources when calculating the cross-spectra.

Symmetrised Dot Pattern Technique

A symmetrised dot pattern (SDP) analysis technique facilitated a study on the way in which human perception of fan far-field noise transformed with changing blade-tip end-plate geometry. Researchers first conceived the symmetrised dot pattern analysis technique for the visual characterisation of speech waveforms in automatic human-voice-recognition algorithms (Pickover, 1986). The symmetrised dot patterns provide a visual representation of the input signal, with pattern features that may be correlated with features of the input signal (Pickover, 1986).

The symmetrised dot pattern analysis technique's advantage over other approaches is its ability to link pattern features with specific physical flow phenomena. The symmetrised dot pattern analysis technique does not simply measure the overall sound power level produced by an input signal's tonal components. It is able to visually represent more subtle features that would otherwise be difficult to characterise. Therefore, the merit of the technique is its ability to perceive otherwise 'unquantifiable' differences in sound signals mimicking the way that humans hear (Schultz, 1978; De Rosier *et al*., 1997; Sottek and Genuit, 2007).

Wu and Chang (2005) used the symmetrised dot pattern analysis technique for fault diagnosis in an internal combustion engine. Sheard *et al.* (2010) also used it as the basis of a stall detection system. However, to the best of our knowledge this is the first application of the symmetrised dot pattern analysis technique to the acoustic characterisation of an axial flow fan. The technique facilitated a qualitative assessment of the way in which human perception of fan far-field noise transformed with changing blade-tip end-plate geometry.

We used an algorithm to map a normalised time waveform into a polar coordinate system to produce the symmetrised dot pattern, Figure 3.6. The algorithm maps a point in the input signal as the polar coordinate's radial component, and the adjacent point as the polar coordinate's angular component. In this way, one may map

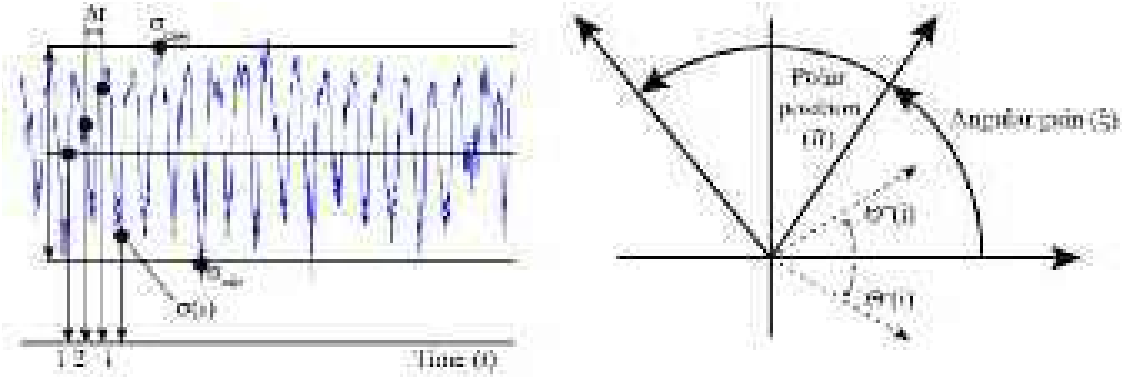

FIGURE 3.6. A schematic illustration of the technique for transforming an input signal into polar coordinates to produce a symmetrised dot pattern.

successive pairs of points from the input signal as single points in a polar coordinate system. Collectively, these points comprise the resultant symmetrised dot pattern.

We can formulate the polar transformation R(i) from waveform to symmetrised dot pattern as:

$$R(i) = \frac{\sigma(i) - \sigma_{\min}}{\sigma_{\max} - \sigma_{\min}} \tag{2}$$

$$\Theta^{+}(i) = \Theta_{0} + \frac{\sigma(i+L) - \sigma_{\min}}{\sigma_{\max} - \sigma_{\min}} \xi \tag{3}$$

$$\Theta^{-}(i) = \Theta_{0} - \frac{\sigma(i+L) - \sigma_{\min}}{\sigma_{\max} - \sigma_{\min}} \xi \tag{4}$$

in which i is the number of dots (i = integer (t/Δt)), with t the time *abscissa* and Δt the sampling time; L is the time lag coefficient; $\sigma(i)$ is the sampled ith sound signal; σ_{max} and σ_{min} are the highest and the lowest value of the original waveform window; Θ_0 is the rotation of the origin angle of any reference line; ξ is the plot angular gain; and Θ^+ and Θ^- are the two angles of the traditional polar space. The input waveform is first normalised by finding the higher (σ_{max}) and lower values (σ_{min}) for the N data points in the window. Therefore, overall signal amplitude, in general, is not a factor in the characterisation.

EXPERIMENTAL DETECTION OF NOISE SOURCES

Span-wise distributions of axial flow coefficient (φ_a) measured 1.2 blade chord downstream of the blade trailing edge illustrate the effect of the studied blade-tip end-plates, Figure 3.7. Adding a blade-tip end-plate significantly modifies the radial distribution of pitch-averaged flow though the blade-to-blade passage. This modification is not just in the blade tip region, but across the majority of the blade span. From this we may conclude that the ability of the studied blade-tip end-plates to control the blade tip-to-casing leakage flow results in boundary layers at the blade root as less prone to separate.

A consequence of the reduction in blade tip-to-casing leakage flow is supressing a hub separation that Bianchi *et al.* (2009) identified when studying the fan *datum* AC90/6. It is perhaps counter-intuitive to conclude that an end-plate fitted to the blade-tip can affect the flow-field at the blade-root. However, it is this ability that illustrated the blade-tip end-plate's influence on boundary layer development over the entire blade span. This influence on boundary layer development has a consequential impact on the migration of boundary layer fluid from the blade hub to tip. This underpins the ability of blade-tip end-plates to influence positively blade tip-to-casing leakage flow and reduces fan far-field noise.

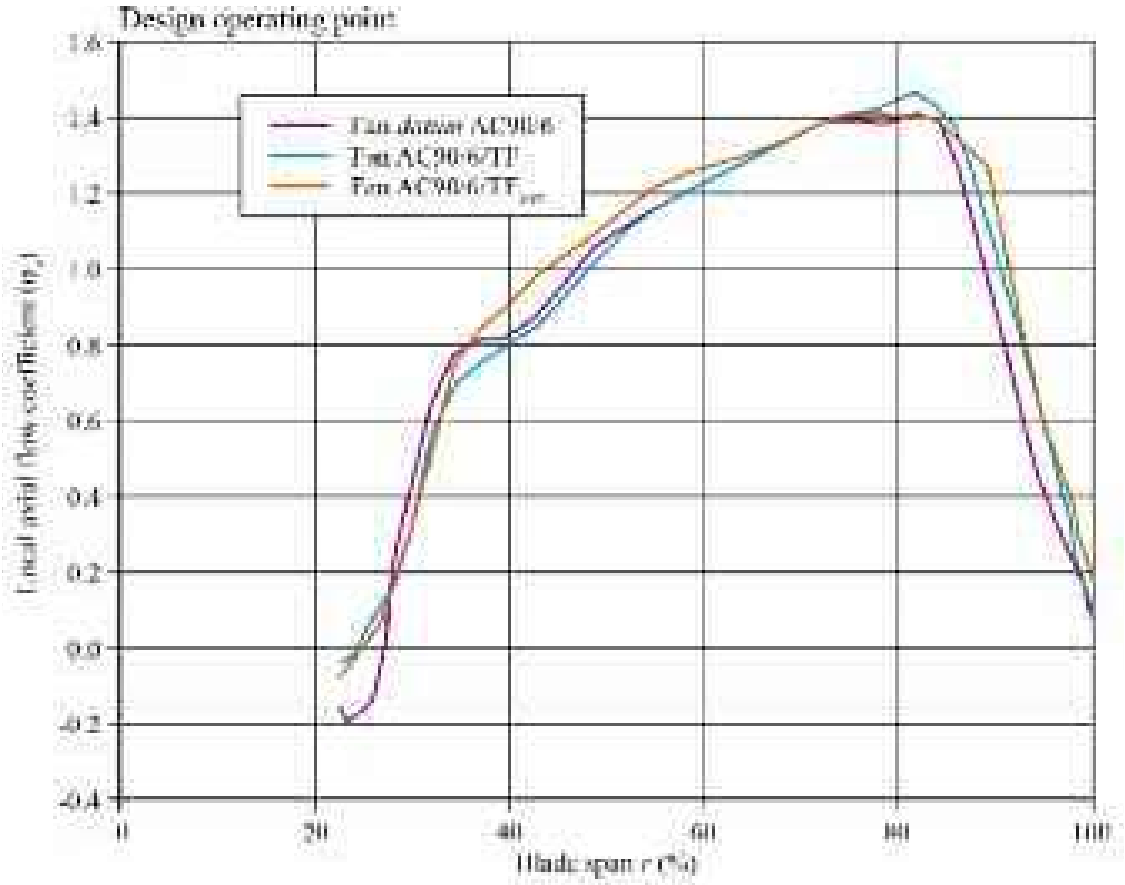

FIGURE 3.7. Span-wise distributions of axial flow coefficient (φ_a) measured 1.2 blade chord downstream of the blade trailing edge illustrating the effect of the studied blade-tip end-plates on span-wise distribution of flow though the blade-to-blade passage.

Span-wise Dissection of Noise Sources: Fan *Datum* AC90/6

Bianchi *et al.* (2009) studied the span-wise distribution of near-field noise sources and the correlation of near- and far-field noise. Bianchi *et al.* (2009) concluded that the fan *datum* AC90/6, AC90/6/TF and AC90/6/TF$_{VTE}$ exhibited distinctly different near-field aerodynamic and far-field acoustic behaviour. By studying the three fans, Bianchi *et al.* (2009) were able to identify the far-field acoustic consequences of the identified near-field noise sources.

Bianchi *et al.*'s (2009) coherence analysis is effective as a consequence of its ability to identify coherent features within the data when those features have only very low energy. Therefore, we are able to identify coherent features in the data that we may have overlooked using other analysis techniques. In the programme of work reported in this chapter we present an analysis of the coherence between data recorded with the traversing microphone and the far-field microphone. We recorded all data at the design operating point, and used the traversing microphone to record data over a range of span-wise locations from blade hub to tip.

To facilitate interpreting the coherence data we present 'maps' of the radial distribution of coherence against normalised frequency. We define normalised fre-

quency (*Sf*) as frequency divided by blade passing frequency. Therefore, for example, a normalised frequency of one is the blade passing frequency. Consider the coherence map for the fan *datum* AC90/6 over the normalised frequency range of zero to seven, Figure 3.8. There is a non-tonal coherent phenomenon in the blade tip's vicinity. We may characterise this coherent phenomena feature at the blade tip as turbulence induced noise (TIN). This occurs as a consequence of the interaction between blade tip-to-casing leakage vortex and the blade wake. The maximum coherence of the turbulence induced noise is 0.6, indicating the uncorrelated nature of this noise source. We would expect this noise source to be uncorrelated as the acoustic emissions emanate from mixing vortices with different structure and rotational frequency.

There is also a second non-tonal coherent phenomenon in the vicinity of the blade hub. We may characterise this coherent phenomena feature at the blade hub as secondary flow noise (SFN). This occurs as a consequence of a blade hub corner stall interacting with the blade-to-blade passage vortex. The maximum turbulence induced noise coherence is 0.6, indicating the noise source's uncorrelated nature. We would expect this noise source to be uncorrelated as the acoustic emissions emanate from mixing two secondary flow features with different structure and rotational frequency.

In addition to the non-tonal coherent phenomenon there are also three tonal coherent phenomena. The first is associated with the fan motor. The fan motor produces isolated tones at normalised frequencies of approximately three and between five and six, Figure 3.8. We may characterise these coherent phenomena features as motor noise (MN). Coherence of the motor noise reduces from 1.0 near the blade hub to 0.4 near the blade tip. We expect this reduction in coherence with increasing blade span as the motor is located behind the blade hub, thus we would expect it to influence the hub more than the tip region.

There is also a second tonal coherent phenomenon. The studied fan is a low-speed fan, with peak velocities typically no more than half the speed of sound. Therefore, the fan rotor is able to induce distortions in the flow-field upstream of the fan. Isolated tones at normalised frequencies of 0.25 and 0.66 characterise the coherence map, Figure 3.8. Cumpsty (1974) first studied the low-frequency tones produced as a consequence of induced distortions in the flow-field upstream of the fan. As these tones were produced by inflow distortions induced in the inflow by the fan rotor's rotation, Cumpsty (1974) characterised them as rotor induced noise. We may characterise this coherent phenomena feature as rotor noise (RN).

The third tonal coherent phenomenon is clearly evident at a normalised frequency of two that becomes progressively more intense as we move from the blade hub to tip. This is the second blade passing frequency, with a maximum coherence of 0.7 at 80 per cent blade span, Figure 3.8. Previous scholars, who have characterised the second blade passing frequency (Magliozzi *et al.*, 1973; Cumpsty, 1974, 1977), concluded that it may be associated with a disturbance of the inflow into the fan. Therefore, this coherence map feature may be ingested noise (IN).

To characterise the coherence map's induced noise feature, it is helpful to consider the coherence at the fan inlet and outlet in the near-hub vicinity, Figure 3.9. The

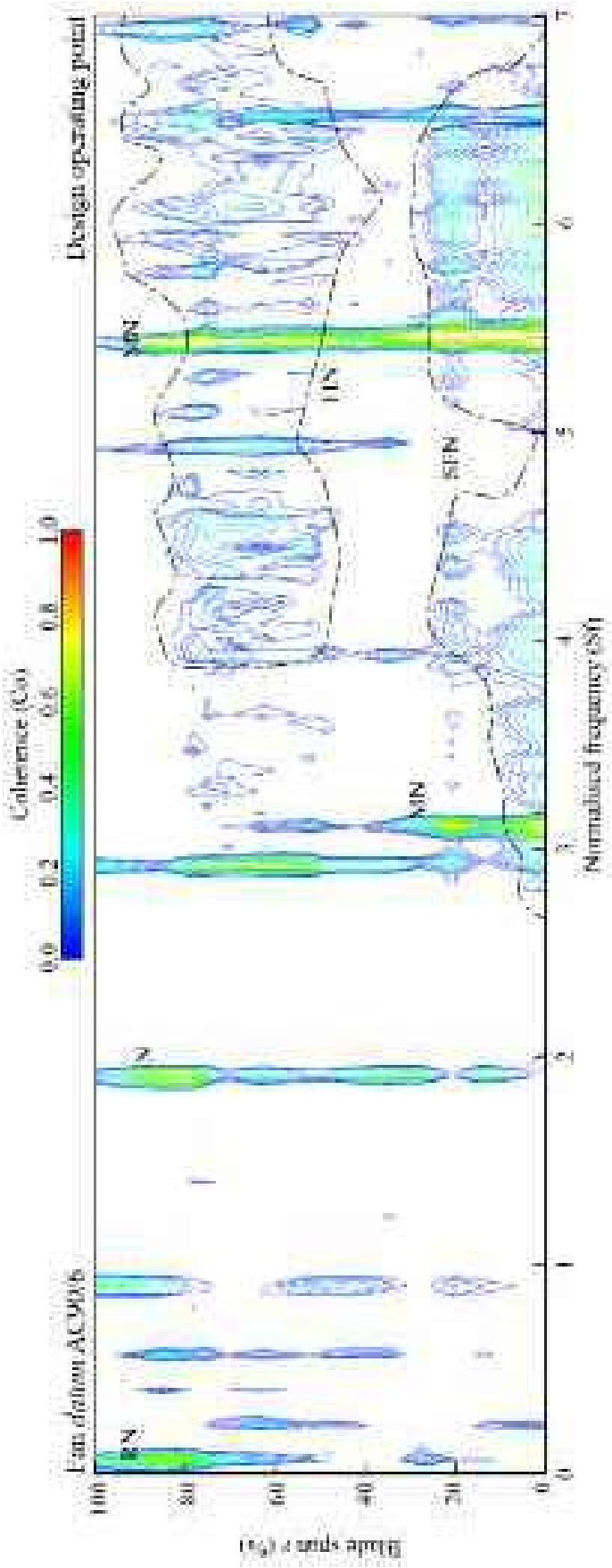

FIGURE 3.8. Fan *datum* AC90/6 span-wise coherence map for normalised frequencies below seven. Normalised frequency (*Sf*) is defined as measured frequency divided by the first blade passing frequency.

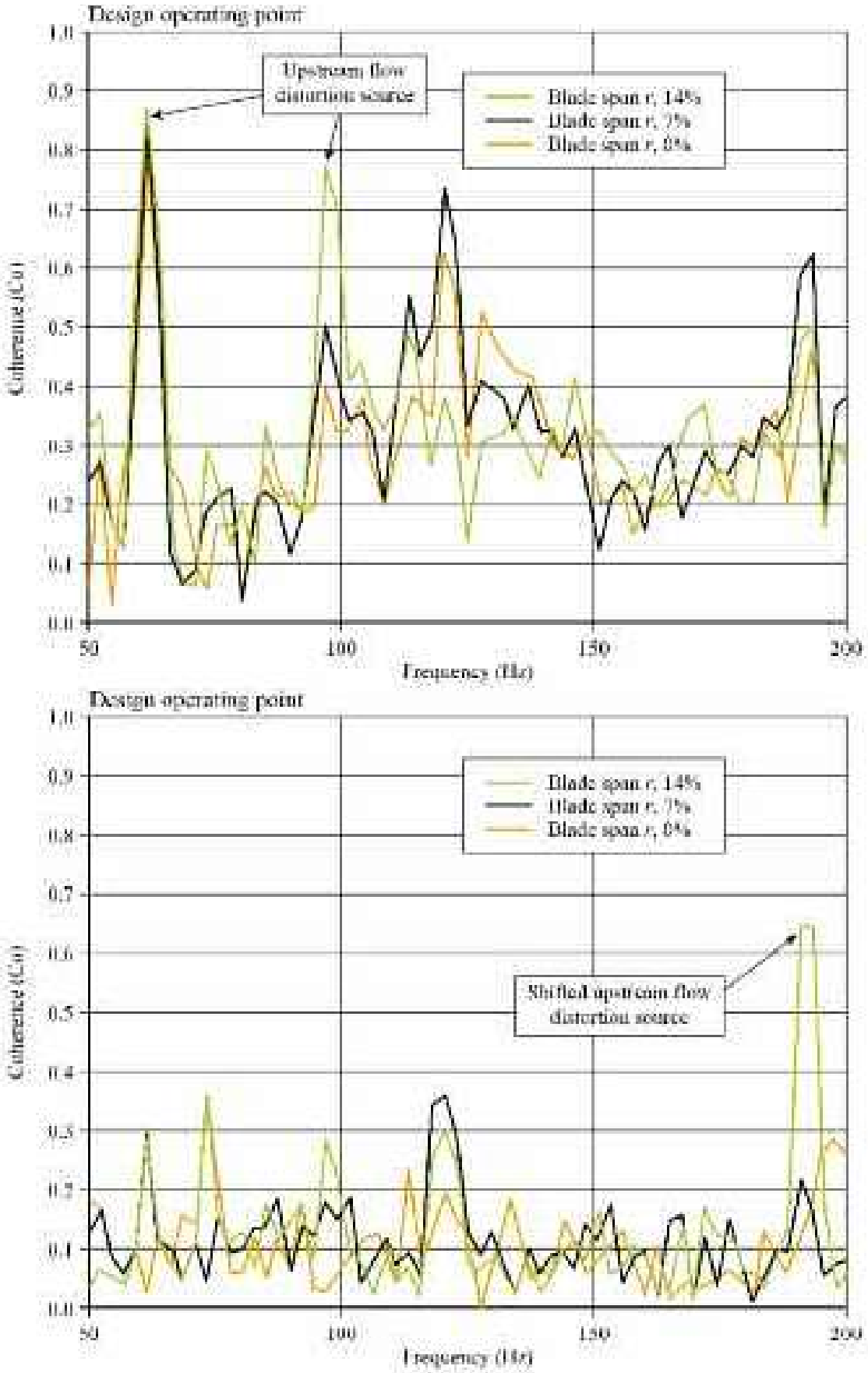

FIGURE 3.9. Fan *datum* AC90/6 inlet (top) and outlet (bottom) coherence spectrum measured at three span-wise locations in the blade hub region at the fan design operating point. The outlet coherence spectrum illustrates the impact of blade hub flow-field features on near-field fan noise.

peak coherence values at the inlet are in the near hub region, with generally lower coherence at the outlet in the hub region. The observation that coherence is more pronounced at the inlet than the outlet indicates that this coherence map feature is ingested noise. We may attribute the ingested noise source's shift in frequency from the inlet to outlet coherence spectra to the scattering of the inlet flow distortions as they pass through the blade-to-blade passage.

We also present coherence data as a map for the fan *datum* AC90/6 over a normalised frequency range of seven to eighteen, Figure 3.10. Non-tonal coherent phenomenon in the vicinity of the blade hub characterises this higher normalised frequency range which is once again secondary flow noise (SFN). We may conceptualise this secondary flow noise as a second noise source associated with the hub corner stall. The interaction of the blade hub corner stall and blade-to-blade passage vortex characterised the first secondary flow noise source. In contrast, we may attribute this noise source to the hub corner stall's unsteady behaviour.

The non-coherent phenomenon over the higher normalised frequency range may be an indication of pseudo noise measured in the near-field. As these purely hydrodynamic pressure fluctuations are not correlated with density fluctuations, they do not propagate coherently as acoustic waves. Therefore, these higher frequency coherent structures may be an indication of low turbulence structures in the near-field that manifest themselves in the far-field as broadband noise. This observation is self-consistent with Quinlan and Bent's conclusions (1998). They studied the mechanisms by which secondary flow features induced fan noise. Quinlan and Bent (1998) concluded that secondary flow features are the primary contributor to broadband noise in axial flow fans at frequencies above 1 kHz. The distribution of coherence over the normalised frequency range from seven to eighteen is relatively even from blade hub to tip. This implies that the blade tip-to-casing leakage vortex must also be contributing to the broadband noise, resulting in a near uniform contribution to fan far-field broadband noise over the entire blade span.

Span-wise Dissection of Noise Sources: fan AC90/6/TF and AC90/6/TF$_{\mathrm{VTE}}$

A lower specific noise level (K_S) than the fan *datum* AC90/6 over the entire fan operating range characterises both fan AC90/6/TF and AC90/6/TF$_{VTE}$, Figure 3.3. The span-wise dissection of noise sources for the fan *datum* AC90/6 provided an insight into the far-field acoustic consequences of the identified near-field noise sources. We used this insight to inform analysis of noise sources for fan AC90/6/TF and AC90/6/TF$_{VTE}$, thus facilitating insight into the reasons for the lower specific noise level. We once again present 'maps' of the radial distribution of coherence against normalised frequency where we recorded all data at the fan's design operating point.

Consider the coherence map for the fan AC90/6/TF over the normalised frequency range of zero to seven, Figure 3.11. The fan AC90/6/TF induced noise (IN) tone was reduced compared to the induced noise tone for fan *datum* AC90/6, Figure 3.8. Generally, the same features as the fan *datum* AC90/6 coherence map characterise the fan AC90/6/TF coherence map, with the exception of the turbulence

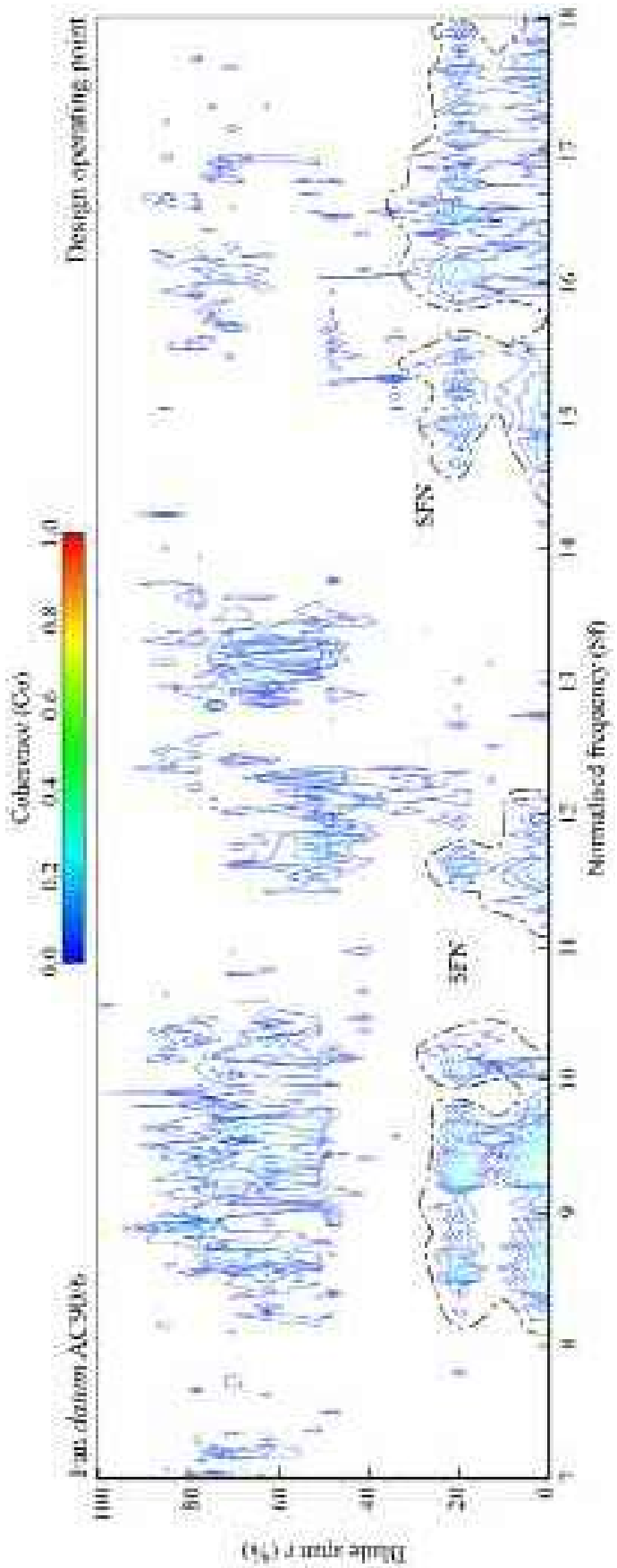

FIGURE 3.10. Fan *datum* AC90/6 span-wise coherence map for normalised frequencies above seven. Normalised frequency (*Sf*) is defined as measured frequency divided by the first blade passing frequency.

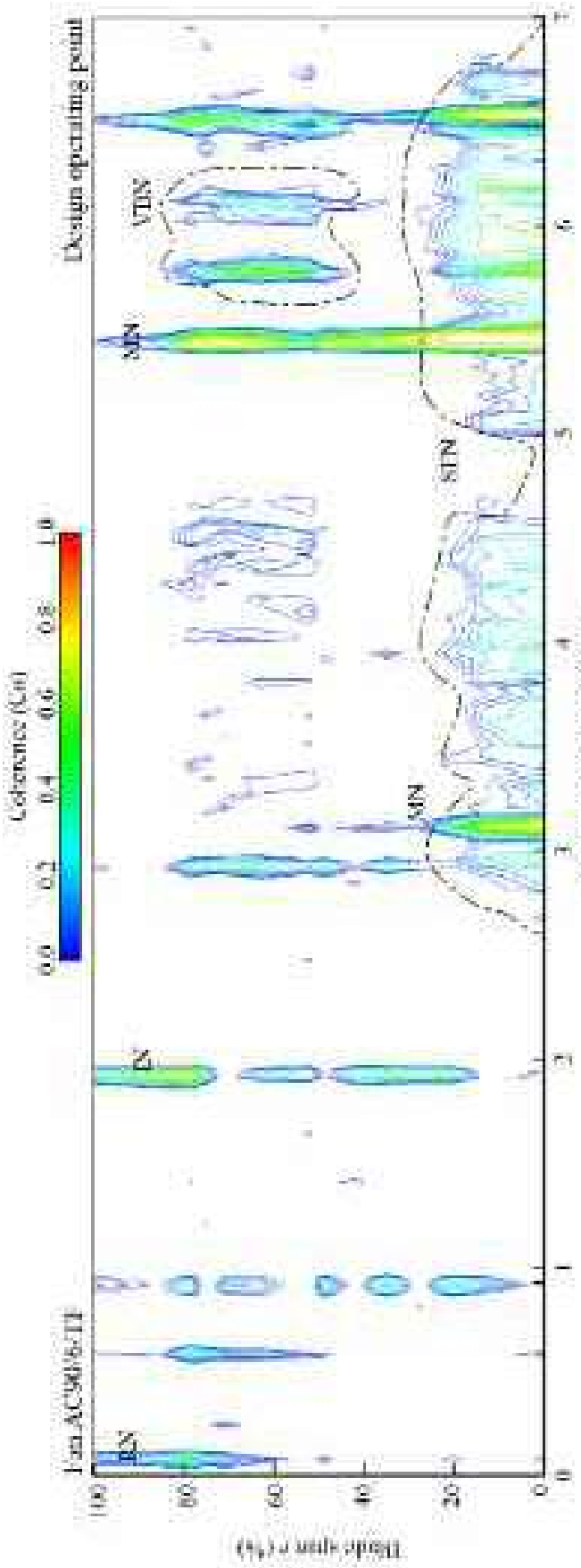

FIGURE 3.11. Fan AC90/6/TF span-wise coherence map for normalised frequencies below seven. Normalised frequency (*Sf*) is defined as measured frequency divided by the first blade passing frequency.

induced noise (TIN) in the vicinity of the blade tip. However, at a normalised frequency of approximately six, a pair of tonal peaks characterises the fan AC90/6/TF coherence map. The span-wise location and frequency of this pair of tonal peaks correlates with the location and bursting frequency of the blade tip-to-casing leakage vortex. Therefore, we characterised this pair of tonal peaks as vortex bursting noise (VBN).

Having identified vortex bursting noise, a further review of the fan AC90/6/TF coherence map indicated that coherence of the hub secondary flow noise (SFN) was generally lower than for the fan *datum* AC90/6. This reduction in secondary flow noise coherence indicates that the addition of a constant thickness blade-tip end-plate results in better control of hub secondary flow features.

Consider the coherence map for the fan AC90/6/TF over the normalised frequency range of seven to eighteen, Figure 3.12. Laurendeau *et al.* (2007) considered this higher frequency range important. Over this higher frequency range Laurendeau *et al.* (2007) concluded that fan far-field noise was linked to the presence of coherence near-field swirling structures. The frequencies of these coherence near-field swirling structures are not linked to a blade passing frequency harmonic. Therefore, they constitute purely aerodynamic noise sources, with no contribution from the interaction of static and rotation components.

The coherence map for the fan AC90/6/TF illustrates that the overall density of coherent structures across the map significantly reduces when compared with the coherence map of the fan *datum* AC90/6. When one studies the two coherence maps it is apparent that the secondary flow noise in the hub region of fan *datum* AC90/6 is still present in the fan AC90/6/TF. The peak coherence reduces over the normalised frequency range eight to ten and eleven to twelve. Over the normalised frequency range of fifteen to eighteen, the coherence of secondary flow noise in the hub region of fan AC90/6/TF has effectively reduced so far that it is no longer coherent. This reduction and elimination of coherent regions of secondary flow noise indicates that the magnitude of the hub separated flow in fan *datum* AC90/6 reduces in fan AC90/6/TF. A reduction in a hub separated flow region's magnitude will result in a reduction in boundary layer flow centrifuged from the blade hub to tip.

Consider the coherence map for the fan AC90/6/TF$_{VTE}$ over the normalised frequency range of zero to seven, Figure 3.13. A significant feature is the absence of coherence in the blade tip region at the blade passing frequency, a normalised frequency of one. This absence is a consequence of the noise source's attenuation originating from the interaction of flow-field features in the blade tip-to-casing flow. The vortex bursting noise also reduces in intensity in comparison with fan AC90/6/TF, and reduces from a double region at a normalised frequency of just below and above six to a single normalised frequency just below six. Therefore, we may conclude that the variable thickness blade-tip end-plate effectively reduces the blade tip-to-casing leakage vortex impact on fan far-field noise.

We developed the variable thickness blade-tip end-plate of fan AC90/6/TF$_{VTE}$ with the specific intention of avoiding breakdown of the blade tip-to-casing leakage vortex. The fan AC90/6/TF$_{VTE}$ coherence map indicates that at a normalised frequency of one and six, blade-tip noise sources have been eliminated. We may con-

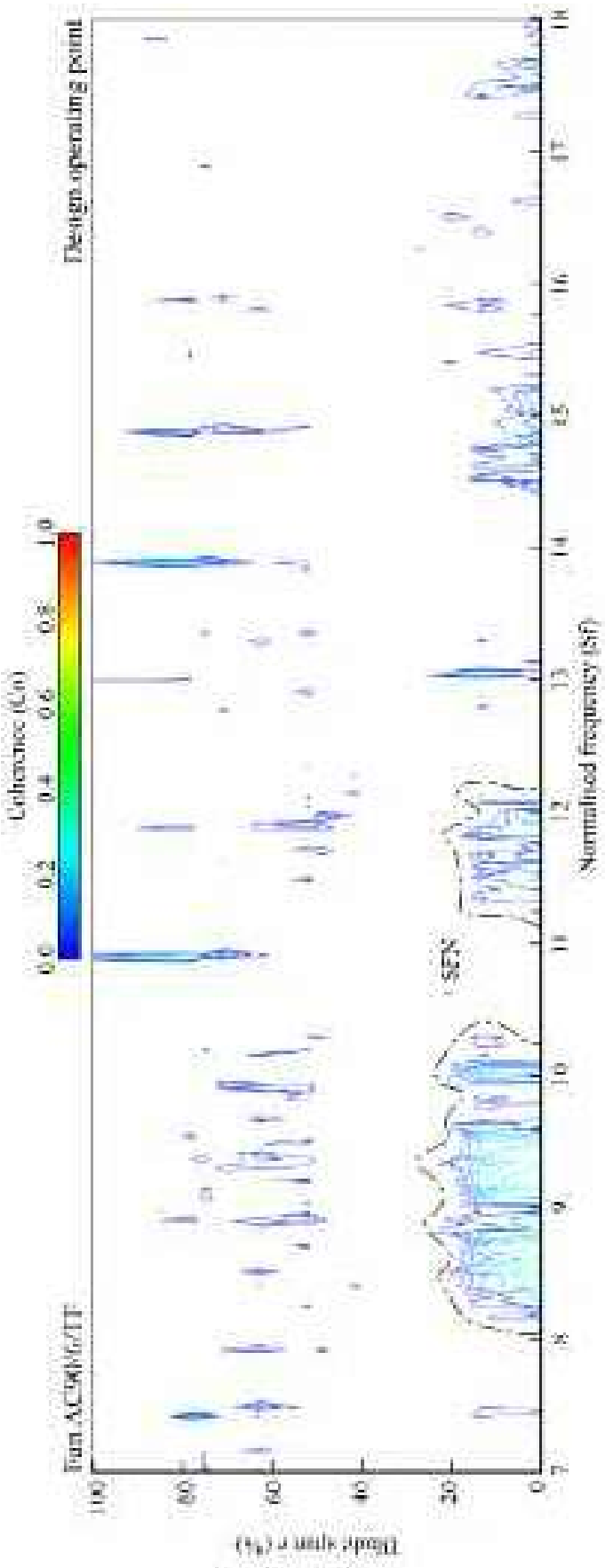

FIGURE 3.12. Fan AC90/6/TF span-wise coherence map for normalised frequencies above seven. Normalised frequency (*Sf*) is defined as measured frequency divided by the first blade passing frequency.

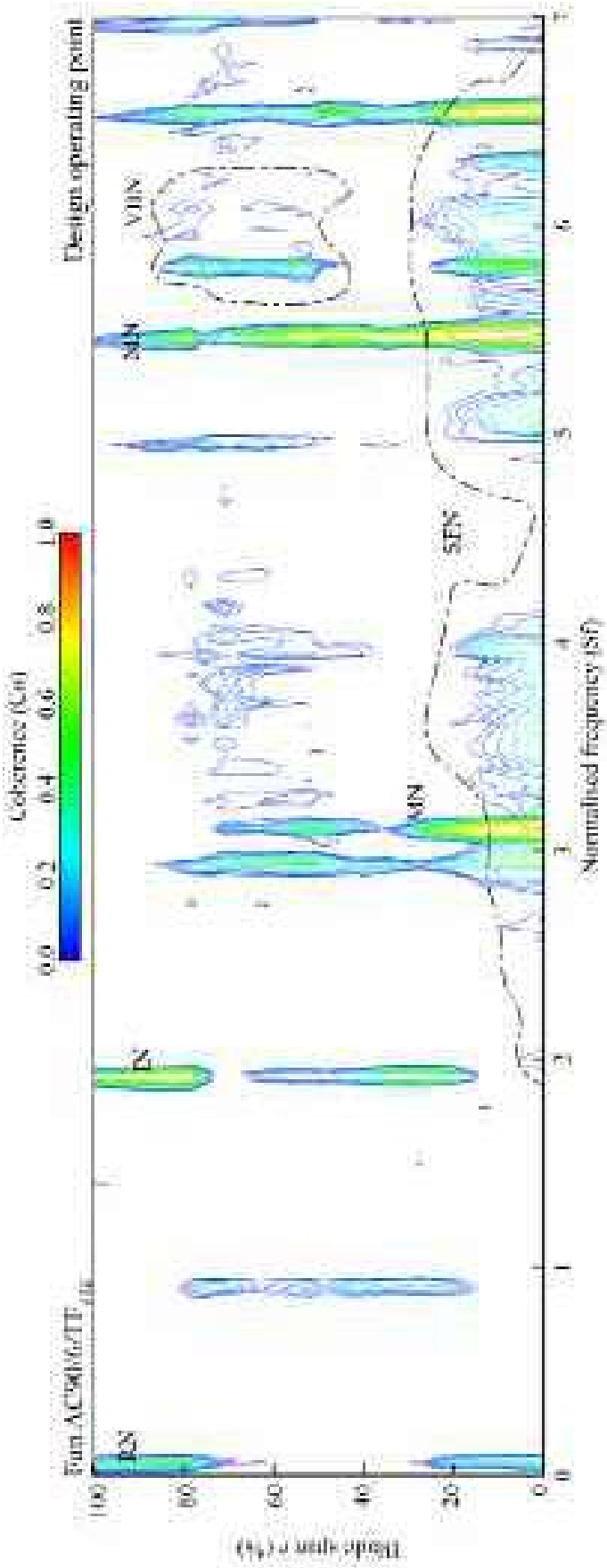

FIGURE 3.13. Fan AC90/6/TF$_{VTE}$ span-wise coherence map for normalised frequencies below seven. Normalised frequency (Sf) is defined as measured frequency divided by the first blade passing frequency.

clude that this is a consequence of the blade tip-to-casing leakage vortex not bursting, with a resultant reduction in fan far-field noise. Therefore, we may conclude that the variable thickness blade-tip end-plate has been effective.

Consider the coherence map for the fan AC90/6/TF$_{VTE}$ over the normalised frequency range of seven to eighteen, Figure 3.14. Over this higher normalised frequency range the fan AC90/6/TF$_{VTE}$ coherence map contains similar features to those in the fan AC90/6/TF coherence map. However, generally higher coherence levels characterise the fan AC90/6/TF$_{VTE}$ coherence map. As has previously been observed, Laurendeau *et al.* (2007) concluded that fan far-field noise was linked to the presence of coherence near-field swirling structures. The implication of this conclusion is that the variable thickness blade-tip end-plate is generating swirling structures in the blade tip-to-casing flow-field. Significantly, the constant thickness blade-tip end-plates do not generate these swirling structures. Therefore, a generally higher coherence that will result in generally higher broadband noise characterises this higher normalised frequency range in the fan AC90/6/TF$_{VTE}$.

The Impact of Blade-tip End-plates on Perceived Noise

Assessing the impact of blade-tip end-plates on perceived fan noise complements the span-wise dissection of noise sources. We chose to assess perceived fan far-field noise using a symmetrised dot pattern (SDP) analysis technique. Researchers first conceived the symmetrised dot pattern analysis technique for the visual characterisation of speech waveforms in automatic human-voice-recognition algorithms.

Our input for the analysis was unsteady pressure measured in the fan far-field for the three studied fans at their design operating point. Fan far-field unsteady pressure measurements for the fans AC90/6/TF and AC90/6/TF$_{VTE}$ were distinctly different from the fan *datum* AC90/6, Figure 3.15. This difference was a consequence of adding the constant and variable thickness blade-tip end-plates.

For each of the studied fans we logged data using the far-field microphone at 65 kHz over twenty seconds, recording approximately 1.3 million data points. These data points then transformed into a symmetrised dot pattern for each of the studied fans, Figure 3.16. We generated the symmetrised dot patterns presented in Figure 3.16 using a plot angular gain (ξ) of 20. We selected this angular gain following a pragmatic trial and error approach, which we adopted as there is no established methodology for using the symmetrised dot pattern analysis technique for characterising fan noise. The chosen angular gain resulted in a stable analysis technique for all three data sets.

Consider the unsteady pressure data for the three studied fans, Figure 3.15. The data for each of the studied fans is visually different, and therefore we would expect each data set to be associated with different tonal and broadband noise levels. The unsteady pressure data for the fan *datum* AC90/6 contains less well defined features than the unsteady pressure data for either the fan AC90/6/TF or AC90/6/TF$_{VTE}$. Therefore, the unsteady pressure data for the fan *datum* AC90/6 is the closest of the

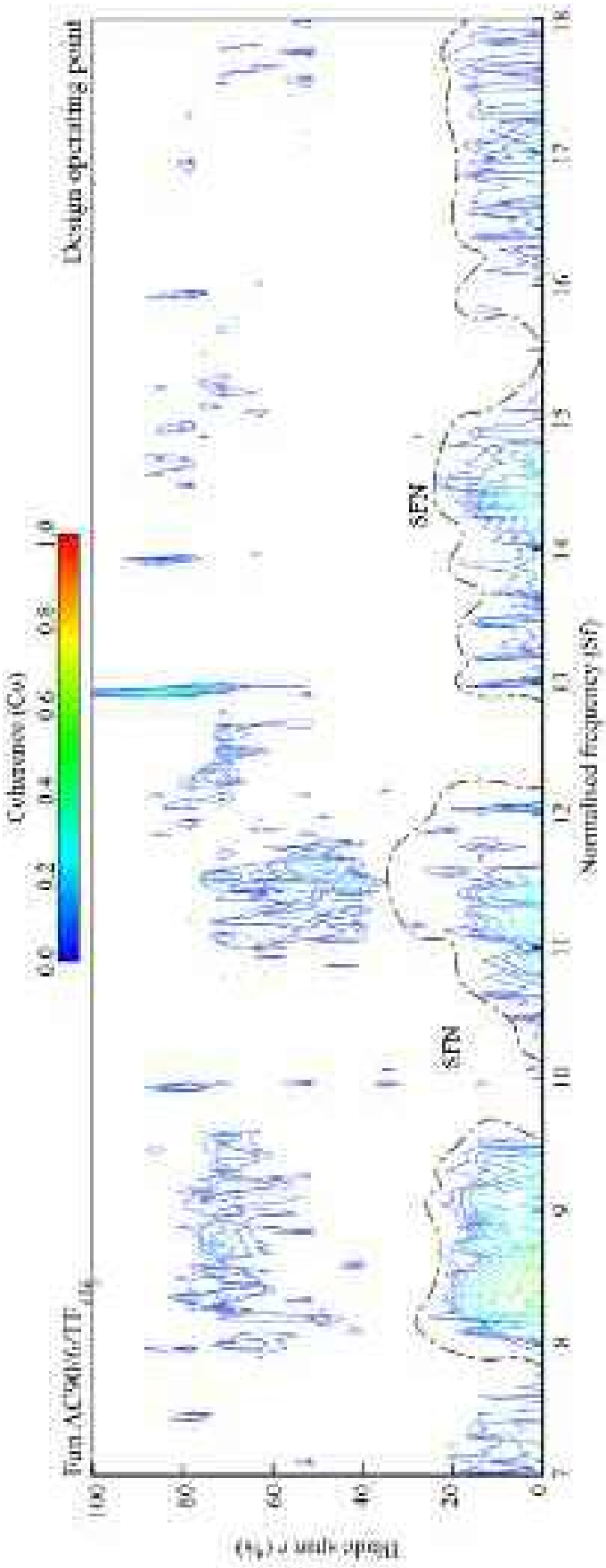

FIGURE 3.14. Fan AC90/6/TF$_{VTE}$ span-wise coherence map for normalised frequencies above seven. Normalised frequency (*Sf*) is defined as measured frequency divided by the first blade passing frequency.

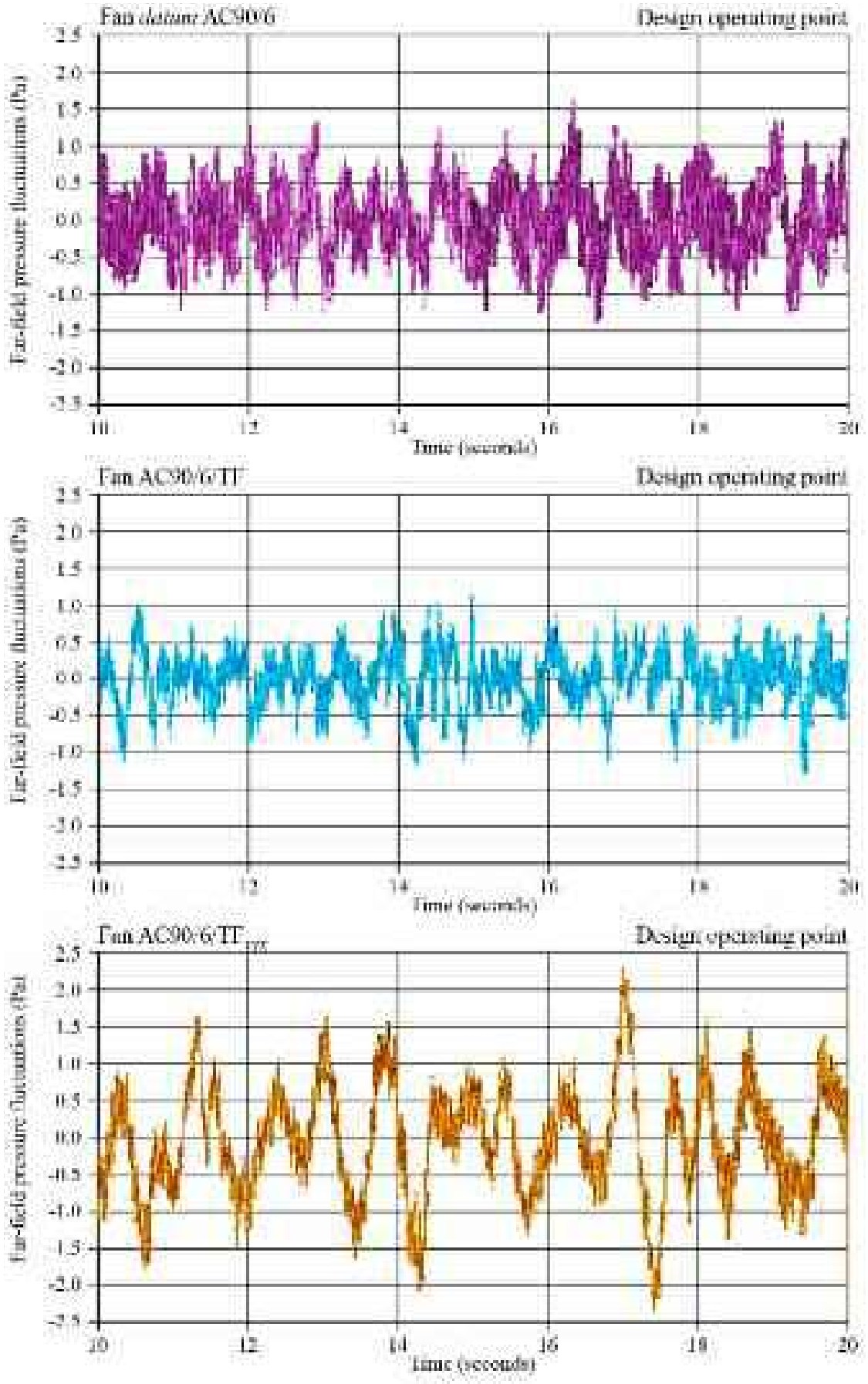

FIGURE 3.15. Unsteady pressure measured in the far-field for the three studied fans at their design operating point. Far-field unsteady pressure measurements were different from the fan *datum* AC90/6 as a consequence of adding the constant and variable thickness blade-tip end-plates.

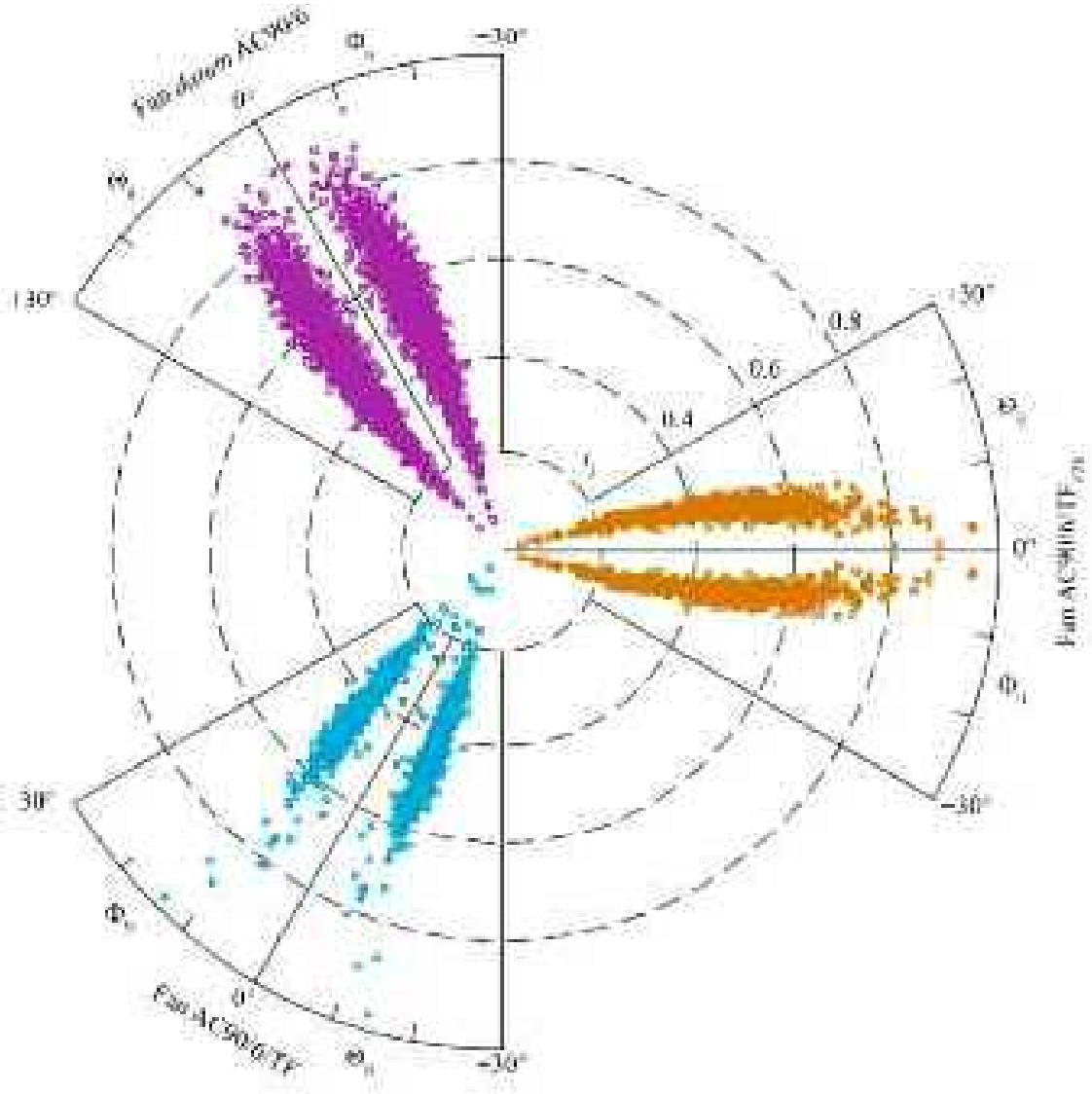

FIGURE 3.16. Symmetrised dot patterns generated using unsteady pressure measured in the far-field for the three studied fans at their design operating point. The three symmetrised dot patterns each cover a different area with a variation in the dispersion of the dots that comprise the pattern.

studied fans to white noise. In this context we define white noise as a random signal with a constant power spectral density. In contrast, the fan AC90/6/TF and AC90/6/TF$_{VTE}$ unsteady pressure signals are more characteristic of pink noise. In this context we define pink noise as a signal where each octave contains an equal amount of acoustic energy. The name arises from the pink appearance of visible light with this power spectrum. This variation in the unsteady pressure data used as input to the symmetrised dot pattern analysis technique will result in a difference between the generated symmetrised dot patterns.

Consider the symmetrised dot patterns for the three studied fans, Figure 3.16. The dot diffusion was larger for the fan *datum* AC90/6 then either fan AC90/6/TF or AC90/6/TF$_{VTE}$. The fan *datum* AC90/6 symmetrised dot patterns dispersed around its base and the boundary was not well defined. In contrast, the fan AC90/6/TF symmetrised dot pattern was concentrated over a smaller area with less dispersion and a

more clearly defined boundary. The fan AC90/6/TF$_{VTE}$ symmetrised dot pattern was closer to the fan *datum* AC90/6 than the fan AC90/6/TF symmetrised dot pattern, but with less dot dispersion.

We may interpret the differences between the three symmetrised dot patterns within the context of Pickover's (1986) conclusions that the human 'acceptability' of noise correlates with the smallest symmetrised dot pattern area of dots. Therefore, a human observer would qualitatively perceive the noise from both the fan AC90/6/TF and AC90/6/TF$_{VTE}$ as more acceptable than the noise from the fan *datum* AC90/6. Thus, adding both constant thickness and variable thickness blade-tip end-plates improves the acceptability of fan far-field fan noise. This improvement in acceptability of fan far-field noise is in addition to reducing the absolute level of specific fan noise, Figure 3.3. Therefore, the blade-tip end-plates both reduce and make more acceptable fan far-field noise.

CONCLUSIONS

In this chapter we applied an experimental methodology that we developed to facilitate assessment of fan acoustic performance. The research focused on the association of flow-field features in the blade tip-to-casing region with blade-tip end-plate design features. We were able to establish that the presence of blade-tip end-plates influenced the blade-to-blade flow-field over the entire blade span. We measured the flow coefficient's span-wise distributions 1.2 blade chords downstream of the studied fan. When we analysed the flow coefficient's span-wise distributions, the results indicated that the presence of a blade-tip end-plate resulted in a boundary layer at the blade root that was less likely to separate.

A consequence of hub boundary layers that are less likely to separate is reduced fluid volume centrifuged up the blade pressure surface towards the blade-tip. Reducing the tendency of the hub boundary layers to separate also resulted in suppressing a hub separation bubble, eliminating a possible near-field flow-field feature that had negative far-field acoustic consequences.

We analysed the role of coherent vortical structures and blade tip-to-casing leakage flow features as noise sources using a novel symmetrised dot pattern (SDP) visualisation of fan far-field noise. The symmetrised dot pattern visualisation technique facilitated a study of the way in which human perception of fan far-field noise transforms as we changed the blade-tip treatment. We produced the symmetrised dot patterns using an algorithm that maps a normalised time waveform derived from a fan far-field noise measurement onto a radial component with the adjacent point mapping onto an angular component. The resulting symmetrised dot pattern shapes provided a qualitative assessment of human acceptability of fan far-field noise associated with the studied fan both with and without fitted blade-tip end-plates.

Previous researchers who have applied the symmetrised dot pattern technique have concluded that the human ear finds noise more acceptable if the noise is correlated with the smallest area of dots in the associated symmetrised dot pattern. Consequently, one may use the area of symmetrised dot patterns as a proxy for the

human ears' perception of the acceptability of a fan's far-field noise. Although somewhat subjective, the applications into which we fit the studied fan are invariably within close proximity to people. As such, it is reasonable to accept that the fan far-field noise acceptability, as well as its overall level, is important. We found that the studied fan with a fitted blade-tip end-plate resulted in a smaller symmetrised dot pattern area than without an end-plate.

The presence of blade-tip end-plates reduces the absolute level of fan far-field noise as a consequence of both reducing the blade-tip leakage flow rate and influencing the development of boundary layers and secondary flow features in the blade hub region. Additionally, the acceptability of fan far-field noise improves with adding a blade-tip end-plate which constitutes a secondary benefit associated with applying blade-tip end-plates.

REFERENCES

ISO 5801:2007 (2007), *Industrial Fans: Performance Testing Using Standardised Airways.*

ISO 10302:1996 (1996), *Fans for General Purposes. Methods of Noise Testing.*

Bianchi, S., Sheard, A.G., Kinghorn, I.R., Corsini, A. and Rispoli, F. (2009), 'Experimental Development of a Measurement Technique to Resolve the Radial Distribution of Fan Aeroacoustic Emissions', *Noise Control Engineering Journal*, vol. 57, pp. 360–369.

Corsini, A. and Sheard, A.G. (2007), 'Tip End-plate Concept Based on Leakage Vortex Rotation Number Control', *Journal of Computer Applied Mechanics*, vol. 8, pp. 21–37.

Corsini, A., Rispoli, F., Sheard, A.G. and Kinghorn, I.R. (2006), 'Investigation of Improved Blade-tip Concept for Axial Flow Fan', *Proceedings of the 51st American Society of Mechanical Engineers Gas Turbine and Aeroengine Congress*, Barcelona, Spain, 8–11 May, paper no. GT2006-90592.

Cumpsty, N.A. (1974), 'Sum and Difference Tones from Turbo-machines', *Journal of Sound and Vibration*, vol. 32, pp. 383–386.

Cumpsty, N.A. (1977), 'A Critical Review of Turbomachinery Noise', *Transactions of the ASME, Journal of Fluids Engineering*, vol. 99, pp. 278–293.

De Rosier, B., Normand, M.D. and Peleg, M. (1997), 'Effect of Lag on the Symmetrised Dot Pattern (SDP) Displays of the Mechanical Signatures of Crunchy Cereal Foods', *Journal of the Science of Food and Agriculture*, vol. 75, pp. 173–178.

Fukano, T. and Jang, C. (2004), 'Tip Clearance Noise of Axial Flow Fans Operating at Design and Off-design Condition', *Journal of Sound and Vibration*, vol. 275, pp. 1027–1050.

Fukano, T., Takamatsu, Y. and Kodama, Y. (1986), 'The Effects of Tip Clearance on the Noise of Low-pressure Axial and Mixed Flow Fans', *Journal of Sound and Vibration*, vol. 105, pp. 291–308.

Ganz, U.W., Joppa, P.D. and Scharpf, D.F. (1998), *Boeing 18-inch Fan Rig Broadband Noise Test*, Report NASA CR-1998-208704.

Garg, A.K. and Leibovich, S. (1979), 'Spectral Characteristics of Vortex Breakdown Flowfields', *Physics of Fluids*, vol. 22(11), pp. 2053–2064.

Holste, F. and Neise, W. (1997), 'Noise Source Identification in a Prop Fan Model by Means of Acoustical Near Field Measurements', *Journal of Sound and Vibration*, vol. 203, pp. 641–665.

Inoue, M., Kuroumaru, M. and Furukawa, M. (1986), 'Behaviour of Tip Leakage Flow Behind an Axial Compressor Rotor', *Transaction of the ASME, Journal of Engineering for Gas Turbines and Power*, vol. 108, pp. 7–14.

Ito, T., Suematsu, Y. and Hayase, T. (1985), 'On the Vortex Breakdown Phenomena in a Swirling Pipe-flow', *Memoirs of the Faculty of Engineering, Nagoya University*, vol. 37, pp. 117–172.

Kameier, F. and Neise, W. (1997), 'Rotating Blade Flow Instability as a Source of Noise in Axial Turbo-machines', *Journal of Sound and Vibration*, vol. 203, pp. 833–853.

Laurendeau, E., Jordan, P., Delville, J. and Bonnet, J. (2007), 'Near Field–Far Field Correlations in Subsonic Jets: What Can They Tell Us?', *Proceedings of the 13th AIAA/CEAS Aeroacoustics Conference*, Rome, Italy, 21–23 May, paper no. 2007-3614.

Leggat, L.J. and Siddon, T.E. (1978), 'Experimental Study of Aeroacoustic Mechanism of Rotor-vortex Interactions', *Journal of the Acoustical Society of America*, vol. 64, pp. 1070–1077.

Longhouse, R.E. (1978), 'Control Tip-vortex Noise of Axial Flow Fans by Rotating Shrouds', *Journal of Sound and Vibration*, vol. 58, pp. 201–214.

Magliozzi, B., Johnson, B.V., Hanson, D.B. and Metzger, F.B. (1973) 'Noise and Wake Structure Measurements in a Subsonic Tip Speed Fan – Tabulation and Plots of Test Data', NASA Technical Report CR-132259, 23 July.

Marcinowski, H. (1953), 'Einfluss des Laufradspalts und der Luftfuehrung bei einem Kuehlgeblaese axialer Bauart', *Motortechnische Zeitschrift*, vol. 14, pp. 259–262.

Miles, J.H. (2006), 'Procedure for Separating Noise Sources in Measurements of Turbofan Engine Core Noise', NASA Report No. TM-2006-214352.

Mongeau, L., Thompson, D.E. and McLaughlin, D.K. (1995), 'A Method for Characterizing Aerodynamic Sound Sources in Turbo-machines', *Journal of Sound and Vibration*, vol. 181, pp. 369–389.

Mugridge, B.D. and Morfey, C.L. (1972), 'Sources of Noise in Axial Flow Fan', *Journal of the Acoustical Society of America*, vol. 51, pp. 1411–1426.

Nelson, D.A. and Cooper, B.A. (1999), 'A "Reduced-Noise Gas Flow Design Guide" for NASA Glenn Research Center', *Proceedings of INTERNOISE 99, the International Congress on Noise Control Engineering*, Fort Lauderdale, FL, USA, 6–8 December, vol. 1, pp. 77–82.

Pickover, C.A. (1986), 'On the Use of Symmetrized Dot Patterns for the Visual Characterization of Speech Waveforms and Other Sampled Data', *Journal of the Acoustical Society of America*, vol. 80, pp. 955–960.

Quinlan, D.A. and Bent, P.H. (1998), 'High Frequency Noise Generation in Small Axial Flow Fans', *Journal of Sound and Vibration*, vol. 218, pp. 177–204.

Ribner, H. (1969), 'Quadrupole Correlations Governing the Pattern of Jet Noise', *Journal of Fluid Mechanics*, vol. 38, pp. 1–24.

Schultz, T.J. (1978), 'Synthesis of Social Surveys on Noise Annoyance', *Journal of the Acoustical Society of America*, vol. 64, pp. 377–405.

Sheard, A.G., Corsini, A. and Bianchi, S. (2010), 'A Method of Detecting Stall in an Axial Fan', Patent No. GB 2,468,571 B, 24 December.

Sottek, R. and Genuit, K. (2007), 'Sound Quality Evaluation of Fan Noise Based on Hearing-related Parameters', *Proceedings of the 3rd International Symposium of Fan Noise*, Lyon, France, 17–19 September.

Spall, R.E., Gatski, T.B. and Grosch, C.E. (1987), 'A Criterion for Vortex Breakdown', *Physics of Fluids*, vol. 30, pp. 3434–3440.

Uchida, S., Nakamura, Y. and Ohsawa, M. (1985), 'Experiments on the Axisymmetric Vortex Breakdown in a Swirling Air Flow', *Transactions of the Japan Society for Aeronautical Space Sciences*, vol. 27, pp. 206–216.

Welch, P.D. (1967), 'The use of Fast Fourier Transform for the Estimation of Power Spectra: a Method Based on Time Averaging Over Short, Modified Periodograms', *IEEE Transactions on Audio and Electroacoustics*, vol. 15(2), pp. 70–73.

Wright, S.E. (1976), 'The Acoustic Spectrum of Axial Flow Machines', *Journal of Sound and Vibration*, vol. 45, pp. 165–223.

Wu, J.D. and Chuang, C.Q. (2005), 'Fault Diagnosis of Internal Combustion Engines using Visual Dot Patterns of Acoustic and Vibration Signals', *Independent Non-destructive Testing and Evaluation (NDT&E) International*, vol. 38, pp. 605–614.

Chapter 4

Experimental Aeroacoustic Studies on Improved Tip Configurations for Passive Control of Noise Signatures in Low-Speed Axial Fans

S. Bianchi, A. Corsini, F. Rispoli and A.G. Sheard

ABSTRACT

The chapter develops the near- and far-field correlation technique presented in Chapter 2 and coherence analysis technique presented in Chapter 3. Analysing the resultant coherence maps facilitated the dissection of fan blade span-wise noise sources. We calculated coherence by correlating fan near- and far-field acoustic measurements. We then created coherence maps by plotting coherence against blade span and frequency. The difference between coherence maps for the studied fan without blade-tip end-plates and with each of the studied end-plate geometries then enabled us to associate end-plate geometry with features on the coherence maps. We identified a total of six separate noise sources. The first occurred when the electric motor driving the fan. The second occurred with ingested noise from the fan inlet plenum. The third occurred with rotor induced noise. The fourth occurred with turbulence induced noise. The fifth occurred with secondary flow noise. The sixth occurred with the blade tip-to-casing leakage vortex bursting. Identifying span-wise noise sources and their association with blade-tip end-plates geometry enabled us to associate specific end-plate features with specific noise sources. We found changes in blade-tip end-plate geometry to have a significant effect on the multiple vortices induced in the blade tip-to-casing leakage flow by the end-plate's presence. Therefore, analysing the coherence maps provided an insight into the acoustic far-field consequences of aerodynamic near-field flow-field features. Analysing coherence maps clarified the far-field acoustic effect of blade-tip end-plate geometry and facilitated insight into the physical flow-field mechanisms responsible for fan far-field noise.

This chapter is a revised and extended version of Bianchi, S., Corsini, A., Rispoli, F. and Sheard, A.G. (2009), 'Experimental Aeroacoustic Studies on Improved Tip Configurations for Passive Control of Noise Signature in Low-Speed Axial Fan', *Transactions of the ASME, Journal of Vibration and Acoustics*, vol. 131, paper no. 061007, pp. 1–10.

NOMENCLATURE

Latin letters

BPF	blade-passing frequency [Hz]
Co	numerical value of the coherence function
f	frequency [Hz]
IN	inflow ingested noise
K_s	specific noise level, $K_s = SPL - 10\log_{10}(V \cdot \Delta p_{tot}^2)$
ℓ	blade chord
L	tip vortex length scale
MN	motor noise
Δp_{stat}	static pressure [Pa]
r	non-dimensional span
$\bar{r}$	non-dimensional radius
R_c	casing radius
Ro	Rossby number ($u/L\Omega$)
RN	rotor alone noise
SFN	secondary flow noise
SPL	sound pressure level
$\Im$	non-dimensional frequency (f/BPF)
t	blade pitch
TIN	turbulence-induced noise
u	characteristic velocity
VBN	noise-source region
V	volume flow rate

Greek letters

η_{tot}	total efficiency
Ω	tip leakage vortex rotation rate scale
σ_h	hub-to-casing diameter ratio

INTRODUCTION

Large axial flow air movement fans are classically used in applications in close proximity to populated areas. The generated tonal and broadband noise typically constitutes the dominant noise source of any system within which they are installed. Researchers in the 1970s, particularly Wright (1976) and Cumpsty (1977), have studied the link between the fan rotors' aerodynamic features and their acoustic emissions. Their findings have enhanced general understanding of axial turbomachinery aeroacoustics. Cumpsty (1977) concluded that, with the exception of the low-frequency range of high-speed machines, the mechanisms that determine broadband noise in subsonic fans are the same as those in supersonic tip-speed fans and compressors. Therefore, the design variables that impact tonal and broadband noise

are similar both for fans designed for aerospace and air movement application (Ganz *et al.*, 1998). According to Wright (1976), this is because of the prominence of rotor noise that originates from turbulent boundary layers.

When studying the acoustic performance of fans and compressors, both Cumpsty (1977) and Holste and Neise (1997) observed that the radiated acoustic energy was small compared with the energy transferred from blades to working fluid. The human ear is highly sensitive, able to perceive very low levels of acoustic energy that if transferred into useful work would result in an increase in aerodynamic efficiency so small it would be immeasurable. Consequently, it is challenging to characterise the far-field acoustic effect of near-field aerodynamic cause. Those scholars who have studied the link between near-field aerodynamic cause and far-field acoustic effect have identified significant unsteady or periodic forces, volume displacements and non-linear flow-features as dominant noise sources. These noise sources arise as a consequence of inflow-turbulence, impeller induced flow-features and features within the blade tip-to-casing flow-field (Sharland, 1964; Fukano *et al.*, 1977a, 1977b).

Researchers regard a fan's blade tip-to-casing flow as particularly important as it interacts with both wakes and blade-to-blade passage secondary flows. The blade tip-to-casing flow is one of the most significant sources of fan noise (Cumpsty, 1977; Nelson and Cooper, 1999). Several studies have attempted to resolve the causal aerodynamic relationship between fan blade-to-blade flow-field structures and fan far-field noise. Marcinowski (1953), the first researcher to study noise associated with tip dynamics, demonstrated that increases in broadband noise levels occur with increasing tip clearance. The largest changes in noise level were apparent at frequencies greater than the blade-passing frequency.

In contrast to Marcinowski (1953), Mugridge and Morfey (1972) argued that an optimum tip clearance exists when broadband noise is at a minimum due to the countervailing effects of the tip clearance flow and the blade-passage vortex. However, Longhouse (1978) did not confirm this result. He searched for a practical solution to the cooling fans' tip clearance noise and concluded that the unstable blade-tip vortex impacted the adjacent blade pressure side. He obtained the lowest noise levels with the smallest possible tip clearance. Fukano and Jang (2004) reported similar findings; whereas, Kameier and Neise's (1997) experiments demonstrated that, with the smallest possible tip clearance, noise reduced over a limited frequency range, close to the blade passage frequency. However, random noise actually increased.

During the past decade, researchers have proposed technical concepts to facilitate assessing air movement fan aeroacoustic properties. Researchers based their experimental techniques, to varying degrees, on previous fan (Leggat and Siddon, 1978; Bianchi *et al.*, 2009a, 2009b), radial pump rotor (Mongeau *et al.*, 1995) and turbofan engine (Kameier and Neise, 1997; Miles, 2006) studies. These researchers share a common goal- to isolate and identify the aerodynamic flow features responsible for the fan or the compressors' aeroacoustic signature. By isolating the individual noise sources, researchers aim to identify their individual acoustic signature, their spectral distribution along the blade span and ultimately their contribution to overall far-field fan or compressor noise.

Isolating and characterising individual noise sources is challenging; however, some scholars have successfully elucidated aspects of the flow-field physics. Leggat and Siddon (1978) studied the interaction between a naturally occurring vortex and axial fan noise. They used a cross-correlation between a near-field pressure probe located in the blade tip region and the noise recorded by a far-field microphone. Mongeau *et al.* (1995) investigated the noise emitted by a ducted centrifugal pump. They used a 'noise-to-noise' cross-correlation between the pump casing and the far-field. Kameier and Neise (1997) measured the blade tip-to-casing clearance flow generated noise for a ducted low-speed axial fan. They used a 'noise-to-noise' cross-correlation as a detection tool for rotating flow instabilities. Miles (2006) developed a test rig at the NASA Glenn Research Centre that he used for measuring the core-noise of a turbofan engine. He used an array of four far-field microphones. He arranged the microphones around the turbofan inlet and correlated the measured noise with turbofan near-field pressure perturbations.

Laurendeau *et al.* (2007) studied near-field to far-field acoustic and pressure correlations in subsonic jets. They concluded that the far-field acoustic spectrum consists of a combination of low and high frequency features. The low-frequency features occurred with aerodynamic features in the near-field. The high frequency features occurred with acoustic pressure fluctuations in the near-field. Laurendeau *et al.* (2007) concluded that unsteady pressure fluctuations in the near-field represent both the aerodynamic cause and the acoustic effect of fan far-field noise in different frequency ranges.

This chapter presents the results of a research programme to develop the near- and far-field correlation technique presented in Chapter 2 and coherence analysis technique presented in Chapter 3. Analysing the resultant coherence maps facilitated the dissection of fan blade span-wise noise sources that enables us to clarify the acoustic effect of blade-tip end-plate geometry. The analysis facilitated insight into the physical flow-field mechanisms responsible for fan far-field noise, which is an essential pre-cursor to developing a more detailed understanding of the aeroacoustic mechanisms at play along the blade span. Detailed understanding of span-wise aeroacoustic mechanisms thus facilitates developing blade-tip end-plates that more effectively minimise fan far-field noise.

METHODOLOGY

Our research objective was first, to develop a methodology to characterise the aeroacoustic noise sources along the fan blade span. Second, we wanted to confirm the difference in aeroacoustic emissions that result from using different blade-tip end-plate geometry. Third, we wanted to demonstrate the reliability of the developed measurement technique by correlating experimental results from the blade-tip region with results reported in Chapter 2.

The developed measurement technique enabled us to isolate and identify the aerodynamic flow features responsible for the fan's aeroacoustic signature. By iso-

lating the individual noise sources we aim to identify their individual acoustic signature, their spectral distribution along the blade span and ultimately their contribution to overall far-field fan noise. The resulting experimental technique enabled us to measure noise source distribution along the blade-span. We achieved this span-wise measurement by traversing a near-field microphone from blade hub to blade tip, whilst simultaneously measuring fan far-field noise. We used far-field measurements when the near-field microphone was not present to compensate for the near-field microphone's acoustic effect when present. Lastly, we followed Leggat and Siddon's methodology (1978) to avoid pseudo sound becoming coherent by optimising the near-field microphone's distance from the fan blade trailing edge.

Family of Fans

We conducted the reported research on a family of commercially available cooling fans. The studied fan configuration, coded AC90/6, incorporates a six-blade un-swept rotor, with modified ARA-D profile aerofoils blade, Table 4.1. One may set the blade-pitch angle during final assembly to customise the fan to a desired duty point. We used a direct coupled-induction 400-volt (AC), 3-phase motor to drive the rotor at a constant speed of 950 rpm, resulting in a 44.7 m/s blade tip speed and a 95 Hz blade-passing frequency (BPF). In its original embodiment the studied fan did not include a blade tip end-plate, therefore we used it as a *datum* against which to assess the performance of fan variants with blade tip end-plates. In the reported research we refer to the fan without blade tip end-plates as the fan *datum* AC90/6.

Table 4.1. *The fan* datum *AC90/6 blade geometry and rotor specification.*

	Fan *datum* AC90/6		
Blade geometry	Hub	Mid-span	Tip
Pitch angle (°)	36	58.8	28
Camber angle (°)	46	44	41
Solidity	1.24	0.86	0.30
Fan rotor			
Blade number		6	
Blade tip pitch angle (°)		16–28	
Blade tip stagger angle (°)		74–62	
Hub-to-casing diameter ratio ν		0.22	
Tip diameter (mm)		900.0	
Rotor tip clearance χ (% span)		1.0	
Rated rotational frequency (r/min)		935–950	

Passive Noise-control Devices

In addition to the fan *datum* AC90/6, we studied two fan variants. The first was fitted with a constant thickness blade-tip end-plate and the second with a variable thickness blade-tip end-plate, Figure 4.1. When fitted with a constant thickness blade-tip end-plate, we named the fan AC90/6/TF. When fitted with the variable thickness blade-tip end-plate, we named the fan AC90/6/TF$_{VTE}$. The effect of both the constant and variable thickness blade-tip end-plate is to reduce the blade tip-to-casing clearance-to-thickness ratio, Table 4.2. Reducing the blade tip-to-casing clearance-to-thickness ratio results in a general reduction in flow though the blade tip-to-casing gap and specifically influences the flow-field structures that develop in the clearance flow.

Designs developed for tip-vortex control and drag reduction in aircraft wings and catamaran hulls inspired the constant thickness blade-tip end-plate design. The constant thickness blade-tip end-plate ran along the blade pressure surface, ending at

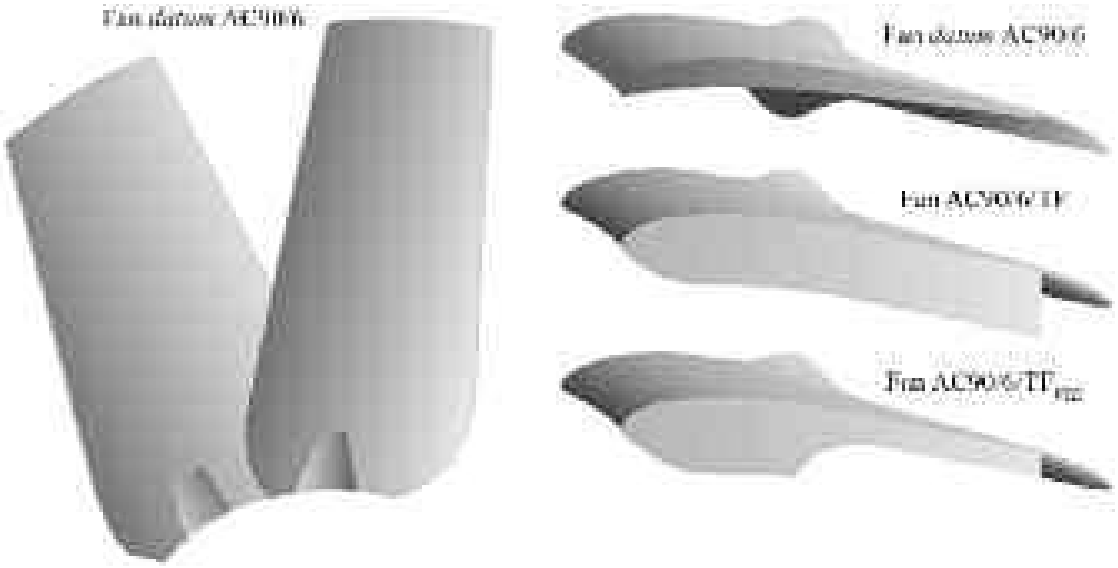

FIGURE 4.1. The studied fan *datum* AC90/6 without a fitted blade-tip end-plate, with a constant thickness blade-tip end-plate, AC90/6/TF and with a variable thickness blade-tip end-plate, AC/6/TF$_{VTE}$.

Table 4.2. *The impact of constant and variable thickness blade-tip end-plates on the blade tip-to-casing clearance-to-thickness ratio.*

	Blade tip-to-casing clearance-to-thickness ratio at the leading edge	Blade tip-to-casing clearance-to-thickness ratio at the trailing edge
Fan *datum* AC90/6	0.53	0.53
Fan AC90/6/TF	0.12	0.12
Fan AC90/6/TF$_{VTE}$	0.12	0.27

the blade trailing edge with a square tail. The addition of this constant thickness blade-tip end-plate resulted in the thickness of the fan AC90/6/TF blade tip increasing by a factor of three compared to the fan *datum* AC90/6. We considered Inoue *et al.*'s (1986) research regarding blade-tip end-plate size for axial compressor blades. They estimated that the optimum blade-tip end-plate size was between 10 and 20 per cent blade span. In practice, we were able to manufacture blades with a blade-tip end-plate size five per cent of blade span. The fan blades were manufactured from injection moulded plastic, with the blade-tip end-plate size the largest the blade manufacturing technique could produce.

Corsini and Sheard (2007) studied both the fan *datum* AC90/6 and AC90/6/TF using a blade-tip vortex 'breakdown criteria' based on Rossby number (Spall *et al.*, 1987). Following Ito *et al.*'s method (1985), they concluded that there is a threshold value of Rossby number below which the vortex rotation cannot reduce if the vortex is to remain stable. Uchida *et al.* (1985) and Garg and Leibovich (1979) defined this critical Rossby number range. Uchida *et al.* (1985) defined a critical Rossby number associated with the breakdown of an axi-symmetric vortex in a swirling flow. Garg and Leibovich (1979) also defined a critical Rossby number associated with an aircraft wing tip vortices' breakdown.

Corsini *et al.* (2006) first presented the fan AC90/6/TF$_{VTE}$ with a more complete treatment of the blade-tip end-plate design methodology presented by Corsini and Sheard (2007). Corsini *et al.* (2006) studied the aerodynamic and acoustic performance of the fan *datum* AC90/6 and fan AC90/6/TF, identifying a breakdown of the fan AC90/6/TF blade tip-to-casing leakage vortex. Vortex breakdown is acoustically productive, and therefore Corsini *et al.* (2006) concluded that a revised blade-tip end-plate design was desirable that avoided leakage vortex breakdown. Corsini and Sheard (2007) developed a blade-tip end-plate design methodology that successfully eliminated the leakage vortex breakdown by adding a variable thickness blade-tip end-plate.

This chapter extends Bianchi *et al.*'s work (2009b) by adding a step between the blade tip and end-plate along the blade suction surface from the blade leading to trailing edge. We added this step to both the fan AC90/6/TF and fan AC90/6/TF$_{VTE}$. The addition of the step resulted in five separate fan configurations:

- the fan *datum* AC90/6, without a fitted blade-tip end-plate;
- the fan AC90/6/TF, with a constant-thickness blade-tip end-plate;
- the fan AC90/6/TF$_{VTE}$, with a variable-thickness end-plate;
- the fan AC90/6/TF$_{step}$, with a constant-thickness blade-tip end-plate plus step; and
- the fan AC90/6/TF$_{VTE\ step,}$ with a variable-thickness blade-tip end-plate plus step.

We studied both the aerodynamic and acoustic performance of all five configurations in order to compare the performance of the stepped configurations with the same configuration without the step, and with the *datum* configuration.

Flow Conditions

The studied fan blade tip pitch angle is adjustable and may be set to a pitch angle between 16 and 28 degrees. In practical application the blade tip pitch angle is typically set to 28 degrees as this maximises flow rate for a given system pressure. In the research reported in this chapter, we conducted the majority of the experimental measurements with the fan blade tip pitch angle to 28 degrees. We selected 28 degrees because it is typical of the angle used in practical application and because it results in the highest blade loading. A highly loaded blade results in the blade tip-to-casing vortex having the most significant effect on both fan aerodynamic and acoustic performance (Holste and Neise, 1997). In addition to the experimental measurements with a blade tip pitch angle of 28 degrees, we also conducted a limited number of measurements with blade tip pitch angles of 16 and 24 degrees. We undertook these lower angle tests to place the 28 degree measurements into context and to assist with their interpretation.

The impact of the blade tip-to-casing vortex on both fan aerodynamic and acoustic performance results in the application of blade-tip end-plates changing not only the fan's acoustic performance, but also the aerodynamic performance. Consequently, the fan *datum* AC90/6 generates a different pressure at a constant flow rate when fitted with each of the studied blade-tip end-plates. To facilitate the comparison of fan performance data when fitted with different blade-tip end-plates, we chose to define three operating points, and their respective volume flow rates, Table 4.3. The design operating point volume flow rate is typical of that required when one installs the fan over the cooling unit's tube bank. The peak pressure flow rate is typical of that required when the tube bank has become partially blocked following a period of in-service operation. The maximum flow operating point volume flow rate is typical of the flow rate associated with the lowest pressure loss tube banks currently operating in service.

Bianchi *et al.* (2009a) measured the performance characteristics of the fan *datum* AC90/6, AC90/6/TF and AC90/6/TF$_{VTE}$. We measured the performance characteristics of the fan AC90/6/TF$_{step}$ and AC90/6/TF$_{VTE\ step}$ in accordance with ISO 5801:2007 requirements (2007). The measured performance characteristics illustrate the impact on pressure rise of blade-tip end-plate geometry, Figure 4.2. The addition

Table 4.3. *The operating points used when characterising the studied fan's performance with and without fitted blade-tip end-plates. The authors measured performance characteristics in a Type D standardised airway (ducted inlet, ducted outlet) in accordance with ISO 5801:2007 requirements (2007).*

Operating point	Volume flow rate (m^3/s)	Studied blade tip pitch angle (°)
Maximum flow	7.0	28
Design	6.5	28
Peak pressure	5.6	28

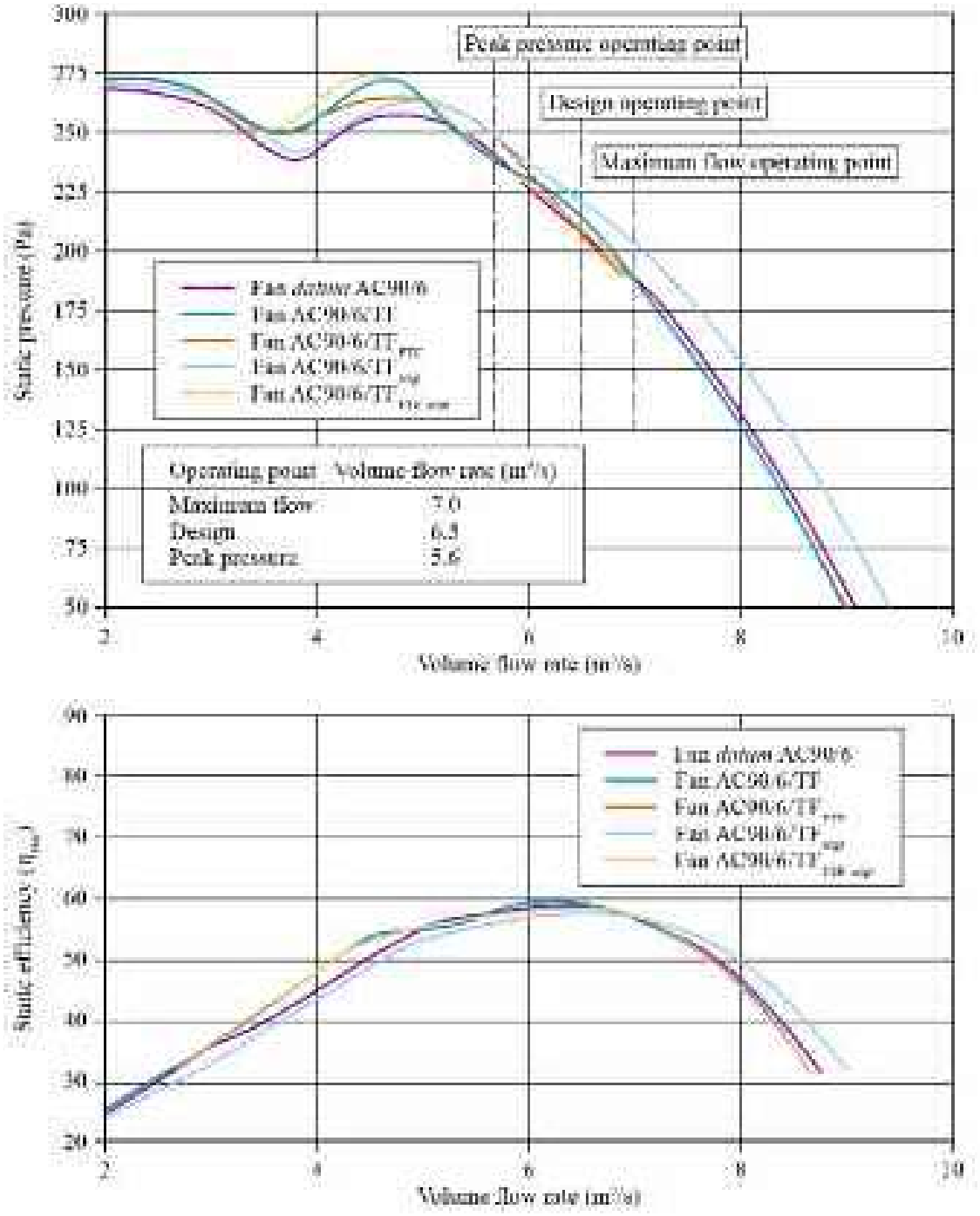

FIGURE 4.2. The performance characteristics of fan *datum* AC90/6 without a fitted blade-tip end-plate, with a constant thickness blade-tip end-plate, AC90/6/TF, with a variable thickness blade-tip end-plate, AC/6/TF$_{VTE}$, with a constant thickness blade-tip end-plate and step, AC90/6/TF$_{step}$ and with a variable thickness blade-tip end-plate and step, AC/6/TF$_{VTE\ step}$. The authors measured performance characteristics with the blade tip pitch angle set to 28 degrees in a Type D standardised airway (ducted inlet, ducted outlet) in accordance with ISO 5801:2007 requirements (2007).

of the four studied blade-tip end-plates results in a change in blade loading. That change is typically an increase in blade loading over the majority of the fan operating range. We would expect blade-tip noise sources to become more acoustically productive with increasing blade loading. Therefore, an increase in blade loading will offset partially any reduction in fan far-field noise attributed to adding a blade-tip end-plate. We must conservatively assess the reduction in fan far-field noise if one neglects increased blade loading. Therefore, despite fan far-field noise serving as a blade loading function, we chose to neglect the change in pressure rise with the change in blade-tip treatment.

We may assess the validity of our assumption that we may neglect change in pressure rise with change in blade-tip treatment by considering fan specific noise level (K_S), Figure 4.3. The four studied fans with blade-tip end-plates demonstrate lower specific noise levels than the fan *datum* AC90/6. As pressure rise increases towards the fan's peak pressure operating point, both fan AC90/6/TF and AC90/6/TF$_{VTE}$ specific noise levels increased from a minimum that occurs with a pressure rise close to the fan's design operating point. The same trend in specific noise level is evident for the fans AC90/6/TF$_{step}$ and AC90/6/TF$_{VTE\ step}$. It is noted-

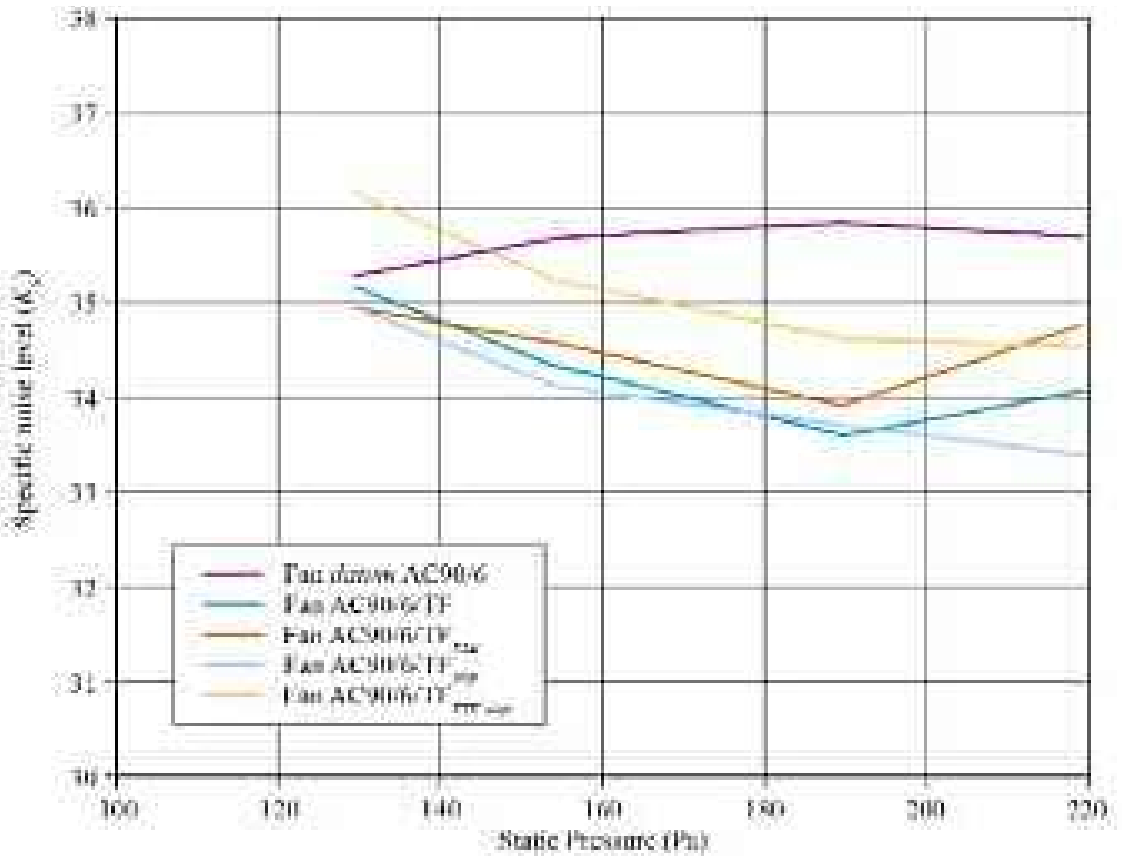

FIGURE 4.3. Specific noise level (K_S) over the fan's operating range for the fan *datum* AC90/6 without a fitted blade-tip end-plate, with a constant thickness blade-tip end-plate, AC90/6/TF, with a variable thickness blade-tip end-plate, AC/6/TF$_{VTE}$, with a constant thickness blade-tip end-plate and step, AC90/6/TF$_{step}$ and with a variable thickness blade-tip end-plate and step, AC/6/TF$_{VTE\ step}$. The authors measured specific noise level with the blade tip pitch angle set to 28 degrees.

worthy that the step feature has a more positive impact when fitted to the constant thickness, as opposed to the variable thickness blade-tip end-plate.

Axial fans classically exhibit an increase in the amplitude of discrete frequency tones as they approach stall (Fukano *et al.*, 1986). Therefore, we expected the increase in specific noise level as the four studied fans with blade-tip end-plates move from their design to peak pressure operating point. However, specific noise levels remain lower than that of fan *datum* AC90/6 over the entire fan operating range despite the increase in blade loading associated with having fitted a blade-tip end-plate. This reduction gives confidence in the effectiveness of the blade-tip end-plates.

EXPERIMENTAL METHODS

We conducted the experimental measurements in an anechoic chamber in accordance with ISO 10302:1996 requirements (1996) following Bianchi *et al.*'s method (2009a). We made acoustic measurements using microphones at the fan inlet and the outlet, recording the near- and far-field signals on two channels of a data acquisition system. An aerofoil louver in the top of the anechoic chamber inlet section facilitated the fan flow rate's variation. We aerodynamically optimised the fan inlet bell mouth profile to provide uniform and un-separated flow into the fan. The fan was connected to the outside environment via up- and down-stream plenums. These plenums were designed to minimise in-flow non-uniformities and we treated them acoustically to both minimise noise transmission from the external environment and its reflection inside plenum ductwork. We also covered the anechoic chamber walls with foam panels to further reduce noise transmission from the external environment.

Cross-correlating the near- and far-field measurements to differentiate near-field noise sources from the far-field noise enabled us to avoid pseudo sound, which degrades measurement accuracy. Pseudo sound is turbulence-generated noise that one records in the near-field, but it decays so quickly that it does not contribute to the far-field noise. Mugridge and Morfey (1972), Holste and Neise (1997), Miles (2006) and Laurendeau *et al.* (2007) have successfully used the cross-correlation technique we adopted in the present study to correct pseudo sound in exhaust flows.

Near-field Acoustic Measurement Technique

Following Bianchi *et al.*'s method (2009a), we made near-field measurement at the fan outlet by mounting a microphone on a 10 mm radial traversing mechanism 10 per cent blade chord downstream of the blade trailing edge, Figure 4.4. We then used the traversing mechanism to move the near-field microphone from the blade hub to tip, in radial steps corresponding to two per cent of blade span. This facilitated the span wise measurement of near-field fan noise. Bianchi *et al.* (2009a) provide a more complete description of the near-field acoustic measurement technique.

FIGURE 4.4. Microphone arrangement for inlet near-field measurements (left) and outlet near-field measurements (middle) of fan noise (Bianchi *et al.*, 2009a). The microphone used for outlet near-field measurements could be traversed from the blade hub to tip, right.

Far-field Acoustic Measurements Technique

Again, following Bianchi *et al.*'s method (2009a), we measured far-field noise six fan diameters from the fan exhaust, as recommended by Leggat and Siddon (1978) when measuring a fan's far-field noise without any obstructions downstream of the fan. Leggat and Siddon (1978) studied the directivity of fan noise in a semi-reverberant environment concluding that the maximum noise levels were coincident with the fan axis, immediately downstream of the exhaust. In the research reported in this chapter, we chose to place the far-field microphone at an angle 30 degrees from the fan axis, Figure 4.5. This was to avoid the possibility of the fan exhaust flow impacting directly on the far-field microphone. Our logic was that the anechoic chamber within which we made our measurements was not infinitely large. Consequently, there was a possibility that the fan would induce flow-field features within the anechoic chamber itself that may have acoustic consequences. Bianchi *et al.* (2009a) provide a more complete description of the near-field acoustic measurement technique.

EXPERIMENTAL RESULTS

Bianchi *et al.* (2009a) studied the span-wise distribution of near-field noise sources and the correlation of near- and far-field noise. Bianchi *et al.*'s (2009a) coherence analysis is effective as a consequence of its ability to identify coherent features within the data when those features have only very low energy. Therefore, Bianchi *et al.* (2009a) were able to identify coherent features in the data that others may have overlooked using different analysis techniques. In the programme of work reported in this chapter, we present an analysis of the coherence between data recorded with the traversing microphone and the far-field microphone. We recorded all data at the design operating point. Unless otherwise stated, we used the traversing microphone to record data over a range of span-wise locations from blade hub to tip.

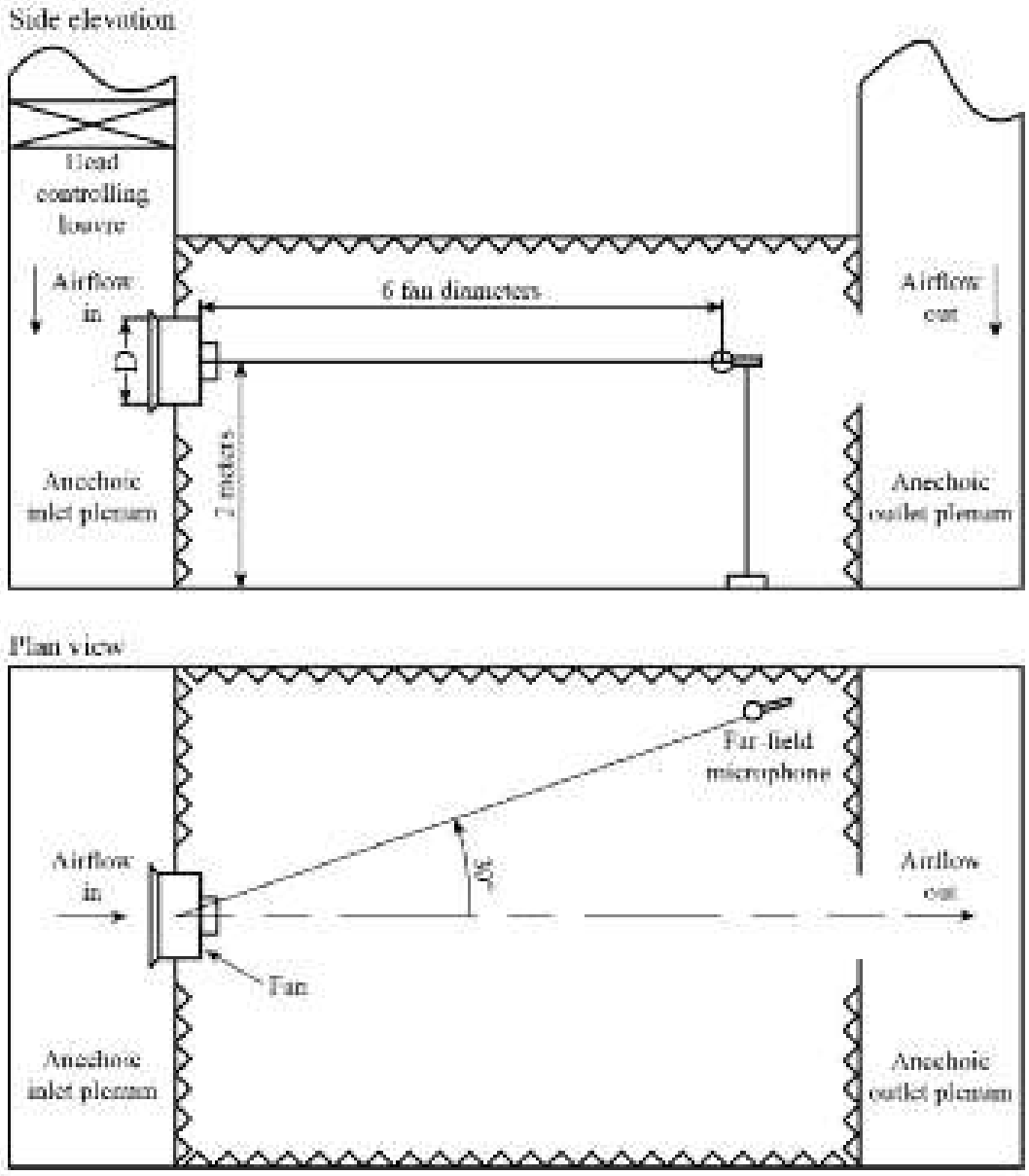

FIGURE 4.5. Microphone arrangement for outlet far-field measurements of fan noise in the anechoic chamber used for near- and far-field fan outlet noise measurements.

Dissection of Rotor-noise Sources

To facilitate interpreting the coherence data, Bianchi *et al.* (2009b) presented 'maps' of the radial distribution of coherence against normalised frequency. Bianchi *et al.* (2009b) define normalised frequency (*Sf*) as frequency divided by blade passing frequency. Therefore, for example, a normalised frequency of one is the blade passing frequency. In their analysis Bianchi *et al.* (2009b) examined coherence maps for the fan *datum* AC90/6, AC90/6/TF and AC90/6/TF$_{VTE}$ over a normalised frequency range from zero to eighteen. In this chapter we extend Bianchi *et al.*'s coherence analysis (2009b) as we examine coherence maps for the five studied fan configurations over a normalised frequency range of zero to seven.

Consider the coherence map for the fan *datum* AC90/6, Figure 4.6. There is a non-tonal coherent phenomenon in the blade tip's vicinity. Bianchi *et al.* (2009b) characterised this coherent phenomena feature at the blade tip as turbulence induced noise (TIN). The turbulence induced noise occurs as a consequence of the interaction between blade tip-to-casing leakage vortex and the blade wake. The maximum coherence of the turbulence induced noise is 0.6, indicating the uncorrelated nature of this noise source. We would expect this noise source to be uncorrelated as the acoustic emissions emanate from mixing vortices with different structure and rotational frequency.

There is also a second non-tonal coherent phenomenon in the vicinity of the blade hub. Bianchi *et al.* (2009b) characterised this coherent phenomena feature at the blade hub as secondary flow noise (SFN). This occurs as a consequence of a blade hub corner stall interacting with the blade-to-blade passage vortex. The maximum coherence of the turbulence induced noise is 0.6, indicating this noise source's uncorrelated nature. We would expect this noise source to be uncorrelated as the acoustic emissions emanate from mixing two secondary flow features with different structure and rotational frequency.

In addition to the non-tonal coherent phenomenon, Bianchi *et al.* (2009b) isolated three tonal coherent phenomena. The first is associated with the fan motor. The fan motor produces isolated tones at normalised frequencies of approximately three and between five and six, Figure 4.6. We may characterise these coherent phenomena features as motor noise (MN). Motor noise coherence reduces from 1.0 near the blade hub to 0.4 near the blade tip. We expect this reduced coherence with increasing blade span as the motor is located behind the blade hub and therefore, we would expect it to influence the hub more than the tip region.

There is also a second tonal coherent phenomenon. The studied fan is a low-speed fan, with peak velocities typically no more than half the speed of sound. Therefore, the fan rotor is able to induce distortions in the flow-field upstream of the fan. Isolated tones at normalised frequencies of 0.25 and 0.66 characterise the coherence map, Figure 4.6. Cumpsty (1974) first studied the low-frequency tones produced as a consequence of induced distortions in the flow-field upstream of the fan. As the inflow distortions induced in the inflow by the fan rotor's rotation produced these tones, Cumpsty (1974) characterised them as rotor induced noise. We may characterise this coherent phenomena feature as rotor noise (RN).

The third tonal coherent phenomenon is clearly evident at a normalised frequency of two that becomes progressively more intense as we move from the blade hub to tip. This is the second blade passing frequency, with a maximum coherence of 0.7 at 80 per cent blade span, Figure 4.6. Previous scholars who have characterised the second blade passing frequency (Magliozzi *et al.*, 1973; Cumpsty, 1974, 1977), concluded that it may occur with an inflow disturbance into the fan. Therefore, this coherence map feature may be ingested noise (IN).

Consider the coherence map for the fan AC90/6/TF, Figure 4.7. The fan AC90/6/TF induced noise (IN) tone was reduced compared to the induced noise tone for fan *datum* AC90/6, Figure 4.6. Generally, the same features as the fan *datum* AC90/6 coherence map characterise the fan AC90/6/TF coherence map, with the

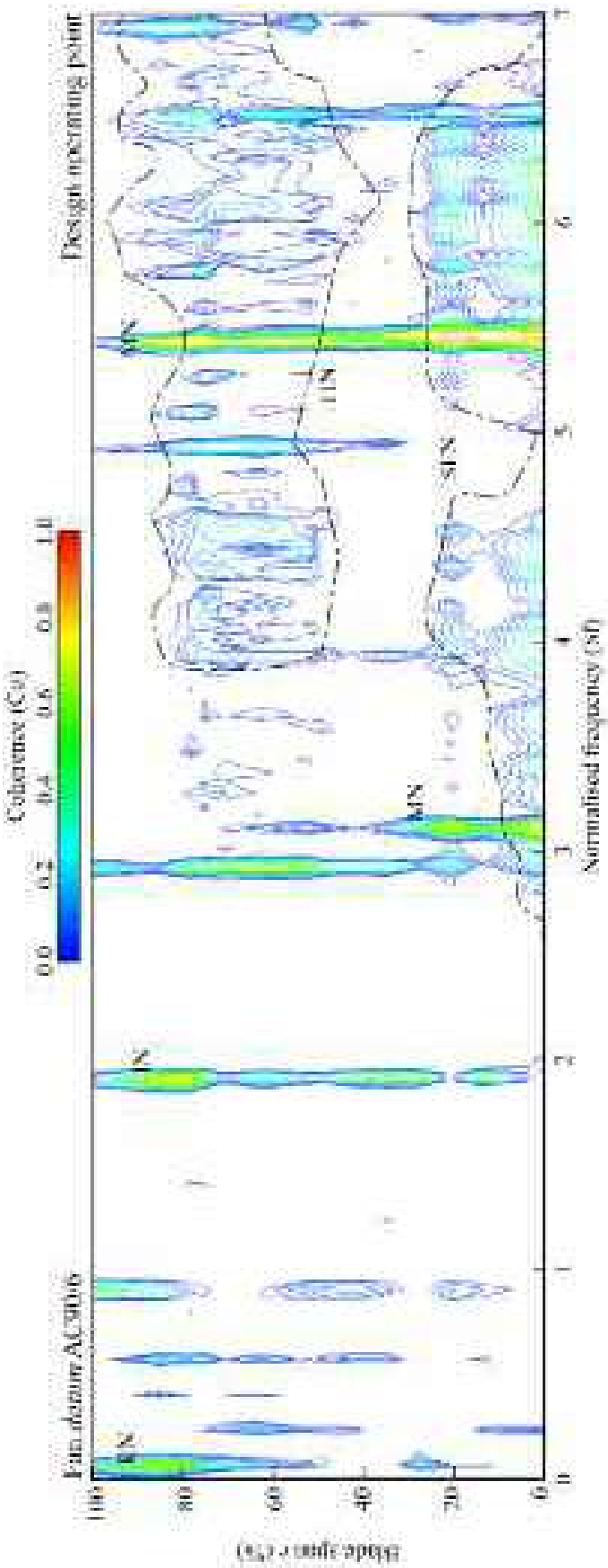

FIGURE 4.6. Fan *datum* AC90/6 span-wise map of normalised frequency (*Sf*), defined as measured frequency divided by the first blade passing frequency for normalised frequencies below seven. The map presents a span-wise distribution of coherence between near-field noise measured at the fan outlet and far-field noise (Bianchi *et al.*, 2009b).

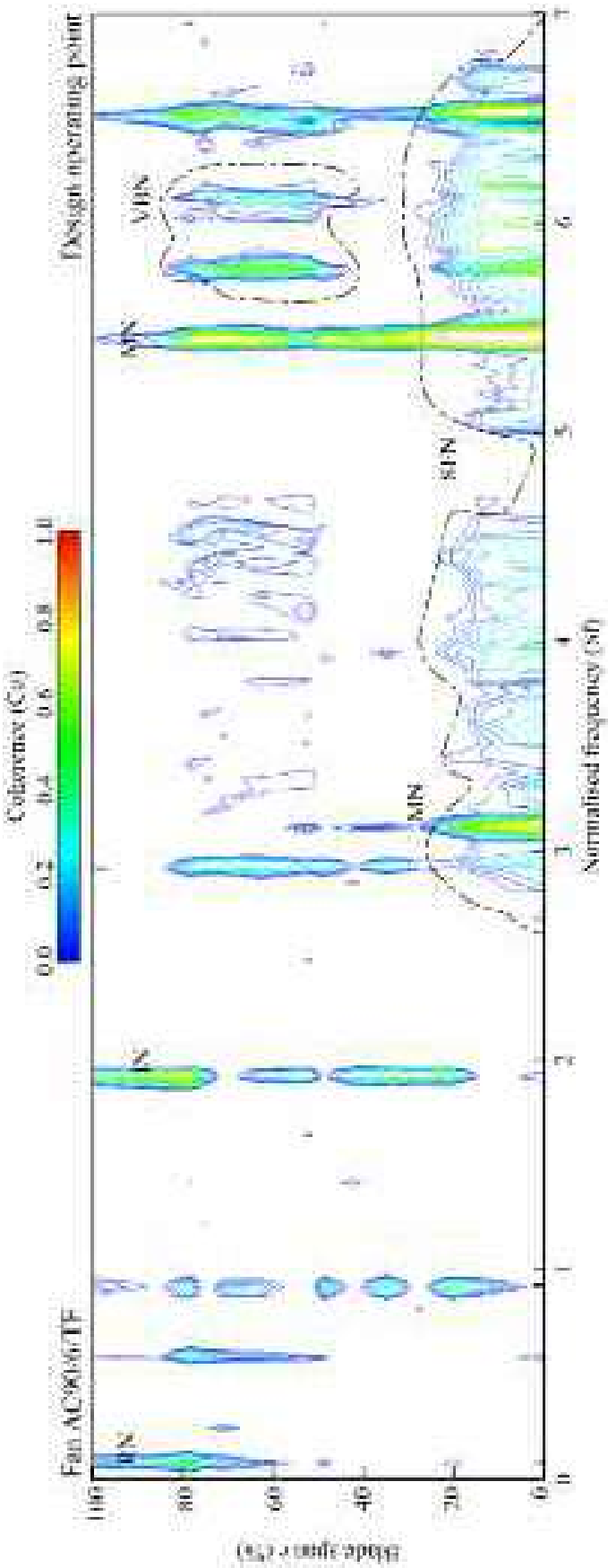

FIGURE 4.7. Fan AC90/6/TF span-wise coherence map for normalised frequencies below seven, Bianchi *et al.* (2009b). Normalised frequency (*Sf*) is defined as measured frequency divided by the first blade passing frequency.

exception of the turbulence induced noise (TIN) in the blade tip's vicinity. However, at a normalised frequency of approximately six, a pair of tonal peaks characterise the fan AC90/6/TF coherence map. The span-wise location and frequency of this pair of tonal peaks correlate with the blade tip-to-casing leakage vortex's location and bursting frequency. Therefore, Bianchi *et al.* (2009b) characterised this pair of tonal peaks as vortex bursting noise (VBN).

Having identified vortex bursting noise, a further review of the fan AC90/6/TF coherence map indicates that coherence of the hub secondary flow noise (SFN) was generally lower than for the fan *datum* AC90/6. This reduction in secondary flow noise coherence indicates that adding a constant thickness blade-tip end-plate results in better control of hub secondary flow features.

Consider the coherence map for the fan AC90/6/TF$_{VTE}$, Figure 4.8. A significant feature is the absence of coherence in the blade tip region at the blade passing frequency, a normalised frequency of one. This is as a consequence of a noise source attenuation originating from flow-field features interacting in the blade tip-to-casing flow. The vortex bursting noise also reduces in intensity in comparison with fan AC90/6/TF, and reduces from a double region at a normalised frequency of just below and above six to a single normalised frequency just below six. Therefore, Bianchi *et al.* (2009b) concluded that the variable thickness blade-tip end-plate effectively reduces the blade tip-to-casing leakage vortex impact on fan far-field noise.

We developed the variable thickness blade-tip end-plate for fan AC90/6/TF$_{VTE}$ to specifically avoid blade tip-to-casing leakage vortex breakdown. The fan AC90/6/TF$_{VTE}$ coherence map indicates that at a normalised frequency of one and six blade-tip noise sources have been eliminated. We may conclude that eliminating these noise sources is as a consequence of the blade tip-to-casing leakage vortex not bursting, with a resultant reduction in fan far-field noise. Therefore, we may conclude that the variable thickness blade-tip end-plate was effective.

Adding a step to the constant and variable thickness blade-tip end-plates was intended to introduce a step-expansion into the end-plate geometry. A step-expansion is a way to weaken organised vortical structures and therefore has the potential to make those structures less acoustically productive. Consider the coherence map for the fan AC90/6/TF$_{step}$ Figure 4.9. The tonal components are more coherent when compared to the tonal components of the coherence map for fan AC90/6/TF. In contrast, one of the two tonal peaks that occurs with vortex bursting noise has almost disappeared and the second peak's coherence is much reduced. The step feature also results in the coherent phenomena at the blade hub associated with secondary flow noise becoming slightly less coherent. Eliminating one vortex breakdown noise tone and reducing the coherence of the second combines with reducing the coherence of the secondary flow noise. Together they indicate that the step feature has reduced the overall coherence of noise sources linked to blade tip-to-casing flow.

Consider the coherence maps for the fan AC90/6/TF$_{VTE\ step}$ Figure 4.10. As with the constant thickness end-plate, the tonal components are more coherent when compared to the tonal components of the coherence map for fan AC90/6/TF$_{VTE}$. In contrast to the constant thickness blade-tip end-plate, the step feature does not reduce the tonal peaks' intensity that we associated with vortex bursting noise. A non-tonal

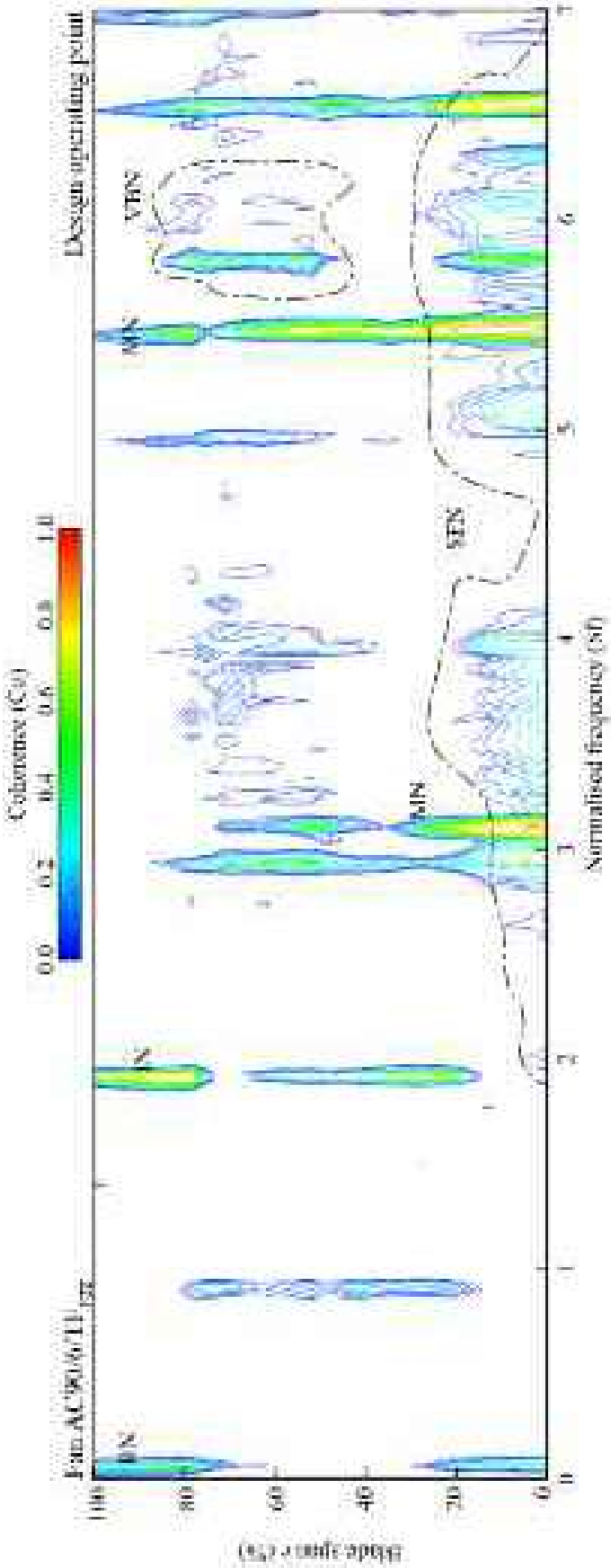

FIGURE 4.8. Fan AC90/6/TF$_{VTE}$ span-wise coherence map for normalised frequencies below seven, Bianchi *et al.* (2009b). Normalised frequency (*Sf*) is defined as measured frequency divided by the first blade passing frequency.

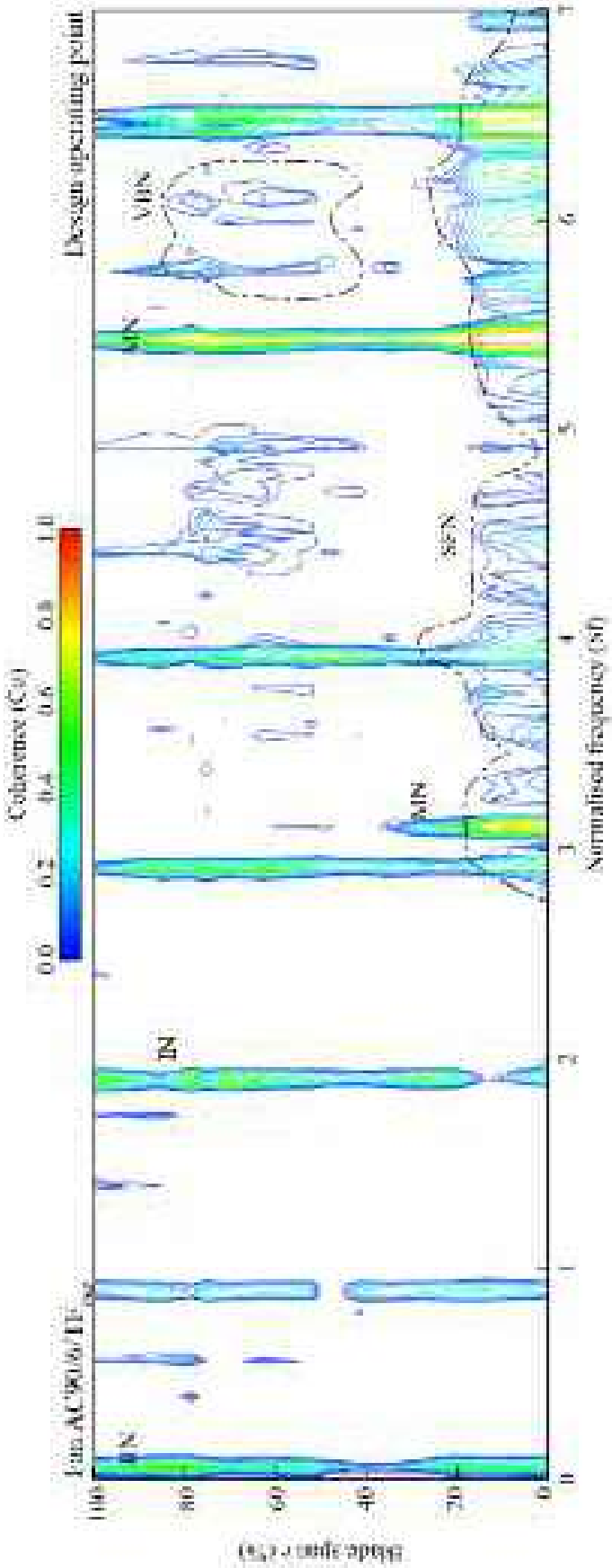

FIGURE 4.9. Fan AC90/6/TF$_{step}$ span-wise coherence map for normalised frequencies below seven. Normalised frequency (*Sf*) is defined as measured frequency divided by the first blade passing frequency.

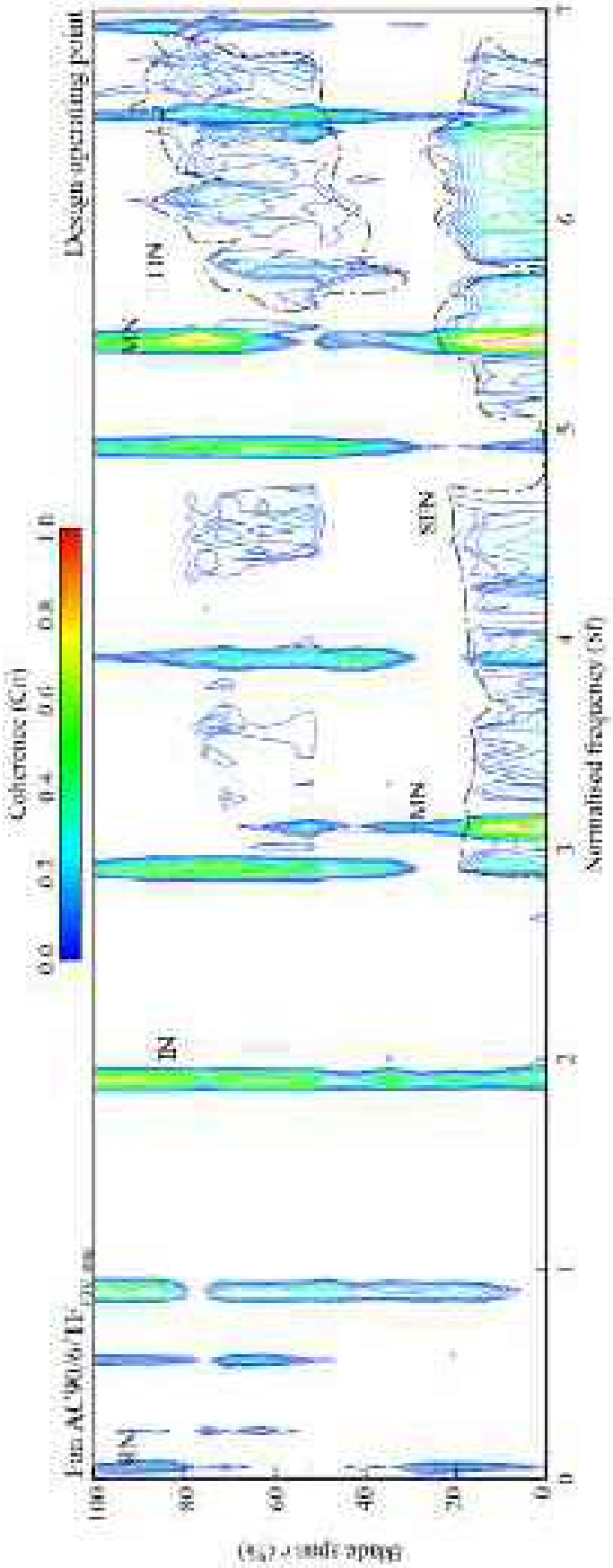

FIGURE 4.10. Fan AC90/6/TF$_{VTE,step}$ span-wise coherence map for normalised frequencies below seven. Normalised frequency (Sf) is defined as measured frequency divided by the first blade passing frequency.

coherent phenomenon in the blade tip's vicinity over a normalised frequency range of approximately five and a half to seven characterises the coherence map for fan AC90/6/TF$_{VTE\ step}$. A similar feature that Bianchi *et al.* (2009b) associated with turbulence induced noise characterises the fan *datum* AC90/6 coherence map. The turbulence induced noise occurs as a consequence of the interaction between blade tip-to-casing leakage vortex and the blade wake. Further, a larger and more coherent hub feature that occurs with secondary flow noise characterises the fan AC90/6/TF$_{VTE\ step}$ coherence map. In combination, the presence of the turbulence induced noise and increase in coherence of the secondary flow noise indicates that the step feature has made the variable thickness blade-tip end-plate more, not less acoustically productive.

A step-expansion is a way to weaken organised vortical structures and therefore has the potential to make those structures less acoustically productive. When we compare the specific noise level of fans AC90/6/TF and AC90/6/TF$_{step}$, it is apparent that the step feature has been effective for the fan AC90/6/TF, Figure 4.3. The specific noise level is consistently lower with the step feature than without. However, the step feature has not resulted in a universally beneficial effect when combined with the variable thickness blade-tip end-plate. Specific noise level is slightly lower at the high pressure operating point, but actually higher at low pressure operating points. We may conclude that the presence of the step feature does act as a mixing enhancer for the blade tip-to-casing flow-field features. However, it appears that the step feature introduces a cascade of smaller vortical structures that are collectively acoustically productive enough to increase fan far-field noise.

Influence of Operating Condition on Tonal Noise

We conducted the coherence analysis with data from the studied fan's design operating point. The design operating point volume flow rate is typical of that required when one installs the fan over the cooling unit's tube bank. However, one may use the fan at both a peak pressure and maximum flow operating point, Table 4.3. As these operating points bracket the design operating point, it is helpful to study coherence of all three. The change in coherence with operating point for the previously identified noise sources provides an additional insight into the flow-field physics.

Consider the outlet coherence spectrum measured at a span-wise location in the blade tip region at the maximum flow operating point for the five studied fan configurations, Figure 4.11. The studied fan's blade passing frequency is 95 Hz, with coherent tones evident at the blade passing frequency and its second and third harmonic. An effect of the blade-tip end-plates is to shift the peak coherence from odd to even blade passing frequency harmonics. The impact of the step feature is apparent, with both the constant and variable thickness blade-tip end-plates occurring with higher coherence at the first and third harmonic of blade passing frequencies. In contrast, the step feature results in reducing coherence at the second harmonic of blade passing frequency.

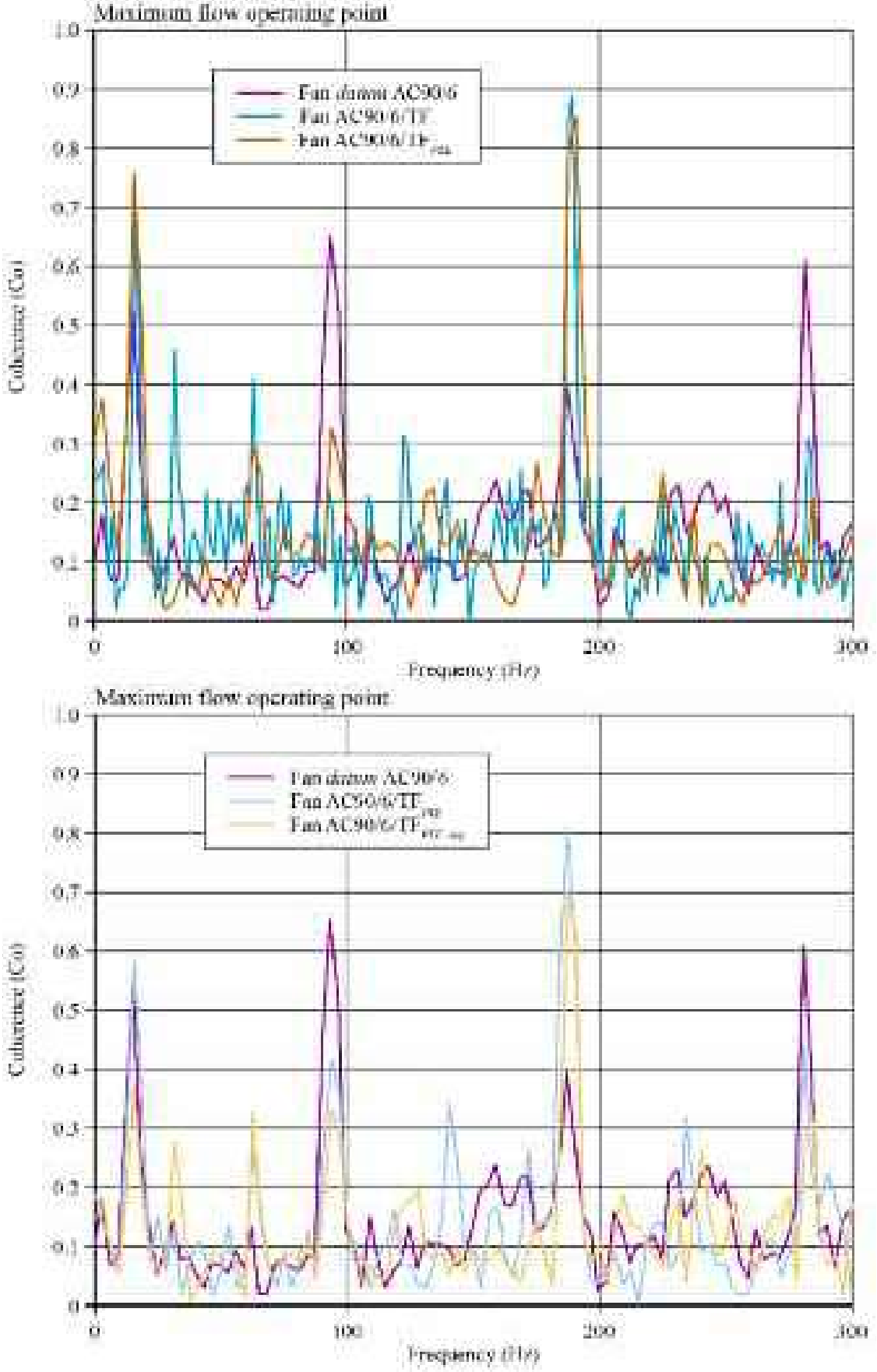

FIGURE 4.11. Fan outlet coherence spectrum measured at a span-wise location in the blade tip region at the fan maximum flow operating point. The outlet coherence spectrum illustrates the impact of blade-tip end-plates on near-field fan noise.

Consider the outlet coherence spectrum measured at a span-wise location in the blade tip region at the design operating point for the five studied fan configurations, Figure 4.12. The shift from maximum flow to design operating point results in an increased blade loading. This resulted in the fan AC90/6/TF and AC90/6/TF$_{VTE}$ coherence reducing at the second harmonic of blade passing frequency from over 0.8 to 0.55 and 0.7 respectively. Adding the step feature had little impact on the constant thickness blade-tip end-plate coherence. However, the variable thickness blade-tip end-plate coherence increased from 0.3 to 0.6 at the blade passing frequency. Therefore, the increase in blade loading resulted in fan AC90/6/TF$_{VTE\ step}$ tonal far-field noise that we may associate with a change in the blade tip-to-casing flow-field features.

Consider the outlet coherence spectrum measured at a span-wise location in the blade tip region at the peak pressure operating point for the five studied fan configurations, Figure 4.13. The shift from the design to peak pressure operating point results in a further increased blade loading. A striking effect of this change in blade loading is the loss of coherence for the fan AC90/6/TF$_{VTE}$ at the second blade passing frequency. For the other four studied fan configurations the second harmonic of blade passing frequency has the highest coherence. However, increasing coherence at frequencies higher than the second harmonic of blade passing frequency generally characterises the fan AC90/6/TF$_{VTE}$ coherence.

At the third harmonic of blade passing frequency both the fan *datum* AC90/6 and AC90/6/TF coherence increased. At the blade passing frequency the change in blade loading did not result in a change in coherence for the blade-tip end-plates with the step feature. At the design operating point fan *datum* AC90/6 coherence of 0.4 characterised the second harmonic of blade passing frequency. This increased to 0.75 at the peak pressure operating point. In contrast, both the constant and variable thickness blade-tip end-plate coherence remained constant at around 0.8 for both operating points. The increased coherence of the fan *datum* AC90/6 to a level similar to that of the four fan configurations with blade-tip end-plates may be significant. It may indicate that at higher blade loading blade-tip end-plates become less effective at reducing tonal fan far-field noise.

Influence of Operating Condition on Broadband Noise

We may also complement the analysis of outlet coherence spectrum in the blade tip region by analysing the operating point's influence on fan near-field noise. The change in fan near-field noise with operating point provides insight into the flow-field physics.

Consider the outlet near-field narrowband and broadband sound pressure level (L_P) spectrum measured at a span-wise location in the blade tip region and at the maximum flow operating point for the five studied blade-tip end-plates, Figures 4.14 and 4.15. The blade-tip end-plates without the step feature are ineffective in the narrowband, with sound power levels similar to that of the fan *datum* AC90/6. The blade-tip end-plates have some impact on the broadband, with the fan AC90/6/TF and AC90/TF$_{VTE}$ exhibiting lower sound power levels than the fan *datum* AC90/6.

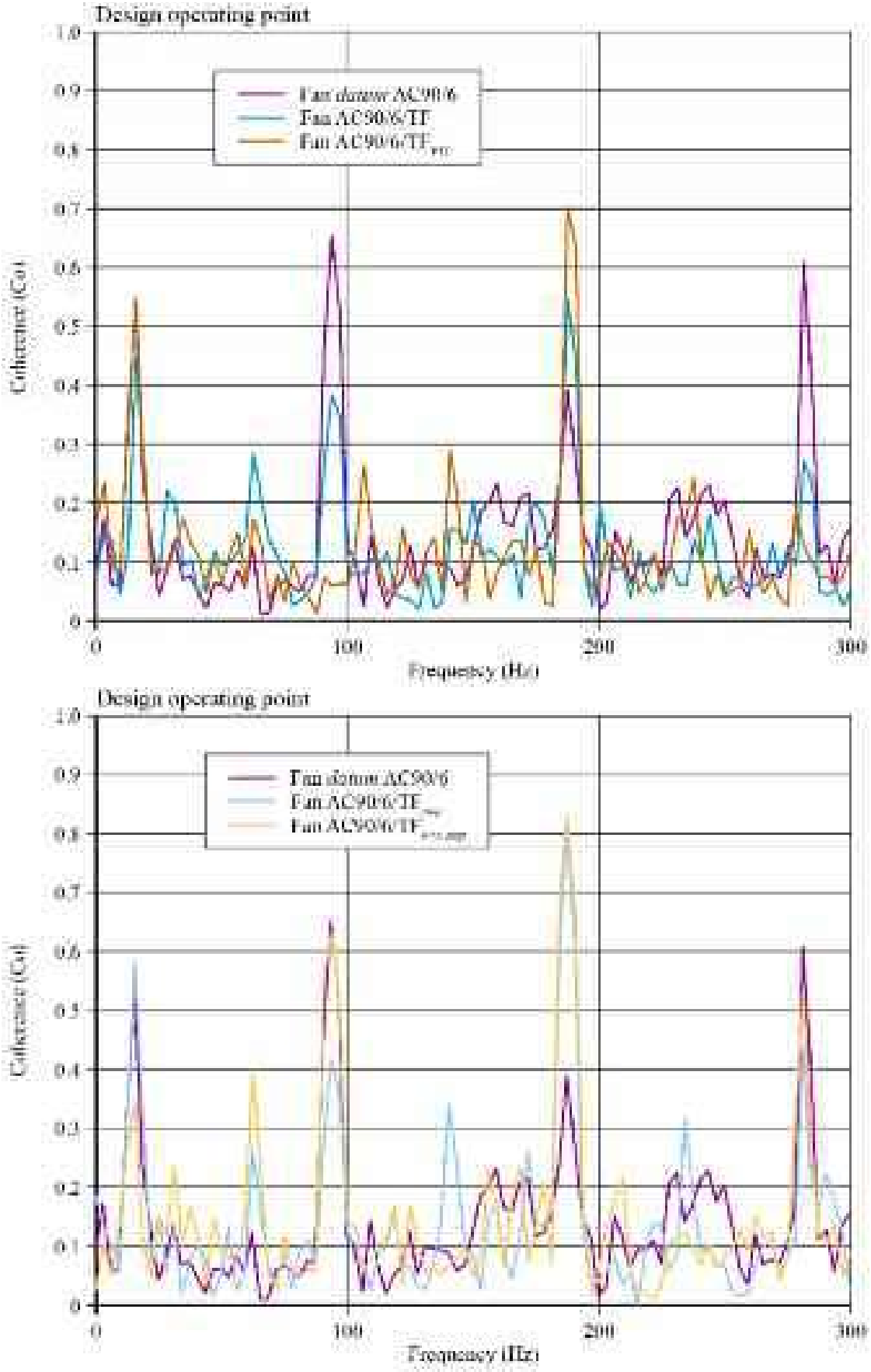

FIGURE 4.12. Fan outlet coherence spectrum measured at a span-wise location in the blade tip region at the fan design operating point. The outlet coherence spectrum illustrates the impact of blade-tip end-plates on near-field fan noise.

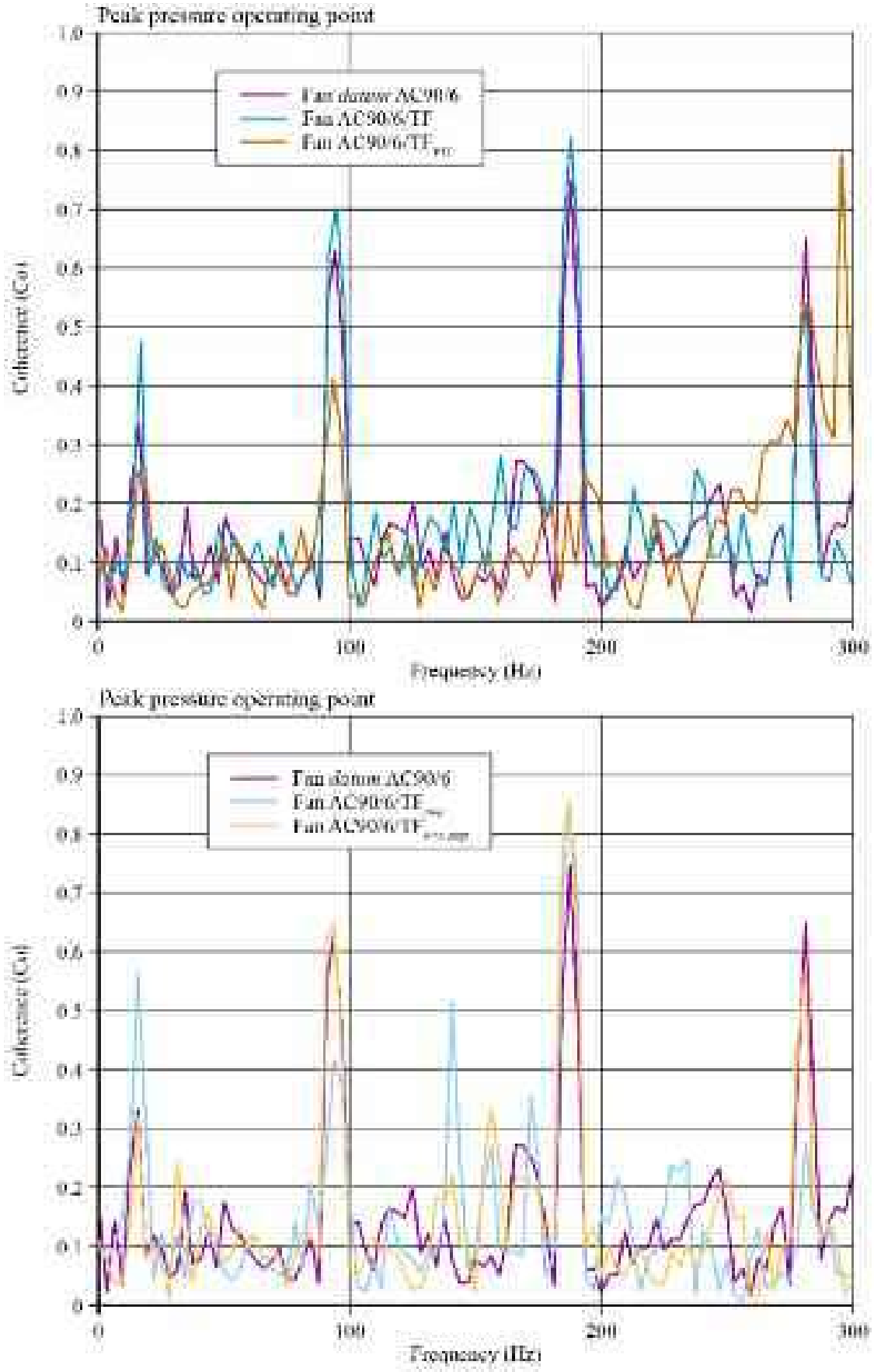

FIGURE 4.13. Fan outlet coherence spectrum measured at a span-wise location in the blade tip region at the fan peak pressure operating point. The outlet coherence spectrum illustrates the impact of blade-tip end-plates on near-field fan noise.

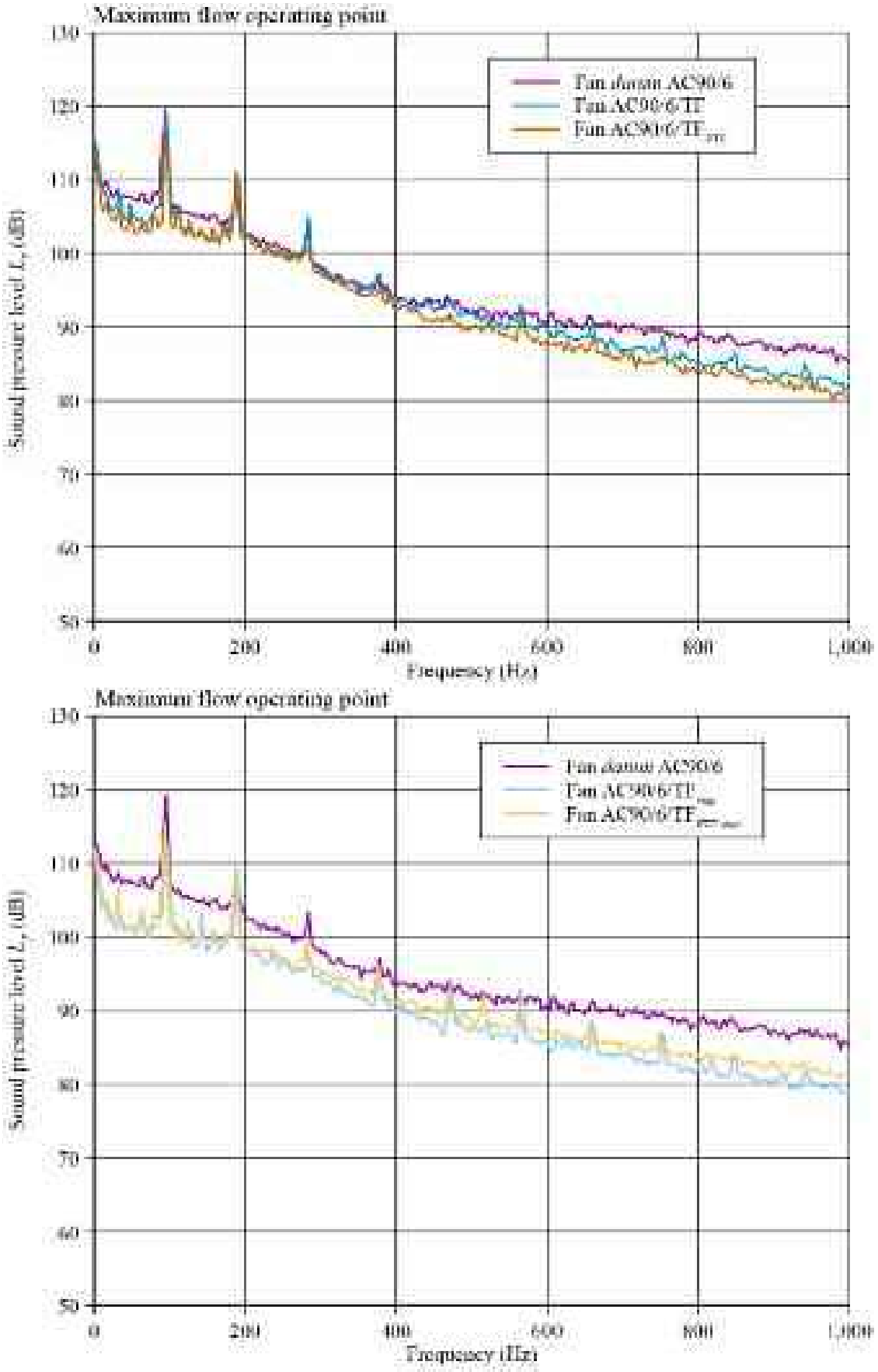

FIGURE 4.14. Outlet near-field narrowband sound pressure level (L_P) spectrum measured at a span-wise location in the blade tip region and at the fan maximum flow operating point for the five studied blade-tip end-plates. The narrowband sound pressure level illustrates the blade-tip end-plates' impact on the near-field narrowband sound pressure level spectrum.

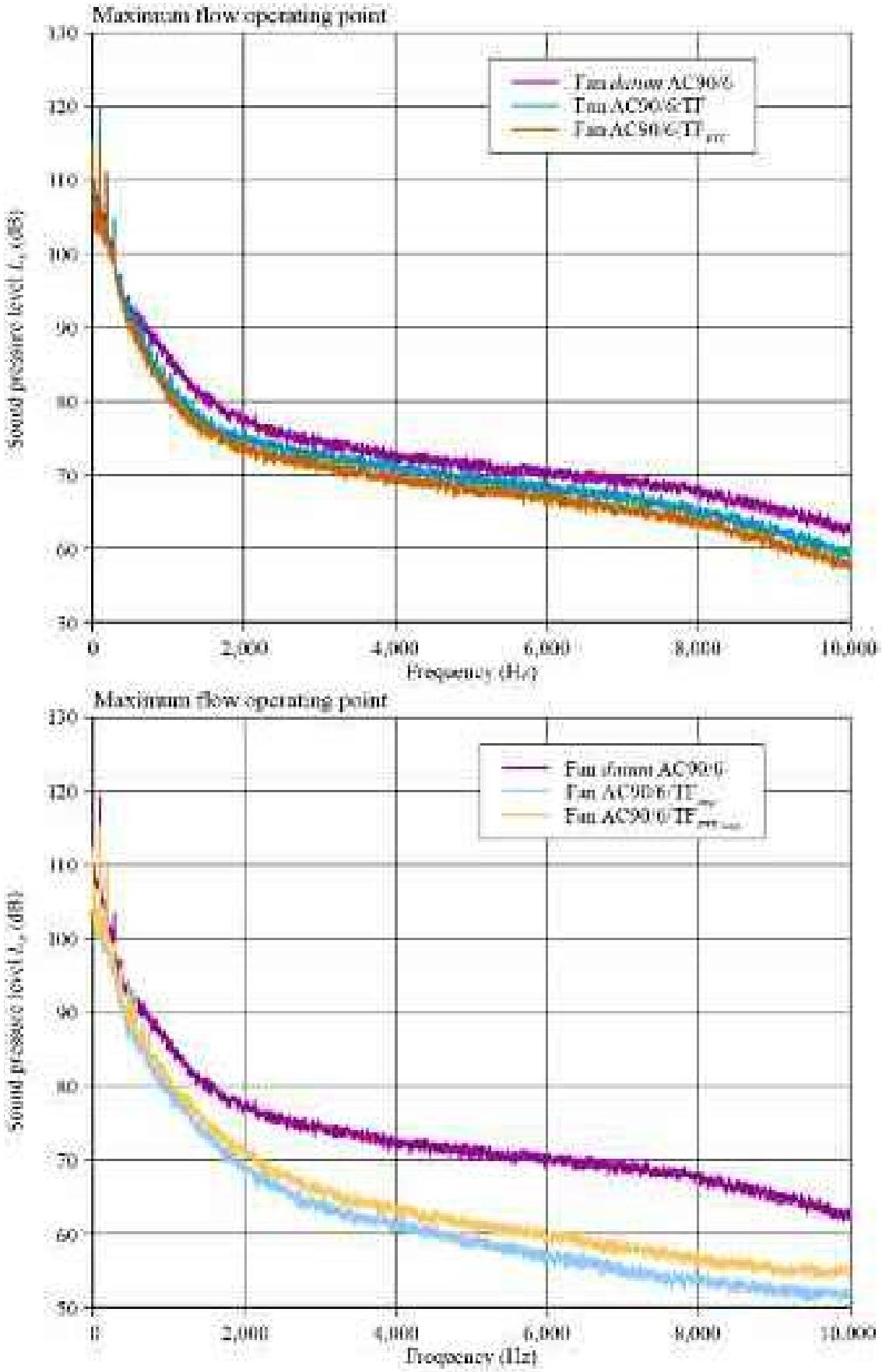

FIGURE 4.15. Outlet near-field broadband sound pressure level (L_P) spectrum measured at a span-wise location in the blade tip region and at the fan maximum flow operating point for the five studied blade-tip end-plates. The broadband sound pressure level illustrates the blade-tip end-plates' impact on the near-field broadband sound pressure level spectrum.

When we add the step feature, both the constant and variable thickness blade-tip end-plates exhibit a reduction in narrowband sound pressure level. This reduction continues into the broadband with both fans AC90/6/TF$_{step}$ and AC90/6/TF$_{VTE\ step}$ exhibiting significantly lower sound pressure levels than the fan *datum* AC90/6. This reduction in broadband sound pressure level indicates that at the maximum flow operating point the step feature is effective.

Consider the outlet near-field narrowband and broadband sound pressure level (L_P) spectrum measured at a span-wise location in the blade tip region and at the design operating point for the five studied blade-tip end-plates, Figures 4.16 and 4.17. The shift from maximum flow to design operating point results in the fan AC90/6/TF narrowband sound pressure level reducing relative to that of the fan AC90/6/TF$_{VTE}$. In the broadband the fan AC90/6/TF$_{VTE}$ still exhibits lower sound pressure levels than either the fan *datum* AC90/6 or AC90/6/TF. However, the difference between the three reduces at the design operating point.

The change in operating point from maximum flow to design did not change the effect of the step feature. Both the constant and variable thickness blade-tip end-plates exhibited lower sound pressure levels over the narrowband. However, once again the difference was reduced between the fan *datum* AC90/6, AC90/6/TF$_{step}$ and AC90/6/TF$_{VTE\ step}$ sound pressure level. Despite this reduction in effectiveness, we may associate the step feature with controlling turbulent mixing of flow-field features in the blade tip-to-casing region.

The change in operating point had a similar effect in the broadband to that in the narrowband. The step feature was still able to induce a reduction in broadband noise compared to that of the fan *datum* AC90/6. However, as with the narrowband, the shift from the maximum flow to design operating point degraded the reduction. This degradation is due likely to the step feature becoming less effective at mixing the small scale vortical flow-field feature in the blade tip-to-casing region. These near-field features then propagate more effectively to the far-field and increase fan far-field noise.

Consider the outlet near-field narrowband and broadband sound pressure level (L_P) spectrum measured at a span-wise location in the blade tip region and at the peak pressure operating point for the five studied blade-tip end-plates, Figures 4.18 and 4.19. The shift from the design to peak pressure operating point resulted in improving the acoustic performance of all four fan configurations with blade-tip end-plates in comparison with fan *datum* AC90/6. This improvement was apparent in both the narrowband and the broadband. This result was somewhat unexpected, as it indicates that the reduction in near-field noise that occurs with the step feature is relatively independent of fan operating condition.

Influence of Blade Angle on Tip Noise

We may also complement the analysis of outlet coherence spectrum in the blade tip region by analysing the influence of blade angle on fan near-field noise. The change in fan near-field noise with blade angle also provides an additional insight

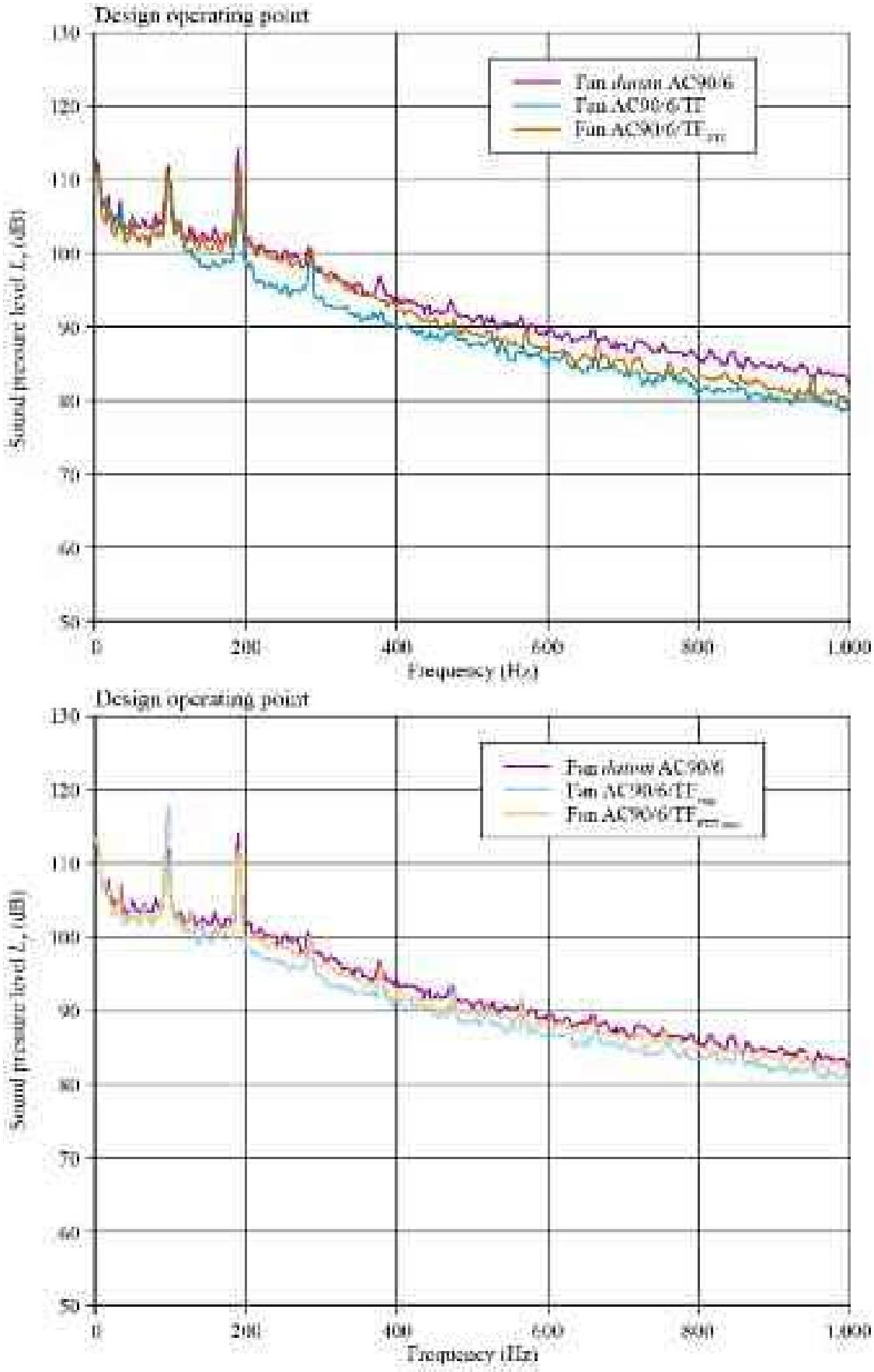

FIGURE 4.16. Outlet near-field narrowband sound pressure level (L_P) spectrum measured at a span-wise location in the blade tip region and at the fan design operating point for the five studied blade-tip end-plates. The narrowband sound pressure level illustrates the blade-tip end-plates' impact on the near-field narrowband sound pressure level spectrum.

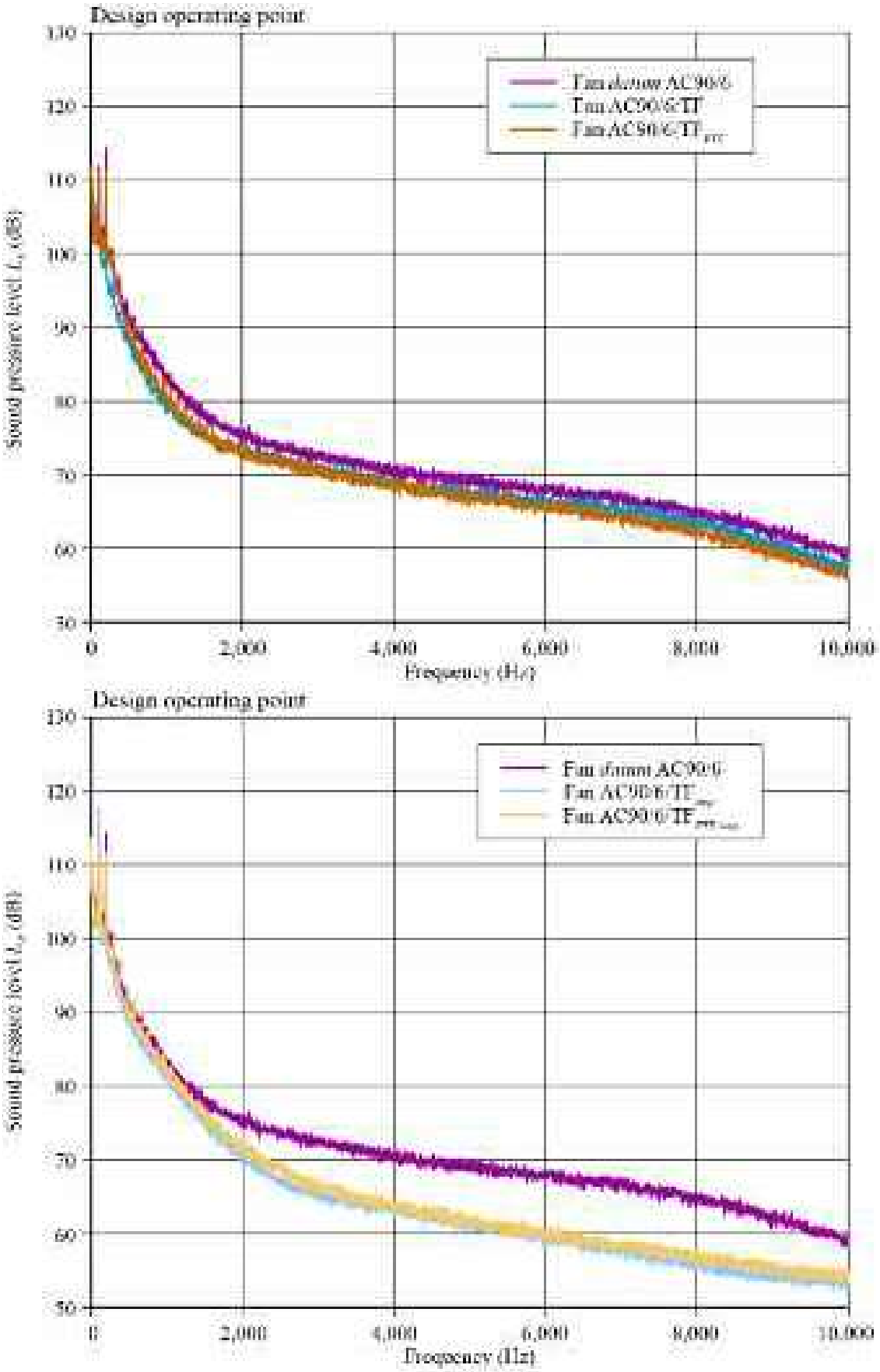

FIGURE 4.17. Outlet near-field broadband sound pressure level (L_P) spectrum measured at a span-wise location in the blade tip region and at the fan design operating point for the five studied blade-tip end-plates. The broadband sound pressure level illustrates the blade-tip end-plates' impact on the near-field broadband sound pressure level spectrum.

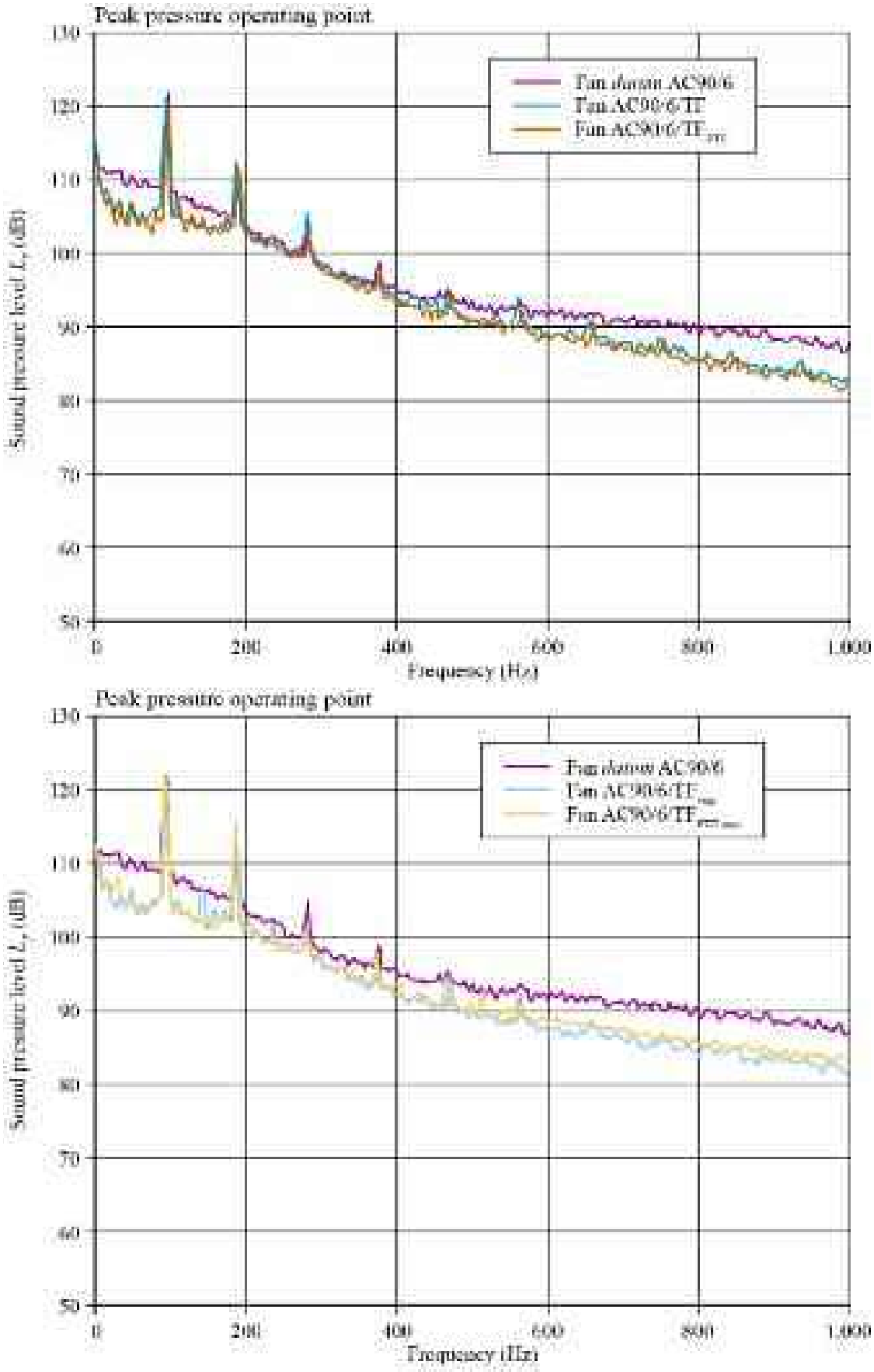

FIGURE 4.18. Outlet near-field narrowband sound pressure level (L_P) spectrum measured at a span-wise location in the blade tip region and at the fan peak pressure operating point for the five studied blade-tip end-plates. The narrowband sound pressure level illustrates the blade-tip end-plates' impact on the near-field narrowband sound pressure level spectrum.

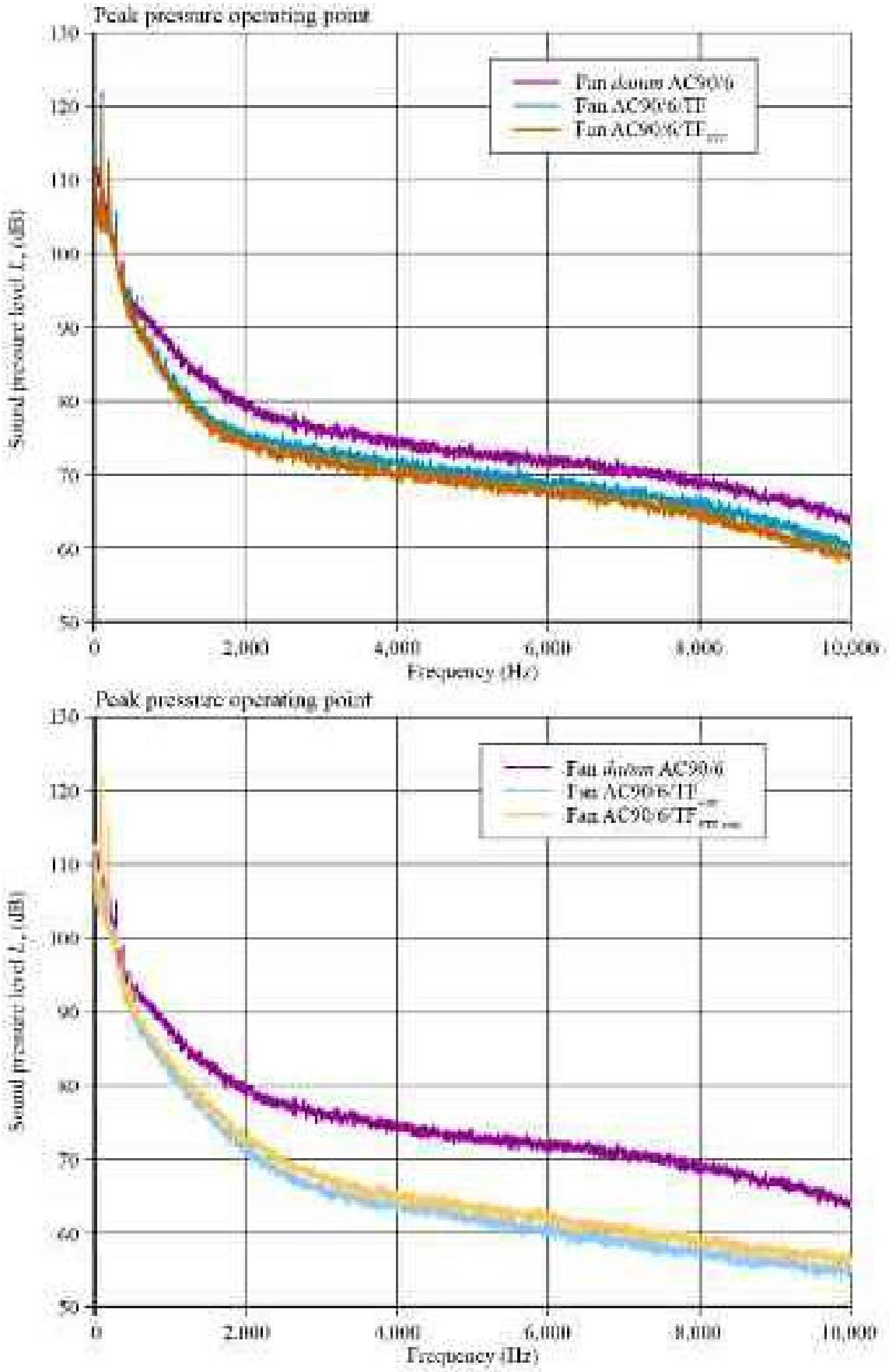

FIGURE 4.19. Outlet near-field broadband sound pressure level (L_P) spectrum measured at a span-wise location in the blade tip region and at the fan peak pressure operating point for the five studied blade-tip end-plates. The broadband sound pressure level illustrates the blade-tip end-plates' impact on the near-field broadband sound pressure level spectrum.

into the flow-field physics. We undertook the previous analysis of the influence of operating point on fan near-field noise with a blade angle of 28 degrees at each of the studied operating points. In this analysis we conducted all measurements at the design operating point for each of the studied blade angles, 16, 24 and 28 degrees.

Consider the outlet near-field narrowband sound pressure level (L_P) spectrum measured at a span-wise location in the blade tip region and at a blade angle of 16 degrees for the five studied blade-tip end-plates, Figure 4.20. The blade passing frequency and second harmonic of blade passing frequency was significantly reduced for the fan AC90/6/TF$_{step}$ in comparison with the other three fan configurations with blade-tip end-plates. Also noteworthy is that the third harmonic of blade passing frequency has all but merged with the broadband noise. There is some evidence of the third harmonic of blade passing frequency for the fan AC90/6/TF, but for all other configurations it has effectively merged with the broadband noise. Although there are other minor variations between the sound power level exhibited by the five studied fan configurations, the blade-tip end-plates are largely ineffective at this blade angle.

Consider the outlet near-field narrowband sound pressure level (L_P) spectrum measured at a span-wise location in the blade tip region and at a blade angle of 24 degrees for the five studied blade-tip end-plates, Figure 4.21. Increasing blade angle from 16 to 24 degrees results in a slight reduction in blade passing frequency sound pressure level for the fan AC90/6/TF and AC90/6/TF$_{step}$. However, the most significant change is at higher frequencies for the fan AC90/6/TF$_{step}$ which exhibits consistently lower sound pressure level with frequency than the other studied fan configurations. These lower sound pressure levels indicate that at a blade angle of 24 degrees the step feature is having a more beneficial effect on the constant thickness than variable thickness blade-tip end-plate.

Consider the outlet near-field narrowband sound pressure level (L_P) spectrum measured at a span-wise location in the blade tip region and at a blade angle of 28 degrees for the five studied blade-tip end-plates, Figure 4.22. At a blade angle of 24 degrees only the fan AC90/6/TF$_{step}$ exhibited lower sound pressure levels than the fan *datum* AC90/6. The other three fan configurations with blade-tip end-plates exhibited sound pressure levels similar to that of fan *datum* AC90/6. However, when we increased the blade angle to 28 degrees, all four fan configurations with blade-tip end-plate exhibited lower sound pressure levels than the fan *datum* AC90/6. Both tonal and broadband sound pressure level reduced for all four fan configurations with blade-tip end-plates. The most significant reduction occurred with the fan AC90/6/TF$_{step}$, indicating that the step feature can be effective at reducing near-field noise and therefore has the potential to reduce fan far-field noise.

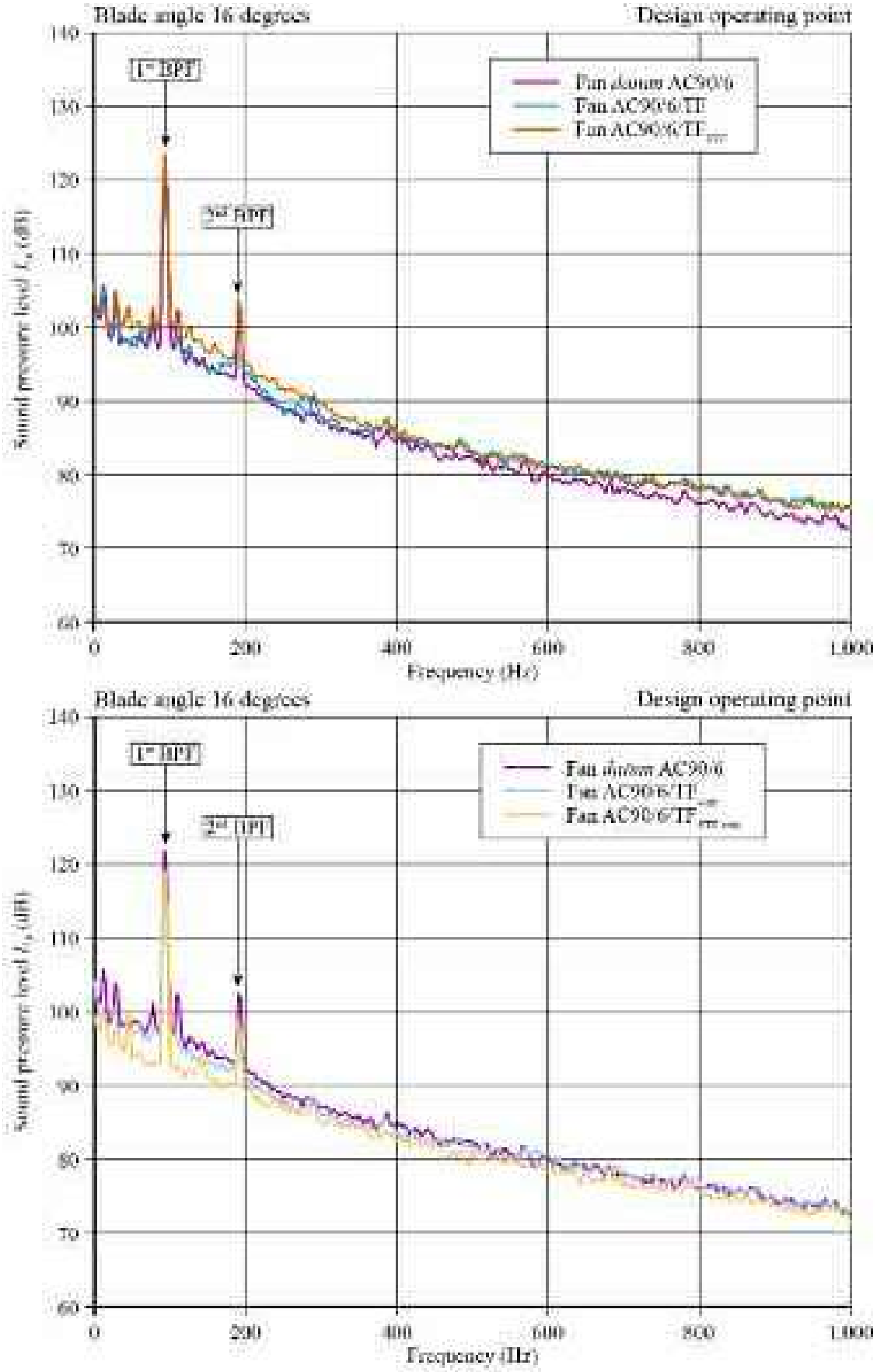

FIGURE 4.20. Outlet near-field narrowband sound pressure level (L_p) spectrum measured at a span-wise location in the blade tip region and at the fan design operating point for the five studied blade-tip end-plates. The studied blade tip pitch angle in the reported research was 28 degrees. The authors measured this data with a blade tip pitch angle of 16 degrees.

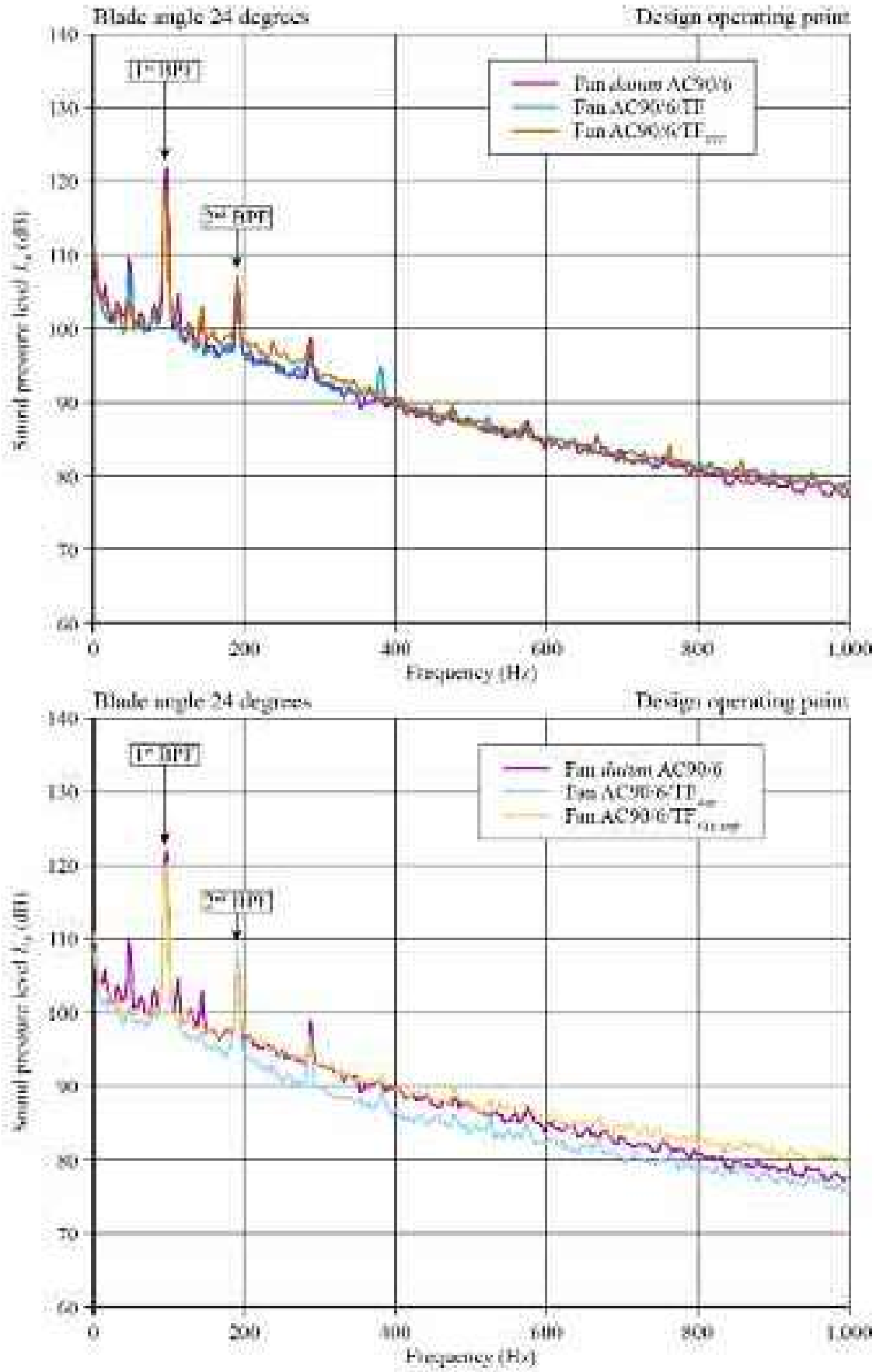

FIGURE 4.21. Outlet near-field narrowband sound pressure level (L_P) spectrum measured at a span-wise location in the blade tip region and at the fan design operating point for the five studied blade-tip end-plates. The studied blade tip pitch angle in the reported research was 28 degrees. The authors measured this data with a blade tip pitch angle of 24 degrees.

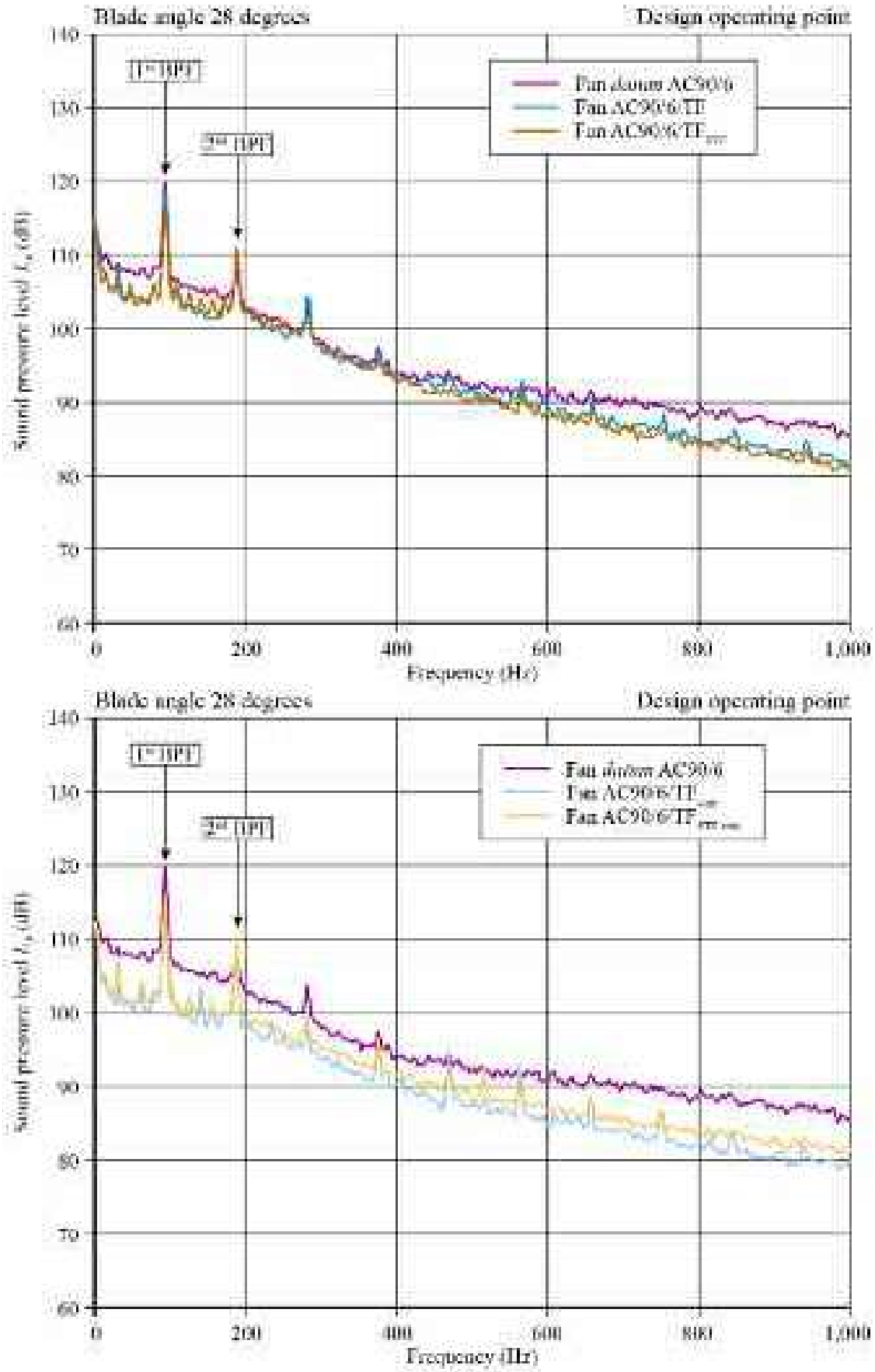

FIGURE 4.22. Outlet near-field narrowband sound pressure level (L_P) spectrum measured at a span-wise location in the blade tip region and at the fan design operating point for the five studied blade-tip end-plates. The studied blade tip pitch angle in the reported research was 28 degrees. The authors measured this data with a blade tip pitch angle of 28 degrees.

CONCLUSIONS

In this chapter we applied an experimental methodology developed to facilitate assessing fan acoustic performance, focusing on the tonal noise's span-wise variation. This focus on tonal noise was a consequence of the blade passing frequency and it's second, third and fourth harmonics dominating the fan far-field noise spectra. The fifth and sixth harmonics were evident in the data, but were tonally less important as they had reduced in magnitude to the point where they effectively merged with the broadband noise.

We used a coherence function that involves normalising the signal, highlighting highly coherent events, irrespective of energy content. Highlighting highly coherent events made the technique effective at isolating coherent regions in the coherence maps. We created coherence maps by plotting coherence against blade span and frequency. The coherence analysis identified six distinct coherent regions, each associated with a different combination of span-wise location and frequency.

We may regard the first three coherent regions as generally occurring with the studied fan, with or without a fitted blade-tip end-plate. The first occurred with noise which the electric motor driving the fan generated. We mounted the fan impeller directly on the motor shaft, and consequently, acoustic measurements included the motor's contribution. The second occurred with ingested noise from the fan inlet plenum. The inlet plenum boundary layer's interaction with the blade-to-blade flow-field in the blade-tip region was acoustically productive. The third occurred with rotor only noise. The rotor only noise is primarily a single tone at the blade passing frequency.

The fourth coherent region provides an insight into the likely in-service effectiveness of blade-tip end-plate designs as it is generated by turbulence in the in-flow. In practice, engineers install the studied fan over a tube bank with flow drawing across it and into the fan inlet. Consequently, the in-service installation occurs with significantly higher inlet turbulence levels than those that occur with a laboratory test. The relative susceptibility of different blade-tip end-plate designs to turbulence induced noise provides a measure of their likely effectiveness in-service.

The fifth and sixth coherent regions occur with specific flow features in the blade-to-blade flow-field that blade-tip end-plate presence induces. The fifth occurred with secondary flow noise. The blade-hub secondary flow vortex presence is responsible for this noise source. The sixth occurred as a consequence of the blade-tip leakage vortex's bursting. The blade-tip leakage vortex may either pass out of the blade-to-blade passage without bursting, or burst in the blade-to-blade passage. Bursting in the blade-to-blade passage is acoustically productive.

The difference between coherence maps for the studied fan with and without blade-tip end-plates enabled us to associate end-plate geometry with features on the coherence maps. Changes in blade-tip end-plate geometry had a significant effect on the flow features induced in the blade-to-blade flow-field. Therefore, analysing the coherence maps provided an insight into the acoustic far-field consequences of aerodynamic near-field flow-field features and thus facilitated an insight into the physical mechanisms responsible for fan far-field noise.

REFERENCES

ISO 5801:2007 (2007), *Industrial Fans: Performance Testing Using Standardised Airways.*

ISO 10302:1996 (1996), *Fans for General Purposes. Methods of Noise Testing.*

Bianchi, S., Sheard, A.G., Kinghorn, I.R., Corsini, A. and Rispoli, F. (2009a), 'Experimental Development of a Measurement Technique to Resolve the Radial Distribution of Fan Aeroacoustic Emissions', *Noise Control Engineering Journal*, vol. 57, pp. 360–369.

Bianchi, S., Corsini, A., Rispoli, F. and Sheard, A.G. (2009b), 'Detection of Aerodynamic Noise Sources in Low-speed Axial Fans with Tip End-plates', *Proceedings of the IMechE Part C, Journal of Mechanical Engineering Science*, vol. 223, pp. 1379–1392.

Corsini, A. and Sheard, A.G. (2007), 'Tip End-plate Concept Based on Leakage Vortex Rotation Number Control', *Journal of Computational and Applied Mechanics*, vol. 8, pp 21–37.

Corsini, A., Rispoli, F., Sheard, A.G. and Kinghorn, I.R. (2006), 'Investigation of Improved Blade-tip Concept for Axial Flow Fan', *Proceedings of the 51st American Society of Mechanical Engineers Gas Turbine and Aeroengine Congress*, Barcelona, Spain, 8–11 May, paper no. GT2006-90592.

Cumpsty, N.A. (1974), 'Sum and Difference Tones from Turbomachines', *Journal of Sound and Vibration*, vol. 32, pp. 383–386.

Cumpsty, N.A. (1977), 'A Critical Review of Turbomachinery Noise', *Transactions of the ASME, Journal of Fluids Engineering*, vol. 99, pp. 278–293.

Fukano, T. and Jang, C. (2004), 'Tip Clearance Noise of Axial Flow Fans Operating at Design and Off-design Condition', *Journal of Sound and Vibration*, vol. 275, pp. 1027–1050.

Fukano, T., Kodama, Y. and Takamatsu, Y. (1977a), 'Noise Generated by Low Pressure Axial Flow Fans I – Modelling of the Turbulent Noise', *Journal of Sound and Vibration*, vol. 50, pp. 63–74.

Fukano, T., Kodama, Y. and Takamatsu, Y. (1977b), 'Noise Generated by Low Pressure Axial Flow Fans II – Effects of Number of Blades, Chord Length and Camber of Blade', *Journal of Sound and Vibration*, vol. 50, pp. 75–88.

Fukano, T., Takamatsu, Y. and Kodama, Y. (1986), 'The Effects of Tip Clearance on the Noise of Low-pressure Axial and Mixed Flow Fans', *Journal of Sound and Vibration*, vol. 105, pp. 291–308.

Ganz, U.W., Joppa, P.D. and Scharpf, D.F. (1998), *Boeing 18-inch Fan Rig Broadband Noise Test*, Report NASA CR-1998-208704.

Garg, A.K. and Leibovich, S. (1979), 'Spectral Characteristics of Vortex Breakdown Flowfields', *Physics of Fluids*, vol. 22, pp. 2053–2064.

Holste, F. and Neise, W. (1997), 'Noise Source Identification in a Prop Fan Model by Means of Acoustical Near Field Measurements', *Journal of Sound and Vibration*, vol. 203, pp. 641–665.

Inoue, M., Kuroumaru, M. and Furukawa, M. (1986), 'Behavior of Tip Leakage Flow Behind an Axial Compressor Rotor', *Transaction of the ASME, Journal of Gas Turbine and Power*, vol. 108, pp. 7–14.

Ito, T., Suematsu, Y. and Hayase, T. (1985), 'On the Vortex Breakdown Phenomena in a Swirling Pipe-flow', *Memoirs of the Faculty of Engineering, Nagoya University*, vol. 37, pp. 117–172.

Kameier, F. and Neise, W. (1997), 'Rotating Blade Flow Instability as a Source of Noise in Axial Turbomachines', *Journal of Sound and Vibration*, vol. 203, pp. 833–853.

Laurendeau, E., Jordan, P., Delville, J. and Bonnet, J. (2007), 'Nearfield-Farfield Correlations in Subsonic Jets: What Can They Tell Us?', *Proceedings of the 13th AIAA/CEAS Aeroacoustics Conference*, Rome, Italy, 21–23 May, paper no. 2007-3614.

Leggat, L.J. and Siddon, T.E. (1978), 'Experimental Study of Aeroacoustic Mechanism of Rotor-vortex Interactions', *Journal of the Acoustical Society of America*, vol. 64, pp. 1070–1077.

Longhouse, R.E. (1978), 'Control Tip-vortex Noise of Axial Flow Fans by Rotating Shrouds', *Journal of Sound and Vibration*, vol. 58, pp. 201–214.

Magliozzi, B., Johnson, B.V., Hanson, D.B. and Metzger, F.B. (1973) 'Noise and Wake Structure Measurements in a Subsonic Tip Speed Fan – Tabulation and Plots of Test Data', NASA Technical Report CR-132259, 23 July.

Marcinowski, H. (1953), 'Einfluss des Laufradspalts und der Luftfuehrung bei einem Kuehlgeblaese Axialer Bauart', *Motortechnische Zeitschrift*, vol. 14, pp. 259–262.

Miles, J.H. (2006), 'Procedure for Separating Noise Sources in Measurements of Turbofan Engine Core Noise', Report NASA/TM-2006-214352.

Mongeau, L., Thompson, D.E. and McLaughlin, D.K. (1995), 'A Method for Characterizing Aerodynamic Sound Sources in Turbomachines', *Journal of Sound and Vibration*, vol. 181, pp. 369–389.

Mugridge, B.D. and Morfey, C.L. (1972), 'Sources of Noise in Axial Flow Fan', *Journal of the Acoustical Society of America*, vol. 51, pp. 1411–1426.

Nelson, D.A. and Cooper, B.A. (1999), 'A "Reduced-noise Gas Flow Design Guide" for NASA Glenn Research Center', *Proceedings of INTERNOISE 99, the International Congress on Noise Control Engineering*, Fort Lauderdale, FL, USA, 6–8 December, vol. 1, pp. 77–82.

Sharland, I.J. (1964), 'Sources of Noise in Axial Flow Fans', *Journal of Sound and Vibration*, vol. 1, pp. 302–322.

Spall, R.E., Gatski, T.B. and Grosch, C.E. (1987), 'A Criterion for Vortex Breakdown', *Physics of Fluids*, vol. 30, pp. 3434–3440.

Uchida, S., Nakamura, Y. and Ohsawa, M. (1985), 'Experiments on the Axisymmetric Vortex Breakdown in a Swirling Air Flow', *Transactions of the Japan Society for Aeronautical Space Sciences*, vol. 27, pp. 206–216.

Wright, S.E. (1976), 'The Acoustic Spectrum of Axial Flow Machines', *Journal of Sound and Vibration*, vol. 45, pp. 165–223.

Chapter 5

Far-field Radiation of Tip Aerodynamic Sound Sources in Axial Fans Fitted with Passive Noise Control Features

S. Bianchi, A. Corsini, F. Rispoli and A.G. Sheard

ABSTRACT

The chapter extends the near- and far-field correlation technique presented in Chapter 2 to include fan far-field acoustic measurements at different azimuthal positions, thus extending the original correlation technique to a directivity analysis. We placed a microphone ten per cent blade chord down-stream of the studied fan blades' trailing edge. We then varied the microphone's span-wise location in steps of two per cent from blade hub to blade tip. At each span-wise location, we made measurements of far-field noise on the fan centre line and 30, 45, 60, 75 and 90 degrees off the fan centre line. We made near- and far-field acoustic measurements simultaneously, thus the experimental technique was able to provide data sets of near- and far-field noise over a range of far-field azimuthal positions that we could correlate to establish the far-field directivity of near-field noise sources. We used the directivity analysis to characterise the directivity of fan far-field noise with and without blade-tip end-plates fitted. By filtering fan far-field noise measurements, we established the tone's directivity that occurs with the blade passing frequency, the second, third and fourth harmonics of blade passing frequency and high frequency noise above 1 kHz. The directivity analysis confirmed that fan far-field noise was anisotropic, both tonally and in the broadband, enabling us to establish the change in directivity associated with changes in blade-tip end-plate geometry. The analysis complemented the span-wise coherence analysis presented in Chapter 4, providing additional insight into the impact of end- plate geometry on fan far-field noise. The directivity analysis clarifies the acoustic effect of blade-tip end-plate geometry, thus facilitating insight into the physical flow-field mechanisms responsible for fan far-field noise.

This chapter is a revised and extended version of Bianchi, S., Corsini, A., Rispoli, F. and Sheard, A.G. (2011), 'Far-field Radiation of Tip Aerodynamic Sound Sources in Axial Fans Fitted with Passive Noise Control Features', *Transactions of the ASME, Journal of Vibration and Acoustics*, vol. 133, paper no. 051001, pp. 1–11.

NOMENCLATURE

Latin letters

BPF	blade-passing frequency [Hz]
Co	numerical value of the coherence function
f^{co}	duct cut-off frequency [Hz]
f^{co}_{mn}	mode cut-off frequency [Hz]
K_s	specific noise level
ℓ	blade chord
L	tip vortex length scale
m	circumferential mode
n	radial mode
Δp_{tot}	rotor total pressure rise
r	non-dimensional span
rv	radial distance from the vortex axis
Ro	Rossby number
SPL	Sound pressure level [dB]
SWL(A)	'A' weighted sound power level
t	blade pitch
v	vortex axial velocity at R

Greek letters

β_{LV}	leakage vortex angle to the blade chord
Ω	tip leakage vortex rotation rate scale
σ_h	hub-to-casing diameter ratio
η_{stat}	efficiency based on static pressure rise
κ_p	local specific sound pressure level
Ψ	local pressure rise coefficient
τ	rotor tip clearance

INTRODUCTION

An on-going market requirement to reduce the far-field noise generated by air movement fans has resulted in interest within the air movement and control community in methods to minimise fan noise. Researchers in the 1970s, particularly Wright (1976) and Cumpsty (1977), have studied the link between the fan rotors' aerodynamic features and their acoustic emissions. Their findings have enhanced general understanding of axial turbomachinery aeroacoustics. Cumpsty (1977) concluded that, with the exception of the low-frequency range of high-speed machines, the mechanisms that determine broadband noise in subsonic fans are the same as those in supersonic tip-speed fans and compressors. Therefore, the design variables that impact tonal and broadband noise are similar both for fans designed for aerospace and air movement application (Ganz *et al.*, 1998). According to Wright (1976),

this is because of the prominence of rotor noise that originates from turbulent boundary layers.

Researchers regard a fan's blade tip-to-casing flow as particularly important as it interacts with both wakes and blade-to-blade passage secondary flows. Therefore, researchers recognise blade tip-to-casing flow as one of the most significant sources of fan noise (Cumpsty, 1977; Nelson and Cooper, 1999). Several studies have attempted to resolve the causal aerodynamics relationship between fan blade-to-blade flow-field structures and fan far-field noise. Marcinowski (1953), the first researcher to study noise associated with tip dynamics, demonstrated that increases in broadband noise levels occur with increasing tip clearance. The largest changes in noise level were apparent at frequencies greater than the blade-passing frequency.

Despite the interest within both the air movement and control and academic communities, there is no general consensus on the noise generating mechanisms associated with the blade tip-to-casing flow (Jordan and Gervais, 2008). Some scholars have studied the azimuthal distribution of aerodynamically generated sound, identifying two independent processes that are at play. These processes result in the radiation of high-frequency noise, with a short stream-wise life-span towards the side of the jet axis. In contrast, the low-frequency noise emits with a significantly longer stream-wise life-span and is concentrated along the jet axis (Mankbadi and Liu, 1984; Tam *et al.*, 1996; Laurendeau *et al.*, 2007). This azimuthal distribution of low- and high-frequency noise is self-consistent with Lighthill's (1952, 1954) conclusions. He observed that coherent flow structures are responsible for the spectrally dependent nature of far-field noise radiation patterns. The far-field noise has a directional maximum at 45 degrees from the jet axis, or slightly less as a consequence of a quadrupolar convection effect. In contrast, the small-scale random turbulent eddies contributed to the far-field noise via a nearly isotropic radiation across the broadband (Lighthill, 1952, 1954).

When conceptualising the exhaust flow from a fan as a jet, Shah *et al.* (2007a, 2007b) studied the effect of exit swirl. Their experimental work focused on the signature of the subsonic exhaust from from a swirl tube in a nacelle configuration. Shah *et al.* (2007a, 2007b) demonstrated that the swirl-flow acoustics have specific angular radiation patterns that may be related to the induced swirl level. Specifically, they concluded that at the high turning vane angles typically favoured by air movement fan designers, the breakdown of the swirling flow results in changing the directivity of fan far-field noise. It is likely that similar directional mechanisms will apply when multiple vortex pairs release themselves from the rotating blade-to-blade passages that characterise a fan's exhaust flow.

Studies on transonic fans (Heidelberg *et al.*, 1997; Julliard *et al.*, 2000; Tester and De Mercato, 2006) have shown that the fan noise radiates along an azimuthal pattern driven by the blade passing frequency. For transonic fans we may conceptualise this azimuthal pattern as a net result of the interaction between the rotating blades and flow passing through the fan. For air movement fans we offer only tentatively this interpretation of the origin of a fan's azimuthal far-field noise pattern. Despite this caveat the conceptualisation provides a basis for characterising the

mechanisms responsible for air movement fan azimuthal far-field noise patterns. This conceptualisation is necessary as the extant literature contains few studies that have specifically explored the mechanisms responsible for air movement fan azimuthal far-field noise patterns. Therefore, there is a need to establish a link between fan far-field noise directivity and aerodynamic flow-field features in the near-field.

This chapter presents an extension of the near- and far-field correlation technique presented in Chapter 2 to include fan far-field acoustic measurements at different azimuthal positions. This extends the original correlation technique to a directivity analysis which clarifies the acoustic effect of blade-tip end-plate geometry. Thus, it facilitates insight into the physical flow-field mechanisms responsible for fan far-field noise. This insight complements the research reported in Chapters 3 and 4, further clarifying the physical flow-field mechanisms responsible for fan far-field noise. A detailed understanding of the physical flow-field mechanisms responsible for fan far-field noise thus facilitates the development of blade-tip end-plates that more effectively minimise fan far-field noise.

FAMILY OF FANS UNDER INVESTIGATION

We conducted the reported research on a family of commercially available cooling fans. The studied fan configuration, coded AC90/6, incorporates a six-blade un-swept rotor, with modified ARA-D profile aerofoil blades, Table 5.1. One may set the blade-pitch angle during final assembly to customise the fan to a desired duty point. We used a direct coupled-induction 400-volt (AC), 3-phase motor to drive the rotor at a constant speed of 950 rpm, resulting in a 44.7 m/s blade tip speed and a 95 Hz blade passing frequency (BPF). In its original embodiment the studied fan did not include a blade-tip end-plate and therefore we used it as a *datum* against which to as-

Table 5.1. *The fan* datum *AC90/6 blade geometry and rotor specification.*

	Fan *datum* AC90/6		
Blade geometry	Hub	Mid-span	Tip
Pitch angle (°)	36	58.8	28
Camber angle (°)	46	44	41
Solidity	1.24	0.86	0.30
Fan rotor			
Blade number		6	
Blade tip pitch angle (°)		16–28	
Blade tip stagger angle (°)		74–62	
Hub-to-casing diameter ratio σ		0.22	
Tip diameter (mm)		900.0	
Rotor tip clearance τ (% span)		1.0	
Rated rotational frequency (r/min)		935–950	

sess the performance of fan variants with blade-tip end-plates. Therefore, in the reported research we refer to the fan without blade-tip end-plates as the fan *datum* AC90/6.

Passive Noise-control Devices

In addition to the fan *datum* AC90/6, we studied two fan variants. We fitted the first with a constant thickness blade-tip end-plate and the second with a variable thickness blade-tip end-plate, Figure 5.1. When fitted with a constant thickness blade-tip end-plate, we named the fan AC90/6/TF. When fitted with the variable thickness blade-tip end-plate, we named the fan AC90/6/TF$_{VTE}$.

Designs developed for tip-vortex control and drag reduction in aircraft wings and catamaran hulls inspired the constant thickness blade-tip end-plate design. The constant thickness blade-tip end-plate ran along the blade pressure surface, ending at the blade trailing edge with a square tail. The addition of this constant thickness blade-tip end-plate resulted in increasing the thickness of the fan AC90/6/TF blade tip by a factor of three compared to the fan *datum* AC90/6. We considered Inoue *et al.*'s (1986) research regarding the blade-tip end-plate's size for axial compressor blades. They estimated that the optimum blade-tip end-plate size was between 10 and 20 per cent blade span. In practice, we were able to manufacture blades with a blade-tip end-plate size five per cent of blade span. The fan blades were manufactured from injection moulded plastic, with the size of the blade-tip end-plate the largest the blade manufacturing technique could produce.

Corsini and Sheard (2007) studied both the fan *datum* AC90/6 and AC90/6/TF using a blade-tip vortex 'breakdown criteria' based on Rossby number (Spall *et al.*,

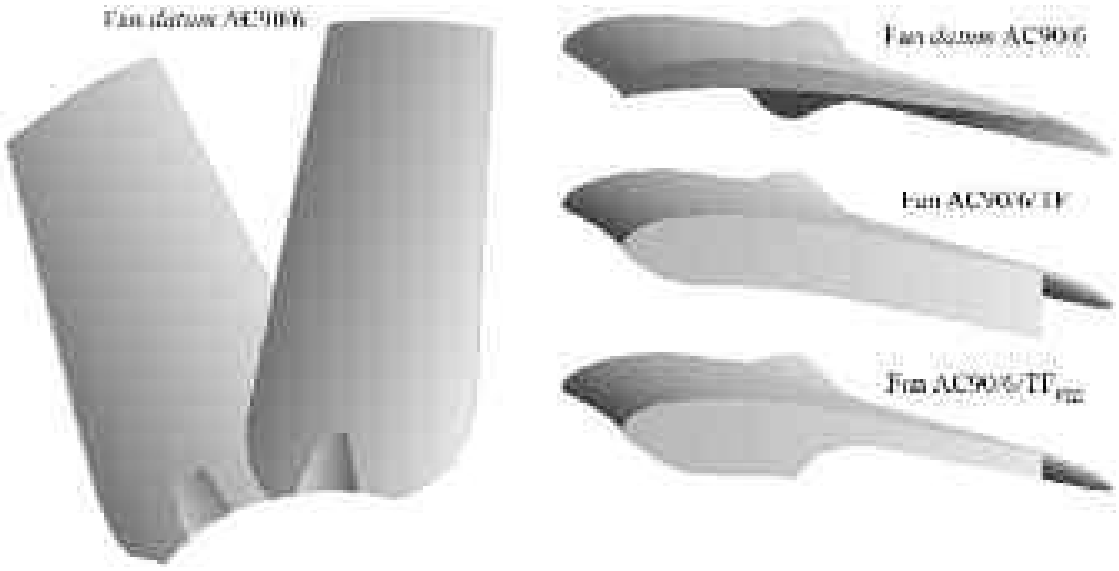

FIGURE 5.1. The studied fan *datum* AC90/6 without a fitted blade-tip end-plate, with a constant thickness blade-tip end-plate, AC90/6/TF and with a variable thickness blade-tip end-plate, AC/6/TF$_{VTE}$.

1987). Following Ito *et al.*'s method (1985), they concluded that there is a threshold value of Rossby number below which vortex rotation cannot reduce if the vortex is to remain stable. We used the critical Rossby number range that Uchida *et al.* (1985) and Garg and Leibovich (1979) defined. Uchida *et al.* (1985) defined a critical Rossby number associated with the breakdown of an axi-symmetric vortex in a swirling flow. Garg and Leibovich (1979) also defined a critical Rossby number associated with an aircraft wing tip vortices' breakdown.

Corsini *et al.* (2006) studied the fan *datum* AC90/6 and fan AC90/6/TF's aerodynamic and acoustic performance, identifying a breakdown of the fan AC90/6/TF blade tip-to-casing leakage vortex. Vortex breakdown is acoustically productive, and therefore Corsini *et al.* (2006) concluded that a revised blade-tip end-plate design was desirable that avoided leakage vortex breakdown. Corsini and Sheard (2007) developed a blade-tip end-plate design methodology that successfully eliminated the leakage vortex breakdown by adding a variable thickness blade-tip end-plate. When fitted with this variable thickness blade-tip end-plate, we named the fan AC90/6/TF$_{VTE}$.

Flow Conditions

The studied fan blade tip pitch angle is adjustable and one may set it to a pitch angle between 16 and 28 degrees. In practical application, one typically sets the blade tip pitch angle to 28 degrees as this maximises flow rate for a given system pressure. In the research reported in this chapter, we conducted the experimental measurements with the fan blade tip pitch angle set to 28 degrees. We selected 28 degrees both because it is typical of the angle used in practical application and because it results in the highest blade loading. A highly loaded blade results in the blade tip-to-casing vortex having the most significant effect on both fan aerodynamic and acoustic performance (Holste and Neise, 1997).

The impact of the blade tip-to-casing vortex on both fan aerodynamic and acoustic performance results in the application of blade-tip end-plates changing not only the fan's acoustic performance, but also the aerodynamic performance. Consequently, the fan *datum* AC90/6 generates a different pressure at a constant flow rate when fitted with each of the studied blade-tip end-plates. To facilitate the comparison of fan performance data when fitted with different blade-tip end-plates, we chose to define three operating points, and their respective volume flow rates, Table 5.2. The design operating point volume flow rate is typical of that required when the fan is installed over a cooling unit's tube bank. The peak pressure flow rate is typical of that required when the tube bank has become partially blocked following a period of in-service operation. The maximum flow operating point volume flow rate is typical of the flow rate that occurs with the lowest pressure loss tube banks currently operating in service.

Bianchi *et al.* (2009a) measured the performance characteristics of the studied fan in accordance with ISO 5801:2007 requirements (2007). The performance characteristics of the studied fan illustrate the impact on pressure rise of blade-tip

Table 5.2. *The operating points used when characterising the studied fan's performance with and without fitted blade-tip end-plates. The authors measured performance characteristics in a Type D standardised airway (ducted inlet, ducted outlet) in accordance with ISO 5801:2007 requirements (2007).*

Operating point	Volume flow rate (m^3/s)	Studied blade tip pitch angle (°)
Maximum flow	7.0	28
Design	6.5	28
Peak pressure	5.6	28

end-plate geometry, Figure 5.2. Therefore, the addition of both the constant and variable thickness blade-tip end-plates results in an increase in blade loading. We would expect blade-tip noise sources to become more acoustically productive with increasing blade loading. Therefore, an increase in blade loading will offset partially any reduction in fan far-field noise attributed to adding a blade-tip end-plate. We must conservatively assess the reduction in fan far-field noise if one neglects increased blade loading. Therefore, despite fan far-field noise serving as a blade loading function, we chose to neglect the change in pressure rise with the change in blade-tip treatment.

We may assess the validity of our assumption by assessing fan A weighted sound power level (L_W) and specific noise level (K_S), Figure 5.3. Both the fans AC90/6/TF and AC90/6/TF$_{VTE}$ demonstrate lower A weighted sound power and specific noise levels than the fan *datum* AC90/6. As pressure rise increases towards the fan's peak pressure operating point, both fan AC90/6/TF and AC90/6/TF$_{VTE}$ noise levels increased from a minimum that occurs with a pressure rise close to the fan's design operating point. Axial fans classically exhibit an increase in the amplitude of discrete frequency tones as they approach stall (Fukano *et al.*, 1986). Therefore, we expected the increase in noise level as the fans AC90/6/TF and AC90/6/TF$_{VTE}$ moved from their design to peak pressure operating point. However, specific noise levels remain lower than that of fan *datum* AC90/6 over the entire fan operating range despite the increase in blade loading that occurs with having fitted a blade-tip end-plate. This reduction gives confidence in the effectiveness of the blade-tip end-plates.

METHODOLOGY

We conducted the experimental measurements in an anechoic chamber in accordance with ISO 10302:1996 requirements (1996) following Bianchi *et al.*'s method (2009a). We made acoustic measurements using microphones at the fan outlet, recording the near- and far-field signals on two channels of a data acquisition system. An aerofoil louver in the top of the anechoic chamber inlet section facilitated variation of fan flow rate. We aerodynamically optimised the fan inlet bell mouth profile to provide uniform and unseparated flow into the fan. The fan was connected to the outside environment via up- and down-stream plenums. These plenums were

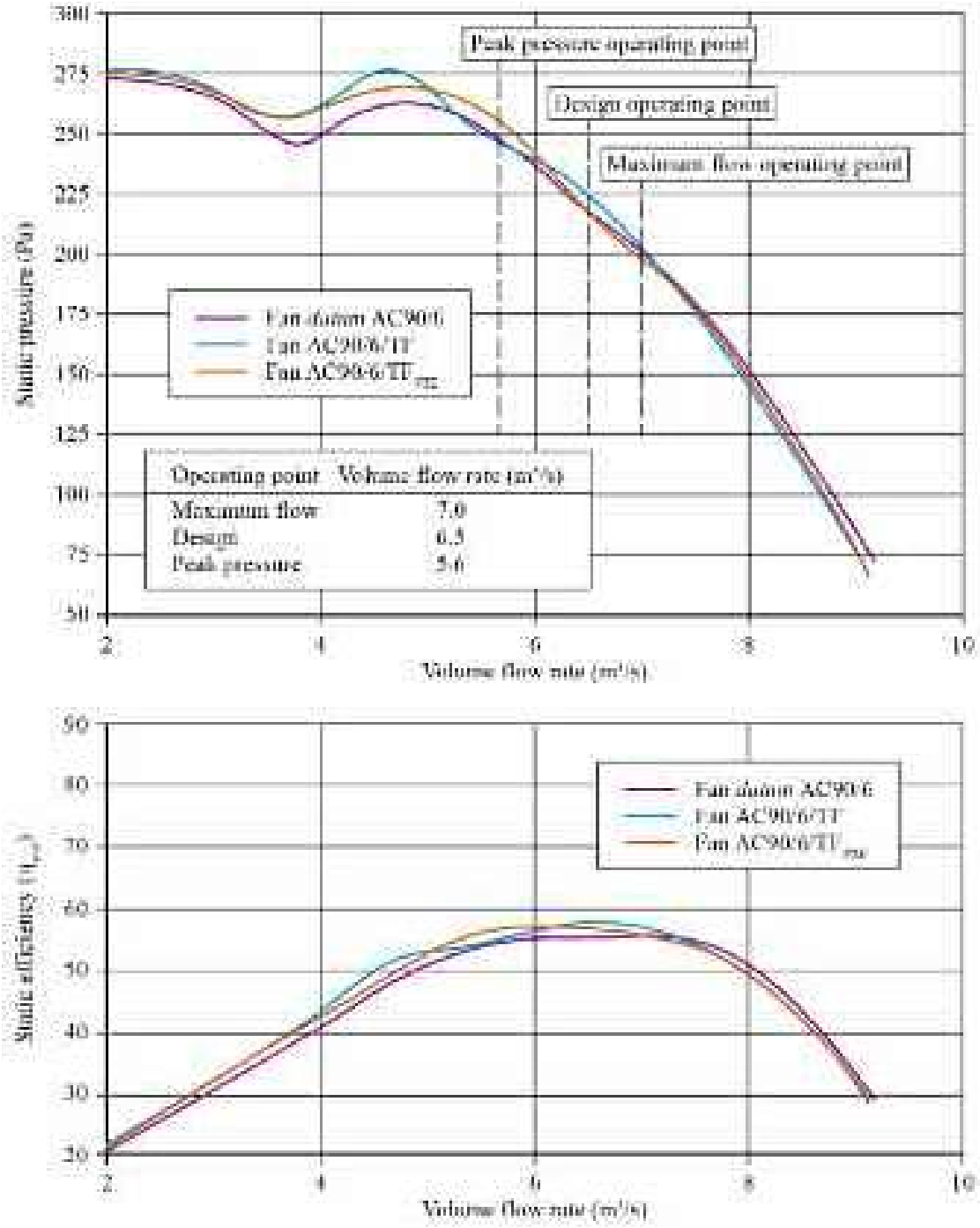

FIGURE 5.2. The performance characteristics of the studied fan *datum* AC90/6 without a fitted blade-tip end-plate, with a constant thickness blade-tip end-plate, AC90/6/TF and with a variable thickness blade-tip end-plate, AC/6/TF$_{VTE}$. Bianchi *et al.* (2009a) measured performance characteristics with the blade tip pitch angle set to 28 degrees in a Type D standardised airway (ducted inlet, ducted outlet) in accordance with ISO 5801:2007 requirements (2007).

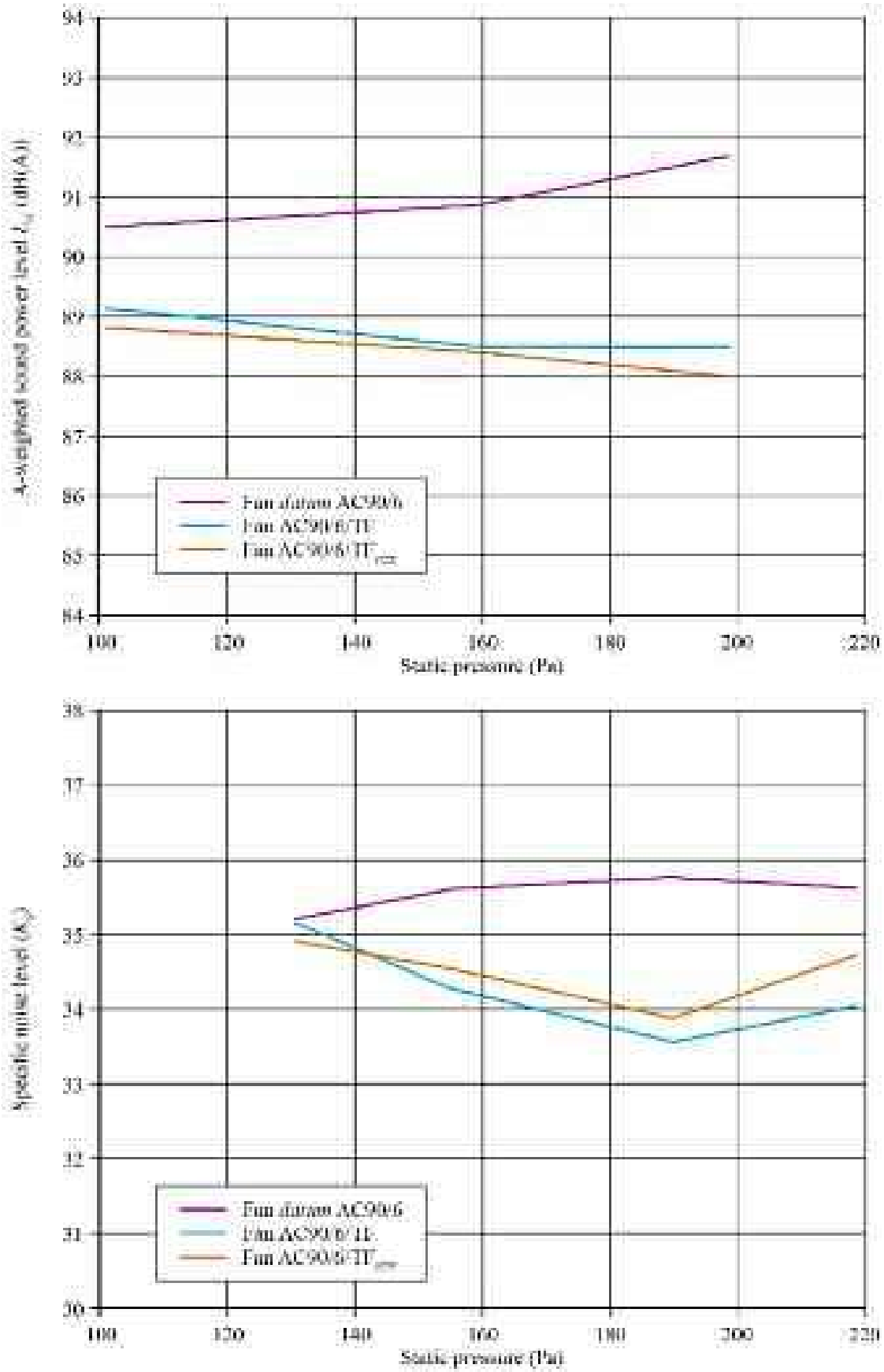

FIGURE 5.3. The A weighted sound power level (L_W) and specific noise level (K_S) over the fan's operating range for the fan *datum* AC90/6 without a fitted blade-tip end-plate, with a constant thickness blade-tip end-plate, AC90/6/TF and with a variable thickness blade-tip end-plate, AC/6/TF$_{VTE}$. The authors made all measurements with the blade tip pitch angle set to 28 degrees.

designed to minimise in-flow non-uniformities and were acoustically treated to both minimise noise transmission from the external environment and its reflection inside plenum ductwork. We also covered the anechoic chamber walls with foam panels to further reduce noise transmission from the external environment.

Near-field Acoustic Measurement Technique

We made near-field measurements at the fan outlet by mounting a microphone on a 10 mm radial traversing mechanism 10 per cent blade chord downstream of the blade trailing edge. We then used the traversing mechanism to move the near-field microphone from the blade hub to tip, in radial steps corresponding to two per cent of blade span. Thus, the traversing microphone facilitated the span-wise measurement of near-field fan noise.

We conducted hot-wire anemometer measurements to determine the flow velocity at each of the exhaust span-wise microphone locations. As the exhaust microphone was located immediately downstream of the blade trailing edge, we chose to calibrate the traversing microphone in a dedicated test rig. We measured the background noise in the test rig with no flow, and then induced the airflow corresponding to each of the microphone's span-wise locations. This facilitated calculation of self-induced noise correction factors for the traversing microphone.

Far-field Acoustic Measurements Technique

We measured far-field noise two metres from the fan exhaust, Figure 5.4. Leggat and Siddon (1978) studied the directivity of fan noise in a semi-reverberant environment concluding that the maximum noise levels were coincident with the fan axis, immediately downstream of the exhaust. In the research reported in this chapter we chose to measure fan fan-field noise coincident with the fan axis on the fan centre line and at 30, 45, 60, 75 and 90 degrees off the fan centre line. Flow velocities at each far-field microphone were low enough for us to reasonably ignore them, with the exception of measurements we made on the fan centre line. We corrected each far-field measurement for wind noise using a correction factor provided by the microphone manufacturer (Brüel & Kjær, 2006).

We made near- and far-field acoustic measurements simultaneously in the near- and far-field with the near-field microphone at each span-wise location. After completing the measurements, we moved the far-field microphone to the next azimuthal position. We made the near- and far-field measurements again with the near-field microphone at each span-wise location. In this way, the experimental technique was able to provide data sets of near- and far-field noise over a range of far-field azimuthal positions that we could correlate to establish the far-field directivity of near-field noise sources. We were then able to use the directivity analysis to characterise the fan far-field noise's directivity with and without blade-tip end-plates fitted.

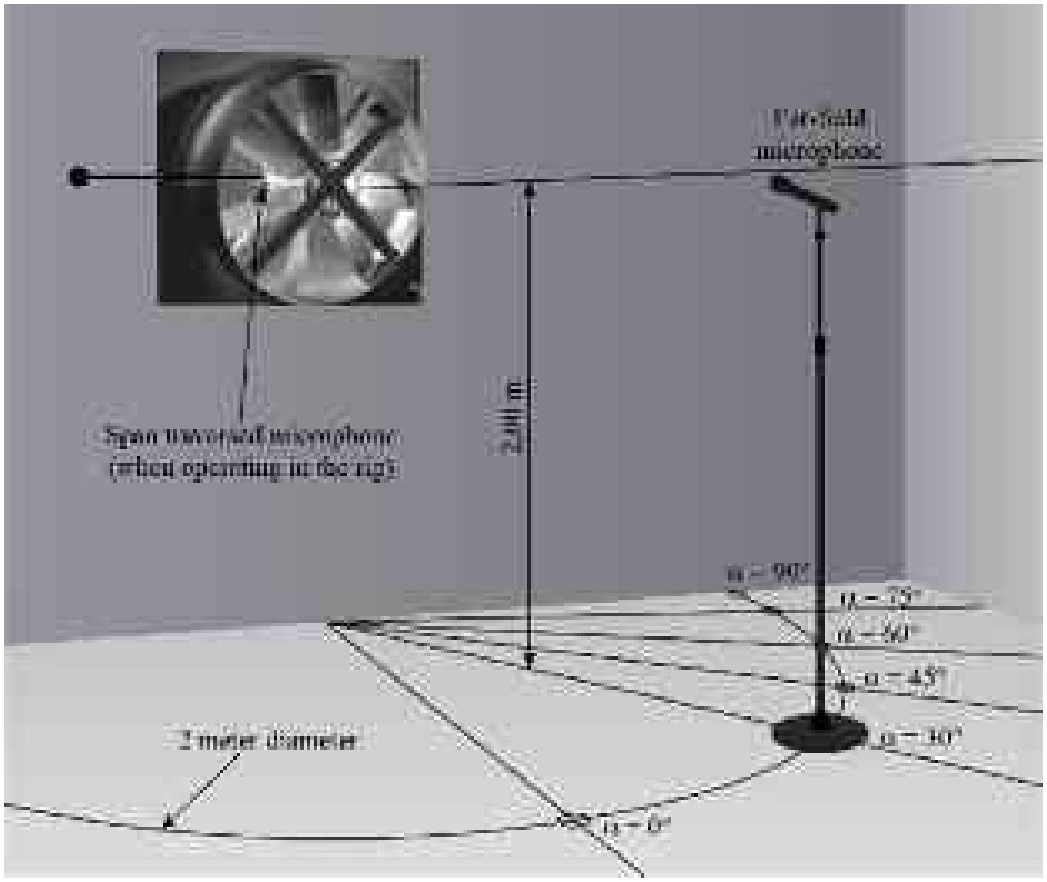

FIGURE 5.4. Microphone arrangement for outlet far-field measurements of fan noise in the anechoic chamber used for near- and far-field fan outlet noise measurements.

For each near- and far-field measurement we computed the narrowband spectra 50 to 10 kHz using a constant bandwidth of 3.15 Hz. Following Bianchi *et al.*'s method (2009a), we cross-correlated the near- and far-field signals that we took with the far-field microphone 30 degrees of the fan centre line. Subsequently we cross-correlated the near- and far-field measurements to facilitate the identification of near-field noise sources responsible for far-field noise. The cross-correlation enabled us to avoid pseudo sound degrading the accuracy of the measurements. Pseudo sound is turbulence-generated noise that is recorded in the near-field, but decays so quickly that it does not contribute to the far-field noise. Mugridge and Morfey (1972), Holste and Neise (1997), Miles (2006) and Laurendeau *et al.* (2007) have successfully used the cross-correlation technique we adopted in the present study to correct for pseudo sound in exhaust flows.

Fan Acoustic Modes

Before moving on a directivity analysis, it is helpful to characterise the circumferential and radial acoustic modes for the studied fan when installed in the anechoic chamber. The fan's modal characteristics are driven by the interaction of the rotating

blades and static components down-stream of the fan blades. The resultant modal characteristics provide a context within which we may interpret the far-field directivity of near-field noise sources.

We may identify these modes from a study of the interaction of the fan's rotating blades with the acoustic media passing though the fan and static components in the fan exhaust. For a fan operating at a fixed operation point we may perform a circumferential mode decomposition of the fan noise at the fan exhaust plane. This circumferential mode decomposition enables us to identify circumferential and radial acoustic modes, cut-off frequency and radiation angles at the blade passing frequency and its second, third and four harmonics (Blake, 1986).

In order to characterise the studied fan's modal characteristics, we calculated the first ten modes, their cut-off frequencies and their radiation angles, Table 5.3. In this context, we define radiation angle as the angle from the fan centre line. The sixth circumferential mode (m = 6, Table 5.3) is the rotor-locked mode that results in a low-frequency tone produced as a consequence of induced distortions in the flow-field upstream of the fan. As this tone is produced by inflow distortions induced in the inflow by the fan rotor's rotation, we characterise it as rotor noise (RN). It is noteworthy that the higher circumferential modes propagate at lower radiation angles. This is in marked contrast to the radiation angle for each individual mode that increases with each harmonic of blade passing frequency.

TOTAL SOUND PRESSURE LEVEL DIRECTIVITY

Our directivity analysis starts with a review of the azimuthal distribution of outlet sound pressure level (L_P) cross-spectra between the near- and far-field, Figure 5.5. We generated the azimuthal distribution distributions at the studied fan's design operating point. The azimuthal distribution illustrates that the highest sound pressure

Table 5.3. *Circumferential and radial acoustic modes, cut-off frequencies and radiation angles at the blade passing frequency and its second, third and four harmonic.*

Circumferential modes M	Radial modes n	Cut-off frequency (Hz) f^{co}_{mn}	Radiation angle Φ_{mn} (degrees) BPF	2^{nd} BPF	3^{rd} BPF	4^{th} BPF
0	1	189.05	29.7	81.6	81.4	81.4
2	0	378.10	14.4	29.6	48.1	82.7
2	1	422.73	12.8	26.3	41.7	62.5
2	2	534.71	10.1	20.5	31.7	44.5
4	0	756.20	7.1	14.3	21.8	29.7
4	1	779.47	6.9	13.9	21.2	28.8
4	2	845.46	6.4	12.8	19.4	26.3
6	0	1134.30	4.7	9.5	14.4	19.3
6	1	1149.95	4.7	9.4	14.2	19.0
6	2	1195.66	4.5	9.0	13.6	18.3

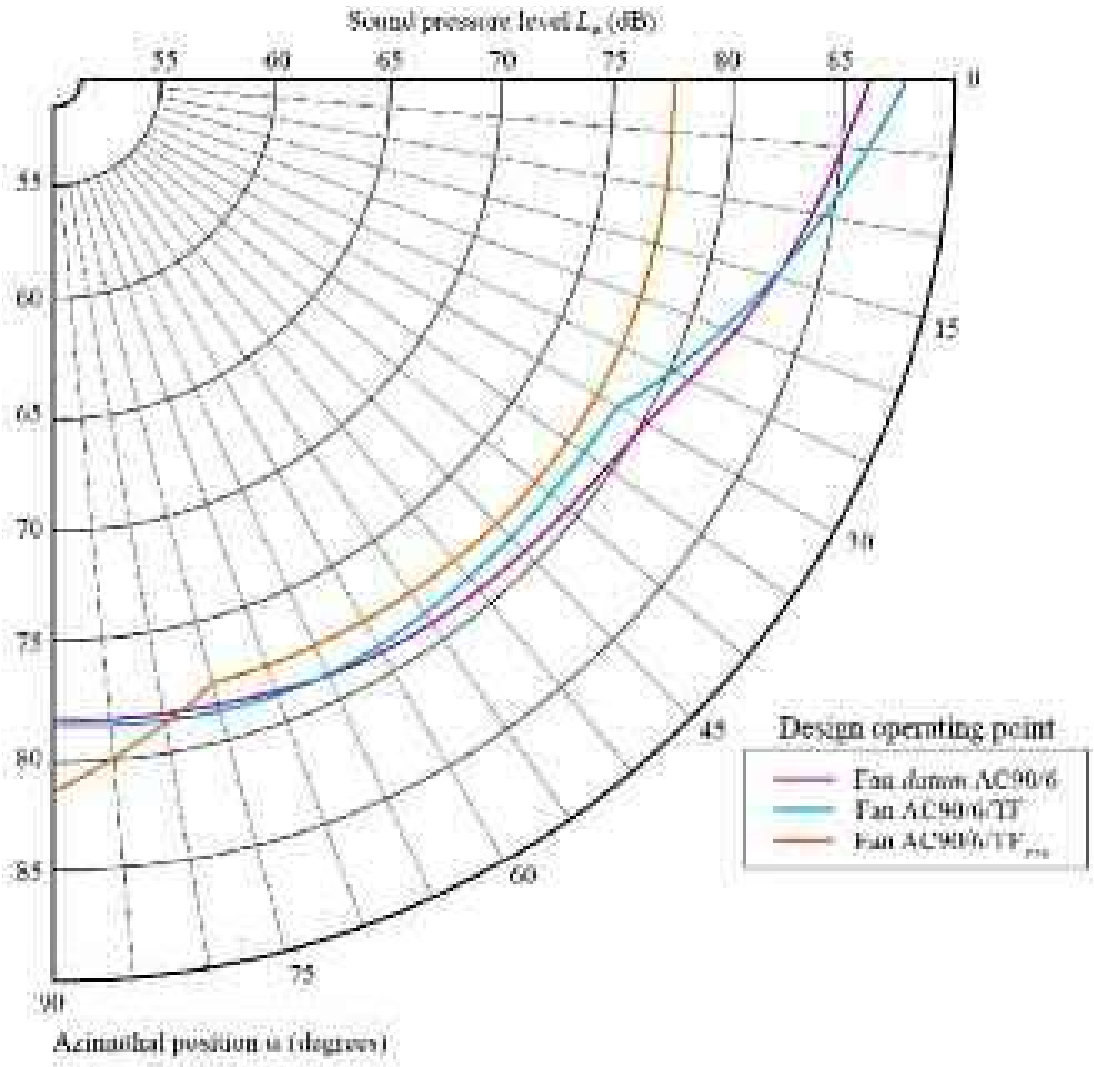

FIGURE 5.5. Measured far-field directivity of the integrated sound pressure level (L_p) for the three studied fans. The peak values of integrated sound pressure level for the fan *datum* AC90/6 and AC90/6/TF are at zero degrees, on the fan axis indicating a dipolar noise source in the fan outlet. In contrast, the integrated sound pressure level for the fan AC90/6/TF$_{VTE}$ is more uniform with azimuthal position.

levels for the fan *datum* AC90/6 and AC90/6/TF are at zero degrees, on the fan axis. The maximum levels are 86 dB and 87 dB respectively. This result is self-consistent with Leggat and Siddon's results (1978) and indicates that the fan *datum* AC90/6 and AC90/6/TF are behaving like dipolar noise sources. Within this context a monopole noise source is a source which radiates sound equally well in all directions. A dipole noise source consists of two monopole sources of equal strength, but opposite phase and separated by a small distance compared with the wavelength of sound. Just as two opposite phase monopoles comprise a dipole, two opposite dipoles comprise a quadrupole noise source.

In contrast to the fans *datum* AC90/6 and AC90/6/TF, the highest sound pressure level for the fan AC90/6/TF$_{VTE}$ occurred at 90 degrees. The maximum level was 82 dB at 90 degrees, but only 77 dB at zero degrees, on the fan axis. Additionally, when one studies the azimuthal distribution of the fan AC90/6/TF$_{VTE}$, it is noticeably

more isotropic than the fan *datum* AC90/6 or AC90/6/TF. Within this context, we define an isotropic noise source as a noise source that has the same value when measured in different directions. We may attribute this isotropic behaviour to the variable thickness blade-tip end-plate inducing a shift in acoustic emissions from higher to lower frequency.

Spectral Directivity

In the programme of work reported in this chapter we present a directivity analysis to characterise the directivity of fan far-field noise with and without blade-tip end-plates fitted. To facilitate the analysis, we present measured far-field directivity 'maps' of the sound pressure level spectrum.

Consider the directivity map for the fan *datum* AC90/6, Figure 5.6. The directivity map indicates that both tonal and broadband noise is anisotropic. We recorded the highest sound pressure levels at zero degrees on the fan axis, with a second peak at 30 degrees. This observation is self-consistent with Wright (1976) and Leggat and Siddon's (1978) conclusions. It indicates that the fan *datum* AC90/6 is behaving like

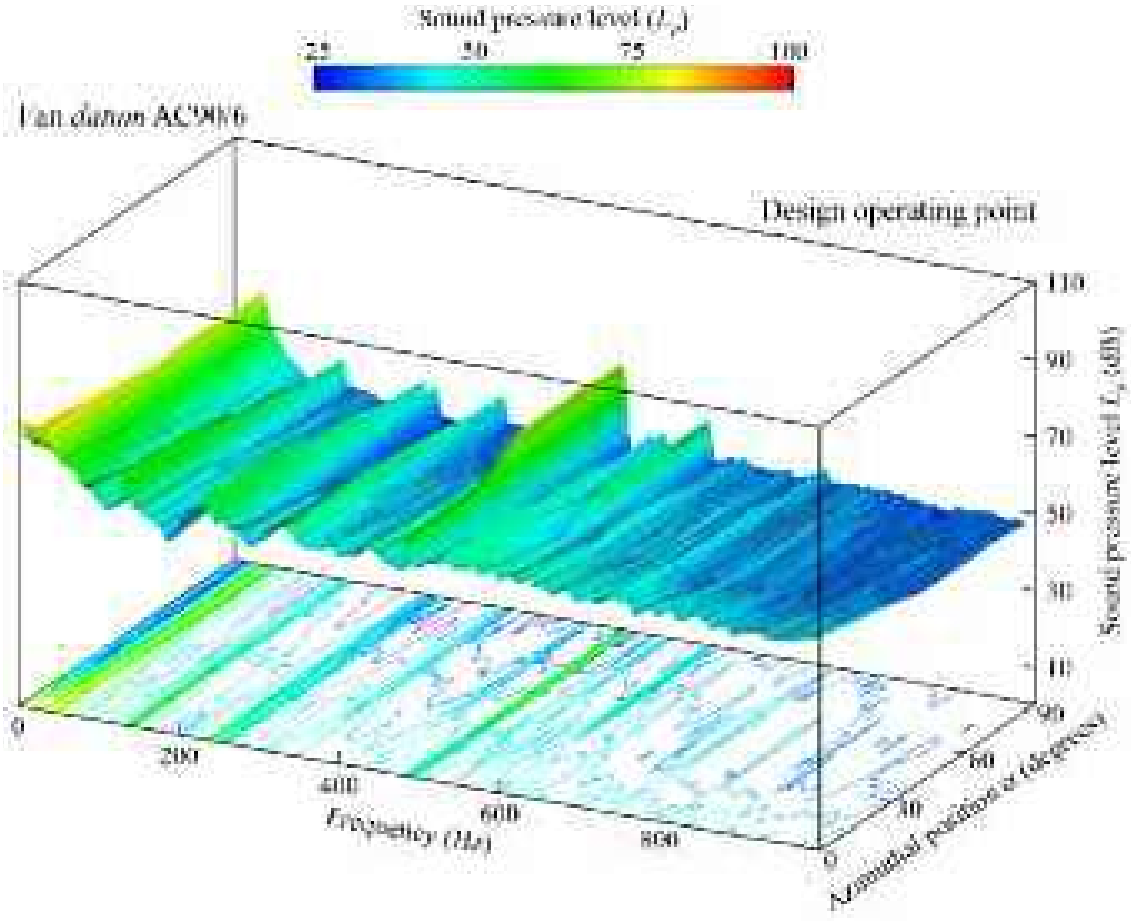

FIGURE 5.6. Measured far-field directivity of the sound pressure level (L_p) spectrum for the fan *datum* AC90/6 illustrating that the sound pressure level spectrum is anisotropic with azimuthal position.

a dipolar noise source. When we study the directivity map further it is apparent that there are identifiable features, the first of which we may associate with the blade passing frequency. We may associate the second to sixth with the blade passing frequencies' second, third, four, fifth and sixth harmonic. The directivity map indicates that the blade passing frequency and its second harmonic are isotropic. In contrast, the third to sixth harmonics exhibit reducing sound pressure level with increasing azimuthal angle.

The directivity map also includes some tonal features at 550 Hz and 650 Hz that are not blade passing frequency harmonics. Bianchi *et al.* (2009b) previously identified these tones and associated them with the electric motor that drives the fan. As these tones are not aerodynamically induced we do not consider them when assessing the far-field acoustic directivity of near-field flow-field features.

Consider the directivity map for the fan AC90/6/TF, Figure 5.7. The directivity map indicates that the fan AC90/6/TF's acoustic characteristics are essentially similar to the fan *datum* AC90/6 up to the fourth harmonic of blade passing frequency. Above the fourth harmonic of blade passing frequency there is a reduction in the sound pressure level at zero degrees on the fan axis. There is also a slight increase in the sound pressure level at 90 degrees for all tonal features.

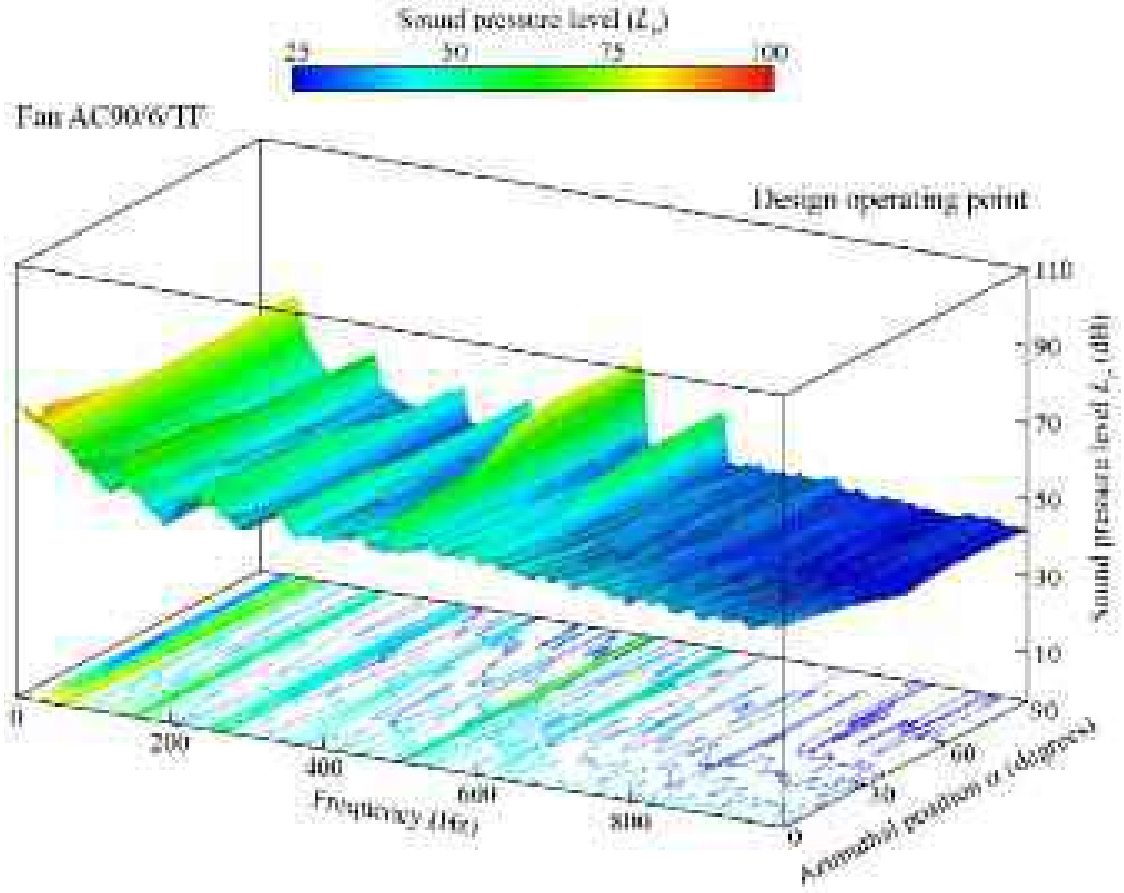

FIGURE 5.7. Measured far-field directivity of the sound pressure level (L_P) spectrum for the fan AC90/6/TF illustrating that the sound pressure level spectrum is anisotropic with azimuthal position.

Consider the directivity map for the fan AC90/6/TF$_{VTE}$, Figure 5.8. The directivity map indicates that both broadband and tonal sound pressure levels are different to those of both fan *datum* AC90/6 and AC90/6/TF at frequencies above the blade passing frequency. In the frequency range from 600 Hz to 1 kHz, the sound pressure level reduces at zero degrees on the fan axis. Additionally, tonal features are apparent that correlate with blade passing frequency harmonics above the sixth harmonic. This may indicate that the dipole characteristic of both the fan *datum* AC90/6 and AC90/6/TF has changed to a quadrupole characteristic for the fan AC90/6/TF$_{VTE}$.

The only difference between the fan AC90/6/TF and AC90/6/TF$_{VTE}$ is the change from a constant to variable thickness blade-tip end-plate. Therefore, we may assume the change from a dipole to a quadrupole noise source occurs as a consequence of the change in end-plate geometry. We may gain an additional insight into this change by considering the sound pressure level spectra at zero degrees, on the fan axis and at 90 degrees, Figure 5.9. At zero degrees, on the fan axis the fan AC90/6/TF exhibits the highest sound pressure level at the first blade passing frequency. In contrast, the fan AC90/6/TF$_{VTE}$ exhibits the lowest. At 90 degrees the sound pressure levels at the first blade passing frequency are similar for the three studied fan geometries.

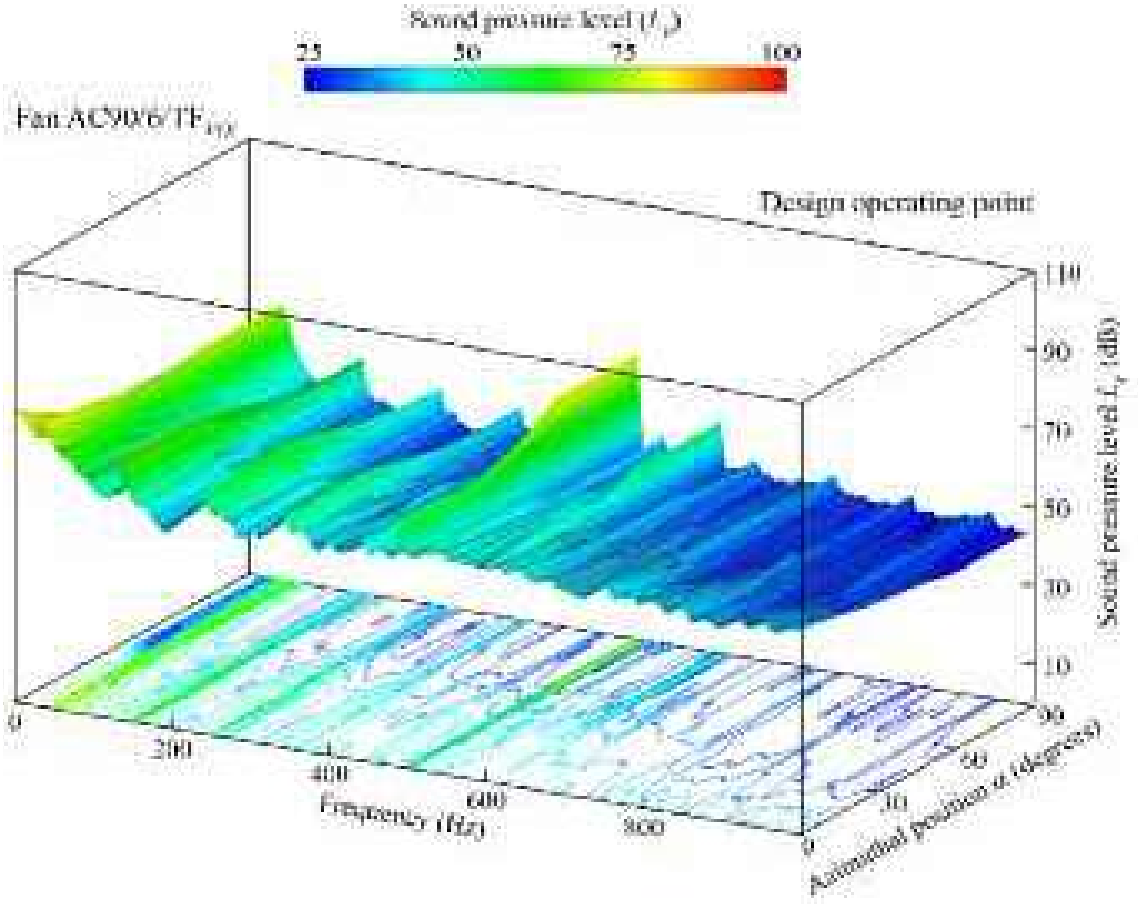

FIGURE 5.8. Measured far-field directivity of the sound pressure level (L_p) spectrum for the fan AC90/6/TF$_{VTE}$ illustrating that the sound pressure level spectrum is anisotropic with azimuthal position.

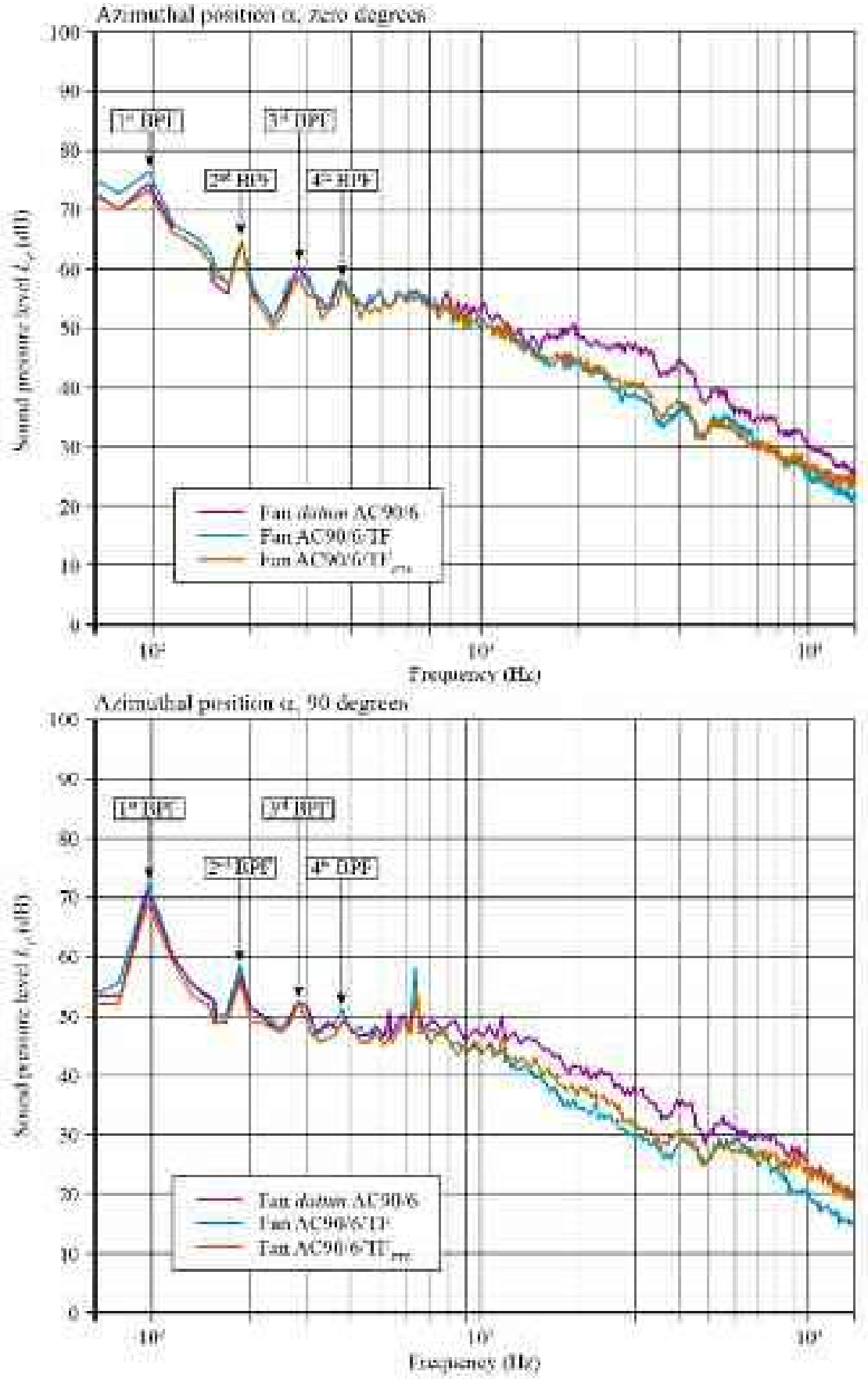

FIGURE 5.9. Outlet near-field narrowband sound pressure level (L_P) spectrum measured at a span-wise location in the blade tip region for the fan's *datum* AC90/6, AC90/6/TF and AC90/6/TF$_{VTE}$. The authors made measurements at the fan design operating point and present them at both zero and 90 degree azimuthal positions.

When we consider the broadband, the fans AC90/6/TF and AC90/6/TF$_{VTE}$ both exhibit lower sound pressure levels than the fan *datum* AC90/6 at zero degrees on the fan axis. At 90 degrees, the fan AC90/6/TF$_{VTE}$ is initially characterised by lower sound pressure levels than the fan AC90/6/TF. However, above 5 kHz the fan AC90/6/TF$_{VTE}$ sound pressure level increases back to the level of the fan *datum* AC90/6.

Tonal Noise Directivity

The directivity analysis for the three studied fans provided an insight into the azimuthal far-field acoustic consequences of near-field noise sources. We associated the fans AC90/6/TF and AC90/6/TF$_{VTE}$ with tones that merged with the broadband after the fourth harmonic of blade passing frequency. The tones merged with the broadband irrespective of azimuthal position. The only exception was a tone at 650 Hz that we associated with motor noise. Given the significance of the blade passing frequency and its second, third and fourth harmonics, we chose to analyse the directivity of sound pressure level at each, Figure 5.10.

Consider the azimuthal distribution of sound pressure level at the blade passing frequency, Figure 5.10. The fan AC90/6/TF has the highest sound power level at zero degrees, on the fan axis and then fell steadily as the azimuthal angle increased to 90 degrees. In contrast, the AC90/6/TF$_{VTE}$ sound pressure level remained almost constant as the azimuthal angle increased. It increased abruptly between 75 and 90 degrees, thus indicating a near-field flow-field phenomenon that influences the radiated noise's directivity at the blade passing frequency.

Our directivity analysis started with a review of the azimuthal distribution of overall outlet sound pressure level, Figure 5.5. The azimuthal distribution of sound pressure level at the blade passing frequency is similar in form to the overall distribution, Figure 5.10. However, the blade passing frequency integrated sound pressure levels are lower than the overall integrated sound power levels. The fan *datum* AC90/6 is 10 dB lower, the fan AC90/6/TF is 7 dB lower and the fan AC90/6/TF$_{VTE}$ is 5 dB lower.

Consider the azimuthal distribution of sound pressure level at the second harmonic of blade passing frequency, Figure 5.10. The fan *datum* AC90/6 and AC90/6/TF azimuthal distribution of sound pressure level at the second harmonic are similar to those exhibited at the blade passing. The only difference is that overall sound pressure levels are lower at the second harmonic. In contrast, the fan AC90/6/TF$_{VTE}$ sound pressure level falls steadily from zero degrees on the fan axis to 75 degrees where it then rises from 75 degrees to 90 degrees.

We may conceptualise the fan AC90/6/TF$_{VTE}$ azimuthal sound pressure level distribution at the second harmonic as resulting from a combination of two noise sources. The first noise source is on-axis and the second is at 90 degrees. This conceptualisation is self-consistent with the theory that the fan AC90/6/TF$_{VTE}$ acoustic emissions result from the superposition of longitudinal dipole and lateral quadrupole

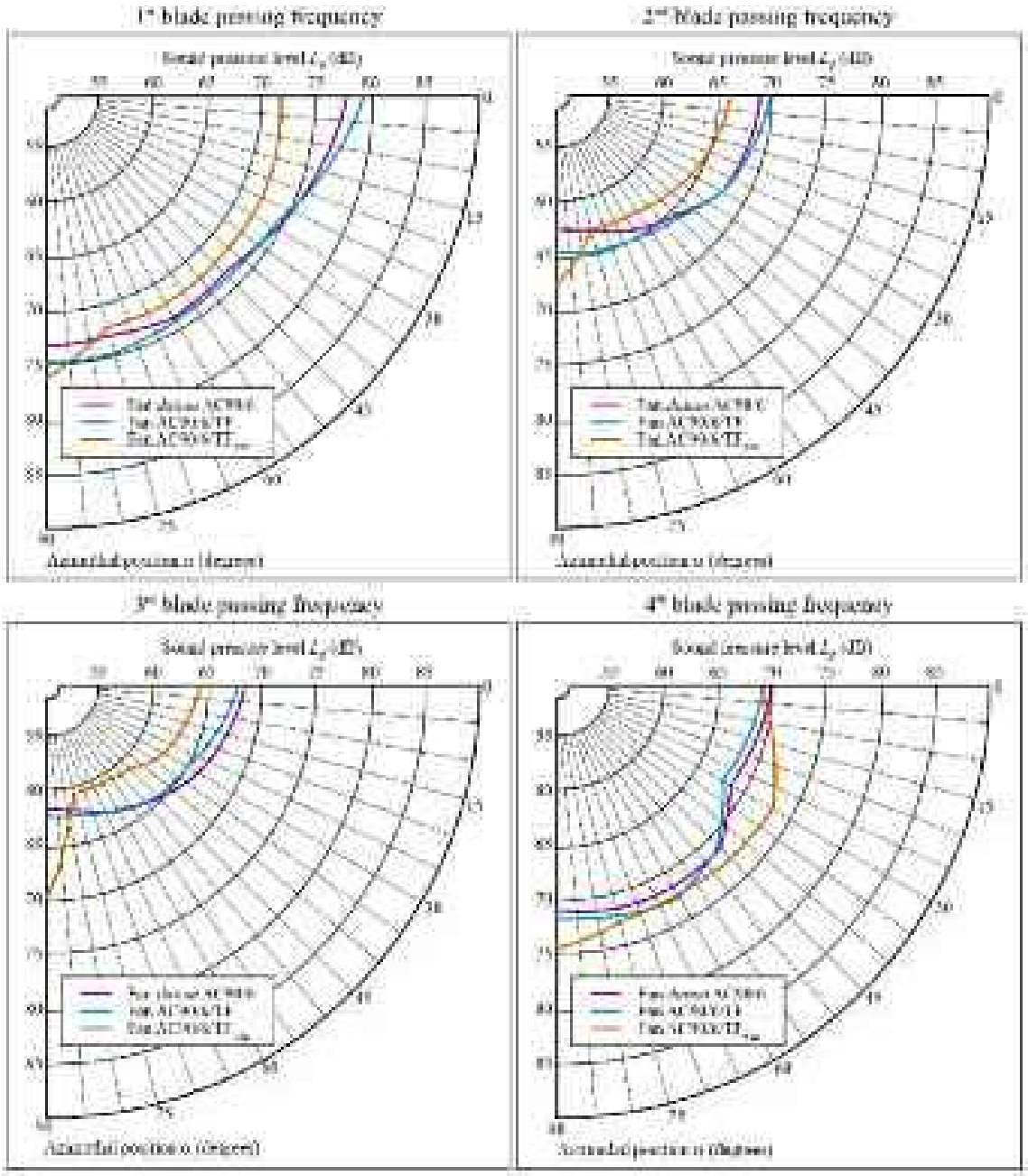

FIGURE 5.10. Measured narrowband far-field directivity of the sound pressure level (L_p) measured at a span-wise location in the blade tip region for the fans *datum* AC90/6, AC90/6/TF and AC90/6/TF$_{VTE}$. The authors made measurements at the fan design operating point and present them at the blade passing frequency and its second, third and fourth harmonic.

noise sources. It is noteworthy that the second harmonic of blade passing frequency is 187 Hz, slightly lower than this mode's 189 Hz cut-off frequency, Table 5.3. This implies that the mode's cut-off frequency did not affect the blade passing frequency and its second harmonic propagation.

Consider the azimuthal distribution of sound pressure level at the third harmonic of blade passing frequency, Figure 5.10. Both the fan *datum* AC90/6 and

AC90/6/TF azimuthal distributions of sound pressure level are reduced and more anisotropic than at either the blade passing frequency or its second harmonic. At the third harmonic of blade passing frequency the resultant azimuthal distributions are closer to those of a theoretical dipolar noise source. In contrast, the fan AC90/6/TF$_{VTE}$ azimuthal distribution maintains its twin-lobe form. This supports the theory that acoustic emissions result from the superposition of longitudinal dipole and lateral quadrupole noise sources.

Consider the azimuthal distribution of sound pressure level at the fourth harmonic of blade passing frequency, Figure 5.10. The azimuthal distribution of sound pressure level for all three of the studied fans were significantly different to those of either the blade passing frequency, the second and third harmonic. The azimuthal distributions for the fan *datum* AC90/6 and AC90/6/TF now exhibit and angular shift at 30 and 45 degrees with the maximum sound pressure level at 60 degrees. The fan AC90/6/TF$_{VTE}$ azimuthal distribution also includes an angular shift at 30 degrees, with the increase in sound pressure level between 75 and 90 degrees now less dominant.

The change in the azimuthal distributions characteristics at the fourth harmonic of blade passing frequency was unexpected. This change may be a consequence of the fourth harmonic of blade passing frequency coinciding with the centre frequency of Wright's (1976) spectrum. Wright (1976) characterised the vortex responsible for the acoustic emissions from load-dependent flow, specifically characterising its spectrum. For the studied fan, the -20 dB threshold is at a frequency of 395.2 Hz. This implies that the change in azimuthal distribution of the fourth harmonic of blade passing frequency is a consequence of the choice of fan design variables (Widnall, 1969; Wright, 1976).

Our earlier modal analysis indicates that the modes at 189 and 378 Hz will be significant at the fourth harmonic of blade passing frequency, Table 5.3. The computed angles of incidence for these modes are 81.4 and 82.7 degrees respectively. Rising sound pressure levels between 75 and 90 degrees characterise the fan AC90/6/TF$_{VTE}$ azimuthal distribution. From this we may infer that there is a constructive interference of these two modes as a consequence of the flow-field physics occurring with the variable thickness blade-tip end-plate.

Broadband Noise Directivity

The tonal noise analysis for the three studied fans provided a further insight into the azimuthal far-field acoustic consequences of near-field noise sources. The azimuthal distribution of sound pressure level varied from harmonic to harmonic. To complement this analysis, we examined broadband noise by calculating the logarithmic sum of sound power level for frequencies from 1 kHz to 10 kHz, Figure 5.11.

Consider the azimuthal distribution of broadband sound pressure level, Figure 5.11. Both the constant and variable thickness blade-tip end-plates result in a significant decrease in broadband noise at all azimuthal positions. This illustrates the benefit of blade-tip end-plates. Irrespective of the end-plate design, the broadband sound

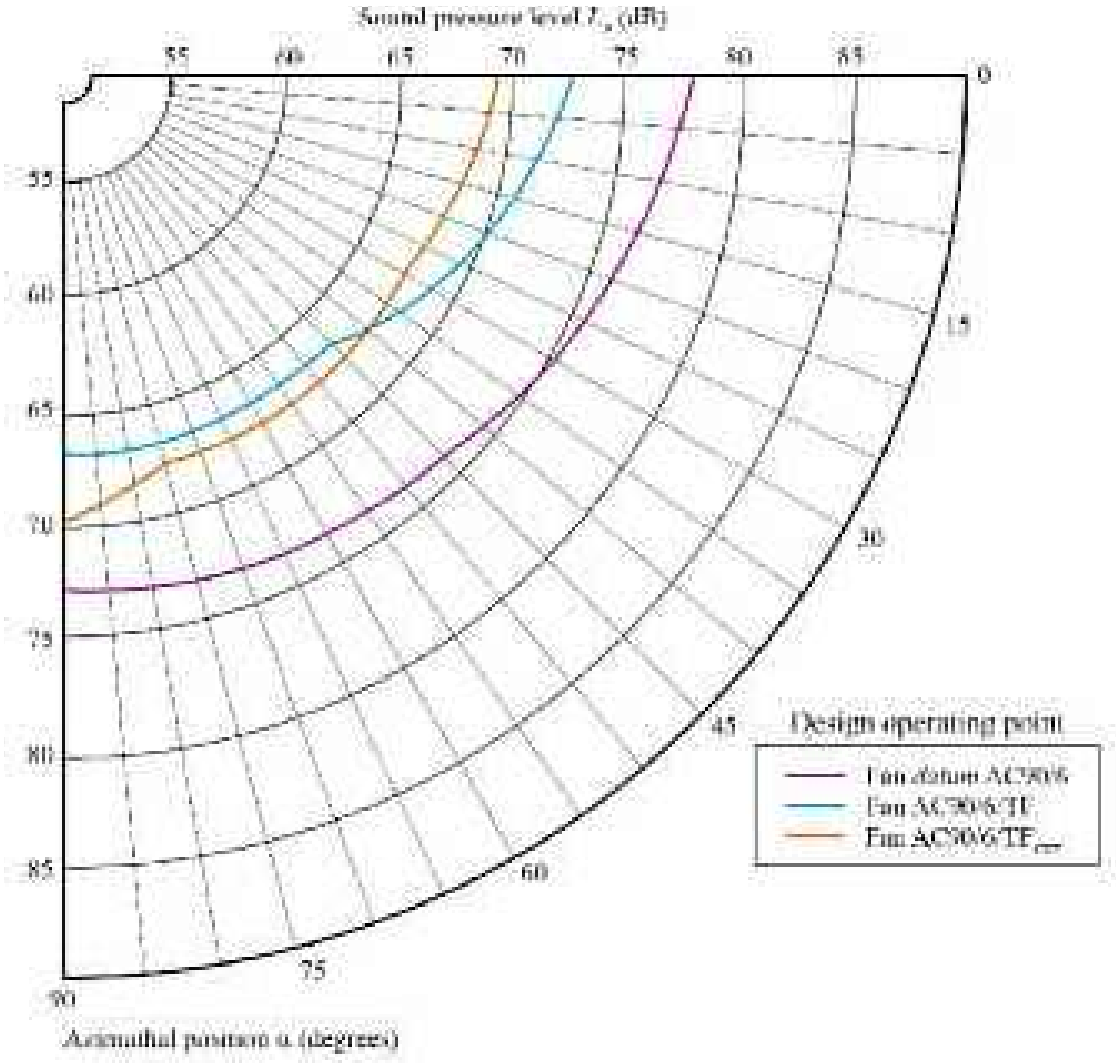

FIGURE 5.11. Measured broadband far-field directivity of the sound pressure level (L_P) measured at a span-wise location in the blade tip region for the fans *datum* AC90/6, AC90/6/TF and AC90/6/TF$_{VTE}$. The authors made measurements at the fan design operating point.

pressure level decreases. However, if we focus on the azimuthal distributions of the fans AC90/6/TF and AC90/6/TF$_{VTE}$, it is apparent that there are different mechanisms at play.

The analysis of the blade passing frequency and its second, third and fourth harmonics has already indicated that there are different mechanisms at play. An on-axis radiation characterises the fan AC90/6/TF, whilst more spherical radiation patterns characterise the fan AC90/6/TF$_{VTE}$. We may associate these more spherical radiation patterns with the acoustic emissions from small-scale vortical structures. If this is the case, these structures are likely to originate as a consequence of blade-tip flow-field features induced by the presence of the variable thickness blade-tip end-plate. We determined broadband noise by calculating the logarithmic sum of sound power level for frequencies from 1 kHz to 10 kHz. At frequencies above 1 kHz, all calculated modes are in-play, Table 5.3. The tendency of these modes will be to influence the sound pressure level at higher angles off the fan axis.

Discussion of Tonal and Broadband Directivity Results

Scholars have studied the near-field aerodynamic cause of far-field acoustic effect since the 1950s. Lighthill (1954) studied jet noise, and more recently Shah *et al.* (2007a, 2007b) have studied swirling-flow noise. These scholars were able to identify a causal relationship between small-scale random turbulent structures in the near-field and far-field noise. They associated high-frequency far-field noise with nearly-isotropic radiation. They associated large-scale coherent eddies with directional radiation, with the radiation angle dependent on their rotational frequency.

The exhaust flow from the studied fans is a swirling flow that contains small-scale swirling flow-field features. We postulate that the fan AC90/6/TF$_{VTE}$ far-field tonal and broadband noise is strongly influenced by these flow-field features. We have previously observed that the dipole characteristic of both the fan *datum* AC90/6 and AC90/6/TF changed to a quadrupole characteristic for the fan AC90/6/TF$_{VTE}$. Shah *et al.* (2007a) concluded that a quadrupole source's acoustic signature, in a low Mach number flow may be attributed to the turbulent mixing of swirling flow-field features. This mixing scatters the dipolar noise source.

Given the above we hypothesise that the directivity of the fan AC90/6/TF$_{VTE}$ far-field tonal and broadband noise may be a consequence of the blade-tip end-plate geometry. The variable thickness blade-tip end-plate may have affected the blade tip-to-casing flow-field, thus avoiding blade tip-to-casing leakage vortex bursting. The variable thickness blade-tip end-plate would achieve this by augmenting the blade tip-to-casing leakage vortex swirl level. This augmentation would increase the vortex rotational frequency as it progresses from blade leading to trailing edge. Mankbadi and Liu (1984) studied the sound generated by swirling flow-field features in a turbulent jet. They concluded that features that did not burst were discernable by the azimuthal switching of the directional components of the acoustic emissions. They switched from on-axis to radial radiation. Mankbadi and Liu's (1984) conclusions therefore support our hypothesis that the fan AC90/6/TF$_{VTE}$ far-field tonal and broadband noise results as a consequence of the blade-tip end-plate geometry

Detection of Aerodynamic Noise Sources

The spectral, tonal and broadband directivity analysis provides an insight into the studied fan's flow-field physics. However, if we are to link near-field flow-field features with their far-field acoustic consequences we must identify individual near-field flow-field features and identify their far-field effect. Jordan and Gervais (2008) developed a noise source localisation technique. We may use this technique to identify the near- to far-field coupling mechanism.

We applied Jordan and Gervais's (2008) noise source localisation technique when mapping the span-wise distribution of sound pressure level. The map presents the span-wise distributions of coherence between near-field noise measured at the fan outlet and far-field noise. We positioned the far-field microphone 30 degrees off the fan centre line. We integrated the measured data in two ways, first from 50 Hz to

10 kHz and, second from 1 kHz to 10 kHz. The first integration represents a narrow-to-broadband integration and the second a broadband integration.

Consider the narrow-to-broadband integration of sound pressure level from 50 Hz to 10 kHz, Figure 5.12. A sound pressure level peaking at 120 dB at 35 per cent blade span characterises the fan *datum* AC90/6. We may associate this sound pressure level peak with a hub separation that centrifuges up to approximately 30 per cent blade span. A second peak at 85 per cent blade span characterises the fan *datum* AC90/6. This span-wise location is self-consistent with the blade tip-to-casing leakage vortex location that is driven radially inwards from the blade tip by the blade-to-blade passage vortex.

A different span-wise feature than the fan *datum* AC90/6 characterises the sound pressure level's narrow-to-broadband integration for the fan AC90/6/TF. The hub separation is still apparent, but at 29 per cent and not 35 per cent blade span. This reduction in span-wise position indicates that the hub separation's magnitude has reduced. Additionally, the peak in sound pressure level we associated with the blade tip-to-casing leakage vortex at 85 per cent blade span is absent. This absence indicates that the constant thickness blade-tip end-plate is effective at supressing near-field flow-field features that are responsible for fan far-field noise.

Similar span-wise features to the fan AC90/6/TF characterise the sound pressure level's narrow-to-broadband integration for the fan AC90/6/TF$_{VTE}$. The hub separation has moved inward slightly to 27 per cent blade span, but is essentially similar to the fan AC90/6/TF. Lower sound pressure levels than either the fan *datum* AC90/6 or AC90/6/TF characterise the mid-span from 40 to 80 per cent blade span. The peak in sound pressure level we associated with the blade tip-to-casing leakage vortex at 85 per cent fan *datum* AC90/6 blade span that was absent for fan AC90/6/TF is also absent for the fan AC90/6/TF$_{VTE}$.

Consider the broadband integration of sound pressure level from 1 kHz to 10 kHz, Figure 5.12. Large scale coherent vortices characterise the span-wise distribution of sound pressure level for both the fan *datum* AC90/6 and fan AC90/6/TF. The hub separation is similar for both fans at 35 per cent blade-span. However, over the mid-span from 50 to 80 per cent blade span, sound pressure level that is 2 dB higher than the fan *datum* AC90/6 characterise the fan AC90/6/TF. In the blade tip region both the fan *datum* AC90/6 and fan AC90/6/TF have span-wise distributions of sound pressure level characterised by rapidly increasing sound pressure levels. The peak value for the fan AC90/6/TF is approximately 126 dB. Counter- intuitively, it is only 1 dB lower than the fan *datum* AC90/6.

Similar span-wise features to the fan *datum* AC90/6 and fan AC90/6/TF characterise the broadband integration of sound pressure level for the fan AC90/6/TF$_{VTE}$. The hub separation is still evident at 30 per cent blade-span, but now 5 dB quieter than either the fan *datum* AC90/6 or fan AC90/6/TF. In the blade tip region similar span-wise features also characterise the fan AC90/6/TF$_{VTE}$. However, the peak sound pressure level is approximately 4 dB lower than the fan *datum* AC90/6 or fan AC90/6/TF.

The source localisation technique that we applied to the narrow-to-broadband and broadband integrations was able to facilitate the identification of near- to far-field coupling mechanisms. To complement the narrow-to-broadband and broadband

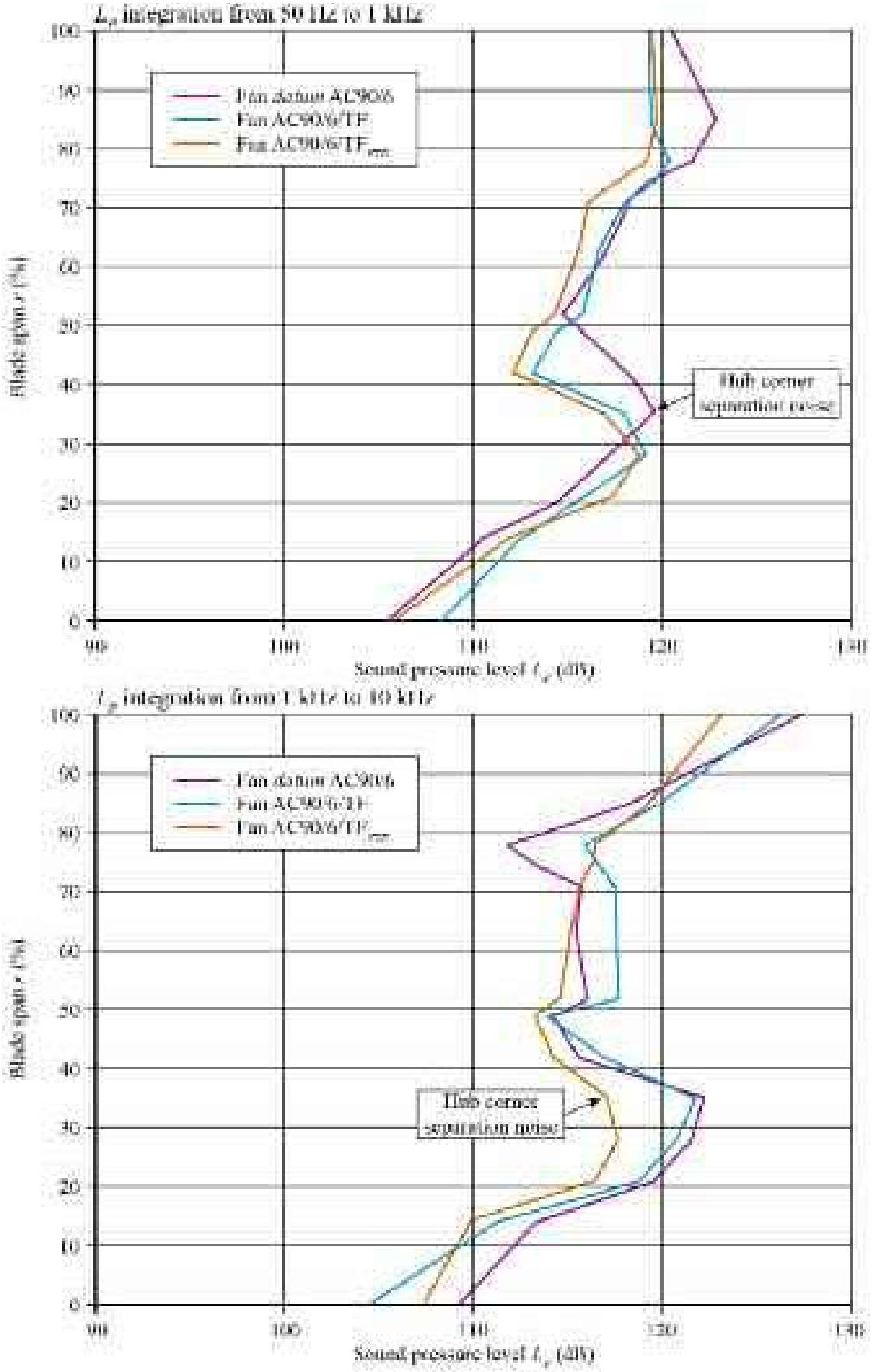

FIGURE 5.12. Span-wise maps of circumferentially averaged sound pressure level (L_p). The map presents measurement that the authors made at the design operating point of the narrow-to-broadband integration of sound pressure level from 50 Hz to 1 kHz and broadband integration of sound pressure level from 1 kHz to 10 kHz.

integrations, we conducted five further tonal integrations. The first was at the blade passing frequency, Figure 5.13. The second was at the fifth harmonic of blade passing frequency, Figure 5.14. The third was at the sixth harmonic of blade passing frequency, Figure 5.15. The fourth was at the seventh harmonic of blade passing frequency, Figure 5.16. The fifth was at the eighth harmonic of blade passing frequency, Figure 5.17. This series of integrations facilitates an analysis of the evolution of span-wise features with frequency.

Consider the evolution of the fan *datum* AC90/6 span-wise features. The dominant tonal noise source at all considered frequencies are in the hub and tip regions. We associate these with coherent vortex shedding. The hub separation is responsible for the coherent vortex shedding that results in a peak sound pressure level at 30 per cent blade span at the blade passing frequency. The hub separation results in a peak sound pressure level at 40 per cent blade span at the harmonics of blade passing frequency. In the tip region the coherent vortex shedding produces a peak in sound pressure level at 85 per cent blade span at the blade passing frequency. At the harmonics of blade passing frequency the sound pressure level does not peak at 85 per cent blade span, but continues to rise to the blade tip.

Consider the evolution of the fan AC90/6/TF span-wise features. The dominant tonal noise source at all considered frequencies are the same as those of fan *datum* AC90/6. However, there are differences between the two and therefore we may conclude that the constant thickness blade-tip end-plate affects the far-field tonal noise

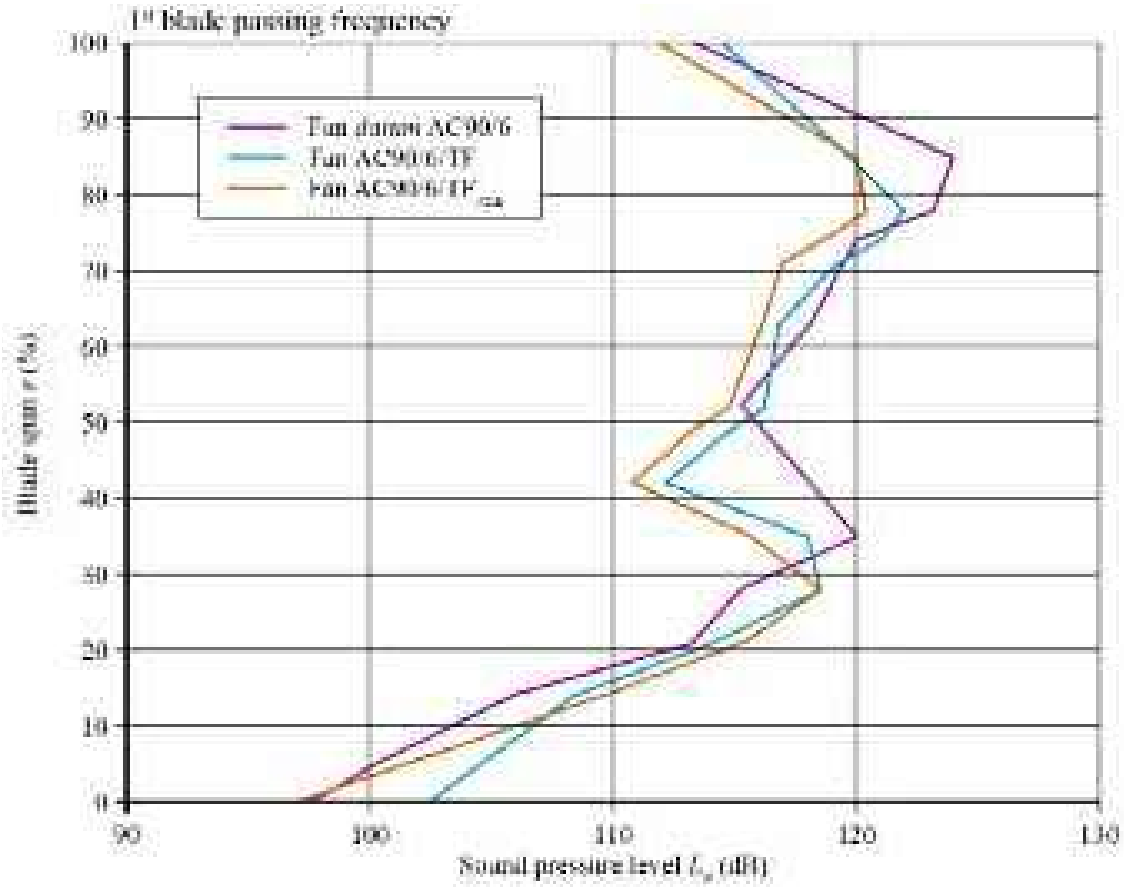

FIGURE 5.13. Measured span-wise cross-spectrum between near- and far-field sound pressure level (L_P) for the fan *datum* AC90/6, AC90/6/TF and AC90/6/TF$_{VTE}$. The authors made measurements at the fan design operating point and present them at the blade passing frequency.

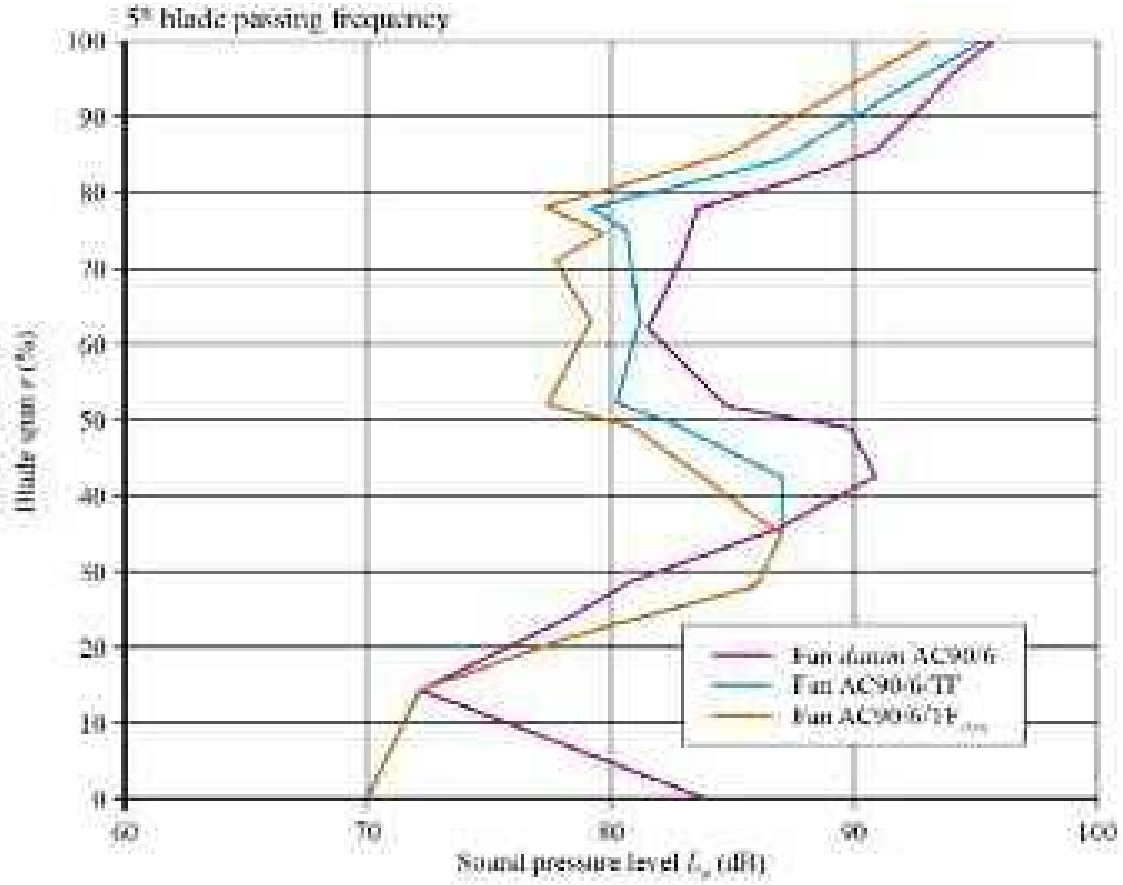

FIGURE 5.14. Measured span-wise cross-spectrum between near- and far-field sound pressure level (L_P) for the fan *datum* AC90/6, AC90/6/TF and AC90/6/TF$_{VTE}$. The authors made measurements at the fan design operating point and present them at the fifth harmonic of blade passing frequency.

over the entire blade span. Consider the evolution of the fan AC90/6/TF$_{VTE}$ span-wise features. The dominant tonal noise source at all considered frequencies are the same as those of fan *datum* AC90/6 and AC90/6/TF. However, the sound pressure level is generally lower than either the fan *datum* AC90/6 or AC90/6/TF. Again this indicates that the variable thickness blade-tip end-plate affects the far-field tonal noise over the entire blade span, and that this influence results in lower fan far-field tonal noise.

We completed research reported in this chapter with one final directivity analysis based on a local specific sound pressure level (κ_p). The local specific sound pressure level constitutes a measure of noise source effectiveness that accounts for the actual span-wise distribution of aerodynamic load from blade hub to tip. We defined local specific sound pressure level using the same approach Fukano *et al.* (1986) used when defining a global sound power coefficient. At each elemental blade section we computed local specific sound pressure level by subtracting the total pressure rise delivered to the air flow from the near-to-far-field cross-spectra SPL(r). The local specific sound pressure level κ_p at a blade span (r) reads as:

$$\kappa_p(r) = SPL(r) - 10\log\left(\Psi^2(r)\right)$$

where Ψ is the local total pressure rise coefficient normalised by the blade tip velocity.

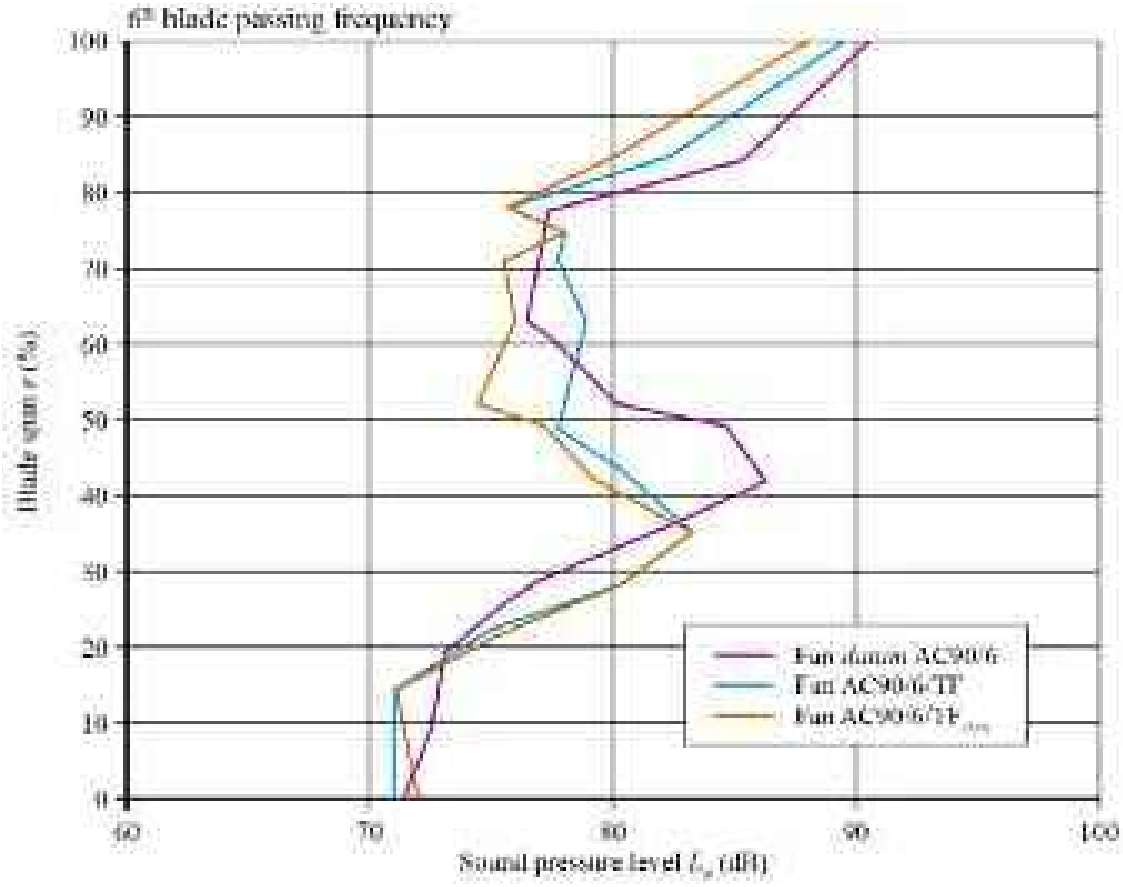

FIGURE 5.15. Measured span-wise cross-spectrum between near- and far-field sound pressure level (L_P) for the fan *datum* AC90/6, AC90/6/TF and AC90/6/TF$_{VTE}$. The authors made measurements at the fan design operating point and presents them at the sixth harmonic of blade passing frequency.

Consider the span-wise distribution of local specific sound pressure level for the three studied fans 30 degrees and 90 degrees off the fan axis, Figure 5.18. We may associate the mid-span region from 25 to 75 per cent blade span with vortex shedding. Longhouse (1978) first studied the acoustic significance of vortex shedding in relatively lightly loaded fans. He concluded that it is responsible for up to 5 dB of overall fan noise. Longhouse (1978) identified the importance of Tollmien-Schlichting instabilities as the flow-field mechanism responsible for vortex shedding noise.

A Tollmien-Schlichting instability is a stream-wise instability which arises in a viscous boundary layer. It is one of the more common methods by which a laminar boundary layer transitions to a turbulent boundary layer. Instabilities are initiated when some disturbance, for example, sound interacts with leading edge roughness in a process known as receptivity. These instabilities are slowly amplified as they move downstream. When they grow large enough, nonlinearities take over and the flow transitions from laminar to turbulent. They go on to interact with the blade wake in the trailing edge region, generating acoustic waves.

An analysis of local specific sound pressure level in the mid-span region facilitates identifying vortex shedding noise sources in this mid-span region. At 30 degrees off the fan axis the span-wise distribution of local specific sound pressure level for the three studied fans is constant. The fan AC90/6/TF$_{VTE}$ exhibits a lower local

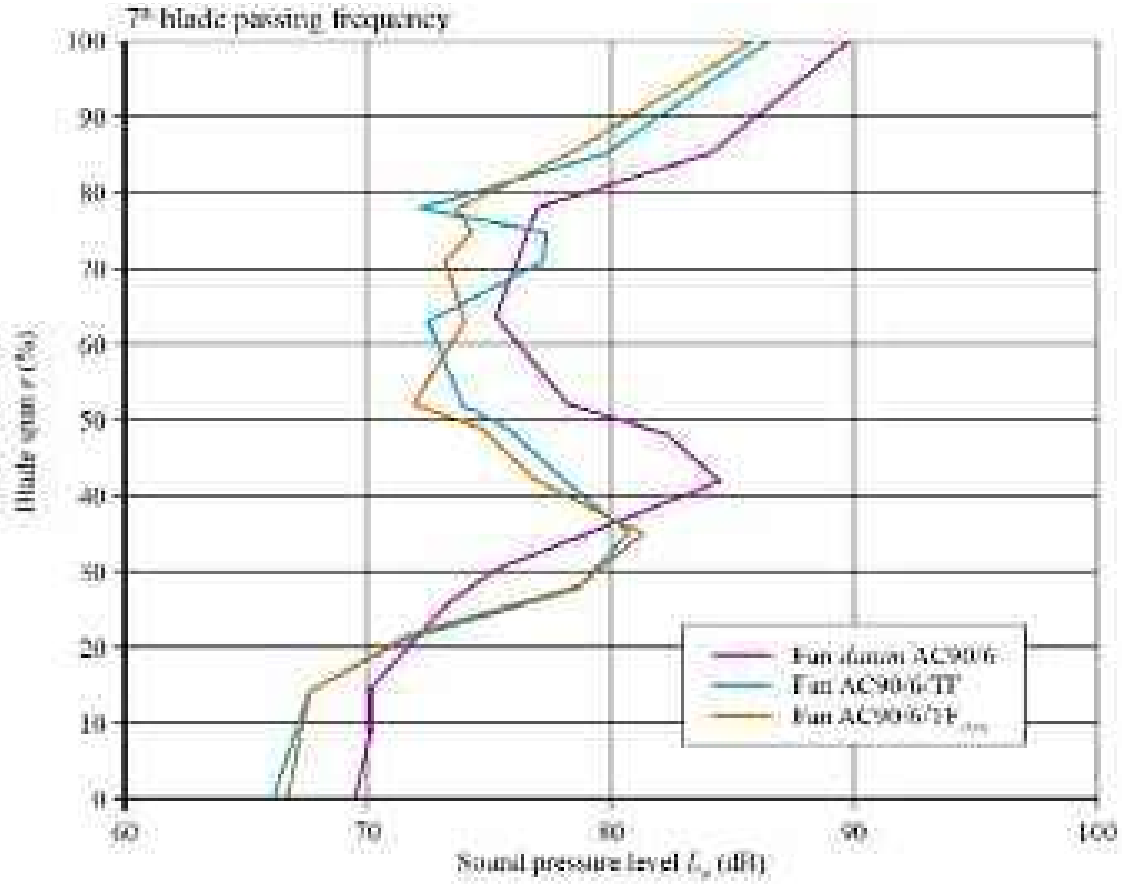

FIGURE 5.16. Measured span-wise cross-spectrum between near- and far-field sound pressure level (L_P) for the fan *datum* AC90/6, AC90/6/TF and AC90/6/TF$_{VTE}$. The authors made measurements at the fan design operating point and present them at the seventh harmonic of blade passing frequency.

specific sound pressure level than the fan *datum* AC90/6 and AC90/6/TF over the entire mid-span. From this we may conclude that vortex shedding noise was not the dominant noise source on or near the fan axis.

At 90 degrees off the fan axis the local specific sound pressure level decreases with increasing blade-span, therefore increasing blade load. In contrast to the 30 degree off fan axis, the fan AC90/6/TF$_{VTE}$ local specific sound pressure level was higher than either the fan *datum* AC90/6 or AC90/6/TF. Nash *et al.* (1999) made a similar observation when studying vortex shedding noise that occurred with boundary layer instability on aerofoils.

There are significant differences between the span-wise distributions of local specific sound pressure level at 30 degrees and 90 degrees off the fan axis. When previously analysing the far-field directivity of integrated sound pressure level, we observed that the fan *datum* AC90/6 and AC90/6/TF exhibited a dipole characteristic. In contrast, the fan AC90/6/TF$_{VTE}$ exhibited a quadrupole characteristic. We may attribute the fan AC90/6/TF$_{VTE}$ quadrupole characteristic to a reduction in the mid-span vortex shedding. We conclude that this reduction is driven by the variable thickness blade-tip end-plate geometry and its impact on the boundary layers, not just in the blade tip region, but over the entire blade span.

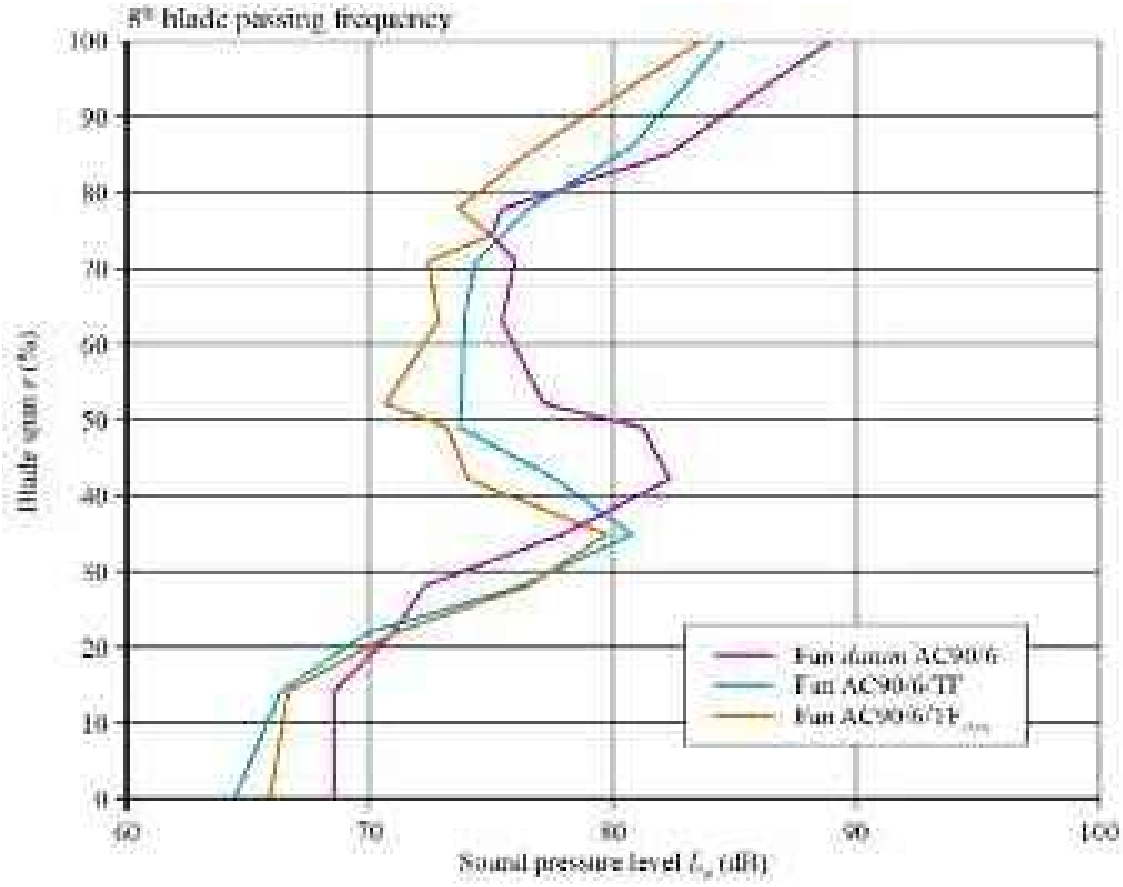

FIGURE 5.17. Measured span-wise cross-spectrum between near- and far-field sound pressure level (L_P) for the fan *datum* AC90/6, AC90/6/TF and AC90/6/TF$_{VTE}$. The authors made measurements at the fan design operating point and present them at the eighth harmonic of blade passing frequency.

Focusing on the blade tip region, an end-plate will have a primary effect on the blade tip-to-casing leakage vortex, and its associated acoustic productivity. The span-wise distributions of local specific sound pressure level at 30 degrees off the fan axis illustrate how the fan AC90/6/TF and AC90/6/TF$_{VTE}$ local specific sound pressure levels fall between 95 and 98 per cent blade span. The near-field noise generated in this blade tip region is coherent as a consequence of the blade tip-to-casing leakage vortex swirl.

Consider the blade tip region's span-wise distribution of local specific sound pressure level 90 degrees off the fan axis for the fan AC90/6/TF$_{VTE}$. It is significantly different to the distribution 30 degrees off the fan axis. There are two factors that contribute to this difference. First is the blade tip-to-casing leakage vortex trajectory and second, the tip-to-casing vortex direction of rotation as it exits the blade-to-blade passage. Both factors affect the blade tip-to-casing leakage vortex. When compared to the fan *datum* AC90/6 or AC90/6/TF, the fan AC90/6/TF$_{VTE}$ features a reduction in vortex axial velocity. When reviewing problems in flow acoustics, Möhring *et al.* (1983) concluded that vortex axial velocity is the primary factor that affects acoustic emissions off the fan axis. Therefore, we may conclude that reduced vortex axial velocity is responsible for the increase in fan AC90/6/TF$_{VTE}$'s local specific sound pressure level in the blade tip region 90 degrees off the fan axis.

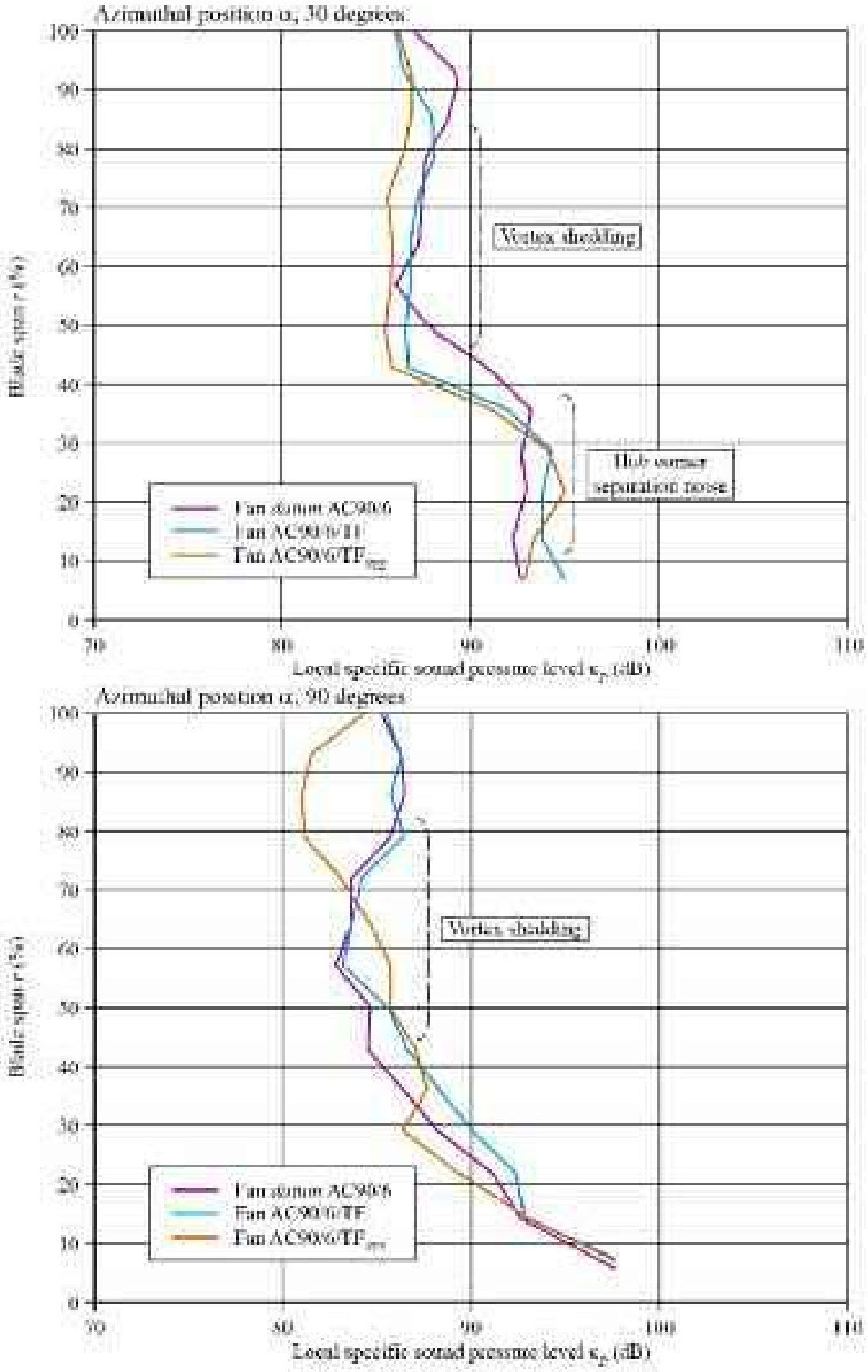

FIGURE 5.18. Span-wise maps of local specific sound pressure level (κ_p) for the fan *datum* AC90/6, AC90/6/TF and AC90/6/TF$_{VTE}$. The authors made measurements at the fan design operating point and present them at both 30 and 90 degree azimuthal positions.

CONCLUSIONS

In this chapter we extended the near- and far-field correlation technique presented in Chapter 2 and coherence analysis technique presented in Chapter 3 to include fan far-field acoustic measurements at different azimuthal positions. The resultant experimental methodology has proven effective, facilitating the dissection of aeroacoustic noise sources. It is the dissection of aeroacoustic noise sources that constitutes elucidating the near-field physical flow mechanisms that we then correlate with fan far-field noise. By extending the correlation technique and coherence analysis technique to include fan far-field acoustic measurements at different azimuthal positions, the original correlation technique extends to a directivity analysis.

We placed a microphone ten per cent blade chord down-stream of the studied fan blades' trailing edge. We then varied the microphone's span-wise location in steps of two per cent from blade hub to blade-tip. At each span-wise location we measured far-field noise on the fan centre line and 30, 45, 60, 75 and 90 degrees off the fan centre line. We also made near- and far-field acoustic measurements simultaneously. This enabled the experimental methodology to provide data sets of near- and far-field noise over a range of far-field azimuthal positions that we could correlate to establish the near-field noise sources' far-field directivity.

We used the directivity analysis to characterise the fan far-field broadband noise's directivity with and without fitted blade-tip end-plates. By filtering fan far-field noise measurements, we established the directivity of the blade passing frequency, the second, third and fourth harmonics of blade passing frequency and high frequency noise above 1 kHz.

The broadband directivity analysis confirmed that fan far-field noise was anisotropic. The studied fan without a fitted blade-tip end-plate behaved as a dipolar broadband noise source. Including a blade-tip end-plate resulted in the fan continuing to behave as a dipolar noise source, or to become a more anisotropic noise source with the difference occurring with specific features of the blade-tip end-plate geometry. We correlated the broadband noise with the degree of swirl in the exhaust flow with large-scale coherent structures superimposing a dipolar noise source and smaller random turbulent structures superimposing a lateral quadra-pole noise source.

The directivity analysis reported in this chapter complements the span-wise coherence analysis presented in Chapter 4, providing additional insight into the impact of end-plate geometry on fan far-field noise. It clarifies the acoustic effect of blade-tip end-plate geometry and thus, the analysis facilitates insight into the blade-tip end-plate geometry's impact on fan far-field noise. A comparative consideration of the directivity analysis of the studied fan both with and without a fitted blade-tip end-plate provided a basis for identifying near-field physical flow-field mechanisms responsible for fan far-field noise.

REFERENCES

ISO 5801:2007 (2007), *Industrial Fans: Performance Testing Using Standardised Airways.*

ISO 10302:1996 (1996), *Fans for General Purposes. Methods of Noise Testing*.

Bianchi, S., Sheard, A.G., Kinghorn, I.R., Corsini, A. and Rispoli, F. (2009a), 'Experimental Development of a Measurement Technique to Resolve the Radial Distribution of Fan Aeroacoustic Emissions', *Noise Control Engineering Journal*, vol. 57, pp. 360–369.

Bianchi, S., Corsini, A., Rispoli, F. and Sheard, A.G. (2009b), 'Detection of Aerodynamic Noise Sources in Low-speed Axial Fans with Tip End-plates', *Proceedings of IMechE Part C, Journal of Mechanical Engineering Science*, vol. 223, pp. 1379–1392.

Blake, W.K. (1986), *Mechanics of Flow-induced Sound and Vibration, Vol. II*, Academic Press, Orlando, FL, USA.

Brüel & Kjær (2006), *4954 ¼ inch Prepolarized Free-field Microphone Manual*.

Corsini, A. and Sheard, A.G. (2007), 'Tip End-plate Concept Based on Leakage Vortex Rotation Number Control', *Journal of Computational and Applied Mechanics*, vol. 8, pp. 21–37.

Corsini, A., Rispoli, F., Sheard, A.G. and Kinghorn, I.R. (2006), 'Investigation of Improved Blade-tip Concept for Axial Flow Fan', *Proceedings of the 51st American Society of Mechanical Engineers Gas Turbine and Aeroengine Congress*, Barcelona, Spain, 8–11 May, paper no. GT2006-90592.

Cumpsty, N.A. (1977), 'A Critical Review of Turbomachinery Noise', *Transactions of the ASME, Journal of Fluids Engineering*, vol. 99, pp. 278–293.

Fukano, T., Takamatsu, Y. and Kodama, Y. (1986), 'The Effects of Tip Clearance on the Noise of Low-pressure Axial and Mixed Flow Fans', *Journal of Sound and Vibration*, vol. 105, pp. 291–308.

Ganz, U.W., Joppa, P.D. and Scharpf, D.F. (1998), *Boeing 18-inch Fan Rig Broadband Noise Test*, Report NASA CR-1998-208704.

Garg, A.K. and Leibovich, S. (1979), 'Spectral Characteristics of Vortex Breakdown Flowfields', *Physics of Fluids*, vol. 22, pp. 2053–2064.

Heidelberg, L.J., Sutliff, D.L. and Nallasamy, M. (1997), 'Azimuthal Directivity of Fan Tones Containing Multiple Mode', *Proceedings of the 3rd AIAA / CEAS Aeroacoustics Conference*, Atlanta, GA, USA, 12–14 May, paper no. AIAA-97-1587.

Holste, F. and Neise, W. (1997), 'Noise Source Identification in a Prop Fan Model by Means of Acoustical Near Field Measurements', *Journal of Sound and Vibration*, vol. 203, pp. 641–665.

Inoue, M., Kuroumaru, M. and Furukawa, M. (1986), 'Behaviour of Tip Leakage Flow Behind an Axial Compressor Rotor', *Transaction of the ASME, Journal of Engineering for Gas Turbines and Power*, vol. 108, pp. 7–14.

Ito, T., Suematsu, Y. and Hayase, T. (1985), 'On the Vortex Breakdown Phenomena in a Swirling Pipe-flow', *Memoirs of the Faculty of Engineering, Nagoya University*, vol. 37, pp. 117–172.

Jordan, P. and Gervais, Y. (2008), 'Subsonic Jet Aeroacoustics: Associating Experiments, Modelling and Simulations', *Experiments in Fluids*, vol. 44, pp. 1–21.

Julliard, J., Antoine, H., Lozachmeur, C. and Roure, A. (2000), 'Active Control of the Directivity of Fan Tones Noise', *Proceedings of the RTO AVT Symposium on Active Control Technology for Enhanced Performance Operational Capabilities of Military Aircraft, Land Vehicles and Sea Vehicles*, Braunschweig, Germany, 8–11 May.

Laurendeau, E., Jordan, P., Delville, J. and Bonnet, J. (2007), 'Nearfield-farfield Correlations in Subsonic Jets: What Can They Tell Us?', *Proceedings of the 13th AIAA/CEAS Aeroacoustics Conference*, Rome, Italy, 21–23 May, paper no. 2007-3614.

Leggat, L.J. and Siddon, T.E. (1978), 'Experimental Study of Aeroacoustic Mechanism of Rotor-vortex Interactions', *Journal of the Acoustical Society of America*, vol. 64, pp. 1070–1077.

Lighthill, M.J. (1952), 'On Sound Generated Aerodynamically. I. General Theory', *Proceedings of the Royal Society of London A,* vol. 211, pp. 564–587.

Lighthill, M.J. (1954), 'On Sound Generated Aerodynamically. II. Turbulence as a Source of Sound', *Proceedings of the Royal Society of London A*, vol. 222, pp. 1–32.

Longhouse, R.E. (1978), 'Control Tip-vortex Noise of Axial Flow Fans by Rotating Shrouds', *Journal of Sound and Vibration*, vol. 58, pp. 201–214.

Mankbadi, R. and Liu, J.T.C. (1984), 'Sound Generated Aerodynamically Revisited: Large-scale Structures in a Turbulent Jet as a Source of Sound', *Philosophical Transactions of the Royal Society of London A,* vol. 311, pp. 183–217.

Marcinowski, H. (1953), 'Einfluss des Laufradspalts und der Luftfuehrung bei einem Kuehlgeblaese axialer Bauart', *Motortechnische Zeitschrift*, vol. 14, pp. 259–262.

Miles, J.H. (2006), 'Procedure for Separating Noise Sources in Measurements of Turbofan Engine CoreNoise', NASA/TM-2006214352.

Möhring, W., Muller, E. and Obermeier, F. (1983), 'Problems in Flow Acoustics', *Review of Modern Physics*, vol. 55, pp. 707–724.

Mugridge, B.D. and Morfey, C.L. (1972), 'Sources of Noise in Axial Flow Fan', *Journal of the Acoustical Society of America*, vol. 51, pp. 1411–1426.

Nash, E.C., Lowson, M.V. and McAlpine, A. (1999), 'Boundary-layer Instability Noise on Aerofoils', *Journal of Fluid Mechanics*, vol. 382, pp. 27–61.

Nelson, D.A. and Cooper, B.A. (1999), 'A "Reduced-Noise Gas Flow Design Guide" for NASA Glenn Research Center', *Proceedings of INTERNOISE 99, the International Congress on Noise Control Engineering*, Fort Lauderdale, FL, USA, 6–8 December, vol. 1, pp. 77–82.

Shah, P.D., Mobed, D., Spakovszky, Z. and Brooks, T.F. (2007a), 'A Novel Turbomachinery Air-brake Concept for Quiet Aircraft', *Proceedings of the 52nd American Society of Mechanical Engineers Gas Turbine and Aeroengine Congress*, Montreal, Canada, 14–17 May, paper no. GT2007-27635.

Shah, P.D., Mobed, D., Spakovszky, Z. and Brooks, T.F. (2007b), 'Aeroacoustics of Drag Generating Swirling Exhaust Flows', *Proceedings of the 13th AIAA/CEAS Aeroacoustics Conference (28th AIAA Aeroacoustics Conference)*, Rome, Italy, 21–23 May, paper no. AIAA-2007-3714.

Spall, R.E., Gatski, T.B. and Grosch, C.E. (1987), 'A Criterion for Vortex Breakdown', *Physics of Fluids*, vol. 30, pp. 3434–3440.

Tam, C.K.W., Golebiowski, M. and Seiner, J.M. (1996), 'On the Two Components of Turbulent Mixing Noise from Supersonic Jets', *Proceedings of the 2nd AIAA/CEAS Aeroacoustics Conference*, State College, PA, USA, 6–8 May, paper no. AIAA 96–1716.

Tester, B.J. and De Mercato, L. (2006), 'Far-field Directivity of Rotor-alone Tones Radiated from Fan Intakes with Spliced Liners for Different Intake Shapes, with Flow', *Proceedings of the 12th AIAA/CEAS Aeroacoustics Conference (27th AIAA Aeroacoustics Conference)*, Cambridge, MA, USA, 8–10 May, paper no. AIAA 2006-2456.

Uchida, S., Nakamura, Y. and Ohsawa, M. (1985), 'Experiments on the Axisymmetric Vortex Breakdown in a Swirling Air Flow', *Transactions of the Japan Society for Aeronautical and Space Sciences*, vol. 27, pp. 206–216.

Widnall, S.E. (1969), 'A Correlation of Vortex Noise Data from Helicopter Main Rotors', *Journal of Aircraft*, vol. 6, pp. 279–281.

Wright, S.E. (1976), 'The Acoustic Spectrum of Axial Flow Machines', *Journal of Sound and Vibration*, vol. 45, pp. 165–223.

Chapter 6

Experimental Study on the Self-noise of a Turbulent Round Jet Investing a Cambered Aerofoil

S. Bianchi, A. Corsini and A.G. Sheard

ABSTRACT

The chapter presents an experimental technique developed to facilitate assessing a fan's acoustic performance for application in compact cooling units. The experimental technique provides insight into the far-field consequences of near-field flow features induced in the flow by a blade-tip end-plate. We placed ten microphones at the tip of a single fan blade, grouped together at the leading edge, mid-chord and trailing edge. We mounted the instrumented blade in an anechoic chamber and measured the interaction noise with a jet impacting the blade. Although the blade did not move, we reproduced the fan design operating point Mach number, Reynolds number and blade incidence angel in the static frame of reference. This 'frozen rotor' technique enabled us to correlate the chord-wise near-field measurements with far-field measurements made 30 degrees off the fan centre line. We made near- and far-field measurements simultaneously. The experimental technique provided data sets of chord-wide distributions of near-field noise that we then correlated with far-field noise. We made measurements with and without a fitted blade-tip end-plate. This facilitated insight into the far-field acoustic consequences of near-field flow features induced in the flow by the blade-tip end-plate. We found that this chord-wise correlation of near- and far-field noise was distinctly different for the studied fan without a fitted blade tip end-plate and when fitted with an end-plate. The developed correlation technique relies on a measure of chord-wise noise taken on a stationary and isolated blade. We did not model the rotational effects, and consequently, the measurement technique models only part of the flow-field physics. The developed frozen rotor experimental technique has proven effective, facilitating the identification of near-field noise sources unique to each of the tested fan configurations. The correlation technique was also effective as it facilitated identifying the far-field acoustic consequences of the near-field noise sources.

This chapter is a revised and extended version of Bianchi, S., Corsini, A. and Sheard, A.G. (2013), 'Experimental Study on the Self-noise of a Turbulent Round Jet Investing a Cambered Aerofoil', *Periodica Polytechnique, Mechanical Engineering,* vol. 57(1), pp. 45–62.

NOMENCLATURE

Latin letters

BPF	blade-passing frequency [Hz]
c	blade chord position
D_n	nozzle passage diameter
f	frequency (Hz)
H	nozzle height
ℓ	blade chord
L	blade length
LE	leading edge
MD	mid-chord
PS	pressure side
r_{xy}	cross correlation coefficient
St	Strouhal Number (fL/U_j)
SPL	sound pressure level [SPL]
SS	suction side
TE	trailing edge
U_e	exhaust velocity
U_j	jet average velocity
U_c	convection velocity

Greek letters

α	blade customary angle of attack
α_L	wind tunnel correction factor of the angle attack
α_T	blade corrected angle of attack
γ^2	numerical value of the coherence function
λ_s	source length scale
θ	flow angle of deviation from the nozzle axis

INTRODUCTION

The research presented in this chapter is part of an on-going research stream (Bianchi *et al.*, 2009). The purpose is to develop experimental techniques to facilitate assessment of the acoustic performance of a fan developed for application in compact cooling units. The experimental techniques provide insight into the far-field consequences of near-field flow features induced in the flow by blade-tip end-plates. Turbulent flow ingested into a fan or compressor is a source of aerodynamically generated noise. A desire to better understand the mechanisms responsible for fan and compressor noise has encouraged scholars to study and model noise generation processes. Lighthill's (1954) acoustic analogy stated that turbulent fluctuations in free space are inefficient noise radiators at low flow Mach numbers. This inefficiency is due to the turbulent sources' quadrupolar-type character from which the radiated

acoustic intensity scales with Mach number raised to the eighth power. However, Curle (1955) observed that in the presence of a solid boundary, the surface dipoles lead to acoustic intensity scaling with Mach number raised to the sixth power. The result is that the blade-to-blade flow-field within a fan or compressor generates higher noise levels as the flow field is characterised by blade and casing surfaces.

Brooks *et al.* (1989) considered the effect of solid boundaries. They studied a NACA 0012 aerofoil in a low speed wind tunnel. Brooks *et al.* (1989) measured the aerofoil's training edge noise in a uniform free stream flow, and then moved on to analyse the flow's behaviour in close proximity to the blade surface. Brooks *et al.* (1989) were able to identify five mechanisms responsible for generating aerofoil self-noise. They concluded that these mechanisms were sensitive to flow-field features, with noise related to the way in which features interact with the aerofoil.

Magliozzi *et al.* (1973) were able to develop an insight into the physical mechanisms responsible for the noise associated with interaction of a solid body and an unsteady flow. When conducting static tests, Magliozzi *et al.* (1973) demonstrated that the dominant noise source arises from the interaction between ingested turbulence and the rotor blades. When a turbulent eddy passes the edge of a solid body, the turbulent fluctuations radiate acoustic energy, with Ffowcs Williams and Hawkings (1969) concluding that the acoustic intensity scales with Mach number raised to the fifth power. Therefore, we may conclude that in the absence of other noise-generating mechanisms, the trailing edge and blade tip-to-casing gap are the most significant aerodynamic noise sources.

Blake and Gershfeld (1989) concluded that a potential source of both tonal and broadband noise is ingested turbulence. The inflow turbulence can be of atmospheric origin, or be generated by the inlet duct and casing boundary layers. The inlet duct and casing boundary layer interacts with the flow-field features in the blade tip region. The flow field's blade tip region has the potential to be more acoustically productive than other flow field regions. This is a consequence of the higher peripheral blade velocity and Mach number.

Marcinowski (1953) first suggested the importance of blade tip noise in low speed fans. Blade tip noise is a self-induced noise mechanism that occurs with the blade tip-to-casing leakage vortex. Marcinowski (1953) concluded that blade tip noise contributes to broadband noise, with the blade tip geometry influencing frequency distribution of acoustic emissions. Subsequently, Lowson (1972) confirmed Marcinowski's (1953) conclusion that an increase in broadband noise levels correlated with an increasing tip clearance. He observed the largest increase in broadband noise at frequencies higher than the blade-passing frequency.

If frequency remains high compared to the blade-passing frequency, the noise generated by a blade's rotation in a turbulent flow is similar to that of an isolated aerofoil. Variations of incidence angle lead to similar blade load fluctuations. If the turbulence length scale is such that only one blade chops a given eddy, the noise is usually broadband. Magliozzi *et al.* (1991) and Fedala *et al.* (2006) concluded that the random elementary surface pressure field fluctuations around an aerofoil correspond to dipolar noise sources. These noise sources result from coherent vortices impacting rigid surfaces and are usually concentrated on the leading edge.

The basis for extending rectilinear motion theory to rotating motion is the assumption that the acoustic frequencies are greater than the rotational frequency. If this assumption is correct we can ignore rotational effects and treat the blade as an aerofoil in rectilinear motion at each instant of time. Blake and Gershfeld (1989) base this approach on isolated aerofoil linearised aerodynamic theory. The far-field noise radiated by an aerofoil is related to the turbulent velocity field by a transfer function which is independent of the aerodynamic flow characteristics. We can determine this transfer function for an isolated aerofoil and can then apply results to a rotating blade. Winkler *et al.* (2007) first proposed this approach for characterising the trailing edge noise of a highly cambered NACA five digit aerofoil. Roger and Moreau (2004) characterised the aerofoil at a zero degree angle of attack, with and without a boundary layer tripping. The approach facilitates a study of the aerodynamic cause of blade acoustic emissions that would otherwise have been challenging. A limitation of this approach is that this measurement technique neglects the blade aerodynamic interaction with other blades.

Some scholars have focused their research on better understanding the origin of trailing edge noise. They have chosen to focus their research around elucidating the flow-field physics in the blade tip's trailing edge region. Kendall (1978) measured the noise at a stationary aerofoil's tip using a directional microphone system. George and Kim (1977) were the first to present a physical model of the blade tip noise generation mechanism. Amiet (1975, 1976) studied the interaction between turbulence and an isolated aerofoil, presenting a comparison of experimental measurement on NACA aerofoils in rotorcrafts. Similarly, Brooks and Marcolini (1986) and Brooks *et al.* (1989), attempted to correlate the noise that stationary aerofoil section models generated with helicopter rotor noise. A review of these scholars' work enables us to identify three possible noise sources in a cambered aerofoil's blade tip region subjected to a turbulent inflow:

- the jet-like blade tip-to-casing flow may generate sound when leaving the clearance region either directly or by interacting with the blade tip edge;
- the blade tip-to-casing leakage vortex may feed unsteady perturbations into the blade wall pressure field that may become noise sources at the blade tip edge;
- in addition to the two self-generated noise sources above, a further noise source may be an interaction noise associated with ingestion of incoming turbulence or flow-field structures in the blade tip region.

Grilliat and Jacob (2007) discussed possible noise sources in a single isolated cambered aerofoil's blade tip region subjected to a turbulent inflow. Ganz *et al.*'s (1998) similar study indicated that fan blade tip noise is not a significant sound source, although they also concluded that it is difficult to identify the role of tip clearance noise among other noise sources on a representative fan test rig. Other studies on rotating rigs have resulted in different conclusions about the magnitude of blade tip clearance noise (Fukano *et al.*, 1977a, 1977b; Fukano and Jang, 2004), with some scholars studying blade tip-to-casing flow control (Khourrami and Choudari,

2001; Corsini and Sheard, 2007). Despite the progress made by these researchers, they have not been able to conclusively identify the dominant noise sources in a cambered aerofoil's blade tip region subjected to a turbulent inflow.

This chapter presents the results of a research programme that aims to isolate the interaction effects between the turbulent flow produced by a jet and a cambered aerofoil's tip. In the reported research we did not consider blade rotation, instead mounting the aerofoil in a fixed position relative to the inflow jet. We corrected the relative inflow angle and velocity to correctly model inlet incidence angle, Mach number and Reynolds number. We made near-field surface measurements of aerofoil wall pressure on both the aerofoil pressure and suction surface at ten chord-wise locations from aerofoil leading to trailing edge at a constant span-wise location in the blade tip region.

We complemented our experimental measurements by analysing the collected data, correlating measured near-field unsteady pressure with measured far-field noise. Our objective was to establish a causal relationship between near-field pressure fluctuations on the aerofoil surface and far-field noise. We took the far-field measurements in an anechoic chamber with the medium within the chamber at rest. We based this experimental approach on Winkler *et al.*'s method (2007). They developed a linear aerodynamic and acoustic theory for isolated aerofoils and extended that theory to a finite span blade's interaction with a fully turbulent jet. We adopted the near- to far-field correlation technique of Mongeau *et al.* (1995) that has been extensively adopted by scholars studying subsonic jets.

METHODOLOGY

We mounted the studied aerofoils in the core of a round jet blowing into an anechoic chamber, Figure 6.1. This jet emanated from a circular nozzle at the end of a convergent duct upstream of the aerofoil. We aligned the jet's centre line with the aerofoil tip, Figure 6.2. The jet's position relative to the aerofoil enabled us to simulate the fan design operating point blade-tip inlet incidence angle, Mach number and Reynolds number. We made near- and far-field measurements using the method originally developed by Winkler *et al.* (2007) and applied to air movement fans by Bianchi *et al.* (2008a).

For far-field measurements we used a Bruel & Kijaer 1/3" microphone protected with a foam ball. The microphone was located in the anechoic chamber 1.2 fan diameters downstream from the blade trailing edge, and followed Leggat and Siddon's recommendation (1978) to place it 30 degrees off the jet centre line.

For near-field measurements we used GRAS Type 40PS surface microphones designed for installation on an aerofoil's curved surfaces, Figure 6.3. These microphones are 2.8 mm thick, with a frequency range up to 20 kHz and a dynamic range up to 136 dB. We acquired both near- and far-field microphone signals using a dBFA-AREVA Symphonie acquisition card. We then used the near- and far-field signals to compute auto- and cross-spectra with a 3.125 Hz bandwidth.

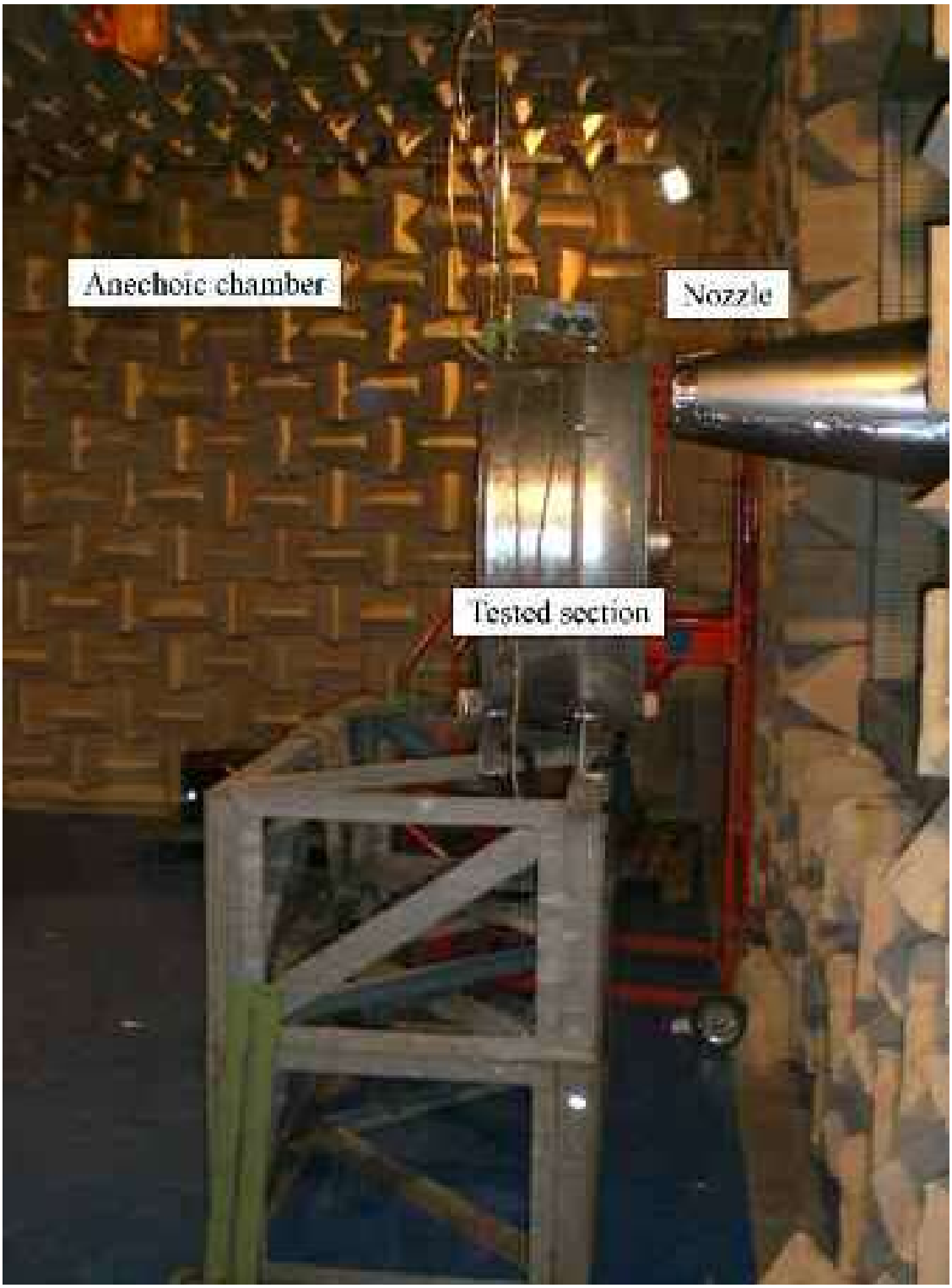

FIGURE 6.1. The 'frozen rotor' test rig in the anechoic chamber within which the authors made acoustic measurements. The test rig uses a jet of air to simulate the design operating point flow-field conditions in the aerofoil-tip region.

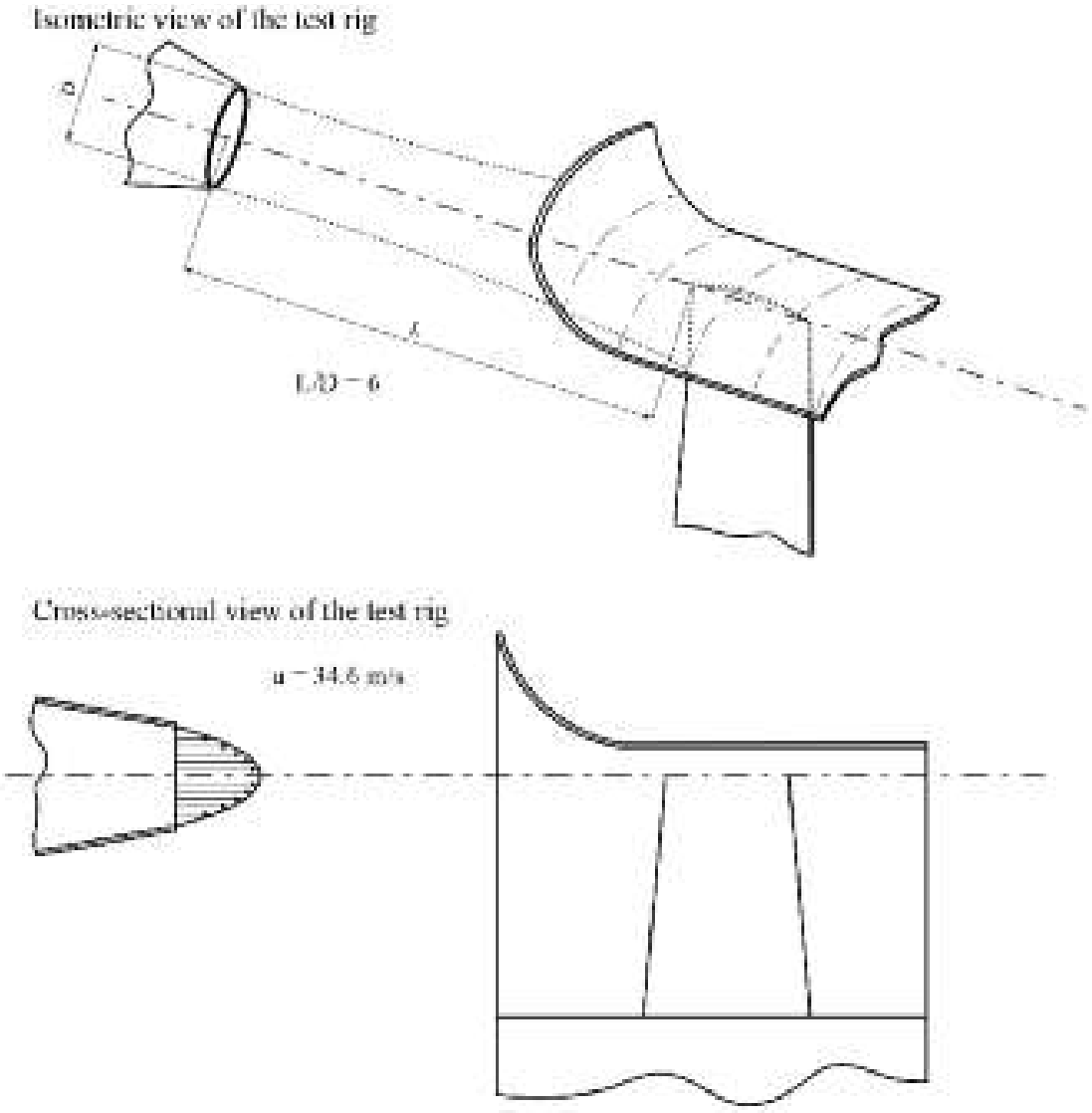

FIGURE 6.2. Isometric and cross-sectional views of the 'frozen rotor' test rig. The test rig uses a jet of air to simulate the design operating point flow-field conditions in the aerofoil-tip region.

Aerodynamic Characterisation of the Round Jet

Scholars working within the aerospace community have characterised jets. Ashforth-Frost and Jambunathan (1996) and Cornaro *et al*. (1999) studied the effects of jet orientation, nozzle diameter and Reynolds number. Both published comprehensive reviews of the jet flow's aerodynamic characteristics. These reviews are a welcome contribution to the air movement and control community. Generally, they characterise jets over a Reynolds number range appropriate for application with an air movement fan. Specifically, their characterisation of nozzle geometry facilitates the design of a jet with kinematics suitable for application in the research reported in this chapter.

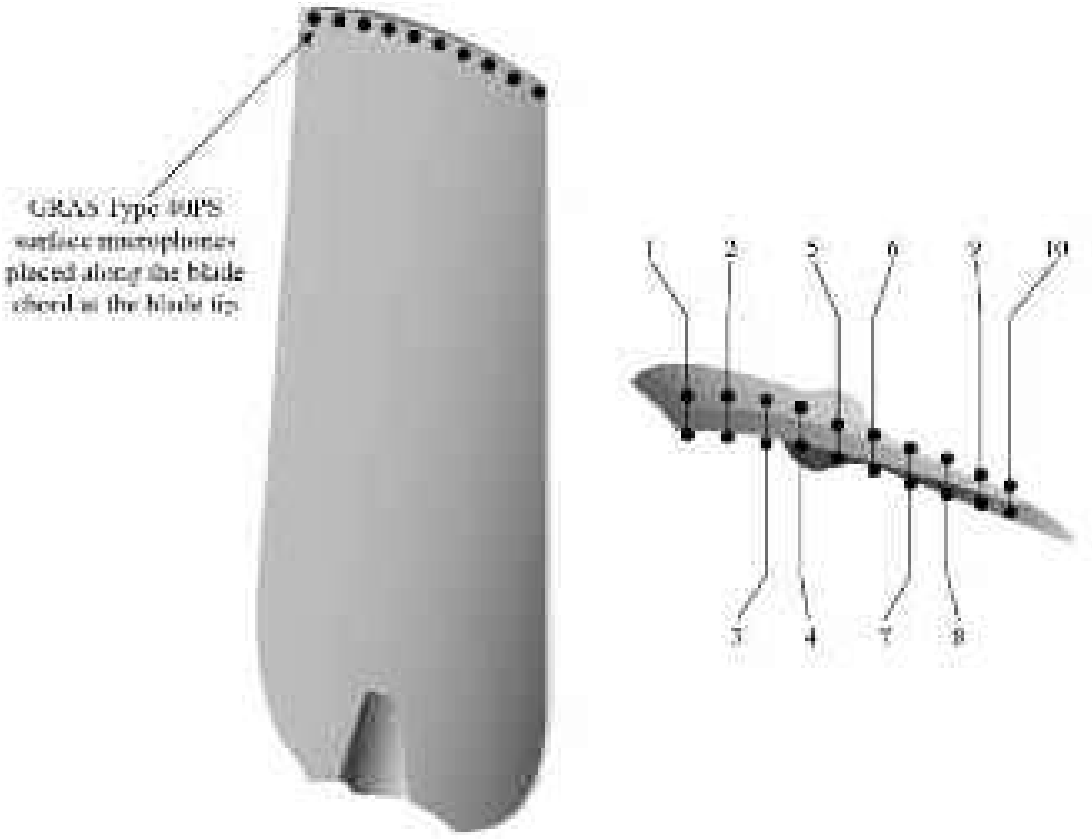

FIGURE 6.3. Location of the microphones fitted in the aerofoil-tip region from leading to trailing edge. These microphones were used to make near-field acoustic measurements on both the blade suction and pressure surface.

The experimental programme reported in this chapter commenced with the nozzle design and characterisation of the resultant nozzle jet. The flow through the nozzle is a function of the air's viscosity and density, which drives through the nozzle to produce the jet. We used Ashforth-Frost and Jambunathan (1996) and Cornaro *et al.*'s (1999) method to define the geometry of a nozzle that would produce the required jet characteristics. Narasimha *et al.* (1973) commented on the validity of reducing the nozzle's width to obtain a more uniform exit velocity from the jet. However, we chose to use a circular nozzle to maintain a symmetrical exit flow from the jet, Figure 6.2.

Ashforth-Frost and Jambunathan (1996) and Cornaro *et al.* (1999) recommended a logarithmic exit flow velocity profile. In an attempt to modify the exit flow velocity profile, we used Coles' (1956) 'law of the wake' to derive the nozzle geometry. The final exit flow velocity profile from the jet was characteristic of fully developed pipe-flow. Despite not fully complying with Ashforth-Frost and Jambunathan (1996) and Cornaro *et al.*'s (1999) recommendations, we used this profile for the research reported in this chapter.

We placed the nozzle that we used to produce the jet six nozzle diameters upstream of the aerofoil leading edge, Figure 6.2. The jet exiting the nozzle was fully turbulent. Conditions at the nozzle exit were:

- dynamic pressure, 0.75 kPa.;
- static pressure, 101.31 kPa.;
- Reynolds number, 5.15×10^5; and
- relative Mach number, 0.12.

Family of Fans under Investigation

We conducted the reported research on a family of commercially available cooling fans. The studied fan configuration, coded AC90/6, incorporates a six-blade un-swept rotor, with modified ARA-D profile aerofoil blades, Table 6.1. In its original embodiment the studied fan did not include a blade tip end-plate. We used it as a *datum* against which to assess the fan's performance when fitted with a blade tip end-plate. Therefore, we refer to the fan without a blade-tip end-plate as the fan *datum* AC90/6, Figure 6.4. In addition to the fan *datum* AC90/6, we studied a variant of the fan fitted with a variable thickness blade-tip end-plate named AC90/6/TF_{VTE}, Figure 6.4. Corsini and Sheard (2007) presented the fan AC90/6/TF_{VTE} blade-tip end-plate design methodology.

Flow Conditions

The studied fan blade tip pitch angle is adjustable and may be set to a pitch angle between 16 and 28 degrees. In practical application the blade tip pitch angle is typically set to 28 degrees as this maximises flow rate for a given system pressure. In the research reported in this chapter we conducted the experimental measurements with the fan blade tip pitch angle to 28 degrees. We selected 28 degrees both because

Table 6.1. *The fan* datum *AC90/6 blade geometry and rotor specification.*

	Fan *datum* AC90/6		
Blade geometry	Hub	Mid-span	Tip
Pitch angle (°)	36	58.8	28
Camber angle (°)	46	44	41
Solidity	1.24	0.86	0.30
Fan rotor			
Blade number		6	
Blade tip pitch angle (°)		16–28	
Blade tip stagger angle (°)		74–62	
Hub-to-casing diameter ratio σ		0.22	
Tip diameter (mm)		900.0	
Rotor tip clearance τ (% span)		1.0	
Rated rotational frequency (r/min)		935–950	

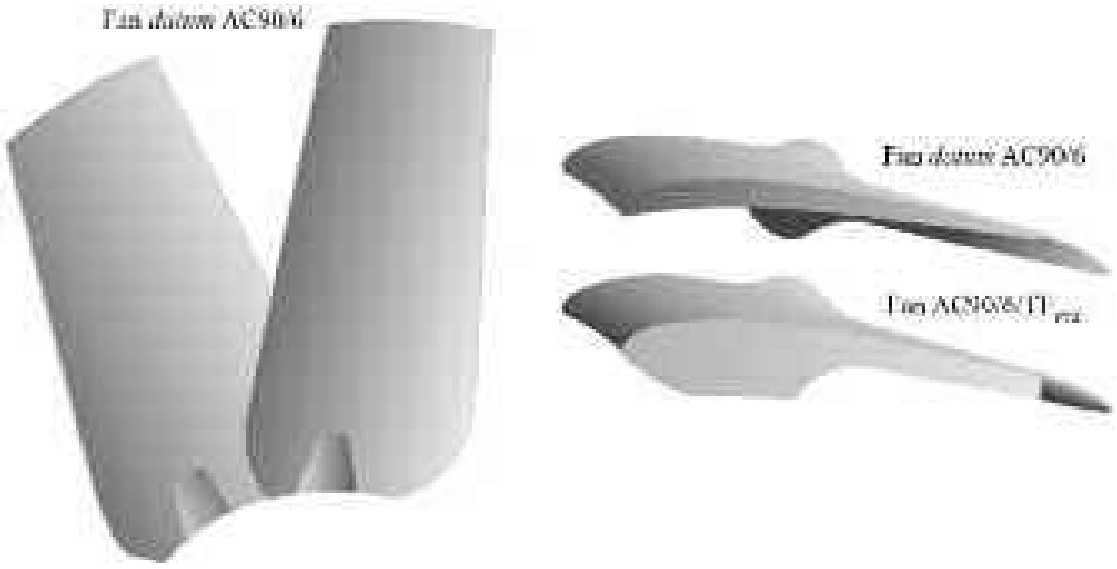

FIGURE 6.4. The studied fan *datum* AC90/6 without a fitted blade-tip end-plate and with a variable thickness blade-tip end-plate, AC/6/TF$_{VTE}$.

it is typical of the angle used in practical application and because it results in the highest blade loading. A highly loaded blade results in the blade tip-to-casing vortex having the most significant effect on both fan aerodynamic and acoustic performance (Holste and Neise, 1997).

Because we used an isolated aerofoil, we corrected the impeller blade's angular setting and jet air speed. The correction simulated, in the static frame of reference, the air inlet angle and velocity for the fan's design operating point with a 28 degree blade angle. Brooks *et al.* (1989) developed the correction technique for application with a NACA 012 aerofoil. Bianchi *et al.* (2008a, 2008b) then generalised this correction technique for application with the family of fans under investigation in the research reported in this chapter.

Aerofoil Aerodynamic Corrections

Aerofoil testing in a finite-size jet plume results in flow deflection and downwash. This deflection and downwash reduces the flow's angle of attack, a phenomena similar to that exhibited by a finite-sized wind tunnel (Brooks and Marcolini, 1986). Brooks *et al.*'s (1989) method for testing aerofoil sections in a finite-size wind tunnel uses lifting surface theory to develop a two-dimensional open tunnel correction factor for the angle of attack and camber. We corrected our static aerofoil angle using Brooks *et al.*'s (1989) correction factor λ that reads as:

$$\lambda = (1 + 2\sigma)^2 + \sqrt{12\sigma}$$

with:

$$\sigma = \left(\frac{\pi^2}{48}\right)\left(\frac{l}{H}\right)^2$$

where l is the aerofoil chord and H is the nozzle height.

We were able to use the above formula for correction factor to calculate the required change in angle for our static aerofoil as 1.83 degrees. By correcting the aerofoil angle, we were able to reproduce the blade-tip incidence angle that occurs with a blade angle of 28 degrees with the fan operating at its design operating point.

In our research, we required the aerofoil and jet to simulate rotational effects. As the blade was not rotating, the boundary layer thickness was reduced. We were able to induce a thicker boundary layer by changing the aerofoil's angle of attack by applying a second aerofoil angle correction factor following Bianchi *et al.*'s (2008 a, 2008b) method.

EXPERIMENTAL TECHNIQUE

We derived our data analysis technique from Brooks and Marcolini's (1986) broadband noise analysis technique. Near-field noise must pass though this jet shear layer before reaching the far-field microphone. Using Brooks and Marcolini's (1986) analysis technique, we were able to correct the measured data to account for the jet shear layer's effect.

We logged the signals from both near- and far-field microphones at a sampling rate of 50 kHz, giving a Nyquist frequency of 25 kHz. To avoid aliasing, we filtered all measured data at 20 kHz and constrained our analysis to frequencies below 20 kHz. We estimated the overall measurement uncertainty as:

- ΔV =1000 mV ± 12 mV (20:1) on signal voltage; and,
- ΔG = 200 dB ± 2.4 dB (20:1) on signal gain.

Using the microphone calibration certificates, we estimated the error in our Fourier transform to be 0.1 – 0.2 dB at 1 kHz and 2 dB at 10 kHz. We estimated the error in our Fourier transform in accordance with ISO IEC60651 requirements (1979).

Fourier Analysis

We calculated near- to far-field signal auto- and cross-spectra using a signal post-process suite with a constant bandwidth of 3.15 Hz. We used the near-field microphone to measure unsteady pressure fluctuations on the blade surface. Our auto- and cross-spectra established the transfer function that couples the pressure fluctuation due to unsteady flow in the near-field with noise in the far-field. Pseudo sound degrades the quality of this transfer function. However, in an anechoic chamber, the

pseudo sound's transfer function has a shorter decay time than the transfer function that couples the pressure fluctuation in the near-field with noise in the far-field (Laurendeau *et al.*, 2007). By following Leggat and Siddon's (1978) recommendation, we were able to position the far-field microphone to avoid pseudo sound becoming coherent.

In our research, we correlated unsteady near-field pressure measurements with far-field acoustic measurements. When endeavouring to identify noise sources, engineers find it helpful to identify a correlation domain that they can use to identify flow regions in the near-field that impact sound in the far-field. A cross-correlation between near- and far-field signals is helpful in this regard. It facilitates the identification of causal relationships between near-field noise sources and the radiated sound in any given direction. Thus, the cross-correlation provides quantitative information on noise source distribution, their local spectra and the scale of their coherence. If a strong harmonic coupling exists between a noise source in the near-field and far-field spectra, the resulting correlation function does not decay quickly, but is periodic in nature.

We derived a coherence function in accordance with Miles's procedure (2006). We set the threshold for signal coherence at 95 per cent of the value that we obtained with a white noise Brüel & Kjær Type 4204 calibrated noise source. This procedure ensured that only coherent sources contributed to the cross-spectra. In contrast, the auto-spectra comprised both coherent and incoherent sources.

The 'Causality Method'

The measurement technique we have developed and present in this chapter relies on a near-field measurement of unsteady pressure. The validity of our measurement technique depends on our ability to use near-field measurement of unsteady pressure to dissect noise sources. Miles (2006), Laurendeau *et al.* (2007) and Bianchi *et al.* (2009) have concluded that near-field measurements provide a valuable insight into the flow-field physics. Ribner (1964) was able to demonstrate that in addition to the 'purely hydrodynamic' contributions, the near-field also comprises an 'acoustic' component. These acoustic components are related to the progressive pressure fluctuations that propagate to the far-field.

Laurendeau *et al.* (2007) conducted a study on subsonic jet noise. The near-field pressure measurements were under similar velocity gradients around the aerofoils to those that are the subject of study in this chapter. Ribner (1964) studied the relationship between near-field unsteady pressure and the dynamics of noise sources. He observed that a first-order approximation of Lighthill's (1954) source term is related to the pressure Laplacian in incompressible flows. Moreover, Laurendeau *et al.* (2007) noted that the near-field spectrum combines low and high frequency components. The fan or compressor's aerodynamic signature dominates the low frequency. Acoustic-pressure fluctuations dominate the high frequency range.

Bianchi *et al.* (2009) used Laurendeau *et al.*'s (2007) approach. They correlated near-field unsteady pressure measurements with fan far-field noise. They made near-field measurements 10 per cent blade chord downstream of the trailing edge of a fan

containing the same blades that are the subject of the research in this chapter. Bianchi *et al.* (2009) were able to identify the far-field 'acoustic effect' of near-field 'aerodynamic cause' and provide insight into the coupling mechanisms.

The research reported in this chapter aims to build on the reported research reviewed above. We aim to correlate the near-field unsteady pressure fluctuations on the blade surface at different chord-wise locations with far-field noise measured 30 degrees off the fan axis. This combination of chord-wise near-field and its correlation with far-field noise constitutes our 'causality method' for localising noise sources. This causality method identifies the coupling mechanism's structure that drives the link between near-field unsteady pressure and far-field noise.

We positioned the near-field microphones at ten locations on the aerofoil chord. We grouped the microphones together around the aerofoil leading edge, in the mid-chord region and at the trailing edge. The grouping is significant as the choice of locations was driven by our expectation that these three locations would be the location of noise sources that transmit to the far-field. When characterising the jet plume, we positioned the far-field microphone on the fan centre line and plus and minus 30, 45, 60 and 90 degrees off the centre line. When characterising the chord-wise distribution of noise sources, we used one far-field microphone 30 degrees off the fan axis. We made all near-field measurements and the far-field measurement simultaneously.

We used the far-field microphone to measure fan far-field noise. However, we may characterise the near-field microphones as making near-field measurements of unsteady pressure. In effect, the near-field microphones served as unsteady pressure sensors. Therefore, the resulting near- and far-field measurement technique enabled us to generate data sets of chord-wise distribution of near-field unsteady pressure and far-field noise. From each data set we were able to derive the far-field noise that occurred with the chord-wise distributions of unsteady pressure. By repeating this process for each of the studied fan configurations, we were able to establish the far-field directivity of chord-wise distributions of near-field unsteady pressure with and without a fitted blade-tip end-plate.

There is an issue with using near-field unsteady pressure measurements to identify noise sources in the aerofoil blade-tip region. The measured unsteady pressure includes the beginning of an acoustic response to the near-field's hydrodynamic component. This response is at specific frequencies only as the pressure field's hydrodynamic behaviour is a function of frequency. We may identify a low frequency acoustic response more easily than a high frequency response due to the reflection of low frequencies on rigid wall surfaces. Therefore, the spectrum of the near-field unsteady pressure comprises a low frequency range. In this low frequency range, pressure perturbations are largely dominated by the hydrodynamic signature of the largest scale of the jet plume turbulence. In contrast, progressive acoustic fluctuations dominate the high frequency range. Consequently, measured near-field unsteady pressure comprises a mix of aerodynamic cause and acoustic effect in different frequency ranges.

We recognised that it was necessary to separate aerodynamic cause and acoustic effect in different frequency ranges when processing near-field unsteady pressure measurements. We were able to separate them by correlating the near-field

unsteady pressure measurements with far-field acoustic measurements. Using this correlation, it is possible to extract information relating to two separate phenomena. The first is the mechanism by which hydrodynamic near-field cause couples with the acoustic far-field effect. The second is the mechanism by which the high frequency hydrodynamic near-field noise source distribution develops. The far-field correlation with the hydrodynamic near-field provides an insight into the characteristics of the near-field noise sources.

Physical interpretation of the unsteady pressure measurements made in the near-field is challenging. We can best approximate the dynamics of the near-field unsteady pressure using a linear hyperbolic differential equation. In contrast, a nonlinear hydrodynamic pressure field drives sound production, which we may approximate using elliptic equations. In addition to these fundamental modelling issues, there is a further challenge relating to the near-field's hyperbolic dynamics. These dynamics impede the interpretation of near-field measurements. Finally, turbulence complicates interpretation of near-field measurements made in regions characterised by vortex formation and motion, such as the aerofoil tip region.

Undoubtedly, there are difficulties that occur with physically interpreting near-field unsteady pressure measurements. Never the less, our 'causality method' has the potential to provide the insight into the physical mechanisms underpinning the near-field aerodynamic cause of far-field acoustic effect. However, our causality method utilises measurements made on a static aerofoil downstream of a jet. Therefore, in addition to the challenges we have already discussed, we must also account for shear layers, which the jet introduces into the flow-field.

When studying jet characteristics, Guitton *et al.* (2007) developed an empirical model. This model accounted for both the flow velocity dependence and spectral decay of the near-field's hydrodynamic and acoustic components. Guitton *et al.* (2007) proposed a set of criteria that we may use to predict the point of transition from hydrodynamic to acoustic dominance. Using Guitton *et al.*'s (2007) empirical model, Laurendeau *et al.* (2007, 2008) characterised the transition point from hydrodynamic to acoustic dominance. This transition point occurs at a Strouhal Number (St) of approximately 1.3 for the near-field to far-field distance between microphones. The Strouhal number (St) is a describing oscillating flow mechanisms. For Strouhal numbers of one or more viscosity dominates fluid flow, resulting in the fluid's collective oscillating movement.

We wished to ensure that that our analysis was focused on near-field acoustic features that had the potential to correlate with far-field acoustic measurements. Therefore, we decided to limit our data analysis by considering Strouhal numbers above five. This limit also ensured similarity of static aerofoil acoustic emissions with the same aerofoil when assembled into a fan and rotating.

EXPERIMENTAL RESULTS

We analysed the chord-wise distributions of near-field unsteady pressure and their correlation with far-field noise. The difficulty associated with establishing the

near-field aerodynamic cause of far-field acoustic effect resulted in no single analysis technique that was sufficient. Therefore, we selected three complementary analysis techniques:

- An analysis of chord-wise maps of near- to far-field coherence (γ^2) over a range of Strouhal numbers from 5 to 40. We made all measurements with the far-field microphone at an azimuthal position of 30 degrees off the fan axis.
- An analysis of chord-wise near- to far-field coherence (γ^2) over a range of Strouhal numbers from 0 to 90. We made measurements at the leading edge, mid-chord and trailing edge of the blade suction and pressure surface. We made all measurements with the far-field microphone at an azimuthal position of 30 degrees.
- An analysis of chord-wise near- to far-field cross-correlation coefficient (r_{xy}) over a 0.4 second time period. We made measurements at the leading edge, mid-chord and trailing edge of the blade suction and pressure surface. We made all measurements with the far-field microphone at an azimuthal position of 30 degrees.

We applied the three analysis techniques to measured data that we obtained with blades fitted to our test rig from the fan *datum* AC90/6 and fan AC90/6/TF$_{VTE}$. We wished to differentiate data that we obtained from the fans *datum* AC90/6 and AC90/6/TF$_{VTE}$ from data that we obtained from individual static blades which we tested as part of the research reported in this chapter. Therefore, we chose to refer to individual blades as aerofoils. Thus we conducted the research reported in this chapter using aerofoil *datum* AC90/6 and aerofoil AC90/6/TF$_{VTE}$ mounted in the jet plume's core.

Jet Noise Characterisation

Before commencing measurements with aerofoil *datum* AC90/6 and aerofoil AC90/6/TF$_{VTE}$ installed, we first established the jet plume's acoustic characteristics. We measured far-field directivity of the integrated sound pressure level (L_P) for the jet plume with no aerofoil fitted in the test rig, Figure 6.5. The far-field directivity illustrates that the jet noise peaks were at an azimuthal position of ninety degrees. This result was unexpected as purely subsonic jets generate acoustic wave fronts that originate from the regions where mixing layers merge. Kandula and Vu (2003) and Bogey and Bailly (2005) studied the noise sources that occur with subsonic jets. They concluded that the dominant noise sources are typically in the jet's core region, resulting in jet noise peaks on the jet axis. We attribute the difference between our results and those of Kandula and Vu (2003) and Bogey and Bailly (2005) to the presence of the test section's inlet bell-mouth, Figure 6.1.

We continued our characterisation of the jet plume without a fitted aerofoil. We analysed the far-field integrated sound pressure level (L_P) at 30 and 90 degree azimuthal positions, and the coherence spectrum between the two signals, Figure 6.6.

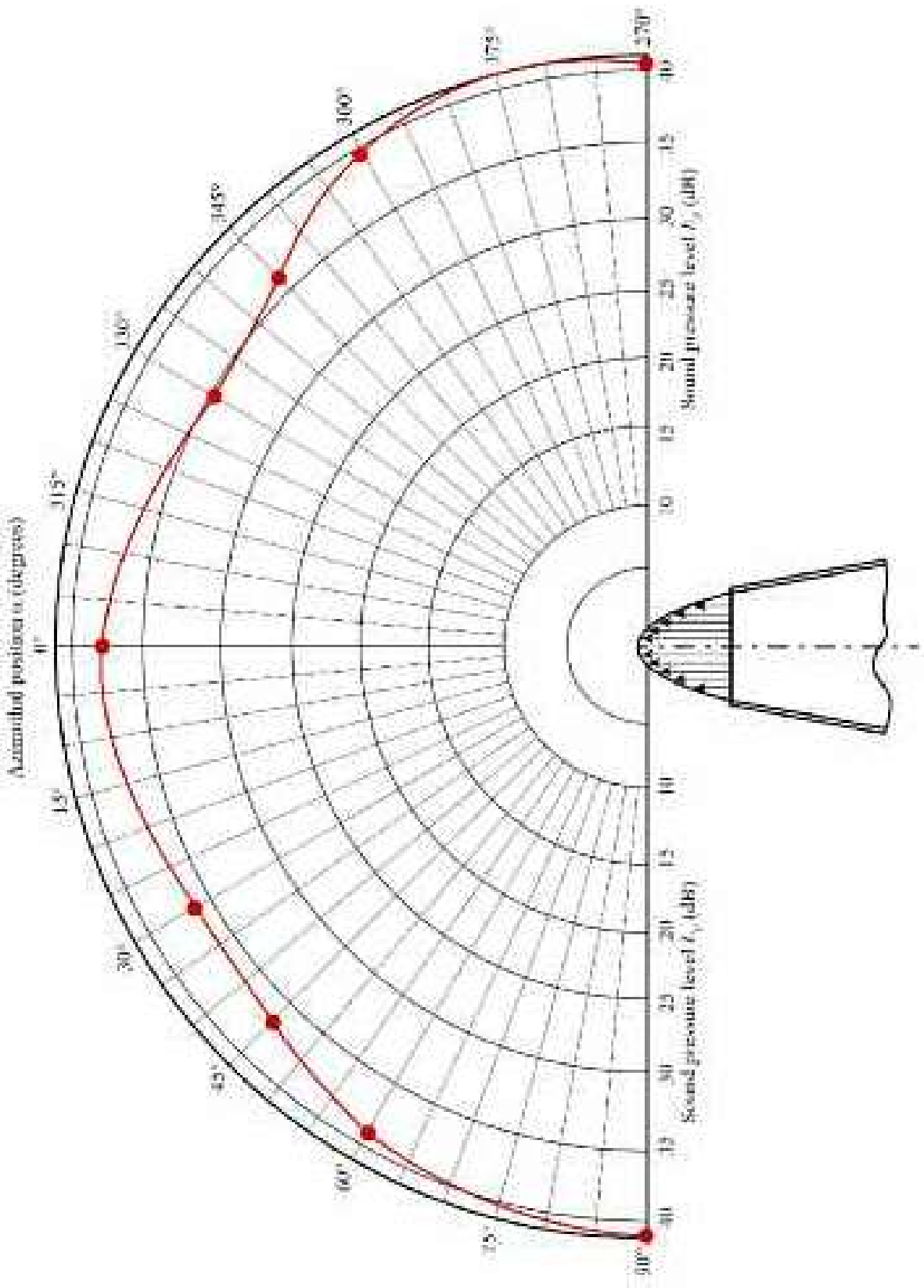

FIGURE 6.5. Measured far-field directivity of the integrated sound pressure level (L_p) for the jet with no aerofoil fitted in the test rig. This initial measurement of jet noise without an aerofoil present facilitated the characterisation of the background noise introduced by the jet plume. The symbols indicate the far-field microphone's azimuthal positions.

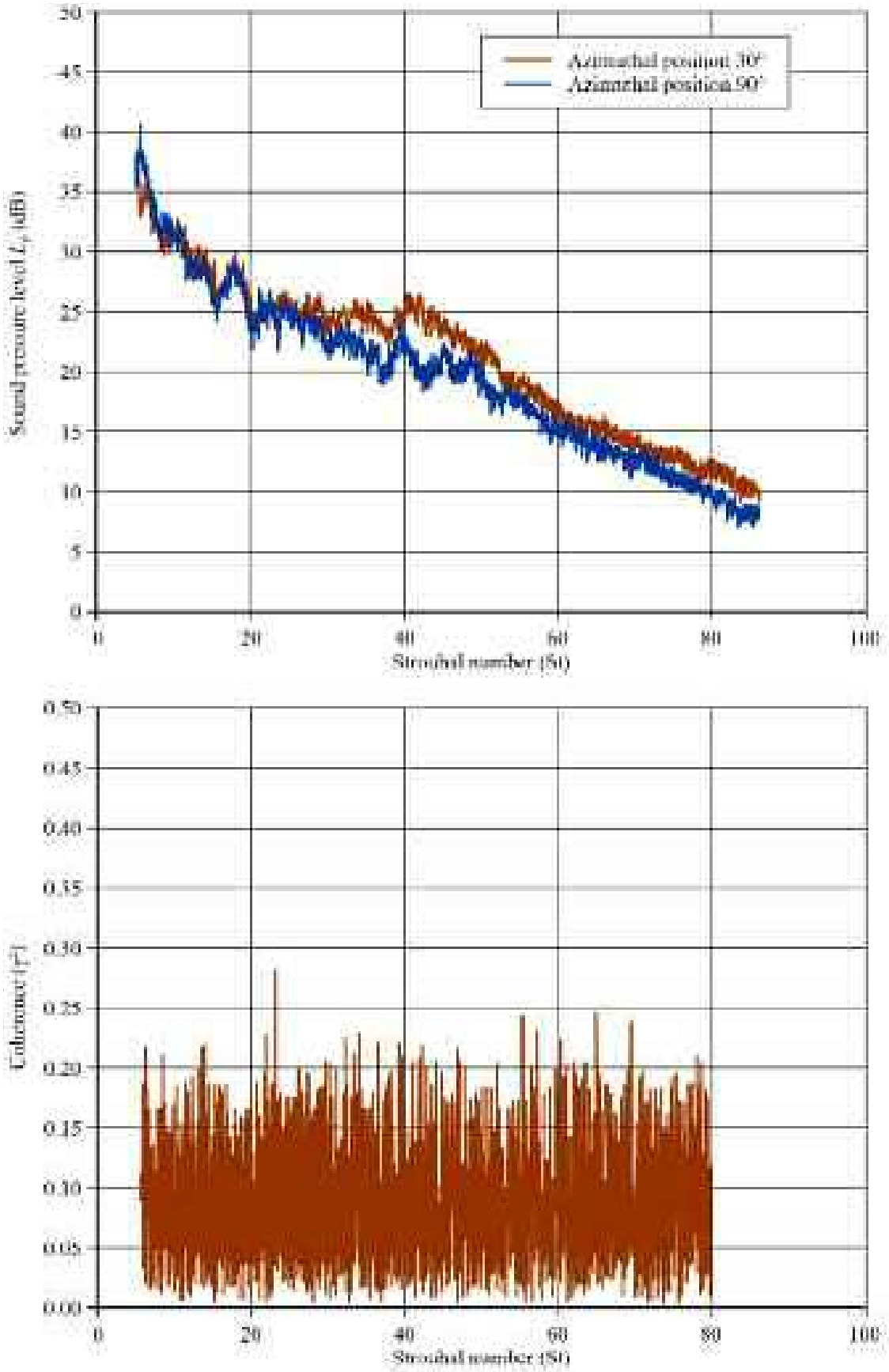

FIGURE 6.6. Measured integrated sound pressure level (L_P) at 30 and 90 degree azimuthal positions for the jet with no aerofoil fitted in the test rig, and the coherence spectrum between the signals measured at 30 and 90 degree azimuthal positions.

The sound pressure level trend with Strouhal number at 30 and 90 degree azimuthal positions are in good agreement. There are two exceptions to the good agreement. The first is in the Strouhal number range 30 to 55. The second is for Strouhal numbers below 10. We may associate Strouhal numbers below 10 with the jet plume acoustic emissions radiating 90 degrees off the fan axis.

A higher sound pressure level at a 30 degree rather than a 90 degree azimuthal position characterise the Strouhal number range 30 to 55. We attribute this discrepancy to the jet plume's turbulent mixing. Jacob *et al.* (2005) and Wang *et al.* (2009) studied the turbulent mixing of jet plumes. They concluded that turbulent mixing in free space produces broadband noise or an elevated narrow band region. Therefore, we may attribute the higher sound pressure level in the Strouhal number range 30 to 55 to the jet plume's turbulent mixing in free space.

We have previously attributes these jet noise peaks at azimuthal positions ninety degrees from the fan axis to the presence of the test section's inlet bell-mouth. Although not ideal, the test rig and its bell mouth comprise a fan casing and its inlet. Therefore, we may consider the impact of the test section's inlet bell-mouth integral with the aerofoils. It is the acoustic performance of both that we are studying, not one or other in isolation.

We calculated the coherence spectra between the sound pressure level measurements at 30 and 90 degree azimuthal positions. We wished to study the coherence between the two in an effort to quantify the average coherence of jet plume noise. By quantifying the average coherence of jet plume noise, we were able to establish an appropriate threshold value of coherence. This was necessary to facilitate an analysis of coherence data generated from measured data with an aerofoil present. The coherence between the sound pressure level measurements at 30 and 90 degree azimuthal positions was typically less than 0.2. Therefore, we chose a coherence threshold of 0.2 for use in our subsequent analysis.

Aerofoil *datum* AC90/6

Having characterised the jet plume with no aerofoil fitted in the test rig, we installed the aerofoil *datum* AC90/6. We recorded data sets of chord-wide distributions of near-field unsteady pressure and far-field noise with the far-field microphone 30 degrees of the fan axis. Before commencing our analysis, it is worthwhile to pause and reflect on the fact that correlation does not imply causation. We emphasise that a correlation between two variables does not necessarily imply that one causes the other. Therefore we cannot use correlation to infer a causal relationship between variables. This caveat does not imply that correlations cannot indicate the potential existence of causal relationships between aerodynamic cause and acoustic effect. However, we may only indirectly elucidate the underlying flow-field physics. Given the limitations of our analysis technique, we chose to limit our analysis to the chord wise distribution of near-field unsteady pressure measurements.

Consider the chord-wise map of near-to-far-field coherence (γ^2) for the aerofoil *datum* AC90/6, Figure 6.7. The aerofoil pressure surface results indicate coherence

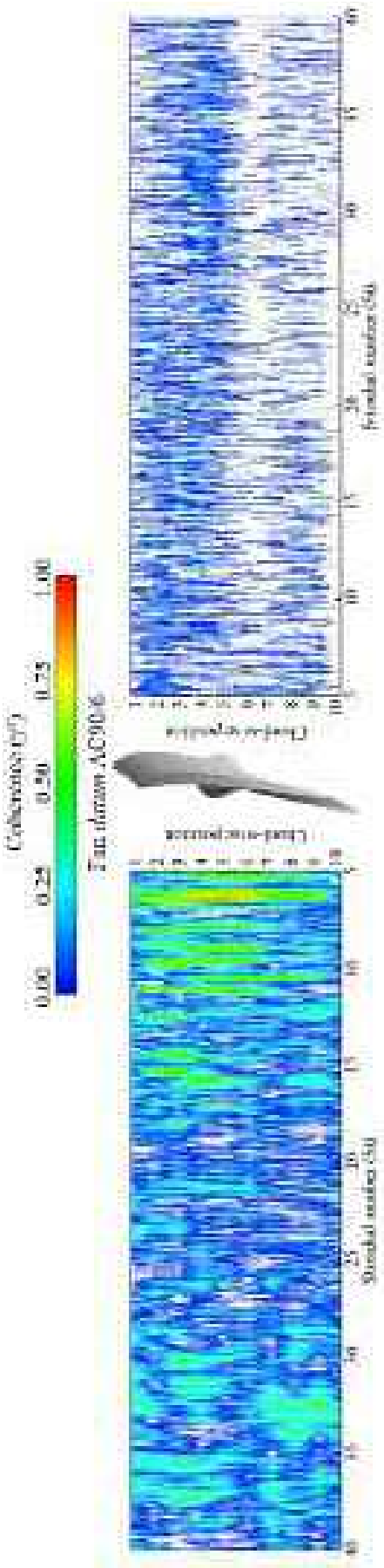

Figure 6.7. Chord-wise map of near- to far-field coherence (γ^2) for the aerofoil *datum* AC90/6 with all signals measured with the far-field microphone at an azimuthal position of 30 degrees.

levels above our threshold on 0.2 on the pressure surface from over a Strouhal number range from 5 to 16. At the aerofoil's leading edge there are coherent tones over a Strouhal number range of 5 to 11. We may attribute these tones to the turbulent inflow from the jet plume onto the aerofoil leading edge. This turbulent inflow affects the inflow and leading edge boundary layer interaction.

The chord-wise map of near-to-far-field coherence exhibits tonal peaks immediately upstream of the aerofoil mid-chord region. This is the location where the primary blade tip-to-casing leakage vortex passes through the blade tip-to-casing gap (Bianchi *et al.*, 2009). It is also the location at which the blade tip-to-casing leakage vortex has its maximum momentum and therefore, highest rotational frequency. A review of the chord-wise map of near-to-far-field coherence indicates that all chord-wise locations constitute noise sources over a Strouhal number range from 5 to 7. However, the chord-wise positions 4, 5 and 6 occur with peaks in coherence indicating that they may be the locations of noise sources. Over a Strouhal number range from 11 to 12, the chord-wise positions 6, 7 and 8 occur with peaks in coherence. These coherence peaks indicate that we may associate these chord-wise locations with higher frequency noise sources.

We may hypothesis that over a range of Strouhal numbers from 5 to 16, two phenomena may characterise the aerofoil *datum* AC90/6. The tonal noise sources over a Strouhal number ranging from 5 to 7 characterise the first phenomena. These noise sources are distributed along the entire aerofoil chord from leading to trailing edge. We may hypothesise that these noise sources are related to two phenomena: the leading edge boundary layer flow and inlet flow interaction, plus the interaction of the blade tip-to-casing leakage vortex with the blade-to-blade passage flow. These two phenomena are related as they result in acoustic emissions over the same frequency ranges that merge as they radiate to the far-field. The resulting tones in the far-field are at Strouhal numbers of 5, 8 and 11, plus the Strouhal number range 6.3 to 6.8. We may attribute these noise sources to blade aerodynamic loading. In this case the aerofoil is not rotating and consequently, we attribute these noise sources to the interaction of the leading edge flow and jet generated turbulence.

As previously stated, we may hypothesis that over a range of Strouhal numbers from 5 to 16, two phenomena characterise the aerofoil *datum* AC90/6. The tonal noise sources over the full Strouhal number range from 5 to 16 characterise the second phenomena. These noise sources originate from the blade tip-to-casing leakage flow, and the skewing of that leakage flow as it migrates from aerofoil leading to trailing edge. The resultant tones in the far-field are at Strouhal numbers 5.5, 6.5 and 9, 10.8 and 15.2.

At Strouhal numbers above 15, coherence regions are sparse as a consequence of the tonal noise sources' reduced magnitude and the resultant dominance of broadband noise. Despite the broadband noise's general dominance, there are noise sources at chord-wise positions 1, 2, 3, 4 and 5. At Strouhal numbers 33 and 35, the noise sources were localised in the aerofoil trailing edge region at chord-wise positions 7, 8, 9 and 10.

We may hypothesise that at Strouhal numbers below 10, phenomena originating at the aerofoil leading edge characterise the aerofoil *datum* AC90/6. In contrast, at

Strouhal numbers above 10, phenomena that manifest themselves at the aerofoil trailing edge characterise the aerofoil *datum* AC90/6. These trailing edge phenomena may be attributes to the blade tip-to-casing leakage flow interaction with fan casing boundary level. Further, we may hypothesise that noise sources at Strouhal numbers above 30 may occur with aerofoil trailing edge noise.

Consider the chord-wise map of near-to-far-field coherence (γ^2) for the aerofoil *datum* AC90/6, Figure 6.7. The aerofoil suction surface results indicate that coherent noise sources may occur with the aerofoil tip-to-casing leakage flow's chord-wise evolution. We may attribute the resultant noise sources to the interaction of the aerofoil tip-to-casing leakage flow and casing boundary layer. As the aerofoil tip-to-casing leakage vortex migrates from aerofoil leading to trailing edge, the resultant noise sources are characteristic of turbulent flow. The result is broadband noise at the aerofoil trailing edge. The result is a coherence map with no significant tonal peaks. The only exception is at the chord-wise position 4 over a Strouhal number range from 15 to 40. The coherence is 0.3, above our threshold value of 0.2, but still low and therefore characteristic of a relatively insignificant noise source.

The chord-wise map of near-to-far-field coherence for the aerofoil *datum* AC90/6 facilitated an analysis of the chord-wise distribution of noise sources that radiate to the far-field. We may complement this analysis by examining coherence function spectra at chord-wise positions 1, 5 and 10, Figure 6.8. Consider the coherence function spectra at chord-wise positions 1 on the aerofoil pressure surface. One tonal peak at a Strouhal number of 7.5 and a series of smaller peaks over a Strouhal number range from 30 to 42 characterise the coherence spectra. Consider the coherence function spectra at chord-wise positions 5 on the aerofoil pressure surface. Peaks in the coherence spectra shift to lower frequencies than at chord-wise positions 1, with a general reduction in coherence at higher frequencies.

Consider the coherence function spectra at chord-wise positions 10 on the aerofoil pressure surface. A tonal peak at a Strouhal number of 32 characterise the coherence spectra. We hypothesise that the same phenomena is responsible for the tonal peaks at Strouhal numbers of 7.5 and 32 at the chord-wise positions 1 and 10. We consider it most likely that the phenomenon responsible for these tonal peaks is ingested turbulence. The tonal peaks over a Strouhal number range from 30 to 42 at chord-wise position 1 have decreased in coherence by chord-wise position 10.

A tonal peak's shift from lower to higher frequency characterises the shift from chord-wise position 1 to 10. Laurendeau *et al.* (2007) studied the noise sources associated with subsonic jets, identifying the mechanisms responsible for the correlation of near- and far-field noise. Laurendeau *et al.* (2007) specifically studied the shift of tonal peaks from lower to higher frequency as they migrate from leading to trailing edge. They concluded that the shift occurred as a consequence of lower frequency harmonics that radiate to the far-field. These become progressively less efficient when radiating to the far-field as they migrate from aerofoil leading to trailing edge.

At chord-wise position 1 the aerofoil mounted microphone was subjected to turbulence that occurs with the casing boundary layer. The resulting flow-field is highly unsteady and we may characterise it as having a Kelvin-Helmholtz mixing-layer structure. At chord-wise position 10, we may characterise the casing boundary

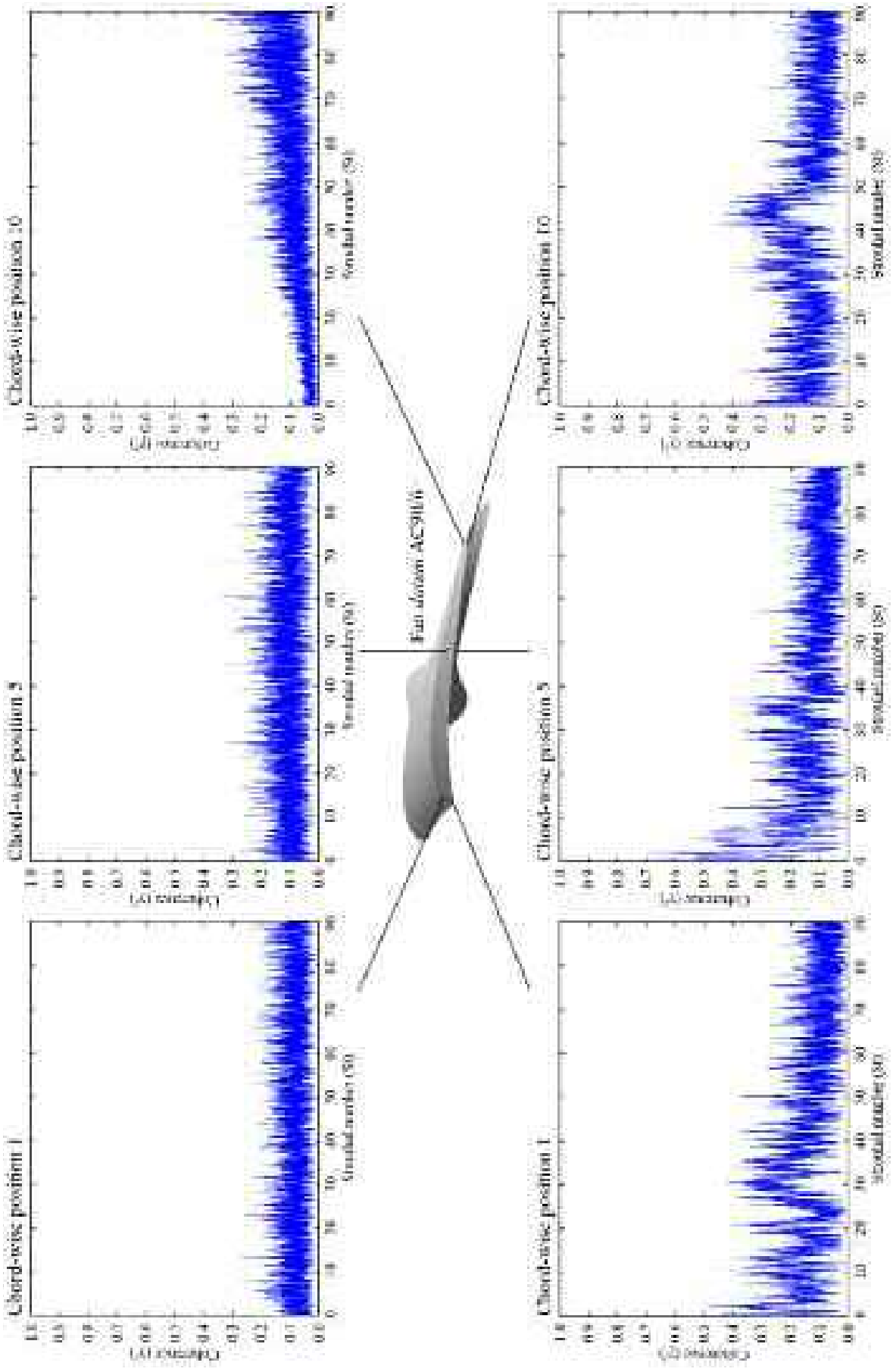

Figure 6.8. Chord-wise near- to far-field coherence (γ^2) for the aerofoil *datum* AC90/6 at the leading edge, mid-chord and trailing edge of the aerofoil suction and pressure surface with all signals measured with the far-field microphone at an azimuthal position of 30 degrees.

layer as a fully developed turbulent boundary layer. The dominant tone is at a Strouhal number of 45. Once again, this observation is self-consistent with Laurendeau *et al.*'s (2007) conclusions that this shift from an essentially broadband noise source to one with a higher frequency tone may occur. This is a consequence of taking measurements in a region where hydrodynamic effects dominated. Consequently, there is no established acoustic signal and therefore we are unable to measure it.

Consider the coherence functions spectra at chord-wise positions 1, 5 and 10 on the aerofoil suction surface. The coherence spectra are distinctly different to those measured on the pressure surface. At chord-wise positions 1 and 5, the coherence is almost constantly below 0.2 from low to high Strouhal numbers. At chord-wise position 10, the coherence spectra is 0.1 at low Strouhal numbers, and then rises linearly with Strouhal number to 0.2 at a Strouhal number of 40. We may attribute the generally lower coherence levels on the aerofoil suction surface to the reduced influence of the Kelvin-Helmholtz mixing-layer structure. The instabilities associated with the Kelvin-Helmholtz mixing-layer structure are not typically this low. However, in this instance it would appear that the blade tip-to-casing leakage vortex constitutes the dominant noise source. The blade tip-to-casing leakage vortex is chaotic, and consequently, masks all other noise sources. We name this effect a 'turbulent shield'. Brown and Clifford (1976) have reported a similar masking phenomenon. They concluded the only near-field noise source that propagated to the far-field occurred with the blade tip-to-casing leakage flow passing though the blade tip-to-casing gap.

We may complement the chord-wise map of near-to-far-field coherence and coherence spectra by analysing the cross-correlation coefficient at chord-wise positions 1, 5 and 10, Figure 6.9. The peak's presence in the cross-correlation coefficient correlates with a match between the near- and far-field measurements for a defined time delay. We presented cross-correlation coefficients over a time delay from 3.4 to 3.8×10^{-3} seconds. We selected this time delay as it covered a range of time delays that occur with a peak value of cross-correlation coefficient.

Miles (2006, 2010) developed a procedure for separating noise sources. He concluded that a peak in the cross-correlation coefficient is characteristic of different *cause-effect* and *effect-effect* mechanisms. At time delays lower than the peak in the cross-correlation coefficient, the noise source travels at the speed of sound from the near- to far-field. At time delays higher than the peak in the cross-correlation coefficient, the noise source travels at the average flow-field velocity.

Consider the cross-correlation coefficients at chord-wise positions 1, 5 and 10 on the aerofoil suction surface. The cross-correlation coefficient exhibits a single positive peak, in contrast to the pressure surface that we may characterise as exhibiting a double positive and negative peak. The reason for the change from single to double peak is not apparent. When Miles (2010) studied noise sources, he concluded that a possible mechanism for the change may be that the relative magnitude of acoustic signals decreases away from the jet axis.

The unexpected change from a double to single peak from pressure to suction surface encouraged us to analyse the pressure surface cross-correlation coefficients further. We chose to derive the positive and negative peak values for pressure surface

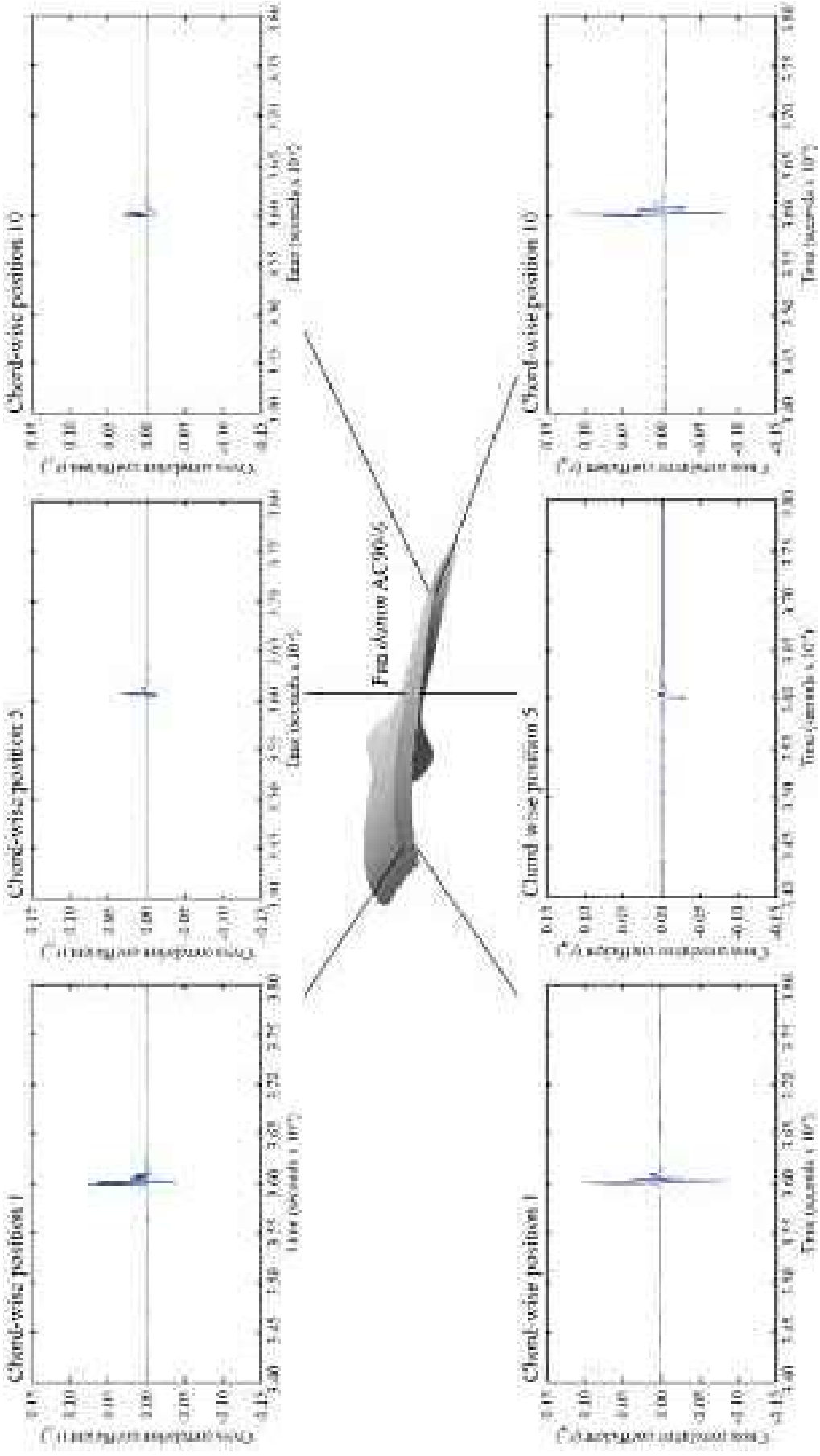

FIGURE 6.9. Chord-wise near- to far-field cross-correlation coefficient (r_{xy}) for the aerofoil *datum* AC90/6 at the leading edge, mid-chord and trailing edge of the aerofoil suction and pressure surface with all signals measured with the far-field microphone at an azimuthal position of 30 degrees.

cross-correlation coefficients and their associated time delay, Table 6.2. We define the time delay as:

$$\Delta\tau(f_L)\big|_{peak} = \tau(f_L)\big|_{peak} - \tau_{ref}$$

with time delay calculated relative to a reference time delay (τ_{ref}) of 3.6×10^{-3} seconds. We chose this reference time delay as all peaks occur close to this value. By subtracting this reference time delay we are able to better interpret the data in Table 6.2. We may use the time delay in conjunction with an estimate of the jet's convection velocity to calculate a length scale that occurs with the peaks in cross-correlation coefficients. With a time delay or 3.6×10^{-3} seconds and an assumption that the jet's convection velocity is 20 metres per second, 60 per cent of the jet's average velocity, we obtain a length scale l_s of 0.15 metres. Strouhal numbers from 1 to 5 have a length scale of 0.23 metres to 0.12 metres, covering the range of the length scale that occurs with the cross-correlation coefficients.

Miles (2010) derived the delay time for direct and indirect noise. He assumed that the delay time depends only on the difference between the entropy's travel time to the turbulent border that surrounds the aerofoil and the acoustic travel time to the same position. In our analysis, we chose to ignore other possible mechanisms that may impact time delay. From the turbulent border that surrounds the aerofoil, we may assume all signals acoustic. Therefore, they travelled along the same path to the far-field microphone and consequently, we may estimate time delay as:

$$\Delta\tau = \tau_s - \tau_a \approx L_j/v_j - L_j/c_j = (L_j/c_j)(1 - M_j) \,/\, M_j \approx \; L_j/v_s$$

where:

L_j is the distance between the microphone and blade trailing edge;
n_j is the speed of flow impinging the blade;
c_j is the speed of sound between the microphone and blade trailing edge;
M_j is the local flow Mach number, and;
n_s is the speed of entropy transmission at the turbulent boundary layer.

The difference in the measured time delay for the direct and indirect aerodynamic noise, $\Delta\tau$ was approximately 0.02×10^{-3} seconds, Table 6.2. Using the above equation, we obtain a delay time between 0.02×10^{-3} to 0.05×10^{-3} seconds depending on the assumptions we made when selecting values for the involved parameters. Therefore, this agreement between the measured data in Table 6.2 and the calculated delay time is reasonable.

We now re-examine the cross-correlation coefficient at chord-wise positions 1, 5 and 10, Figure 6.9. Positive and negative cross-correlation coefficient double peaks characterise the pressure surface. Positive cross-correlation coefficient single peaks characterise the suction surface. With a single peak, we are not able to use Miles' (2010) method to determine the separation of direct and indirect noise. Despite this reservation, we are able to clearly identify the time delay on both pressure and suc-

Table 6.2. *Time delays and peak values of cross correlation coefficients for the aerofoil* datum *AC90/6 at three chord-wise positions on the aerofoil pressure surface.*

	Time (x 10^{-3} seconds)	Peak
Chord-wise position 1	3.601	+ 0.1020
	3.603	– 0.0950
	3.605	+ 0.0380
	3.606	– 0.0974
	3.609	+ 0.0151
	No data	No data
Chord-wise position 5	3.600	No peak
	3.601	No peak
	3.602	No peak
	3.603	No peak
	3.606	No peak
	3.609	No peak
Chord-wise position 10	3.599	+ 0.0800
	3.602	+ 0.1180
	3.603	– 0.0760
	3.606	+ 0.0350
	3.607	– 0.0250
	No data	No data

tion surface at each chord-wise location. Consider the positive and negative cross-correlation coefficient peaks at chord-wise position 1 on the pressure and suction surface. We may hypothesise that on the negative peak present on the pressure surface, a turbulent structure on the suction surface absorbed it. The same effect is evident at chord-wise position 10, with both positive and negative peaks further reduced on the suction surface. The aerofoil's trailing edge region is known to be a turbulent region. Therefore, it is apparent that the size of cross-correlation coefficient peaks reduces as we move from aerofoil leading to trailing edge. This supports the hypothesis that a turbulent structure on the suction surface absorbed suction surface peaks.

Turbulent interaction with the acoustic waves that occur with jet noise attenuate near-field noise (Miles, 2010). Therefore, we may hypothesise about the possible mechanisms responsible for the negative peak in the cross-correlation coefficient. Consider the negative peak in the aerofoil pressure surface cross-correlation coefficient at chord-wise position 10. This negative peak may be primarily a consequence of indirect noise that a turbulent structure on the suction surface absorbs. We may associate the turbulent structure with the leakage flow through the aerofoil tip-to-casing gap or the interactions of that leakage flow with the casing boundary layer. If the research community accepts our hypothesis, then there may be an alternative sound absorption mechanism: vortex shedding from rigid surfaces (Bechert, 1980).

Bechert (1980) concluded that the *Kutta condition* is crucial to the vortex shedding from a rigid surface. When the *Kutta condition* is satisfied there is vortex shedding and that vortex shedding extracts acoustic energy from the sound field in

the vortex's near vicinity. Therefore, vortex shedding may be responsible for the absence of suction surface negative cross-correlation coefficient peaks. This hypothesis implies that higher frequency aerofoil broadband noise may not be omni-directional. Our hypothesis is self-consistent with Laurendeau *et al.* (2007) and Tinney and Jordan (2008). However, it is possible that at the higher frequencies associated with broadband noise there is still some hydrodynamic impact. Therefore, we may not be studying a purely acoustic mechanism. If hydrodynamic effects remain significant, then we compromise our interpretation of the chord-wise distribution of noise sources. We could undertake a more complete analysis with additional chord-wise measurements and complementary sets of span-wise acoustic measurements. The additional data would facilitate a better insight into the flow-field physics.

Aerofoil AC90/6/TF$_{VTE}$

Having characterised the aerofoil *datum* AC90/6, we went on to characterise the aerofoil AC90/6/TF$_{VTE}$. Once again, we recorded data sets of chord-wide distributions of near-field unsteady pressure and far-field noise with the far-field microphone 30 degrees off the fan axis.

Consider the chord-wise map of near-to-far-field coherence (γ^2) for the aerofoil AC90/6/TF$_{VTE}$, Figure 6.10. The regions of coherence on both aerofoil pressure and suction surface are reduced compared with the aerofoil *datum* AC90/6. Despite this caveat, the aerofoil AC90/6/TF$_{VTE}$ distribution of noise sources is broadly similar to that of the aerofoil *datum* AC90/6. We may characterise this aerofoil pressure surface distribution tonal noise sources over a Strouhal number range from 5 to 20 where aerofoil AC90/6/TF$_{VTE}$'s tonal noise sources have a lower coherence then similar noise sources that occur with the aerofoil *datum* AC90/6. An example of this is the tonal noise source at a Strouhal number of 1. This has a coherence of 0.3 for the aerofoil AC90/6/TF$_{VTE}$. In contrast, a coherence of 0.7 for the aerofoil *datum* AC90/6 characterises the same Strouhal number.

A tonal noise source that has the same coherence of 0.5 for both the aerofoil AC90/6/TF$_{VTE}$ and *datum* AC90/6 characterises the pressure surface at a Strouhal number of 1. This was unanticipated as one would expect the blade loading's chord-wise distribution to affect noise sources in the blade tip region. When one fits the variable thickness blade-tip end-plate to the blade tip, the blade loading's chord-wise distribution changes. When we study the chord-wise distribution of aerofoil AC90/6/TF$_{VTE}$ noise sources, it is apparent that they are concentrated from the aerofoil leading edge to mid-chord. The highest coherence of 0.7 at chord-wise position 4 and a Strouhal number of 15 characterise the aerofoil AC90/6/TF$_{VTE}$ pressure surface. This coherence peak may be a consequence of the variable thickness blade-tip end-plate control of blade tip-to-casing leakage swirl. According to Corsini *et al.* (2010), this control results in the blade tip-to-casing leakage vortex's instability that develops at a chord-wise location approximately coincident with chord-wise position 4.

Consider the chord-wise map of near-to-far-field coherence for the aerofoil AC90/6/TF$_{VTE}$, suction surface, Figure 6.10. Once again, as with the aerofoil *datum*

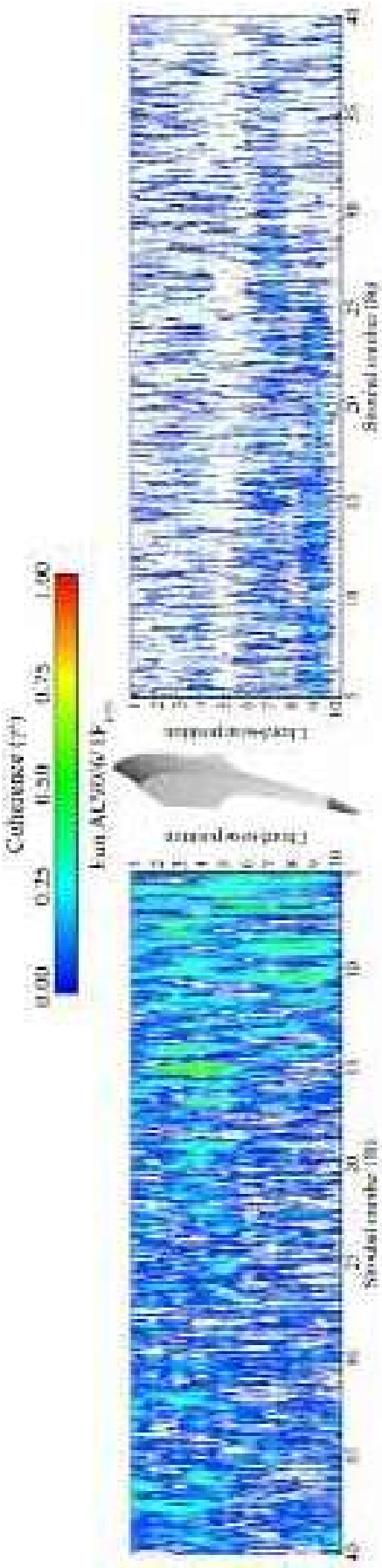

FIGURE 6.10. Chord-wise map of near- to far-field coherence (γ^2) for the aerofoil AC90/6/TF$_{VTE}$ with all signals measured with the far-field microphone at an azimuthal position of 30 degrees.

AC90/6 few tonal features characterise the suction surface of aerofoil AC90/6/TF$_{VTE}$, therefore we may regard the noise as broadband. The coherent regions that are present over aerofoil *datum* AC90/6's suction surface remain discernable over the aerofoil AC90/6/TF$_{VTE}$'s suction surface. However, the peak coherence has moved from a chord-wise position of 4 to 9. Bianchi *et al.* (2009) studied the aerofoil AC90/6/TF$_{VTE}$ concluding that blade tip-to-casing leakage vortex development is a dominate noise source in the blade tip region. The presence of the variable thickness blade-tip end-plate has a primary impact on the tip-to-casing leakage vortex development, and its resultant acoustic emissions.

When we study the chord-wise map of aerofoil AC90/6/TF$_{VTE}$ suction surface coherence, it is apparent that coherence levels are generally lower than aerofoil *datum* AC90/6. We may attribute this general reduction to the presence of the variable thickness blade-tip end-plate. We may hypothesise that the variable thickness blade-tip end-plate acts as a mixing enhancer in the blade tip region. An increase in vortex shedding and the associated transformation of tonal into broadband noise that transmits less efficiently to the far-field accompanies the enhanced mixing. Bechert (1980) studied jet noise and demonstrated that an increase in near-field broadband noise is linked with an increase in the jet flow rotating turbulence. However, there is no published research that establishes the existence of this link between broadband noise and rotating turbulence through blade rows. Therefore, we may only hypothesise that an increase in vortex shedding accompanies enhanced mixing. Further, we may only hypothesise that the associated transformation of tonal into broadband noise then transmits less efficiently to the far-field.

We may complement our analysis of the aerofoil AC90/6/TF$_{VTE}$ coherence maps by comparing the coherence spectra at chord-wise positions 1, 5 and 10. Consider the coherence spectra for aerofoil AC90/6/TF$_{VTE}$, Figure 6.11, and aerofoil *datum* AC90/6, Figure 6.8. The aerofoil AC90/6/TF$_{VTE}$ exhibits characteristics that are broadly similar to those of aerofoil *datum* AC90/6. This observation is true for both the aerofoil pressure and suction surface. Although the characteristics are broadly similar, coherence levels are generally lower for the aerofoil AC90/6/TF$_{VTE}$ when compared to those of aerofoil *datum* AC90/6. However, there is a difference between the coherence levels of the aerofoil AC90/6/TF$_{VTE}$ and those of aerofoil *datum* AC90/6. We may associate the aerofoil AC90/6/TF$_{VTE}$ with increasingly lower coherence levels as the Strouhal number reduces. This phenomenon is most evident at chord-wise position 5 on both the pressure and suction surface. It is only chord-wise position 10 for aerofoil AC90/6/TF$_{VTE}$ that we associate with higher coherence than aerofoil *datum* AC90/6, and then only at Strouhal numbers over 40.

Again, we study cross-correlation coefficients, this time comparing them for the aerofoil AC90/6/TF$_{VTE}$, Figure 6.12, with aerofoil *datum* AC90/6, Figure 6.9. When we study the cross-correlation coefficients for the aerofoil AC90/6/TF$_{VTE}$, it is apparent that single peaks on both the pressure and suction surface characterise them. In contrast, single peaks characterise the aerofoil *datum* AC90/6's suction surface. A single peak characteristic does not enable noise sources that occur with direct and indirect noise to separate. Despite this limitation, we may infer that the aerofoil AC90/6/TF$_{VTE}$ is associated with acoustic absorption at chord-wise position 10 on

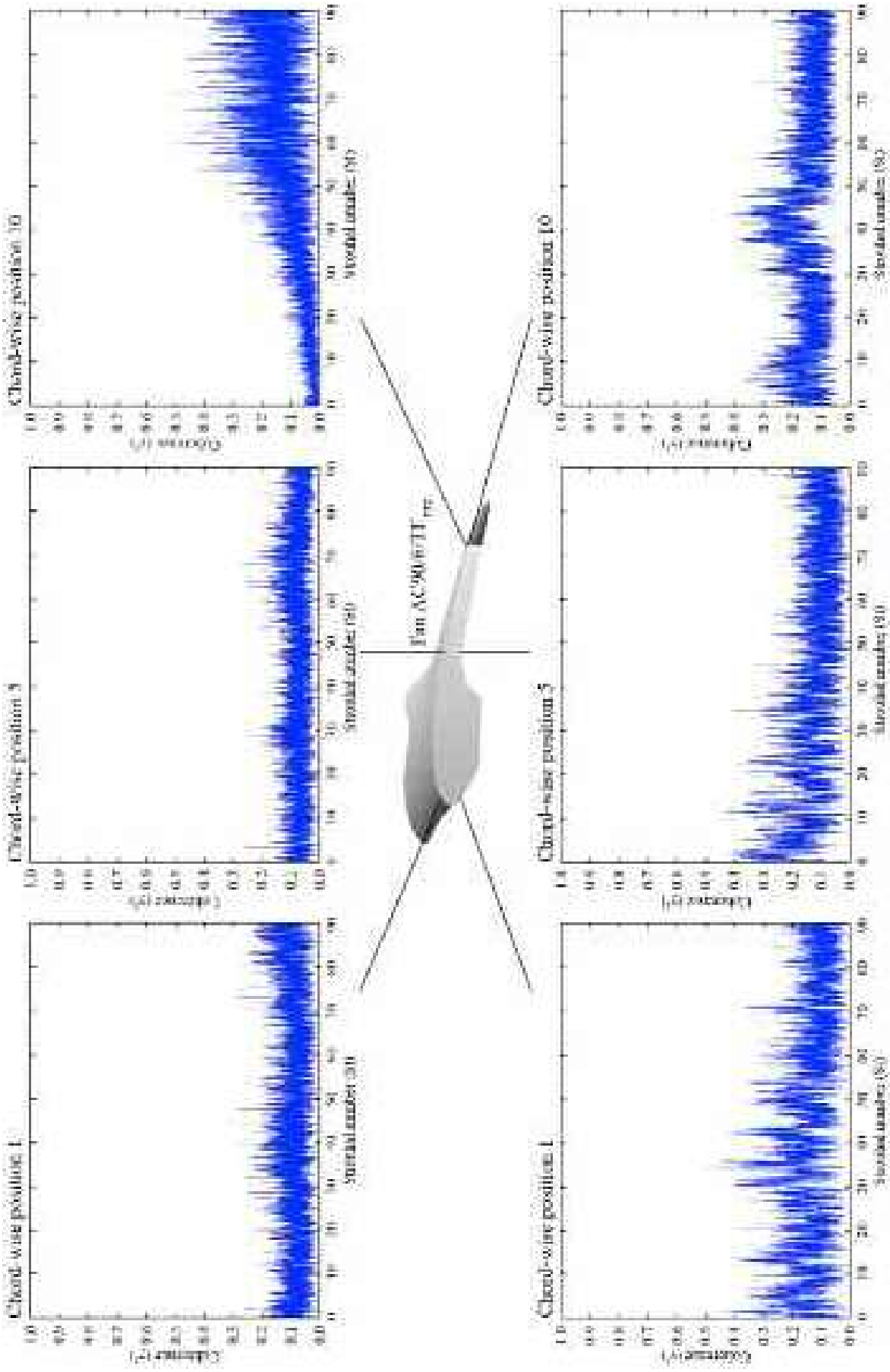

FIGURE 6.11. Chord-wise near- to far-field coherence (γ^2) for the aerofoil AC90/6/TF$_{VTE}$ at the leading edge, mid-chord and trailing edge of the aerofoil suction and pressure surface with all signals measured with the far-field microphone at an azimuthal position of 30 degrees.

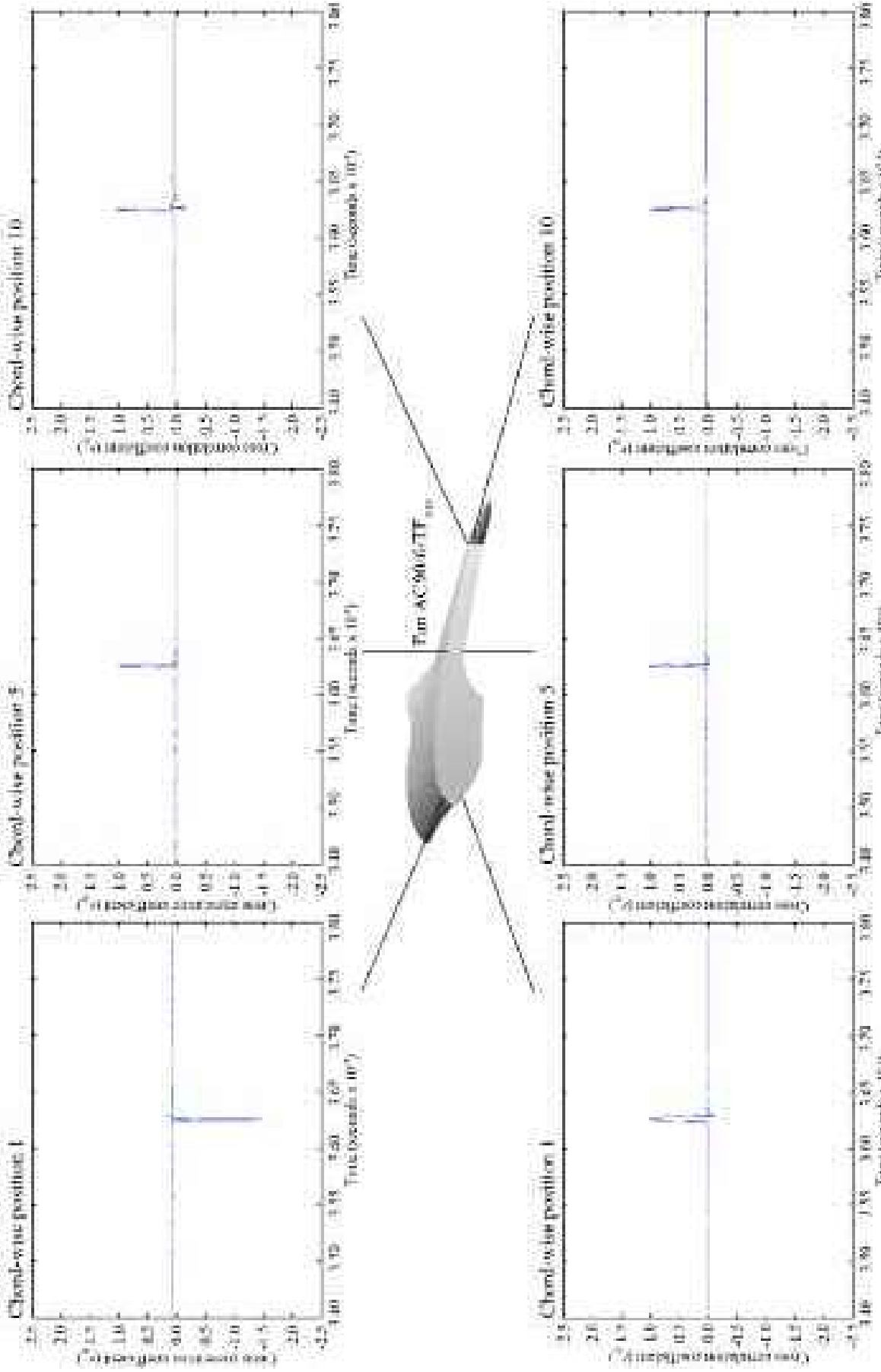

FIGURE 6.12. Chord-wise near- to far-field cross-correlation coefficient (r_{xy}) for the aerofoil AC90/6/TF$_{VTE}$ at the leading edge, mid-chord and trailing edge of the aerofoil suction and pressure surface with all signals measured with the far-field microphone at an azimuthal position of 30 degrees.

the suction surface. We characterise separated flow or vortex shedding with acoustic absorption driven by changes in the flow-field features induced by the presence of the variable thickness blade-tip end-plate.

Fukano *et al.* (1977a) studied the noise generated by low pressure axial flow fans, developing a model for their turbulence induced noise. Fukano *et al.* (1977a) concluded that near-field noise should increase linearly with vortex scale. Within the context of the research reported in this chapter, this linear increase should scale with increasing blade tip-to-casing gap. The results presented in this chapter did not show a linear increase with increasing vortex scale. This absence is probably a consequence of the aerofoil not moving relative to the casing. The frozen aerofoil results in a significant change in momentum transfer in the blade tip-to-casing gap. Additionally, because the aerofoil is not rotating boundary layer fluid is not centrifuged up the aerofoil. This centrifuging of fluid up the aerofoil is a factor known to impact the flow-field features that develop in the blade tip-to-casing gap. Therefore, our analysis is ultimately limited by the limitations of a frozen rotor experimental technique.

CONCLUSIONS

The chapter presents an experimental methodology developed to facilitate assessing a fan's acoustic performance that we developed for application in compact cooling units. We placed ten microphones at the blade-tip of a single fan blade. We mounted the instrumented blade in an anechoic chamber and measured the interaction noise with a jet impacting the blade. Although the blade did not move, we reproduced the Mach number, Reynolds number and blade incidence angel in the static frame of reference. This 'frozen rotor' technique enabled us to correlate ten chord-wise near-field acoustic measurements with a far-field acoustic measurement made 30 degrees off the fan centre line. We developed this experimental methodology to provide insight into the far-field consequences of near-field flow features induced in the flow by blade-tip end-plates.

We made the near- and far-field acoustic measurements simultaneously. This enabled the experimental methodology to provide data sets of chord-wide distributions of near-field unsteady pressure that we correlated with far-field noise. We repeated near- and far-field measurements with and without a fitted blade-tip end-plate. This allowed us to establish the far-field consequences of changes in near-field flow-features induced by the presence of the blade-tip end-plate.

This chord-wise correlation of near- and far-field noise was distinctly different for the studied aerofoil without a fitted blade-tip end-plate and when fitted with an end-plate. For the aerofoil without a fitted blade-tip end-plate, the predominant noise source occurred with the blade-tip leakage flow towards the blade trailing edge. The blade-tip leakage flow's intensity as a noise source is directly related to the fan casing boundary layer's thickness, with a thicker boundary layer resulting in increased fan far-field broadband noise.

When fitted with a blade-tip end-plate, the chord-wise near-field unsteady pressure measurements indicated that the blade surface in the blade-tip region acted as a

mixing enhancer. This mixing enhancer resulted in the absorption of near-field noise as a consequence of vortex shedding through the blade tip-to-casing gap. This vortex shedding resulted in an increase in the local turbulence level that transformed harmonic tonal noise into broadband high frequency noise. The correlation between near- and far-field indicated that this broadband high frequency noise was more easily attenuated than the original harmonic noise. Consequently, the broadband high frequency noise did not transmit to the far-field as efficiently as the original harmonic noise, with the result that when fitted with a blade-tip end-plate, aerofoil far-field noise reduced.

The developed frozen rotor experimental technique has proven effective, enabling us to identify near-field noise sources unique to each of the tested fan configurations. The correlation technique also facilitated identification of the far-field acoustic consequences of the identified near-field noise sources. Finally, we were also able to identify a mechanism by which blade-tip end-plates modify the blade tip-to-casing flow that results in a change from harmonic to broadband noise.

REFERENCES

ISO IEC60651, IEC/EN-61672-1 (1979), *Calibration Rules for Hardware in Noise Measurements*.

Amiet, R.K. (1975), 'Acoustic Radiation from an Airfoil in a Turbulent Stream', *Journal of Sound and Vibration*, vol. 41, pp. 407–420.

Amiet, R.K. (1976), 'Noise Due to Turbulent Flow Past a Trailing Edge', *Journal of Sound and Vibration*, vol. 47(3), pp. 387–393.

Ashforth-Frost, S. and Jambunathan, K. (1996), 'Effect of Nozzle Geometry and Semi-confinement on the Potential Core of a Turbulent Axi-symmetric Free Jet', *International Communications in Heat and Mass Transfer*, vol. 23(2), pp. 155–162.

Bechert, D.W. (1980), 'Sound Absorption Caused by Vorticity Shedding, Demonstrated with a Jet Flow', *Journal of Sound and Vibration*, vol. 70(3), pp. 389–405.

Bianchi, S, Corsini, A., Rispoli, F. and Sheard, A.G. (2008a), 'Experimental Investigation of the Near-field Aeroacoustic Noise Sources of a Low Speed Axial Fan', *Proceedings of the XIX Biannual Symposium on Measuring Techniques in Turbomachinery*, Saint Genesius Rode, Belgium, 7–8 April.

Bianchi, S., Corsini, A., Rispoli, F. and Sheard, A.G. (2008b), 'Near-field Aeroacoustic Experimental Investigation in Low Speed Axial Fans', *Proceedings of the American Society of Mechanical Engineers Noise Control and Acoustics Division NoiseCon2008*, Dearborn, MI, USA, 28–30 July.

Bianchi, S., Corsini, A., Rispoli, F. and Sheard, A.G. (2009), 'Experimental Aeroacoustic Studies on Improved Tip Configurations for Passive Control of Noise-Signature in Low-speed Axial Fan', *Transactions of the ASME, Journal of Vibration & Acoustics*, vol. 131, paper no. 061007, pp. 1–10.

Blake, W.K. and Gershfeld, J.L. (1989), 'The Aeroacoustics of Trailing Edges', in Gad-el-Hak, M. (Ed.), *Frontiers in Experimental Fluid Mechanics*, Springer-Verlag, Berlin, pp. 457–532.

Bogey, C. and Bailly, C. (2005), 'Investigation of Sound Sources in Subsonic Jets using Causality Methods on LES Data', *Proceedings of the 11th AIAA/CEAS Aeroacoustics Conference (26th AIAA Aeroacoustics Conference)*, Monterey, CA, USA, 23–25 May 2005, paper no. AIAA 2005-2885.

Brooks, T.F. and Marcolini, M.A. (1986), 'Airfoil Tip Vortex Formation Noise', *AIAA Journal*, vol. 24(2), pp. 246–252.

Brooks, T.F., Pope D.S. and Marcolini, M.A. (1989), 'Airfoil Self Noise and Prediction', NASA Reference Publication 1218.

Brown, E.H. and Clifford, S.F. (1976), 'On the Attenuation of Sound by Turbulence', *Journal of the Acoustical Society of America,* vol. 60(4), pp. 788–794.

Coles, D. (1956), 'The Law of the Wake in the Turbulent Boundary Layer', *Journal of Fluid Mechanics,* vol. 1, pp. 191–226.

Cornaro, C.C., Fleischer, A.S. and Goldstein, R.J. (1999), 'Flow Visualization of a Round Jet Impinging on Cylindrical Surfaces', *Experimental Thermal and Fluid Science,* vol. 20(2), pp. 66–78.

Corsini, A. and Sheard, A.G. (2007), 'Tip End-plate Concept Based on Leakage Vortex Rotation Number Control', *Journal of Computational and Applied Mechanics*, vol. 8(1), pp. 21–37.

Corsini, A., Rispoli, F. and Sheard, A.G. (2010), 'Shaping of Tip End-plate to Control Leakage Vortex Swirl in Axial Flow Fans', *Transactions of ASME, Journal of Turbomachinery*, vol. 132(3), paper no. 031005, pp. 1–9.

Curle, N. (1955), 'The Influence of Solid Boundaries upon Aerodynamic Sound', *Proceedings of the Royal Society*, vol. A20, pp. 505–514.

Fedala, D., Kouidri, S., Rey, R., Carolus, T. and Schneider, M. (2006), 'Incident Turbulence Interaction Noise from an Axial Fan', *Proceedings of the 12th AIAA/CEAS Aeroacoustics Conference (27th AIAA Aeroacoustics Conference)*, Cambridge, MA, USA, 8–10 May, paper no. AIAA 2006-2477.

Ffowcs Williams, J.E. and Hawkings, D.L. (1969), 'Sound Generated by Turbulence and Surfaces in Arbitrary Motion', *Philosophical Transactions of the Royal Society*, vol. A264, pp. 321–342.

Fukano, T. and Jang, C. (2004), 'Tip Clearance Noise of Axial Flow Fans Operating at Design and Off-design Condition', *Journal of Sound and Vibration*, vol. 275, pp. 1027–1050.

Fukano, T., Kodama, Y. and Takamatsu, Y. (1977a), 'Noise Generated by Low Pressure Axial Flow Fans I – Modelling of the Turbulent Noise', *Journal of Sound and Vibration*, vol. 50, pp. 63–74.

Fukano, T., Kodama, Y. and Takamatsu, Y. (1977b), 'Noise Generated by Low Pressure Axial Flow Fans II – Effects of Number of Blades, Chord Length and Camber of Blade', *Journal of Sound and Vibration*, vol. 50, pp. 75–88.

Ganz, U.W., Joppa, P.D. and Scharpf, D.F. (1998), *Boeing 18-inch Fan Rig Broadband Noise Test*, Report NASA CR-1998-208704.

George, A.R. and Kim, Y.N. (1977), 'High-frequency Broadband Rotor Noise', *AIAA Journal*, vol. 15(4), pp. 538–545.

Grilliat, J. and Jacob, M.C. (2007), 'Tip Leakage Experiment – Part One: Aerodynamic and Acoustic Measurements', *Proceedings of the 13th AIAA/CEAS Aeroacoustic Conference (28th AIAA Aeroacoustics Conference)*, Rome, Italy, 21–23 May, paper no. AIAA 2007-3684.

Guitton, A., Jordan, P., Laurendeau, E. and Delville, J. (2007), 'Velocity Dependence of the Near Pressure Field of Subsonic Jets: Understanding the Associated Source Mechanisms', *Proceedings of the 13th AIAA/CEAS Aeroacoustic Conference (28th AIAA Aeroacoustics Conference)*, Rome, Italy, 21–23 May, paper no. AIAA 2007-3661.

Holste, F. and Neise, W. (1997), 'Noise Source Identification in a Prop Fan Model by Means of Acoustical Near Field Measurements', *Journal of Sound and Vibration*, vol. 203, pp. 641–665.

Jacob, M.C., Boudet, J., Casalino, D. and Michard, M. (2005), 'A Rod-airfoil Experiment as Benchmark for Broadband Noise Modelling', *Theoretical and Computational Fluid Dynamics*, vol. 19, pp. 171–196.

Kandula, M. and Vu, B. (2003), 'On the Scaling Laws for Jet Noise in Subsonic and Supersonic Flow', *Proceedings of the 9th AIAA/CEAS Aeroacoustics Conference and Exhibition*, Hilton Head, SC, USA, 12–14 May, paper no. AIAA 2003-3288.

Kendall, J.M. (1978), 'Measurements of Noise Produced by Flow Past Lifting Surfaces', *Proceedings of the 16th AIAA Aerospace Meeting*, Huntsville, AL, 16–18 January, paper no. 78-239.

Khourrami, M.R. and Choudari, M. (2001), 'A Novel Approach for Reducing Rotor Tip-clearance Induced Noise in Turbofan Engines', *Proceedings of the 7th AIAA/CEAS Aeroacoustics Conference*, Maastricht, The Netherlands, 28–30 May, paper no. AIAA 2001-2148.

Laurendeau, E., Jordan, P., Delville, J. and Bonnet, J. (2007), 'Nearfield-farfield Correlations in Subsonic Jets: What Can They Tell Us?', *Proceedings of the 13th AIAA/CEAS Aeroacoustics Conference*, Rome, Italy, 21–23 May, paper no. 2007-3614.

Laurendeau, E., Jordan, P., Delville, J. and Bonnet, J.-P. (2008), 'Source Mechanism Identification by Near Field-far Field Pressure Correlations in Subsonic Jets', *International Journal of Aeroacoustics*, vol. 7, pp. 41–68.

Leggat, L.J. and Siddon, T.E. (1978), 'Experimental Study of Aeroacoustic Mechanism of Rotor-vortex Interactions', *Journal of the Acoustical Society of America*, vol. 64, pp. 1070–1077.

Lighthill, M.J. (1954), 'On Sound Generated Aerodynamically. II: Turbulence as a Source of Sound', *Proceedings of the Royal Society A*, vol. 222, pp. 1–32.

Lowson, M.V. (1972), 'Some Experiments on Fan Noise and their Implication', *Journal of the Acoustical Society of America*, vol. 52(1A), p. 165.

Magliozzi, B., Johnson, B.V., Hanson, D.B. and Metzger, F.B. (1973) 'Noise and Wake Structure Measurements in a Subsonic Tip Speed Fan – Tabulation and Plots of Test Data', NASA Technical Report CR-132259, 23 July.

Magliozzi, B., Hanson, D.B. and Amiet, R.K. (1991), 'Propeller and Propfan Noise', in *Aeroacoustics of Flight Vehicles: Theory and Practice. Volume 1: Noise Sources*, NASA Langley Research Center, Cleveland, OH, USA, vol. 1, pp. 1–64.

Marcinowski, H. (1953), 'Einfluss des Laufradspalts und der Luftfuehrung bei einem Kuehlgeblaese axialer Bauart', *Motortechnische Zeitschrift*, vol. 14, pp. 259–262.

Miles, J.H. (2006), 'Procedure for Separating Noise Sources in Measurements of Turbofan Engine Core Noise', *Proceedings of the 12th AIAA/CEAS Aeroacoustics Conference (27th AIAA Aeroacoustics Conference)*, Cambridge, MA, USA, 8–10 May, paper no. AIAA 2006-2580.

Miles, J.H. (2010), 'Core Noise Diagnostics of Turbofan Engine Noise Using Correlation and Coherence Functions', *Journal of Propulsion and Power*, vol. 26(2), pp. 303–316.

Mongeau, L., Thompson, D.E. and McLaughlin, D.K. (1995), 'A Method for Characterizing Aerodynamic Sound Sources in Turbomachines', *Journal of Sound and Vibration*, vol. 181, pp. 369–389.

Narasimha, R., Narayan, K.Y. and Parthassarathi, S.P. (1973), 'Parametric Analysis of Turbulent Wall Jets in Still Air', *Aeronautical Journal,* vol. 77, pp. 355–359.

Ribner, H.S. (1964), 'The Generation of Sound by Turbulent Jets', *Advances in Applied Mechanics*, vol. 8, pp. 103–182.

Roger, M. and Moreau, S. (2004), 'Broadband Self-noise from Loaded Fan Blades', *AIAA Journal*, vol. 42(3), pp. 536–544.

Tinney, C.E. and Jordan, P. (2008), 'The Near Pressure Field of Co-axial Subsonic Jets', *Journal of Fluid Mechanics*, vol. 611, pp. 175–204.

Wang, M., Moreau, S., Iaccarino, G. and Roger, M. (2009), 'LES Prediction of Wall-pressure Fluctuations and Noise of a Low-speed Airfoil', *Aeroacoustics*, vol. 8(3), pp. 177–198.

Winkler, J., Temel, F.Z. and Carolus, T. (2007), 'Concepts, Design and Characterization of a Small Aeroacoustic Wind Tunnel Facility with Application to Fan Blade Measurements', *Proceedings of the 3rd International Symposium of Fan Noise*, Lyon, France, 17–19 September.

Chapter 7

Tip End-plate Concept Based on Leakage Vortex Rotation Number Control

A. Corsini and A.G. Sheard

ABSTRACT

The chapter presents a computational analysis of a fan's blade-to-blade flow-field which we developed for application in compact cooling units. The computational analysis provides insight into the studied fan's flow-field with and without fitted blade-tip end-plates. We predicted the blade-to-blade flow-field for a *datum* fan AC90/6 without blade-tip end-plates, and the fan AC/90/6/TF incorporated a constant thickness end-plate. Following a computational analysis of both, we developed an end-plate design methodology. We applied the constant thickness end-plate in an early attempt to reduce fan noise, with experimental measurements of fan far-field noise confirming that the end-plate was effective. The computational analysis indicated that at the fan design operating point the presence of the constant thickness blade-tip end-plate reduced the blade tip-to-casing leakage flow and therefore the intensity of the associated leakage vortex. We concluded that the decreased intensity was responsible for the reduced fan far-field noise. However, reduced leakage vortex intensity also resulted in it bursting, a flow-field feature known to be acoustically productive. We developed a design methodology that enhanced vortex swirl using a variable thickness blade-tip end-plate that prevented vortex bursting. When we incorporated the variable thickness blade-tip end-plate into the fan *datum* AC90/6, we named the resultant fan AC90/6/TF$_{VTE}$. We undertook the computational analysis using a Reynolds-Averaged Navier–Stokes (RANS) simulation with non-linear k-ε turbulence model in low-Reynolds number formulation. Although well proven, the simulation was not able to model unsteady effects and therefore models only part of the flow-field physics. The blade-tip end-plate design methodology utilises the computational analysis to establish blade tip leakage vortex swirl level and then varies end-plate geometry to enhance swirl level. Thus, the design methodology ensures that the blade tip-to-casing leakage vortex does not burst, therefore minimising its acoustic emissions.

This chapter is a revised and extended version of Corsini, A. and Sheard, A.G. (2007), 'Tip End-plate Concept Based on Leakage Vortex Rotation Number Control', *Journal of Computational and Applied Mechanics*, vol. 8, pp. 21–37.

NOMENCLATURE

Latin letters

B	tip-gap pressure drop
D	near-design condition
D_h	hub diameter
D_c	casing diameter
f_f	friction factor
H_n	normalised helicity
ℓ	blade chord
N_c	normal to the chord
Δp_{stat}	static pressure [Pa]
P	near-peak pressure condition
p_t	total pressure
Ro	Rossby number
Re_{gap}	leakage-flow Reynolds number
r_v	radial distance from the vortex axis
V_a	axial velocity at rv
s_c	chord-wise position
SDP	symmetrised dot pattern
Sf	normalised frequency (f/1BPF)
SWL	sound power level
t	blade pitch
t_{ep}	end-plate thickness distribution
TLV	tip leakage vortex
v, w	absolute and relative velocities
w_{Ln}	leakage-flow bulk velocity

Greek letters

β_{LV}	leakage vortex angle to the blade chord
ζ	total loss coefficient
η	efficiency
σ_h	hub-to-casing diameter ratio
ν_t	turbulent viscosity
ξ_i	absolute vorticity vector
Φ	global flow coefficient
τ	rotor tip clearance
Ω	rotation rate in the wing-tip vortices
τ_{gap}	gap height
ρ	air density

Subscripts and superscripts

a, p, r	axial, peripheral and radial
c	casing wall
h	hub wall
i	Cartesian component index
in	inlet section
mol	molecular quantity
s	streamwise component
$\bar{}$	pitch-averaged value
0	total quantities

INTRODUCTION

Non-linear interaction of flow-field features characterise the blade-to-blade flow-field in a fan or compressor's blade-tip region. The blade tip-to-casing leakage vortex interacts with both casing boundary layers and blade-to-blade passage secondary flow features. The resulting flow-field determines the fan or compressor's operating margin, as both are classically tip limited as a consequence of blade span-wise loading and loss distribution. In addition to defining fan or compressor operating margin, flow-field features collectively contribute to a fan or compressor's acoustic signature (Fukano and Takamatsu, 1986; Storer and Cumpsty, 1991; Furukawa *et al.*, 1999).

Ganz *et al.* (1998) studied the mechanisms that govern the flow-field physics in the blade tip region, concluding that they apply both to compressors developed for aerospace application and fans developed for air movement application. The reduction in performance that occurs with the presence of the associated flow-field features has resulted in both aerospace compressor and air movement fan designers seeking techniques to minimise the adverse effects on operating margin that occurs with blade tip-to-casing leakage flow. Their objective is to manage the blade tip-to-casing clearance flow with the desired outcome of reduced self-generated noise without sacrificing either operating margin or efficiency. Designers can achieve this objective either by reducing blade tip-to-casing leakage flow rate or by enhancing primary- to secondary-flow momentum transfer.

In an attempt to improve compressor performance, researchers first experimented with casing treatments in the early 1970s utilising grooves (Takata and Tsukuda, 1977; Smith and Cumpsty, 1984), and more recently stepped gaps in the blade tip region (Thompson *et al.*, 1998). These casing treatments improved the compressors' stable operating range by reducing blade tip leakage flow intensity. The air movement and control community has historically favoured using passive noise control techniques when attempting to minimise low-speed fan noise. The intent of these passive techniques is to influence positively dominant noise generation mechanisms. The air movement and control community have most widely adopted blade-tip appendages as their passive noise control technique. Researchers have

studied extensively fan blade-tip appendage design (Jensen, 1986; Quinlan and Bent, 1998; Longet, 2003; Mimura, 2003; Belady, 2004; Uselton *et al.*, 2008). They have advocated using blade-tip appendages as a technique for noise control in both fans and compressors.

This chapter presents a new design procedure for determining a blade-tip end-plate's optimum thickness distribution. This variable thickness blade-tip end-plate controls the tip-to-casing leakage vortex rotation number's chord-wise evolution. Control of leakage vortex rotation number is a passive control mechanism that enables a designer to avoid leakage vortex breakdown by controlling the swirling flow in the blade tip region. When controlling the swirling flows in an aircraft wing's tip region (Spall *et al.*, 1987) or in a combustor (Escudier, 1987), the proposed design procedure rationale advocates linking blade-tip end-plate geometry and the blade tip-to-casing leakage vortex near-axis swirl. This linkage facilitates leakage vortex control and thus, avoids it bursting (Jones *et al.*, 2001; Herrada and Shtern, 2003). One implements this noise-by-flow control design procedure by reconfiguring the blade-tip end-plate and thus influencing the momentum transfer from the leakage flow. The procedure also forces some waviness in the leakage vortex trajectory, as in delta-wing platforms (Srigrarom and Kurosaka, 2000).

FAMILY OF FANS UNDER INVESTIGATION

We conducted the reported research on a family of commercially available cooling fans. The studied fan configuration, coded AC90/6, incorporates a six-blade un-swept rotor, with modified ARA-D profile aerofoil blades, Table 7.1. One may set the blade-pitch angle during final assembly to customise the fan to a desired duty point. We used a direct coupled-induction 400-volt (AC), 3-phase motor to drive the rotor at a constant speed of 950 rpm, resulting in a 44.7 m/s blade tip speed and a 95

Table 7.1. *The fan* datum *AC90/6 blade geometry and rotor specification.*

	Fan *datum* AC90/6		
Blade geometry	Hub	Mid-span	Tip
Pitch angle (°)	36	58.8	28
Camber angle (°)	46	44	41
Solidity	1.24	0.86	0.30
Fan rotor			
Blade number		6	
Blade tip pitch angle (°)		16–28	
Blade tip stagger angle (°)		74–62	
Hub-to-casing diameter ratio σ		0.22	
Tip diameter (mm)		900.0	
Rotor tip clearance τ (% span)		1.0	
Rated rotational frequency (r/min)		935–950	

Hz blade-passing frequency (BPF). In its original embodiment the studied fan did not include a blade-tip end-plate, thus we used it as a *datum* against which to assess the performance of fan variants with blade-tip end-plates. Therefore, in the reported research we refer to the fan without blade-tip end-plates as the fan *datum* AC90/6.

In addition to the fan *datum* AC90/6, we studied a fan variant fitted with a constant thickness blade-tip end-plate, Figure 7.1, which we named AC90/6/TF. The designs developed for tip-vortex control and drag reduction in aircraft wings and catamaran hulls inspired the constant thickness blade-tip end-plate design, which ran along the blade pressure surface, ending at the blade trailing edge with a square tail. This addition resulted in the thickness of the fan AC90/6/TF blade tip increasing by a factor of three compared to the fan *datum* AC90/6. We considered the blade-tip end-plate size for axial compressor blades using Inoue *et al.*'s (1986) research. They estimated that the optimum blade-tip end-plate size was between 10 and 20 per cent blade span. In practice, we were able to manufacture blades with a blade-tip end-plate size five per cent of blade span. The fan blades were manufactured from injection moulded plastic, with the blade-tip end-plate size the largest the blade manufacturing technique could produce.

Flow Conditions

The studied fan blade tip pitch angle is adjustable and may be set to a pitch angle between 16 and 28 degrees. In practical application, the blade tip pitch angle is typically set to 28 degrees as this maximises flow rate for a given system pressure. In the research reported in this chapter, we conducted the computational analysis of fan performance and blade-to-blade flow-field with the fan blade tip pitch angle set to 28 degrees. We selected 28 degrees both because it is typical of the angle used in

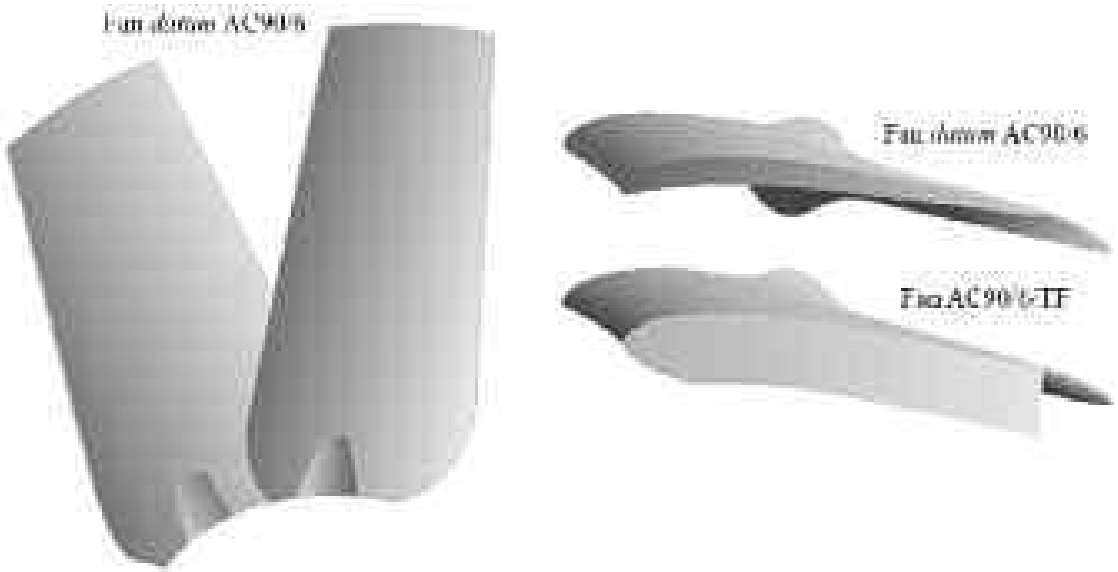

FIGURE 7.1. The studied fan *datum* AC90/6 without a fitted blade-tip end-plate and with a constant thickness blade-tip end-plate, AC90/6/TF.

practical application and because it results in the highest blade loading. A highly loaded blade results in the blade tip-to-casing vortex having the most significant effect on both fan aerodynamic and acoustic performance (Holste and Neise, 1997).

The impact of the blade tip-to-casing leakage vortex on both fan aerodynamic and acoustic performance results in the application of blade-tip end-plates changing not only the fan's acoustic performance, but also the aerodynamic performance. Consequently, the fan *datum* AC90/6 generates a different pressure at a constant flow rate when fitted with a blade-tip end-plate. To facilitate the comparison of fan performance data when fitted with different blade-tip end-plates we chose to define three operating points, and their respective volume flow rates, Table 7.2. The design operating point volume flow rate is typical of that required when one installs the fan over the cooling unit's tube bank. The peak pressure flow rate is typical of that required when the tube bank has become partially blocked following a period of in-service operation. The maximum flow operating point volume flow rate is typical of the flow rate that occurs with the lowest pressure loss tube banks currently operating in service.

Leakage-vortex Breakdown Detection

Corsini *et al.* (2006) studied the fan *datum* AC90/6 and fan AC90/6/TF and have empirically established the aerodynamic and acoustic performance of both. Assessing acoustic performance at both the design and peak pressure operating points indicated that the constant thickness blade-tip end-plate resulted in a three to four dB reduction in far-field noise, Table 7.3. Corsini *et al.* (2006) concluded that the constant thickness blade-tip end-plate fitted to the fan AC90/6/TF was effective at reducing the blade tip-to-casing flow rate over the fan's operating range. A consequence of this reduction was a diminution of three-dimensional flow-field features through the blade-to-blade passage, reducing fan AC90/6/TF far-field noise.

Despite the success of the constant thickness blade-tip end-plate in reducing fan far-field noise, Corsini *et al.* (2006) identified that the blade tip-to-casing leakage vortex burst. Vortex bursting is known to be acoustically productive, so the fan AC90/6/TF's far-field noise could be lower by avoiding vortex bursting.

Table 7.2. *The operating points used when characterising the studied fan's performance with and without fitted blade-tip end-plates. The authors measured performance characteristics in a Type D standardised airway (ducted inlet, ducted outlet) in accordance with ISO 5801:2007 requirements (2007).*

Operating point	Volume flow rate (m^3/s)	Studied blade tip pitch angle (°)
Maximum flow	7.0	28
Design	6.5	28
Peak pressure	5.6	28

Table 7.3. *Experimentally measured fan aerodynamic and acoustic performance for the fan* datum *AC90/6 and AC90/6/TF at both the design and peak pressure operating points (Corsini* et al.*, 2006).*

Operating point	*datum* AC90/6		AC90/6/TF	
	Δp_{stat} (Pa)	η (%)	Δp_{stat} (Pa)	η (%)
Design	134.8	49.0	126.2	51.0
Peak pressure	184.4	44.0	179.4	49.0
	unweighted SWL (dB)	A-weighted SWL (dB(A))	unweighted SWL (dB)	A-weighted SWL (dB(A))
Design	72.4	70.8	70.2	66.9
Peak pressure	72.7	71.8	69.7	67.4

Numerical Procedure and Vortex Breakdown

In this chapter we report the results of a computational analysis using a Reynolds-Averaged Navier–Stokes (RANS) simulation. We used the same numerical procedure as Borello *et al*. (2003), and therefore will describe the modelling procedure only briefly here. We modelled the fan incompressible three-dimensional turbulent flow-field in a rotating frame of reference with a non-linear k-ε turbulence model. We utilised a topology-free low-Reynolds variant of the chosen turbulence model (Craft *et al*., 1996). Corsini and Rispoli (2004) previously validated this modelling approach in both transonic compressor cascade flows and high-pressure air movement fan rotors.

Using the above numerical procedure, we predicted the fan AC90/6/TF blade-to-blade flow-field, focusing on the flow-field through the blade tip-to-casing gap. We may visualise vortex bursting via a study of three-dimensional streamlines through the blade tip-to-casing gap, Figure 7.2. The streamlines illustrate development of the leakage vortex, and specifically the chord-wise position at which vortex breakdown commences. The streamlines indicate that the blade-tip end-plate obstructs blade pressure-surface flow migrations through the blade tip-to-casing gap. This obstruction results in a *vena contracta* effect that results in the blade-tip end-plate inducing an anti-vortex effect in blade tip-to-casing clearance flow. The fan AC90/6/TF leakage vortex streamlines illustrate that the reduced blade tip-to-casing gap leakage flow rate influences the swirl-to-axial velocity ratio, Figure 7.2. At approximately mid-blade chord, this change in swirl-to-axial velocity ratio results in a bubble type unseparated vortex core developing. As this unseparated vortex core moves towards the blade trailing edge, it goes on to separate from the blade surface.

Development followed by separation is indicative of blade tip-to-casing leakage vortex breakdown (Lucca-Negro and O'Doherty, 2001). According to Leibovich (1978), we may conceptualise a bursting vortex as a bubble type vortex core as a consequence of the vortex swirl level. According to both Escudier and Zehnder

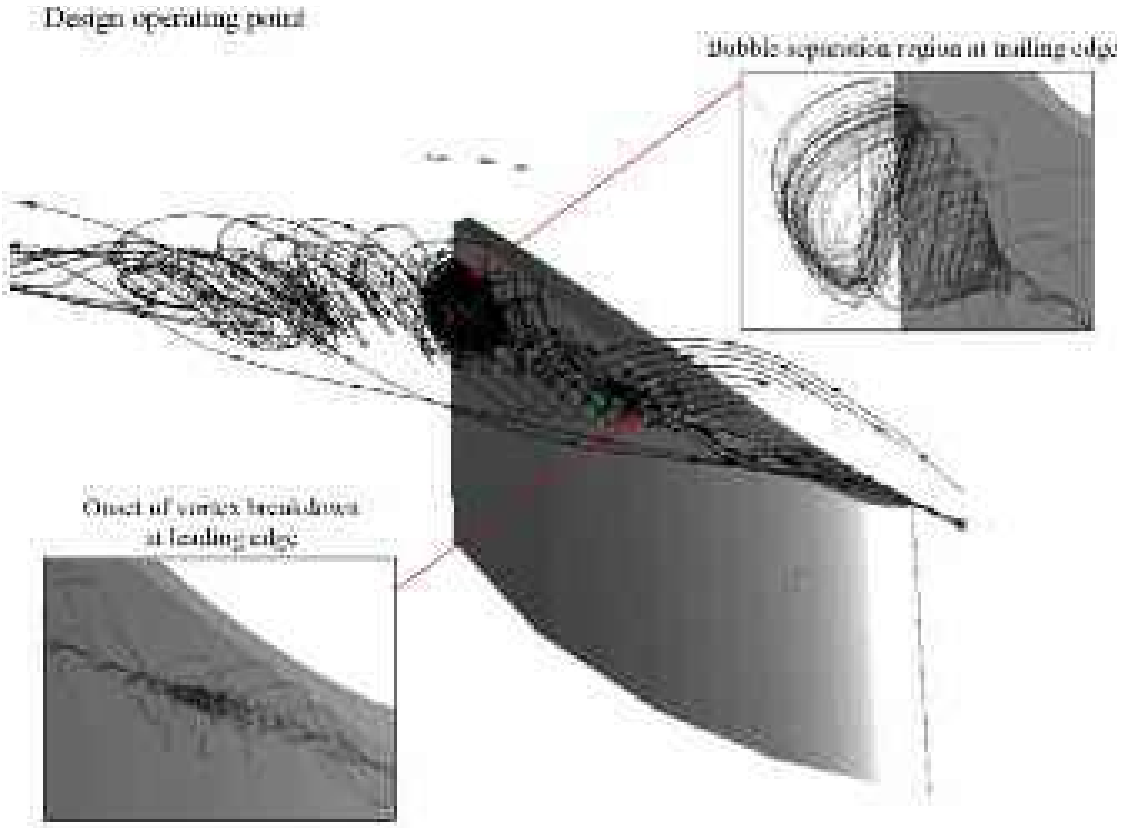

FIGURE 7.2. A three-dimensional presentation of numerically predicted streamlines through the fan AC90/6/TF blade tip-to-casing gap at the design operating point illustrating development of the leakage vortex.

(1982) and Inoue and Furukawa (2002), we may associate the stability of the bubble form of vortex breakdown with the vortex swirl level. A lower swirl level is associated with a lower stability. This assertion supports our interpretation of the bubble separation core as evidence of blade tip-to-casing leakage vortex breakdown. If we accept this interpretation, we may characterise the mid-chord bubble-core as the onset of the bursting phenomena.

We may test our assertion that the mid-chord bubble-core constitutes the onset of the bursting phenomena by considering blade tip-to-casing leakage flow axial velocity. A review of numerically predicted streamlines through the fan AC90/6/TF blade tip-to-casing gap, in combination with iso-surfaces of leakage vortex zero axial velocity, facilitate a study of leakage flow axial velocity, Figure 7.3. There is a small zero axial velocity iso-surface at approximately mid-blade chord that is coincident with the unseparated vortex core. We may associate this zero axial velocity iso-surface with the onset of vortex breakdown, a conclusion self-consistent with Spall *et al.*'s (1987) conclusions. It was Spall *et al.* (1987) who first identified the presence of a stagnation point along a vortex axis as a necessary pre-condition for breakdown. Towards the blade trailing edge there is a larger zero axial velocity iso-surface which characterises the region over which the blade tip-to-casing leakage vortex is actually breaking down.

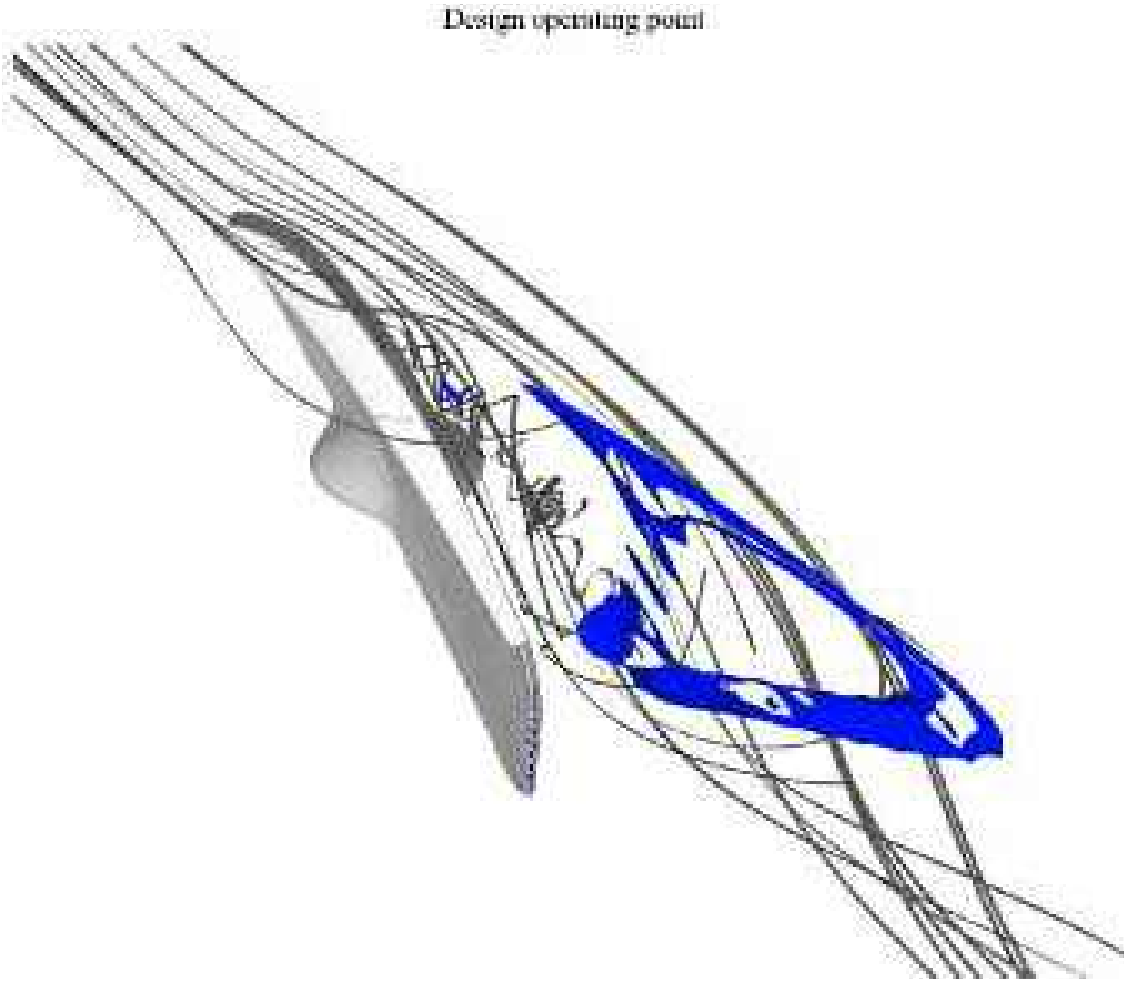

FIGURE 7.3. A three-dimensional presentation of numerically predicted streamlines through the fan AC90/6/TF blade tip-to-casing gap at the design operating point with iso-surfaces of leakage vortex zero axial velocity coloured blue.

VORTEX BREAKDOWN ROSSBY NUMBER ANALYSIS

Scholars have studied vortex breakdown, linear stability, phase velocity and wave tapping (Benjamin, 1962; Leibovich, 1978; Tsai and Widnall, 1980). Their focus has been on identifying a critical condition that occurs with the on-set of vortex breakdown by using vortex swirl based parameters. Leibovich (1978) studied vortex breakdown, conceptualising it as a change in vortex structure initiated by a variation in the ratio of tangential to axial velocity components. Ito *et al.* (1985) conducted a theoretical study of unsteady and steady vortex breakdown and characterised vortex breakdown using the Rossby number. We define the Rossby number as:

$$Ro = V_a / (r_v \Omega) \tag{1}$$

in which:

V_a = velocity;
r_v = length, and
Ω = rotation rate.

Spall *et al.* (1987) extended Ito *et al.*'s (1985) work by developing a vortex breakdown criterion based on the Rossby number. Spall *et al.* (1987) proposed scale definitions for the velocity distribution consistent with swirling flows, leading-edge vortices and unconfined trailing wing-tip vortices. In the research reported in this chapter, we adopted Spall *et al.*'s (1987) approach for application to the blade tip-to-casing leakage vortex typical of fans and compressors. We chose to define Spall *et al.*'s (1987) parameters as:

- r_v is the radial distance from the vortex axis at which the swirl velocity is a maximum, corresponding to Leibovich's (1984) characteristic viscous length scale;
- V_a (= w_{aTLV}) is the axial velocity at r_v, and
- Ω is the rotation rate of the blade tip-to-casing leakage vortices that is driven by the vortex's assumed solid-body rotation at the vortex centre.

The choice of axial velocity at the radial distance from the vortex axis at which the swirl velocity is a maximum is consistent with the swirl scale Ωr_v (= w_{pTLV}) and the critical Rossby number values reported in the extant literature. Uchida *et al.* (1985) defined a critical Rossby number of 0.64 for confined axi-symmetric vortex breakdown. Garg and Leibovich (1979) defined a critical Rossby number of 0.60 for a wing-tip vortex with bubble- or spiral-type vortex breakdown.

We calculated the chord-wise distribution of the blade tip-to-casing leakage vortex Rossby number for the fan *datum* AC90/6 and AC90/6/TF, Figure 7.4. When operating at its design operating point, the fan AC90/6/TF Rossby number falls to a critical value at 50 per cent blade chord. It then goes on to recover, finally falling below the critical value at a 75 per cent blade chord. When operating at the peak pressure operating point, the fan AC90/6/TF Rossby number remains above the critical value, and therefore avoids vortex bursting. In contrast, the fan *datum* AC90/6 Rossby number remains above the critical value at the design operating point, but falls below at 70 per cent blade chord at the peak pressure operating point.

The chord-wise locations of critical Rossby number for the fan AC90/6/TF were self-consistent with the previously identified locations of vortex zero axial velocity, Figure 7.3. The locations of vortex zero axial velocity at 50 per cent matches the point at which the Rossby number falls to a critical value, and then recovers, Figure 7.4. The larger zero axial velocity iso-surface towards the trailing edge characterises the region over which the blade tip-to-casing leakage vortex actually breaks down. This region matches the 75 per cent chord-wise point at which the Rossby number falls below a critical value.

The agreement between the locations of vortex zero axial velocity and the critical Rossby number indicates that the Rossby number is a useful parameter. Therefore, we may base the blade-tip end-plate geometry modification on control of the blade tip-to-casing leakage vortex Rossby number. Changes to the blade-tip end-plate

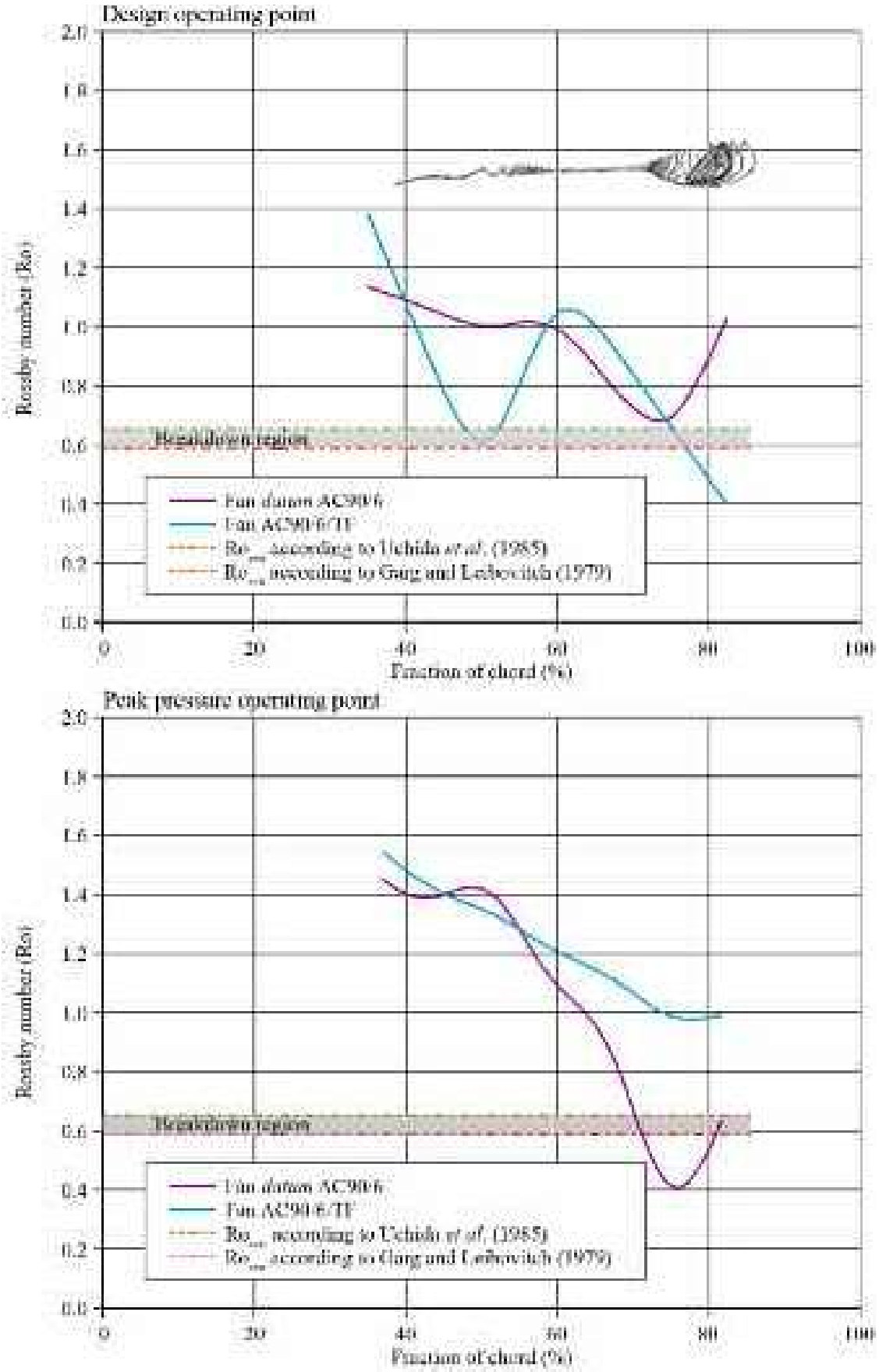

FIGURE 7.4. Chord-wise evolution of numerically predicted blade tip-to-casing leakage vortex Rossby number (*Ro*) at the fan design and peak pressure operating point for the fan *datum* AC90/6 and AC90/6/TF.

geometry result in enhancing or reducing the vortex near-axis swirl that in turn increase or reduce the Rossby number. Therefore, changing blade-tip end-plate geometry to maintain the Rossby number above a critical value provides a basis upon which to optimise end-plate geometry to avoid vortex bursting.

NEW BLADE-TIP END-PLATE DESIGN

The purpose of developing a new blade-tip end-plate design is to avoid blade tip-to-casing leakage vortex bursting. Vortex bursting is known to be acoustically productive, and therefore if the blade tip-to-casing leakage vortex does not burst, fan far-field noise should reduce. The new blade-tip end-plate design procedure varied only one parameter, blade-tip end-plate thickness along the blade chord. By varying blade-tip end-plate thickness along the blade chord, our objective was to maintain the blade tip-to-casing Rossby number above its critical value, thus avoiding vortex bursting.

Our rationale for varying blade-tip end-plate thickness along the blade chord was that reducing end-plate thickness would enhance near-axis swirl (Jones *et al.*, 2001; Herrada and Shtern, 2003) by influencing momentum transfer from the leakage flow and forcing some waviness into the leakage-vortex trajectory (Srigrarom and Kurosaka, 2000). Therefore, our design procedure required us to calculate the blade-tip end-plate thickness distribution, $t_{ep}(s_c)$. We calculated thickness distribution by combining a simplified expression for the blade tip-to-casing gap pressure drop and a stability criterion for the blade tip-to-casing leakage vortex (TLV). We defined the stability criterion as a safe chord-wise distribution of the Rossby number.

We modelled the pressure losses within the tip gap at each chord-wise position (s_c) by modelling the blade tip-to-casing leakage flow as a two dimensional flow orthogonal to the chord line, Figure 7.5. We expressed the pressure drop as a function of:

- the blade tip-to-casing gap height (τ_{gap}) and width (τ);
- the kinetic energy of the leakage flow, as given by the leakage velocity component normal to the chord $(w_{Ln})^2$;
- the friction factor (f_f) which is itself a function of leakage-flow Reynolds number, $Re_{gap} = f(\tau_{gap}, w_{Ln})$ velocity scale; and
- the end-plate thickness $t_{ep}(s_c)$.

We chose to manage the dependence of the friction factor (f_f) on the chord-wise position (s_c) by scaling the value for the leakage-flow bulk velocity (w_{Ln}). This enabled us to define the pressure drop through the blade tip-to-casing gap at each chord-wise position (s_c) as:

$$dp(s_c) = \frac{f_f(Re_{gap})}{2\tau_{gap}} t_{ep}(s_c) w_{Ln}^2(s_c) \tag{2}$$

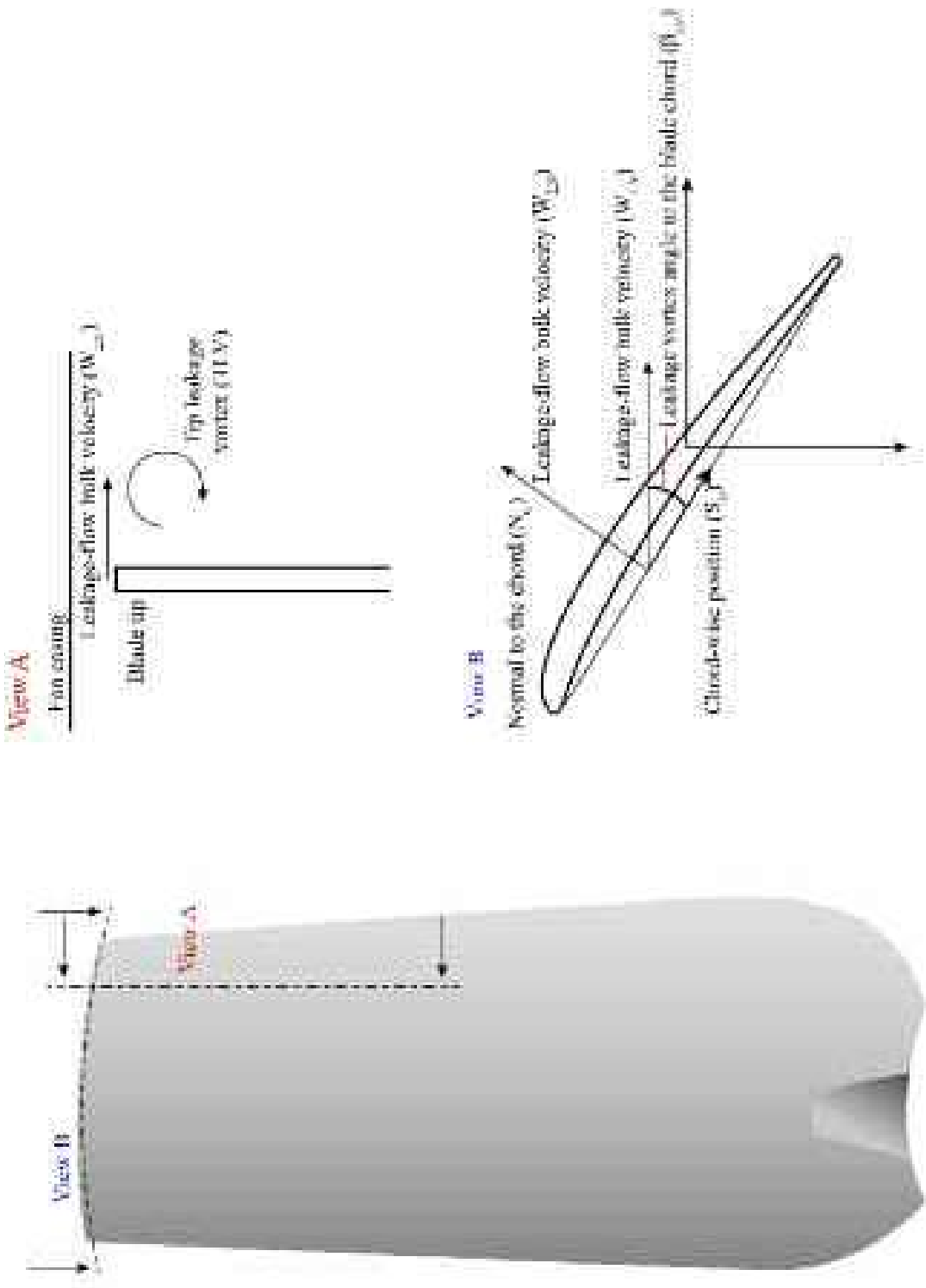

FIGURE 7.5. Definition of the coordinate system used to model the blade-tip end-plate geometry and its effect on momentum transfer to the blade tip-to-casing leakage vortex.

We then used Equation 2 to derive an expression for the chord-wise chord gradient of blade tip-to casing gap pressure loss:

$$\frac{dp}{ds_c} = \rho \frac{f_f(Re_{gap})}{2\tau_{gap}} \frac{d\,[t_{ep}(s_c) w_{Ln}^2(s_c)]}{ds_c} \tag{3}$$

By rearranging Equation 3, we were able to formulate a correlation between the blade-tip end-plate thickness and the blade tip-to-casing leakage flow:

$$A_w \frac{dt_{ep}(s_c)}{ds_c} + A_{Ro} t_{ep}(s_c) = B \tag{4}$$

in which:

B is the blade tip-to-casing gap pressure drop, and
A_w is a function of the definition of a velocity scale for the leakage flow.

The coefficient A_{Ro} is made proportional to the chord-wise gradient of blade tip-to-casing leakage-flow velocity normal to the blade chord (w_{Ln}) as follows:

$$A_{Ro} \propto \frac{dw_{Ln}(s_c)}{ds_c} \tag{5}$$

Using the chord-wise gradient of blade tip-to-casing leakage flow bulk velocity, $w_{Ln}(s_c)$, we may now define an explicit dependency on the chord-wise gradient of the Rossby number. We then use this dependency in our correlation between the thickness of the blade-tip end-plate and the blade tip-to-casing leakage flow, allowing us to express the Rossby number chord-wise gradient as:

$$\frac{dRo}{ds_c} = \left.\frac{dRo}{ds_c}\right|_{TLVstable} = \frac{1}{r_v \Omega} \frac{dw_L(s_c)}{ds_c} \tag{6.1}$$

in which the blade tip-to-casing leakage flow velocity ($w_L(s_c)$) approximates the axial velocity of the leakage vortex (w_{aTLV}) at its periphery.

Assuming a uniform direction of the blade tip-to-casing leakage flow along the blade tip chord, we can rearrange Equation 6.1 to express the blade tip-to-casing leakage flow velocity normal to the chord, $w_{Ln}(s_c)$ as follows:

$$\frac{1}{r_v \Omega} \frac{dw_L(s_c)}{ds_c} \cong \frac{1}{r_v \Omega} \frac{1}{sen(\beta_L)} \frac{dw_{Ln}(s_c)}{ds_c} \tag{6.2}$$

It is then possible to establish the blade-tip end-plate thickness distribution according to any stable Rossby number gradient value as:

$$\left.\frac{dRo}{ds_c}\right|_{TLVstable} = \frac{1}{r_v \Omega} \frac{dw_L(s_c)}{ds_c} \propto \frac{1}{r_v \Omega} \frac{1}{sen(\beta_L)} A_{Ro} \tag{6.3}$$

We conducted a parametric analysis of blade-tip end-plate thickness distribution by solving Equation 4, Figure 7.6. We conducted the parametric analysis in two ways. First, we assumed a constant blade tip-to-casing gap pressure drop gradient (B) whilst varying the Rossby number gradient (A_{Ro}). Second, we assumed a constant Rossby number gradient (A_{Ro}) and varied the blade tip-to-casing gap pressure drop gradient (B). We used the new blade-tip end-plate design procedure to define the thickness distribution of a new variable thickness blade-tip end-plate. When fitted to the fan *datum* AC90/6, we named the resultant fan AC90/6/TF$_{VTE}$, Figure 7.7.

EXPERIMENTAL ASSESSMENT OF BLADE-TIP END-PLATE PERFORMANCE

Bianchi *et al*. (2009) measured the performance characteristics of the fan *datum* AC90/6, AC90/6/TF and AC90/6/TF$_{VTE}$ in accordance with ISO 5801: 2007 requirements (2007). The studied fans' performance characteristics illustrate the impact on pressure rise of blade-tip end-plate geometry, Figure 7.8. The impact of constant and variable thickness blade-tip end-plates on both static pressure and efficiency is small, but significant. The fan AC90/6/TF static pressure is approximately two per cent lower than the fan *datum* AC90/6 at the design operating point, Table 7.2. We may conclude that this reduction occurs as a consequence of interaction between the blade tip-to-casing clearance flow and the blade suction surface near-surface boundary layer fluid (Gbadebo *et al*., 2006). The fan AC90/6/TF$_{VTE}$ exhibits performance closer to that of the fan *datum* AC90/6, with increasing pressure rise as it is throttled from its maximum flow to peak pressure operating point.

The efficiency of the three studied fans is significantly different over the fan's operating range. At their maximum flow operating point all three fans have a similar efficiency. As they are throttled towards their design operating point, both the constant and variable thickness blade-tip end-plates result in an increased efficiency compared to the fan *datum* AC90/6. Further, both end plates resulted in the peak efficiency point shifting from the maximum flow operating point to the design operating point. Therefore, we may conclude that both blade-tip end-plates have had a positive effect on efficiency. In combination, they both increase efficiency and shift peak efficiency towards the design operating point.

A way to validate the quality of a computational analysis of the blade-to-blade flow-field is to predict the overall performance of the studied fan. We may reasonably assume that if we are able to predict overall fan performance accurately, we may also accurately predict flow-field features in the blade-to-blade passage. Therefore, we used our computational analysis to predict performance of the three studied fans, Table 7.4. The predicted static pressure and efficiency for the three studied fans was within the uncertainty of the measured performance. Thus, we concluded that our initial assumption was valid. We could use the computational analysis as input to our new design procedure for determining the blade-tip end-plates' optimum thickness distribution.

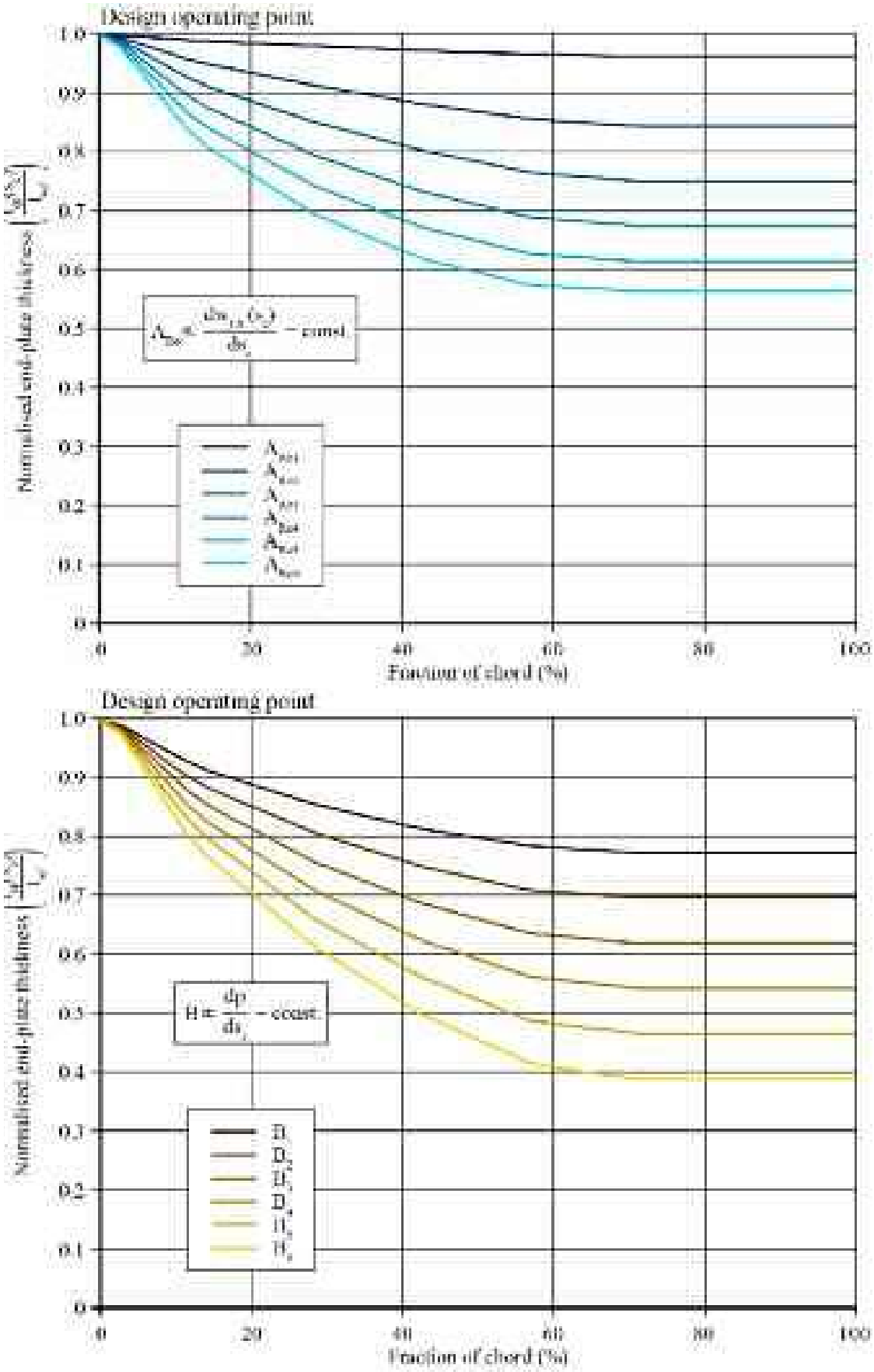

FIGURE 7.6. Parametric analysis of blade-tip end-plate thickness distribution for: top, increasing Rossby number gradient (A_{Ro}) and; bottom, increasing gap pressure-drop gradient (B).

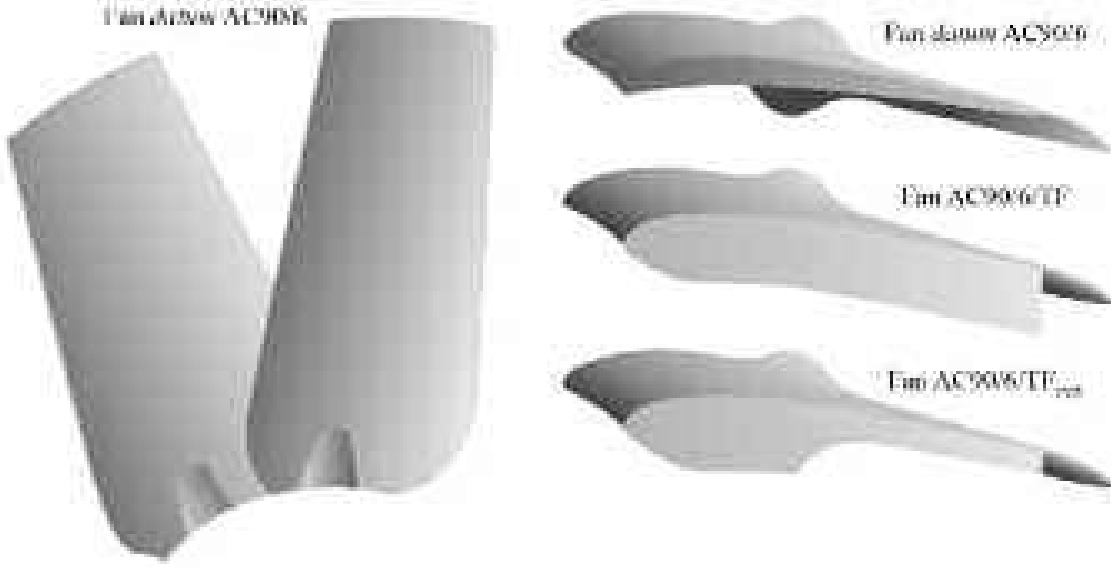

FIGURE 7.7. The studied fan *datum* AC90/6 without a fitted blade-tip end-plate, with a constant thickness blade-tip end-plate, AC90/6/TF and with a variable thickness blade-tip end-plate, AC/6/TF$_{VTE}$.

Table 7.4. *Experimentally measured (Bianchi* et al.*, 2009) and predicted fan aerodynamic performance for the fan* datum *AC90/6, AC90/6/TF and AC90/TF*$_{\mathrm{VTE}}$ *at the design operating point.*

	Measurements		Predictions	
	Δp_{stat} (Pa)	η (%)	Δp_{stat} (Pa)	η (%)
datum AC90/6	134.8	49.0	133.3	51.0
AC90/6/TF	126.2	51.0	126.1	50.4
AC90/6/TF$_{VTE}$	129.0	52.0	128.2	51.6

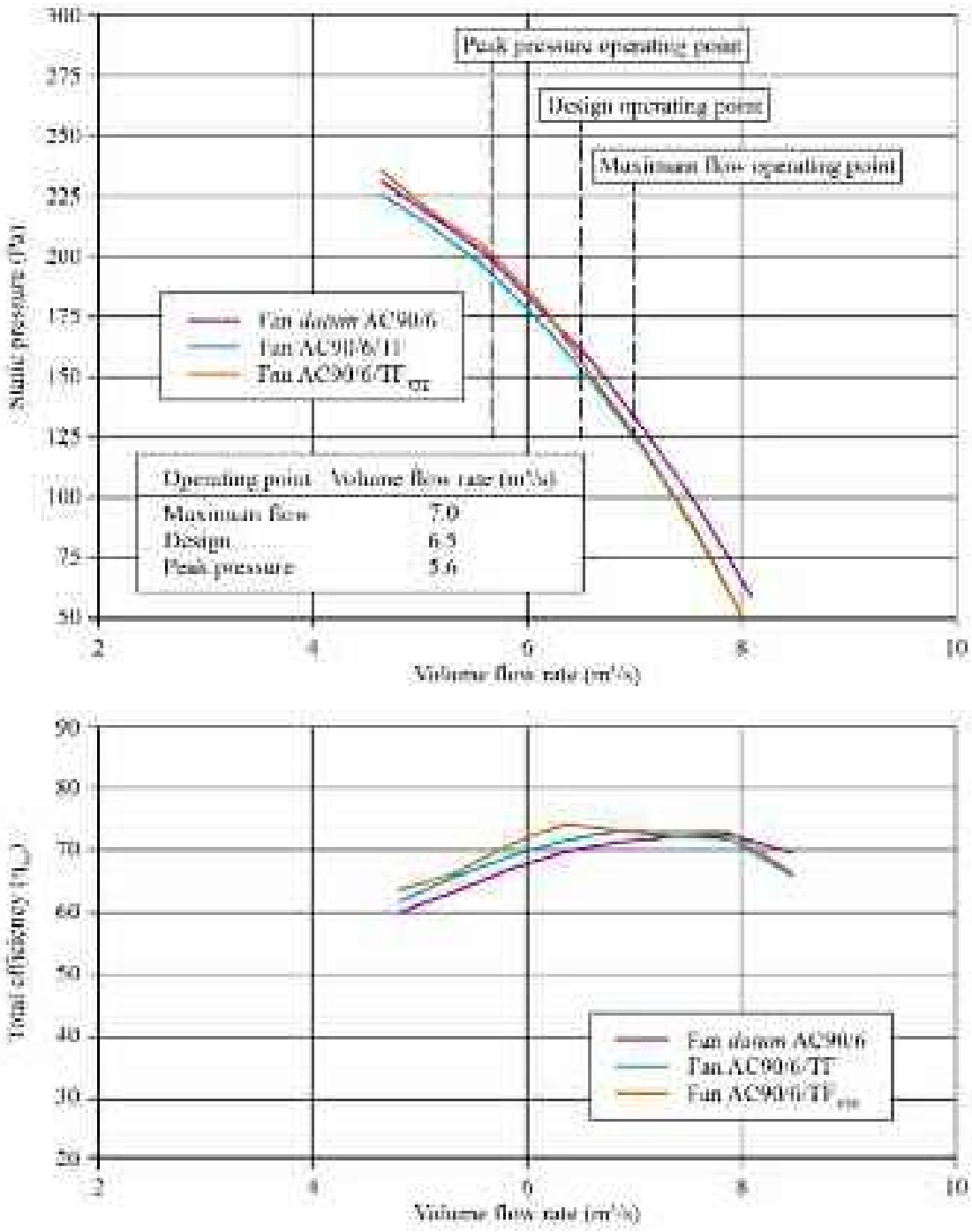

FIGURE 7.8. The performance characteristics of the studied fan *datum* AC90/6 without a fitted blade-tip end-plate, with a constant thickness blade-tip end-plate, AC90/6/TF and with a variable thickness blade-tip end-plate, AC/6/TF$_{VTE}$. Bianchi *et al*. (2009) measured the performance characteristics with the blade tip pitch angle set to 28 degrees in a Type D standardised airway (ducted inlet, ducted outlet) in accordance with ISO 5801:2007 requirements (2007).

CONCLUSIONS

In this chapter we presented an initial computational analysis of the blade-to-blade flow-field for the studied fan both without a blade-tip end-plate, coded fan *datum* AC90/6, and with a constant thickness blade-tip end-plate, coded fan AC90/6/TF. We undertook the computational analysis using a Reynolds-Averaged Navier–Stokes (RANS) simulation with a non-linear k-ε turbulence model in low-Reynolds number formulation.

A limitation of RANS simulations is that they are not able to model unsteady effects and therefore model only part of the flow-field physics. We considered this acceptable in analysing the studied fan geometries because the RANS model was the subject of extensive application specific development. We adapted the eddy-viscosity closure model to maximise accuracy when predicting the blade-tip leakage vortex's roll up under a pressure gradient influence. Additionally, the RANS model utilised an anisotropy-resolving turbulence model with a numerical diffusivity scheme previously proven to model the dominant large-scale flow features' non-isotropy.

The experimental results reported in Chapters 2, 3, 4, 5 and 6 had established the importance of the blade-tip leakage vortex, and therefore the computational analysis focused on the flow-field in the blade-tip region. The computational analysis indicated that at the fan's design point, the presence of the constant thickness blade-tip end-plate reduced the over-tip blade leakage flow and therefore the blade-tip leakage vortex's intensity. We concluded that this reduction in intensity was responsible for reducing fan far-field noise. However, the reduction in intensity resulted in the blade-tip leakage vortex bursting. This is a flow-field feature that researchers know is acoustically productive.

We used computational analysis to characterise the chord-wise distribution of blade-tip leakage vortex Rossby number. The Rossby number quantifies vortex rotation. There is a threshold value of the Rossby number below which vortex rotation cannot reduce if the vortex is to remain stable. The computational analysis indicated that for the fan *datum* AC90/6 blade-tip leakage vortex, the Rossby number remained above the threshold value and did not burst. However, the fan AC/90/6/TF blade-tip leakage Rossby number fell below the threshold value at approximately 90 per cent chord and did burst.

A realisation that the blade-tip end-plate resulted in the fan AC90/6/TF blade-tip leakage vortex bursting was the insight we required to refine the blade-tip end-plate design. By reducing the blade-tip end-plate's chord-wise thickness towards the blade's trailing edge, the blade-tip leakage vortex's vorticity could increase. Increasing blade-tip leakage vortex vorticity would ensure its Rossby number remained above the threshold value needed to avoid vortex bursting. Avoiding vortex bursting would eliminate the acoustic emissions that occurred with it and therefore should reduce fan far-field noise.

Thus, the blade-tip end-plate design methodology utilises the computational analysis to establish blade-tip leakage vortex swirl level and then varies end-plate geometry to enhance swirl level. The design methodology produces a blade-tip end-

plate design that ensures the blade-tip leakage vortex does not burst, minimising acoustic emissions from the vortex. When the authors fitted the studied fan with the new variable thickness blade-tip end-plate, they coded it fan AC90/6/TF$_{VTE}$.

REFERENCES

ISO 5801:2007 (2007), *Industrial Fans: Performance Testing Using Standardised Airways.*

Belady, C.L. (2004), 'Winglet-Enhanced Fan', Patent No. US 6,776,578 B2, 17 August.

Benjamin, T.B. (1962), 'The Theory of Vortex Breakdown', *Journal of Fluid Mechanics*, vol. 14, pp. 583–629.

Bianchi, S., Sheard, A.G., Kinghorn, I.R., Corsini, A. and Rispoli, F. (2009), 'Experimental Development of a Measurement Technique to Resolve the Radial Distribution of Fan Aeroacoustic Emissions', *Noise Control Engineering Journal*, vol. 57, pp. 360–369.

Borello, D., Corsini, A. and Rispoli, F. (2003), 'A Finite Element Overlapping Scheme for Turbomachinery Flows on Parallel Platforms', *Computers and Fluids*, vol. 3, pp. 1017–1047.

Corsini, A. and Rispoli, F. (2004), 'Using Sweep to Extend Stall-free Operational Range in Sub-sonic Axial Fan Rotors', *Proceedings of the IMechE Part A, Journal of Power and Energy*, vol. 218, pp. 129–139.

Corsini, A., Rispoli, F., Sheard, A.G. and Kinghorn, I.R. (2006), 'Investigation of Improved Blade-tip Concept for Axial Flow Fan', *Proceedings of the 51st American Society of Mechanical Engineers Gas Turbine and Aeroengine Congress*, Barcelona, Spain, 8–11 May, paper no. GT2006-90592.

Craft, T.J., Launder, B.E. and Suga, K. (1996), 'Development and Application of a Cubic Eddy-viscosity Model of Turbulence', *International Journal of Heat and Fluid Flow*, vol. 17, pp. 108–155.

Escudier, M. (1987), 'Confined Vortices in Flow Machinery', *Annual Review of Fluid Mechanics*, vol. 19, pp. 27–52.

Escudier, M. and Zehnder, N. (1982), 'Vortex Flow Regimes', *Journal of Fluid Mechanics*, vol. 115, pp. 105–121.

Fukano, T. and Takamatsu, Y. (1986), 'The Effects of Tip Clearance on the Noise of Low-pressure Axial and Mixed Flow Fans', *Journal of Sound and Vibration*, vol. 105, pp. 291–308.

Furukawa, M., Inoue, M., Kuroumaru, M., Saiki, K. and Yamada, K. (1999), 'The Role of Tip Leakage Vortex Breakdown in Compressor Rotor Aerodynamics', *Transactions of the ASME, Journal of Turbomachinery*, vol. 121, pp. 469–480.

Ganz, U.W., Joppa, P.D. and Scharpf, D.F. (1998), *Boeing 18-inch Fan Rig Broadband Noise Test*, Report NASA CR-1998-208704.

Garg, A.K. and Leibovich, S. (1979), 'Spectral Characteristics of Vortex Breakdown Flowfields', *Physics of Fluids*, vol. 22(11), pp. 2053–2064.

Gbadebo, S.A., Cumpsty, N.A. and Hynes, T.P. (2006), 'Interaction of Tip Clearance Flow and Three-dimensional Separations in Axial Compressors', *Proceedings of the 51st American Society of Mechanical Engineers Gas Turbine and Aeroengine Congress*, Barcelona, Spain, 8–11 May, paper no. GT2006-90071.

Herrada, M.A. and Shtern, V. (2003), 'Vortex Breakdown Control by Adding Near-axis Swirl and Temperature Gradients', *Physical Review E, Non-Linear Sofy Matter Physics*, vol. 68(1), paper no. 041202, pp. 1–8.

Holste, F. and Neise, W. (1997), 'Noise Source Identification in a Prop Fan Model by Means of Acoustical Near Field Measurements', *Journal of Sound and Vibration*, vol. 203, pp. 641–665.

Inoue, M. and Furukawa, M. (2002), 'Physics of Tip Clearance Flow in Turbomachinery', *Proceedings of the ASME2002 Joint US – European Fluids Engineering Division Conference*, Montreal, Quebec, Canada, 14–18 July, paper no. FEDSM2002-31184, pp. 777–789.

Inoue, M., Kuroumaru, M. and Furukawa, M. (1986), 'Behavior of Tip Leakage Flow Behind an Axial Compressor Rotor', *Transactions of the ASME, Journal of Engineering for Gas Turbines and Power*, vol. 108, pp. 7–14.

Ito, T., Suematsu, Y. and Hayase, T. (1985), 'On the Vortex Breakdown Phenomena in a Swirling Pipe-flow', *Memoirs of the Faculty of Engineering, Nagoya University*, vol. 37, pp. 117–172.

Jensen, C.E. (1986), 'Axial-flow Fan', Patent No. US 4,630,993, 23 December.

Jones, M.C., Hourigan, K. and Thompson, M.C. (2001), 'The Generation and Suppression of Vortex Breakdown by Upstream Swirl Perturbations', *Proceedings of 14th Australian Fluid Mechanics Conference*, Adelaide, Australia, 10–14 December, pp. 347–350.

Leibovich, S. (1978), 'The Structure of Vortex Breakdown', *Annual Review of Fluid Mechanics*, vol. 10, pp. 221–246.

Leibovich, S. (1984), 'Vortex Stability and Breakdown: Survey and Extension', *AIAA Journal*, vol. 22, pp. 1192–1206.

Longet, C.M.L. (2003), 'Axial Flow Fan with Noise Reducing Means', Patent No. US 2003/0123987 A1, 3 July.

Lucca-Negro, O. and O'Doherty, T. (2001), 'Vortex Breakdown: A Review', *Progress in Energy and Combustion Science*, vol. 27, pp. 431–481.

Mimura, M. (2003), 'Axial Flow Fan', Patent No. US 6,648,598 B2, 18 November.

Quinlan, D.A. and Bent, P.H. (1998), 'High Frequency Noise Generation in Small Axial Flow Fans', *Journal of Sound and Vibration*, vol. 218, pp. 177–204.

Smith, G.D.J. and Cumpsty, N.A. (1984), 'Flow Phenomena in Compressor Casing Treatment', *Transactions of the ASME, Journal of Engineering for Gas Turbines and Power*, vol. 106, pp. 532–541.

Spall, R.E., Gatski, T.B. and Grosch, C.E. (1987), 'A Criterion for Vortex Breakdown', *Physics of Fluids*, vol. 30, pp. 3434–3440.

Srigrarom, S. and Kurosaka, M. (2000), 'Shaping of Delta-wing Platform to Suppress Vortex Breakdown', *AIAA Journal*, vol. 38, pp. 183–186.

Storer, J.A. and Cumpsty, N.A. (1991), 'Tip Leakage Flow in Axial Compressors', *Transactions of the ASME, Journal of Turbomachinery*, vol. 113, pp. 252–259.

Takata, H. and Tsukuda, Y. (1977), 'Stall Margin Improvement by Casing Treatment – Its Mechanism and Effectiveness', *Transactions of the ASME, Journal of Engineering for Power*, vol. 99, pp. 121–133.

Thompson, D.W., King, P.I. and Rabe, D.C. (1998), 'Experimental and Computational Investigation on Stepped Tip Gap Effects on the Flowfield of a Transonic Axial-flow Compressor Rotor', *Transactions of the ASME, Journal of Turbomachinery*, vol. 120, pp. 477–486.

Tsai, C-Y. and Widnall, S.E. (1980), 'Examination of Group-velocity Criterion for Breakdown of Vortex Flow in a Divergent Duct', *Physics of Fluids*, vol. 23, pp. 864–870.

Uchida, S., Nakamura, Y. and Ohsawa, M. (1985), 'Experiments on the Axisymmetric Vortex Breakdown in a Swirling Air Flow', *Transactions of the Japan Society for Aeronautical Space Sciences*, vol. 27, pp. 206–216.

Uselton, R.B., Cook, L.J. and Wright, T. (2008), 'Fan with Reduced Noise Generation', Patent No. US 7,351,041 B2, 1 April.

Chapter 8

Development of Improved Blade Tip Endplate Concepts for Low-noise Operation in Industrial Fans

A. Corsini, F. Rispoli and A.G. Sheard

ABSTRACT

The chapter presents a computational analysis of the studied fan's blade-to-blade flow-field with and without blade-tip end-plates fitted. The analysis verifies the effectiveness of the end-plate design methodology presented in Chapter 7. We predicted the blade-to-blade flow-field for a *datum* fan AC90/6 without blade-tip end-plates, and two fan variants with different end-plate geometries. The fan AC90/6/TF incorporated a constant thickness end-plate and the fan AC90/6/TF$_{VTE}$ incorporated a variable thickness end-plate. The computational analysis indicated that the variable thickness blade-tip end-plate design successfully avoided blade tip-to-casing leakage vortex bursting. Assessing aerodynamic performance demonstrated an improved pressure developing capability and efficiency that we may attribute to the leakage vortex not bursting. However, noise measurements indicated that the variable thickness blade-tip end-plate resulted in an overall noise level approximately 0.5 dB higher than that occurring with the constant thickness end-plate. The computational analysis showed that the variable thickness end-plate induced the presence of multiple organised vortical structures. In breaking down, these vortical structures were acoustically productive enough to result in increased overall fan far-field noise. We undertook the computational analysis using a Reynolds-Averaged Navier–Stokes (RANS) simulation with non-linear k-ε turbulence model in a low-Reynolds number formulation. Although well proven, the simulation was not able to model unsteady effects and therefore models only part of the flow-field physics. Despite this caveat we conclude that the blade-tip end-plate design methodology was effective, in that it avoided blade tip-to-casing leakage vortex bursting, but was not effective at reducing overall fan far-field noise. In order to take advantage of the lower noise that occurs with a leakage vortex that does not burst, we conclude that the acoustic consequences of other organised vortical structures must be minimised.

This chapter is a revised and extended version of Corsini, A., Rispoli, F. and Sheard, A.G. (2007), 'Development of Improved Blade Tip Endplate Concepts for Low-noise Operation in Industrial Fans', *Proceedings of the IMechE Part A, Journal of Power and Energy*, vol. 221, pp. 669–681.

NOMENCLATURE

Latin letters

D	design operating point
E_Ω	rotational kinetic energy
H_ν	normalised helicity
k	turbulent kinetic energy
ℓ	chord length
l_ε	turbulence length scale
p	static pressure
Δp_{stat}	static pressure variation [Pa]
r	non-dimensional span
SWL	sound power level
t	blade pitch
TI	turbulence intensity
TE	trailing edge
TLV	tip-leakage vortex
v, w	absolute and relative velocities
x, y, z	cartesian coordinates

Greek letters

δ^+	normalised distance from the wall
ζ	total loss coefficient
η	efficiency
σ_h	hub-to-casing diameter ratio
ν_t	turbulent viscosity
ξ_i	absolute vorticity vector
Φ	global flow coefficient (annulus area-averaged axial velocity normalised by Uc)
τ	rotor tip clearance

Subscripts and superscripts

a, p, r	axial, peripheral and radial
c	casing wall
h	hub wall
i	Cartesian component index
in	inlet section
mol	molecular quantity
s	streamwise component
$\bar{}$	pitch-averaged value
0	total quantities

INTRODUCTION

The specifications for low-speed fans intended for air movement application routinely includes a requirement for large blade tip-to-casing gaps. These large gaps are typically to facilitate the fan's operation in the event of an emergency when they are required to clear hot gas and smoke from either a building or tunnel system. By incorporating larger blade tip-to-casing gaps at ambient temperature during routine operation, operators may be confident that the gap will not close to zero when clearing hot gas and smoke during high temperature emergency operation.

One disadvantage of larger blade tip-to-casing gaps is that they have a detrimental effect on the fan's aerodynamic performance (Fukano and Takamatsu, 1986; Storer and Cumpsty, 1991; Furukawa *et al.*, 1999). Larger blade tip-to-casing gaps also result in larger over-tip leakage flow that results in higher fan noise. The blade tip-to-casing clearance flow is acoustically productive as a consequence of the blade tip-leakage vortex itself, and its interaction with turbulent boundary layers and blade-to-blade passage secondary flow features (Quinlan and Bent, 1998; Jang *et al.*, 2003; Fukano and Jang, 2004; Vad *et al.*, 2006).

In practice, designers working within the air movement and control community minimise blade tip-to-casing gap size for each application. As it is impossible to reduce further minimum blade tip-to-casing gap sizes for any given application, there is interest in design methods and techniques that facilitate tip-clearance noise reduction. Such design methods and techniques have immediate application in fan design intended for air movement application.

Bianchi *et al.* (2014) reviewed the current state-of-the-art techniques in air movement fan flow and noise control, examining the interaction between aerodynamic cause and acoustic effect. Bianchi *et al.* (2014) went on to consider the application of control technologies that current cause-and-effect theories have inspired. The purpose is two-fold. First, it provides a vision for aerodynamics research over the next decade; and second, it provides air movement fan designers with an insight into the technology available now that they may apply in an on-going effort to reduce fan noise. Bianchi *et al.* (2014) identified two broad categories into which we may divide noise control techniques: active and passive.

Active noise control techniques classically seek to manage the blade tip-to-casing leakage flow by injecting fluid though the casing of both high-speed compressors (Bae *et al.*, 2005) and low-speed flow fans (Roy *et al.*, 2005). In contrast, some scholars studying passive noise control techniques have focused on the application of swept blade-stacking lines (Wadia *et al.*, 1998; Corsini and Rispoli, 2004; Corsini *et al.*, 2004b).

A second passive noise control technique utilises casing treatments. In an attempt to improve compressor performance, researchers first experimented with casing treatments in the early 1970s utilising grooves (Takata and Tsukuda, 1977; Smith and Cumpsty, 1984), and more recently stepped gaps in the blade tip region (Thompson *et al.*, 1998). These casing treatments improved the compressors' stable operating range by reducing the blade tip leakage flow intensity.

The air movement and control community has historically favoured using passive noise control techniques when attempting to minimise low-speed fan noise. The intent of these passive techniques is to influence positively dominant noise generation mechanisms. The passive noise control technique most widely adopted within the air movement and control community are blade-tip appendages. Researchers have studied extensively fan blade-tip appendage design (Jensen, 1986; Quinlan and Bent, 1998; Longet, 2003; Mimura, 2003; Belady, 2004; Uselton *et al.*, 2008). They have advocated using blade-tip appendages as a technique for noise control in both fans and compressors.

Booth *et al.* (1982) and Wadia and Booth (1982) demonstrated that blade-tip appendages could reduce the magnitude of blade tip-to-casing clearance flow. This reduction both increases aerodynamic performance and reduces fan noise. These blade-tip appendages constitute anti-vortex devices. Scholars who have studied their application have reached a consensus that in addition to reducing the volume flow rate of clearance flow, they influence the flow-field structures within the blade tip-to-casing flow. A consequence of this is that the blade-tip noise generation mechanism intensity reduces.

This chapter continues Corsini and Sheard's (2007) research, establishing the effectiveness of their blade-tip end-plate design methodology. In this chapter we present a computational analysis of the fan blade-to-blade flow-field with and without fitted blade-tip end-plates. The computational analysis facilitates a qualitative assessment of the *datum* fan's aerodynamic and acoustic performance with and without fitted blade-tip end-plates. We identify structures within the blade tip-to-casing leakage flow by studying the rotational kinetic energy and turbulent kinetic energy distributions. We further analysed the identified structures by studying helicity and total pressure loss distributions. We complemented our qualitative computational analysis with quantitative experimental measurements of overall aerodynamic and acoustic fan performance. These measurements enabled us to associated individual structures within the blade tip-to-casing leakage flow with changes in fan performance, thus enabling us to link aerodynamic cause with acoustic effect.

FAMILY OF FANS UNDER INVESTIGATION

We conducted the reported research on a family of commercially available cooling fans. The studied fan configuration, coded AC90/6, incorporates a six-blade un-swept rotor, with modified ARA-D profile aerofoil blades, Table 8.1. One may set the blade-pitch angle during final assembly to customise the fan to a desired duty point. We used a direct coupled-induction 400-volt (AC), 3-phase motor to drive the rotor at a constant speed of 950 rpm, resulting in a 44.7 m/s blade tip speed and a 95 Hz blade-passing frequency (BPF). In its original embodiment, the studied fan did not include a blade-tip end-plate, therefore, we used it as a *datum* against which to assess the performance of fan variants with blade-tip end-plates. Thus, in the reported research we refer to the fan without blade-tip end-plates as the fan *datum* AC90/6.

Fan Blade-tip End-plates

In addition to the fan *datum* AC90/6, we studied two fan variants. The first was fitted with a constant thickness blade-tip end-plate and the second with a variable thickness blade-tip end-plate, Figure 8.1. When fitted with a constant thickness blade-tip end-plate, we named the fan AC90/6/TF. When fitted with the variable thickness blade-tip end-plate, we named the fan AC90/6/TF_{VTE}.

The designs developed for tip-vortex control and drag reduction in aircraft wings and catamaran hulls inspired the constant thickness blade-tip end-plate design, which ran along the blade pressure surface, ending at the blade trailing edge

Table 8.1. *The fan* datum *AC90/6 blade geometry and rotor specification.*

	Fan *datum* AC90/6		
Blade geometry	Hub	Mid-span	Tip
Pitch angle (°)	36	58.8	28
Camber angle (°)	46	44	41
Solidity	1.24	0.86	0.30
Fan rotor			
Blade number		6	
Blade tip pitch angle (°)		16–28	
Blade tip stagger angle (°)		74–62	
Hub-to-casing diameter ratio σ		0.22	
Tip diameter (mm)		900.0	
Rotor tip clearance τ (% span)		1.0	
Rated rotational frequency (r/min)		935–950	

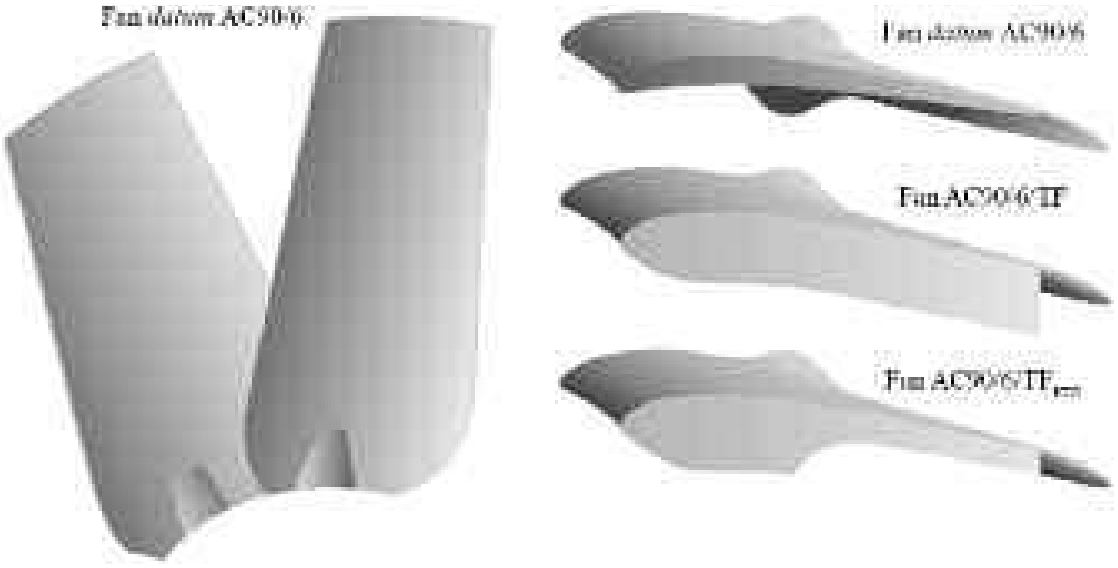

FIGURE 8.1. The studied fan *datum* AC90/6 without a fitted blade-tip end-plate, with a constant thickness blade-tip end-plate, AC90/6/TF and with a variable thickness blade-tip end-plate, AC90/6/TF_{VTE}.

with a square tail. This addition resulted in the thickness of the fan AC90/6/TF blade tip increasing by a factor of three compared to the fan *datum* AC90/6. We characterised the blade-tip end-plate size for axial compressor blades using Inoue *et al.*'s (1986) research. They estimated that the optimum blade-tip end-plate size was between 10 and 20 per cent blade span. In practice, we were able to manufacture blades with a blade-tip end-plate size five per cent of blade span. The fan blades were manufactured from injection moulded plastic, with the blade-tip end-plate size serving as the largest the blade manufacturing technique could produce.

Corsini and Sheard (2007) studied both the fan *datum* AC90/6 and AC90/6/TF using a blade-tip 'vortex breakdown' criteria based on Rossby number (Spall *et al.*, 1987). Following Ito *et al.*'s method (1985) they concluded that there is a threshold value of Rossby number below which the vortex rotation cannot reduce if the vortex is to remain stable. We defined this critical Rossby number range using the critical Rossby numbers defined by Uchida *et al.* (1985) and Garg and Leibovich (1979). Uchida *et al.* (1985) defined a critical Rossby number associated with the breakdown of an axi-symmetric vortex in a swirling flow. Garg and Leibovich (1979) also defined a critical Rossby number associated with an aircraft wing tip vortices' breakdown.

Corsini *et al.* (2006) studied the fan *datum* AC90/6 and fan AC90/6/TF's aerodynamic and acoustic performance, identifying a breakdown of the fan AC90/6/TF blade tip-to-casing leakage vortex. Vortex breakdown is acoustically productive, and therefore Corsini *et al.* (2006) concluded that a revised blade-tip end-plate design was desirable that avoided leakage vortex breakdown. Corsini and Sheard (2007) developed a blade-tip end-plate design methodology that successfully eliminated the leakage vortex breakdown by adding a variable thickness blade-tip end-plate. When fitted with this variable thickness blade-tip end-plate, we named the fan AC90/6/TF$_{VTE}$.

Flow Conditions

The studied fan blade tip pitch angle is adjustable and may be set to a pitch angle between 16 and 28 degrees. In practical application, the blade tip pitch angle is typically set to 28 degrees as this maximises flow rate for a given system pressure. In the research reported in this chapter, we conducted the experimental measurements with the fan blade tip pitch angle set to 28 degrees. We selected 28 degrees both because it is typical of the angle that one uses in practical application and because it results in the highest blade loading. A highly loaded blade results in the blade tip-to-casing vortex having the most significant effect on both fan aerodynamic and acoustic performance (Holste and Neise, 1997).

NUMERICAL PROCEDURE AND AXIAL FAN MODELLING

In the programme of work reported in this chapter, we simulated the blade-to-blade flow-field with a Reynolds-Averaged Navier–Stokes (RANS) based non-linear

code, with two-equation closure (Craft *et al.*, 1996). The two-equation closure was able to cope with non-isotropic and non-equilibrium turbulence effects without a significant increase in the required computational effort. The code utilised a parallel multi-grid (MG) numerical scheme, developed for an in-house finite element method (FEM) code which Borello *et al.* (2003) first proposed. Corsini and Sheard (2007) applied Borello *et al.*'s (2003) numerical procedure to the study of blade-tip endplates, and it is Corsini and Sheard's (2007) procedure that we have further developed during the course of the research reported in this chapter.

The finite element method formulation is based on a stabilised Petrov-Galerkin (PG) method modified for application to three-dimensional equal- and mixed-order spaces of approximation. We used the Petrov-Galerkin scheme to control the instability that affects the advective-diffusive incompressible flow, and the momentum's reaction and turbulent scale equations. The turbulent scale equations relate to Coriolis acceleration (Corsini *et al.*, 2004a). We used equal-order Q1-Q1 and mixed-order Q2-Q1 interpolation for primary turbulent scale equations and constrained secondary variables, implicitly eliminating the undesirable pressure-checker boarding effects. We performed the computational analysis using a hybrid full linear multigrid accelerator running on an overlapping parallel solver (Borello *et al.*, 2001).

In our Reynolds-Averaged Navier–Stokes simulation, we utilised a non-linear k-ε turbulence model in its topology-free low-Reynolds number formulation (Craft *et al.*, 1996). Although a well proven approach for modelling vortex structures (Inoue and Furukawa, 2002), the simulation was not able to model unsteady effects and therefore models only part of the flow-field physics. Despite this caveat, Corsini and Rispoli (2004) were able to validate the modelling approach when they applied it to a compressor application. Corsini and Rispoli (2005) were also able validate the modelling approach in air movement fan applications.

Computational Mesh and Boundary Conditions

The approach we adopted when constructing a computational mesh utilised a non-orthogonal body fitted H-type grid system. We split the mesh into two regions, one in the blade-to-blade region and a second in the blade tip-to-casing gap. In total, the mesh comprised $154 \times 68 \times 58$ nodes in the axial-, pitch- and span-wise directions. In the axial direction 20 per cent of the nodes were distributed upstream of the blade leading edge, 50 per cent were within the blade passage and 30 per cent were downstream of the blade trailing edge. In the span-wise direction, 14 of the 58 nodes were spaced across the blade tip-to-casing gap. All mesh density regions maintained an adequate computational cell aspect ratio toward solid boundaries. The computational grid that we developed for the blade illustrates how mesh density increased in the solid wall's near vicinity, Figure 8.2.

We defined the boundary conditions according to Corsini and Rispoli (2004) and Corsini *et al.*'s (2004b) recommendations. They studied the performance of ducted high-solidity fans. The Dirichlet conditions for the relative velocity components are imposed at the inflow section, half a mid-span chord upstream of the

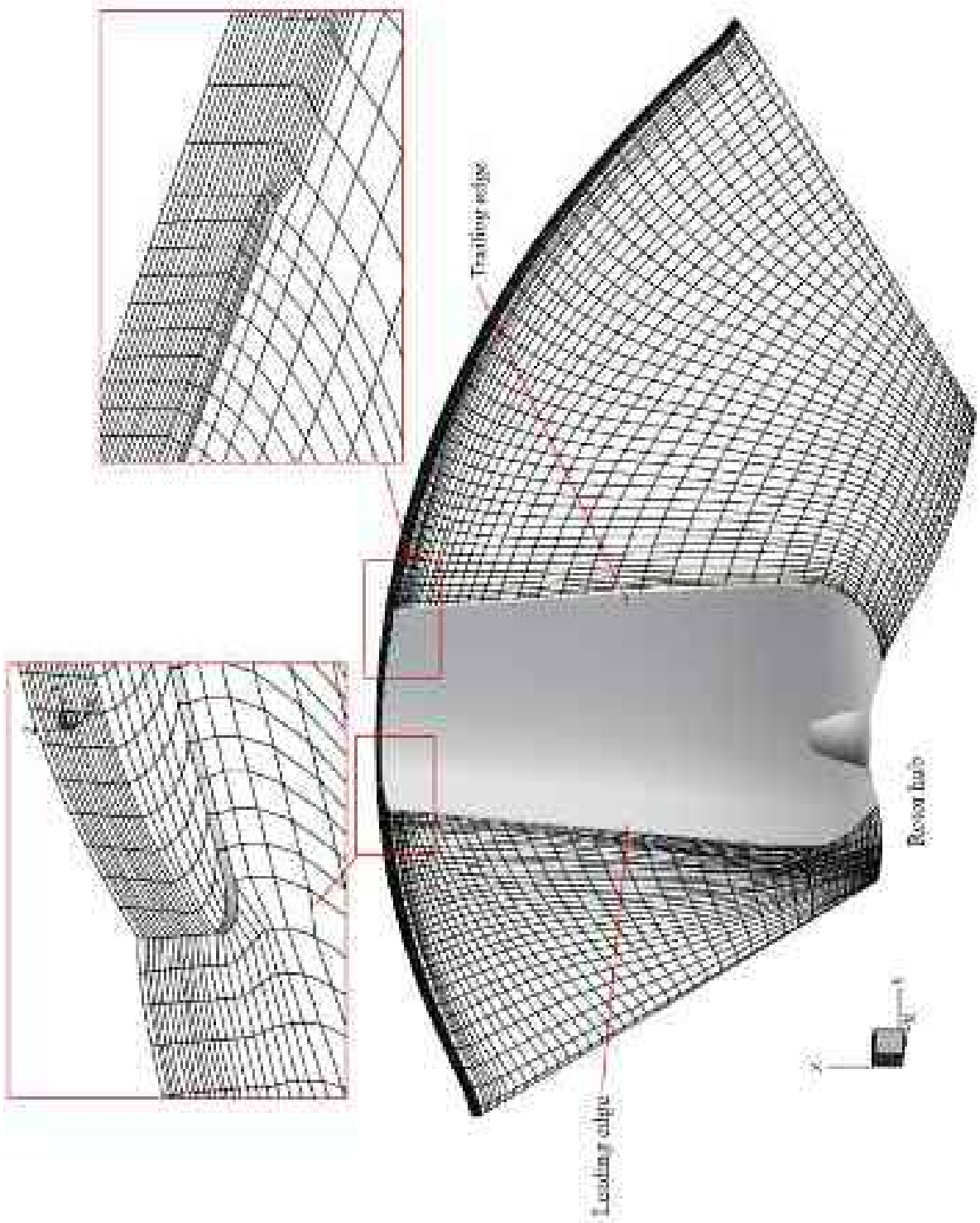

FIGURE 8.2. The computational grid used in the numerical simulations. The mesh was formed by merging a structured H-type grid though the up-stream blade-to-blade passage and down-stream region with a second H-type grid in the blade tip-to-casing region.

leading edge, as obtained from a flow simulation in an annular passage of identical hub-to-casing diameter ratio that includes an upstream spinner cone.

We used a turbulent kinetic energy (k) pitch-wise profile derived from an axi-symmetric turbulence intensity profile previously developed by Corsini and Rispoli (2004). The turbulence intensity profile was a near-uniform six per cent across the annulus, increasing to ten per cent near the casing. We used the turbulent kinetic energy's pitch-wise profile to calculate the radial distribution of dissipation based on a dissipation length scale (l_ε) of one per cent of blade mid-span pitch. We completed the boundary conditions by assuming periodicity both up- and down-stream of the fan blades.

Fan Aerodynamic Performance

The impact of the blade tip-to-casing leakage vortex on both fan aerodynamic and acoustic performance results in applying blade-tip end-plates changing not only the fan's acoustic performance, but also the aerodynamic performance. Gbadebo *et al.* (2006) concluded that this change is a consequence of the interaction between blade tip-to-casing flow and blade suction surface near surface fluid. Consequently, the fan *datum* AC90/6 generates a different pressure at a constant flow rate when fitted with each of the studied blade-tip end-plates. To facilitate the comparison of fan performance data when fitted with different blade-tip end-plates, we chose to define three operating points, and their respective volume flow rates, Table 8.2. The design operating point volume flow rate is typical of that required when one installs the fan over a cooling unit's tube bank. The peak pressure flow rate is typical of that required when the tube bank has become partially blocked following a period of in-service operation. The maximum flow operating point volume flow rate is typical of the flow rate that occurs with the lowest pressure loss tube banks currently operating in service.

Bianchi *et al.* (2009) measured the performance characteristics of the fan *datum* AC90/6, AC90/6/TF and AC90/6/TF$_{VTE}$ in accordance with ISO 5801:2007 requirements (2007). Bianchi *et al.* (2009) observed that the addition of both the constant and variable thickness blade-tip end-plates results in an increase in blade loading. We would expect blade-tip noise sources to become more acoustically productive

Table 8.2. *The operating points used when characterising the studied fan's performance with and without fitted blade-tip end-plates. The authors measured performance characteristics in a Type D standardised airway (ducted inlet, ducted outlet) in accordance with ISO 5801:2007 requirements (2007).*

Operating point	Volume flow rate (m^3/s)	Studied blade tip pitch angle (°)
Maximum flow	7.0	28
Design	6.5	28
Peak pressure	5.6	28

with increasing blade loading. Therefore an increase in blade loading will partially offsets any reduction in fan far-field noise attributed to adding a blade-tip end-plate. We reasoned that we would conservatively assess the reduction in fan far-field noise if we neglect increased blade loading. Therefore, despite fan far-field noise increasing with blade loading, we chose to neglect the change in pressure rise with the change in blade-tip treatment.

We validated the quality of the blade-to-blade flow-field computational analysis using Corsini and Sheard's (2007) method. We predicted the overall performance of the studied fans *datum* AC90/6, AC90/6/TF and AC90/6/TF$_{VTE}$ and compared the predicted performance with Bianchi *et al.*'s (2009) performance measurement, Table 8.3. We may reasonably assume that if we are able to predict overall fan performance accurately, we accurately predict flow-field features in the blade-to-blade passage. The predicted static pressure and efficiency for the three studied fans was within the uncertainty of the measured performance.

BLADE-TIP END-PLATE EFFECTIVENESS

Corsini and Sheard (2007) observed that the constant thickness blade-tip end-plate fitted to fan AC90/6/TF reduced the blade tip-to-casing leakage flow and therefore the intensity of the associated leakage vortex. We may conclude that this reduced intensity was responsible for the reduction in fan AC90/6/TF far-field noise when compared with fan *datum* AC90/6. However, the reduced leakage vortex intensity also resulted in it bursting, a flow-field feature known to be acoustically productive. Corsini and Sheard (2007) developed a design methodology that enhanced vortex swirl using a variable thickness blade-tip end-plate that prevented vortex bursting. When they incorporated the variable thickness blade-tip end-plate into the fan *datum* AC90/6, they named the resultant fan AC90/6/TF$_{VTE}$.

Bianchi *et al.* (2011) measured the fan A-weighted overall sound power and specific noise level across its operating range. As pressure rise increases towards the fan's peak pressure operating point, both fan AC90/6/TF and AC90/6/TF$_{VTE}$ noise levels increased from a minimum that is associated with a pressure rise close to the fan's design operating point. Axial fans classically exhibit an increase in the amplitude of discrete frequency tones as they approach stall (Fukano *et al.*, 1986).

Table 8.3. *Experimentally measured (Bianchi et al., 2009) and predicted fan aerodynamic performance for the fan* datum *AC90/6, AC90/6/TF and AC90/TF*$_{\mathrm{VTE}}$ *at the design operating point.*

	Measurements		Predictions	
	Δp_{stat} (Pa)	η (%)	Δp_{stat} (Pa)	η (%)
datum AC90/6	134.8	49.0	133.3	51.0
AC90/6/TF	126.2	51.0	126.1	50.4
AC90/6/TF$_{VTE}$	129.0	52.0	128.2	51.6

Therefore, we expected the increase in noise level as the fans AC90/6/TF and AC90/6/TF$_{VTE}$ moved from their design to peak pressure operating point. However, specific noise levels remain lower than that of fan *datum* AC90/6 over the entire fan operating range despite the increase in blade loading that occurs with having fitted a blade-tip end-plate.

The reduction A-weighted overall sound power level across the fan operating range gave us confidence in the effectiveness of the blade-tip end-plates. However, the fan AC90/6/TF exhibited slightly lower noise levels than fan AC90/6/TF$_{VTE}$ at all operating points. This indicated that Corsini and Sheard (2007) had developed a blade-tip end-plate design methodology that actually increased far-field fan noise and therefore was not effective. In an attempt to establish why Corsini and Sheard's (2007) blade-tip end-plate design methodology was ineffective, we initiated the programme of work reported in this chapter. We conducted a computational analysis of the studied fan's blade-to-blade flow-field with and without blade-tip end-plates fitted.

Helicity Distributions and Vortex Core Trajectories

We used our computational analysis to study the flow-field features through the blade-to-blade passage of the fan *datum* AC90/6, AC90/6/TF and AC90/6/TF$_{VTE}$. The computational analysis was particularly helpful when visualising the flow-field features that develop through the blade tip-to-casing gap. We may use the computational analysis to compute a range of flow-field parameters. When studying tip-clearance flow-field features, Furukawa *et al.* (1999) and Inoue and Furukawa (2002) studied normalised helicity (H_n). Normalised helicity is a useful parameter as it facilitates visualising blade tip-to-casing leakage vortex core trajectories. Furukawa *et al.* (1999) and Inoue and Furukawa (2002) defined normalised helicity as:

$$H_n = (\xi_i \cdot w_i) / (|\xi||w|)$$

in which:

$i = 1 \ldots 3$
ξ_i and w_i are the Cartesian components of the absolute vorticity and relative velocity vectors; and
$|\xi|$ and $|w|$ and are the norms of these vectors.

When plotting the normalised helicity contours on cross sections for the fan *datum* AC90/6, AC90/6/TF and AC90/6/TF$_{VTE}$, we chose planes at 25, 43, 65, 89 and 120 per cent blade chords from the blade tip's leading edge. Through these planes we then plotted the blade tip-to-casing leakage vortex trajectory, Figure 8.3.

Consider the normalised helicity contours and blade tip-to-casing leakage vortex trajectory for the fan *datum* AC90/6, Figure 8.3. The blade tip-to-casing leakage vortex (TLV1) is well defined, with the vortex trajectory departing from the blade suction surface as it progresses from blade leading to trailing edge. There

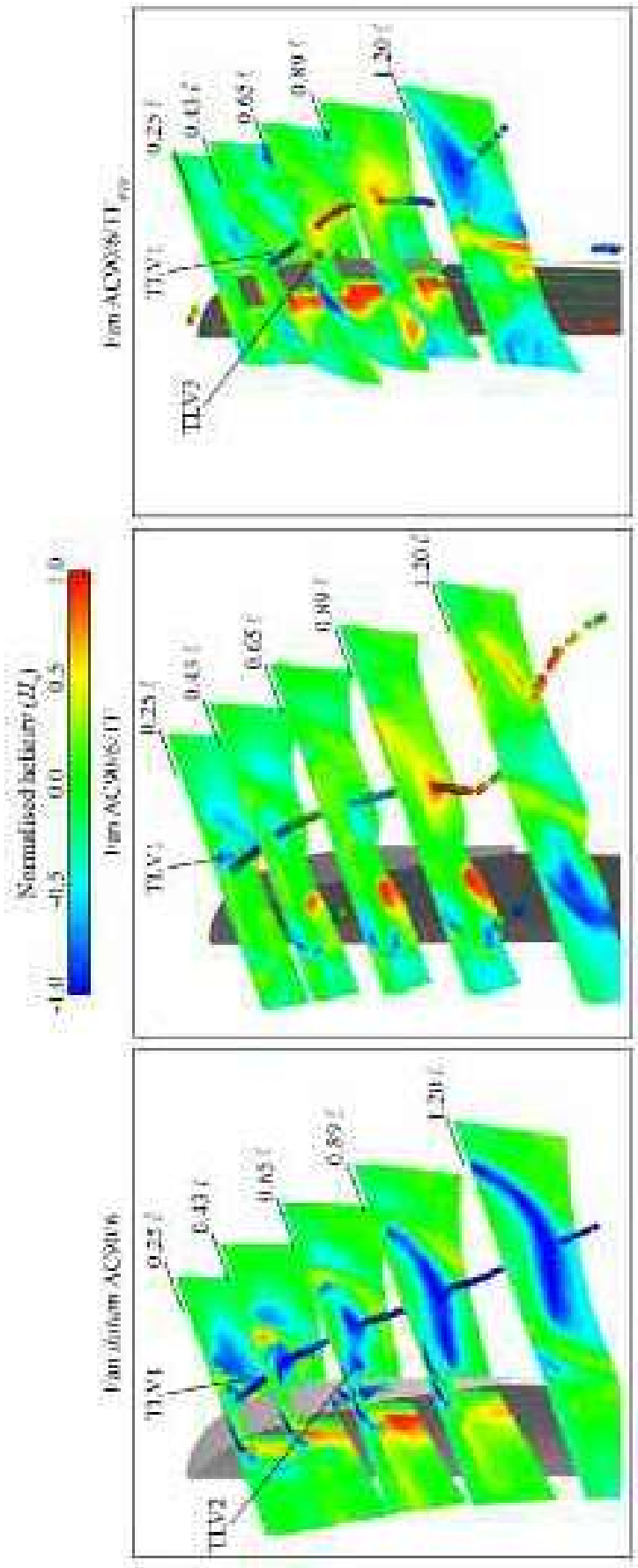

FIGURE 8.3. Three-dimensional normalised helicity (H_n) contours numerically predicted at the fan design operating point. Helicity contours are presented at five chord-wise locations through the fan *datum* AC90/6, AC90/6/TF and AC90/6/TF$_{VTE}$. The blade tip-to-casing leakage vortex core trajectory and normalised helicity illustrate the effect of fitting a constant and variable thickness blade-tip end-plate.

is also evidence of a weaker secondary tip-to-casing leakage vortex (TLV2) that appears close to the suction surface 65 per cent blade chord downstream of the blade leading edge. As this weaker vortex progresses towards the blade trailing edge, it merges into the blade tip-to-casing leakage vortex (TLV1). The result is a well-defined vortex that affects a significant proportion of the blade-to-blade passage in the blade tip region.

Consider the normalised helicity contours and blade tip-to-casing leakage vortex trajectory for the fan AC90/6/TF, Figure 8.3. The helicity contours indicate the presence of a vortex in the blade tip region of the blade pressure surface from 43 to 89 per cent blade chord. This vortex may be the pressure-side leg of a blade-to-blade passage horseshoe vortex, and its presence will be limiting the blade tip-to-casing leakage flow. As we previously observed with fan *datum* AC90/6, the blade tip-to-casing leakage vortex (TLV1) departs from the suction surface. However, its helicity magnitude is generally lower than fan *datum* AC90/6. Further, the secondary tip-to-casing leakage vortex (TLV2) is not apparent in the helicity contours. If it is present at all, it does not merge with the blade tip-to-casing leakage vortex (TLV1), but simply decays.

By mid-chord the helicity contours indicate that the blade tip-to-casing leakage vortex (TLV1) helicity has reduced. This reduction is probably a consequence of the reduced blade tip-to-casing leakage flow rate and the deflection of the vortex core. As it moves towards the blade trailing edge, helicicy falls to zero which we may interpret as evidence of vortex breakdown. After it has broken down the tip-to-casing leakage vortex (TLV1) flow acquires anti-clockwise vorticity as a consequence of the adjacent trailing edge blade tip-to-casing flow. This anti-clockwise vorticity washes out by the time it reaches the blade trailing edge, with no evidence of clockwise- or anti-clockwise helicity.

Consider the normalised helicity contours and blade tip-to-casing leakage vortex trajectory for the fan AC90/6/TF$_{VTE}$, Figure 8.3. The variable thickness blade-tip end-plate has a significant impact on the flow-field in the blade tip region. The onset of the blade tip-to-casing leakage vortex (TLV1) is apparent by 43 per cent blade chord. This is in contrast to the fan *datum* AC90/6 and AC90/6/TF where it is apparent at 25 per cent blade chord. Additionally, the vortex trajectory for fan AC90/6/TF$_{VTE}$ remains relatively close to the blade suction surface when compared to either fan *datum* AC90/6 or AC90/6/TF.

By mid-chord there is evidence that the blade tip-to-casing leakage vortex (TLV1) is interacting with a weak anti-clockwise vortex (TLV3). This vortex is apparent on the blade suction surface at 65 per cent blade chord. This vortex appears to be highly energetic and we may regard it as a leakage jet of blade pressure surface boundary layer fluid. This jet merges with the blade tip-to-casing leakage vortex (TLV1) and as it does so the leakage vortex rotation changes from clockwise- to anti-clockwise. As it moves towards the blade trailing edge, the blade tip-to-casing leakage vortex (TLV1) merges with the trailing edge blade tip-to-casing flow. The trailing edge blade tip-to-casing flows influence is to change the blade tip-to-casing leakage vortex (TLV1) rotation from anti-clockwise to clockwise as it exits the blade-to-blade passage.

We may complement our helicity analysis with an analysis of the chord-wise evolution of the blade tip-to-casing leakage vortex trajectory. A comparison of the vortex trajectories illustrates the impact of the studied blade-tip end-plates on the leakage vortex, Figure 8.4. A feature common to both the leakage vortex (TLV1) trajectory for the fan AC90/6/TF and AC90/6/TF$_{VTE}$ is a sudden change in direction. This change in direction occurs as the vortex rotation direction changes. In contrast, there is no sudden change in direction for the fan *datum* AC90/6 or change in its rotation direction.

When we study leakage vortex trajectories, it is apparent that there are additional organised vortical structures that occur with the fan AC90/6/TF$_{VTE}$. These are evident at the blade leading edge, mid-chord (TLV3) and near the blade trailing edge. The additional organised vortical structures are smaller than the leakage vortex (TLV1) and are relatively weak in comparison. As they are relatively weak, we may assume that they burst, resulting in an increase in fan far-field noise. Bianchi *et al.* (2011) measured the far-field noise of both the fan AC90/6//TF and AC90/6/TF$_{VTE}$ concluding that the fan AC90/6/TF$_{VTE}$ far-field noise was approximately 0.5 dB higher than fan AC90/6/TF. As the fan AC90/6/TF leakage vortex (TLV1) bursts and the fan AC90/6/TF$_{VTE}$ leakage vortex (TLV1) does not burst, Bianchi *et al.* (2011) anticipated that the fan AC90/6/TF$_{VTE}$ would have a lower fan far-field noise.

The fan AC90/6/TF leakage vortex (TLV1) bursts, but the leakage vortex trajectories indicate that it is not associated with any additional organised vortical structures. In contrast, the fan AC90/6/TF$_{VTE}$ leakage vortex (TLV1) does not burst, but the leakage vortex trajectories indicate that it occurs with additional organised vortical structures. Therefore, we may hypothesise that additional organised vortical

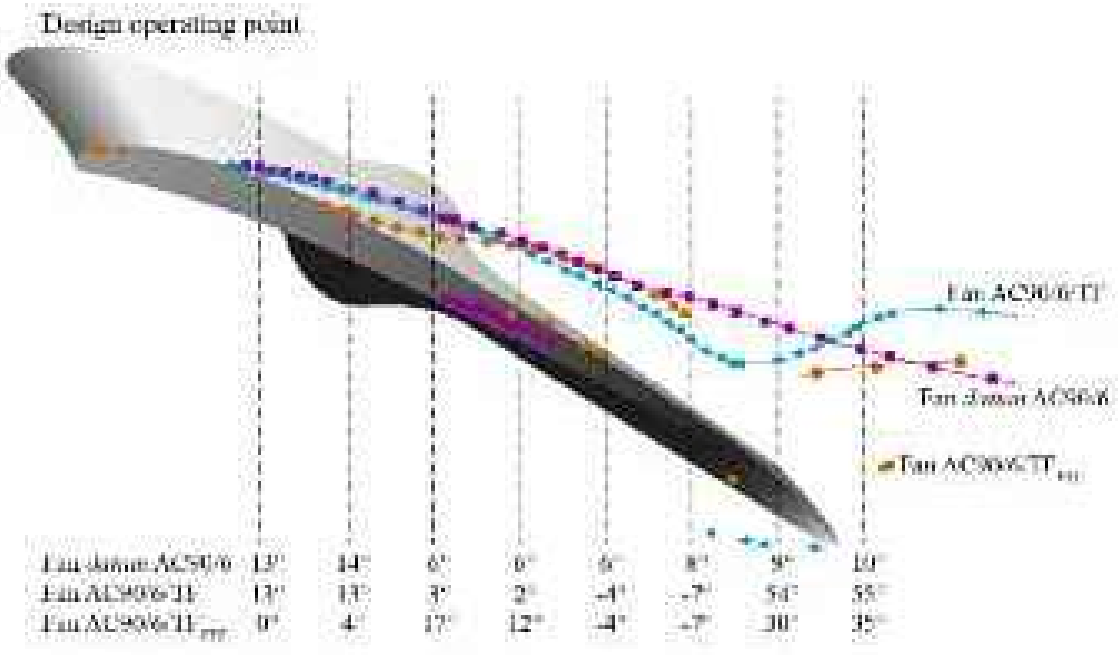

FIGURE 8.4. Chord-wise evolution of the blade tip-to-casing leakage vortex trajectory predicted at the fan design operating condition. A comparison of the vortex trajectories illustrates the impact of the studied blade-tip end-plates on the leakage vortex.

structure bursting that occurs with the fan AC90/6/TF$_{VTE}$ is responsible for the increased fan far-field noise. If we accept this hypothesis, then we may conclude the following. The increase in fan far-field noise that occurs with additional organised vortical structure bursting is greater than the reduction that occurs with the leakage vortex (TLV1) not bursting.

Leakage Flow Energy

The helicity contours and leakage vortex trajectories provided an insight into the nature and extent of blade-to-blade passage flow-field features. The blade tip-to-casing leakage vortex helicity and trajectory were significantly different for each of the three studied fans. We complemented our helicity analysis with an analysis of rotational kinetic energy (E_Ω). Rotational kinetic energy contours are on a cylindrical surface at 99.8 per cent fan radius, within the blade tip-to-casing gap for the three studied fans, Figure 8.5. Our objective with this analysis is to relate tonal noise sources to the blade tip-to-casing leakage vortex energy content.

Consider the rotational kinetic energy contours for the fan *datum* AC90/6, Figure 8.5. High rotational kinetic energy characterises the leakage vortices that appear as a red region near fan *datum* AC90/6's leading edge. The rotational kinetic energy contours clearly illustrate the presence of two leakage vortex. The first relatively close to the blade leading edge departs from the blade suction surface and is characteristic of the blade tip-to-casing leakage vortex (TLV1) identified during the helicity analysis. Additionally, there is a second high rotational kinetic energy feature that initiates downstream of the blade tip-to-casing leakage vortex (TLV1) and remains close to the blade suction surface. We may characterise this feature as the secondary tip-to-casing leakage vortex (TLV2) that we identified during the helicity analysis.

Consider the rotational kinetic energy contours for the fan AC90/6/TF and AC90/6/TF$_{VTE}$, Figure 8.5. It is apparent that the rotational kinetic energy of features that occurs with both the fan AC90/6/TF and AC90/6/TF$_{VTE}$ is lower than for the fan *datum* AC90/6. Therefore, we may conclude that both the constant and variable thickness blade-tip end-plates have reduced the rotational kinetic energy of the blade tip-to-casing leakage vortex (TLV1). This reduction is a consequence of two primary mechanisms. First is a reduction in the momentum transfer from blade pressure to suction surface during the leakage vortex's initial formation. Second is the leakage flow's unfeeding that reduces the momentum transfer to the leakage vortex as it progresses from blade leading to trailing edge.

We continued our analysis of rotational kinetic energy (E_Ω) with an analysis of three-dimensional turbulent kinetic energy (k). We present turbulent kinetic energy contour at the same five chord-wise planes that we used during the helicity analysis. These planes are 25, 43, 65, 89 and 120 per cent blade chords from the blade tip's leading edge. Through these planes we then plotted blade tip-to-casing leakage vortex core trajectory streamlines, Figure 8.6.

The chord-wise evolution of turbulent kinetic energy for the studied fans indicates that differences between the three were concentrated in the blade tip region.

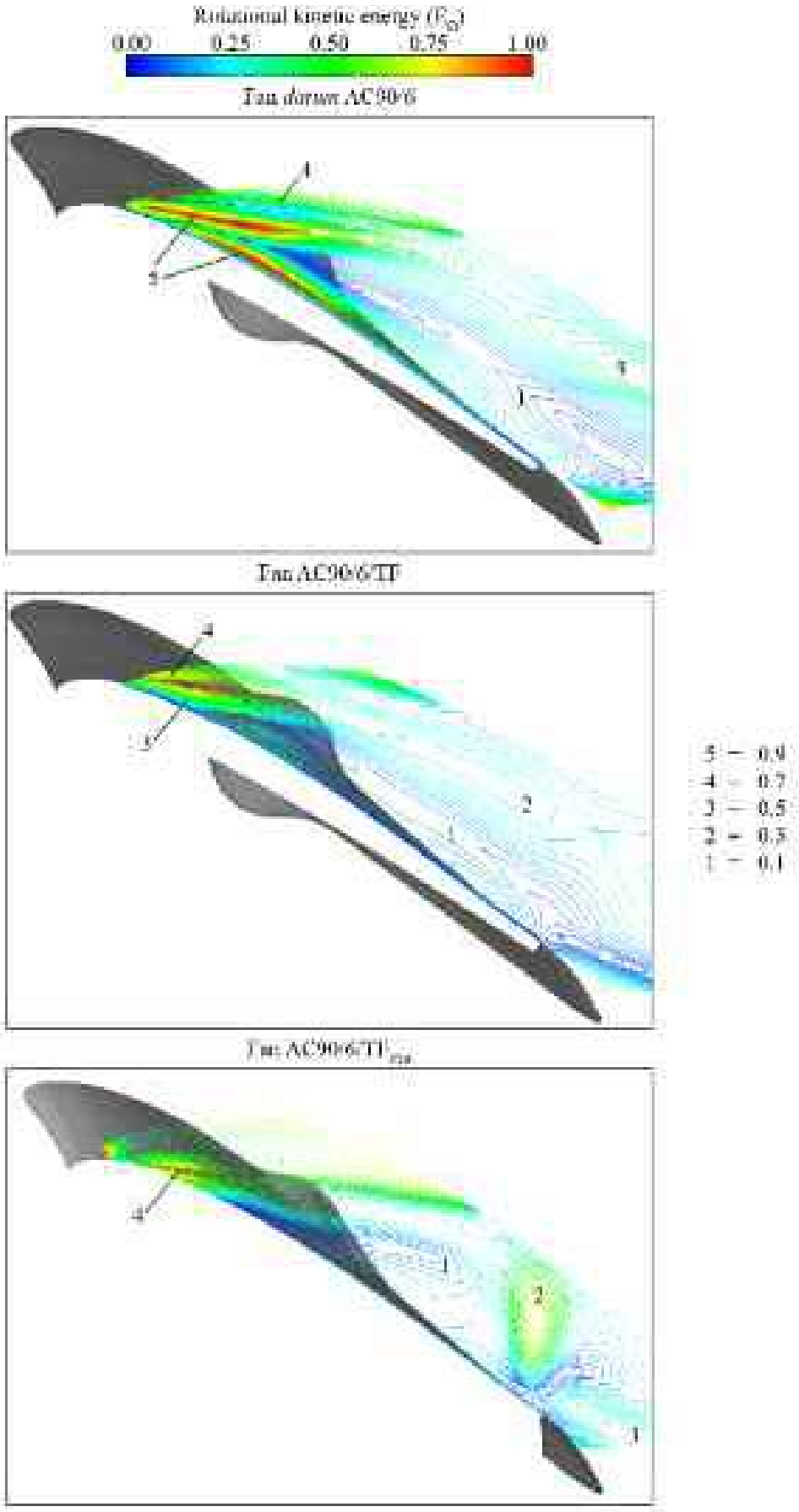

FIGURE 8.5. Two-dimensional rotational kinetic energy (E_Ω) contours numerically predicted at the fan design operating point. Rotational kinetic energy contours are presented on a cylindrical surface at 99.8 per cent fan radius, within the blade tip-to-casing gap. High rotational kinetic energy characterises the leakage vortices, clearly visible as a red region near fan *datum* AC90/6's leading edge.

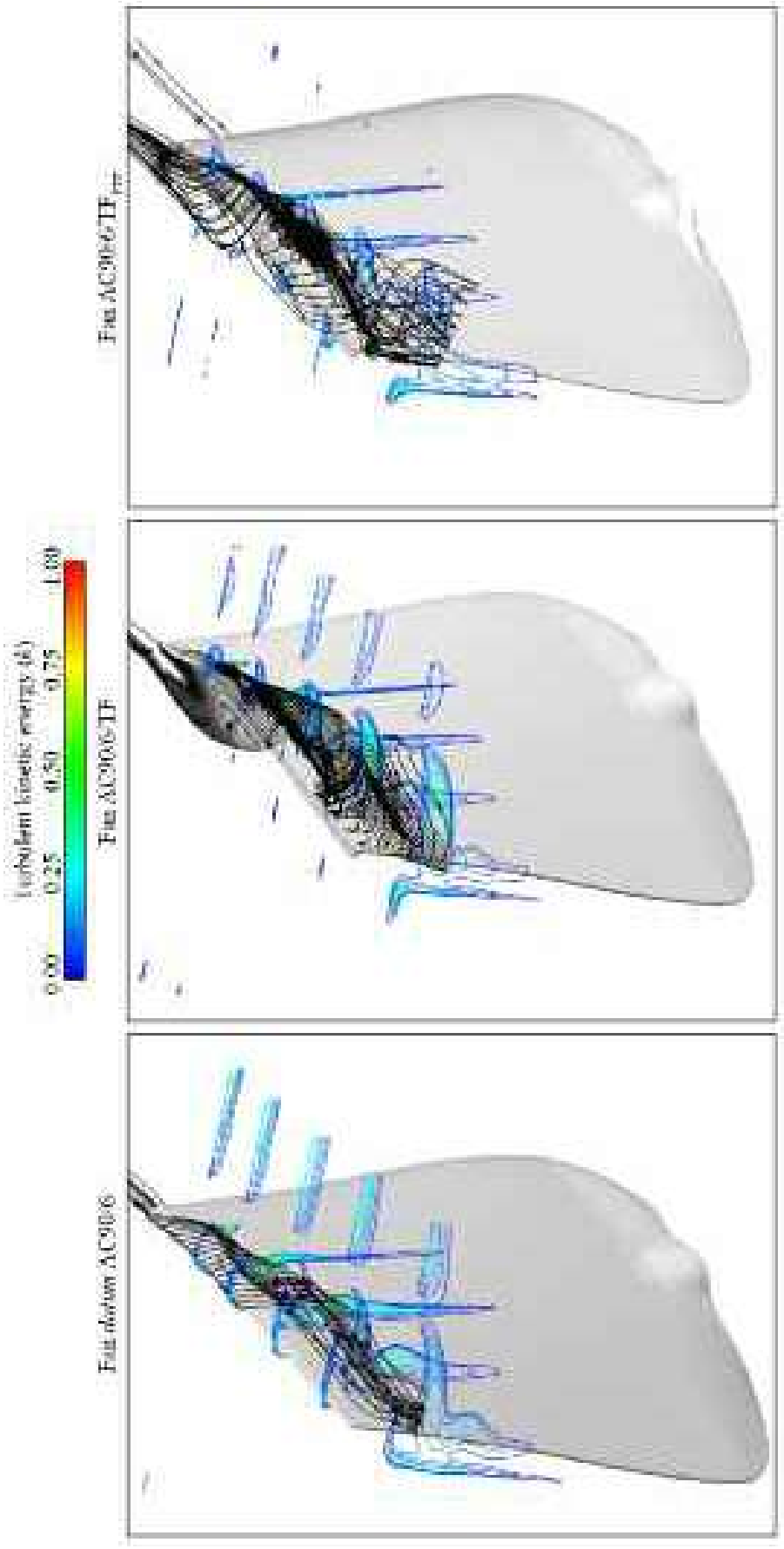

FIGURE 8.6. Three-dimensional turbulent kinetic energy (k) contours numerically predicted at the fan design operating point. Turbulent kinetic energy contours are presented at five chord-wise locations through the fan *datum* AC90/6, AC90/6/TF and AC90/6/TF$_{VTE}$. The blade tip-to-casing leakage vortex core trajectory streamlines illustrate the effect of fitting a constant and variable thickness blade-tip end-plate.

Both the constant and variable thickness blade-tip end-plates reduced blade tip-to-casing leakage flow rate. This reduction in flow rate in turn reduced the peak turbulent kinetic energy associated with vortex cores. The reduced peak turbulent kinetic energy was particularly evident around mid-chord where the blade tip-to-casing leakage vortex rotation changes from clockwise to anti-clockwise. If we consider the streamlines for the fan AC90/6/TF, the change in vortex rotation occurs with streamline expansion, which is characteristic of a separation bubble and we may regard it as evidence of vortex breakdown. When we study the streamlines for the fan AC90/6/TF$_{VTE}$, they also expand and then contract around the mid-chord. This contraction indicates that the variable thickness blade-tip end-plate is able to re-energise the blade tip-to-casing leakage vortex to prevent it from breaking down.

Acoustic Implications

The analysis of helicity contours, leakage vortex trajectories, rotational and turbulent kinetic energy contours provides an insight into the impact of the fitted blade-tip end-plates. The acoustic implications of this impact are linked to each end-plate's role as a mixing enhancement device. By acting as mixing enhancers, the end-plates modify both low and high frequency components which then changes both tonal and broadband acoustic emissions.

We may assess the effectiveness of the studied blade-tip end-plates as mixing enhancement devices by studying iso-surfaces of turbulence intensity. We present turbulent kinetic energy iso-surfaces for two turbulence intensities, 0.3 and 0.6 through the fan *datum* AC90/6, AC90/6/TF and AC90/6/TF$_{VTE}$, Figure 8.7. The fan *datum* AC90/6 occurs with a turbulence intensity of 0.6 concentrated over the blade tip that is present from approximately 25 per cent blade chord to the blade trailing edge. We may associate the blade tip-to-casing leakage vortex with a turbulence intensity of 0.3. When we compare the iso-surfaces of turbulence intensity for the fan *datum* AC90/6 with those of fan AC90/6/TF or AC90/6/TF$_{VTE}$, it is apparent that both occur with peak turbulence intensity near the blade leading edge. The blade tip-to-casing leakage vortex originates near the blade leading edge. Like the fan *datum* AC90/6, a lower turbulence intensity of 0.3 characterises the vortex core trajectories. However, in contrast to the fan *datum* AC90/6, the 0.3 iso-surfaces of turbulence intensity are significantly larger.

We may complement our analysis of turbulence intensity with a study of iso-surfaces of turbulence viscosity. We present iso-surfaces of turbulence viscosity for two normalised turbulence viscosities, 100 and 50, Figure 8.8. The blade-tip end-plates fitted to both the fans AC90/6/TF and AC90/6/TF$_{VTE}$ result in higher levels of turbulence viscosity in the blade tip region when compared to the fan *datum* AC90/6. This indicates that the constant and variable thickness blade-tip end-plates enhance mixing in the blade tip region. They are effective as they enhance the turbulent diffusion within the blade tip-to-casing leakage vortices.

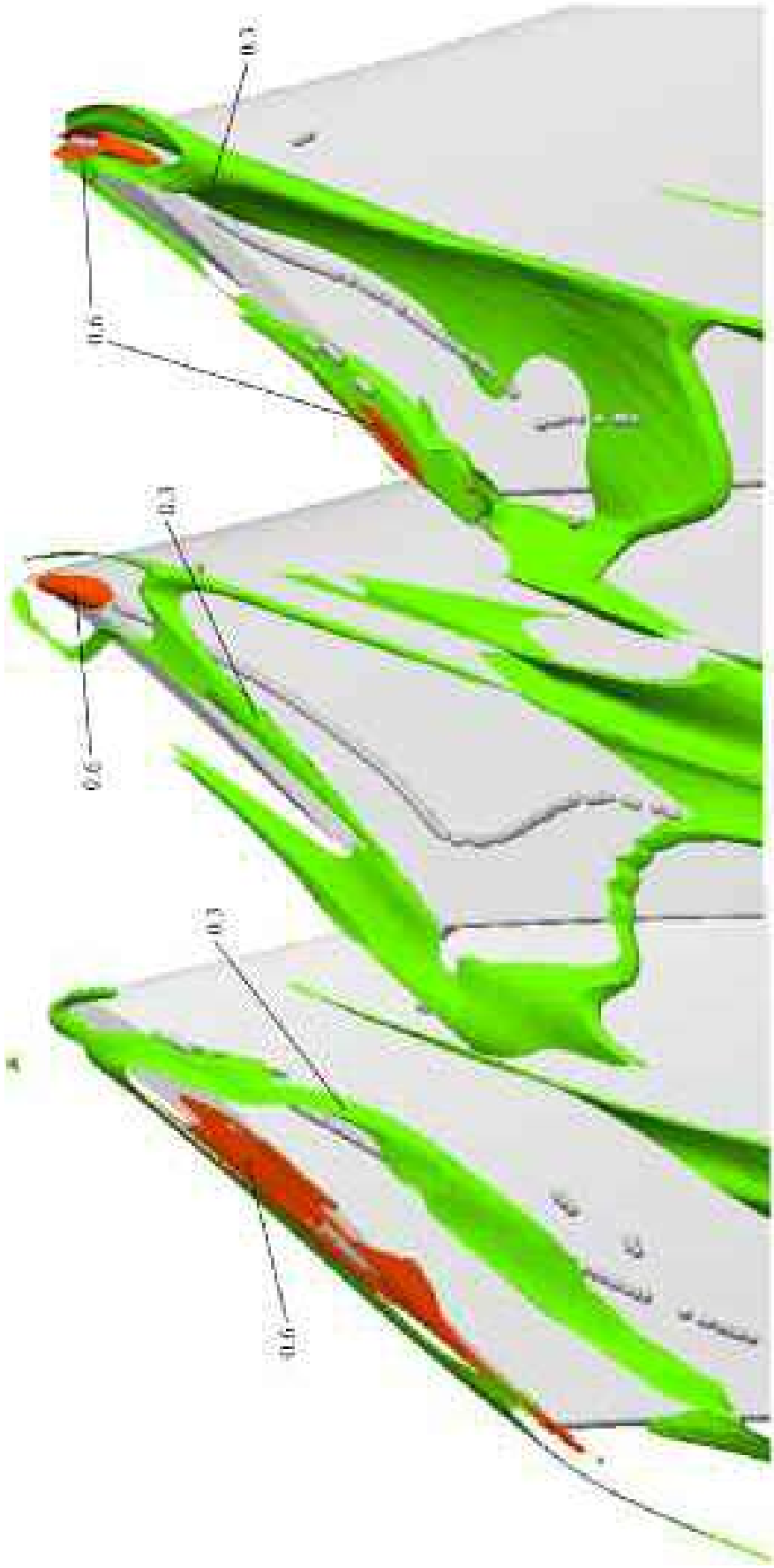

FIGURE 8.7. Three-dimensional turbulence intensity iso-surfaces numerically predicted at the fan design operating point. Turbulence intensity iso-surfaces are presented for two turbulence intensities, 0.3 and 0.6 through the fan *datum* AC90/6, AC90/6/TF and AC90/6/TF_{VTE}.

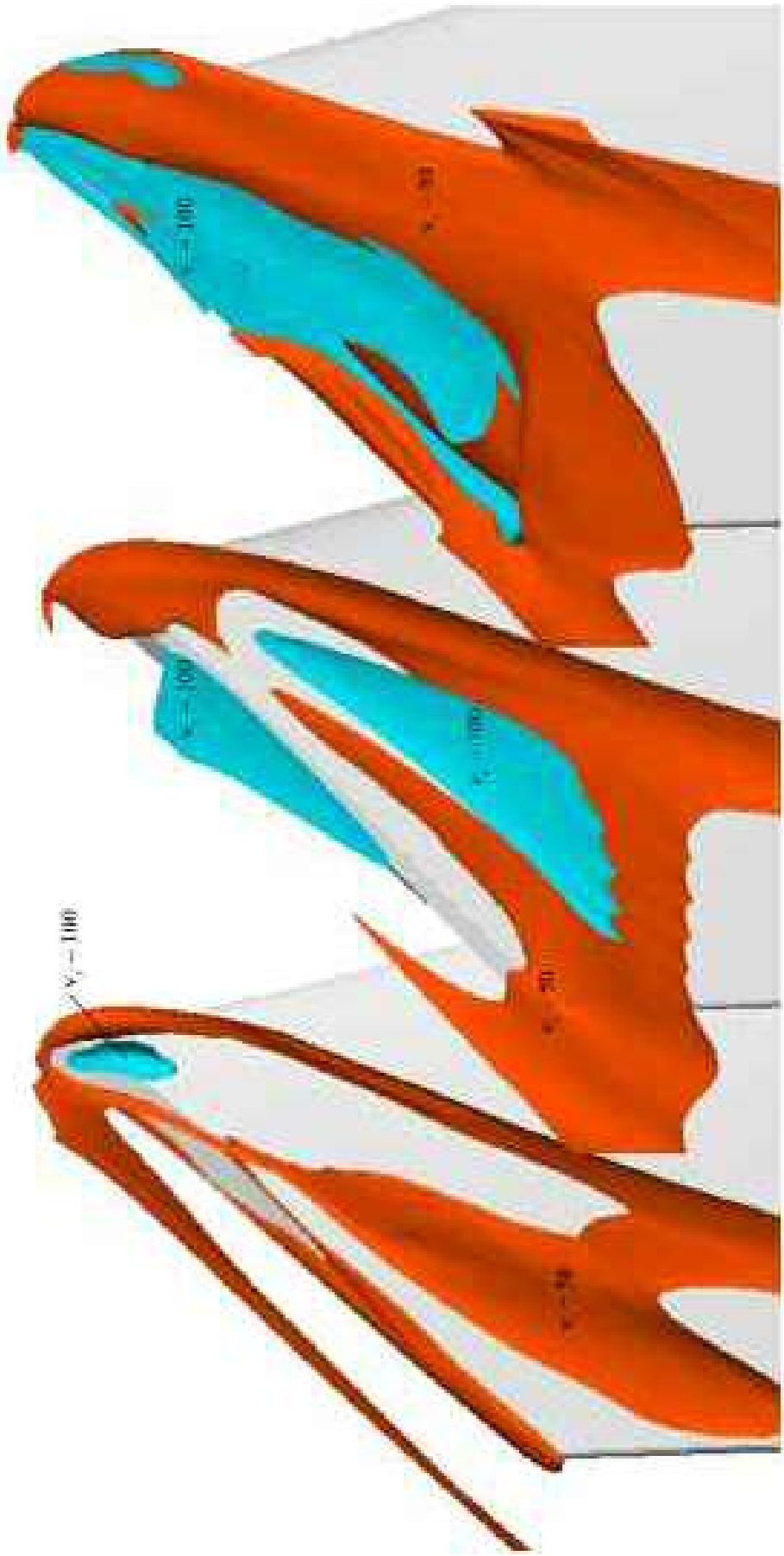

FIGURE 8.8. Three-dimensional normalised turbulence viscosity (ν_t) iso-surfaces numerically predicted at the fan design operating point. Normalised turbulence viscosity iso-surfaces are presented for two normalised turbulence viscosities, 100 and 50 through the fan *datum* AC90/6, AC90/6/TF and AC90/6/TF_{VTE}. The blade-tip endplates fitted to both the fans AC90/6/TF and AC90/6/TF_{VTE} result in higher levels of normalised turbulence viscosity in the blade tip region when compared to the fan *datum* AC90/6 indicating enhanced mixing in the blade tip region.

Consider the iso-surfaces of turbulence viscosity for the three studied fans. It is apparent that the fan *datum* AC90/6 is associated with generally lower levels of turbulence viscosity than either the fan AC90/6/TF of AC90/6/TF$_{VTE}$. Further, the iso-surfaces of turbulence viscosity define the extent of the blade tip-to-casing leakage vortex for each of the three studied fans. The extent of the blade tip-to-casing leakage vortex is significantly larger for the fan AC90/6/TF and AC90/6/TF$_{VTE}$ then the fan *datum* AC90/6. This indicates that the constant and variable thickness blade-tip end-plates are responsible for the convection of large scale flow-field fluctuations downstream of the blade trailing edge.

Khourrami and Choudari (2001) studied approaches to reduce rotor tip clearance induced noise in turbofan engines. They noted that broadband noise could be primarily related to the acoustic emissions from the blade tip-to-casing leakage vortex. Once formed, the leakage vortex is responsible for the convection of large scale flow-field fluctuations downstream of the blade trailing edge. These fluctuations are then responsible for scattering the fan's broadband acoustic emissions.

We completed our analysis by considering helicity over the entire blade span. We present iso-surfaces of helicity over two iso-surfaces, Figure 8.9. Iso-surface one has a helicity of 1.0 and iso-surface 2 has a helicity of –1.0. This span-wise presentation of helicity facilitates an insight into the impact of the constant and variable thickness blade-tip end-plates of the entire blade-to-blade flow-field. Perhaps most surprising is that both blade-tip end-plates have a significant effect in the blade hub region. A hub secondary flow with a helicity of –1.0 characterises the fan *datum* AC90/6. This secondary flow feature is not evident in the iso-surfaces of helicity for either the fan AC90/6/TF or AC90/6/TF$_{VTE}$. Therefore, we conclude that the application of blade-tip end-plates has a positive effect over the enter blade span, specifically reducing the magnitude hub separated flow regions.

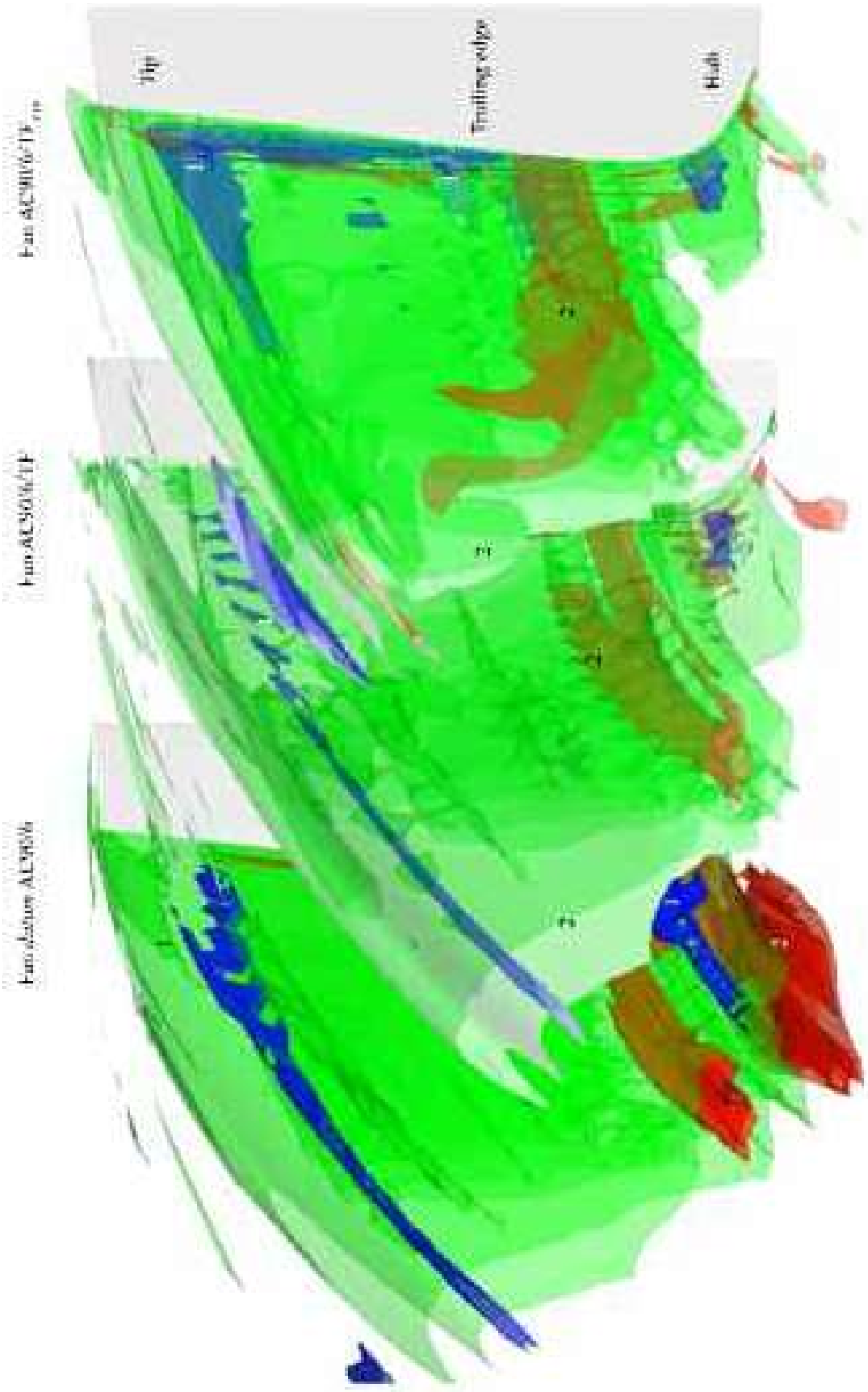

FIGURE 8.9. Three-dimensional helicity (H_n) iso-surfaces numerically predicted at the fan design operating point. Helicity is presented over two iso-surfaces. Iso-surface 1 has a helicity of 1.0 and iso-surface 2 has a helicity of −1.0. The iso-surfaces are shown over three blades, one from each of the studied fans: *datum* AC90/6, AC90/6/TF and AC90/6/TF$_{VTE}$.

CONCLUSIONS

In this chapter we presented a computational analysis of the blade-to-blade flow-field for the studied fan both without a blade-tip end-plate, fan *datum* AC90/6, and with a constant thickness blade-tip end-plate, fan AC90/6/TF and with a variable thickness blade-tip end-plate, fan AC90/6/TF_{VTE}. We undertook the computational analysis using a Reynolds-Averaged Navier–Stokes (RANS) simulation with a non-linear k-ε turbulence model in low-Reynolds number formulation. The purpose of the computational analysis was to establish the effectiveness of the blade-tip end-plate design methodology that we used to design the variable thickness blade-tip end-plate.

The computational analysis indicated that the variable thickness blade-tip end-plate design successfully avoided blade-tip leakage vortex bursting. Assessing aerodynamic performance demonstrated an improved pressure developing capability and fan efficiency that we may attribute to the blade-tip leakage vortex not bursting. However, noise measurements indicated that the variable thickness blade-tip end-plate resulted in an overall broadband noise level approximately 0.5 dB higher than that occurring with the constant thickness end-plate.

We used the computational analysis to calculate the blade-tip leakage flow's helicity. In this context, we define helicity as the projection of vorticity along the local relative velocity vector. Helicity is a useful parameter as it provides an insight into the criteria needed for vortex bursting. When we studied the helicity contours, we found that the variable thickness end-plate induced the presence of multiple organised vortical structures. These vortical structures did burst, with the breakdown acoustically productive enough to result in increased overall fan far-field noise.

Despite the variable thickness end-plate successfully preventing the blade-tip leakage vortex bursting, we conclude that the breakdown of other organised vortical structures is responsible for the increased broadband noise. This increase occurs in spite of the blade-tip leakage vortex not bursting, a result that supports the existence of a strong linkage between bursting coherent swirling structures and fan far-field noise. Therefore, the blade-tip end-plate design methodology was effective, in that it avoided bursting the blade-tip leakage vortex, but was not effective at reducing overall fan far-field noise.

REFERENCES

ISO 5801:2007 (2007), *Industrial Fans: Performance Testing Using Standardised Airways.*

Bae, J.W., Breuer, K.S. and Tan, C.S. (2005), 'Active Control of Tip Clearance Flow in Axial Compressors', *Transactions of the ASME, Journal of Turbomachinery*, vol. 127, pp. 352–362.

Belady, C.L. (2004), 'Winglet-Enhanced Fan', Patent No. US 6,776,578 B2, 17 August.

Bianchi, S., Corsini, A., Rispoli, F. and Sheard, A.G. (2011), 'Far-field Radiation of Tip Aerodynamic Sound Sources in Axial Fans Fitted with Passive Noise Control Features', *Transactions of the ASME, Journal of Vibration & Acoustics*, vol. 133, paper no. 051001, pp. 1–11.

Bianchi, S., Corsini, A. and Sheard, A.G. (2014), 'A Critical Review of Passive Noise Control Techniques in Industrial Fans', *Transactions of the ASME, Journal of Engineering for Gas Turbines & Power*, vol. 136(4), paper no. 044001, pp. 1–10.

Booth, T.C., Hepworth, H.K. and Dodge, P.R. (1982), 'Rotor-tip Leakage: Part I—Basic Methodology', *Transactions of the ASME, Journal of Engineering for Gas Turbines and Power*, vol. 104(1), pp. 154–161.

Borello, D., Borrelli, P., Quagliata, E. and Rispoli, F. (2001), 'A Multi-grid Additive and Distributive Parallel Algorithm for FEM Turbomachinery CFD', *Proceedings of the European Congress on Computational Methods in Applied Sciences (ECCOMAS CFD 2001)*, Swansea, UK, 4–7 September.

Borello, D., Corsini, A. and Rispoli, F. (2003), 'A Finite Element Overlapping Scheme for Turbomachinery Flows on Parallel Platforms', *Computers and Fluids*, vol. 3, pp. 1017–1047.

Corsini, A. and Rispoli, F. (2004), 'Using Sweep to Extend Stall-free Operational Range in Axial Fan Rotors', *Proceedings of the IMechE Part A, Journal of Power and Energy*, vol. 218, pp. 129–139.

Corsini, A. and Rispoli, F. (2005), 'Flow Analyses in a High-pressure Axial Ventilation Fan with a Non-linear Eddy-viscosity Closure', *International Journal of Heat and Fluid Flow*, vol. 26, pp. 349–361.

Corsini, A. and Sheard, A.G. (2007), 'Tip End-plate Concept Based on Leakage Vortex Rotation Number Control', *Journal of Computational and Applied Mechanics*, vol. 8, pp. 21–37.

Corsini, A., Rispoli, F. and Santoriello, A. (2004a), 'A New Stabilized Finite Element Method for Advection-Diffusion-Reaction Equations using Quadratic Elements', in Vad, J., Lajos, T. and Schilling, R. (Eds), *Modelling Fluid Flow: The State of the Art*, Springer-Verlag, Berlin, Germany.

Corsini, A., Rispoli, F., Sheard, A.G. and Kinghorn, I.R. (2004b), 'The Aerodynamic Interaction of Tip Leakage and Mainstream Flows in a Fully Ducted Axial Fan', *Proceedings of the 49th American Society of Mechanical Engineers Gas Turbine and Aeroengine Congress*, Vienna, Austria, 14–17 June, paper no. GT2004-53408.

Corsini, A., Rispoli, F., Sheard, A.G. and Kinghorn, I.R. (2006), 'Investigation of Improved Blade-tip Concept for Axial Flow Fan', *Proceedings of the 51st American Society of Mechanical Engineers Gas Turbine and Aeroengine Congress*, Barcelona, Spain, 8–11 May, paper no. GT2006-90592.

Craft, T.J., Launder, B.E. and Suga, K. (1996), 'Development and Application of a Cubic Eddy-viscosity Model of Turbulence', *International Journal of Heat and Fluid Flow*, vol. 17, pp. 108–155.

Fukano, T. and Jang, C. (2004), 'Tip Clearance Noise of Axial Flow Fans Operating at Design and Off-design Condition', *Journal of Sound and Vibration*, vol. 275, pp. 1027–1050.

Fukano, T. and Takamatsu, Y. (1986), 'The Effects of Tip Clearance on the Noise of Low-pressure Axial and Mixed Flow Fans', *Journal of Sound and Vibration*, vol. 105, pp. 291–308.

Furukawa, M., Inoue, M., Saiki, K. and Yamada, K. (1999), 'The Role of the Tip Leakage Vortex Breakdown in Compressor Rotor Aerodynamics', *Transactions of the ASME, Journal of Turbomachinery*, vol. 121, pp. 469–480.

Garg, A.K. and Leibovich, S. (1979), 'Spectral Characteristics of Vortex Breakdown Flowfields', *Physics of Fluids*, vol. 22(11), pp. 2053–2064.

Gbadebo, S.A., Cumpsty, N.A. and Hynes, T.P. (2006), 'Interaction of Tip Clearance Flow and Three-dimensional Separations in Axial Compressors', *Proceedings of the 51st American Society of Mechanical Engineers Gas Turbine and Aeroengine Congress*, Barcelona, Spain, 8–11 May, paper no. GT2006-90071.

Holste, F. and Neise, W. (1997), 'Noise Source Identification in a Prop Fan Model by Means of Acoustical Near Field Measurements', *Journal of Sound and Vibration*, vol. 203, pp. 641–665.

Inoue, M. and Furukawa, M. (2002), 'Physics of Tip Clearance Flow in Turbomachinery', *Proceedings of the ASME2002 Joint US – European Fluids Engineering Division Conference*, Montreal, Quebec, Canada, 14–18 July, paper no. FEDSM2002-31184, pp. 777–789.

Inoue, M., Kuroumaru, M. and Furukawa, M. (1986), 'Behavior of Tip Leakage Flow Behind an Axial Compressor Rotor', *Transactions of the ASME, Journal of Engineering for Gas Turbines and Power*, vol. 108, pp. 7–14.

Ito, T., Suematsu, Y. and Hayase, T. (1985), 'On the Vortex Breakdown Phenomena in a Swirling Pipe-flow', *Memoirs of the Faculty of Engineering, Nagoya University*, vol. 37, pp. 117–172.

Jang, C.M., Fukano, T. and Furukawa, M. (2003), 'Effects of the Tip Clearance on Vortical Flow and its Relation to Noise in an Axial Flow Fan', *JSME Transaction Series B*, vol. 46(3), pp. 356–365.

Jensen, C.E. (1986), 'Axial-flow Fan', Patent No. US 4,630,993, 23 December.

Khourrami, M.R. and Choudari, M. (2001), 'A Novel Approach for Reducing Rotor Tip-clearance Induced Noise in Turbofan Engines', *Proceedings of the 7th AIAA/CEAS Aeroacoustics Conference*, Maastricht, The Netherlands, 28–30 May, paper no. AIAA 2001-2148.

Longet, C.M.L. (2003), 'Axial Flow Fan with Noise Reducing Means', Patent No. US 2003/0123987 A1, 3 July.

Mimura, M. (2003), 'Axial Flow Fan', Patent No. US 6,648,598 B2, 18 November.

Quinlan, D.A. and Bent, P.H. (1998), 'High Frequency Noise Generation in Small Axial Flow Fans', *Journal of Sound and Vibration*, vol. 218, pp. 177–204.

Roy, B., Chouhan, M. and Kaundinya, K.V. (2005), 'Experimental Study of Boundary Layer Control Through Tip Injection on Straight and Swept Compressor Blades', *Proceedings of the 50th American Society of Mechanical Engineers Gas Turbine and Aeroengine Congress*, Reno, NV, USA, 6–9 June, paper no. GT2005-68304.

Smith, G.D.J. and Cumpsty, N.A. (1984), 'Flow Phenomena in Compressor Casing Treatment', *Transactions of the ASME, Journal of Engineering for Gas Turbines and Power*, vol. 106, pp. 532–541.

Spall, R.E., Gatski, T.B. and Grosch, C.E. (1987), 'A Criterion for Vortex Breakdown', *Physics of Fluids*, vol. 30, pp. 3434–3440.

Storer, J.A. and Cumpsty, N.A. (1991), 'Tip Leakage Flow in Axial Compressors', *Transactions of the ASME, Journal of Turbomachinery*, vol. 113, pp. 252–259.

Takata, H. and Tsukuda, Y. (1977), 'Stall Margin Improvement by Casing Treatment – Its Mechanism and Effectiveness', *Transactions of the ASME, Journal of Engineering and Power*, vol. 99, pp. 121–133.

Thompson, D.W., King, P.I. and Rabe, D.C. (1998), 'Experimental and Computational Investigation on Stepped Tip Gap Effects on the Flowfield of a Transonic Axial-flow Com-

pressor Rotor', *Transactions of the ASME, Journal of Turbomachinery*, vol. 120, pp. 477–486.

Uchida, S., Nakamura, Y. and Ohsawa, M. (1985), 'Experiments on the Axisymmetric Vortex Breakdown in a Swirling Air Flow', *Transactions of the Japan Society for Aeronautical Space Sciences*, vol. 27, pp. 206–216.

Uselton, R.B., Cook, L.J. and Wright, T. (2008), 'Fan with Reduced Noise Generation', Patent No. US 7,351,041 B2, 1 April.

Vad, J., Koscso, G., Gutermuth, M., Kasza, Z., Tabi, T. and Csorgo, T. (2006), 'Study of the Aeroacoustic and Aerodynamic Effects of Soft Coating upon Airfoil', *JSME International Journal Series C Mechanical Systems, Machine Elements and Manufacturing*, vol. 49(3), pp. 648–656.

Wadia, A.R., Szucs, P.N. and Crall, D.W. (1998), 'Inner Workings of Aerodynamic Sweep', *Transactions of the ASME, Journal of Turbomachinery*, vol. 120(4), pp. 671–682.

Wadia, R.A. and Booth, T.C. (1982), 'Rotor-tip Leakage: Part II—Design Optimization Through Viscous Analysis and Experiment', *Transactions of the ASME, Journal of Engineering for Gas Turbines and Power*, vol. 104(1), pp. 162–169.

Chapter 9

Shaping of Tip End-plate to Control Leakage Vortex Swirl in Axial Flow Fans

A. Corsini, F. Rispoli and A.G. Sheard

ABSTRACT

The chapter builds on the computational analysis presented in Chapter 8, studying flow-field features in the blade tip region induced by the presence of blade-tip end-plates. We predicted the blade-to-blade flow-field for a *datum* fan AC90/6 without blade-tip end-plates, and two fan variants with different end-plate geometries. The fan AC90/6/TF incorporated a constant thickness end-plate and the fan AC90/6/TF$_{VTE}$ incorporated a variable thickness end-plate. The variable thickness blade-tip end-plate design was successful in that it avoided the breakdown of the blade tip-to-casing leakage vortex. Additionally, fan pressure developing capability and efficiency were improved. However, overall fan far-field noise increased slightly. An analysis of the flow-field's evolution in the blade tip region indicated that by avoiding leakage vortex breakdown, the variable thickness end-plate occurred with lower losses, explaining the improvement in fan pressure developing capability and efficiency. However, a redistributed flow in the blade tip region resulted in creating multiple organised vortical structures that are acoustically productive. We studied the blade-tip flow-field by conducting a computational analysis using a Reynolds-Averaged Navier–Stokes (RANS) simulation with a non-linear k-ε turbulence model in low-Reynolds number formulation. Although well proven, the simulation was not able to model unsteady effects and therefore is inherently limited as it models only part of the flow-field physics. Despite the limitation of the adopted computational approach, the resulting blade-to-blade flow-field prediction provided a useful insight into the flow-field physics. A realisation that organised vortical structures were acoustically productive resulted in recognising that the blade-tip end-plate required redesign. The redesigned blade-tip end-plate must still minimise the blade tip-to-casing leakage vortex's intensity whilst ensuring that it does not burst. It must also avoid generating organised vortical structures.

This chapter is a revised and extended version of Corsini, A., Rispoli, F. and Sheard, A.G. (2010), 'Shaping of Tip End-plate to Control Leakage Vortex Swirl in Axial Flow Fans', *Transactions of the ASME, Journal of Turbomachinery*, vol. 132, paper no. 031005, pp. 1–9.

NOMENCLATURE

Latin letters

D	near-design condition
D_h	hub diameter
D_c	casing diameter
f_f	friction factor
H_n	normalised helicity
k	turbulent kinetic energy
ℓ	blade chord
l_ε	turbulence length scale
Δp_{stat}	static pressure [Pa]
p_t	total pressure
P	near-peak pressure condition
Ro	Rossby number
Re_{gap}	leakage-flow Reynolds number
r_v	radial distance from the vortex axis
V_a	axial velocity at r
s_c	chord wide position
SWL	sound power level
t	blade pitch
t_{ep}	end-plate thickness distribution
TLV	tip leakage vortex
v, w	absolute and relative velocities
w_{Ln}	leakage-flow bulk velocity

Greek letters

β_{LV}	leakage-flow skewing angle
ζ	total loss coefficient
η	efficiency
σ_h	hub-to-casing diameter ratio
ξ_i	vorticity vector
φ_a	axial flow coefficient
φ_r	radial flow coefficient
ψ	swirl flow coefficient
τ	rotor tip clearance
τ_{gap}	gap height

Subscripts and superscripts

a, p, r	axial, peripheral and radial
c	casing wall
h	hub wall
i	Cartesian component index
in	inlet section
mol	molecular quantity
s	streamwise component
$\bar{}$	pitch-averaged value
0	total quantities

INTRODUCTION

Three mechanisms dominate the flow-field physics in an axial fan or compressor's blade-tip region. First, there is the non-linear interaction of blade tip-to-casing leakage flow features. Second, there is interaction of skewed end-wall boundary layer flow features with the leakage flow. Third, there is interaction of blade passage secondary flow features with the leakage flow. These three mechanisms result in a complex flow-field in the blade tip region that drives both blade span-wise loading and the blade-to-blade passage loss distribution. This combination of loading and loss distribution ultimately determines both fan and compressors' operating margin and aeroacoustic signature (Fukano *et al.*, 1986; Storer and Cumpsty, 1991; Furukawa *et al.*, 1999).

Ganz *et al.* (1998) studied the mechanisms that govern flow-field physics in the blade tip region and concluded that they apply both to compressors developed for aerospace application and fans developed for air movement application. The reduction in performance that occurs with the presence of these flow-field mechanisms has resulted in both air movement fan and aerospace compressor designers seeking techniques to minimise the adverse effects on operating margin that occurs with blade tip-to-casing leakage flow. Their objective is to manage the blade tip-to-casing leakage flow with the desired outcome a reduction in self-generated noise without sacrificing either operating margin or efficiency. One may achieve this objective either by reducing blade tip-to-casing leakage flow rate or by enhancing primary- to secondary-flow momentum transfer.

In an attempt to improve compressor performance, researchers first experimented with casing treatments in the early 1970s utilising grooves (Takata and Tsukuda, 1977; Smith and Cumpsty, 1984), and more recently stepped gaps in the blade tip region (Thompson *et al.*, 1998). These casing treatments improved the compressors' stable operating range by reducing the intensity of blade tip-to-casing leakage flow. Air movement fan designers have historically favoured a casing treatment comprising an annular ring of recirculating vanes over the blades' leading edge (Karlsson and Holmkvist, 1986). During the past decade, several researchers have proposed passive noise-control concepts based on modifications to the blade tip by means of anti-vortex appendages. Quinlan and Bent (1998) have proposed end-plates, and others have proposed various solutions in patents for air movement fans (Jensen, 1986; Longet, 2003; Mimura, 2003; Uselton *et al.*, 2008).

This chapter presents an analysis of a variable thickness blade-tip end-plate design for application with subsonic axial fan blades. This variable thickness blade-tip end-plate controls the chord-wise evolution of the blade tip-to-casing leakage vortex rotation number (Sheard *et al.*, 2009). Controlling the leakage vortex rotation number is a passive control mechanism that enables a designer to avoid leakage vortex breakdown by controlling the swirling flow in the blade tip region. When controlling the swirling flows in an aircraft wing's tip region (Spall *et al.*, 1987) or a combustor (Escudier, 1987), the proposed design procedure rationale advocates linking blade-tip end-plate geometry and the blade tip-to-casing leakage vortex near-axis swirl to

control the leakage vortex in order to avoid it bursting (Jones *et al.*, 2001; Herrada and Shtern, 2003). One implements this noise-by-flow control design procedure by reconfiguring the blade-tip end-plate and thus influencing the momentum transfer from the leakage flow. The procedure also forces some waviness in the leakage vortex trajectory, as in delta-wing platforms (Srigrarom and Kurosaka, 2000).

FAMILY OF FANS UNDER INVESTIGATION

We conducted the reported research on a family of commercially available cooling fans. The studied fan configuration, coded AC90/6, incorporates a six-blade unswept rotor, with modified ARA-D profile aerofoil blades, Table 9.1. One may set the blade-pitch angle during final assembly to customise the fan to a desired duty point. We used a direct coupled-induction 400-volt (AC), 3-phase motor to drive the rotor at a constant speed of 950 rpm, resulting in a 44.7 m/s blade tip speed and a 95 Hz blade-passing frequency (BPF). In its original embodiment, the studied fan AC90/6 did not include a blade tip end-plate, therefore we used it as a *datum* against which to assess the performance of fan variants with blade-tip end-plates. In the reported research we refer to the fan without blade-tip end-plates as the fan *datum* AC90/6.

In addition to the fan *datum* AC90/6, we studied a fan variant fitted with a constant thickness blade-tip end-plate that we named AC90/6/TF, Figure 9.1. Designs developed for tip-vortex control and drag reduction in aircraft wings and catamaran hulls inspired the constant thickness blade-tip end-plate design, which ran along the blade pressure surface, ending at the blade trailing edge with a square tail. The addition of this constant thickness blade-tip end-plate resulted in the thickness of the fan AC90/6/TF blade tip increasing by a factor of three compared to the fan *datum* AC90/6. We considered the blade-tip end-plate size for axial compressor blades using Inoue *et al.*'s (1986) research. They estimated that the optimum blade-tip end-plate

Table 9.1. *The fan* datum *AC90/6 blade geometry and rotor specification.*

	Fan *datum* AC90/6		
Blade geometry	Hub	Mid-span	Tip
Pitch angle (°)	36	58.8	28
Camber angle (°)	46	44	41
Solidity	1.24	0.86	0.30
Fan rotor			
Blade number		6	
Blade tip pitch angle (°)		16–28	
Blade tip stagger angle (°)		74–62	
Hub-to-casing diameter ratio σ		0.22	
Tip diameter (mm)		900.0	
Rotor tip clearance τ (% span)		1.0	
Rated rotational frequency (r/min)		935–950	

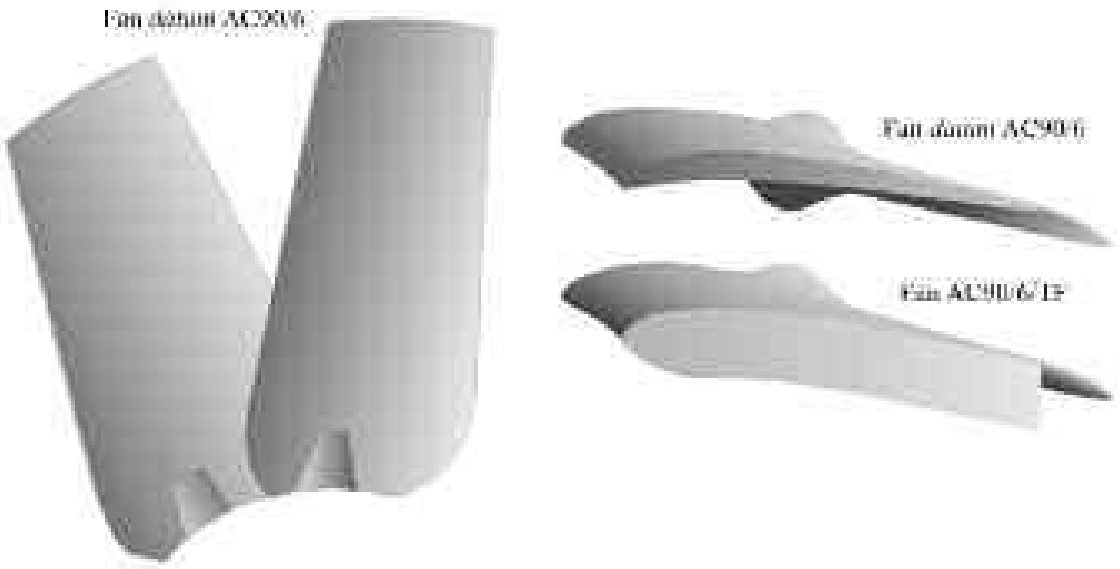

FIGURE 9.1. The studied fan *datum* AC90/6 without a fitted blade-tip end-plate and with a constant thickness blade-tip end-plate, AC90/6/TF.

size was between 10 and 20 per cent blade span. In practice, we were able to manufacture blades with a blade-tip end-plate size five per cent of blade span. The fan blades were manufactured from injection moulded plastic, with the blade-tip end-plate size serving as the largest the blade manufacturing technique could produce.

Flow Conditions

The studied fan blade tip pitch angle is adjustable and may be set to a pitch angle between 16 and 28 degrees. In practical application the blade tip pitch angle is typically set to 28 degrees as this maximises flow rate for a given system pressure. In the research reported in this chapter, we conducted the experimental measurements with the fan blade tip pitch angle set to 28 degrees. We selected 28 degrees both because it is typical of the angle that one uses in practical application and because it results in the highest blade loading. A highly loaded blade results in the blade tip-to-casing leakage vortex having the most significant effect on both fan aerodynamic and acoustic performance (Holste and Neise, 1997).

The impact of the blade tip-to-casing leakage vortex on both fan aerodynamic and acoustic performance results in the application of blade-tip end-plates changing not only the fan's acoustic performance, but also the aerodynamic performance. Consequently, the fan *datum* AC90/6 generates a different pressure at a constant flow rate when fitted with a studied blade-tip end-plate. To facilitate the comparison of fan performance data when fitted with different blade-tip end-plates, we chose to define three operating points, and their respective volume flow rates, Table 9.2. The design operating point volume flow rate is typical of that required when one installs the fan over a cooling unit's tube bank. The peak pressure flow rate is typical of that required

Table 9.2. *The operating points used when characterising the studied fan's performance with and without fitted blade-tip end-plates. The authors measured performance characteristics in a Type C standardised airway (ducted inlet, ducted outlet) in accordance with ISO 5801:2007 requirements (2007).*

Operating point	Volume flow rate (m^3/s)	Studied blade tip pitch angle (°)
Maximum flow	8.0	28
Design	7.0	28
Peak pressure	6.0	28

when the tube bank has become partially blocked following a period of in-service operation. The maximum flow operating point volume flow rate is typical of the flow rate that occurs with the lowest pressure loss tube banks currently operating in service.

Background Investigation

Corsini and Sheard (2007) characterised the chord-wise distribution of blade-tip leakage vortex Rossby number. The Rossby number has a threshold value below which the vortex rotation cannot reduce if the vortex is to remain stable. Corsini and Sheard (2007) concluded that for the fan *datum* AC90/6, the blade-tip leakage vortex Rossby number remained above the threshold value and did not burst. However, the fan AC90/6/TF blade-tip leakage vortex Rossby number fell below the threshold value at approximately 90 per cent chord and did burst. Although vortex bursting is acoustically productive, the fan AC90/6/TF was both more efficient and exhibited a lower far-field noise level than the fan *datum* AC90/6, Table 9.3. This improvement was evident at both the studied fan's design and peak pressure operating point.

Vortex bursting is acoustically productive and the addition of a constant thickness blade-tip end-plate resulted in the leakage vortex bursting. As such, we might reasonably have expected the fan AC90/6/TF to have exhibited a higher far-field noise level than the fan *datum* AC90/6. However, the fan AC90/6/TF far-field noise levels were lower than the fan *datum* AC90/6 noise levels. Insight into the reasons why required an insight into the flow-field's nature in the blade tip region. The complexity of the blade tip flow-field made an experimental evaluation challenging, and therefore we opted to undertake a numerical simulation of the blade-to-blade flow-field for both fan *datum* AC90/6 and fan AC90/6/TF.

NUMERICAL PROCEDURE AND AXIAL FAN MODELLING

In the programme of work reported in this chapter, we simulated the blade-to-blade flow-field with a Reynolds-Averaged Navier–Stokes (RANS) based non-linear code, with a two-equation closure (Craft *et al.*, 1996). The two-equation closure was able to cope with non-isotropic and non-equilibrium turbulence effects without a significant increase in the required computational effort. The code utilised a parallel

Table 9.3. *Experimentally measured fan aerodynamic and acoustic performance for the fan* datum *AC90/6 and AC90/6/TF at both the design and peak pressure operating points (Corsini* et al.*, 2006).*

Operating point	*datum* AC90/6		AC90/6/TF	
	Δp_{stat} (Pa)	η (%)	Δp_{stat} (Pa)	η (%)
Design	134.8	49.0	126.2	51.0
Peak pressure	184.4	44.0	179.4	49.0
	Unweighted SWL (dB)	A-weighted SWL (dB(A))	Unweighted SWL (dB)	A-weighted SWL (dB(A))
Design	72.4	70.8	70.2	66.9
Peak pressure	72.7	71.8	69.7	67.4

multi-grid (MG) numerical scheme, developed for an in-house finite element method (FEM) code which Borello *et al.* (2003) first proposed. Corsini and Sheard (2007) applied Borello *et al.*'s (2003) numerical procedure to the study of blade-tip end-plates with Corsini *et al.* (2007) refining the procedure. It is Corsini *et al.*'s (2007) numerical procedure that that we have used during the course of the research reported in this chapter.

The finite element method formulation is based on a stabilised Petrov-Galerkin (PG) method modified for application to three-dimensional equal- and mixed-order spaces of approximation. We used the Petrov-Galerkin scheme to control the instability that affects the advective-diffusive incompressible flow, and the momentum's reaction and turbulent scale equations. The turbulent scale equations relate to Coriolis acceleration, Corsini *et al.* (2004a). We used equal-order Q1-Q1 and mixed-order Q2-Q1 interpolation for primary turbulent scale equations and constrained secondary variables, implicitly eliminating the undesirable pressure-checker boarding effects. We performed the computational analysis using a hybrid full linear multi-grid accelerator running on an overlapping parallel solver (Borello *et al.*, 2001).

In our Reynolds-Averaged Navier–Stokes simulation, we utilised a non-linear k-ε turbulence model in its topology-free low-Reynolds number formulation (Craft *et al.*, 1996). Although a well proven approach for modelling vortex structures (Inoue and Furukawa, 2002), the simulation was not able to model unsteady effects and therefore models only part of the flow-field physics. Despite this caveat, Corsini and Rispoli (2004) were able to validate the modelling approach when they applied it to a compressor application. Corsini and Rispoli (2004) were also able to validate the modelling approach in an air movement fan application.

Computational Mesh and Boundary Conditions

The approach we adopted when constructing a computational mesh utilised a non-orthogonal body fitted H-type grid system. We split the mesh into two regions,

one in the blade-to-blade region and a second in the blade tip-to-casing gap. In total, the mesh comprised $154 \times 68 \times 58$ nodes in the axial-, pitch- and span-wise directions. In the axial direction, 20 per cent of the nodes were distributed upstream of the blade leading edge, 50 per cent were within the blade passage and 30 per cent were downstream of the blade trailing edge. In the span-wise direction, 14 of the 58 nodes were spaced across the blade tip-to-casing gap. All mesh density regions maintained an adequate computational cell aspect ratio toward solid boundaries.

We defined the boundary conditions according to Corsini and Rispoli (2004) and Corsini *et al.*'s (2004b) recommendations regarding ducted high-solidity fan performance. The Dirichlet conditions for the relative velocity components are imposed at the inflow section, half a mid-span chord upstream of the leading edge, as obtained from a flow simulation in an annular passage of identical hub-to-casing diameter ratio that includes an upstream spinner cone.

We used a turbulent kinetic energy (k) pitch-wise profile derived from an axisymmetric turbulence intensity profile previously developed by Corsini and Rispoli (2004). The turbulence intensity profile was a near-uniform six per cent across the annulus, increasing to ten per cent near the casing. We used the turbulent kinetic energy's pitch-wise profile to calculate the radial distribution of dissipation based on a dissipation length scale (l_e) of one per cent of blade mid-span pitch. We completed the boundary conditions by assuming periodicity both up- and down-stream of the fan blades.

Leakage Vortex Breakdown

Using the above numerical procedure Corsini and Sheard (2007) predicted the fan AC90/6/TF blade-to-blade flow-field, focusing on the flow-field through the blade tip-to-casing gap. They visualised vortex bursting via a study of three-dimensional streamlines through the blade tip-to-casing gap. The streamlines illustrated development of the leakage vortex, and specifically the chord-wise position at which vortex breakdown commences. Corsini and Sheard (2007) concluded that the streamlines indicated that the blade-tip end-plate obstructs blade pressure-surface flow migrations through the blade tip-to-casing gap. This obstruction resulted in a *vena contracta* effect that resulted in the blade-tip end-plate inducing an anti-vortex effect in blade tip-to-casing clearance flow. The fan AC90/6/TF leakage vortex streamlines illustrated that the reduced blade tip-to-casing gap leakage flow rate influenced the swirl-to-axial velocity ratio. At approximately mid-blade chord, this change in swirl-to-axial velocity ratio resulted in a bubble type unseparated vortex core developing. As this unseparated vortex core moved towards the blade trailing edge, it went on to separate from the blade surface.

Corsini and Sheard (2007) concluded that the streamlines towards the blade trailing edge were indicative of a reduced blade tip-to-casing gap leakage flow rate. This reduction altered the swirl-to-axial velocity ratio and this change resulted in the bubble type unseparated vortex core first developing and then going on to separate. This development followed by separation is indicative of blade tip-to-casing leakage vortex breakdown (Lucca-Negro and O'Doherty, 2001). According to Leibovich

(1978), we may conceptualise the bursting of a bubble type vortex core as a consequence of the vortex swirl level. According to both Escudier and Zehnder (1982) and Inoue and Furukawa (2002), we may associate the stability of the bubble form of vortex breakdown with the vortex swirl level. The assertions of Leibovich (1978), Escudier and Zehnder (1982) and Inoue and Furukawa (2002) support Corsini and Sheard's (2007) interpretation of the bubble separation core as evidence of blade tip-to-casing leakage vortex breakdown.

Corsini and Sheard (2007) tested their assertion that the mid-chord bubble-core constitutes the onset of vortex bursting by studying blade tip-to-casing leakage flow axial velocity. They concluded that there was a small zero axial velocity iso-surface at approximately mid-blade chord that is coincident with the unseparated vortex core. Corsini and Sheard (2007) associated this zero axial velocity iso-surface with the onset of vortex breakdown, a conclusion self-consistent with Spall *et al.*'s (1987) conclusions. It was Spall *et al.* (1987) who first identified the presence of a stagnation point along a vortex axis as a necessary pre-condition for breakdown. Towards the blade trailing edge, Corsini and Sheard (2007) identified a larger zero axial velocity iso-surface which they concluded characterised the region over which the blade tip-to-casing leakage vortex was actually breaking down.

Corsini *et al.* (2007) extended Corsini and Sheard's (2007) study using a computational analysis to compute a range of flow-field parameters. They observed that when studying tip-clearance flow-field features, Furukawa *et al.* (1999) and Inoue and Furukawa (2002) studied normalised helicity (H_n). Normalised helicity is a useful parameter as it facilitates visualisation of blade tip-to-casing leakage vortex core trajectories. Furukawa *et al.* (1999) and Inoue and Furukawa (2002) defined normalised helicity as:

$$H_n = (\xi_i \cdot w_i) / (|\xi||w|)$$

in which:

$i = 1 \ldots 3$
ξ_i and w_i are the Cartesian components of the absolute vorticity and relative velocity vectors; and
$|\xi|$ and $|w|$ and are the norms of these vectors.

When plotting the normalised helicity contours on cross sections for the fan *datum* AC90/6 and AC90/6/TF, Corsini *et al.* (2007) plotted the blade tip-to-casing leakage vortex trajectory, Figure 9.2. The blade tip-to-casing leakage vortex is well defined, with the vortex trajectory departing from the blade suction surface as it progresses from blade leading to trailing edge. There is also evidence of a weaker secondary tip-to-casing leakage vortex that appears close to the suction surface 65 per cent blade chord downstream of the blade leading edge. As the two vortex progress towards the blade trailing edge, they merge into the blade tip-to-casing leakage vortex. The result is a well-defined vortex that affects a significant proportion of the blade-to-blade passage in the blade tip region.

Corsini *et al.* (2007) also considered the leakage vortex trajectory for the fan AC90/6/TF, Figure 9.2. As they had previously observed when considering fan *datum* AC90/6, the blade tip-to-casing leakage vortex departs from the suction surface. However, the secondary tip-to-casing leakage vortex is not apparent. If it is present at all it does not merge with the blade tip-to-casing leakage vortex, but simply decays.

VORTEX BREAKDOWN ROSSBY NUMBER ANALYSIS

Scholars have studied vortex breakdown, linear stability, phase velocity and wave tapping (Benjamin, 1962; Leibovich, 1978; Tsai and Widnall, 1980). Their focus has been on identifying a critical condition that is indicative of the onset of vortex breakdown by using vortex swirl based parameters. Leibovich (1978) studied vortex breakdown, conceptualising it as a change in vortex structure initiated by a variation in the ratio of tangential to axial velocity components. Ito *et al.* (1985) conducted a theoretical study of unsteady and steady vortex breakdown and characterised vortex breakdown using the Rossby number. Corsini and Sheard (2007) defined the Rossby number as:

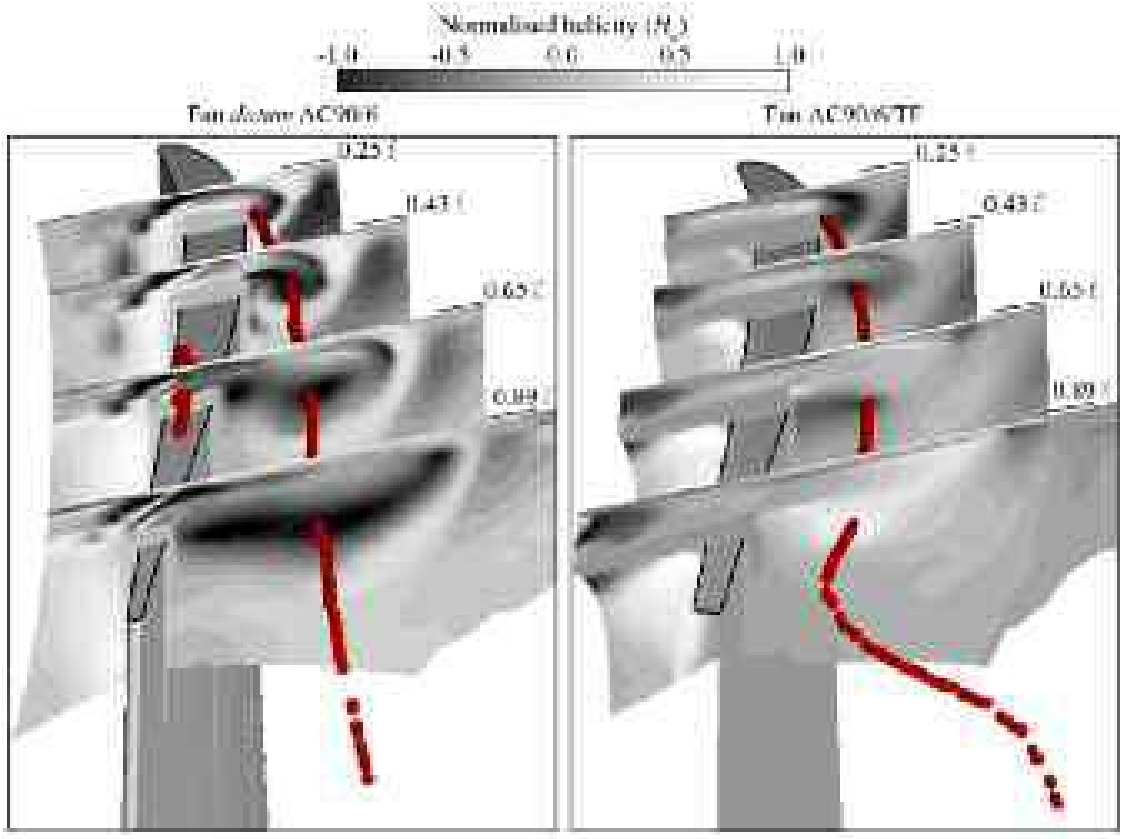

FIGURE 9.2. Three-dimensional normalised helicity (H_n) contours numerically predicted by Corsini *et al.* (2007) at the fan design operating point. Helicity contours are presented at four chord-wise locations through the fan *datum* AC90/6 and AC90/6/TF. The blade tip-to-casing leakage vortex core trajectory illustrates the effect of fitting a constant thickness blade-tip end-plate.

$$Ro = V_a / (r_v \, \Omega) \tag{1}$$

in which:

V_a = velocity;
r_v = length, and
Ω = rotation rate.

Spall *et al.* (1987) extended the work of Ito *et al.* (1985) developing a vortex breakdown criterion based on the Rossby number. Spall *et al.* (1987) proposed scale definitions for the velocity distribution consistent with swirling flows, leading-edge vortices and unconfined wing-tip vortices. Corsini and Sheard (2007) adopted Spall *et al.*'s (1987) approach, adapting it for application to the blade tip-to-casing leakage vortex typical of fan and compressors. Corsini and Sheard (2007) chose to define Spall *et al.*'s (1987) parameters as:

- r_v is the radial distance from the vortex axis at which the swirl velocity is a maximum, corresponding to Leibovich's (1984) characteristic viscous length scale;
- V_a (= w_{aTLV}) is the axial velocity at r_v, and
- Ω is the rotation rate of the blade tip-to-casing leakage vortices that is driven by the vortex's assumed solid-body rotation at the vortex centre.

The choice of axial velocity at the radial distance from the vortex axis at which the swirl velocity is maximum is consistent with the swirl scale $\Omega \, r_v$ (= w_{pTLV}) and the critical Rossby number values reported in the extant literature. Uchida *et al.* (1985) defined a critical Rossby number of 0.64 for confined axi-symmetric vortex breakdown. Garg and Leibovich (1979) defined a critical Rossby number of 0.60 for a wing-tip vortex with bubble- or spiral-type vortex breakdown.

Corsini and Sheard (2007) calculated the chord-wise distribution of the blade tip-to-casing leakage vortex Rossby number for the fan *datum* AC90/6 and AC90/6/TF, Figure 9.3. The fan AC90/6/TF Rossby number fell to a critical value at 50 per cent blade chord. It then goes on to recover, finally falling below the critical value at 75 per cent blade chord. Corsini and Sheard (2007) concluded that they could base blade-tip end-plate geometry modification on the control of the blade tip-to-casing leakage vortex Rossby number. Changes to the blade-tip end-plate geometry result in the enhanced or reduced vortex near-axis swirl that then increases or reduces the Rossby number. Therefore, changing blade-tip end-plate geometry to maintain the Rossby number above a critical value provides a basis upon which to optimise end-plate geometry to avoid vortex bursting.

Blade-tip End-plate Design Concept

The purpose of developing a new blade-tip end-plate design was to avoid blade tip-to-casing leakage vortex bursting. Vortex bursting is acoustically productive, and

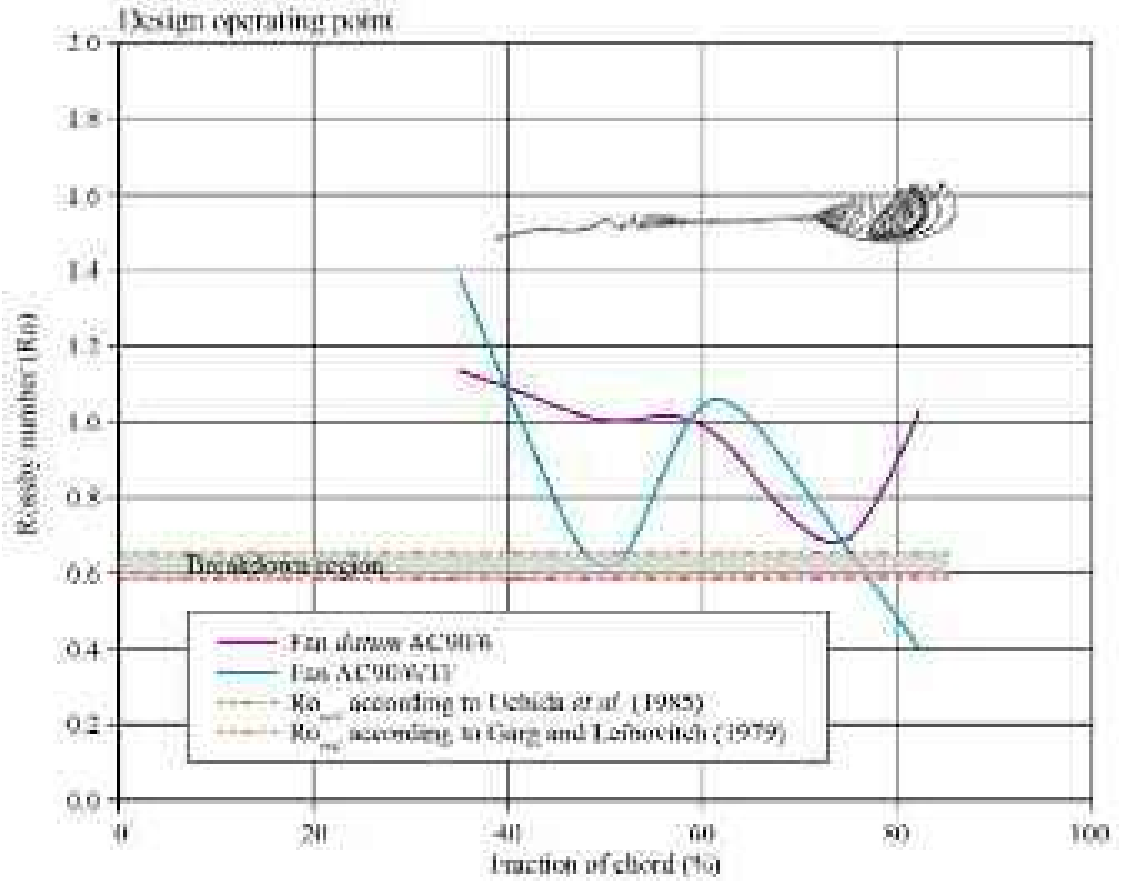

FIGURE 9.3. Chord-wise evolution of numerically predicted blade tip-to-casing leakage vortex Rossby number (*Ro*) for the fan *datum* AC90/6 and AC90/6/TF at their design operating point (Corsini and Sheard, 2007).

therefore if the blade tip-to-casing leakage vortex does not burst, fan far-field noise should reduce. Corsini and Sheard (2007) developed a new blade-tip end-plate design procedure that involved varying only one parameter, blade-tip end-plate thickness along the blade chord, with the objective of maintaining the blade tip-to-casing Rossby number at its critical value to avoid vortex bursting.

Corsini and Sheard's (2007) rationale for varying blade-tip end-plate thickness along the blade chord was that reducing end-plate thickness would enhance near-axis swirl (Jones *et al.*, 2001; Herrada and Shtern, 2003). Near-axis swirl was enhanced as a consequence of influencing momentum transfer from the leakage flow and forcing some waviness into the leakage vortex trajectory (Srigrarom and Kurosaka, 2000). Therefore, the new design procedure required Corsini and Sheard (2007) to calculate the blade-tip end-plate thickness distribution.

Corsini and Sheard (2007) calculated blade-tip end-plate thickness distribution by combining a simplified expression for the blade tip-to-casing gap pressure drop and a stability criterion for the leakage vortex. They defined the stability criterion as a safe chord-wise distribution of the Rossby number. A variable thickness characterised the resulting blade-tip end-plate, and when fitted to the fan *datum* AC90/6, they named it fan AC90/6/TF$_{VTE}$, Figure 9.4.

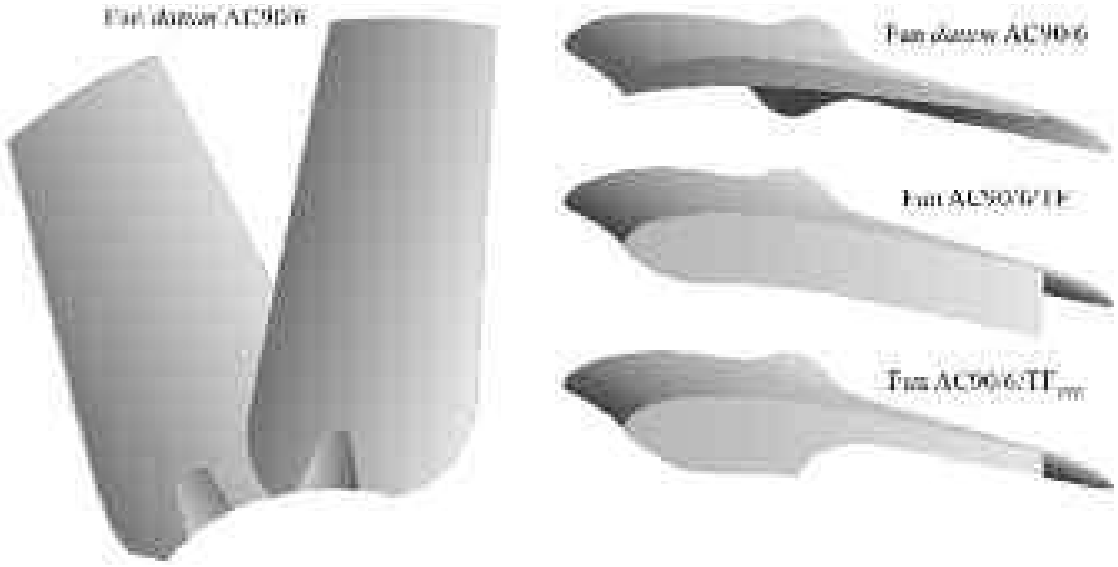

FIGURE 9.4. The studied fan *datum* AC90/6 without a fitted blade-tip end-plate, with a constant thickness blade-tip end-plate, AC90/6/TF and with a variable thickness blade-tip end-plate, AC90/6/TF$_{VTE}$.

THE IMPACT OF BLADE-TIP END-PLATES ON AERODYNAMIC PERFORMANCE

Bianchi *et al.* (2011) measured the A-weighted overall sound power and specific noise level of fan *datum* AC90/6, AC90/6/TF and AC90/6/TF$_{VTE}$. Both fan AC90/6/TF and AC90/6/TF$_{VTE}$ specific noise levels remained lower than that of fan *datum* AC90/6 over the entire fan operating range. However, the fan AC90/6/TF exhibited slightly lower specific noise levels than fan AC90/6/TF$_{VTE}$ at all operating points. This indicated that Corsini and Sheard (2007) had developed a blade-tip end-plate design methodology that actually increased fan far-field noise and was therefore ineffective. Corsini *et al.* (2007) studied the fan *datum* AC90/6, AC90/6/TF and AC90/6/TF$_{VTE}$ attempting to evaluate:

- helicity distributions;
- blade tip-to-casing leakage vortex trajectories;
- rotational and turbulent kinetic energy distributions;
- turbulence intensity distributions; and,
- turbulence viscosity distributions.

Corsini *et al.* (2007) concluded that the variable thickness blade-tip end-plate induced the creation of multiple organised vortical structures. They speculated that these vortical structures did break down, and were acoustically productive enough to result in increased overall fan far-field noise. This increase was in spite of the blade-tip-to-casing leakage vortex not bursting.

The multiple organised vortical structures responsible for the increase in fan AC90/6/TF$_{VTE}$ far-field noise originated in the blade tip-to-casing gap. To better understand why these organised vortical structures are created, we require an insight

into the blade tip-to-casing flow-field physics. Therefore, in the research reported in this chapter, we chose to survey six flow-field parameters:

- leakage flow axial velocity distributions;
- leakage flow skewing angle;
- axial flow coefficient distributions;
- radial flow coefficient distributions;
- swirl coefficient distributions; and,
- total pressure loss coefficient distributions.

Before analysing these flow-field parameters, we calculated the chord-wise distribution of the blade tip-to-casing leakage vortex Rossby number for the fan AC90/6/TF$_{VTE}$, Figure 9.5. Corsini and Sheard (2007) had previously calculated the chord-wise distribution of the blade tip-to-casing leakage vortex Rossby number for the fan AC90/6/TF, Figure 9.3. A comparison of the two provides a context for an analysis of flow-field parameters.

There are significant differences between the chord-wise distributions of blade tip-to-casing leakage vortex Rossby number for the fan AC90/6/TF and AC90/6/TF$_{VTE}$. The variable thickness blade-tip end-plate fitted in fan AC90/6/TF$_{VTE}$

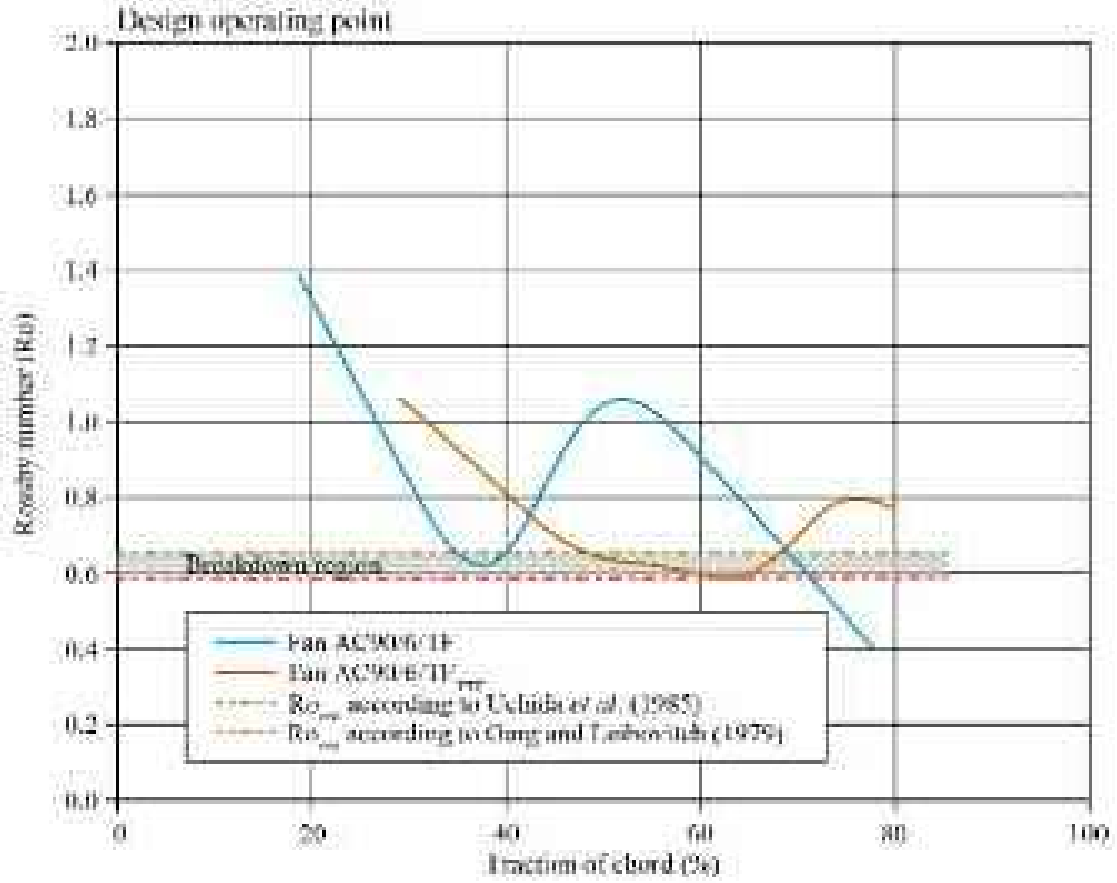

FIGURE 9.5. Chord-wise evolution of numerically predicted blade tip-to-casing leakage vortex Rossby number (*Ro*) for fan AC90/6/TF and AC90/6/TF$_{VTE}$ at their design operating point.

results in the Rossby number falling more slowly with increasing blade chord. The minimum Rossby number is at approximately 60 per cent blade chord, and then goes on to rise towards the blade trailing edge. Corsini and Sheard (2007) developed the variable thickness blade-tip end-plate geometry to maintain the fan AC90/6/TF$_{VTE}$ Rossby number above a critical value associated with vortex bursting. Our analysis of fan AC90/6/TF$_{VTE}$ indicates that the Rossby number did remain above this critical value. However, the Rossby number falls close to the critical value at mid-chord and falls again near the blade trailing edge.

Leakage Flow Survey

Corsini *et al.* (2007) identified organised vortical structures originating at the blade leading edge, mid-chord and blade trailing edge of the fan AC90/6/TF$_{VTE}$. The Rossby number falling close to a critical value may be responsible for creating these organised vortical structures. To test this hypothesis we studied the chord-wise blade tip-to-casing clearance distribution of leakage flow axial velocity (w_{LV}) and leakage flow skewing angle (β_{LV}). We define leakage flow axial velocity as blade tip-to-casing leakage flow velocity normal to the blade chord, normalised by the average blade-to-blade passage velocity. We define leakage flow skewing angle as the angle between the leakage flow and blade chord.

We studied the chord-wise distribution of leakage flow axial velocity and leakage flow skewing angle at four chord-wise locations. The first was 15 per cent blade chord downstream of the blade leading edge. The second was 30, the third 55 and the fourth 75 per cent chord downstream of the blade leading edge. We present these leakage flow axial velocity distributions and leakage flow skewing angle in Figures 9.6, 9.7, 9.8 and 9.9.

Consider the leakage flow axial velocity distributions and leakage flow skewing angle at 15 per cent blade chord, Figure 9.6. The fan *datum* AC90/6 and AC90/6/TF have similar leakage flow axial velocities across the blade tip-to-casing gap. The leakage flow axial velocity is positive over the majority of the blade tip-to-casing gap which indicates that the leakage vortex is established. In contrast, the fan AC90/6/TF$_{VTE}$ is negative over the majority of the blade tip-to-casing gap which indicates that the leakage vortex is not established. When we review the leakage flow skewing angles it is apparent that the fan AC90/6/TF$_{VTE}$ behaves differently to the fan *datum* AC90/6 or AC90/6/TF. In comparison to fan *datum* AC90/6 and AC90/6/TF, it occurs with under turning at 20 per cent blade tip-to-casing clearance and over turning at the blade tip. This under and over turning indicates that the leakage vortex is not established.

Consider the leakage flow axial velocity distributions and leakage flow skewing angle at 30 per cent blade chord, Figure 9.7. The fan *datum* AC90/6 and AC90/6/TF leakage flow axial velocities are essentially similar to those at 15 per cent blade chord. In contrast the fan AC90/6/TF$_{VTE}$ leakage flow axial velocity is now close to zero across the entire blade tip-to-casing gap. This zero velocity is indicative that the leakage vortex is on the verge of establishing itself. When we review the leakage

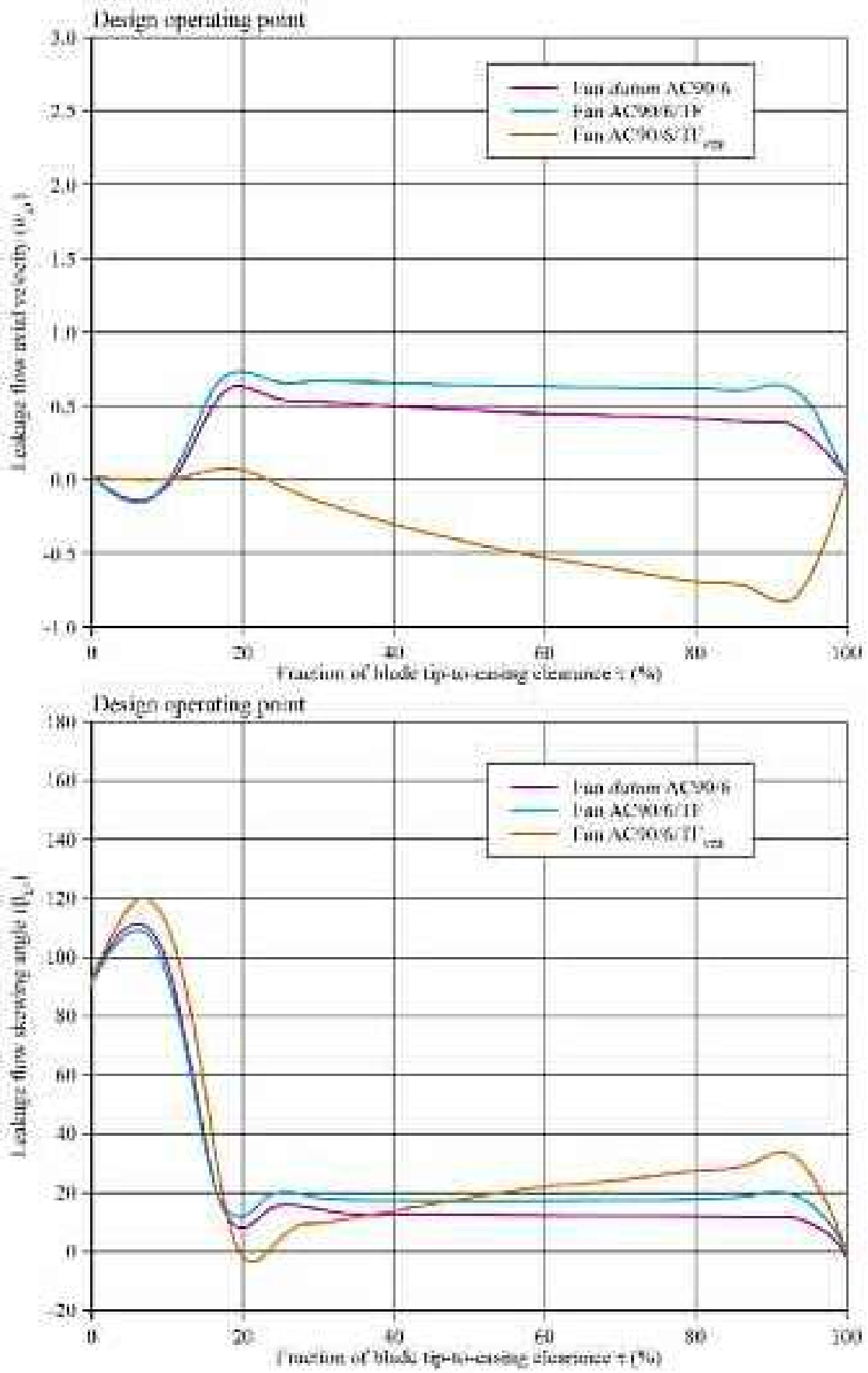

FIGURE 9.6. Evolution of the blade tip-to-casing leakage vortex axial velocity (w_{LV}) and leakage-flow skewing angle (β_{LV}). Leakage vortex axial velocity and leakage-flow skewing angle are predicted at the fan design operating point through the blade tip-to-casing gap 15 per cent chord downstream of the blade leading edge. The change in vortex axial velocity and leakage-flow skewing angle illustrates the impact of

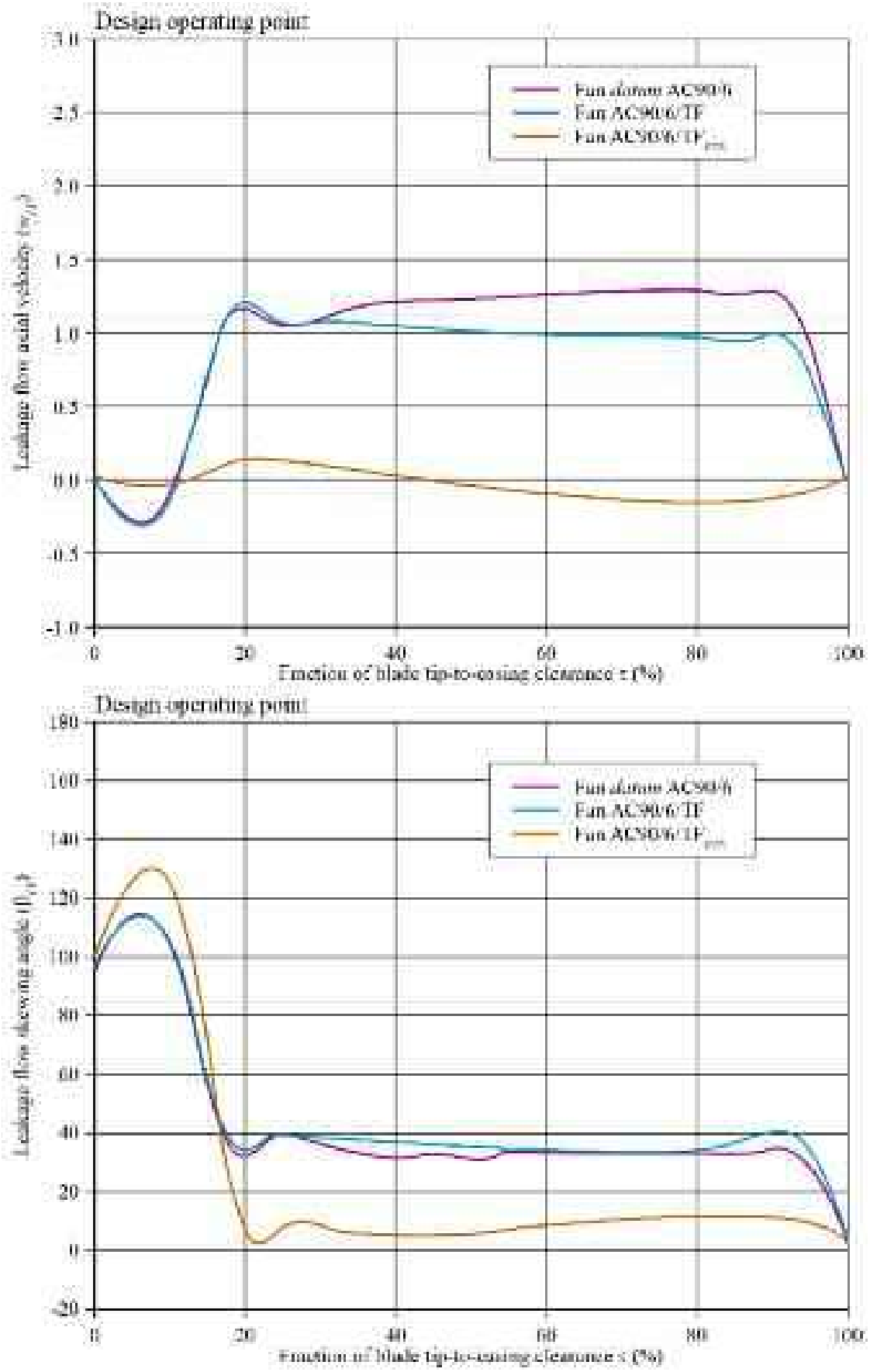

FIGURE 9.7. Evolution of the blade tip-to-casing leakage vortex axial velocity (w_{LV}) and leakage-flow skewing angle (β_{LV}). Leakage vortex axial velocity and leakage-flow skewing angle are predicted at the fan design operating point through the blade tip-to-casing gap 30 per cent chord downstream of the blade leading edge. The change in vortex axial velocity and leakage-flow skewing angle illustrates the impact of

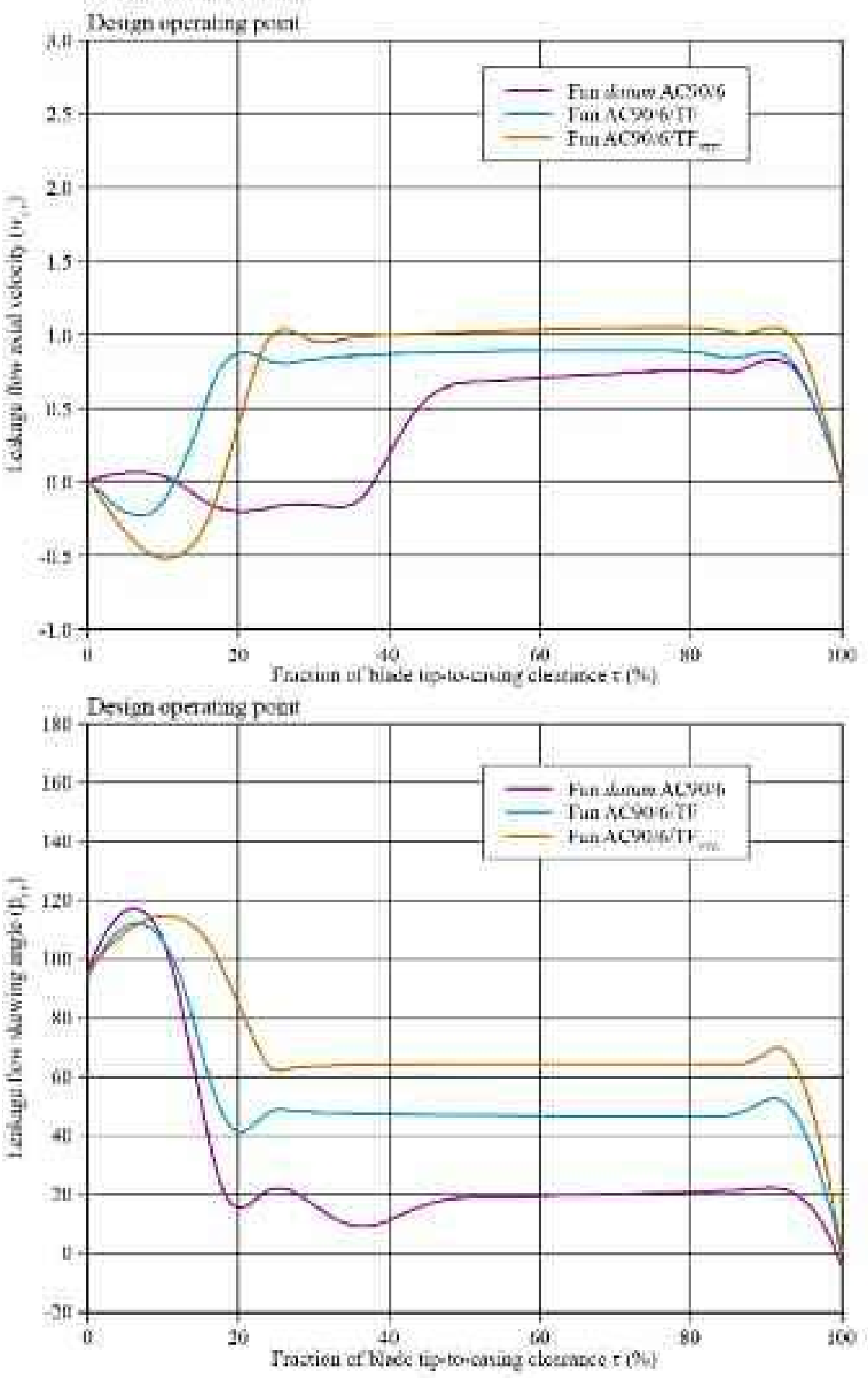

FIGURE 9.8. Evolution of the blade tip-to-casing leakage vortex axial velocity (w_{LV}) and leakage-flow skewing angle (β_{LV}). Leakage vortex axial velocity and leakage-flow skewing angle are predicted at the fan design operating point through the blade tip-to-casing gap 55 per cent chord downstream of the blade leading edge. The change in vortex axial velocity and leakage-flow skewing angle illustrates the impact of

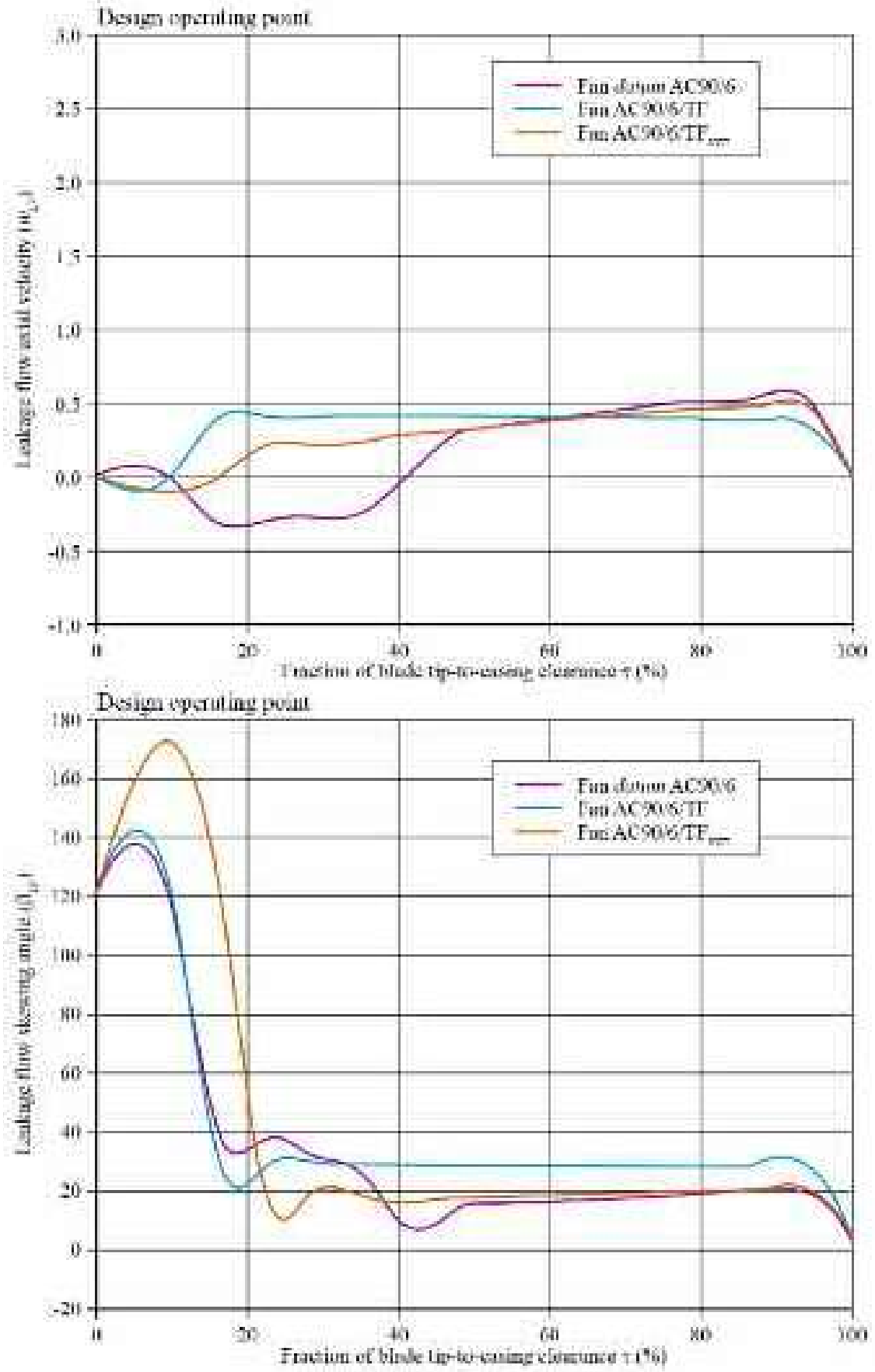

FIGURE 9.9. Evolution of the blade tip-to-casing leakage vortex axial velocity (w_{LV}) and leakage-flow skewing angle (β_{LV}). Leakage vortex axial velocity and leakage-flow skewing angle are predicted at the fan design operating point through the blade tip-to-casing gap 75 per cent chord downstream of the blade leading edge. The change in vortex axial velocity and leakage-flow skewing angle illustrates the impact of

flow skewing angles, it is apparent that the fan AC90/6/TF$_{VTE}$ is still under turning at 20 per cent blade tip-to-casing clearance, but no longer over turning at the blade tip. This indicates that the leakage vortex is in the process of establishing itself.

Consider the leakage flow axial velocity distributions and leakage flow skewing angle at 55 per cent blade chord, Figure 9.8. The fan AC90/6/TF$_{VTE}$ blade-tip end-plate thickness has reduced by 55 per cent blade chord. A result of this is that the now established leakage vortex momentum is augmented. Thus, we see leakage flow axial velocities over the majority of the blade tip-to-casing clearance that are higher than either the fan *datum* AC90/6 or AC90/6/TF. When we review the leakage flow skewing angles, it is apparent that the fan AC90/6/TF$_{VTE}$ is now associated with higher skewing angles than either the fan *datum* AC90/6 or AC90/6/TF.

Consider the leakage flow axial velocity distributions and leakage flow skewing angle at 75 per cent blade chord, Figure 9.9. The fan AC90/6/TF$_{VTE}$ has once again changed its leakage flow axial velocity relative to either the fan *datum* AC90/6 or AC90/6/TF. It now has an almost linear progression of leakage flow axial velocity across the blade tip-to-casing clearance. When we review the leakage flow skewing angles, it is now similar to that of the fan *datum* AC90/6 and AC90/6/TF over the majority of the blade tip-to-casing clearance.

Influence of Span-wise Rotor Flow Behaviour

The chord-wise distribution of leakage flow axial velocity and leakage flow skewing angle through the blade tip-to-casing clearance provide an insight into leakage vortex development. However, the distributions alone do not provide an insight into the leakage vortex magnitude. We may assess the magnitude of the leakage vortex for the three studied fans by calculating the blade tip-to-casing leakage flow rate as a percentage of the flow rate though the fan, Table 9.4. Both the constant and variable thickness blade-tip end-plates result in the leakage flow rate reducing by over 25 per cent, and therefore they both reduce the leakage flow rate. However, when we compare the leakage flow rate for fan AC90/6/TF and AC90/6/TF$_{VTE}$, it is apparent that the fan AC90/6/TF$_{VTE}$ reduces leakage flow rate further. Therefore, we may conclude that the variable thickness blade-tip end-plate is the most effective at minimising blade tip-to-casing leakage vortex magnitude.

Table 9.4. *Blade tip-to-casing leakage flow-rate as a percentage of the flow-rate through the three studied fans when operating at their design operating point.*

Datum AC90/6	AC90/6/TF	AC90/6/TF$_{VTE}$
Leakage flow/inflow (%)	Leakage flow/inflow (%)	Leakage flow/inflow (%)
1.40	1.03	0.95

The change in leakage flow rate that occurs with adding a constant or variable thickness blade-tip end-plate will result in a change in the fan blade-to-blade flow field. We may assess the impact of a blade-tip end-plate by studying the circumferentially averaged span-wise distributions of axial (φ_a) and radial (φ_r) flow coefficients. Our objective was to facilitate an assessment of the impact of blade-tip end-plates on the overall fan performance. Therefore, we chose to calculate the distributions at a plane 20 per cent chord downstream of the blade trailing edge, Figure 9.10.

Consider the span-wise distribution of axial flow coefficient. The constant and variable thickness blade-tip end-plates are characterised by lower blade tip-to-casing clearance flow rates than the fan *datum* AC90/6. The span-wise distributions of axial flow coefficient indicate that both the fan AC90/6/TF and AC90/6/TF$_{VTE}$ have higher axial flow coefficients from 70 to 100 per cent blade-span. Higher axial flow coefficients are indicative of a lower leakage flow rate.

Consider the span-wise distribution of radial flow coefficient. An effect of fitting a blade-tip end-plate is a reduced size of separated flow in the blade root region. This reduction results in less flow centrifuging from blade root to tip, and therefore a change in the span-wise flow distribution. The span-wise distributions of radial flow coefficient indicate that the three studied fans perform in a similar manner up to 30 per cent blade span. This implies that differences between the span-wise flow distributions are not evident 20 per cent downstream of the blade leading edge. At approximately 95 per cent blade span, the fan AC90/6/TF$_{VTE}$ features a larger radial flow coefficient than either the fan *datum* AC90/6 or AC90/6/TF. The design criteria for the variable thickness blade-tip end-plate are based on controlling leakage vortex swirl level, and therefore we would expect a larger radial flow coefficient at the blade tip.

We may gain an insight into leakage vortex swirl level by studying span-wise distributions of swirl coefficient (ψ), Figure 9.11. Once again, we chose to calculate the distributions at a plane 20 per cent chord downstream of the blade trailing edge. The span-wise distribution of swirl coefficient for the fan AC90/6/TF$_{VTE}$ exhibits a higher peak at approximately 85 per cent blade span than either the fan *datum* AC90/6 or AC90/6/TF. This higher peak is indicative of the variable thickness blade-tip end-plate inducing a higher leakage vortex swirl level. Therefore, it is indicative of the effectiveness of the variable thickness blade-tip end-plate design methodology.

Our analysis has focused on leakage flow axial velocity distributions and leakage flow skewing angle distributions, axial flow, radial flow and swirl coefficient distributions. It has provided an insight into the blade tip-to-casing clearance flow-field features and clarified the impact of both constant and variable thickness blade-tip end-plates. We may complement this analysis with a study of three-dimensional total pressure-loss coefficient (ζ) contours. When combined with leakage vortex trajectories, three-dimensional total pressure-loss coefficient contours provide an insight into the impact of blade-tip end-plate on the entire blade-to-blade flow-field. We define total pressure-loss coefficient ζ as:

$$\zeta = \bar{p}_{0in} - p_0 / 0.5\rho\bar{w}^2_{in}, \tag{2}$$

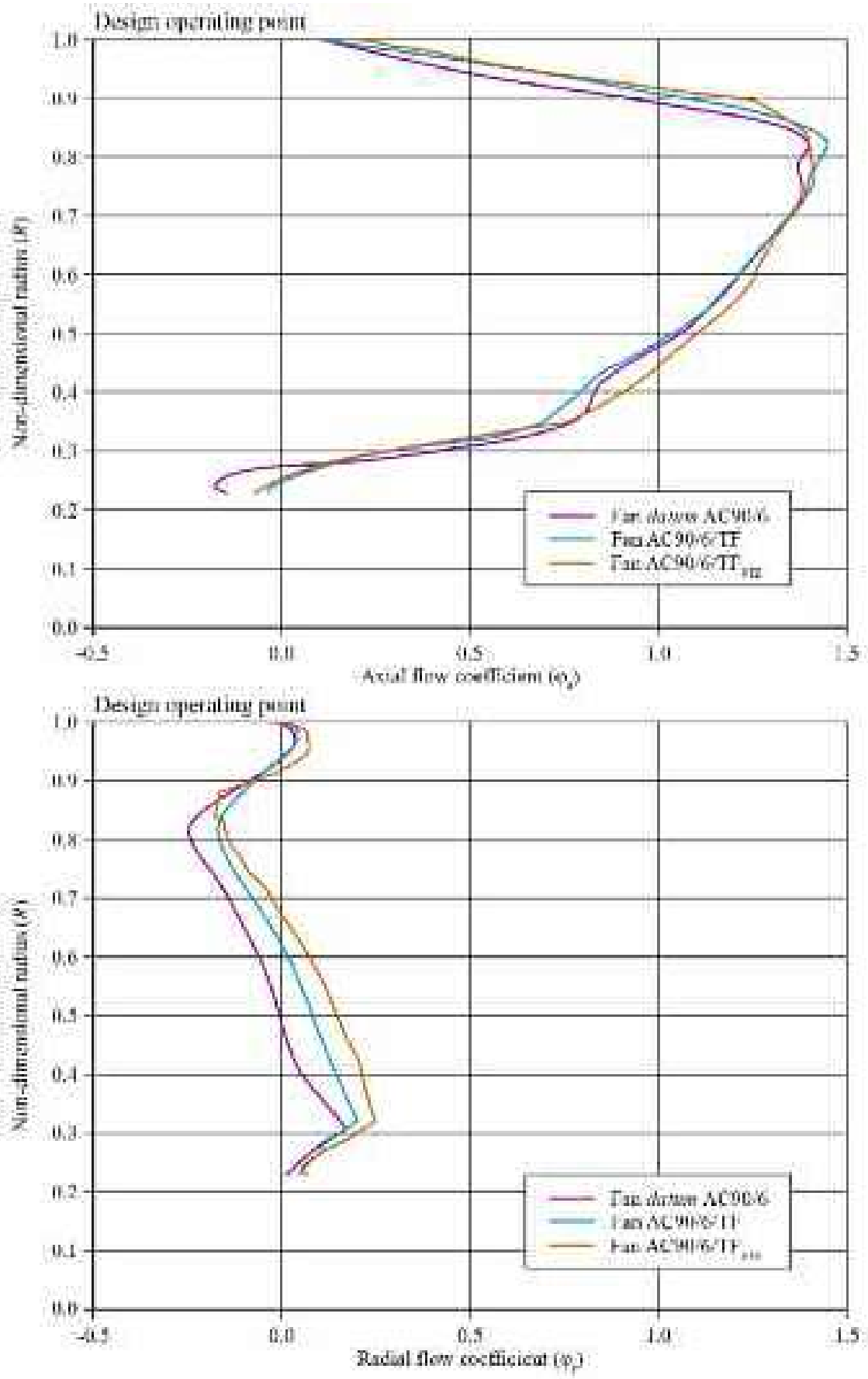

FIGURE 9.10. Span-wise evolution of numerically predicted axial (φ_a) and radial (φ_r) flow coefficient at the fan design operating point for the fan *datum* AC90/6, AC90/6/TF and AC90/6/TF$_{VTE}$. Axial and radial flow coefficients are predicted 20 per cent blade chord downstream of the blade trailing edge.

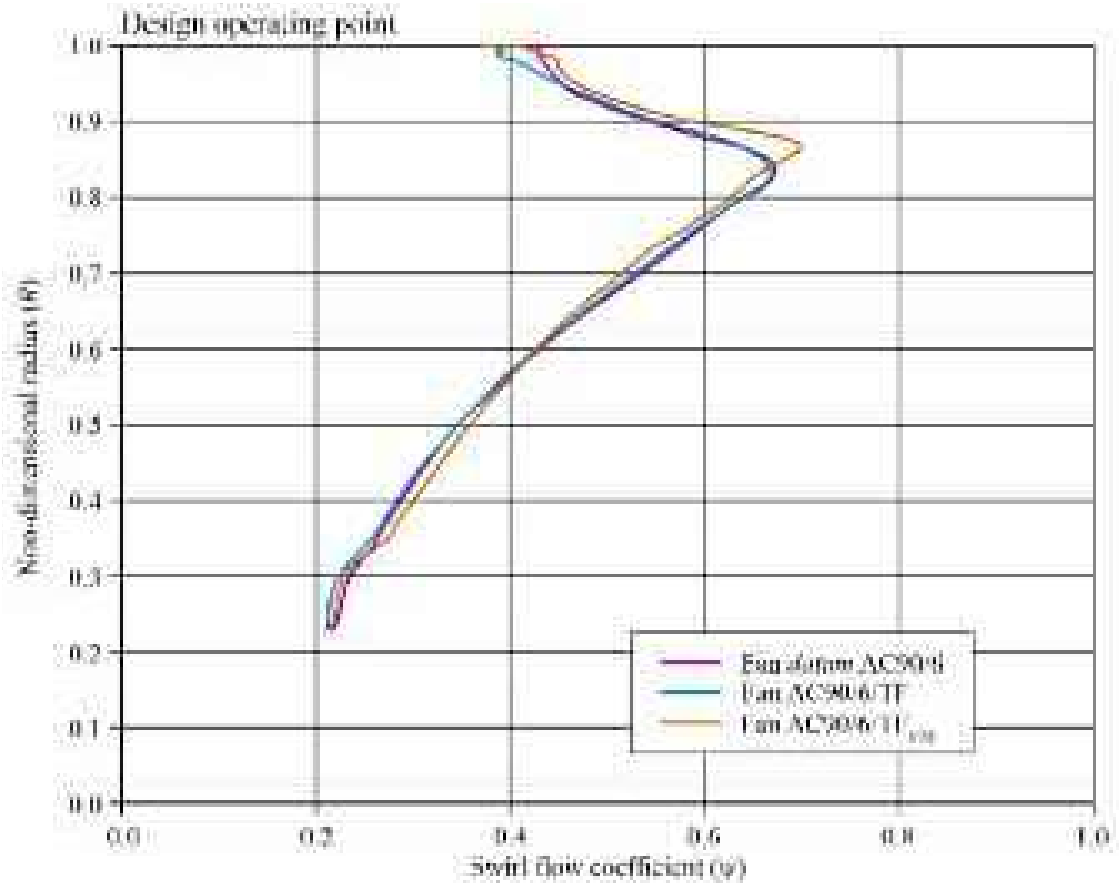

FIGURE 9.11. Span-wise evolution of numerically predicted swirl flow coefficient at the fan design operating point for the fan *datum* AC90/6, AC90/6/TF and AC90/6/TF$_{VTE}$. Swirl flow coefficients are predicted 20 per cent blade chord downstream of the blade trailing edge.

where p_0 is the local total pressure; and $\bar{p}_{0in}$ and $0.5\rho\bar{w}^2_{in}$ are, respectively, the reference circumferentially averaged relative total and dynamic pressures. We computed these pressures at 50 per cent blade span at the fan inlet. We calculated the total loss coefficient distribution within the blade-to-blade passage. We present them for the fan *datum* AC90/6, AC90/6/TF and AC90/6/TF$_{VTE}$ over axial planes 25, 65 and 120 per cent blade chord downstream of the blade leading edge, Figure 9.12.

At the axial plane 25 per cent blade chord downstream of the blade leading edge, total pressure loss distributions are similar for the three studied fans. We may associate fan *datum* AC90/6, AC90/6/TF and AC90/6/TF$_{VTE}$ with loss cores concentrated in the hub region. At the axial plane 65 per cent blade chord downstream of the blade leading edge, total pressure loss distributions in the blade tip region are now different for the three studied fans. Each total pressure loss distribution is characteristic of the fan's blade tip-to-casing leakage vortex. The fan AC90/6/TF is the only studied fan where we saw bursting of the leakage vortex, thus we associate this with a larger total pressure loss core.

At the axial plane 120 per cent blade chord downstream of the blade leading edge, it is evident that the blade-tip end-plates affect fan span-wise loss distribution. The constant thickness blade-tip end-plate results in a thinner wake and smaller hub loss core. The variable thickness blade-tip end-plate total pressure loss distributions

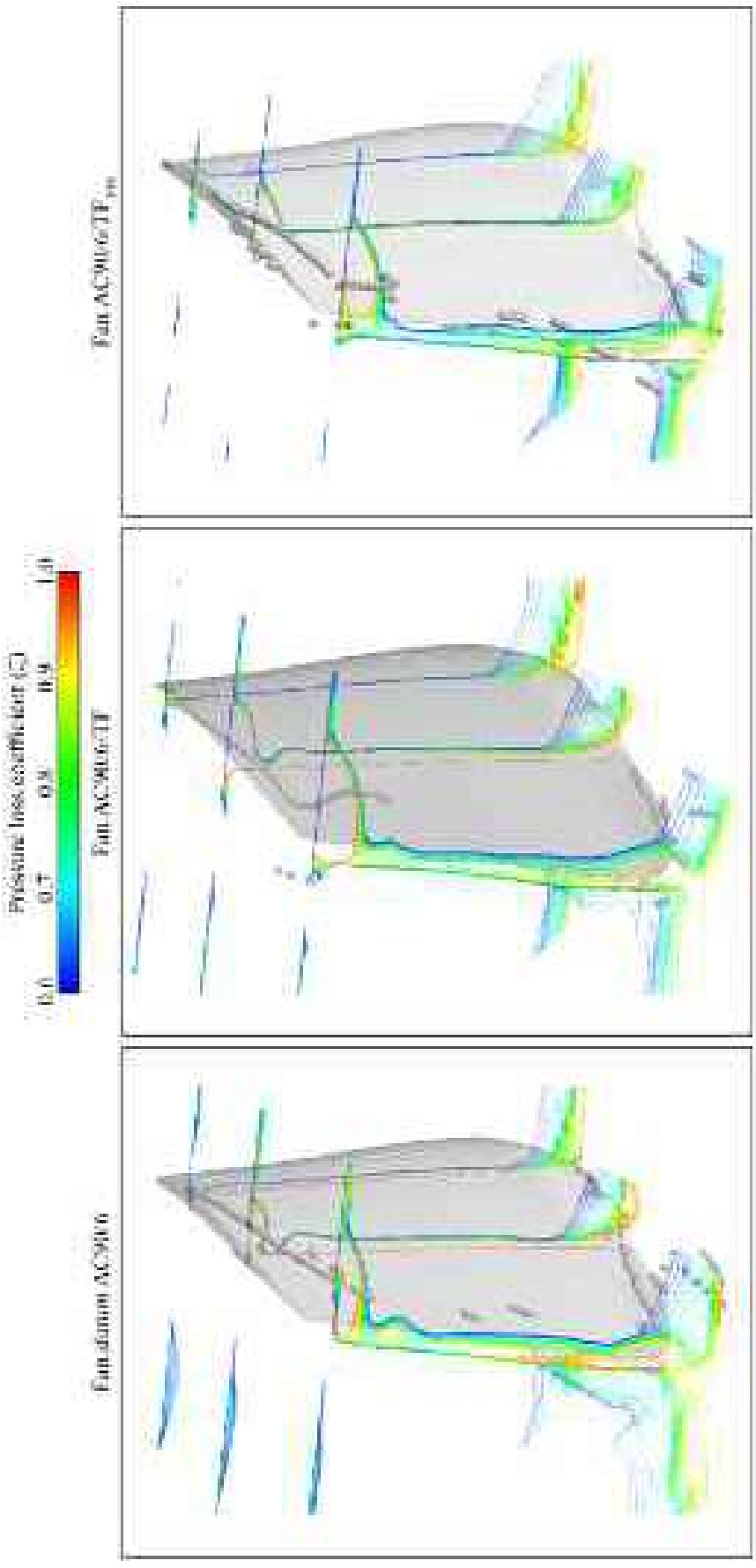

FIGURE 9.12. Three-dimensional total pressure-loss coefficient (ζ) contours numerically predicted at the fan design operating point. Total pressure-loss coefficient contours are presented at three chord-wise locations through the fan *datum* AC90/6, AC90/6/TF and AC90/6/TF$_{VTE}$ illustrating the effect of constant and variable thickness blade-tip end-plates.

in the blade tip region indicate that leakage vortex loss core is smaller than that of the fan *datum* AC90/6. This reduction is evident at both 65 and 120 blade chord and is a consequence of the reduced three-dimensional redistribution of flow within the blade-to-blade passage. This reduced rearrangement occurs as a consequence of the reduced blade tip-to-casing clearance leakage flow rate.

We associate the fan AC96/6/TF$_{VTE}$ with generally smaller total pressure loss cores at the blade hub and tip then either the fan *datum* AC90/6 or AC90/6/TF. These smaller total pressure loss cores result in a higher fan efficiency and pressure developing capability. Therefore, the variable thickness blade-tip end-plate is an aerodynamic success, avoiding bursting of the leakage vortex and improving overall fan performance. However, Corsini *et al.* (2007) concluded that the variable thickness blade-tip end-plate induced the creation of multiple organised vortical structures. Although the blade tip-to-casing leakage vortex did not break down, these vortical structures did. Their breakdown was acoustically productive enough to result in increased overall fan far-field noise. Therefore, we may conclude that the variable thickness blade-tip end-plate was an aerodynamic success, but an acoustic failure.

CONCLUSIONS

In this chapter we presented a computational analysis of the blade-to-blade flow-field for the studied fan both without a blade-tip end-plate, coded fan *datum* AC90/6, and with a constant thickness blade-tip end-plate, coded fan AC90/6/TF and with a variable thickness blade-tip end-plate, coded fan AC90/6/TF$_{VTE}$. We undertook the computational analysis using a Reynolds-Averaged Navier–Stokes (RANS) simulation with a non-linear k-ε turbulence model in low-Reynolds number formulation.

The computational analysis indicated that the variable thickness blade-tip end-plate design had been successful in that it avoided blade-tip-to-casing leakage vortex breakdown. Experimental measurements confirmed that the fan pressure developing capability and efficiency had improved. However, acoustic measurements indicated that overall fan far-field noise increased. We used the computational analysis to calculate the distribution of total pressure loss coefficients in the blade-to-blade passage of the fan *datum* AC90/6, fan AC90/6/TF and fan AC90/6/TF$_{VTE}$. Distributions of total pressure loss coefficients are useful because they characterise the evolution of blade boundary layers. Thus, they facilitate identifying the three-dimensional swirling cores that are a feature of the flow-fields acoustically productive organised vortical structures.

Analysis of total pressure loss coefficient distributions confirmed that the highest loss regions always coincided with the blade-tip leakage vortex core. The multiple organised vortical structures were weak in comparison and therefore aerodynamically insignificant compared to the blade-tip leakage vortex. Despite the low loss of the multiple organised vortical structures, they proved to be disproportionately acoustically productive.

A realisation that the multiple organised vortical structures induced in the blade-tip region by the variable thickness blade-tip end-plate were disproportion-

ately acoustically productive resulted in a break-through in conceptual thinking. The blade-tip end-plate requires redesign to avoid the creation of organised vortical structures. Further, the redesign must minimise the swirling intensity and size of vortices in the blade-tip region while ensuring that they do not burst.

REFERENCES

ISO 5801:2007 (2007), *Industrial Fans: Performance Testing Using Standardised Airways.*

Benjamin, T.B. (1962), 'The Theory of Vortex Breakdown', *Journal of Fluid Mechanics*, vol. 14, pp. 583–629.

Bianchi, S., Corsini, A., Rispoli, F. and Sheard, A.G. (2011), 'Far-field Radiation of Tip Aerodynamic Sound Sources in Axial Fans Fitted with Passive Noise Control Features', *Transactions of the ASME, Journal of Vibration & Acoustics*, vol. 133, paper no. 051001, pp. 1–11.

Borello, D., Borrelli, P., Quagliata, E. and Rispoli, F. (2001), 'A Multi-grid Additive and Distributive Parallel Algorithm for FEM Turbomachinery CFD', *Proceedings of the European Congress on Computational Methods in Applied Sciences (ECCOMAS CFD 2001)*, Swansea, UK, 4–7 September.

Borello, D., Corsini, A. and Rispoli, F. (2003), 'A Finite Element Overlapping Scheme for Turbomachinery Flows on Parallel Platforms', *Computers and Fluids*, vol. 32, pp. 1017–1047.

Corsini, A. and Rispoli, F. (2004), 'Using Sweep to Extend Stall-free Operational Range in Sub-sonic Axial Fan Rotors', *Proceedings of the IMechE Part A, Journal of Power and Energy*, vol. 218, pp. 129–139.

Corsini, A. and Sheard, A.G. (2007), 'Tip End-plate Concept Based on Leakage Vortex Rotation Number Control', *Journal of Computational and Applied Mechanics*, vol. 8, pp. 21–37.

Corsini, A., Rispoli, F. and Santoriello, A. (2004a), 'A New Stabilized Finite Element Method for Advection-Diffusion-Reaction Equations using Quadratic Elements', in Vad, J., Lajos, T. and Schilling, R. (Eds), *Modelling Fluid Flow: The State of the Art*, Springer-Verlag, Berlin, Germany.

Corsini, A., Rispoli, F., Sheard, A.G. and Kinghorn, I.R. (2004b), 'The Aerodynamic Interaction of Tip Leakage and Mainstream Flows in a Fully Ducted Axial Fan', *Proceedings of the 49th American Society of Mechanical Engineers Gas Turbine and Aeroengine Congress*, Vienna, Austria, 14–17 June, paper no. GT2004-53408.

Corsini, A., Rispoli, F., Sheard, A.G. and Kinghorn, I.R. (2006), 'Investigation of Improved Blade-tip Concept for Axial Flow Fan', *Proceedings of the 51st American Society of Mechanical Engineers Gas Turbine and Aeroengine Congress*, Barcelona, Spain, 8–11 May, paper no. GT2006-90592.

Corsini, A., Rispoli, F. and Sheard, A.G. (2007), 'Development of Improved Blade-tip End-plate Concepts for Low-noise Operation in Industrial Fans', *Proceedings of the IMechE Part A, Journal of Power and Energy*, vol. 221, pp. 669–681.

Craft, T.J., Launder, B.E. and Suga, K. (1996), 'Development and Application of a Cubic Eddy-viscosity Model of Turbulence', *International Journal of Heat and Fluid Flow*, vol. 17, pp. 108–155.

Escudier, M. (1987), 'Confined Vortices in Flow Machinery', *Annual Review of Fluid Mechanics*, vol. 19, pp. 27–52.

Escudier, M. and Zehnder, N. (1982), 'Vortex Flow Regimes', *Journal of Fluid Mechanics*, vol. 115, pp.105–121.

Fukano, T., Takamatsu, Y. and Kodama, Y. (1986), 'The Effects of Tip Clearance on the Noise of Low Pressure Axial and Mixed Flow Fans', *Journal of Sound and Vibration*, vol. 105(2), pp. 291–308.

Furukawa, M., Inoue, M., Kuroumaru, M., Saiki, K. and Yamada, K. (1999), 'The Role of Tip Leakage Vortex Breakdown in Compressor Rotor Aerodynamics'. *Transactions of the ASME, Journal of Turbomachinery*, vol. 121, pp. 469–480.

Ganz, U.W., Joppa, P.D. and Scharpf, D.F. (1998), *Boeing 18-inch Fan Rig Broadband Noise Test*, Report NASA CR-1998-208704.

Garg, A.K. and Leibovich, S. (1979), 'Spectral Characteristics of Vortex Breakdown Flowfields', *Physics of Fluids*, vol. 22, pp. 2053–2064.

Herrada, M.A. and Shtern, V. (2003), 'Vortex Breakdown Control by Adding Near-axis Swirl and Temperature Gradients', *Physical Review E, Non-Linear Soft Matter Physics*, vol. 68(1), paper no. 041202, pp. 1–8.

Holste, F. and Neise, W. (1997), 'Noise Source Identification in a Prop Fan Model by Means of Acoustical Near Field Measurements', *Journal of Sound and Vibration*, vol. 203, pp. 641–665.

Inoue, M. and Furukawa, M. (2002), 'Physics of Tip Clearance Flow in Turbomachinery', *Proceedings of the ASME2002 Joint US – European Fluids Engineering Division Conference*, Montreal, Quebec, Canada, 14–18 July, paper no. FEDSM2002-31184, pp. 777–789.

Inoue, M., Kuroumaru, M. and Furukawa, M. (1986), 'Behavior of Tip Leakage Flow Behind an Axial Compressor Rotor', *Transactions of the ASME, Journal of Engineering for Gas Turbines and Power*, vol. 108, pp. 7–14.

Ito, T., Suematsu, Y. and Hayase, T. (1985), 'On the Vortex Breakdown Phenomena in a Swirling Pipe-flow', *Nagoya University, Faculty of Engineering, Memoirs*, vol. 37(2), pp. 117–172.

Jensen, C.E. (1986), 'Axial-flow Fan', Patent No. US 4,630,993, 23 December.

Jones, M.C., Hourigan, K. and Thompson, M.C. (2001), 'The Generation and Suppression of Vortex Breakdown by Upstream Swirl Perturbations', *Proceedings of 14th Australian Fluid Mechanics Conference*, Adelaide, Australia, 10–14 December, pp. 347–350.

Karlsson, S. and Holmkvist, T. (1986), 'Guide Vane Ring For a Return Flow Passage in Axial Fans and a Method of Protecting It', US Patent No. 4,602,410, 29 July.

Leibovich, S. (1978), 'The Structure of Vortex Breakdown', *Annual Review of Fluid Mechanics*, vol. 10, pp. 221–246.

Leibovich, S. (1984), 'Vortex Stability and Breakdown: Survey and Extension', *AIAA Journal*, vol. 22, pp. 1192–1206.

Longet, C.M.L. (2003), 'Axial Flow Fan with Noise Reducing Means', Patent No. US 2003/0123987 A1, 3 July.

Lucca-Negro, O. and O'Doherty, T. (2001), 'Vortex Breakdown: A Review', *Progress in Energy and Combustion Science*, vol. 27, pp. 431–481.

Mimura, M. (2003), 'Axial Flow Fan', Patent No. US 6,648,598 B2, 18 November.

Quinlan, D.A. and Bent, P.H. (1998), 'High Frequency Noise Generation in Small Axial Flow Fans', *Journal of Sound and Vibration*, vol. 218, pp. 177–204.

Sheard, A.G., Corsini, A. and Rispoli, F. (2009), 'A Meridional Fan'. Patent No. GB 2 452 104 B, 22 July.

Smith, G.D.J. and Cumpsty, N.A. (1984), 'Flow Phenomena in Compressor Casing Treatment', *Transactions of the ASME, Journal of Engineering for Gas Turbines and Power*, vol. 106, pp. 532–541.

Spall, R.E., Gatski, T.B. and Grosch, C.E. (1987), 'A Criterion for Vortex Breakdown', *Physics of Fluids*, vol. 30, pp. 3434–3440.

Srigrarom, S. and Kurosaka, M. (2000), 'Shaping of Delta-wing Planform to Suppress Vortex Breakdown', *AIAA Journal*, vol. 38, pp. 183–186.

Storer, J.A. and Cumpsty, N.A. (1991), 'Tip Leakage Flow in Axial Compressors', *Transactions of the ASME, Journal of Turbomachinery*, vol. 113, pp. 252–259.

Takata, H. and Tsukuda, Y. (1977), 'Stall Margin Improvement by Casing Treatment – Its Mechanism and Effectiveness', *Transactions of the ASME, Journal of Engineering and Power*, vol. 99, pp. 121–133.

Thompson, D.W., King, P.I. and Rabe, D.C. (1998), 'Experimental and Computational Investigation on Stepped Tip Gap Effects on the Flowfield of a Transonic Axial-flow Compressor Rotor', *Transactions of the ASME, Journal of Turbomachinery*, vol. 120, pp. 477–486.

Tsai, C.Y. and Widnall, S.E. (1980), 'Examination of Group-Velocity Criterion for Breakdown of Vortex Flow in a Divergent Duct', *Physics of Fluids*, vol. 23, pp. 864–870.

Uchida, S., Nakamura, Y. and Ohsawa, M. (1985), 'Experiments on the Axisymmetric Vortex Breakdown in a Swirling Air Flow', *Transactions of the Japan Society for Aeronautical Space Sciences*, vol. 27, pp. 206–216.

Uselton, R.B., Cook, L.J. and Wright, T. (2008), 'Fan with Reduced Noise Generation', Patent No. US 7,351,041 B2, 1 April.

Chapter 10

Aerodynamic Performance of BladeTip End-plates Designed for Low-noise Operation in Axial Flow Fans

A. Corsini, F. Rispoli and A.G. Sheard

ABSTRACT

The chapter presents a computational analysis of the blade-to-blade flow-field of the studied fan with blade-tip end-plates incorporating a step along the blade chord at the intersection of the blade-tip and end-plate. We introduced this step in response to the research presented in Chapter 8 and 9. The studied blade-tip end-plate induced the creation of multiple organised vortical structures that we concluded to have increased fan far-field noise. In this chapter we incorporate a step into the blade-tip end-plate to provide an additional mechanism to weaken the multiple organised vortical structures' intensity as we aimed to reduce fan far-field noise. We predicted the blade-to-blade flow-field for a *datum* fan AC90/6 without blade-tip end-plates, and four variants of the fan with different end-plate geometries. The fan AC90/6/TF incorporated a constant thickness end-plate. The fan AC90/6/TF$_{step}$ incorporated a constant thickness end-plate with a step between the blade suction surface and end-plate. The fan AC90/6/TF$_{VTE}$ incorporated a variable thickness end-plate. The fan AC90/6/TF$_{VTE\ step}$ incorporated a variable thickness end-plate with a step between the blade suction surface and end-plate. When we studied the predicted blade-to-blade flow-field for the *datum* fan AC90/6 and four variants with different end-plate geometries it was apparent that an incoming horseshoe vortex characterised the pressure surface. In contrast the blade tip-to-casing leakage vortex characterised the suction surface. The pressure side horseshoe vortex acted as a vena contractor, reducing the leakage mass flow rate over the blade tip. However, introducing the step into the end-plate appeared to make the organised vortical structures more acoustically productive, not less, resulting in an increase in fan far-field noise. We undertook the computational analysis using a Reynolds-Averaged Navier–Stokes (RANS) simulation with non-linear k-ε turbulence model in low-Reynolds number

This chapter is a revised and extended version of Corsini, A., Rispoli, F. and Sheard, A.G. (2009), 'Aerodynamic Performance of Blade Tip End-plates Designed for Low-noise Operation in Axial Flow Fans', *Transactions of the ASME, Journal of Fluids Engineering*, vol. 131, paper no. 081101, pp. 1–13.

formulation. Although well proven, the simulation was not able to model unsteady effects and therefore models only part of the flow-field physics. The step end-plate concept does constitute a mechanism for weakening organised vortical structures, but additionally, constitutes a mechanism for making those structures more acoustically productive. Therefore, we concluded that it was ineffective in this application.

NOMENCLATURE

Latin letters

C_p	static pressure coefficientt
Δe_m	non dimensional mechanical energy loss through the gap
H_n	normalised helicity
K_s	specific noise level [dB]
ℓ	chord length
L_W	sound power level [dB]
p	static pressure
Δp_{stat}	static pressure rise [Pa]
Ro	Rossby number
t	blade pitch
TE	trailing edge
TLV	tip-leakage vortex
V_a	vortex axial velocity scale
v_c	convection velocity
v, w	absolute and relative velocities
x, y, z	cartesian coordinates

Greek letters

β_{LV}	leakage-flow skewing angle
δ^+	normalised distance from the wall
ζ	total loss coefficient
η	efficiency
σ_h	hub-to-casing diameter ratio
τ	rotor tip clearance
ω	leakage flow's vortex vector

Subscripts and superscripts

a, p, r	axial, peripheral and radial
c	casing wall
h	hub wall
i	Cartesian component index
in	inlet section
mol	molecular quantity
s	streamwise component
$\bar{}$	pitch-averaged value
0	total quantities

INTRODUCTION

The effect of geometry on aerodynamic efficiency and acoustic signature are primary considerations for engineers during the design of both low-speed fans for air movement application and high-speed fans for aerospace application. When we consider the acoustic emissions from a gas turbine developed for aerospace application, the fan is the most significant noise source (Ganz *et al.*, 1998). Therefore, an objective when designing high-speed fans for aerospace application is to optimise the blade design to minimise fan noise.

Researchers have studied extensively the link between a fan's aerodynamic features and its acoustic emissions. In particular, Wright (1976) and Cumpsty's (1977) research has enhanced the community's understanding of axial turbomachinery aeroacoustics. Cumpsty (1977) concluded that, with the exception of high speed machine low-frequency range, the mechanisms that determine broadband noise in subsonic fans is the same as that in supersonic tip-speed fans and compressors. According to Wright (1976), this is due to the prominence of rotor noise that originates from turbulent boundary layers.

The blade tip-to-casing clearance flow is acoustically productive as a consequence of the blade tip-to-casing leakage vortex itself, and its interaction with turbulent boundary layers and blade-to-blade passage secondary flow features (Quinlan and Bent, 1998; Jang *et al.*, 2003; Fukano and Jang, 2004). When studying fan noise, scholars have concluded that the most acoustically productive features are associated with the blade tip-to-casing clearance flow (Fukano *et al.*, 1986; Storer and Cumpsty, 1991; Furukawa *et al.*, 1999).

In an attempt to improve compressor performance, researchers first experimented with casing treatments in the early 1970s utilising grooves (Takata and Tsukuda, 1977; Smith and Cumpsty, 1984), and more recently stepped gaps in the blade tip region (Thompson *et al.*, 1998). These casing treatments improved the compressors' stable operating range by reducing the blade tip leakage flow's intensity. An alternative way to reduce the blade tip-to-casing leakage vortex's intensity is to utilise a swept blade-stacking line (Wadia *et al.*, 1998; Corsini and Rispoli, 2004). However, when reviewing passive noise control techniques, Bianchi *et al.* (2014) concluded that the greatest reduction in noise low-speed fans has been a consequence of applying passive noise control techniques.

The air movement and control community has historically favoured using passive noise control techniques when attempting to minimise low-speed fan noise. The intent of these passive techniques is to influence positively dominant noise generation mechanisms. The passive noise control technique most widely adopted within the air movement and control community are blade-tip appendages. Researchers have studied extensively the design of fan blade-tip appendages (Jensen, 1986; Quinlan and Bent, 1998; Longet, 2003; Mimura, 2003; Uselton *et al.*, 2008). These blade-tip appendages constitute anti-vortex devices, with those scholars who have studied their application reaching a consensus that they influence the blade tip-to-casing flow. A consequence of this influence is reduced intensity of blade-tip noise generation mechanisms.

This chapter continues the work of Corsini and Sheard (2007) and Corsini *et al.* (2007, 2010). We study the impact on blade-tip end-plate performance of a step along the blade chord at the blade-tip and end-plate's intersection. Corsini *et al.* (2007) concluded that blade-tip end-plates induced the creation of multiple organised vortical structures, which are responsible for an increase in fan far-field noise. In this chapter, we assess the technical merits of a step as a passive noise control technique by computing Powell's (1963, 1964) sound-source distributions. These sound-source distributions facilitated identifying the location of primary noise sources in the blade-tip region.

FAMILY OF FANS UNDER INVESTIGATION

We conducted the reported research on a family of commercially available cooling fans. The studied fan configuration, coded AC90/6, incorporates a six-blade un-swept rotor, with modified ARA-D profile aerofoil blades, Table 10.1. One may set the blade-pitch angle during final assembly to customise the fan to a desired duty point. We used a direct coupled-induction 400-volt (AC), 3-phase motor to drive the rotor at a constant speed of 950 rpm, resulting in a 44.7 m/s blade tip speed and a 95 Hz blade-passing frequency (BPF). In its original embodiment, the studied fan did not include a blade-tip end-plate and therefore we used it as a *datum* against which to assess the performance of fan variants with blade-tip end-plates. Therefore, in the reported research we refer to the fan without blade-tip end-plates as the fan *datum* AC90/6.

Table 10.1. *The fan* datum *AC90/6 blade geometry and rotor specification.*

	Fan *datum* AC90/6		
Blade geometry	Hub	Mid-span	Tip
Pitch angle (°)	36	58.8	28
Camber angle (°)	46	44	41
Solidity	1.24	0.86	0.30
Fan rotor			
Blade number		6	
Blade tip pitch angle (°)		16–28	
Blade tip stagger angle (°)		74–62	
Hub-to-casing diameter ratio σ		0.22	
Tip diameter (mm)		900.0	
Rotor tip clearance τ (% span)		1.0	
Rated rotational frequency (r/min)		935–950	

End-plate Configurations

In addition to the fan *datum* AC90/6, we studied two fan variants. The first we fitted with a constant thickness blade-tip end-plate and the second with a variable thickness blade-tip end-plate, Figure 10.1. When fitted with a constant thickness blade-tip end-plate the fan, we name the fan AC90/6/TF. When fitted with the variable thickness blade-tip end-plate, we named the fan AC90/6/TF$_{VTE}$.

Designs developed for tip-vortex control and drag reduction in aircraft wings and catamaran hulls inspired the constant thickness blade-tip end-plate design. The constant thickness blade-tip end-plate ran along the blade pressure surface, ending at the blade trailing edge with a square tail. The addition of this constant thickness blade-tip end-plate resulted in the thickness of the fan AC90/6/TF blade tip increasing by a factor of three compared to the fan *datum* AC90/6. We considered the blade-tip end-plate size for axial compressor blades using Inoue *et al.*'s (1986) research. They estimated that the optimum blade-tip end-plate size was between 10 and 20 per cent blade span. In practice, we were able to manufacture blades with a blade-tip end-plate size five per cent of blade span. The fan blades were manufactured from injection moulded plastic, with the blade-tip end-plate size serving as the largest the blade manufacturing technique could produce.

Corsini and Sheard (2007) studied both the fan *datum* AC90/6 and AC90/6/TF using a blade-tip vortex 'breakdown criteria' based on the Rossby number (Spall *et al.*, 1987). Following Ito *et al.*'s method (1985), they concluded that there is a threshold value of Rossby number below which the vortex rotation cannot reduce if the vortex is to remain stable. We defined this critical Rossby number range using the critical Rossby numbers defined by Uchida *et al.* (1985) and Garg and Leibovich (1979). Uchida *et al.* (1985) defined a critical Rossby number associated with the breakdown of an axi-symmetric vortex in a swirling flow. Garg and Leibovich

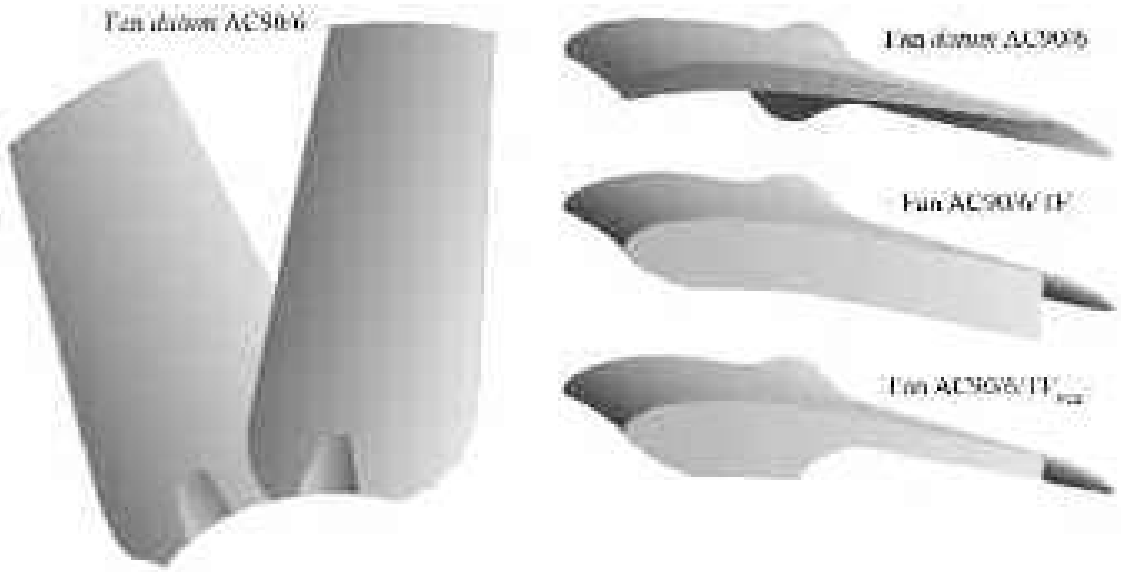

FIGURE 10.1. The studied fan *datum* AC90/6 without a fitted blade-tip end-plate, with a constant thickness blade-tip end-plate, AC90/6/TF and with a variable thickness blade-tip end-plate, AC90/6/TF$_{VTE}$.

(1979) also defined a critical Rossby number associated with an aircraft wing tip vortices' breakdown.

By considering the critical Rossby number, Corsini *et al.* (2007) concluded that for the fan *datum* AC90/6, the blade-tip leakage vortex did not burst. However, the fan AC90/6/TF blade-tip leakage vortex did burst, Figure 10.2. Vortex bursting is acoustically productive, with Corsini and Sheard (2007) proposing a variable thickness blade-tip end-plate to avoid vortex bursting.

This chapter extends the work of Corsini *et al.* (2007, 2010) by adding a step between the blade tip and end-plate along the blade suction surface from the blade leading to trailing edge. We added this step to both the fan AC90/6/TF and fan AC90/6/TF$_{VTE}$. The addition of the step resulted in five separate fan configurations:

- the fan *datum* AC90/6, without a fitted blade-tip end-plate;
- the fan AC90/6/TF, with a constant-thickness blade-tip end-plate;
- the fan AC90/6/TF$_{VTE}$, with a variable-thickness end-plate;
- the fan AC90/6/TF$_{step}$, with a constant-thickness blade-tip end-plate plus step; and
- the fan AC90/6/TF$_{VTE\ step,}$ with a variable-thickness blade-tip end-plate plus step.

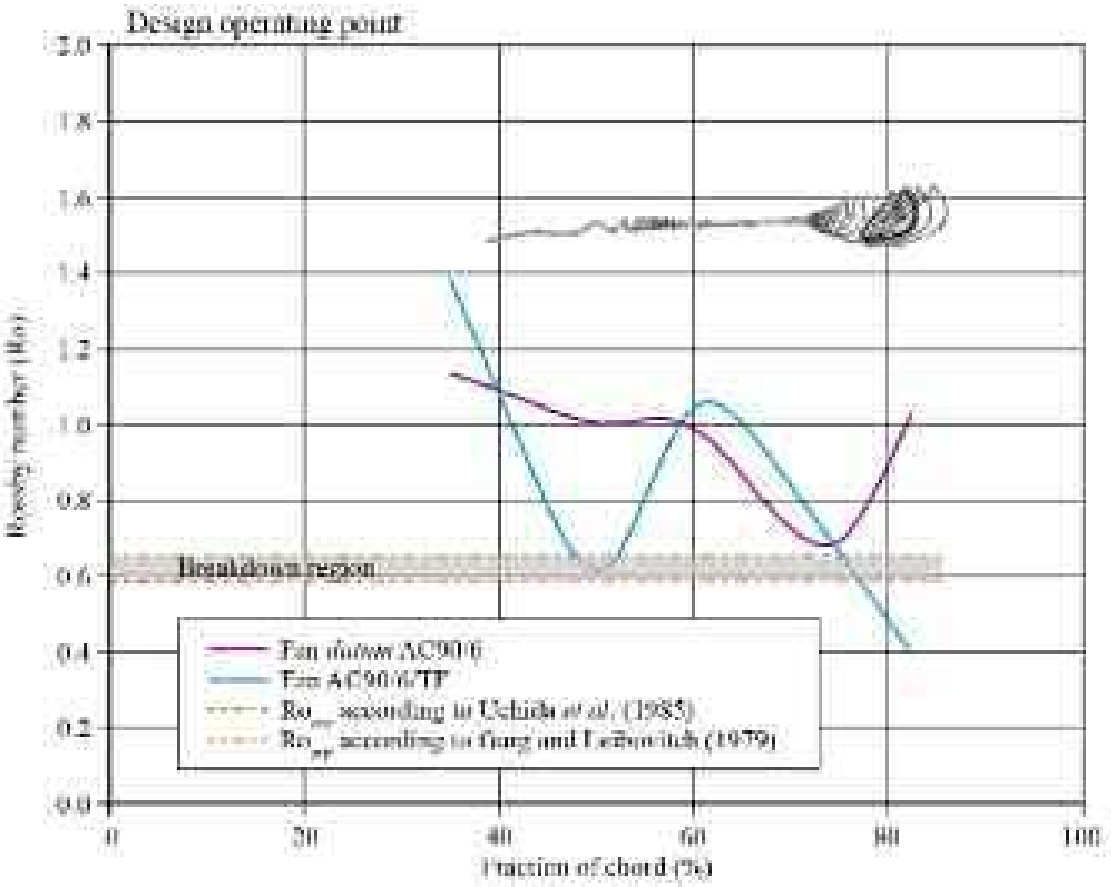

FIGURE 10.2. Chord-wise evolution of numerically predicted blade tip-to-casing leakage vortex Rossby number (*Ro*) at the fan design operating point for the fan *datum* AC90/6 and AC90/6/TF (Corsini and Sheard, 2007).

We studied both the aerodynamic and acoustic performance of all five configurations, both experimentally and by predicting the blade-to-blade flow-field using a numerical method. Thus, we were able to compare the performance of the stepped configurations with both the same configuration without the step, and with the *datum* configuration.

Flow Conditions

The studied fan blade tip pitch angle is adjustable and may be set to a pitch angle between 16 and 28 degrees. In practical application, the blade tip pitch angle is typically set to 28 degrees as this maximises flow rate for a given system pressure. In the research reported in this chapter, we conducted the experimental measurements with the fan blade tip pitch angle to 28 degrees. We selected 28 degrees both because it is typical of the angle that one uses in practical application and because it results in the highest blade loading. A highly loaded blade results in the blade tip-to-casing leakage vortex having the most significant effect on both fan aerodynamic and acoustic performance (Holste and Neise, 1997).

The impact of the blade tip-to-casing leakage vortex on both fan aerodynamic and acoustic performance results in the application of blade-tip end-plates changing not only the fan's acoustic performance, but also aerodynamic performance. Consequently, the fan *datum* AC90/6 generates a different pressure at a constant flow rate when fitted with each of the studied blade-tip end-plates. To facilitate the comparison of fan performance data when fitted with different blade-tip end-plates, we chose to define three operating points, and their respective volume flow rates, Table 10.2. The design operating point volume flow rate is typical of that required when one installs the fan over a cooling unit's tube bank. The peak pressure flow rate is typical of that required when the tube bank has become partially blocked following a period of in-service operation. The maximum flow operating point volume flow rate is typical of the flow rate that occurs with the lowest pressure loss tube banks currently operating in service.

Table 10.2. *The operating points used when characterising the studied fan's performance with and without fitted blade-tip end-plates. The authors measured performance characteristics in a Type D standardised airway (ducted inlet, ducted outlet) in accordance with ISO 5801:2007 requirements (2007).*

Operating point	Volume flow rate (m^3/s)	Studied blade tip pitch angle (°)
Maximum flow	7.0	28
Design	6.5	28
Peak pressure	5.6	28

Aerodynamic Performance

Bianchi *et al.* (2009a) measured the performance characteristics of the fan *datum* AC90/6, AC90/6/TF, AC90/6/TF$_{VTE}$. Bianchi *et al.* (2009b) measured the performance characteristics of the fan AC90/6/TF$_{step}$ and AC90/6/TF$_{VTE\ step}$. They made all measurements in accordance with ISO 5801:2007 requirements (2007). The addition of the constant and variable thickness blade-tip end-plates resulted in increased blade loading. We would expect blade-tip noise sources to become more acoustically productive with increased blade loading. Therefore, an increase in blade loading will partially offset any reduction in fan far-field noise attributed to adding a blade-tip end-plate. We conservatively assess the reduction in fan far-field noise if one neglects an increase in blade loading. Despite fan far-field noise serving as a function of blade loading, we chose to neglect the change in pressure rise with the change in blade-tip treatment.

COMPUTATIONAL AND EXPERIMENTAL METHODOLOGY

In the research reported in this chapter, we focused on both the experimental and computational analysis on the far-field acoustic consequence of near-field flow-field features. We aimed to associate blade-tip end-plate features with specific near-field flow-field features and their far-field acoustic consequences. Therefore, the adopted methodology combined blade-tip flow-field predictions with an experimental assessment of fan far-field acoustic performance.

Near-field Acoustic Measurement Technique

Following Bianchi *et al.*'s (2009a) method, we made near-field measurement at the fan outlet by mounting a microphone on a 10 mm radial traversing mechanism 10 per cent blade chord downstream of the blade trailing edge. We then used the traversing mechanism to move the near-field microphone from the blade hub to tip, in radial steps corresponding to two per cent of blade span. Thus, the traversing microphone facilitated the span-wise measurement of near-field fan noise.

We conducted hot-wire anemometer measurements to determine the flow velocity at each of the exhaust span-wise microphone locations. As the exhaust microphone was located immediately downstream of the blade trailing edge, we chose to calibrate the traversing microphone in a dedicated test rig. We measured the background noise in the test rig with no flow, and then induced the airflow corresponding to each microphone's span-wise location. This facilitated calculation of self-induced noise correction factors for the traversing microphone.

Far-field Acoustic Measurements Technique

Following Bianchi *et al.*'s method (2009a), we measured far-field noise six fan diameters from the fan exhaust, as recommended by Leggat and Siddon (1978),

when measuring a fan's far-field noise without any obstructions downstream of the fan. Leggat and Siddon (1978) studied the directivity of fan noise in a semi-reverberant environment concluding that the maximum noise levels were coincident with the fan axis, immediately downstream of the exhaust. In the research reported in this chapter, we chose to place the far-field microphone at an angle 30 degrees from the fan axis. We chose to do this to avoid the possibility of the fan exhaust flow impacting directly on the far-field microphone. Our logic was that the anechoic chamber within which we made our measurements was not infinitely large. Consequently, there was a possibility that the fan would induce flow-field features within the anechoic chamber itself that may have acoustic consequences.

By placing the microphone at an angle 30 degrees from the fan axis, we placed it in a location with the lowest flow-field velocity within the anechoic chamber. We considered that low flow-field velocities would result in any flow-field features within the anechoic chamber also having a low impact on measured far-field noise. We selected the location of the far-field microphone following a measurement of flow-field velocity at different locations within the anechoic chamber. The chosen location flow-field velocity was less than 0.1 m/s which we considered negligible.

Numerical Procedure and Axial Fan Modelling

In the programme of work reported in this chapter, we simulated the blade-to-blade flow-field with a Reynolds-Averaged Navier–Stokes (RANS) based non-linear code, with two-equation closure (Craft *et al.*, 1996). The two-equation closure was able to cope with non-isotropic and non-equilibrium turbulence effects without a significant increase in the required computational effort. The code utilised a parallel multi-grid (MG) numerical scheme, developed for an in-house finite element method (FEM) code which Borello *et al.* (2003) first proposed. Corsini and Sheard (2007) applied Borello *et al.*'s (2003) numerical procedure to the study of blade-tip end-plates with Corsini *et al.* (2007) refining the procedure. It is Corsini *et al.*'s (2007) numerical procedure that we have used during the course of the research reported in this chapter.

The finite element method formulation is based on a stabilised Petrov-Galerkin (PG) method modified for application to three-dimensional equal- and mixed-order spaces of approximation. We used the Petrov-Galerkin scheme to control the instability that affects the advective-diffusive incompressible flow, and the momentum's reaction and turbulent scale equations. The turbulent scale equations relate to Coriolis acceleration (Corsini *et al.*, 2004a). We used equal-order Q1-Q1 and mixed-order Q2-Q1 interpolation for primary turbulent scale equations and constrained secondary variables, implicitly eliminating the undesirable pressure-checker boarding effects. We performed the computational analysis using the hybrid full linear multigrid accelerator running on an overlapping parallel solver (Borello *et al.*, 2001).

In our Reynolds-Averaged Navier–Stokes simulations, we utilised a non-linear k-ε turbulence model in its topology-free low-Reynolds number formulation (Craft *et al.*, 1996). Although a well proven approach for modelling vortex structures (Inoue and Furukawa, 2002), the simulation was not able to model unsteady effects

and therefore models only part of the flow-field physics. Despite this caveat, Corsini and Rispoli (2004) were able to validate the modelling approach when they applied it into a compressor application. Corsini and Rispoli (2005) were also able validate the modelling approach in an air movement fan application.

Computational Mesh and Boundary Conditions

The approach we adopted when constructing a computational mesh utilised a non-orthogonal body fitted H-type grid system. We split the mesh into two regions, one in the blade-to-blade region and a second in the blade tip-to-casing gap. In total the mesh comprised $154 \times 68 \times 58$ nodes in the axial-, pitch- and span-wise directions. In the axial direction, 20 per cent of the nodes were distributed upstream of the blade leading edge, 50 per cent were within the blade passage and 30 per cent were downstream of the blade trailing edge. In the span-wise direction, 14 of the 58 nodes were spaced across the blade tip-to-casing gap. All mesh density regions maintained an adequate computational cell aspect ratio toward solid boundaries. The computational grid developed for the blade illustrates how mesh density increased in the solid wall's near vicinity, Figure 10.3.

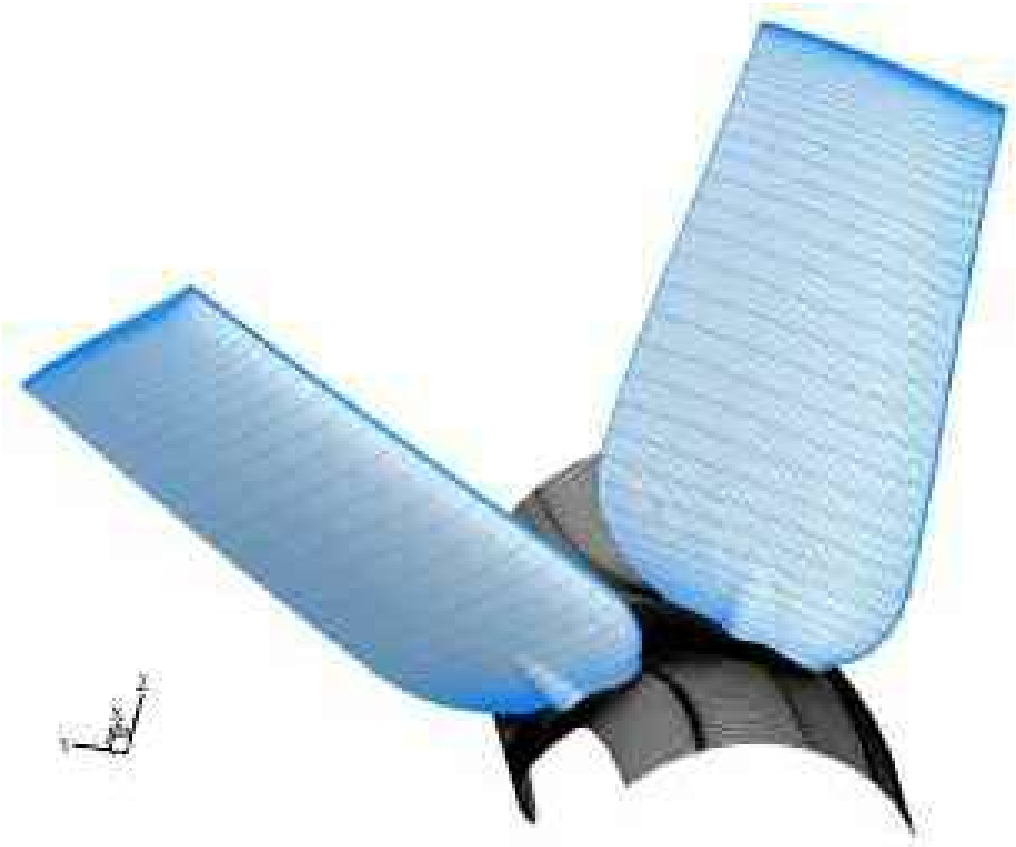

FIGURE 10.3. The computational grid used in the numerical simulations. The mesh was formed by merging a structured H-type grid though the up-stream, blade-to-blade passage and down-stream region with a second H-type grid in the blade tip-to-casing region.

We defined the boundary conditions according to Corsini and Rispoli (2004) and Corsini *et al.*'s (2004b) recommendations. They studied the performance of ducted high-solidity fans. The Dirichlet conditions for the relative velocity components are imposed at the inflow section, half a mid-span chord upstream of the blade leading edge, as obtained from a flow simulation in an annular passage of identical hub-to-casing diameter ratio that includes an upstream spinner cone.

We used a turbulent kinetic energy (k) pitch-wise profile derived from an axisymmetric turbulence intensity profile previously developed by Corsini and Rispoli (2004). The turbulence intensity profile was a near-uniform six per cent across the annulus, increasing to ten per cent near the casing. We used the turbulent kinetic energy's pitch-wise profile to calculate the radial distribution of dissipation based on a dissipation length scale (l_ε) of one per cent of blade mid-span pitch. We completed the boundary conditions by assuming periodicity both up- and down-stream of the fan blades.

AEROACOUSTIC PROPERTIES OF THE BLADE-TIP END-PLATE

We conducted the experimental measurements in an anechoic chamber in accordance with ISO 10302:1996 requirements (1996). We made acoustic measurements using microphones at the fan outlet, recording the near- and far-field signals on two channels of a data acquisition system. An aerofoil louver in the top of the anechoic chamber inlet section facilitated the fan flow rate variation. We aerodynamically optimised the fan inlet bell mouth profile to provide uniform and unseparated flow into the fan. The fan was connected to the outside environment via up- and down-stream plenums. We designed these plenums to minimise in-flow non-uniformities and acoustically treated them to both minimise noise transmission from the external environment and its reflection inside plenum ductwork. We also covered the anechoic chamber walls with foam panels to further reduce noise transmission from the external environment.

Narrowband Spectra Analysis

We commenced our analysis of fan far-field noise with a study of outlet far-field narrowband sound pressure level (L_P) spectrum measured at the fan design operating point. For the sake of clarity, we considered the narrowband sound pressure level spectrum from zero to 1 kHz and from 1 kHz to 5 kHz. The narrowband sound pressure level spectrum from zero to 1 kHz facilitates a study of tonal features. The narrowband sound pressure level spectrum from 1 kHz to 5 kHz facilitates the characterisation of fan broadband noise.

Consider the outlet far-field narrowband sound pressure level (L_P) spectrum from zero to 1 kHz for the fan *datum* AC90/6, AC90/6/TF and AC90/TF$_{VTE}$, Figure 10.4 and fan *datum* AC90/6, AC90/6/TF$_{step}$ and AC90/TF$_{VTE\ step}$, Figure 10.5. We

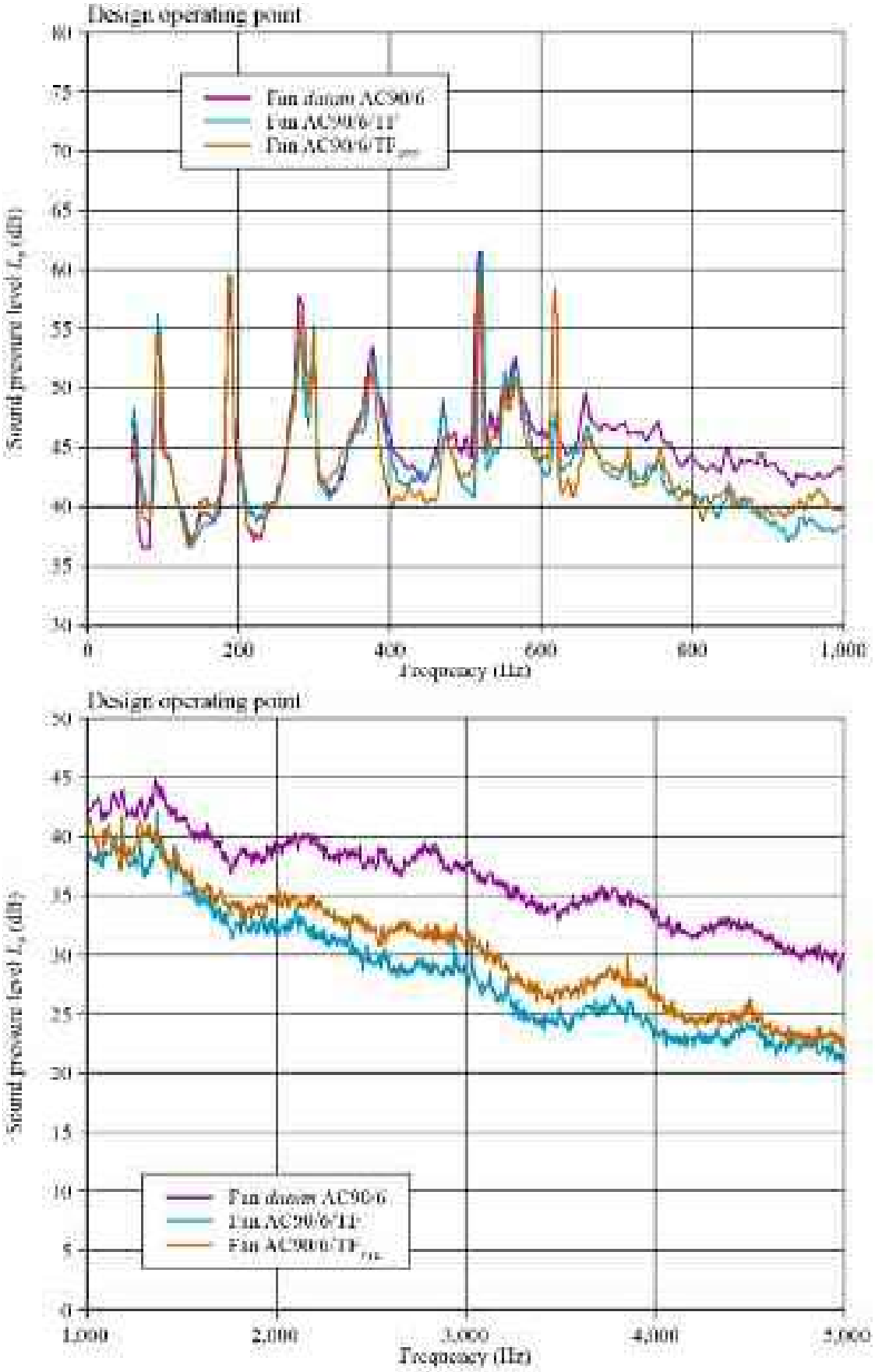

FIGURE 10.4. Outlet far-field narrowband sound pressure level (L_P) spectrum measured at the fan design operating point for the studied blade-tip end-plates. For the sake of clarity, the narrowband sound pressure level spectrum is from zero to 1 kHz and from 1 kHz to 5 kHz. We present measured narrowband sound pressure level spectrum data for the fan *datum* AC90/6, AC90/6/TF and AC90/6/TF$_{VTE}$.

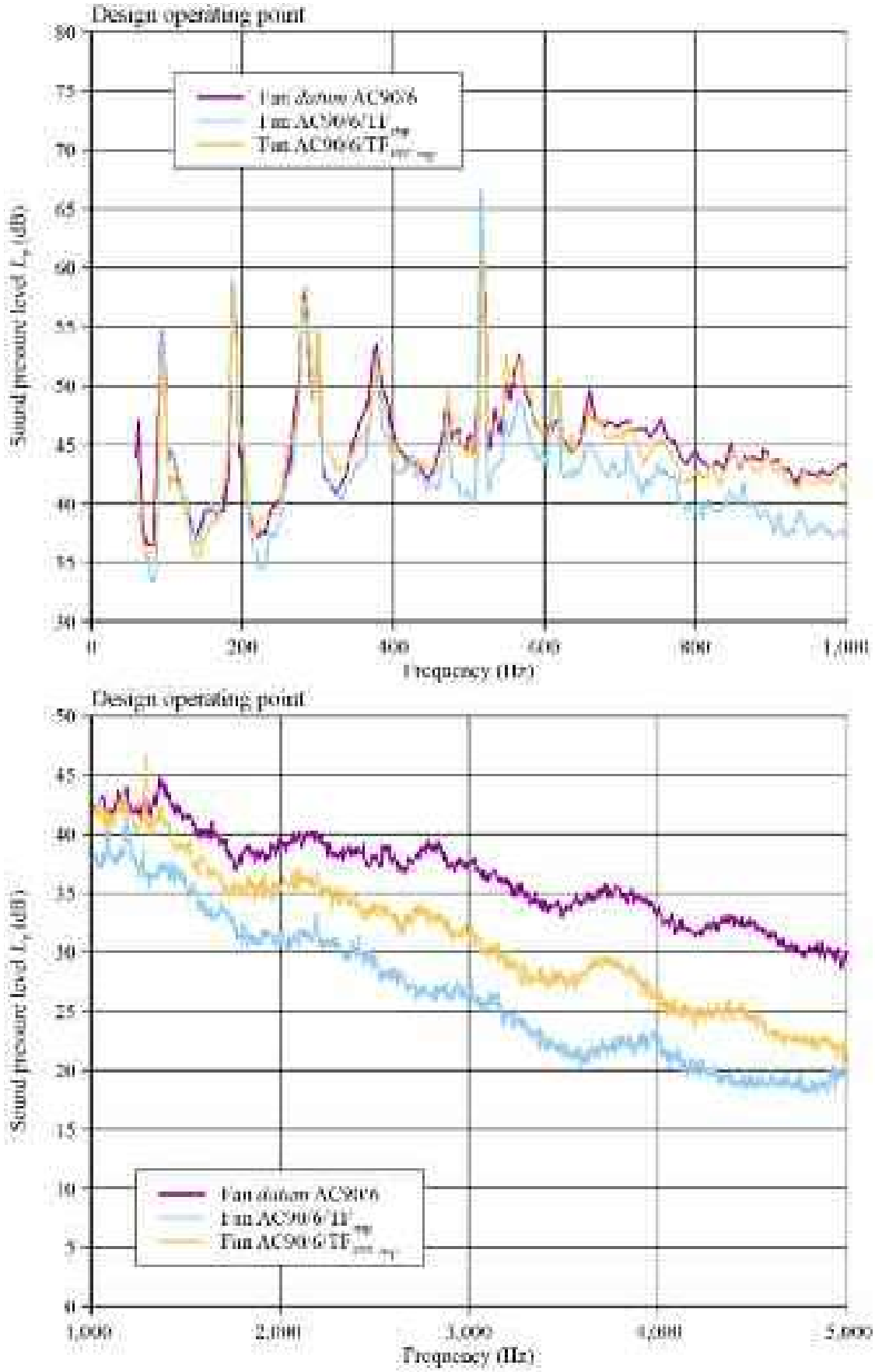

FIGURE 10.5. Outlet far-field narrowband sound pressure level (L_P) spectrum measured at the fan design operating point for the studied blade-tip end-plates. For the sake of clarity, the narrowband sound pressure level spectrum is from zero to 1 kHz and from 1 kHz to 5 kHz. We present measured narrowband sound pressure level spectrum data for the fan *datum* AC90/6, AC90/6/TF$_{step}$ and AC90/6/TF$_{VTE\ step}$.

may group the tonal features into two categories: those associated with the blade passing frequency and its harmonics and those that are not. Blade passing frequency is 95 Hz, with significant tones up to the fourth harmonic and evident up to the sixth harmonic.

The fourth harmonic of blade passing frequency is coincident with the median frequency of Wright's (1976) spectrum for turbulent self-generated noise. This coincidence confirms that self-generated noise sources dominate over interaction noise sources, with the exception of tones we can associate with the fan motor. There are two motor tones: one just above the third and one between the fifth and sixth harmonic of blade passing frequency.

Between tonal features it is apparent that both the constant and variable thickness blade-tip end-plates result in a generally lower sound pressure level. We may associate this improvement with the end-plates' impact on the blade tip-to-casing leakage vortex. Khourrami and Choudari (2001) have linked blade tip-to-casing leakage vortex stability to self-generated broadband noise. The leakage vortex also interacts with blade-to-blade passage secondary flow features and the blade wake, both of which are potentially acoustically productive.

Consider the narrowband sound pressure level spectrum from 1 kHz to 5 kHz for the fans *datum* AC90/6, AC90/6/TF, AC90/6/TF$_{VTE}$, AC90/6/TF$_{step}$ and AC90/6/TF$_{VTE\ step}$. The impact of the blade-tip end-plates becomes apparent at approximately 2 kHz, the frequency at which the sound pressure levels separate. A significant feature of the broadband spectra is the impact of the step feature. The step feature has relatively little impact on the broadband spectra of fan AC90/6/TF$_{VTE\ step}$. In contrast, the broadband spectra of fan AC90/6/TF$_{step}$ is lower than that of fan AC90/6/TF.

We may further characterise the studied fans using Bianchi *et al.*'s (2009a) method to generate outlet sound pressure level cross spectra, Figure 10.6. The outlet sound pressure level cross spectra illustrate the significance of the first, second and third blade passing frequencies. Although the fourth blade passing frequency is discernable, it has all but merged with the broadband noise and therefore we may regard it as an insignificant tonal component of the far-field noise.

Consider the sound pressure level cross spectra at the blade passing frequency for the fans *datum* AC90/6, AC90/6/TF and AC90/6/TF$_{VTE}$. The first blade passing frequency tone is the dominant feature of the sound pressure level cross spectra. The constant thickness blade-tip end-plate has reduced the peak by a little less than 2dB. In contrast, the variable thickness blade-tip end-plate had reduced the peak by approximately 5 dB.

Consider the sound pressure level cross spectra of the second harmonic of blade passing frequency for the fans *datum* AC90/6, AC90/6/TF and AC90/6/TF$_{VTE}$. Bianchi *et al.* (2009b) studied the blade passing frequency's second harmonic. They concluded that this occurred with a disturbance of the inflow into the fan which resulted in a noise source of constant magnitude along the entire blade span from hub to tip. As the noise source occurs as a consequence of a disturbance of the inflow into the fan, it is independent of blade-tip end-plate geometry.

Consider the sound pressure level cross spectra at the third harmonic of blade passing frequency for the fans *datum* AC90/6, AC90/6/TF and AC90/6/TF$_{VTE}$. Both

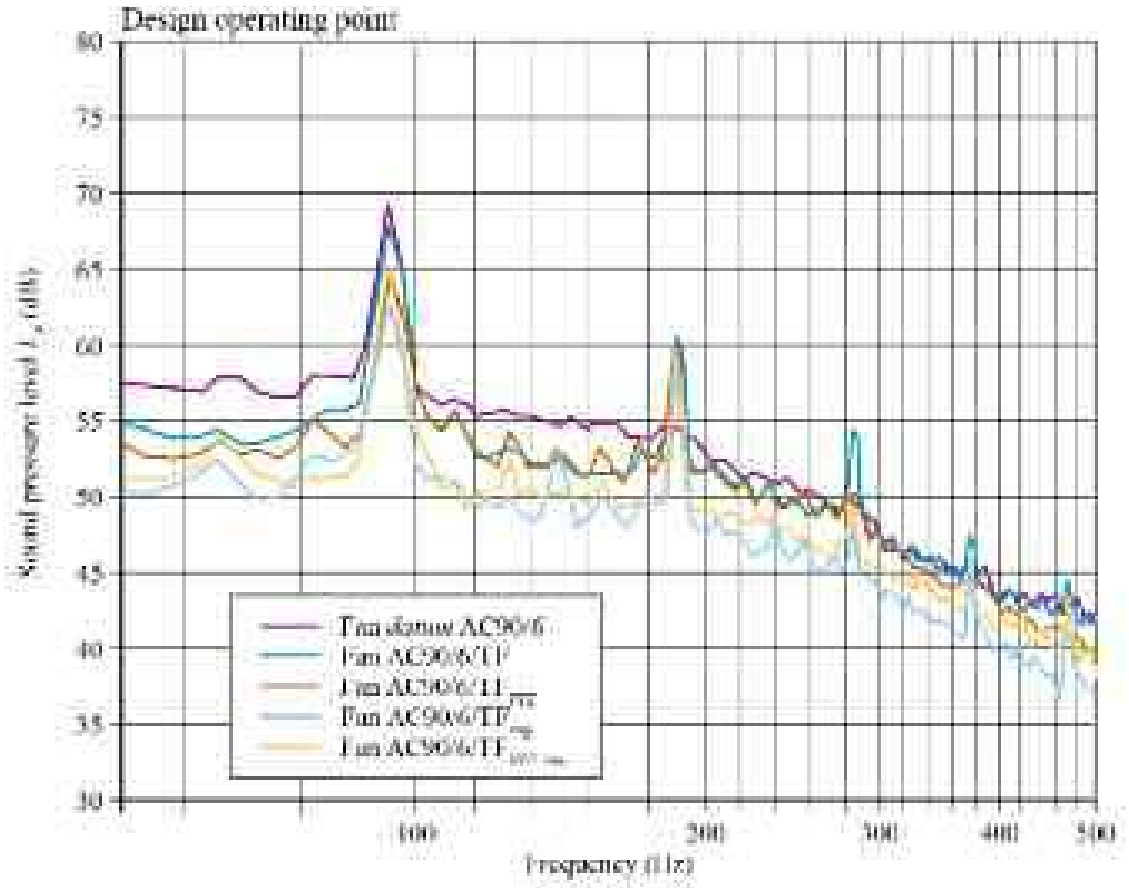

FIGURE 10.6. Outlet near- to far-field sound pressure level (L_P) cross spectrum measured at the fan design operating point for the five studied blade-tip end-plates.

the constant and variable thickness blade-tip end-plates result in an increased sound pressure level cross spectra when compared to the fan *datum* AC90/6.

Consider the sound pressure level cross spectra for the fans AC90/6/TF_{step} AC90/6/$TF_{VTE\ step}$. Adding the step feature to both the constant and variable thickness blade-tip end-plates resulted in a reduced magnitude of both tonal features and broadband noise. The reduction in tonal peaks is a consequence of the blade-tip end-plates controlling the turbulent mixing of the blade tip-to-casing leakage vortex with other flow-field features. The fan AC90/6/TF_{step} exhibited the lowest tonal peak and broadband noise, with an overall noise level approximately 3 dB lower than fan *datum* AC90/6. It is noteworthy that the fan AC90/6/TF_{step} had consistently lower tonal and broadband noise than the fan AC90/6/$TF_{VTE\ step}$. This indicates that the step feature is more effective when applied to the constant thickness than the variable thickness blade-tip end-plate.

Overall Sound Level Analysis

We complemented our analysis of outlet far-field narrowband sound pressure level (L_P) spectrum with a comparison of specific noise level (K_S) over the operating range of each of the studied fan configurations, Figure 10.7. We calculated specific

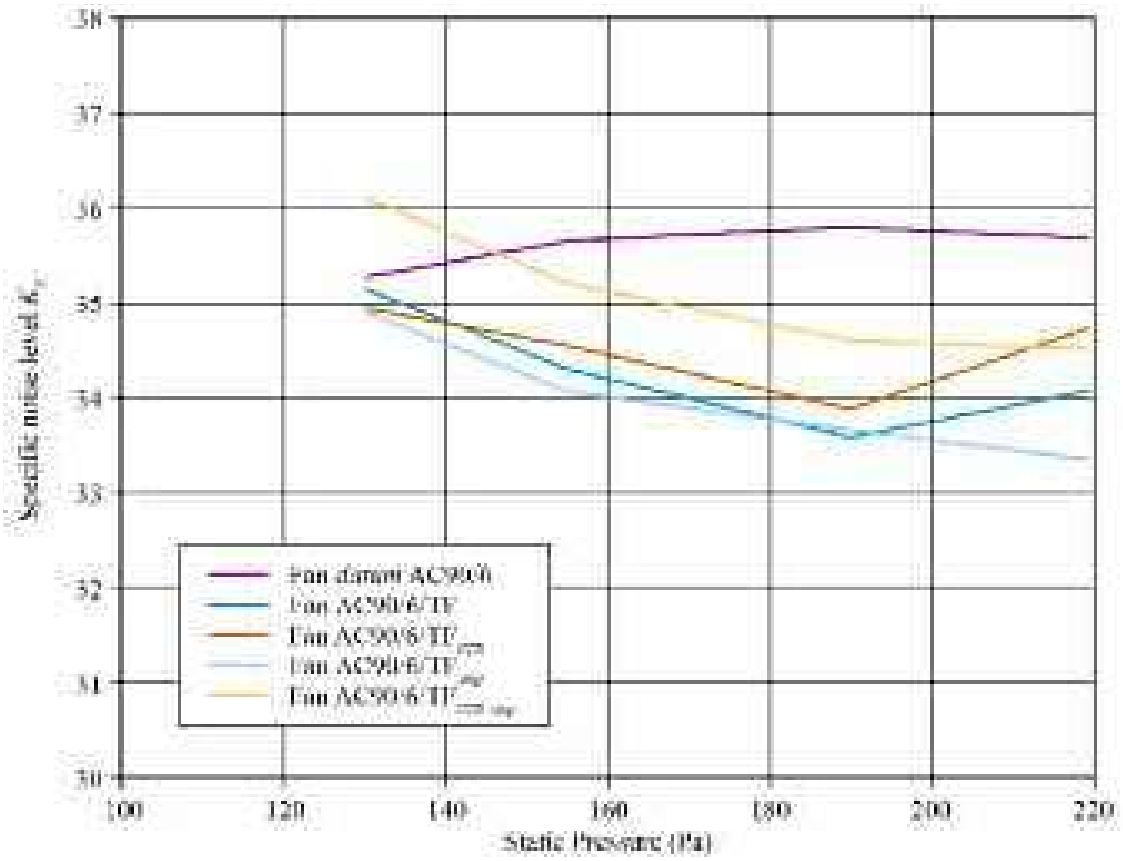

FIGURE 10.7. A comparison of specific noise level (K_S) measured over the operating range of each of the five studied fan configurations.

noise level using Fukano *et al.*'s (1986) method. The step feature results in lower specific noise levels over the entire fan operating range when fitted to the constant thickness blade-tip end-plate. The constant thickness blade-tip end-plate performed consistently better than the variable thickness blade-tip end-plate. However, an unexpected feature of the specific noise level distribution was the reduction as the fans AC90/6/TF$_{step}$ and AC90/6/TF$_{VTE\ step}$ approached stall. As Fukano *et al.* (1986) observed, as a fan approaches stall, the noise sources responsible for tones become more acoustically productive. Therefore, we anticipated that the fans AC90/6/TF$_{step}$ and AC90/6/TF$_{VTE\ step}$ would exhibit increasing specific noise levels as they approached stall.

We complemented our analysis of specific noise level with an analysis of unweighted sound power level (L_W). The analysis of specific noise level indicated that the studied fans did not respond to changing operating point as anticipated. Therefore, we chose to measure un-weighted sound power level at both the design and peak pressure operating points with blade angles of both 24 and 28 degrees, Table 10.3.

Consider the unweighted sound power level at 24 and 28 degrees for each of the studied fan configurations. At the design operating point, a change in blade angle from 24 to 28 degrees resulted in an increase for all five studied fan configurations.

Table 10.3. *Experimentally measured acoustic performance for the five studied fan configurations at their design and peak pressure operating points. The authors made acoustic measurements in accordance with ISO 10302:1996 requirements (1996).*

	Unweighted sound power level L_W (dB)	
Design operating point	24 degrees	28 degrees
datum AC90/6	70.5	72.4
AC90/6/TF	68.1	70.2
AC90/6/TF_{VTE}	68.9	70.5
AC90/6/TF_{step}	69.6	69.9
AC90/6/$TF_{VTE\ step}$	70.2	71.1
Peak pressure operating point	24 degrees	28 degrees
datum AC90/6	73.9	72.8
AC90/6/TF	70.6	69.7
AC90/6/TF_{VTE}	69.4	70.0
AC90/6/TF_{step}	69.7	69.7
AC90/6/$TF_{VTE\ step}$	70.4	71.8

At the peak pressure operating point, a change in blade angle from 24 to 28 degrees resulted in slight decreases for the fans *datum* AC90/6, AC90/6/TF and AC90/6/TF_{VTE}. The fan AC90/6/TF_{step} remains constant and the fan AC90/6/$TF_{VTE\ step}$ increases slightly. When we assess the performance of the five studied fan configurations, it is noteworthy that the fan AC90/6/TF_{step} exhibits an almost constant unweighted sound power level. Therefore, we may conclude that the fan AC90/6/TF_{step} is relatively less sensitive than the other configurations to changes in blade angle and operating point.

BLADE-TIP END-PLATE EFFECTIVENESS

The purpose of the research reported in this chapter is to evaluate the effectiveness of the blade-tip end-plate geometry, and specifically the step feature. We have studied effectiveness through an analysis of measured far-field narrowband sound pressure level spectrum, sound pressure level cross spectra, specific noise level and unweighted sound power level. Our analysis indicates that the step feature results in lower fan far-field noise when fitted to the constant thickness blade-tip end-plate. When fitted to the variable thickness blade-tip end-plate, the step feature results in increased fan far-field noise. We may complement the above analysis of experimental data with a computational analysis.

The computational analysis is particularly helpful when visualising the flow-field features that develop though the blade tip-to-casing gap. We may use it to

compute a range of flow-field parameters. In the research reported in this chapter we chose to compute:

- normalised helicity (H_n) distributions;
- Powell sound-source distributions; and,
- total pressure loss (ζ) distributions.

When studying tip-clearance flow-field features, Furukawa *et al.* (1999) and Inoue and Furukawa (2002) studied normalised helicity (H_n). Normalised helicity is a useful parameter as it facilitates the visualisation of blade tip-to-casing leakage vortex core trajectories. Powell (1963, 1964) sound-source distributions facilitate the identification of predominant noise sources. We may combine three-dimensional total pressure-loss coefficient (ζ) distributions with leakage vortex trajectories. The combination provides an insight into the impact of blade-tip end-plate on the entire blade-to-blade flow-field.

Helicity Distributions and Vortex Core Trajectories

Following Corsini *et al.*'s method (2007), we computed normalised helicity for the five studied fan configurations. We chose to present normalised helicity contours on cross planes at 25, 43, 65, 89 and 120 per cent blade chords from the blade tip's leading edge. Through these planes, we then plotted the blade tip-to-casing leakage vortex trajectory, Figure 10.8.

Consider the normalised helicity contours and blade tip-to-casing leakage vortex trajectory for the fan *datum* AC90/6, Figure 10.8. The blade tip-to-casing leakage vortex (TLV1) is well defined, with the vortex trajectory departing from the blade suction surface as it progresses from blade leading to trailing edge. There is also evidence of a weaker secondary tip-to-casing leakage vortex (TLV2) that appears close to the suction surface 65 per cent blade chord downstream of the blade leading edge. As the vortex progress towards the blade trailing edge, they merge into the blade tip-to-casing leakage vortex (TLV1). The result is a well-defined vortex that affects a significant proportion of the blade-to-blade passage in the blade tip region.

Consider the normalised helicity contours and blade tip-to-casing leakage vortex trajectory for the fan AC90/6/TF, Figure 10.8. The helicity contours indicate the presence of a vortex in the blade tip region of the blade pressure surface from 43 to 89 per cent blade chord. This vortex may be the pressure-side leg of a blade-to-blade passage horseshoe vortex, and its presence will limit the blade tip-to-casing leakage flow. As we previously observed with fan *datum* AC90/6, the blade tip-to-casing leakage vortex departs from the suction surface. However, its helicity magnitude is generally lower than fan *datum* AC90/6. Further, the secondary tip-to-casing leakage vortex is not apparent in the helicity contours. If it is present at all, it does not merge with the blade tip-to-casing leakage vortex, but simply decays.

By mid-chord the helicity contours indicate that the blade tip-to-casing leakage vortex helicity has reduced. This reduction is probably a consequence of the reduced

blade tip-to-casing leakage flow rate and the deflection of the vortex core. As it moves towards the blade trailing edge, helicicy falls to zero which we may interpret as evidence of vortex breakdown. After it has broken down, the tip-to-casing leakage vortex flow acquires anti-clockwise vorticity as a consequence of the adjacent trailing edge blade tip-to-casing flow. This anti-clockwise vorticity washes out by the time it reaches the blade trailing edge, with no evidence of clockwise- or anti-clockwise helicity.

Consider the normalized helicity contours and blade tip-to-casing leakage vortex trajectory for the fan AC90/6/TF$_{VTE}$, Figure 10.8. The variable thickness blade-tip end-plate has a significant impact on the flow-field in the blade tip region. The onset of the blade tip-to-casing leakage vortex is apparent by 43 per cent blade chord. This is in contrast to the fan *datum* AC90/6 and AC90/6/TF where it is apparent at 25 per cent blade chord. Additionally, the vortex trajectory for fan AC90/6/TF$_{VTE}$ remains relatively close to the blade suction surface when compared to either fan *datum* AC90/6 or AC90/6/TF.

By mid-chord there is evidence that the blade tip-to-casing leakage vortex is interacting with a weak anti-clockwise vortex. This vortex is apparent on the blade suction surface at 65 per cent blade chord. This vortex appears to be highly energetic and we may regard it as a leakage jet of blade pressure surface boundary layer fluid. This jet merges with the blade tip-to-casing leakage vortex and as it does so, the leakage vortex rotation changes from clockwise- to anti-clockwise. As it moves towards the blade trailing edge, the blade tip-to-casing leakage vortex merges with the trailing edge blade tip-to-casing flow, changing the blade tip-to-casing leakage vortex rotation from anti-clockwise to clockwise as it exits the blade-to-blade passage.

Consider the normalised helicity contours and blade tip-to-casing leakage vortex trajectory for the fan AC90/6/TF$_{step}$, Figure 10.8. The step feature results in a deceleration of fluid flowing through the blade tip-to-casing gap. A result of this deceleration is that the blade tip-to-casing leakage vortex moves down-stream relative to fan AC90/6/TF. The fan AC90/6/TF$_{step}$ blade tip-to-casing leakage vortex normalised helicity is also generally lower than that of fan AC90/6/TF. The fan AC90/6/TF$_{step}$ blade tip-to-casing leakage vortex remains close to the blade suction surface until the blade trailing edge. Like fan AC90/6/TF, the blade tip-to-casing leakage vortex then changes rotation direction and breaks down.

Consider the normalised helicity contours and blade tip-to-casing leakage vortex trajectory for the fan AC90/6/TF$_{VTE\ step}$, Figure 10.8. The inclusion of the step feature has had a significant impact on the blade tip-to-casing leakage vortex. When compared to the leakage vortex of fan AC90/6/TF$_{VTE}$, a reduction in momentum characterises it. This reduction is a consequence of reduced momentum transfer within the blade tip-to-casing gap to the leakage vortex. As a consequence, the fan AC90/6/TF$_{VTE\ step}$ leakage vortex remains closer to the blade suction surface. Unlike the fan AC90/6/TF$_{VTE}$, it did not reverse its rotational direction. Therefore, we may conclude that the step feature had a more substantive impact on the leakage vortex of fan AC90/6/TF$_{VTE\ step}$ than fan AC90/6/TF$_{step}$. Additionally, the fan AC90/6/TF$_{step}$ and AC90/6/TF$_{VTE\ step}$ are each characterised by lower normalised helicity blade tip-to-casing leakage vortex than fan AC90/6/TF or AC90/6/TF$_{VTE}$. This indicates that in-

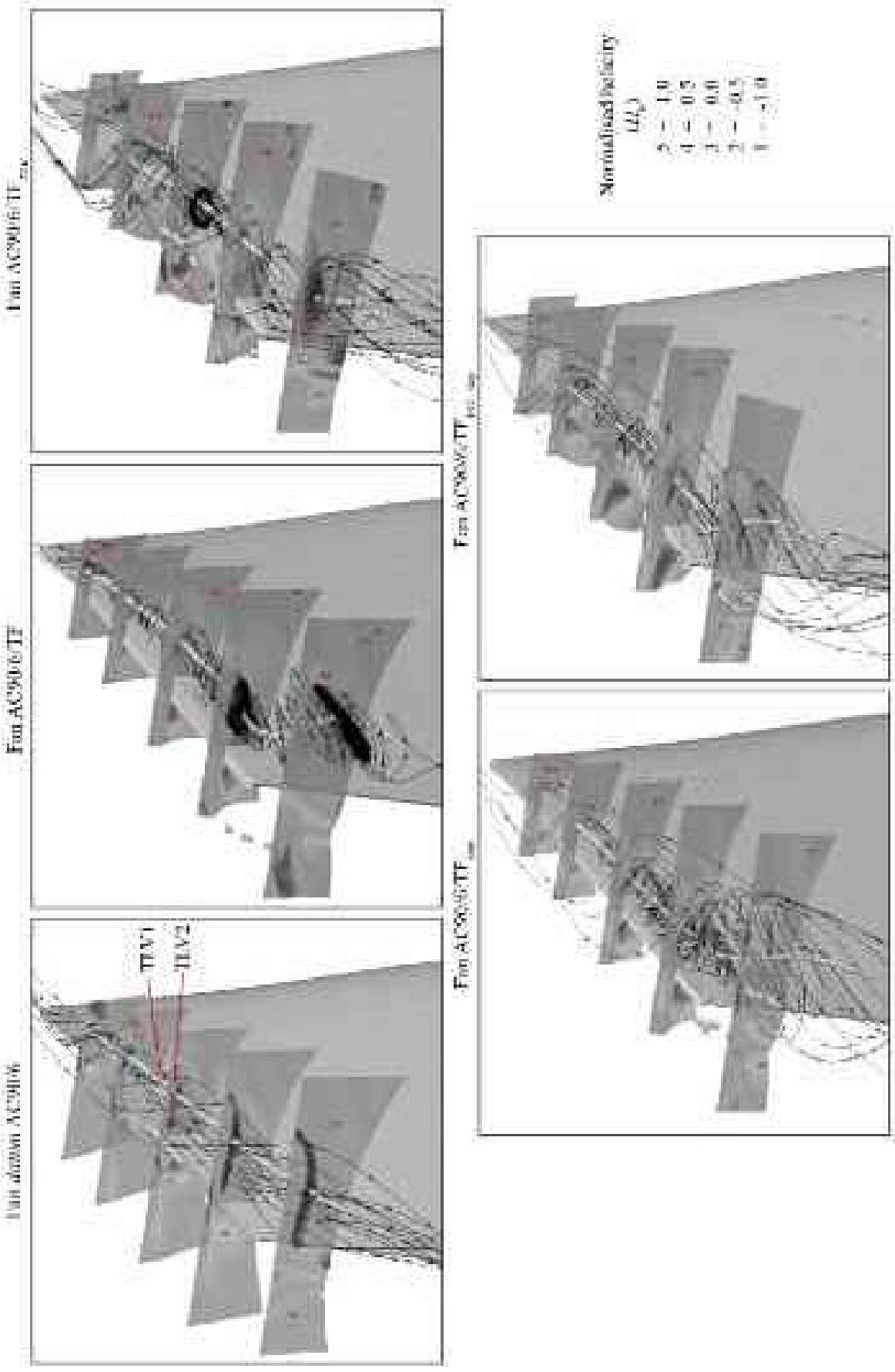

FIGURE 10.8. Three-dimensional normalised helicity (H_n) contours numerically predicted at the fan design operating point. We present helicity contours at five chordwise location through the fan *datum* AC90/6, AC90/6/TF, AC90/6/TF$_{VTE}$, AC90/6/TF$_{step}$ and AC90/6/TF$_{VTE\ step}$. The blade tip-to-casing leakage vortex streamlines illustrate the effect of fitting a constant and variable thickness blade-tip end-plate and a step.

cluding the step feature results in an overall reduction in blade tip-to-casing gap leakage flow rate, and momentum transfer within the gap.

We may complement our helicity study with an analysis of the chord-wise evolution of blade tip-to-casing leakage vortex trajectory. We calculated the vortex core trajectories using Sujudi and Haimes's (1995) critical point theory. Comparing the vortex trajectories illustrates the impact of the studied blade-tip end-plates on the leakage vortex, Figure 10.9. A feature common to both the leakage vortex trajectory for the fan AC90/6/TF and AC90/6/TF$_{VTE}$ is a sudden change in direction, which occurs as the vortex's direction of rotation changes. In contrast, there is no sudden change in direction for the fan *datum* AC90/6 or change in its rotation direction.

Corsini *et al.* (2007) studied leakage vortex trajectories, concluding that there are additional organised vortical structures that occur with the fan AC90/6/TF$_{VTE}$. These are evident at the blade leading edge, mid-chord and near the blade trailing edge. The additional organised vortical structures are smaller than the leakage vortex

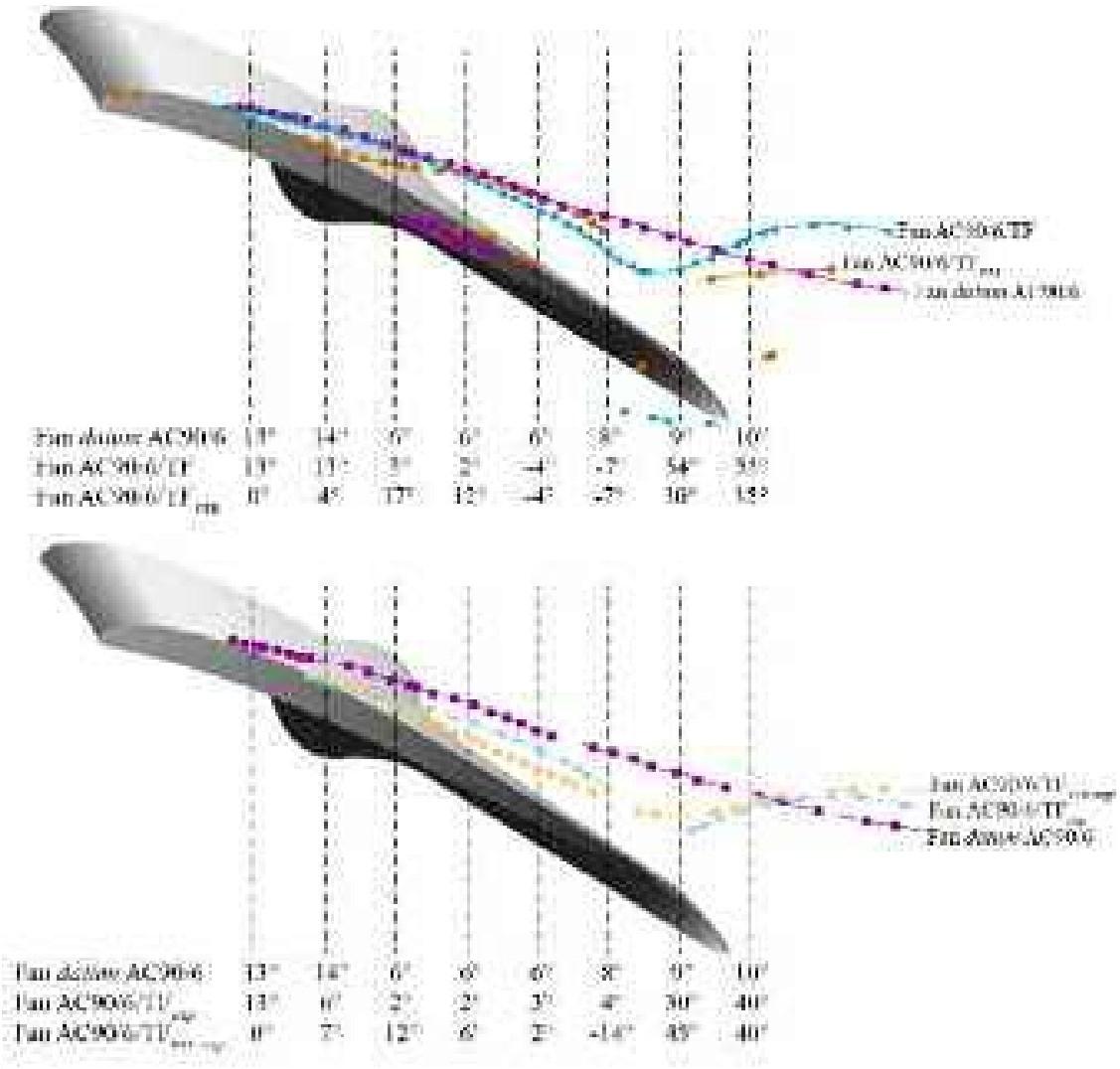

FIGURE 10.9. Chord-wise evolution of the blade tip-to-casing leakage vortex trajectory predicted at the fan design operating point. A comparison of the vortex trajectories illustrates the impact of the studied blade-tip end-plates on the leakage vortex.

and are relatively weak in comparison. As they are relatively weak, we may assume that they burst, resulting in an increase in fan far-field noise. Bianchi *et al.* (2011) measured the far-field noise of both the fan AC90/6//TF and AC90/6/TF$_{VTE}$ concluding that the fan AC90/6/TF$_{VTE}$ far-field noise was approximately 0.5 dB higher than fan AC90/6/TF. As the fan AC90/6/TF leakage vortex bursts and the fan AC90/6/TF$_{VTE}$ leakage vortex does not burst, Bianchi *et al.* (2011) anticipated that the fan AC90/6/TF$_{VTE}$ would have a lower fan far-field noise.

The fan AC90/6/TF leakage vortex bursts, but the leakage vortex trajectories indicate that it does not occur with any additional organised vortical structures. In contrast, the fan AC90/6/TF$_{VTE}$ leakage vortex does not burst, but the leakage vortex trajectories indicate that it occurs with any additional organised vortical structures. Therefore, we may hypothesise that bursting of the additional organised vortical structures that occur with the fan AC90/6/TF$_{VTE}$ is responsible for the increased fan far-field noise. If we accept this hypothesis, then we may conclude the following. The increase in fan far-field noise that occurs with bursting the additional organised vortical structures is greater than the reduction that occurs with the leakage vortex not bursting.

Adding the step feature resulted in two identifiable changes in the leakage vortex trajectories. First, both the fan AC90/6/TF$_{step}$ and AC90/6/TF$_{VTE\ step}$ leakage vortex trajectories shift downstream relative to fan AC90/6/TF and AC90/6/TF$_{VTE}$. We may attribute this shift to the reduction in blade tip-to-casing gap leakage flow rate and the reduced momentum transfer to the leakage vortex in the gap. Second, the leakage vortex trajectories remained closer to the blade suction surface. Again, we may attribute this to the reduced leakage flow rate and reduced momentum transfer.

We complemented our analysis of the chord-wise evolution of the blade tip-to-casing leakage vortex trajectory with an analysis of the blade tip-to-casing gap leakage flow. We calculated chord-wise distributions of leakage vortex axial velocity (w_{LV}) and leakage flow skewing angle (β_{LV}). By averaging both quantities across the blade tip-to-casing gap, we were then able to plot the chord-wise evolution of both parameters, Figure 10.10.

A near constant leakage vortex axial velocity characterises the fan *datum* AC90/6. The absence of a blade-tip end-plate resulted in leakage vortex axial velocity driven by the local blade loading along the blade chord. A relatively uniform leakage vortex axial velocity also characterises the fan AC90/6/TF. A relatively uniform, but consistently lower leakage vortex axial velocity also characterises the fan AC90/6/TF$_{step}$.

In contrast, a reduction in leakage vortex axial velocity over the first 20 per cent of the blade chord each characterise the fan AC90/6/TF$_{VTE}$ and AC90/6/TF$_{VTE\ step}$. From the leading edge to approximately 50 per cent blade chord, the step feature has relatively little impact on leakage vortex axial velocity. Over the rear half of the blade chord, the step feature resulted in the leakage vortex axial velocity remaining relatively low. We may interpret this as a positive impact. The variable thickness blade-tip end-plate itself induces a rapid increase in leakage vortex axial velocity over the blade's rear portion. Therefore, the step feature mitigates a negative aspect that we associate with applying the variable thickness blade-tip end-plate.

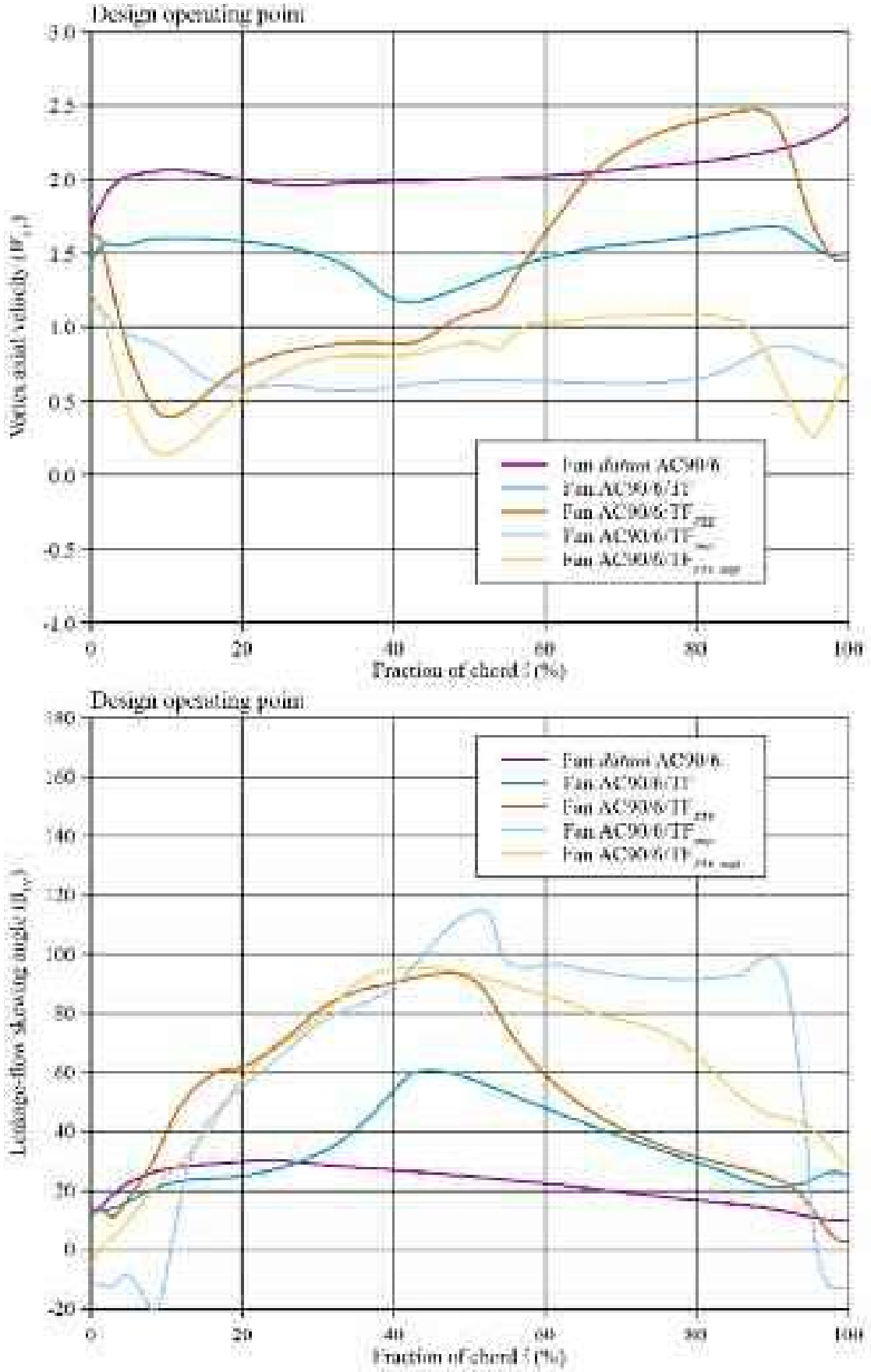

FIGURE 10.10. Chord-wise evolution of the blade tip-to-casing leakage vortex axial velocity (W_{LV}) and leakage-flow skewing angle (β_{LV}) predicted at the fan design operating point. The change in vortex axial velocity and leakage-flow skewing angle illustrates the impact of the studied blade-tip end-plates on the leakage vortex.

A near constant leakage flow skewing angle also characterises the fan *datum* AC90/6. We may associate all four fan configurations with blade-tip end-plates with significantly larger leakage flow skewing angles with significantly larger variations. At mid-chord the fan AC90/6/TF, AC90/6/TF$_{VTE}$ and AC90/6/TF$_{VTE\ step}$ leakage flow skewing angles are orthogonal to the blade chord. These three fan configurations exhibit similar leakage flow skewing angle distributions over the first 50 per cent of the blade chord. Over the rear 50 per cent of the blade chord, fan AC90/6/TF$_{step}$ and AC90/6/TF$_{VTE\ step}$ deviated from the fan AC90/6/TF$_{VTE}$ maintaining a higher leakage flow skewing angle.

Blade-tip Loading Analysis

We complemented our analysis of the blade tip-to-casing gap leakage flow with an analysis of two further parameters. First, we looked at the span-wise evolution of the blade local diffusion factor (DF_{Loc}). Second, we examined the chord-wise evolution of static pressure coefficient (C_P) at the blade tip. Cumpsty (1977) studied the aerodynamic origins of fan far-field noise and concluded that blade tip unloading is a contributory factor in noise generation. Therefore, this analysis of local diffusion factor and static pressure coefficient is useful. It enables us to characterise the extent to which blade-tip end-plates affect blade loading.

Consider the span-wise evolution of local diffusion factor for the five fan configurations, Figure 10.11. The four fan configurations with fitted blade-tip end-plates all feature lower local span-wise distributions of diffusion factor than the fan *datum* AC90/6. Lower local diffusion factors should result in lower fan far-field noise. Measured fan far-field noise for the four fan configurations with fitted blade-tip end-plates at the design operating point were typically 2 dB lower than fan *datum* AC90/6, Table 10.3. However, the largest reduction in measured fan far-field noise relative to the fan *datum* AC90/6 was the fan AC90/6/TF. The fan AC90/6/TF local diffusion factor is typically only 0.02 lower than the fan *datum* AC90/6.

Burdsall and Urban (1971) studied the relationship between diffusion factor and fan far-field noise. The reduction in local diffusion factor of 0.02 is an order of magnitude lower than that needed to explain the 2 dB reduction in fan far-field noise. This observation implies that the measured reductions in fan far-field noise does not occur as a consequence of the blade-tip end-plates reducing blade loading. Therefore, the blade-tip end-plates must be reducing the acoustic productivity of flow-field features in the blade tip region.

Consider the chord-wise evolution of static pressure coefficient for the five fan configurations, Figure 10.11. The four fan configurations with fitted blade-tip end-plates all feature similar chord-wise distributions of static pressure coefficient to the fan *datum* AC90/6. The largest deviations of static pressure coefficient from the fan *datum* AC90/6 occur with fan AC90/6/TF$_{VTE}$. The analysis of leakage vortex axial velocity indicated that the variable thickness end-plate resulted in abrupt changes in leakage vortex axial velocity. These changes will manifest themselves as deviations of static pressure coefficient relative to the fan *datum* AC90/6.

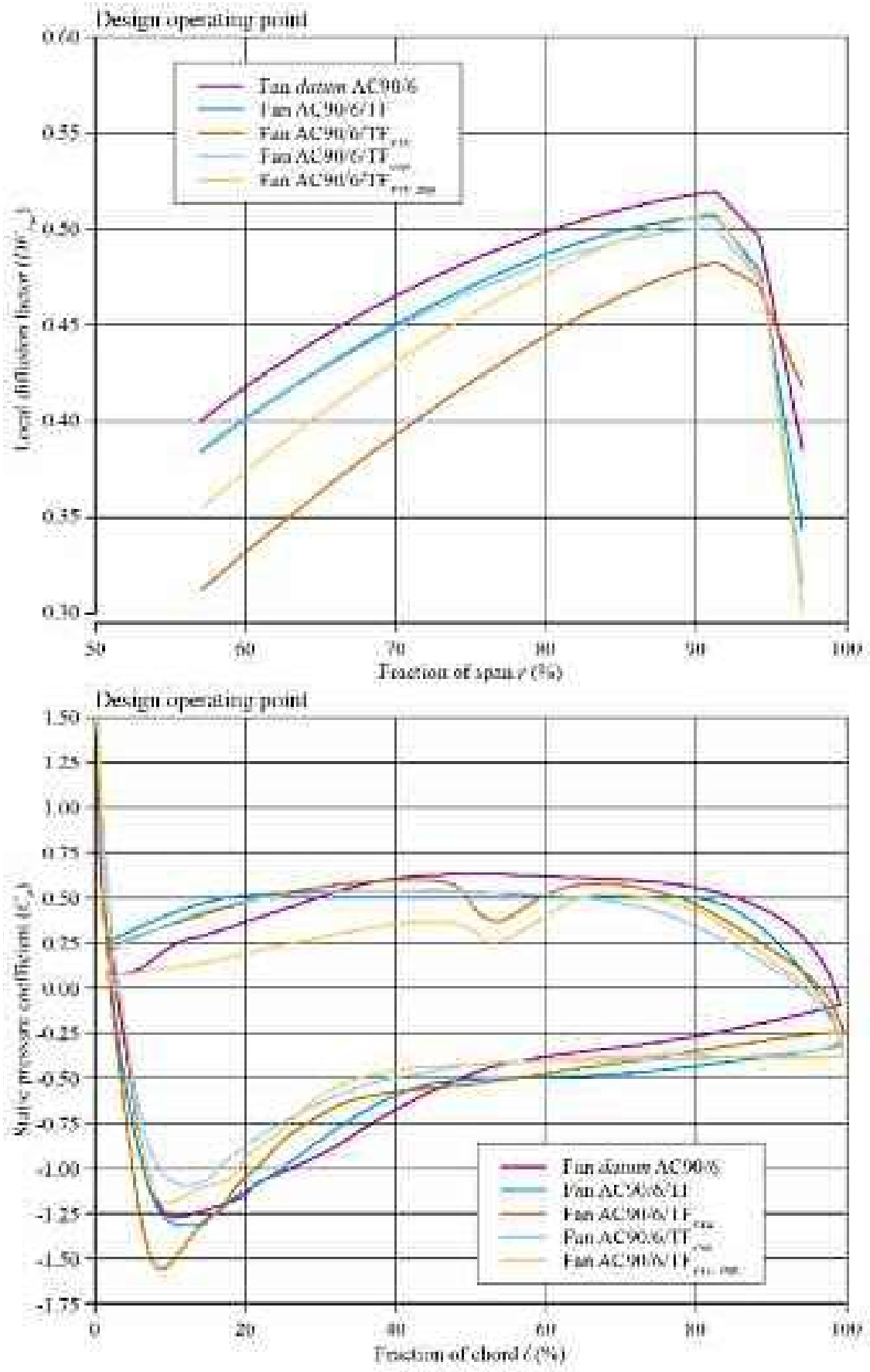

FIGURE 10.11. Span-wise evolution of the blade local diffusion factor (DF_{Loc}) and chord-wise evolution of static pressure coefficient (C_P) predicted at the fan design operating point. The change in blade local diffusion factor and static pressure coefficient illustrates the impact of the studied blade-tip end-plates on the leakage vortex.

Powell's Sound-source Survey

The analysis presented so far has focused on parameters that characterise aerodynamic aspects of the blade-to-blade and blade tip-to-casing flow-field. Presenting these parameters in the qualitative form of three-dimensional images and two-dimensional graphs facilitates an insight into the flow-field physics. However, although we may infer acoustic significance of flow-field features, we are not able to quantify their relative significance. In an effort to quantify the relative acoustic significance of flow-field features, Powell (1963, 1964) characterised the turbulent flow-field motion that is responsible for acoustic emissions. Powell (1963, 1964) discovered that vortex formation and motion is the fundamental noise generation mechanism.

For a relatively high Reynolds number flow with no heat release, we can neglect the entropy and viscous-stress terms in Lighthill's (1952, 1954) acoustic tensor. Consequently, the Reynolds-stress factor becomes the dominant contributor to sound generation. This provides the following sound source term:

$$\nabla \cdot (\omega \times v_c), \tag{1}$$

where ω is the leakage vortex flow's vector and v_c is its convection velocity. Powell (1963) used the same source term to characterise the acoustic productivity of flow-field features.

Powell (1964) developed the concept of a survey to identify the most relevant vortex-generated sound sources in a low-speed flow-field. Arakawa *et al.* (2005) used this sound-source survey technique to generate sound-source intensity maps. Following Arakawa *et al.*'s (2005) method, we numerically predicted Powell's (1964) three-dimensional sound-source distributions. We predicted the distributions in the blade tip-to-casing gap at 99.8 per cent fan radius for the five studied fan configurations, Figure 10.12. We normalised the Powell (1964) sound sources by a global flow time scale based on the casing diameter and the blade tip velocity. This normalisation facilitated a direct comparison of Powell's (1964) sound-source distributions for the five studied fan configurations.

Consider Powell's (1964) sound-source distribution for the fan *datum* AC90/6. The leading edge is associated with a highly concentrated sound source that we may associate with the blade tip-to-casing leakage vortex. There is also evidence of other sound sources over the blade's aft portion and at the blade trailing edge. The peak sound source value occurred over the blade's aft portion as the blade tip-to-casing leakage vortex's momentum peaked. A review of the sound-source distributions for the four fan configurations with fitted blade-tip end-plates indicates that they all occurred with a lower peak sound source value. The step feature resulted in a chord-wise stretching of the flow-field features that occurred with the peak sound source value.

Rotor Loss Behaviour

We may complement our analysis of Powell's (1963, 1964) sound sources with an analysis of three-dimensional total pressure-loss coefficient (ζ) contours. When

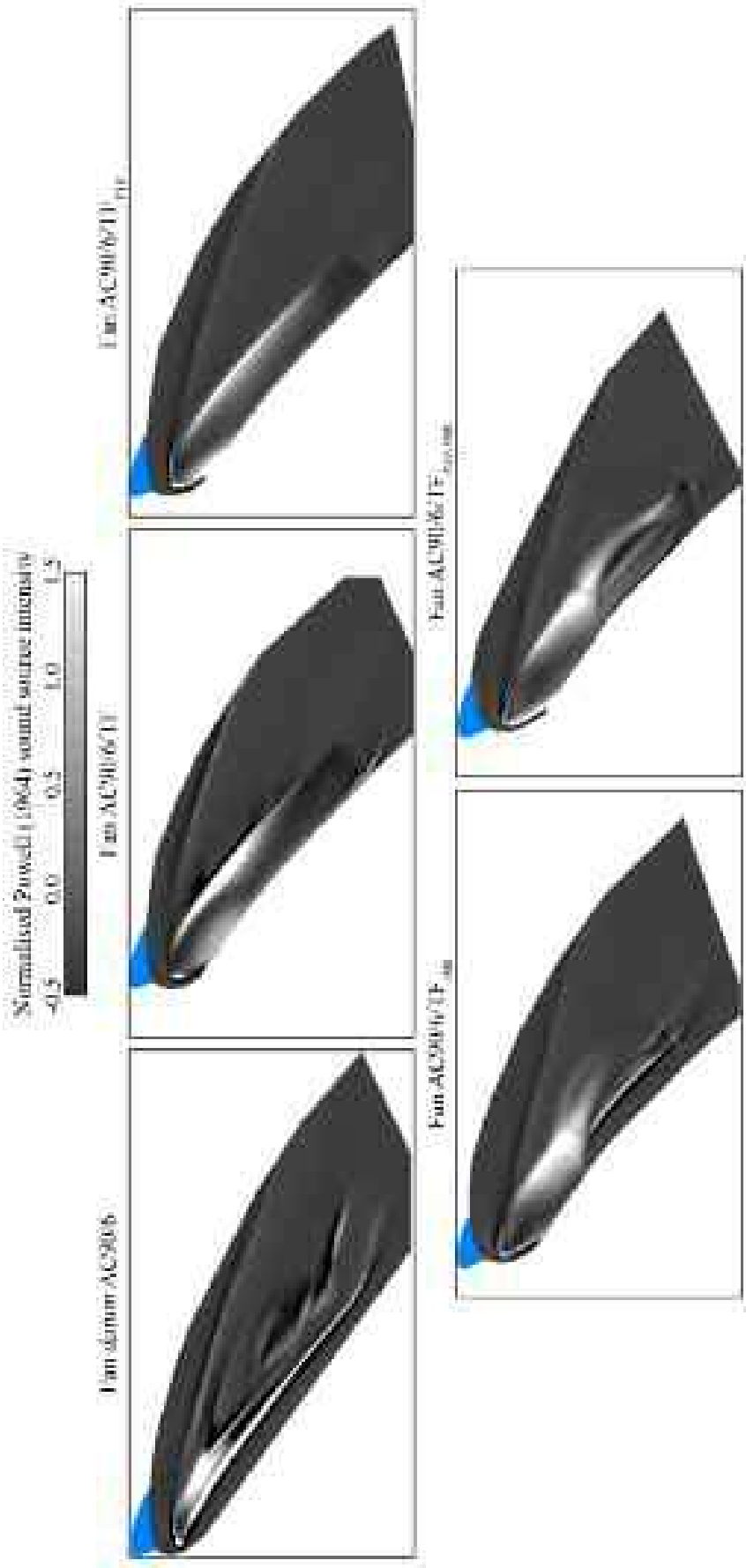

FIGURE 10.12. Three-dimensional Powell (1964) sound-source distributions numerically predicted at the fan design operating point. We present Powell's (1964) sound-source distributions in the blade tip-to-casing gap at 99.8 per cent fan radius for the fan *datum* AC90/6, AC90/6/TF, AC90/6/TF$_{VTE}$, AC90/6/TF$_{step}$ and AC90/6/TF$_{VTE\,step}$ illustrating the effect of changing from a constant to variable thickness blade-tip end-plate and adding a step.

combined with leakage vortex trajectories, three-dimensional total pressure-loss coefficient contours provide an insight into the impact of blade-tip end-plate geometry on the entire blade-to-blade flow-field. Corsini *et al.* (2010) defined total pressure-loss coefficient ζ as:

$$\zeta = \bar{p}_{0in} - p_0 / \, 0.5\rho\bar{w}^2_{in}, \tag{2}$$

where p_0 is the local total pressure; and $\bar{p}_{0in}$ and $0.5\rho\bar{w}^2_{in}$ are, respectively, the reference circumferentially averaged relative total and dynamic pressures. We computed these pressures at 50 per cent blade span at the fan inlet. We calculated the total loss coefficient distribution within the blade-to-blade passage and present them for the five studied fans over axial planes 25, 65 and 120 per cent blade chord downstream of the blade leading edge, Figure 10.13

At the axial plane 25 per cent blade chord downstream of the blade leading edge, total pressure loss distributions are similar for the five studied fans. Fan *datum* AC90/6, AC90/6/TF, AC90/6/TF$_{VTE}$, AC90/6/TF$_{step}$ and AC90/6/TF$_{VTE\,step}$ are all associated with loss cores concentrated in the hub region. At the axial plane 65 per cent blade chord downstream of the blade leading edge, total pressure loss distributions in the blade tip region are now different for the five studied fans. Each total pressure loss distribution is characteristic of the fan's leakage vortex. The fan AC90/6/TF is the only studied fan associated with leakage vortex bursting, and we associate it with a larger total pressure loss core.

At the axial plane 120 per cent blade chord downstream of the blade leading edge, it is evident that the blade-tip end-plates affect fan span-wise loss distribution. The constant thickness blade-tip end-plate results in a thinner wake and smaller hub loss core. The variable thickness blade-tip end-plate total pressure loss distributions in the blade tip region indicate that leakage vortex loss core is smaller than that of the fan *datum* AC90/6. This reduction is evident at both 65 and 120 blade chord and is a consequence of the reduced three-dimensional redistribution of flow within the blade-to-blade passage. This reduced rearrangement occurs as a consequence of the reduction in blade tip-to-casing clearance leakage flow rate.

We associate the fan AC96/6/TF$_{VTE}$ with generally smaller total pressure loss cores at the blade hub and tip than either the fan *datum* AC90/6 or AC90/6/TF. These smaller total pressure loss cores result in a higher fan efficiency and pressure developing capability. A comparison of the fan AC90/6/TF and fan AC90/6/TF$_{step}$ loss distributions illustrates that the step feature results in generally larger loss cores at the blade tip. A comparison of the fan AC90/6/TF$_{VTE}$ and fan AC90/6/TF$_{VTE\,step}$ loss distributions illustrates that the step feature results in generally larger loss cores at the blade hub and tip. Despite the increase in loss core size, the constant and variable thickness blade-tip end-plates were still able to minimise the extent of the fan *datum* AC90/6 hub corner stall.

We complete our analysis with a comparison of the loss of mechanical energy (Δe_m) due to blade tip-to-casing gap leakage flow per unit length of blade-tip chord, Table 10.4. Senoo (1991) developed this parameter by studying the mechanics of blade tip-to-casing clearance losses. Senoo provides a measure of the loss level

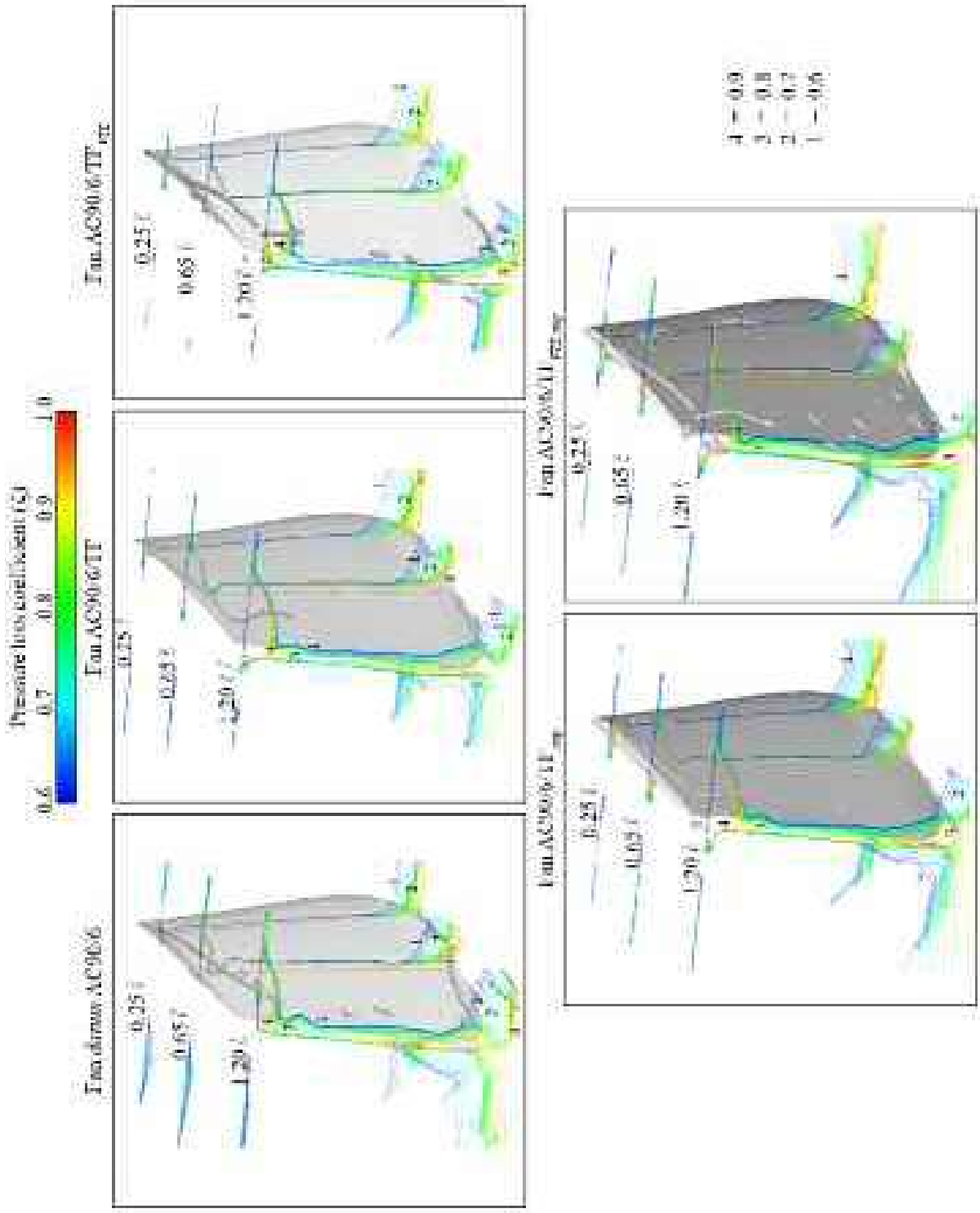

FIGURE 10.13. Three-dimensional total pressure-loss coefficient (ζ) contours numerically predicted at the fan design operating point. We present total pressure-loss coefficient contours at three chord-wise location through the fan *datum* AC90/6, AC90/6/TF, AC90/6/TF$_{VTE}$, AC90/6/TF$_{step}$ and AC90/6/TF$_{VTE\,step}$ illustrating the effect of changing from a constant to variable thickness blade-tip end-plate and adding a step.

Table 10.4. *Loss of mechanical energy (Δe_m) due to blade tip-to-casing gap leakage flow per unit length of blade-tip chord at the fan design operating point.*

	Normalised leakage-flow rate	Δe_m
datum AC90/6	8.9×10^{-3}	18.90×10^{-3}
AC90/6/TF	6.8×10^{-3}	7.90×10^{-3}
AC90/6/TF$_{VTE}$	6.6×10^{-3}	7.91×10^{-3}
AC90/6/TF$_{step}$	5.4×10^{-3}	1.36×10^{-3}
AC90/6/TF$_{VTE\ step}$	5.6×10^{-3}	1.94×10^{-3}

through the blade tip-to-casing gap that facilities comparing blade-tip end-plate effectiveness. Our earlier analysis demonstrated that the blade-tip end-plates each introduced a significant deflection of the blade tip-to-casing leakage flow. This deflection should result in an increase in loss through the blade tip-to-casing gap. A comparison of loss for the five studied fan configurations indicates that the four with blade-tip end-plates occurred with lower loss than the fan *datum* AC90/6. We may attribute this reduction in loss to a general reduction in leakage flow rate and a reduction in the momentum transferred to the blade tip-to-casing leakage vortex.

CONCLUSIONS

In this chapter we present a computational analysis of the studied fan's blade-to-blade flow-field both with and without a fitted blade-tip end-plate. In total, we conducted a computational analysis of five variants of the studied fan:

- the fan *datum* AC90/6, without a fitted blade-tip end-plate;
- the fan AC90/6/TF, with a constant-thickness blade-tip end-plate;
- the fan AC90/6/TF$_{VTE}$, with a variable-thickness end-plate;
- the fan AC90/6/TF$_{step}$, with a constant-thickness blade-tip end-plate plus step; and
- the fan AC90/6/TF$_{VTE\ step,}$ with a variable-thickness blade-tip end-plate plus step.

We undertook the computational analysis using a Reynolds-Averaged Navier–Stokes (RANS) simulation with a non-linear k-ε turbulence model in low-Reynolds number formulation. The purpose of the computational analysis was to establish the effectiveness of the blade-tip end-plate design methodology that we used to design the variable thickness blade-tip end-plate.

The reported research establishes the effectiveness of the fans AC90/6/TF and AC90/6/TF$_{VTE}$ when incorporating a step along the blade chord at the intersection of the blade-tip and the end-plate. The objective of incorporating these stepped blade-tip features was to provide a mechanism to weaken the intensity of the multiple organised vortical structures that had resulted in the relatively poor acoustic

performance of the fan AC90/6/TF_{VTE}. Thus, we hoped that the stepped variant of the fan AC90/6/TF_{VTE} would retain the benefit that occurred with the blade-tip leakage vortex not bursting, but would negate the negative effect of creating multiple organised vortical structures in the process.

We used the computational analysis to calculate Powell's sound-source distributions of blade-tip leakage flow. Powell's sound-source distributions are useful as the Powell's sound-source parameter characterises the vortical motion that is responsible for acoustic emissions. Consequently, one may use an analysis of Powell's sound-source distributions to identify the most productive sound sources in a low-speed flow characterised by the presence of multiple coherent swirling structures.

When we studied Powell's sound-source distributions, we found that they facilitated a qualitative comparison of the fan near-field noise's origin for the studied fan with and without a fitted blade-tip end-plate. The Powell's sound-source distribution for the variable thickness end-plate indicated that a highly skewed blade leading-edge vortex interacting with the blade-tip leakage vortex resulted in the creation of the multiple organised vortical structures.

We studied the Powell's sound-source distributions for both constant and variable thickness blade-tip end-plates with the added step feature. We found that the step constituted an end-plate feature that weakened the intensity of near-field acoustic emissions from the organised vortical structures. This weakening occurred as a consequence of stretching the length of blade chord over which the blade-tip leakage vortex developed, thus reducing the blade tip-to-casing leakage flow rate. Researchers generally consider fan far-field acoustic emissions to be a function of overall blade tip-to-casing leakage flow rate. However, noise measurements indicated that when fitted with the step feature, the studied fan with variable thickness blade-tip end-plate overall broadband noise level was approximately 1.0 dB higher than that occurring with the constant thickness end-plate and no step feature.

REFERENCES

ISO 5801:2007 (2007), *Industrial Fans: Performance Testing Using Standardised Airways.*

ISO 10302:1996 (1996), *Fans for General Purposes. Methods of Noise Testing.*

Arakawa, C., Fleig, O., Makoto, I. and Masakazu, S. (2005), 'Numerical Approach for Noise Reduction of Wind Turbine Blade Tip with Earth Simulator', *Journal of the Earth Simulator*, vol. 2, pp. 11–33.

Bianchi, S., Sheard, A.G., Kinghorn, I.R., Corsini, A. and Rispoli, F. (2009a), 'Experimental Development of a Measurement Technique to Resolve the Radial Distribution of Fan Aeroacoustic Emissions', *Noise Control Engineering Journal*, vol. 57, pp. 360–369.

Bianchi, S., Corsini, A., Rispoli, F. and Sheard, A.G. (2009b), 'Experimental Aeroacoustic Studies on Improved Tip Configurations for Passive Control of Noise Signature in Low-speed Axial Fan', *Transactions of the ASME, Journal of Vibration and Acoustics*, vol. 131, paper no. 061007, pp. 1–10.

Bianchi, S., Corsini, A., Rispoli, F. and Sheard, A.G. (2011), 'Far-field Radiation of Tip Aerodynamic Sound Sources in Axial Fans Fitted with Passive Noise Control Features',

Transactions of the ASME, Journal of Vibration & Acoustics, vol. 133, paper no. 051001, pp. 1–11.

Bianchi, S., Corsini, A. and Sheard, A.G. (2014), 'A Critical Review of Passive Noise Control Techniques in Industrial Fans', *Transactions of the ASME, Journal of Engineering for Gas Turbines & Power*, vol. 136(4), paper no. 044001, pp. 1–10.

Borello, D., Borrelli, P., Quagliata, E. and Rispoli, F. (2001), 'A Multi-grid Additive and Distributive Parallel Algorithm for FEM Turbomachinery CFD', *Proceedings of the European Congress on Computational Methods in Applied Sciences (ECCOMAS CFD 2001)*, Swansea, UK, 4–7 September.

Borello, D., Corsini, A. and Rispoli, F. (2003), 'A Finite Element Overlapping Scheme for Turbomachinery Flows on Parallel Platforms', *Computers and Fluids*, vol. 32, pp. 1017–1047.

Burdsall, E.A. and Urban, R.H. (1971), *Fan-Compressor Noise: Prediction, Research and Reduction Studies*, Pratt and Whitney Aircraft, Defence Technical Information Center, East Hartford, CT, USA.

Corsini, A. and Rispoli, F. (2004), 'Using Sweep to Extend Stall-free Operational Range in Sub-sonic Axial Fan Rotors', *Proceedings of the IMechE Part A, Journal of Power and Energy*, vol. 218, pp. 129–139.

Corsini, A. and Rispoli, F. (2005), 'Flow Analyses in a High-pressure Axial Ventilation Fan with a Non-linear Eddy-viscosity Closure', *International Journal of Heat and Fluid Flow*, vol. 26, pp. 349–361.

Corsini, A. and Sheard, A.G. (2007), 'Tip End-plate Concept Based on Leakage Vortex Rotation Number Control', *Journal of Computational and Applied Mechanics*, vol. 8, pp. 21–37.

Corsini, A., Rispoli, F. and Santoriello, A. (2004a), 'A New Stabilized Finite Element Method for Advection-Diffusion-Reaction Equations using Quadratic Elements', in Vad, J., Lajos, T. and Schilling, R. (Eds), *Modelling Fluid Flow: The State of the Art*, Springer-Verlag, Berlin, Germany.

Corsini, A., Rispoli, F., Sheard, A.G. and Kinghorn, I.R. (2004b), 'The Aerodynamic Interaction of Tip Leakage and Mainstream Flows in a Fully Ducted Axial Fan', *Proceedings of the 49th American Society of Mechanical Engineers Gas Turbine and Aeroengine Congress*, Vienna, Austria, 14–17 June, paper no. GT2004-53408.

Corsini, A., Rispoli, F. and Sheard, A.G. (2007), 'Development of Improved Blade-tip End-plate Concepts for Low-noise Operation in Industrial Fans', *Proceedings of the IMechE Part A, Journal of Power and Energy*, vol. 221, pp. 669–681.

Corsini, A., Rispoli, F. and Sheard, A.G. (2010), 'Shaping of Tip End-plate to Control Leakage-vortex Swirl in Axial-flow Fans', *Transactions of the ASME, Journal of Turbomachinery*, vol. 132, paper no. 031005, pp. 1–9.

Craft, T.J., Launder, B.E. and Suga, K. (1996), 'Development and Application of a Cubic Eddy-viscosity Model of Turbulence', *International Journal of Heat and Fluid Flow*, vol. 17, pp. 108–155.

Cumpsty, N.A. (1977), 'A Critical Review of Turbomachinery Noise', *Transactions of the ASME, Journal of Fluids Engineering*, vol. 99(2), pp. 278–293.

Fukano, T. and Jang, C. (2004), 'Tip Clearance Noise of Axial Flow Fans Operating at Design and Off-design Condition', *Journal of Sound and Vibration*, vol. 275, pp. 1027–1050.

Fukano, T., Takamatsu, Y. and Kodama, Y. (1986), 'The Effects of Tip Clearance on the Noise of Low-pressure Axial and Mixed Flow Fans', *Journal of Sound and Vibration*, vol. 105, pp. 291–308.

Furukawa, M., Inoue, M., Kuroumaru, M., Saiki, K. and Yamada, K. (1999), 'The Role of Tip Leakage Vortex Breakdown in Compressor Rotor Aerodynamics', *Transactions of the ASME, Journal of Turbomachinery*, vol. 121, pp. 469–480.

Ganz, U.W., Joppa, P.D. and Scharpf, D.F. (1998), *Boeing 18-inch Fan Rig Broadband Noise Test*, Report NASA CR-1998-208704.

Garg, A.K. and Leibovich, S. (1979), 'Spectral Characteristics of Vortex Breakdown Flowfields', *Physics of Fluids*, vol. 22, pp. 2053–2064.

Holste, F. and Neise, W. (1997), 'Noise Source Identification in a Prop Fan Model by Means of Acoustical Near Field Measurements', *Journal of Sound and Vibration*, vol. 203, pp. 641–665.

Inoue, M. and Furukawa, M. (2002), 'Physics of Tip Clearance Flow in Turbomachinery', *Proceedings of the ASME2002 Joint US – European Fluids Engineering Division Conference*, Montreal, Quebec, Canada, 14–18 July, paper no. FEDSM2002-31184, pp. 777–789.

Inoue, M., Kuroumaru, M. and Furukawa, M. (1986), 'Behavior of Tip Leakage Flow Behind an Axial Compressor Rotor', *Transactions of the ASME, Journal of Engineering for Gas Turbines and Power*, vol. 108, pp. 7–14.

Jang, C.M., Fukano, T. and Furukawa, M. (2003), 'Effects of the Tip Clearance on Vortical Flow and its Relation to Noise in an Axial Flow Fan', *JSME Transaction Series B*, vol. 46(3), pp. 356–365.

Jensen, C.E. (1986), 'Axial-flow Fan', Patent No. US 4,630,993, 23 December.

Khourrami, M.R. and Choudari, M. (2001), 'A Novel Approach for Reducing Rotor Tip-clearance Induced Noise in Turbofan Engines', *Proceedings of the 7th AIAA/CEAS Aeroacoustics Conference*, Maastricht, The Netherlands, 28–30 May, paper no. AIAA 2001-2148.

Leggat, L.J. and Siddon, T.E. (1978), 'Experimental Study of Aeroacoustic Mechanism of Rotor-vortex Interactions', *Journal of the Acoustical Society of America*, vol. 64, pp. 1070–1077.

Lighthill, M.J. (1952), 'On Sound Generated Aerodynamically. I: General Theory', *Proceedings of the Royal Society A*, vol. 221, pp. 564–587.

Lighthill, M.J. (1954), 'On Sound Generated Aerodynamically. II: Turbulence as a Source of Sound', *Proceedings of the Royal Society A*, vol. 222, pp. 1–32.

Longet, C.M.L. (2003), 'Axial Flow Fan with Noise Reducing Means', Patent No. US 2003/0123987 A1, 3 July.

Mimura, M. (2003), 'Axial Flow Fan', Patent No. US 6,648,598 B2, 18 November.

Powell, A. (1963), 'Mechanisms of Aerodynamic Sound Production', AGARD Report No. 466.

Powell, A. (1964), 'The Theory of Vortex Sound', *Journal of the Acoustical Society of America*, vol. 33, pp. 177–195.

Quinlan, D.A. and Bent, P.H. (1998), 'High Frequency Noise Generation in Small Axial Flow Fans', *Journal of Sound and Vibration*, vol. 218, pp. 177–204.

Senoo, Y. (1991), 'Mechanics on the Tip Clearance Loss of Impeller Blades', *Transactions of the ASME, Journal of Turbomachinery*, vol. 113, pp. 680–685.

Smith, G.D.J. and Cumpsty, N.A. (1984), 'Flow Phenomena in Compressor Casing Treatment', *Transactions of the ASME, Journal of Engineering for Gas Turbines and Power*, vol. 106, pp. 532–541.

Spall, R.E., Gatski, T.B. and Grosch, C.E. (1987), 'A Criterion for Vortex Breakdown', *Physics of Fluids*, vol. 30, pp. 3434–3440.

Storer, J.A. and Cumpsty, N.A. (1991), 'Tip Leakage Flow in Axial Compressors', *Transactions of the ASME, Journal of Turbomachinery*, vol. 113, pp. 252–259.

Sujudi, D. and Haimes, R. (1995), 'Identification of Swirling Flow in 3-D Vector Fields', *Proceedings of the 12th AIAA Computational Fluid Dynamics Conference*, San Diego, CA, USA, 19–22 June, paper no. AIAA-95-1715-CP.

Takata, H. and Tsukuda, Y. (1977), 'Stall Margin Improvement by Casing Treatment – Its Mechanism and Effectiveness', *Transactions of the ASME, Journal of Engineering and Power*, vol. 99, pp. 121–133.

Thompson, D.W., King, P.I. and Rabe, D.C. (1998), 'Experimental and Computational Investigation on Stepped Tip Gap Effects on the Flowfield of a Transonic Axial-flow Compressor Rotor', *Transactions of the ASME, Journal of Turbomachinery*, vol. 120, pp. 477–486.

Uchida, S., Nakamura, Y. and Ohsawa, M. (1985), 'Experiments on the Axisymmetric Vortex Breakdown in a Swirling Air Flow', *Transactions of the Japan Society for Aeronautical Space Sciences*, vol. 27, pp. 206–216.

Uselton, R.B., Cook, L.J. and Wright, T. (2008), 'Fan with Reduced Noise Generation', Patent No. US 7,351,041 B2, 1 April.

Wadia, A.R., Szucs, P.N. and Crall, D.W. (1998), 'Inner Workings of Aerodynamic Sweep', *Transactions of the ASME, Journal of Turbomachinery*, vol. 120(4), pp. 671-682.

Wright, S.E. (1976), 'The Acoustic Spectrum of Axial Flow Machines', *Journal of Sound and Vibration*, vol. 45, pp. 165–223.

Chapter 11

End-plate for Noise-by-flow Control in Axial Fans

A. Corsini and A.G. Sheard

ABSTRACT

The chapter presents a design procedure for blade-tip end-plates that controls the blade tip-to-casing leakage vortex's swirl level. These end-plates are designed to be fitted to the blades of a subsonic axial fan utilised in compact cooling units. We tested a *datum* fan without blade-tip end-plates, and three fan variants with different end-plate geometries. The fan AC90/6/TF incorporated a constant thickness end-plate. The fan AC90/6/TF$_{VTE}$ incorporated a variable thickness end-plate. The fan AC90/6/TF$_{MVB}$ incorporated an end-plate designed using the new design procedure, which successfully exploited a linkage between blade tip-to-casing leakage vortex breakdown and fan acoustic emissions. The link is exploited by first controlling the flow with the specific objectives, minimising blade tip-to-casing leakage vortex intensity; and second, avoiding leakage vortex breakdown. Reconfiguring the end-plate using a multiple-vortex-breakdown criterion for the end-plate design implements this noise-by-flow control design process. We named the resulting blade-tip end-plate MVB, with the fan incorporating the MVB blade tip end-plate named fan AC90/6/TF$_{MVB}$. We have assessed the impact of the MVB end-plate design on fan performance using a numerical simulation of the flow-field in the blade tip region and by experimentally measuring fan aerodynamic and acoustic performance. The reported research verifies the developed design procedure's technical merit, demonstrating that blade tip-to-casing leakage flow control can result in reducing blade-tip flow generated noise. When compared to the fan *datum* AC90/6, the fan AC90/6/TF$_{MVB}$ incorporating the MVB blade-tip end-plate A-weighted far-field sound power level was consistently lower. At the maximum flow operating point is was 4.4 dB(A) lower and respectively, 5.8 dB(A) and 8.2 dB(A) lower at the design and peak pressure operating points. The near-axis broadband far-field sound pressure level for the fan AC90/6/TF$_{MVB}$ was 10 dB lower than the fan *datum* AC90/6.

This chapter is a revised and extended version of Corsini, A. and Sheard, A.G (2013), 'End-plate for Noise-by-flow Control in Axial Fans', *Periodica Polytechnique, Mechanical Engineering*, vol. 57(2), pp. 3–16.

NOMENCLATURE

Latin letters

BPF	blade-passing frequency [Hz]
C_l	local lift coefficient
$C_{l,D}$	design value of local lift coefficient
D_h	hub diameter
D_c	casing diameter
f_f	friction factor
H_n	normalised helicity
K_s	specific noise level
ℓ	blade chord
ℓ_c	blade tip chord
Δp_{tot}	rotor total pressure rise
p	static pressure
r_v	radial distance from the vortex axis
Re_{gap}	leakage-flow Reynolds number
Ro	Rossby number
s_c	chord wide position
SWL	sound power level
t	blade pitch
t_{ep}	end-plate thickness distribution
V_a	axial velocity at r
v_i	vector of sound coherent perturbation velocity
v_m	average velocity through the tip blade section
v, w	absolute and relative velocities
w_{Ln}	leakage-flow bulk velocity
x, y, z	cartesian coordinates

Greek letters

β_{LV}	angle between the leakage jet and the blade chord
Γ	blade circulation
η_{tot}	total efficiency
ν	kinematic viscosity
ν_A	coefficient of acoustic dissipation
ν_t	turbulent viscosity
Π	net dissipation of acoustic energy
ρ	air density
τ	rotor tip clearance
τ_D	design value of blade tip-to-casing clearance
Ω	tip leakage vortex rotation rate scale
ξ_i	absolute vorticity vector

Subscripts and superscripts

a, p, r	axial, peripheral and radial
c	casing wall
h	hub wall
i	Cartesian component index
in	inlet section
mol	molecular quantity
s	streamwise component
$\bar{}$	pitch-averaged value
0	total quantities

INTRODUCTION

The European Union Regulation 327 mandates minimum fan and motor efficiency grades' (FMEGs) for air movement fans. 'Tier 1' FMEGs became legally binding on 1 January, 2013 (Directive 2005/32/EC of the European Parliament and of the Council, 2005). The minimum FMEGs will increase again on 1 January, 2015. The Commission commenced a review of the regulation and its impact in 2014, and will make a decision on future increases in the minimum FMEGs during 2015. This regulatory framework has driven fan manufacturers towards computational methods in an on-going effort to increase fan efficiency.

In parallel to the regulatory framework intended to drive improvements in efficiency, market requirements are driving manufacturers to reduce fan noise. Increasingly, stringent acoustic specifications are a consequence of a requirement to install air movement fans in close proximity to populated areas. The regulatory and market requirements combine into a requirement for improved design methodologies that will deliver both higher efficiency and as a consequence of minimising or eliminating the aerodynamic origins of acoustic noise, lower noise fan designs.

The aerodynamic origin of an air movement fan's acoustic emissions occurs as a consequence of one of two primary mechanisms, interaction and self-generated. Interaction noise occurs as a consequence of rotating components passing static components. Self-generated noise occurs as a consequence of unsteady aerodynamic blade loads (Baad, 1977; Wen-Shiang *et al.*, 1989). Within an air movement fan, its interaction noise is typically less significant than self-generated noise. Turbulent inflow, turbulent boundary layers, separated flow, trailing edge flow from blunt trailing edges, secondary flows and blade tip-to-casing leakage flow drive self-generated noise (Fukano *et al.*, 1986).

When studying the aerodynamic origins of self-generated noise, Akaike *et al.* (1991) observed that the vortical structure near the blade tip in air movement fans is a dominant noise generating mechanism. In his pioneering work, Longhouse (1978) introduced rotating shrouds attached to the blade tips to reduce blade tip-to-casing leakage vortex noise. He concluded that the vortical flow near the blade tip has a dominant effect on both a fan's acoustic emissions and aerodynamic characteristics. Inoue and Kuroumaru (1989), Storer and Cumpsty (1991) and Lakshminarayana *et*

al. (1995) all studied the impact of blade tip-to-casing leakage flow on compressor aerodynamics, concluding that the three-dimensional and unsteady nature of the leakage flow had a primary impact on both noise generated and aerodynamic loss. Within the context of low-speed turbomachinery, engineers generally correlate blade tip-to-casing leakage flow noise with the broadband spectral signature (Longhouse, 1978; Fukano *et al.*, 1986; Kameier and Neise, 1997). Kameier and Neise (1997) highlighted that, in addition to its effect on broadband noise, tip leakage flows can be responsible for narrowband tones at frequencies below the blade passing frequency that coincide with a tip vortex rotational frequency.

During the last two decades, noise control has emerged as a new research field (Gad-el-Hak, 2000; Joslin *et al.*, 2005). The scholars working in this field have proposed numerous noise reduction strategies that they broadly categorise as passive, active or reactive. Recent research programmes have focused on the development of fan designs that aim to minimise noise-by-flow control. One achieves flow control by incorporating passive or active flow control technologies. An example of a passive flow control technology is the chevron mixer for jet noise reduction (Saiyed *et al.*, 2000). An example of an active flow control technology is trailing edge blowing (Brookfield and Waitz, 2000). When considering how to classify noise-by-flow control technologies, Thomas *et al.* (2002) and Joslin *et al.* (2005) base classification on the nature of the linkage between the underlying flow physics and the noise generation mechanisms.

The noise control techniques which air movement fan manufacturers adopt are primarily passive, exploiting a direct linkage between fan geometry and flow features associated with specific noise sources. Those researchers who have studied the application of passive noise control techniques in air movement fans have primarily focused on blade and casing geometry, with the objective of controlling flow features associated with specific noise sources without sacrificing aerodynamic performance. Engineers have long known that the blade tip-to-casing leakage flow is both a dominant noise source and a flow feature that reduces aerodynamic performance. Consequently, passive noise control techniques that focus on reducing the magnitude of leakage flows have the potential to both reduce noise and improve aerodynamic performance.

In an attempt to improve compressor performance, researchers first experimented with casing treatments in the early 1970s utilising grooves (Takata and Tsukuda, 1977; Smith and Cumpsty, 1984), and more recently stepped gaps in the blade tip region (Thompson *et al.*, 1998). These casing treatments improved the compressors' stable operating range by reducing the blade tip leakage flow's intensity. Air movement fan manufacturers have historically favoured a casing treatment comprising an annular ring of recirculating vanes over the blades' leading edge (Karlsson and Holmkvist, 1986). These annular rings stabilise fan performance, but typically also reduce fan efficiency by three to five per cent. This is a reduction that is likely to be unacceptable after 1 January, 2015 when the minimum allowable fan and motor efficiency grades (FMEGs) are increased.

Quinlan and Bent (1998) studied the performance of a small air movement fan. They were able to demonstrate that blade tip anti-vortex appendages developed by

other scholars were an effective passive noise control technology (Longet, 2003: Mimura, 2003; Uselton *et al.*, 2005). Akturk and Camci (2010) reported a novel tip platform extension experimental study that resulted in a more efficient fan with improved acoustic performance as a consequence of flow swirl control. Akturk and Camci (2010) applied their developed flow control methodology to tip leakage flow control in ducted lift fans for vertical take-off and landing applications (Akturk and Camci, 2011a, 2011b). Corsini and Sheard (2007), Corsini *et al.* (2007) and Bianchi *et al.* (2009a, 2009b) investigated the application of profiled end-plates to the blade tips of a family of compact cooling fans, advocating the link between blade tip-to-casing leakage flow and vortex swirl control.

This chapter presents a novel concept and a design procedure derived from the concept for blade-tip end-plate design for subsonic axial fan blades. As a consequence of the role that organised structures in turbulent flow play in the noise generation process, controlling these structures is a key objective in noise suppression (Ffowcs Williams, 1977). Experimental and numerical studies have demonstrated fan noise reduction that results from adopting blade tip-to-casing leakage flow control technologies (Bianchi *et al.*, 2009a, 2009b; Corsini *et al.*, 2010). We speculate on the role of the leakage vortex bursting on an air movement fan's aerodynamic and acoustic performance. When controlling the swirling flows in an aircraft wing's tip region (Spall *et al.*, 1987) or in combustor technologies (Escudier, 1987), the proposed design procedure rationale advocates linking blade-tip end-plate geometry and the leakage vortex near-axis swirl. This linkage facilitates control of the blade-tip vortex to avoid the vortex bursting (Jones *et al.*, 2001; Herrada and Shtern, 2003).

One implements this noise-by-flow control design procedure by reconfiguring the blade-tip end-plate and thus influencing the momentum transfer from the leakage flow. The procedure also forces some waviness in the leakage vortex trajectory, as in delta-wing platforms (Srigrarom and Kurosaka, 2000). The design procedure deliberately varies the blade-tip end-plate thickness to control the leakage vortex rotation number's chord-wise evolution. The design procedure utilises a critical minimum value of the leakage vortex rotation number (Sheard *et al.*, 2009) and induces a sequence of augmentation-diminution of momentum transfer to the leakage vortex up to near-critical swirl conditions (Garg and Leibovich, 1979; Uchida *et al.*, 1985). Thus, the new blade-tip end-plate design procedure results in the blade tip-to-casing leakage vortex swirl level's passive control, based on a succession of breakdown or bursting conditions. By avoiding bursting of the leakage vortex, the resultant blade-tip end-plate produces lower acoustic emissions from the leakage vortex, and consequently, reduces far-field fan noise (Sheard *et al.*, 2009).

FAMILY OF FANS UNDER INVESTIGATION

We conducted the reported research on a family of commercially available cooling fans. The studied fan configuration, coded AC90/6, incorporates a six-blade un-swept rotor, with modified ARA-D profile aerofoil blades, Table 11.1. One may set the blade-pitch angle during final assembly to customise the fan to a desired duty

Table 11.1. *The fan* datum *AC90/6 blade geometry and rotor specification.*

	Fan *datum* AC90/6		
Blade geometry	Hub	Mid-span	Tip
Pitch angle (°)	36	58.8	28
Camber angle (°)	46	44	41
Solidity	1.24	0.86	0.30
Fan rotor			
Blade number		6	
Blade tip pitch angle (°)		16–28	
Blade tip stagger angle (°)		74–62	
Hub-to-casing diameter ratio σ		0.22	
Tip diameter (mm)		900.0	
Rotor tip clearance τ (% span)		1.0	
Rated rotational frequency (r/min)		935–950	

point. We used a direct coupled-induction 400-volt (AC), 3-phase motor to drive the rotor at a constant speed of 950 rpm, resulting in a 44.7 m/s blade tip speed and a 95 Hz blade-passing frequency (BPF). In its original embodiment, the studied fan did not include a blade-tip end-plate, therefore we used it as a *datum* against which to assess the performance of fan variants with blade-tip end-plates. Therefore, in the reported research we refer to the fan without blade-tip end-plates as the fan *datum* AC90/6.

The studied fan blade tip pitch angle is adjustable and may be set to a pitch angle between 16 and 28 degrees. In practical application, the blade tip pitch angle is typically set to 28 degrees as this maximises flow rate for a given system pressure. In the research reported in this chapter, we conducted the experimental measurements with the fan blade tip pitch angle set to 28 degrees. We selected 28 degrees both because it is typical of the angle that one uses in practical application and because it results in the highest blade loading. A highly loaded blade results in the blade tip-to-casing leakage vortex having the most significant effect on both fan aerodynamic and acoustic performance (Holste and Neise, 1997).

The impact of the blade tip-to-casing leakage vortex on both fan aerodynamic and acoustic performance results in the application of blade-tip end-plates changing not only the fan's acoustic performance, but also the aerodynamic performance. Consequently, the fan *datum* AC90/6 generates a different pressure at a constant flow rate when fitted with each of the studied blade-tip end-plates. To facilitate the comparison of fan performance data when fitted with different blade-tip end-plates, we chose to define three operating points, and their respective volume flow rates, Figure 11.1 and Table 11.2. The design operating point volume flow rate is typical of that required when one installs the fan over a cooling unit's tube bank. The peak pressure flow rate is typical of that required when the tube bank has become partially blocked following a period of in-service operation. The maximum flow operating point

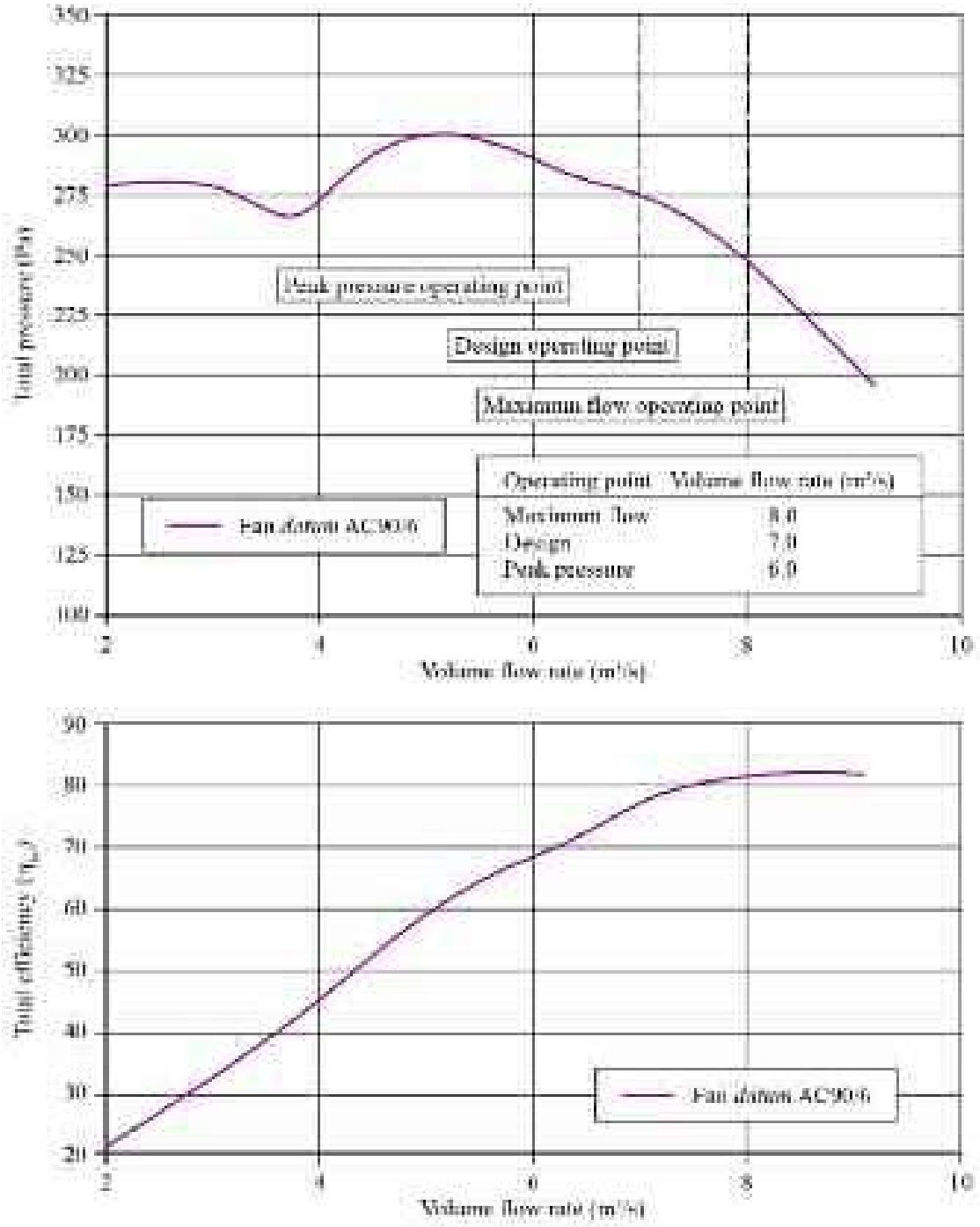

FIGURE 11.1. The performance characteristics of the studied fan *datum* AC90/6 without a fitted blade-tip end-plate. The authors measured performance characteristics with the blade tip pitch angle set to 28 degrees in a Type C standardised airway (ducted inlet, free outlet) in accordance with ISO 5801:2007 requirements (2007).

Table 11.2. *The operating points used when characterising the studied fan's performance with and without fitted blade-tip end-plates. The authors measured performance characteristics in a Type C standardised airway (ducted inlet, ducted outlet) in accordance with ISO 5801:2007 requirements (2007).*

Operating point	Volume flow rate (m^3/s)	Studied blade tip pitch angle (°)
Maximum flow	8.0	28
Design	7.0	28
Peak pressure	6.0	28

volume flow rate is typical of the flow rate that occurs with the lowest pressure loss tube banks currently operating in service.

MULTIPLE VORTEX BREAKDOWN CONCEPT

Breakdown of a blade tip-to-casing leakage vortex is an important phenomenon within swirling flows. The breakdown constitutes a noise source, and consequently, the link between blade tip flow and fan noise has been a subject of interest to scholars for the last two decades. The subject has historically been an active research area for aeronautical engineers (Spall *et al.*, 1987) and combustion engineers (Escudier, 1987). Today, researchers working within the air movement and control community (Jones *et al.*, 2001; Herrada and Shtern, 2003) study the link between blade tip-to-casing leakage flow and fan noise.

Background Studies on Blade-tip End-plates

Corsini and Sheard (2007) studied the aerodynamic and acoustic benefit that occurs with the addition of a blade-tip end-plate. They predicted the fan's performance without a fitted blade-tip end-plate and with a constant thickness blade-tip end-plate. Without a fitted blade-tip end-plate, they named the fan *datum* AC90/6. With a constant thickness blade-tip end-plate, they named the fan AC90/6/TF, Figure 11.2. Following Ito *et al.*'s method (1985), Corsini and Sheard (2007) concluded that there is a threshold value of the Rossby number below which the vortex rotation cannot reduce if the vortex is to remain stable. They identified the critical Rossby number range using the critical Rosby numbers which Uchida *et al.* (1985) and Garg and Leibovich (1979) defined. Uchida *et al.* (1985) defined a critical Rossby number that occurred with the breakdown of an axi-symmetric vortex in a swirling flow. Garg and Leibovich (1979) also defined a critical Rossby number that occurred with an aircraft wing tip vortices' breakdown. Corsini and Sheard (2007) observed the fan AC90/6/TF exhibited a blade tip-to-casing leakage vortex breakdown as the Rossby number fell below the critical Rossby number range, Figure 11.3.

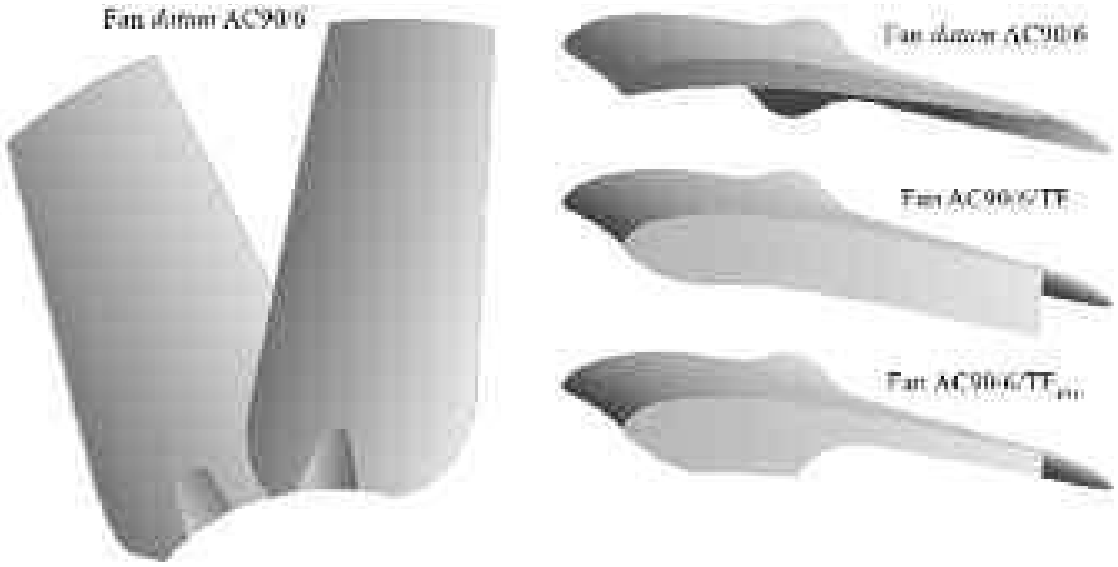

FIGURE 11.2. The studied fan *datum* AC90/6 without a fitted blade-tip end-plate, with a constant thickness blade-tip end-plate, AC90/6/TF and with a variable thickness blade-tip end-plate, AC6/TF$_{VTE}$.

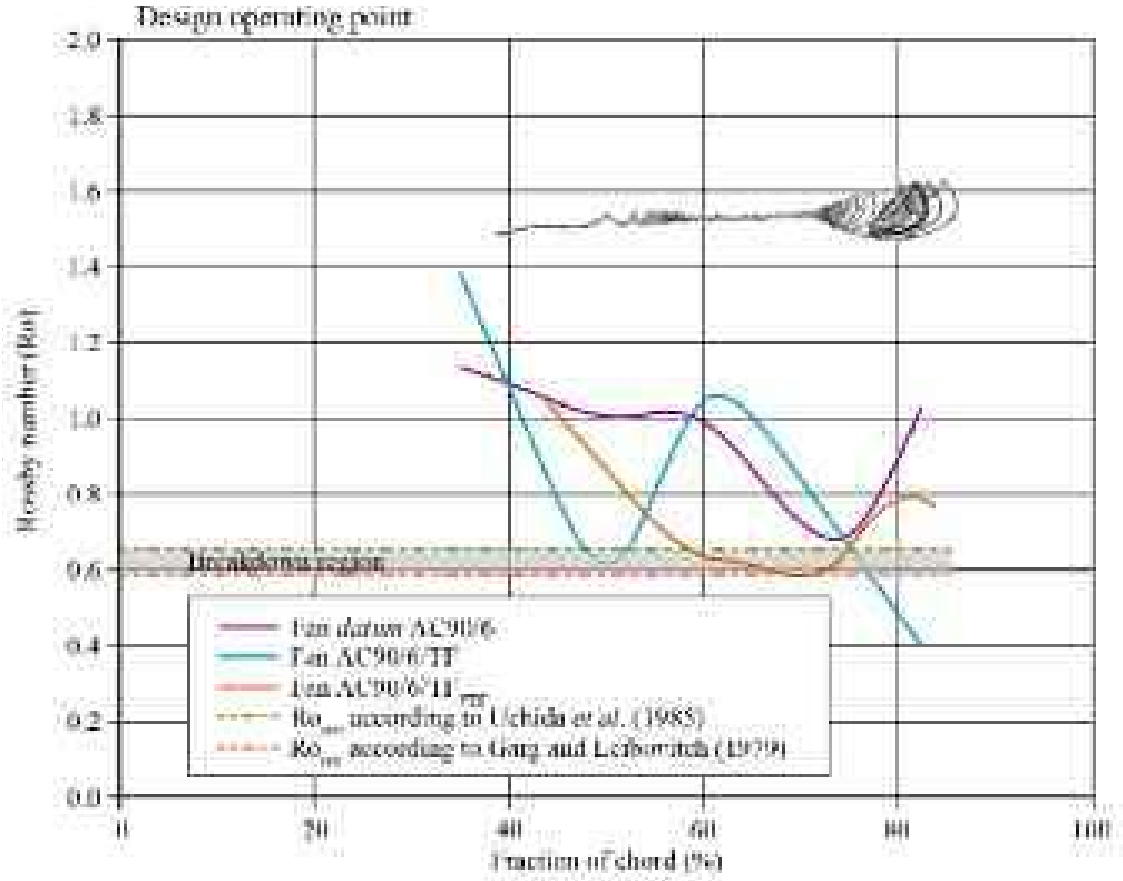

FIGURE 11.3. Chord-wise evolution of numerically predicted blade tip-to-casing leakage vortex Rossby number (*Ro*) at the fan design operating point for the fan *datum* AC90/6 and AC90/6/TF (Corsini and Sheard, 2007) and fan AC90/6/TF$_{VTE}$ (Corsini *et al.*, 2010).

Corsini and Sheard (2007) concluded that for the fan *datum* AC90/6, the blade tip-to-casing leakage vortex Rossby number remained above the threshold value and did not burst. However, the fan AC90/6/TF leakage vortex Rossby number fell below the threshold value at approximately 90 per cent blade chord and did burst. Vortex bursting is acoustically productive, with Corsini and Sheard (2007) proposing a variable thickness blade-tip end-plate that maintained the leakage vortex Rossby number above the required threshold value. When fitted with the variable thickness blade-tip end-plate, they named the studied fan AC90/6/TF$_{VTE}$, Figure 11.2. Corsini *et al.* (2010) studied the fan AC90/6/TF$_{VTE}$, concluding that the blade tip-to-casing leakage vortex Rossby number did remain above the threshold value and that the leakage vortex did not burst, Figure 11.3.

Corsini *et al.* (2007) studied the aerodynamic performance of fan AC90/ 6/TF$_{VTE}$. They concluded that the variable thickness blade-tip end-plate design successfully avoided blade tip-to-casing leakage vortex bursting. Assessing the aerodynamic performance demonstrated an improved pressure developing capability and fan efficiency that we may attribute to the leakage vortex not bursting. However, noise measurements indicated that the variable thickness blade-tip end-plate resulted in a broadband noise level approximately 0.5 dB higher than that associated with the constant thickness end-plate, Table 11.3. Corsini *et al.* (2007) concluded that the variable thickness blade-tip end-plate occurred with the presence of multiple organised vortical structures. These vortical structures did burst, with the breakdown acoustically productive enough to result in the observed increase in overall fan far-field broadband noise.

The work of Corsini *et al.* (2007) was continued by Corsini *et al.* (2009, 2010) who concluded that the multiple organised vortical structures induced in the blade tip region by the variable thickness blade-tip end-plate were disproportionately acoustically productive. Therefore, the blade-tip end-plate required redesign to minimise the swirling intensity and size of vortices in the blade tip region whilst both ensuring that they do not burst and that the blade-tip end-plate design avoids generating organised vortical structures.

Table 11.3. *Experimentally measured aerodynamic and acoustic performance for the fan AC90/6/TF and AC90/6/TF$_{VTE}$ at the peak pressure operating point. The authors made aerodynamic measurements in accordance with ISO 5801:2007 requirements (2007) and acoustic measurements in accordance with ISO 10302:2011 requirements (2011).*

Aerodynamic	Fan AC90/6/TF		Fan AC90/6/TF$_{VTE}$	
	Δp_{tot} (Pa)	η_{tot} (%)	Δp_{tot} (Pa)	η_{tot} (%)
	291.4	66	299.2	68
Acoustic @ 2 meters	unweighted SWL dB	A-weighted SWL dB(A)	unweighted SWL dB	A-weighted SWL dB(A)
	92.2	87.1	91.7	87.6

Rationale and Design Criterion

The reported research's aim is to develop a design process that links blade-tip end-plate design with flow control and fan noise attenuation. Designing the blade-tip end-plate to control the chord-wise evolution of the blade tip-to-casing leakage vortex Rossby number achieves this noise-by-flow control. The resulting blade-tip end-plate design induces sequences of augmentation and diminution of momentum transfer to the leakage vortex up to a near-critical Rossby number (Sheard *et al.*, 2009). The design process exploits a correlation between the blade-tip end-plate thickness $t_{ep}(s_c)$, the leakage vortex kinematics, the local blade loading and the blade tip-to-casing leakage flow's magnitude. We can derive the resultant end-plate thickness from the leakage vortex Rossby number, with the twin objectives of maintaining a stable leakage vortex that does not burst and minimising vortex intensity.

The derivation of blade-tip end-plate geometry follows Spall *et al.*'s method (1987), which proposed scale definitions for the blade tip velocity distribution consistent with swirling flows, leading-edge vortices and unconfined trailing wing-tip vortices. We interpreted Spall *et al.*'s (1987) method in the present study within the context of axial decelerating turbomachinery and consequently, we may express the definition for a confined blade tip-to-casing leakage vortex's Rossby number as:

$$Ro = \frac{V_a}{r_v \Omega}, \tag{1}$$

where we define:

- r_v as the radial distance from the vortex axis at which the swirl velocity is a maximum, in accord with Leibovich's (1982) characteristic viscous length scale;
- Ω as the rotation rate in the blade tip-to-casing leakage vortices near the vortex centre;

and;

- V_a equals the leakage velocity component along the tip vortex axis (w_{La}) as the axial velocity at the radial distance from the vortex axis at which the swirl velocity is a maximum (r_v) is consistent with the swirling velocity scale Ωr_v that equals the vortex peripheral velocity (w_{Lp}).

We extrapolated the algebraic function linking the end-plate thickness to the leakage vortex Rossby number by using classical flow models for the blade tip-to-casing flow. These models are documented in experimental and theoretical studies on the flow in the blade tip region of axial flow compressors, fans and pumps (Rains, 1954; Lakshminarayana, 1970). The proposed approach, although not mathemati-

cally precise, includes all the dominant flow and blade parameters that influence vortex creation in the blade tip-to-casing gap and is in accord with fundamental physical principles.

We defined the radial dimension of the blade tip-to-casing leakage vortex r using Rains' leakage flow model (1954), which establishes a correlation among the vortex's scale, the chord-wise position, the tip gap and the local blade load as:

$$r(s_c) = 0.14\tau\left[\frac{s_c}{\tau}C_l^{0.5}\right]^{0.85}, \tag{2}$$

where,

s_c is the abscissa along the chord;
τ is the tip gap height; and
C_l is the local lift coefficient.

We defined the blade tip-to-casing leakage vortex's rotational velocity (Ω) using Lakshminarayana's model (1970), valid in incompressible flow without accounting for blade rotation effects:

$$\Omega(s_c) = \frac{(1-k)\Gamma}{2\pi r^2}, \tag{3.1}$$

and,

$$\Gamma = 0.5C_l\ell_c v_m, \tag{3.2}$$

$$(1-k) = 0.23 + 7.45\left(\frac{\tau}{s_c}\right), \tag{3.3}$$

where,

Γ is the blade circulation;
ℓ_c is the blade tip chord; and
v_m is the average velocity through the blade tip section which depends on the local incidence and deviation angles.

We approximated the velocity scale (V) by introducing the leakage velocity component along the tip vortex axis w_{La} following Corsini and Sheard's method (2007). Rains (1954) concluded that the blade tip-to-casing flow driven by the pressure gradient across the blade is normal to the blade's camber line, and therefore we can define w_{La} as a function of leakage velocity normal to the blade chord w_{Ln}:

$$V \approx w_{La} = w_{Ln} \sin(\beta_L) \tag{4}$$

with β_L being the angle between the leakage jet and the blade chord, Figure 11.4. Therefore, we may derive the leakage velocity w_{Ln} by introducing a two-dimensional viscous analysis (Wadia and Booth, 1982) as a function of the pressure gradient within the blade tip-to-casing gap at each chord-wise *abscissae* location s_c. The dependence of friction factor f_f on the chord-wise position s_c is fixed by using a scaling value for the leakage flow bulk velocity w_{Ln} that then enables us to define the velocity w_{Ln} as:

$$w_{Ln}(s_c) = \sqrt{\frac{2\tau}{\rho f_f(Re_{gap}) t_{ep}(s_c)} dp(s_c)}, \tag{5}$$

where,

ρf_f is the friction factor which is itself a function of leakage flow Reynolds number, Re_{gap};
τ, is the tip gap height; and
$dp(s_c)$, is the static pressure drop through the tip gap.

Using the model which we defined in Equation 5, we were able to derive a closure equation for a Multiple-Vortex-Breakdown (MVB) blade-tip end-plate design that correlates the geometry of the end-plate with the evolution of blade tip vortex swirl, blade parameters and load conditions. By rearranging Equations (2), (3.1) and (4), the algebraic equation $t_{ep}(s_c) = f(Ro)$ reads as:

$$t_{ep}(s_c) = \Im_{load} \Im_{geo} \left[\frac{\sin(\beta_L)}{V_m Ro(s_c)} \right]^2 s_c^z \tag{6}$$

where $\Im_{load}$ and $\Im_{geo}$ are groups of parameters which respectively describe the influence of blade loading condition at the tip and blade geometry. We use Equation (6) to manage the evolution of the tip leakage flow's swirl level, $Ro(s_c)$, with the target swirl level a function of local lift coefficient. The local lift coefficient is also a function of both blade camber and blade-tip pitch angle. In the reported research, we derived the target swirl level from a numerical analysis of the blade tip-to-casing leakage flow in fan *datum* AC90/6.

The MVB blade-tip end-plate geometry results in a prescribed chord-wise distribution of the Rossby number against the end-plate shape, Figure 11.5. The MVB chord-wise thickness variation is a direct result of the developed design procedure, correlating the main vortical structures' swirl level over the blade tip with the end-plate geometry. When we fitted the studied fan with the MVB blade-tip end-plate, we named the fan AC90/6/TF_{MVB}.

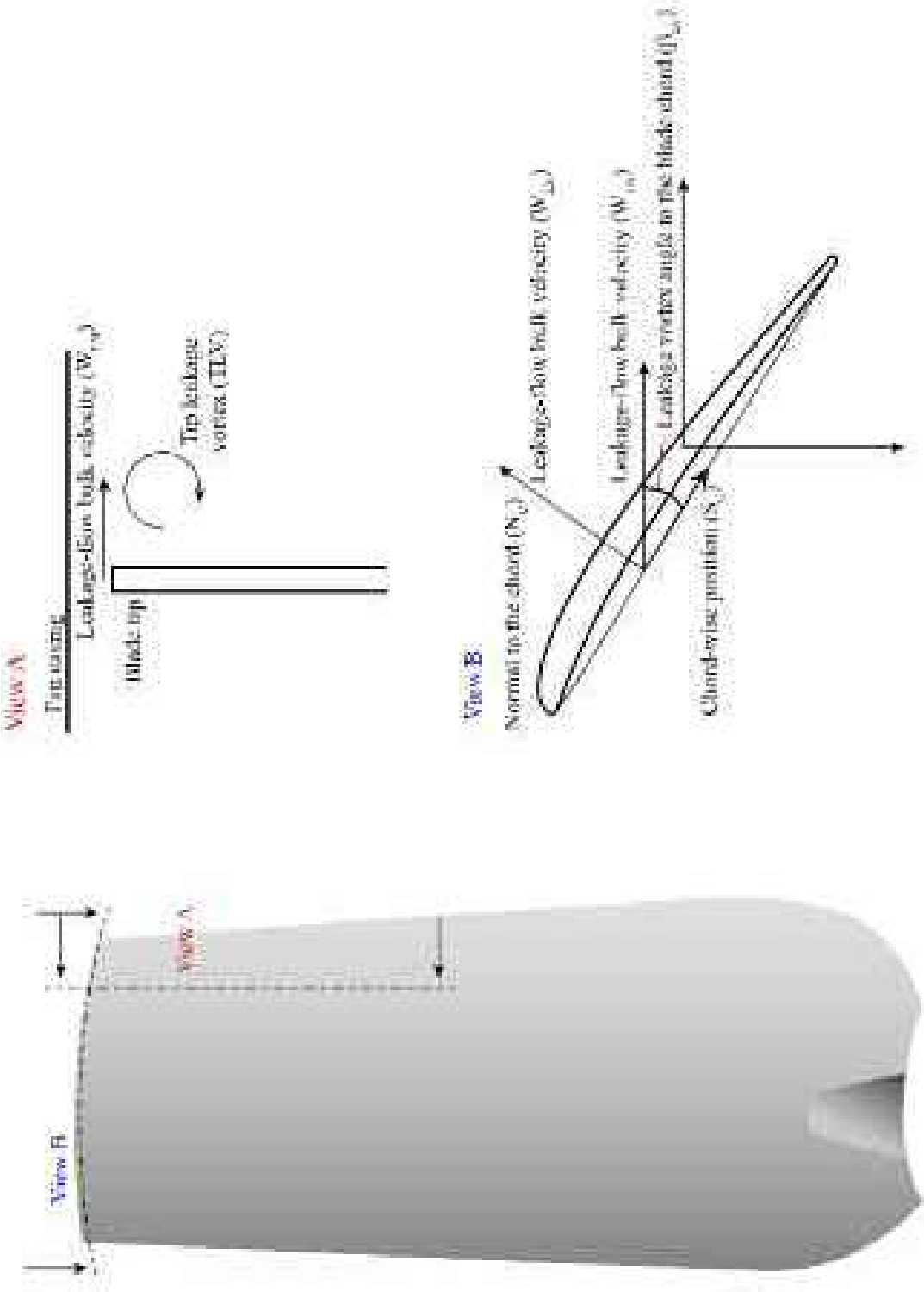

FIGURE 11.4. Definition of the coordinate system used to model the blade-tip end-plate geometry and its effect on momentum transfer to the blade tip-to-casing leakage vortex.

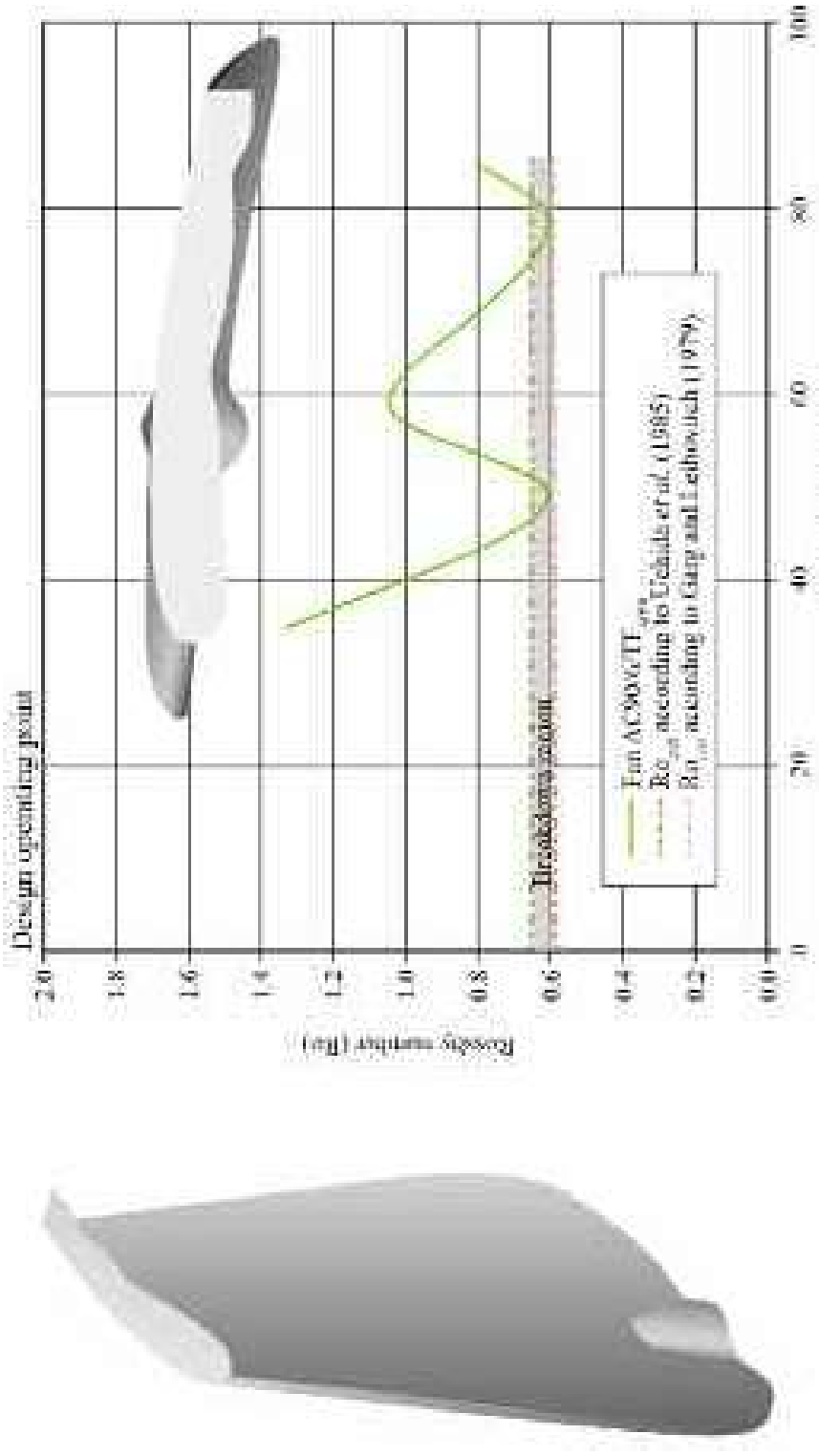

FIGURE 11.5. Chord-wise evolution of numerically predicted blade tip-to-casing leakage vortex Rossby number (*Ro*) at the fan design operating point for the fan AC90/6/TF_{MVB}. A three-dimensional numerical blade model with the MVB blade-tip end-plate illustrates the end-plate's scale relative to the blade.

Multiple-vortex-breakdown Sensitivity Analysis

A sensitivity analysis of the MVB end-plate design identified the influence of blade tip-to-casing clearance τ and blade loading on blade tip feature thickness, Figure 11.6. Blade tip-to-casing clearance was varied from 60 to 140 per cent of design value, τ_D, and blade loading C_l was varied from 55 to 105 per cent of design value, $C_{l,D}$. The MVB design procedure results in an increase in end-plate thickness when the tip leakage flow momentum requires a diminution. Control of the blade tip-to-casing leakage flow swirl level could be required either because of an enlarged blade tip-to-casing gap or because of aerodynamically overloaded blade tip sections. When we compare the relative influence of blade tip-to-casing clearance and blade loading, clearance τ is the more dominant parameter. Increasing clearance to 140 per cent of its design value results in near uniform end-plate thickness, Figure 11.6.

NUMERICAL SURVEY OF THE BLADE-TIP END-PLATE AERODYNAMICS

The flow-field in the studied fan's blade tip-to-casing gap is complex, and consequently, we chose to study the flow-field through a numerical survey. We first present our adopted methodology, followed by the numerical survey results.

Methodology

We solved the Reynolds-Averaged Navier–Stokes equations using an original parallel multi-grid finite element flow solver (Corsini *et al.*, 2006), developed using C++ technology and libMesh libraries (Kirk *et al.*, 2006). We modelled the fluid dynamics of incompressible three-dimensional turbulent flows in a rotating frame of reference with a topology-free low-Reynolds variant of a non-linear k-ε turbulence model (Craft *et al.*, 1996; Corsini and Rispoli, 2005). The finite element solver used second-order approximations for velocity, pressure and turbulence variables. We solved the Navier-Stokes and scale-determining turbulence equations fully coupled with a linear solver based on a preconditioned generalised minimal residual method (GMRES) algorithm. We built the mesh in a non-orthogonal body-fitted coordinate system by merging two structured h-type grid systems:

- a mesh in the main flow region (surrounding the blade); and,
- an embedded mesh in the tip-gap region.

For the fan *datum* AC90/6, the mesh consists of approximately 0.6 million linear hexahedral elements. The axial node distribution consisted of 20 per cent of nodes upstream of the blade leading edge, 50 per cent of nodes in the blade passage and 30 per cent of nodes downstream of the blade passage. We modelled the blade tip-to-casing clearance using 13 cells. The computational grid was clustered towards

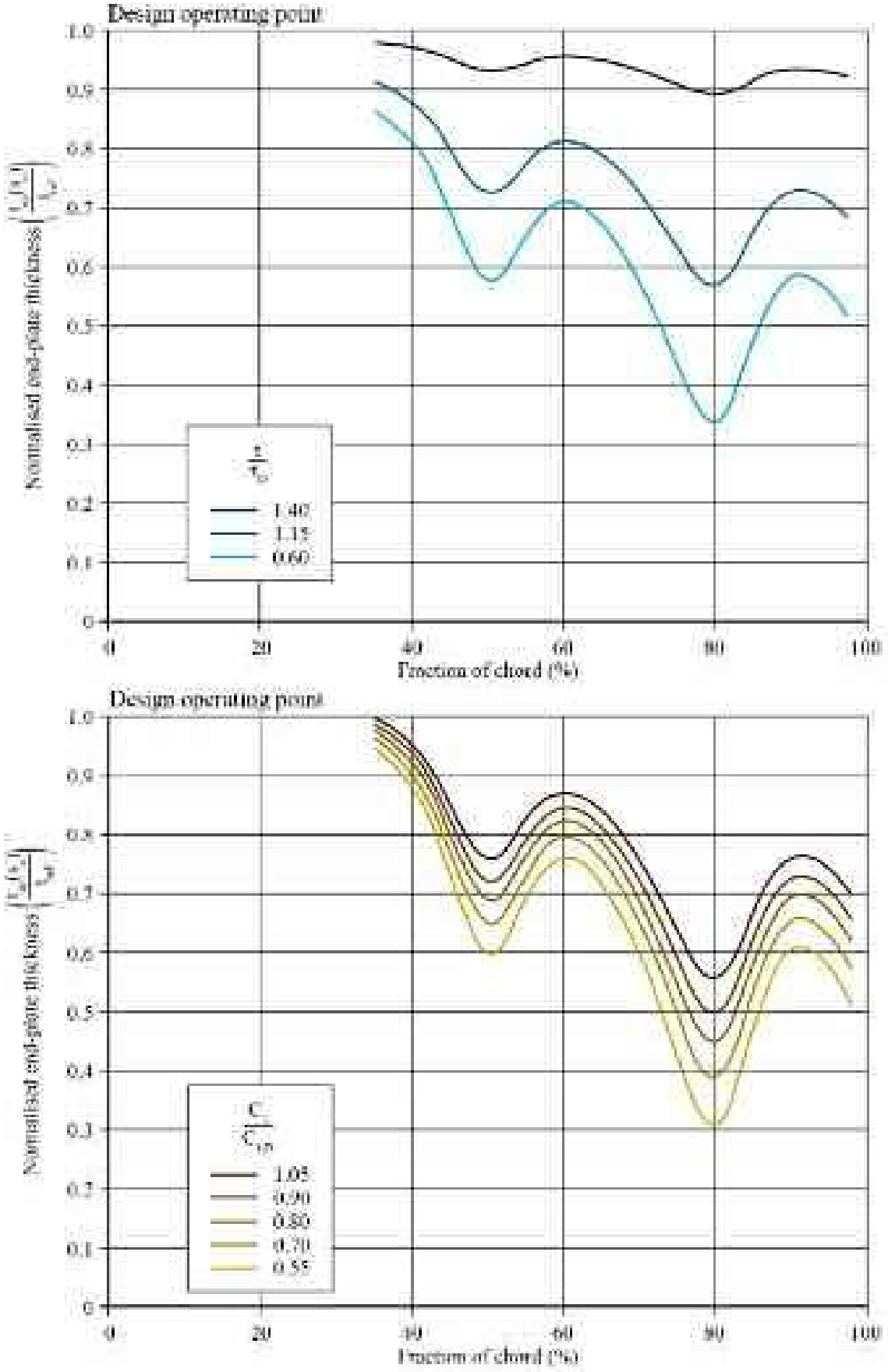

FIGURE 11.6. Parametric analysis of the MVB blade-tip end-plate geometry sensitivity to blade tip-to-casing clearance (τ) and local lift coefficient (C_l).

all solid boundaries, with the ratio of minimum grid spacing on solid walls to mid-span blade chord set at 2×10^{-3} at the blade tip, casing wall and blade surfaces. The grid refinement towards solid surfaces maintained a dimensionless distance value of approximately unity at the first row of nodes from each surface.

We adopted standard boundary condition settings (Corsini and Rispoli, 2004; Corsini *et al.*, 2010) and imposed the Dirichlet conditions for the relative velocity components at the in-flow half a blade mid-span chord upstream of the leading edge. We obtained the inlet velocity profile from flow simulation in an annular passage of the same hub-to-casing diameter ratio as the fan *datum* AC90/6, with the simulation including an up-stream spinner cone. We obtained the inlet distribution of turbulent kinetic energy (k) from an axi-symmetric turbulence intensity profile featuring a nearly uniform value of six per cent in the flow's core region, which increased approaching the end-walls to approximately ten per cent. We based the turbulence energy dissipation's inlet profile on the length scale (l_ε) set to 0.01 of rotor pitch at mid-span. Flow periodicity upstream and downstream of the blading, and Neumann outflow conditions (homogeneous for k and ε, and non-homogeneous for the static pressure), completed the boundary data.

Flow Survey at the Blade Tip

The numerical analysis facilitated a study of the blade tip-to-casing leakage vortex evolution at the design operating point, Figure 11.7. We used a normalised helicity H_n, based on the absolute vorticity as the tip vortex swirl metric. Normalised helicity provides a criterion for detecting vortex bursting (Furukawa *et al.*, 1999; Corsini *et al.*, 2010). We defined normalised helicity H_n as:

$$H_n = (\xi_i \cdot w_i) \,/\, (|\xi|\,|w|) \text{ with } i = 1, \ldots 3, \tag{7}$$

where ξ_i and w_i are the Cartesian components of the absolute vorticity and relative velocity vectors, and $|\xi|$ and $|w|$ are their norms.

When one studies the normalised helicity results for the fan *datum* AC90/6, it is apparent that the helicity field indicates that there is a highly skewed chord-wise vortical structure emanating from the blade chord's first quarter. This vortical structure co-exists with a weak tip separation vortex. Over the blade chord's last quarter, we may characterise the leakage flow by a merging of the tip separation vortex and the leading edge vortex. This merging results in a unique clock-wise vortical structure that affects the blade-to-blade flow-field over the majority of the blade pitch in the tip region.

When one studies the normalised helicity results for the fan AC90/6/TF, it is apparent that the constant thickness end-plate induces a significant change in the blade tip-to-casing leakage flow physics. The leakage vortex normalised helicity reduces as the vortex travels from blade leading to blade trailing edge, and is deflected as a consequence of near-axis swirl weakening. Over the blade chord's last quarter the leakage vortex collapses, producing a bubble-type separation that indicates vortex breakdown (Corsini and Sheard, 2007; Corsini *et al.*, 2010). The separated flow

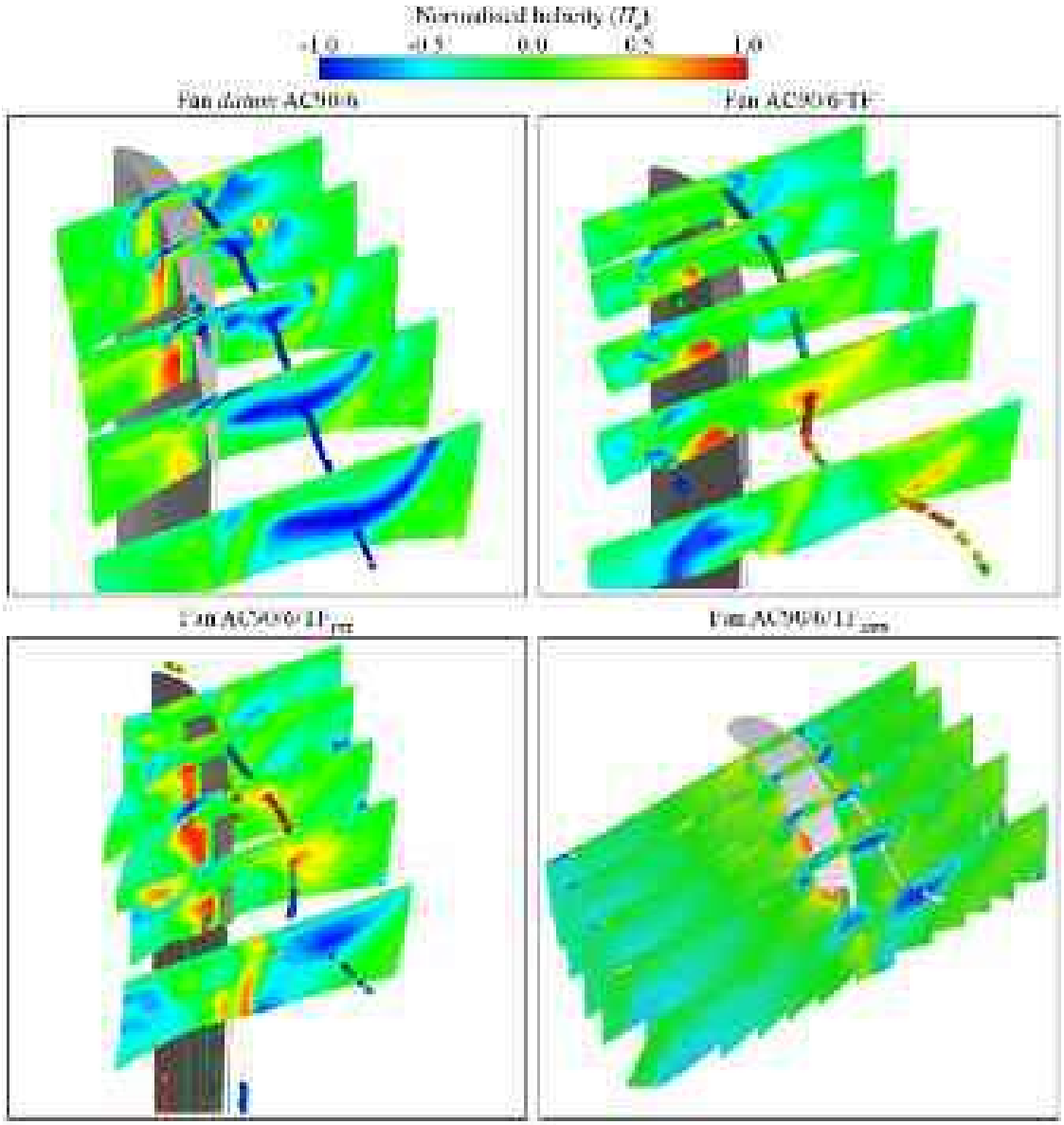

FIGURE 11.7. Three-dimensional normalised helicity (H_n) contours numerically predicted at the fan design operating point. Helicity contours are presented at five chord-wise locations through the fan *datum* AC90/6, AC90/6/TF, AC90/6/TF$_{VTE}$ and AC90/6/TF$_{MVB}$. The blade tip-to-casing leakage vortex core trajectory also illustrates the effect of fitting the three blade-tip end-plates.

evolves into a counter clockwise vortex and immediately downstream of the rotor this vortex washes out. As a result, no coherent vortical structure is evident.

When one studies the normalised helicity results for the fan AC90/6/TF$_{VTE}$, it is apparent that tapering the end-plate thickness shifts the origin of the primary vortical structure downstream in comparison to both the fan *datum* AC90/6 and AC90/6/TF. At mid-chord the reduction of fan AC90/6/TF$_{VTE}$ blade end-plate thickness results in an increase in the primary vortical structure's energy. Additionally, the primary vortical structure drives an anti-clockwise rotating cell from the blade pressure side that interacts with the primary vortical structure. This interaction indicates that the variable thickness end-plate results in a blade tip flow-field that is distinctly different to that as-

sociated with both the fan *datum* AC90/6 and AC90/6/TF. The variable thickness end-plate effectively blocks leakage flow over the blade chord's front half, forcing the leakage flow to the blade chord rear half where the end-plate is tapered. The proposed design concept does not consider this pressure gradient redistribution that manages the Rossby number above a critical value (Corsini and Sheard, 2007). The pressure gradient redistribution appears to be a factor that is at least partly responsible for the increase in fan AC90/6/TF$_{VTE}$ far-field noise when compared with fan AC90/9/TF.

It is apparent that the tip leakage vortex origin is located over the blade chord's first quarter when one studies the normalised helicity results for the fan AC90/6/TF$_{MVB}$. In this regard, the fan AC90/6/TF$_{MVB}$ is similar to the fan AC90/6/TF. The evolution of the normalised helicity contours indicates that the design procedure has produced an end-plate design that does result in flow control that both reduce leakage flow and overall vortical swirl. The normalised helicity contours indicate that a succession of leakage flow momentum enhancements and diminution manage the evolution and convection of the leakage vortex through the blade passage. This both minimises the blade tip-to-casing gap flow rate and results in a leakage vortex that does not burst.

A blade tip-to-casing leakage flow vortex streamline analysis complements the analysis of normalised helicity results, Figure 11.8. Using the leakage vortex streamlines for the fan *datum* AC90/6 as a benchmark for comparison, it is apparent that the presence of a bubble-like separation along the vortex axis affects both the fan AC90/6/TF and AC90/6/TF$_{VTE}$. For the fan AC90/6/TF, this separation occurs as a consequence of excessive leakage flow reduction. For the fan AC90/6/TF$_{VTE}$, this separation occurs as a consequence of a leakage jet at mid-chord interacting with the leakage vortex.

When one studies the leakage vortex streamlines for the fan AC90/6/TF$_{MVB}$, it is apparent that the flow control design procedure has resulted in an effective end-plate. The recirculating flow regions observable in both the fan AC90/6/TF and AC90/6/TF$_{VTE}$ streamlines have been eliminated, and the leakage vortex does not burst. The normalised helicity for the fan AC90/6/TF$_{MVB}$ indicates that the MVB end-plate reduces the complexity of the over-tip vortical structure by permitting only the leakage vortex to pass over the blade tip. Therefore, the MVB end-plate is effective as a consequence of eliminating all but the leakage vortex and managing the leakage vortex's Rossby number to minimise its intensity whilst simultaneously preventing it from bursting.

We may consider the analysis of normalised helicity and leakage vortex streamlines primarily as an analysis of aerodynamic performance. We must complement this aerodynamic analysis by considering the aerodynamic flow features' acoustic consequence. Changes in the blade tip-to-casing flow-field will have acoustic consequences. The change in end-plate geometry may result in an increase in the acoustic energy that occurs with the flow features induced by the end-plates. Alternatively, the sound absorption may increase as a consequence of acoustic waves traversing turbulent flow regions (Guedel, 1985). When considering the impact of blade-tip end-plates, the characteristic time scales that occur with turbulent flow are significantly shorter than those that occur with acoustic waves. Consequently, we may assume that turbulence is both not influenced by the passage of acoustic waves and that

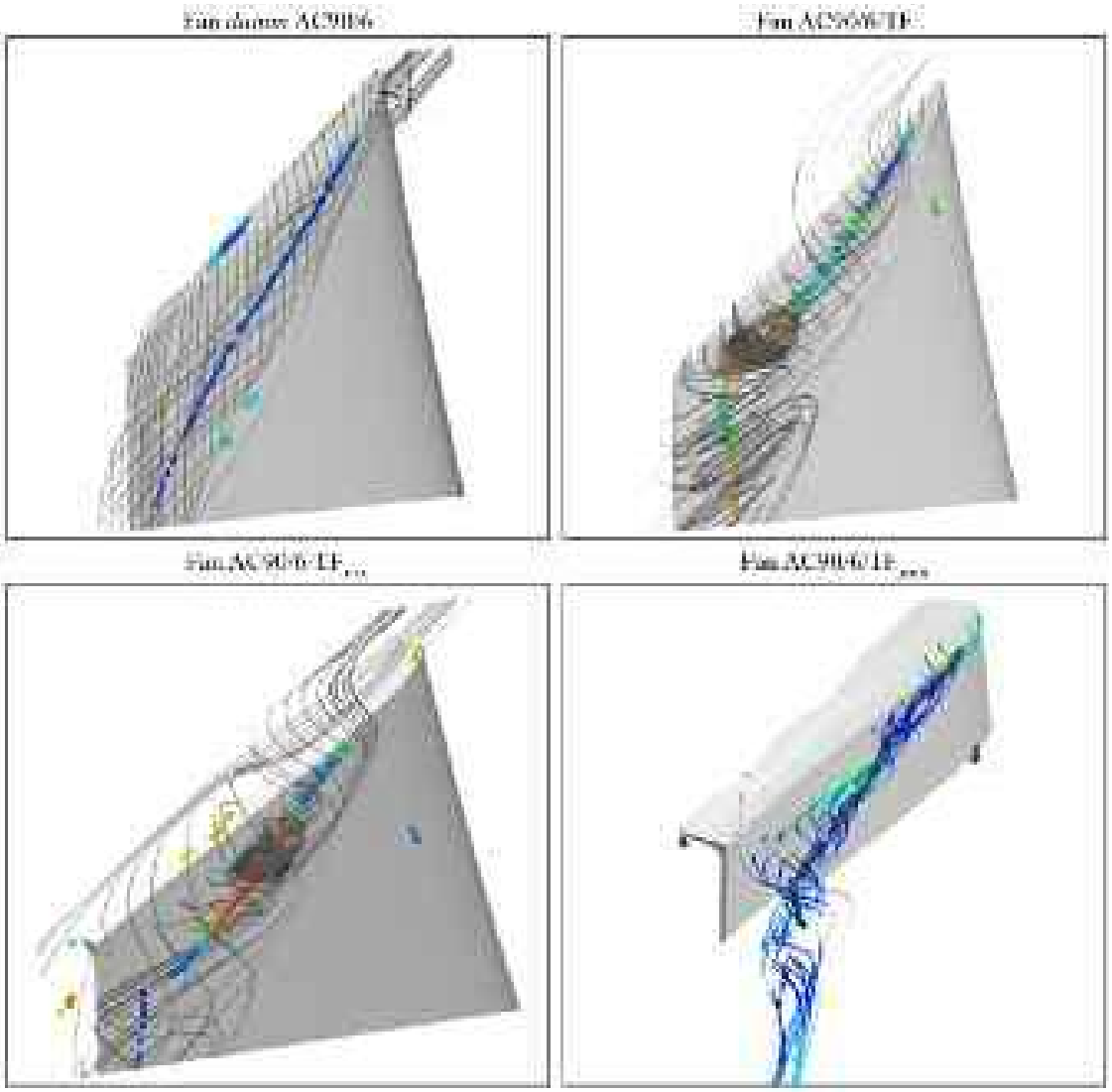

FIGURE 11.8. Three-dimensional blade tip-to-casing leakage vortex streamlines numerically predicted at the fan design operating point. Leakage vortex streamlines are presented through the fan *datum* AC90/6, AC90/6/TF, AC90/6/TF$_{VTE}$ and AC90/6/TF$_{MVB}$. The blade tip-to-casing leakage vortex core trajectory also illustrates the effect of fitting the three blade-tip end-plates.

the turbulence does not absorb acoustic energy. If we accept that acoustic energy generated by blade-tip flow-field features is not absorbed within the blade passage, then we must also accept that acoustic energy generated by flow-field features in the blade tip region transmits to the fan far-field.

In cases where the turbulence characteristic time scale is of the same order of magnitude of the speed of sound, acoustic energy of aerodynamic origin dampens as it propagates through turbulent flow regions. Guedel (1985) studied air movement fan acoustic characteristics and concluded that turbulent shear layers result in sound absorption from rotating and stretching vortical flow features passing though the turbulent shear layer. Before a comparative analysis of the four end-plate designs is possible, it is necessary to establish if the flow-field in the blade tip region does, or does not absorb acoustic energy. Howe (1984) provided a theoretical model for sound absorption in wall turbulent shear flows at low Mach numbers and concluded

that if coherent perturbations of velocity do not influence the turbulent scale-determining quantities, we may express the net dissipation of acoustic energy as:

$$\Pi = \rho_0 \nu_A \left(\frac{\partial v_i}{\partial x_j} \right)^2 , \tag{8.1}$$

where, ρ_0 is the air density in normal condition, v_i is the vector of sound coherent perturbation velocity and ν_A is the coefficient of acoustic dissipation. According to Howe (1984), this net dissipation of acoustic energy coefficient depends on the fluid's local viscosity that we may express as:

$$\nu_A = [2\nu_t + \nu] , \tag{8.2}$$

where, ν_t is the turbulence viscosity, and ν is the air kinematic viscosity.

Following Howe's method (1984), we may complement the previously presented aerodynamic analysis with an analysis of the coefficient of acoustic energy dissipation. When one studies the coefficient of acoustic energy dissipation for the fan *datum* AC90/6, Figure 11.9, it is apparent that the blade tip-to-casing leakage vortex development results in an inviscid swirling core, an observation that is self-consistent with other scholars' conclusions (Storer and Cumpsty, 1991; Corsini and Rispoli, 2004). When one studies the coefficient of acoustic energy dissipation for the fans AC90/6/TF, AC90/6/TF$_{VTE}$ and AC90/6/TF$_{MVB}$, a common theme attributable to all three end-plates is their role as mixing devices that affect the blade tip-to-casing leakage flow (Corsini *et al*., 2007). All three end-plates affect the ratio between axial and peripheral momentum transfer from the leakage vortex that produces unstable structures. As a consequence, the induced vortex instabilities manifest themselves as a loss of rotational coherence that may be related to reduced fan far-field noise.

EXPERIMENTAL SURVEY OF THE BLADE-TIP END-PLATE PERFORMANCE

We felt that the flow-field in the blade tip-to-casing gap was too complex to study experimentally. Consequently, we chose to study the flow-field using a numerical survey. However, it was possible to establish the overall aerodynamic and acoustic performance of the studied fan and the developed blade end-plate configurations. We present the experimental methodology that we adopted, followed by a presentation of aerodynamic and acoustic experimental results.

Methodology

We carried out static and dynamic pressure measurements using a type B test rig, configured in accordance with ISO 5801:2007 (2007), using pressure transducers equally spaced around the casing wall and a standard Pitot-probe. We mounted the

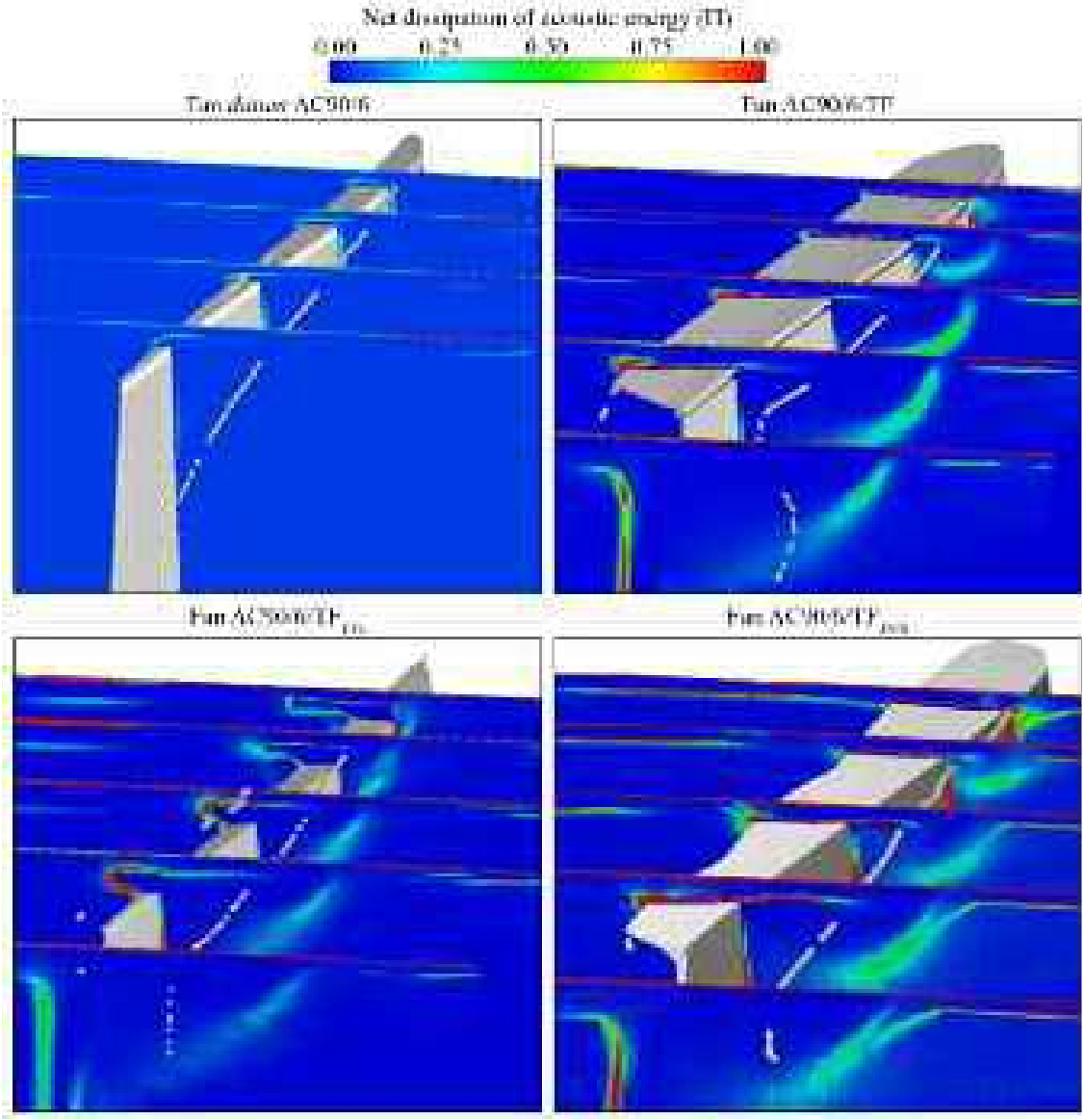

FIGURE 11.9. Three-dimensional net dissipation of acoustic energy (P) contours, numerically predicted at the fan design operating point. Coefficients are presented through the fan *datum* AC90/6, AC90/6/TF, AC90/6/TF$_{VTE}$ and AC90/6/TF$_{MVB}$. The blade tip-to-casing leakage vortex core trajectory also illustrates the effect of fitting the three blade-tip end-plates.

Pitot-probe on a traversing mechanism fixed to the test rig's outer wall. We recorded data using a digital multi-channel micro-manometer with 2 kPa range and a resolution of 1 Pa. The pressure measurement's accuracy was ± 0.5% of reading. We defined fan efficiency as the ratio between the air power (computed using either static or dynamic pressure rise) and the electric input power. We measured the input electric power using an AC power analyser with an accuracy of 0.24 per cent of reading.

We conducted the acoustic measurements in an anechoic chamber originally developed for measuring air movement fan noise in accordance with the ISO 10302:2011 (2011) standard. The anechoic chamber cut-off frequency was 25 Hertz. Bianchi *et al.* provide a more complete description of the facility (Bianchi *et al.*, 2009c). We carried out the acoustic measurements using a type-A configuration with

the fan installed downstream of an acoustically treated plenum chamber with a free outlet. The fan center line was two meters from the floor, in an arrangement similar to that typical of compact cooling fans when installed in-service. We mounted a bell-mouth on the fan inlet to give uniform and unseparated flow into the fan.

We measured the far-field noise six fan diameters from the fan outlet, in accordance with Leggat and Siddon's recommendations (1978). Air-speed measurements at the far-field microphone's location indicated a flow rate of less than one metre per second that we may consider low enough to have only a second order effect on the acoustic measurements that we obtained using the microphone. We set the free-field microphone at the same height as the fan centre line. In all cases, we measured the signals three times for 30 seconds, and averaged the results. We estimated the error in measured noise to be between 0.1–0.2 dB at 1 kHz. To isolate fan aerodynamic noise from motor noise, we conducted a preliminary motor test to establish the motor's spectral signature that we then used to correct subsequent noise measurements.

Aerodynamic Performance

We measured the aerodynamic performance for the following fans: *datum* AC90/6, AC90/6/TF, AC90/6/TF$_{VTE}$ and AC90/6/TF$_{MVB}$, Figure 11.10. An analysis of the total pressure rise characteristic curves indicates that the fan AC90/6/TF$_{MVB}$ performed significantly better than the other fans. The aerodynamic gain associated with the MVB end-plate was approximately a five per cent increase in pressure at the peak pressure operating point and a seven per cent increase in pressure at the design operating point. This improvement in pressure developing capability did not reduce the fan AC90/6/TF$_{MVB}$'s stable operating range that was unchanged compared with the other fans.

An analysis of the efficiency characteristic curves indicates that the four tested fans had essentially similar efficiency characteristics at both the peak pressure and design operating points. As the flow rate throttles from the peak pressure operating point towards stall, there is a small increase in efficiency for fans AC90/6/TF, AC90/6/TF$_{VTE}$ and AC90/6/TF$_{MVB}$ when compared with the fan *datum* AC90/6. This improvement enabled us to infer that the blade tip leakage vortex flow's end-plate control influences the overall secondary flow field in the blade tip region, with a resultant small gain in fan efficiency as the fans approach stall. The fan AC90/6/TF$_{MVB}$ exhibits a one per cent improvement in efficiency compared to the fan *datum* AC90/6 at both the peak pressure and design operating points. As the three fans with end-plates operate at higher flow rates increasingly off-design, their efficiency decreases compared with the fan *datum* AC90/6.

Noise Performance

The MVB end-plate noise analysis focuses on the comparison of the overall acoustic performance that we measured in accordance with ISO 10302:2011 (2011),

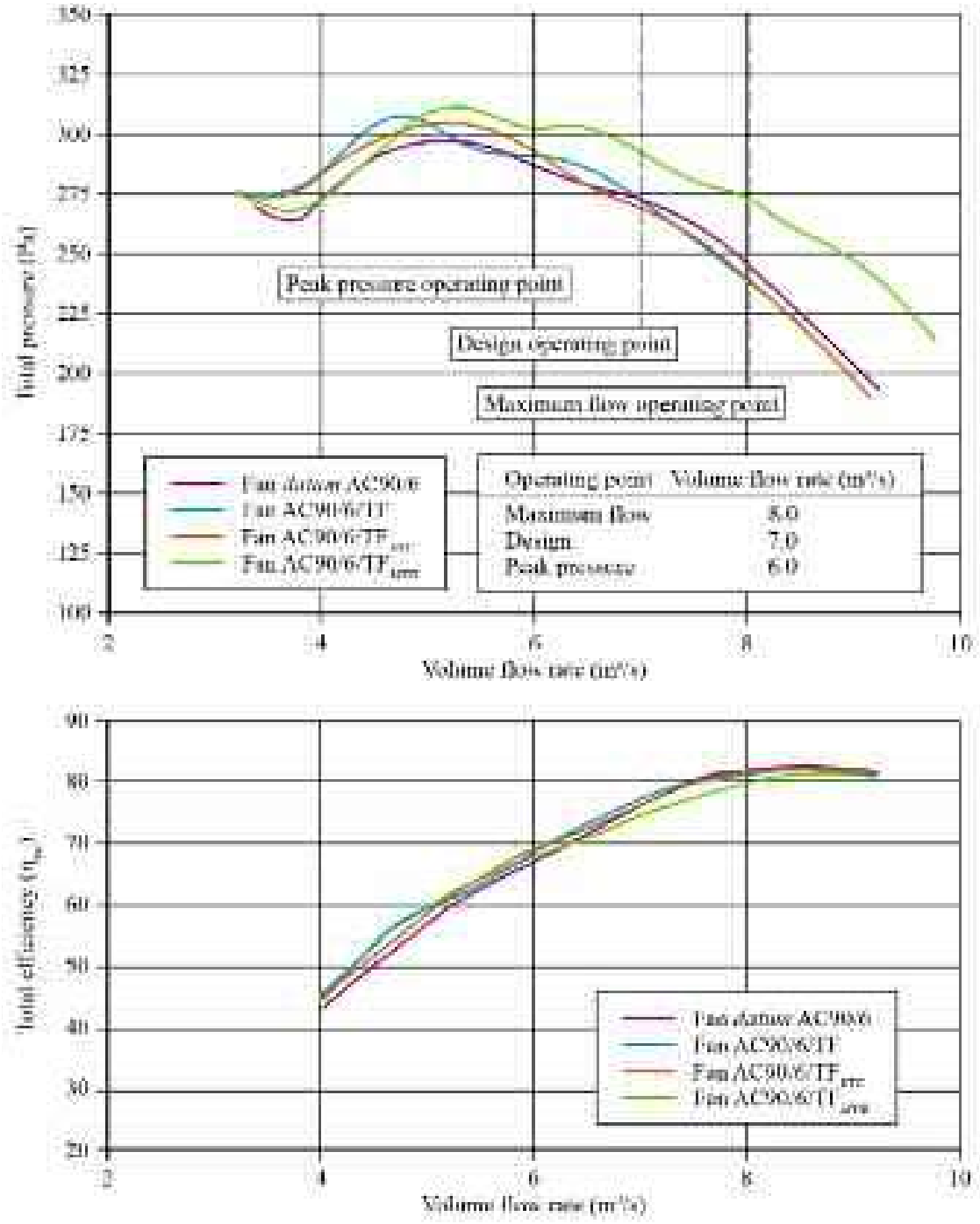

FIGURE 11.10. The performance characteristics of the studied fan *datum* AC90/6 without a fitted blade-tip end-plate, with a constant thickness blade-tip end-plate, AC90/6/TF, with a variable thickness blade-tip end-plate, AC90/6/TF$_{VTE}$ and with the multiple vortex breakdown blade-tip end-plate, AC90/6/TF$_{MVB}$. The authors measured performance characteristics with the blade tip pitch angle set to 28 degrees in a Type C standardised airway (ducted inlet, free outlet) in accordance with ISO 5801:2007 requirements (2007).

Figure 11.11. The four studied fans each had slightly different aerodynamic performance, making it difficult to measure acoustic performance at identical operating points for each fan. We chose to measure the four studied fans' acoustic performance at the design operating point flow rate. This choice resulted in the fans *datum*

AC90/6, AC90/TF and AC90/TF$_{VTE}$ generating a similar pressure rise. However, the fan AC90/TF$_{MVB}$ generated a significantly higher pressure rise, Figure 11.10. Reasonably, we may expect a higher pressure developing fan to be noisier, and therefore our decision to test all four fans at the same flow rate reflects a conservative approach to the comparative analysis of the MVB end-plate performance.

When one studies the narrow-band and A-weighted one-third octave band spectra, a reduction is evident for the fans fitted with end-plates, Figure 11.11. We may speculate that the reduction is correlated with noise generation mechanisms found in all classes of decelerating turbomachinery. To different extents, the end-plates exploit control over the leakage vortices' magnitude, both in terms of radial footprint and rotational energy content. A consequence of this control is primarily reduced tonal noise. In contrast, we may correlate reduced broadband noise with mixing enhancement in the blade tip region where the leakage vortex develops.

Comparing the four studied fans' acoustic performance, Table 11.4, provides insight into the three end-plate concepts' noise reduction potential by comparing the unweighted and A-weighted sound levels at the design and high flow operating points. Consider the A-weighted sound power level of the fan AC90/6/TF$_{MVB}$ and fan *datum* AC90/6. It is evident that the fan AC90/6/TF$_{MVB}$ is characterised by lower A-weighted sound power level at the maximum flow, design and peak pressure operating points. At the maximum flow operating point the fan AC90/6/TF$_{MVB}$ is 4.4 dB(A) quieter. At the design operating point the fan AC90/6/TF$_{MVB}$ is 5.8 dB(A) quieter. At the maximum flow operating point the fan AC90/6/TF$_{MVB}$ is 8.2 dB(A) quieter. We must consider this result within the context of the fan AC90/6/TF$_{MVB}$ delivering a significantly higher total pressure rise than the fan *datum* AC90/6. This higher total pressure rise may be normalised by taking into account specific noise level k_s (Fukano *et al.*, 1978). Reducing the total pressure rise back to that of fan *datum* AC90/6 is equivalent to an additional 0.5 to 1.0 dB reduction in fan AC90/6/TF$_{MVB}$'s noise level.

CONCLUSIONS

In this chapter we presented a new noise-by-flow control concept for the design of blade-tip end-plates for subsonic axial fans. We numerically analysed the resultant end-plate design, and measured the overall performance of fans fitted with the studied end-plates in both aerodynamic and acoustic experimental facilities. This combination of numerical and experimental analysis established the role of end-plates in reducing fan far-field noise, and the role of blade tip-to-casing leakage vortex bursting.

We exploited the noise-by-flow control concept through developing an end-plate design procedure that enabled us to create end-plate geometry that influenced the momentum transfer into the leakage flow. Applying the design procedure resulted in a variation of end-plate thickness with the specific objective of controlling the blade tip-to-casing leakage vortex swirl's chord-wise evolution. The objective in controlling swirl was to manage energy transfer from the leakage flow to the leakage vortex in order to induce a subtraction and addition sequence of near-axis momentum. This enabled the new end-plate design, via purely passive means, to control the blade tip-to-casing leakage vortex swirl level, first minimising vortex intensity and

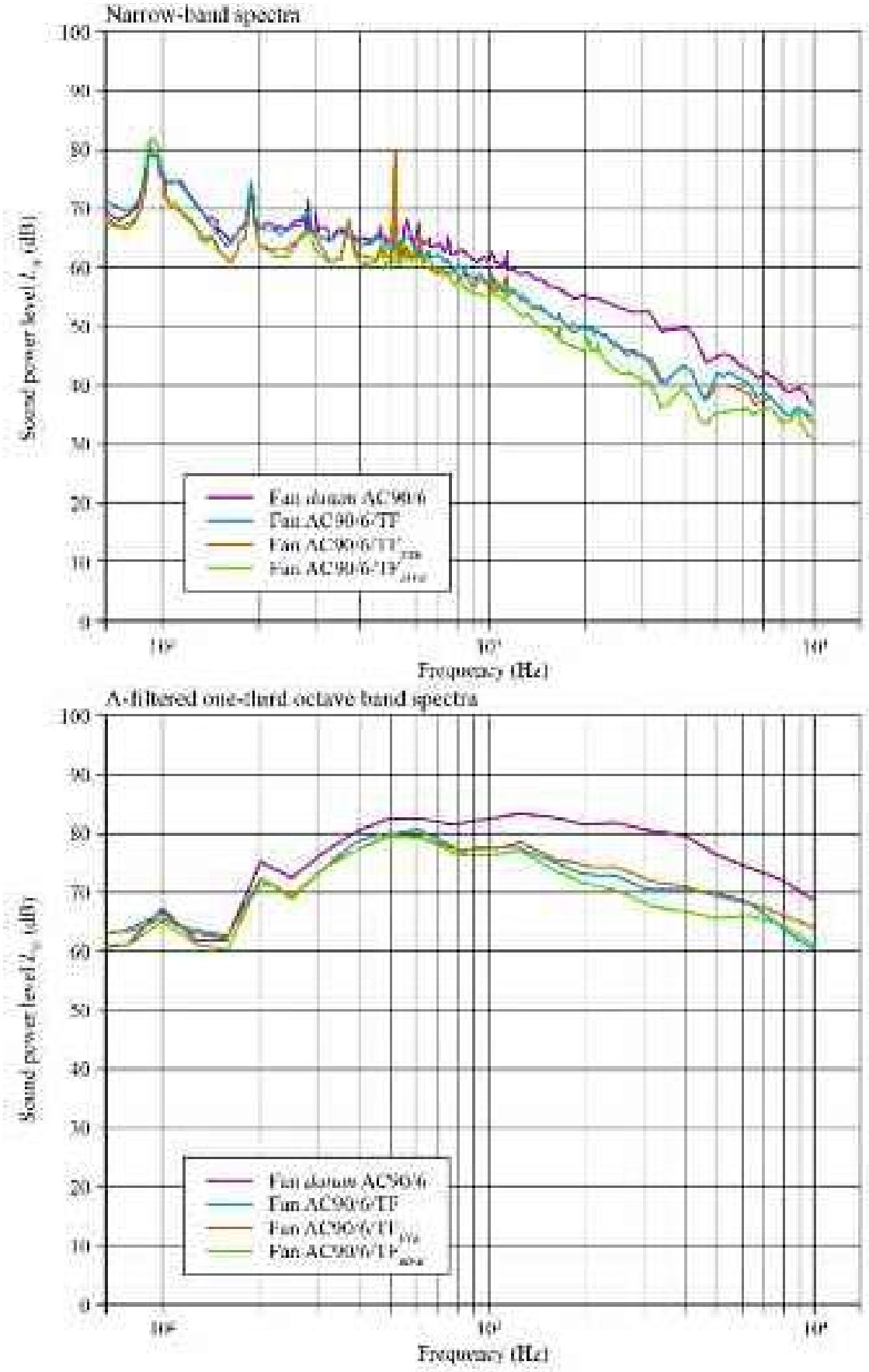

FIGURE 11.11. Outlet far-field sound pressure level (L_P) spectrum measured at the fan design operating point. For the sake of clarity, the authors presented the sound pressure level as both a narrowband and A-filtered one-third octave band spectrum. We provide measured sound pressure level spectrum data for the fan *datum* AC90/6, AC90/6/TF, AC90/6/TF$_{VTE}$ and AC90/6/TF$_{MVB}$.

Table 11.4. *Experimentally measured acoustic performance for the four studied fan configurations at their maximum flow, design and peak pressure operating points. The authors made acoustic measurements in accordance with ISO 10302:2011 requirements (2011)*

	datum AC90/6		AC90/6/TF		AC90/6/TF$_{VTE}$		AC90/6/TF$_{MVB}$	
Operating point	unweighted SWL dB	A-weighted SWL dB(A)	unweighted SWL dB	A-weighted SWL dB(A)	unweighted SWL dB	A-weighted SWL dB(A)	unweighted SWL dB	A-weighted SWL dB(A)
Maximum flow	100,1	92,5	96,7	89,3	99,7	89,1	98,6	88,1
Design	96,8	92,5	96,6	87,9	96,3	87,7	94,7	86,7
Peak pressure	95,4	93,2	92,2	87,1	91,7	87,6	89,9	85,0

second, ensuring that it did not burst. Thus, the design procedure was able to combine the control of vortical structures with a reduced fan far-field noise.

We used flow-field numerical predictions in the blade tip region to provide insight into physical principles underpinning the noise-by-flow control concept. Predicted flow streamlines provided a qualitative assessment of the blade tip leakage flow evolution's kinematics, which is characterised using the Rossby number. The end-plate thickness is varied to ensure that the near-axis swirl diminution-enhancement results in the blade tip-to-casing leakage vortex remaining above a critical Rossby number value so that it did not burst.

We demonstrated blade-tip end-plate concept effectiveness via fan far-field tonal and broad-band noise reduction. We experimentally verified the end-plate designed using the multiple vortex breakdown (MVB) design procedure is 4.4 dB(A) quieter than the fan *datum* AC90/6. At the design operating point the fan AC90/6/TF$_{MVB}$ is 5.8 dB(A) quieter. At the maximum flow operating point the fan AC90/6/TF$_{MVB}$ is 8.2 dB(A) quieter.

REFERENCES

ISO 5801:2007 (2007), *Industrial Fans: Performance Testing Using Standardised Airways.*

ISO 10302:2011 (2011), *Acoustics: Measurement of Airborne Noise Emitted and Structure-Borne Vibration Induced by Small Air-Moving Devices Part 1: Airborne Noise Measurement.*

Akaike, S., Kuroki, S. and Katagiri, M. (1991), 'Noise Reduction of Radiator Cooling Fan for Automobile. Three-dimensional Analysis of the Flow between the Blades of the Fan', *Japan Society of Automotive Engineers*, vol. 22(3), pp. 79–84.

Akturk, A. and Camci, C. (2010), 'Axial Flow Fan Tip Leakage Flow Control using Tip Platform Extensions', *Transactions of the ASME, Journal of Fluids Engineering*, vol. 132(5), pp. 1-10.

Akturk, A. and Camci, C. (2011a), 'Tip Clearance Investigation of a Ducted Fan used in VTOL UAVS. Part 1: Baseline Experiments and Computational Validation', *Proceedings of the 56th American Society of Mechanical Engineers Turbine and Aeroengine Congress*, Vancouver, Canada, 6–10 June, paper no. GT2011-46356.

Akturk, A. and Camci, C. (2011b), 'Tip Clearance Investigation of a Ducted Fan used in VTOL UAVS. Part 2: Novel Treatments via Computational Design and their Experimental Verification', *Proceedings of the 56th American Society of Mechanical Engineers Turbine and Aeroengine Congress*, Vancouver, Canada, 6–10 June, paper no. GT2011-46359.

Baad, P.K. (1977), 'Effects of Acoustic Loading on Axial Flow Fan Noise Generation', *Noise Control Engineering*, vol. 8, pp. 5–15.

Bianchi, S., Corsini, A., Rispoli, F. and Sheard, A.G. (2009a), 'Detection of Aerodynamic Noise Sources in Low-speed Axial Fan with Tip End-plates', *Proceedings of the IMechE Part C, Journal of Mechanical Engineering Science*, vol. 223, pp. 1379–1392.

Bianchi, S., Corsini, A., Rispoli, F. and Sheard, A.G. (2009b), 'Experimental Aeroacoustic Studies on Improved Tip Configurations for Passive Control of Noise Signatures in Low-

speed Axial Fans', *Transactions of the ASME, Journal of Vibration and Acoustics*, vol. 131, pp. 1–10.

Bianchi, S., Sheard, A.G., Kinghorn, I.R., Corsini, A. and Rispoli, F. (2009c), 'Experimental Development of a Measurement Technique to Resolve the Radial Distribution of Fan Aeroacoustic Emissions', *Noise Control Engineering*, vol. 57, pp. 360–369.

Brookfield, J.M. and Waitz, I.A. (2000), 'Trailing Edge Blowing for Reduction of Turbomachinery Fan Noise', *AIAA Journal of Propulsion and Power*, vol. 16(1), pp. 57–64.

Corsini, A. and Rispoli, F. (2004), 'Using Sweep to Extend Stall-free Operational Range in Sub-sonic Axial Fan Rotors', *Proceedings of the IMechE Part A, Journal of Power and Energy*, vol. 218, pp. 129–139.

Corsini, A. and Rispoli, F. (2005), 'Flow Analyses in a High-pressure Axial Ventilation Fan with a Non-linear Eddy-viscosity Closure', *International Journal of Heat and Fluid Flow*, vol. 26, pp. 349–361.

Corsini, A. and Sheard, A.G. (2007), 'Tip End-plate Concept based on Leakage Vortex Rotation Number Control', *Journal of Computational and Applied Mechanics*, vol. 8(1), pp. 21–37.

Corsini, A., Rispoli, F., Santoriello, A. and Tezduyar, T. (2006), 'Improved Discontinuity-capturing Finite Element Techniques for Reaction Effects in Turbulence Computation', *Computational Mechanics*, vol. 38, pp. 356–364.

Corsini, A., Rispoli, F. and Sheard, A.G. (2007), 'Development of Improved Blade-tip End-plate Concepts for Low-noise Operation in Industrial Fans', *Proceedings of the IMechE Part A, Journal of Power and Energy*, vol. 221(5), pp. 669–681.

Corsini, A., Rispoli, F. and Sheard, A.G. (2009), 'Aerodynamic Performance of Blade-tip End-plates Designed for Low-noise Operation in Axial Flow Fans', *Transactions of the ASME, Journal of Fluids Engineering*, vol. 131, paper no. 081101, pp. 1–13.

Corsini, A., Rispoli, F. and Sheard, A.G. (2010), 'Shaping of Tip End-plate to Control Leakage Vortex Swirl in Axial Flow Fans', *Transaction of the ASME, Journal of Turbomachinery*, vol. 132, paper no. 031005, pp. 1–9.

Craft, T.J., Launder, B.E. and Suga, K. (1996), 'Development and Application of a Cubic Eddy-viscosity Model of Turbulence', *International Journal of Heat and Fluid Flow*, vol. 17, pp. 108–155.

Directive 2005/32/EC of the European Parliament and of the Council (2005), 'Establishing a Framework for the Setting of Ecodesign Requirements for Energy-using Products and Amending Council Directive 92/42/EEC and Directives 96/57/EC and 2000/55/EC of the European Parliament and of the Council'.

Escudier, M. (1987), 'Confined Vortices in Flow Machinery', *Annual Review of Fluid Mechanics*, vol. 19, pp. 27–52.

Ffowcs Williams, J.E. (1977), 'Aeroacoustics', *Annual Review of Fluid Mechanics*, vol. 9, pp. 447–468.

Fukano, T., Kodama, Y. and Takamatsu, Y. (1978), '', *Journal of Sound and Vibration*, vol. 56(2), pp. 261–277.

Fukano, T., Takamatsu, Y. and Kodama, Y. (1986), 'The Effects of Tip Clearance on the Noise of Low Pressure Axial and Mixed Flow Fans', *Journal of Sound and Vibration*, vol. 105, pp. 291–308.

Furukawa, M., Inoue, M., Saiki, K. and Yamada, K. (1999), 'The Role of the Tip Leakage Vortex Breakdown in Compressor Rotor Aerodynamics', *Transactions of the ASME, Journal of Turbomachinery*, vol. 121, pp. 469–480.

Gad-el-Hak, M. (2000), *Flow Control: Passive, Active, and Reactive Flow Management*, Cambridge University Press, London, UK.

Garg, A.K. and Leibovich, S. (1979), 'Spectral Characteristics of Vortex Breakdown Flowfields', *Physics of Fluids*, vol. 22(11), pp. 2053–2064.

Guedel, A. (1985), 'Scattering of an Acoustic Field by a Free-jet Shear Layer', *Journal of Sound and Vibration*, vol. 100, pp. 285-304.

Herrada, M.A. and Shtern, V. (2003), 'Vortex Breakdown Control by Adding Near-axis Swirl and Temperature Gradients', *Physical Review E, Statistics, Nonlinear, and Soft Matter Physics*, vol. 68, paper no. 041202, pp. 1–8.

Holste, F. and Neise, W. (1997), 'Noise Source Identification in a Prop Fan Model by Means of Acoustical Near Field Measurements', *Journal of Sound and Vibration*, vol. 203, pp. 641–665.

Howe, M.S. (1984), 'On the Absorption of Sound by Turbulence and Other Hydrodynamic Flows', *I.M.A. Journal of Applied Mathematics*, vol. 32, pp. 187–203.

Inoue, M. and Kuroumaru, M. (1989), 'Structure of Tip Clearance Flow in an Isolated Axial Compressor Rotor', *Transactions of the ASME, Journal of Turbomachinery*, vol. 111, pp. 250–256.

Ito, T., Suematsu, Y. and Hayase, T. (1985), 'On the Vortex Breakdown Phenomena in a Swirling Pipe-flow', *Nagoya University, Faculty of Engineering, Memoirs*, vol. 37(2), pp. 117–172.

Jones, M.C., Hourigan, K. and Thompson, M.C. (2001), 'The Generation and Suppression of Vortex Breakdown by Upstream Swirl Perturbations', *Proceedings of 14th Australian Fluid Mechanics Conference*, Adelaide, Australia, 10–14 December.

Joslin, R.D., Rusell, H.T. and Choudhari, M.M. (2005), 'Synergism of Flow and Noise Control Technologies', *Progress in Aerospace Sciences*, vol. 41, pp. 363–417.

Kameier, F. and Neise, W. (1997), 'Experimental Study of Tip Clearance Losses and Noise in Axial Turbomachines and their Reduction', *Transactions of the ASME, Journal of Turbomachinery*, vol. 119, pp. 460–471.

Karlsson, S. and Holmkvist, T. (1986), 'Guide Vane Ring For a Return Flow Passage in Axial Fans and a Method of Protecting It', US Patent No. 4,602,410, 29 July.

Kirk, B.S., Peterson, J.W., Stogner, R.H. and Carey, G.F. (2006), 'libMesh: A C++ Library for Parallel Adaptive Mesh Refinement/Coarsening Simulations', *Engineering with Computers*, vol. 22, pp. 237–254.

Lakshminarayana, B. (1970), 'Methods of Predicting the Tip Clearance Effects in Axial Flow Turbomachinery', *Journal of Basic Engineering*, vol. 92, pp. 467–482.

Lakshminarayana, B., Zaccaria, M. and Marathe, B. (1995), 'The Structure of Tip Clearance Flow in Axial Flow Compressors', *Transactions of the ASME, Journal of Turbomachinery*, vol. 117, pp. 336–347.

Leggat, L.J. and Siddon, T.E. (1978), 'Experimental Study of Aeroacoustic Mechanism of Rotor-vortex Interactions', *Journal of the Acoustical Society of America*, vol. 64, pp. 1070–1077.

Leibovich, S. (1982), 'Wave Propagation, Instability, and Breakdown of Vortices', in Hornung, H.G. and Müller, E.-A (Eds), *Vortex Motion*, the Proceedings of a Colloquium Held at Gottingen on the Occasion of the 75th Anniversary of the Aerodynamische Versuchsanatalt in November 1982, Springer Fachmedien, Wiesbaden, Germany.

Longet, C.M.L. (2003), 'Axial Flow Fan with Noise Reducing Means', Patent No. US 2003/0123987 A1, 3 July.

Longhouse, R.E. (1978), 'Control Tip-vortex Noise of Axial Flow Fans by Rotating Shrouds', *Journal of Sound and Vibration*, vol. 58, pp. 201–214.

Mimura, M. (2003), 'Axial Flow Fan', US Patent No. 6,648,598 B2, 18 November.

Quinlan, D.A. and Bent, P.H. (1998), 'High Frequency Noise Generation in Small Axial Flow Fans', *Journal of Sound and Vibration*, vol. 218, pp. 177–204.

Rains, D.A. (1954), 'Tip Clearance Flows in Axial Flow Compressors and Pumps', PhD Thesis, California Institute of Technology, http://resolver.caltech.edu/CaltechETD:etd-04152003-112816.

Saiyed, N.H., Bridges, J.E. and Mikkelsen, K.L. (2000), 'Acoustics and Thrust of Separate-flow Exhaust Nozzles with Mixing Devices for High-bypass-ratio Engines', *Proceedings of the 6th Aeroengine Conference and Exhibit*, Lahaina, HI, 12–14 June, paper no. AIAA-2000-1961.

Sheard, A.G., Corsini, A. and Rispoli, F. (2009), 'A Meridional Fan', Patent No. GB 2,452,104 B, 22 July.

Smith, G.D.J. and Cumpsty, N.A. (1984), 'Flow Phenomena in Compressor Casing Treatment', *Transactions of the ASME, Journal of Engineering for Gas Turbines and Power*, vol. 106, pp. 532–541.

Spall, R.E., Gatski, T.B. and Grosch, C.E. (1987), 'A Criterion for Vortex Breakdown', *Physics of Fluids*, vol. 30, pp. 3434–3440.

Srigrarom, S. and Kurosaka, M. (2000), 'Shaping of Delta-wing Planform to Suppress Vortex Breakdown', *AIAA Journal*, vol. 38, pp. 183–186.

Storer, J.A. and Cumpsty, N.A. (1991), 'Tip Leakage Flow in Axial Compressors', *Transactions of the ASME, Journal of Turbomachinery*, vol. 113, pp. 252–259.

Takata, H. and Tsukuda, Y. (1977), 'Stall Margin Improvement by Casing Treatment – its Mechanism and Effectiveness', *Transactions of the ASME, Journal of Engineering for Power*, vol. 99, pp. 121–133.

Thomas, R.H., Choudhari, M.M. and Joslin, R.D. (2002), 'Flow and Noise Control: Review and Assessment of Future Directions', NASA TM-2002-211631, 1 April.

Thompson, D.W., King, P.I. and Rabe, D.C. (1998), 'Experimental and Computational Investigation on Stepped Tip Gap Effects on the Flowfield of a Transonic Axial-flow Compressor Rotor', *Transactions of the ASME, Journal of Turbomachinery*, vol. 120, pp. 477–486.

Uchida, S., Nakamura, Y. and Ohsawa, M. (1985), 'Experiments on the Axisymmetric Vortex Breakdown in a Swirling Air Flow', *Transactions of the Japan Society for Aeronautical and Space Sciences*, vol. 27, pp. 206–216.

Uselton, R.B., Cook, L.J. and Wright, T. (2005), 'Fan with Reduced Noise Generation', US Patent No. 6,872,048 B2, 29 March.

Wadia, A.R. and Booth, T.C. (1982), 'Rotor-Tip Leakage: Part II – Design Optimization Through Viscous Analysis and Experiment', *Transactions of the ASME, Journal of Engineering for Power*, vol. 104, pp. 162–168.

Wen-Shiang, C., Lauchle, G.C. and Thompson, D.E. (1989), 'Subsonic Axial Flow Fan Noise and Unsteady Rotor Force', *Journal of the Acoustical Society of America*, vol. 85(2), pp. 641–647.

Chapter 12

Experimental Characterisation of the Far-field Noise in Axial Fans Fitted with Shaped Tip End-plates

S. Bianchi, A. Corsini and A.G. Sheard

ABSTRACT

The chapter presents an investigation of the far-field noise emissions of a fan with anti-vortex end-plates designed to control the blade tip-to-casing leakage vortex swirl level when installed in a standardised airway. We tested a fan AC90/6 without blade-tip end-plates, and two variants, fan AC90/6/TF and fan AC90/6/TF$_{MVB}$ with different end-plates. The fan AC90/6/TF incorporated a constant thickness end-plate and the fan AC90/6/TF$_{MVB}$ incorporated an end-plate designed using a new noise-by-flow control design procedure. Blade-tip end-plate geometry influences the blade tip-to-casing leakage flow intensity, swirl level and vortex formation. This in turn affects the acoustic emissions of fans fitted with the blade-tip end-plates. We may characterise the impact of blade-tip end-plate design using azimuthal measurements of sound-power and sound-pressure level and spectra. We establish a cause-and-effect relationship between the blade-tip flow features and the radiated sound fields. By studying directivity patterns and using a coherence analysis, we were able to establish that the fan AC90/6/TF$_{MVB}$, incorporating the newly conceived blade-tip end-plate, results in a reduction in both fan tonal and broadband far-field noise. The A-weighted far-field sound power level was consistently lower than fan *datum* AC90/6. At the maximum flow operating point is was 4.4 dB(A) lower and respectively 5.8 dB(A) and 8.2 dB(A) lower at the design and peak pressure operating points. The near-axis broadband far-field sound pressure level for the fan AC90/6/TF$_{MVB}$ was 10 dB lower than the fan *datum* AC90/6. This reduction of near-axis noise correlates with the presence of coherent swirling structures induced by the blade-tip end-plate. The reported research verifies the technical merit of the fan AC90/6/TF$_{MVB}$ incorporating the newly conceived end-plate, providing insight into the flow-field physics underpinning the reduction in fan far-field noise. The newly conceived end-plate effectively minimises blade-tip leakage vortex intensity, avoids

This chapter is a revised and extended version of Bianchi, S., Corsini, A. and Sheard, A.G. (2012), 'Experimental Characterisation of the Far-field Noise in Axial Fans Fitted with Shaped Tip End-plates', *International Scholarly Research Network Mechanical Engineering*, vol. 2012, paper no. 212358, pp. 1–9.

vortex breakdown and additionally induces a blade-tip flow-field feature that reduces fan far-field near-axis noise. It is this combination that results in the low noise of the fan AC90/6/TF_{MVB}.

NOMENCLATURE

Latin letters

BPF	blade-passing frequency [Hz]
f	frequency [Hz]
K_s	specific noise level
ℓ	blade chord
OSWL	overall sound power level
Δp_{tot}	rotor total pressure rise
SWL(A)	'A' weighted sound power level [dB(A)]
SWL	overall sound power level [dB]
SPL	sound pressure level [dB]
t	blade pitch
V	volume flow rate

Greek letters

τ	rotor tip clearance
η_{tot}	total efficiency

INTRODUCTION

Researchers have studied extensively the link between a fan rotor's aerodynamic features and its acoustic emissions. In particular, Wright (1976) and Cumpsty's (1977) research has enhanced the community's understanding of axial turbomachinery aeroacoustics. Cumpsty (1977) concluded that, with the exception of high speed machine low-frequency range, the mechanism that determines broadband noise in subsonic fans is the same as that in supersonic tip-speed fans and compressors. According to Wright (1976), this is due to the prominence of rotor noise that originates from turbulent boundary layers.

Researchers have identified a variety of mechanisms that collectively result in a fan or compressor's noise signatures. The dominant noise sources identified are the fan or compressor blades, which generate noise as a result of turbulent wake shedding. This turbulent wake shedding occurs as a consequence of the interaction between the end-wall boundary layer and the blade tips. The aerodynamic effect of blade tip-to-casing leakage flow on both wakes and secondary flows is also significant. It is this significance that has resulted in the turbomachinery community widely recognising the blade tip-to-casing leakage flow as a significant noise source (Fukano *et al.*, 1986; Holste and Neise, 1997).

Increasingly stringent regulations defining maximum permissibly noise levels have stimulated academics and practitioners alike to pursue the development of concepts and technologies that are likely to reduce fan noise. Research is focused on both controlling noise at its source and attenuating noise as it propagates from its source. Marcinowski (1953), who was the first scholar to study tip-generated noise, demonstrated that increases in broadband noise occur with increased tip-clearance, with the largest changes apparent at frequencies greater than the blade passing frequency.

Mugridge and Morfey (1972) argued that an optimum tip clearance exists at which broadband noise is at a minimum due to the countervailing effect of the blade passage vortex on the tip-clearance flow. However, Longhouse (1978) did not confirm this result as he searched for a practical solution to the tip-clearance noise which cooling fans emit. He concluded that the cause emanated from the unstable blade tip-to-casing leakage vortex which impacted the adjacent blade pressure side. Longhouse obtained the lowest noise levels with the smallest possible tip clearance. Fukano and Jang (2004) reported similar findings. In contrast, Kameier and Neise's (1997) experiments demonstrated that with the smallest possible tip clearance, noise reduced over a limited frequency range, close to the blade passage frequency. However, broadband noise actually increased.

During the past decade, researchers have proposed passive noise-control concepts based on modifications to the blade tip by means of anti-vortex appendages. Quinlan and Bent (1998) have proposed end-plates, and others have proposed solutions in patents for air movement fans (Jensen, 1986; Longet, 2003; Mimura, 2003; Uselton *et al.*, 2008). The present study focuses on a family of commercially available fans intended for application in compact cooling units. Utilising an experimental technique for the span-wise detection of rotor noise sources (Bianchi *et al.*, 2009a), the study compares aeroacoustic performance of a *datum* fan, named fan *datum* AC90/6, without a fitted blade-tip end-plate with the same fan's performance when fitted with blade-tip end-plates.

We fitted the studied fan with two different blade-tip end-plates. When fitted with a constant thickness blade-tip end-plate, we named the fan AC90/6/TF, Figure 12.1. The fan blades were manufactured from injection moulded plastic, with the size of the blade-tip end plate serving as the largest the blade manufacturing technique could produce. Corsini and Sheard (2013) exploited the link between aerodynamic flow features in the blade-tip region and fan acoustic emissions by a design process that aimed to control the blade tip-to-casing leakage flow. We used the design process to design a new blade-tip end-plate, named the Multiple Vortex Breakdown (MVB) end-plate. When we fitted the studied fan with the MVB blade-tip end-plate, we named it fan AC90/6/TF$_{MVB}$, Figure 12.1.

The study's objective is to compare the acoustic merit of fan AC90/6/TF$_{MVB}$ with both the fan *datum* AC90/6 and fan AC90/6/TF. The comparative investigation focuses on an emitted noise assessment in the far-field and considers the overall sound power level variation with the fan's operating condition. Moreover, we explore directivity of the three studied fans' far-field noise by plotting narrowband

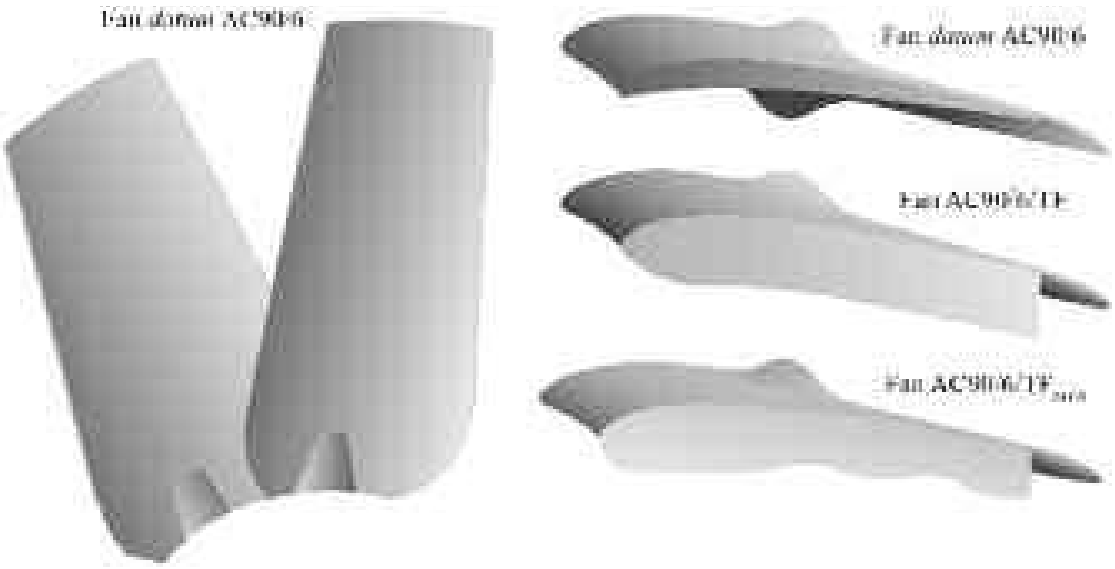

FIGURE 12.1. The studied fan *datum* AC90/6 without a fitted blade-tip end-plate, the fan AC90/6/TF with a constant thickness blade-tip end-plate and the fan AC90/6/TF$_{MVB}$ incorporating a blade-tip end-plate designed using Corsini and Sheard's (2013) noise-by-flow control design procedure.

sound pressure level spectra azimuthal maps from 0 to 90 degrees off the fan axis. The investigation attempts to establish a cause-and-effect relationship between blade-tip flow-field features and the sound field radiation patterns.

FAMILY OF FANS UNDER INVESTIGATION

We conducted the reported research on a family of commercially available cooling fans. The studied fan configuration, named AC90/6, incorporates a six-blade un-swept rotor, with modified ARA-D profile aerofoil blades, Table 12.1. One may set the blade-pitch angle during final assembly to customise the fan to a desired duty point. We used a direct coupled-induction 400-volt (AC), 3-phase motor to drive the rotor at a constant speed of 950 rpm, resulting in a 44.7 m/s blade tip speed and a 95 Hz blade-passing frequency (BPF). In its original embodiment, the studied fan AC90/6 did not include a blade tip end-plate. We used it as a *datum* against which to assess the performance of fan variants with blade-tip end-plates. Therefore, in the reported research we refer to the fan without blade-tip end-plates as the fan *datum* AC90/6.

The studied fan blade tip pitch angle is adjustable and may be set to a pitch angle between 16 and 28 degrees. In practical application, the blade tip pitch angle is typically set to 28 degrees as this maximises flow rate for a given system pressure. In the research reported in this chapter, we conducted the experimental measurements with the fan blade tip pitch angle set to 28 degrees. We selected 28 degrees both because it is typical of the angle that one uses in practical application and because it results in the highest blade loading. A highly loaded blade results in the blade

Table 12.1. *The fan* datum *AC90/6 blade geometry and rotor specification.*

	Fan *datum* AC90/6		
Blade geometry	Hub	Mid-span	Tip
Pitch angle (°)	36	58.8	28
Camber angle (°)	46	44	41
Solidity	1.24	0.86	0.30
Fan rotor			
Blade number		6	
Blade tip pitch angle (°)		16–28	
Blade tip stagger angle (°)		74–62	
Hub-to-casing diameter ratio σ		0.22	
Tip diameter (mm)		900.0	
Rotor tip clearance τ (% span)		1.0	
Rated rotational frequency (r/min)		935–950	

tip-to-casing leakage vortex having the most significant effect on both fan aerodynamic and acoustic performance (Holste and Neise, 1997).

The impact of the blade tip-to-casing leakage vortex on both fan aerodynamic and acoustic performance results in applying blade-tip end-plates changing not only the fan's acoustic performance, but also the aerodynamic performance. Consequently, the fan *datum* AC90/6 generates a different pressure at a constant flow rate when fitted with each of the studied blade-tip end-plates. To facilitate the comparison of fan performance data when fitted with different blade-tip end-plates, we chose to define three operating points, and their respective volume flow rates, Table 12.2. The design operating point volume flow rate is typical of that required when one installs the fan over a cooling unit's tube bank. The peak pressure flow rate is typical of that required when the tube bank has become partially blocked following a period of in-service operation. The maximum flow operating point volume flow rate is typical of the flow rate that occurs with the lowest pressure loss tube banks currently operating in service. In the research reported in this chapter, we studied fan performance at both the design and peak pressure operating points.

Table 12.2. *The operating points used when characterising the studied fan's performance with and without fitted blade-tip end-plates. The authors measured performance characteristics in a Type C standardised airway (ducted inlet, ducted outlet) in accordance with ISO 5801:2007 requirements (2007).*

Operating point	Volume flow rate (m^3/s)	Studied blade tip pitch angle (°)
Maximum flow	8.0	28
Design	7.0	28
Peak pressure	6.0	28

Blade-tip End-plate Theory

Previous researchers working to reduce the drag of aircraft wings and catamarans hulls inspired the concept for the constant thickness blade-tip end-plate. The engineers who had originally developed the fan *datum* AC90/6 were aware that the end-plates fitted to aircraft wings were designed using a vortex control theory. Inoue *et al.* (1986) developed the vortex control theory for application in axial compressors and later, Corsini and Rispoli (2004) applied it to air movement fans. Vortex control theory defines the blade-tip end-plate dimension as a function of the leakage vortex's radius that is to be controlled. We considered Inoue *et al.*'s (1986) research regarding the blade-tip end-plate's size for axial compressor blades. They estimated that the optimum blade-tip end-plate size was between 10 and 20 per cent blade span.

The blades fitted to the fan *datum* AC90/6 are 200 mm long, and therefore following Inoue *et al.*'s (1986) recommendations, the blade-tip end-plate should have been between 20 and 40 mm thick. The fan *datum* AC90/6 blades were manufactured from injection moulded plastic, with the available manufacturing technology limiting the thickness of the blade-tip end-plate that could be moulded to 15 mm. As such, the engineers responsible for developing fan *datum* AC90/6 took a pragmatic approach to blade-tip end-plate design. They made it as large as was possible within the constraints of the available manufacturing technology. When fitted with the resultant constant thickness blade-tip end-plate, we named the studied fan AC90/6/TF.

Corsini and Sheard (2007) studied the aerodynamic and acoustic performance of fan *datum* AC90/6 and fan AC90/6/TF. They characterised the chord-wise distribution of blade tip-to-casing leakage vortex Rossby number. There is a threshold value of the Rossby number below which vortex rotation cannot reduce if the vortex is to remain stable. Corsini and Sheard (2007) concluded that for the fan *datum* AC90/6, the leakage vortex Rossby number remained above the threshold value and did not burst. However, the fan AC90/6/TF leakage vortex Rossby number fell below the threshold value at approximately 90 per cent chord and did burst. Vortex bursting is acoustically productive, with Corsini and Sheard (2007) proposing a variable thickness blade-tip end-plate that maintained the leakage vortex Rossby number above the required threshold value and therefore did not burst. When fitted with the variable thickness blade-tip end-plate, we named the studied fan AC90/6/TF$_{VTE}$.

Corsini *et al.* (2007) studied the aerodynamic performance of fan AC90/6/TF$_{VTE}$. They concluded that the variable thickness blade-tip end-plate design successfully avoided blade tip-to-casing leakage vortex bursting. Assessing the aerodynamic performance demonstrated an improved pressure developing capability and fan efficiency that we may attribute to the leakage vortex not bursting. However, noise measurements made by Corsini and Sheard (2013) indicated that the variable thickness blade-tip end-plate resulted in a broadband noise level approximately 0.5 dB higher than that associated with the constant thickness end-plate. Corsini *et al.* (2007) concluded that the variable thickness blade-tip end-plate occurred with the presence of multiple organised vortical structures. These vortical structures did burst, with the breakdown acoustically productive enough to result in the observed increase in overall fan far-field broadband noise.

The work of Corsini *et al.* (2007) was continued by Corsini *et al.* (2009, 2010) who concluded that that the multiple organised vortical structures induced in the blade tip region by the variable thickness blade-tip end-plate were disproportionately acoustically productive and therefore the blade-tip end-plate required redesign to minimise the swirling intensity and size of vortices in the blade tip region. Whilst minimising intensity and size of vortical structures, the end-plate design must also ensure that neither the blade tip-to-casing leakage vortex nor those organised vortical structures that are created burst. Corsini and Sheard (2013) developed a design process to control the blade-tip leakage flow. They used the design process to design a new blade-tip end-plate, named the Multiple Vortex Breakdown (MVB) end-plate that Sheard *et al.* (2009) patented. When we fitted the studied fan with the MVB blade tip end-plate, we named it fan AC90/6/TF$_{MVB}$.

Experimental Method

We made acoustic measurements in accordance with ISO 10302:2011 requirements (2011). The test-rig was a type-A standardised airway, Figure 12.2, with the fan downstream from a plenum chamber with a free outlet. The rotor centre line was two metres from the floor. The fan inlet bell-mouth was aerodynamically optimised to

FIGURE 12.2. The standardised airway test rig set-up in a semi-anechoic chamber with a Type A (fan downstream from a plenum chamber with a free outlet) fan installation.

provide uniform and unseparated flow into the fan. We acoustically treated the down-stream and upstream plena to minimise noise transmissions from the air stream into the fan and the outside environment. The fan's inlet airflow passed through an aerofoil louver in the top of the facility, enabling us to varying pressure across the fan.

We made fan near- and far-field acoustic measurements using Bianchi *et al.*'s (2011) methodology. Bianchi *et al.* (2011) followed Leggat and Siddon's (1978) recommendations, placing a microphone ten per cent blade chord down-stream of the studied fan blades' trailing edge. We then varied the microphone's span-wise location in steps of two per cent from blade-hub to blade-tip. At each span-wise location we made measurements of far-field noise on the fan centre line and plus and minus 30, 45, 60, 75 and 90 degrees off the fan centre line. We made near- and far-field acoustic measurements simultaneously to provide data sets of near- and far-field noise over a range of far-field azimuthal positions. We then correlated these measurement sets to establish the far-field directivity of near-field noise sources.

EXPERIMENTAL RESULTS

We measured the performance characteristics of the fan *datum* AC90/6, AC90/6/TF and AC90/6/TF$_{MVB}$. We made all measurements in accordance with ISO 5801:2007 requirements (2007). The measured performance characteristics illustrate the impact on pressure rise of blade-tip end-plate geometry, Figure 12.3. The performance characteristics of the three studied fans illustrate that the fan AC90/6/TF$_{MVB}$ has a similar efficiency to both the fan *datum* AC90/6 and AC90/6/TF over its entire operating range. However, it generates approximately a 10 per cent higher pressure rise at its design operating point than either the fan *datum* AC90/6 or AC90/6/TF.

The 10 per cent increase in pressure rise at the fan design operating point indicates that adding the multiple vortex breakdown blade-tip end-plate increased the fan blades' loading. We would expect blade-tip noise sources to become more acoustically productive with increasing blade loading. Therefore, any reduction in fan far-field noise attributed to adding the multiple vortex breakdown blade-tip end-plate will be partially off-set by the increase in blade loading. The reduction in fan far-field noise is consequently conservatively assessed if the increase in blade loading is neglected. Therefore, we chose to neglect the increase in fan AC90/6/TF$_{MVB}$ blade loading.

In addition to the increase in fan far-field noise, there is one additional negative consequence that occurs with an increase in blade loading. The fan AC90/6/TF$_{MVB}$ stalled sooner than either the fan *datum* AC90/6 or AC90/6/TF. The stall was also deeper than either the fan *datum* AC90/6 or AC90/6/TF. As a consequence, if one operated the fan AC90/6/TF$_{MVB}$ in a stalled condition, it would likely suffer a mechanical failure sooner than either the fan *datum* AC90/6 or AC90/6/TF. Despite this caveat, there is still an acceptable margin on flow between the peak pressure operating point and the fan AC90/6/TF$_{MVB}$ stall point. Therefore, we concluded that the increase in pressure developing capability of the fan AC90/6/TF$_{MVB}$ was a positive development.

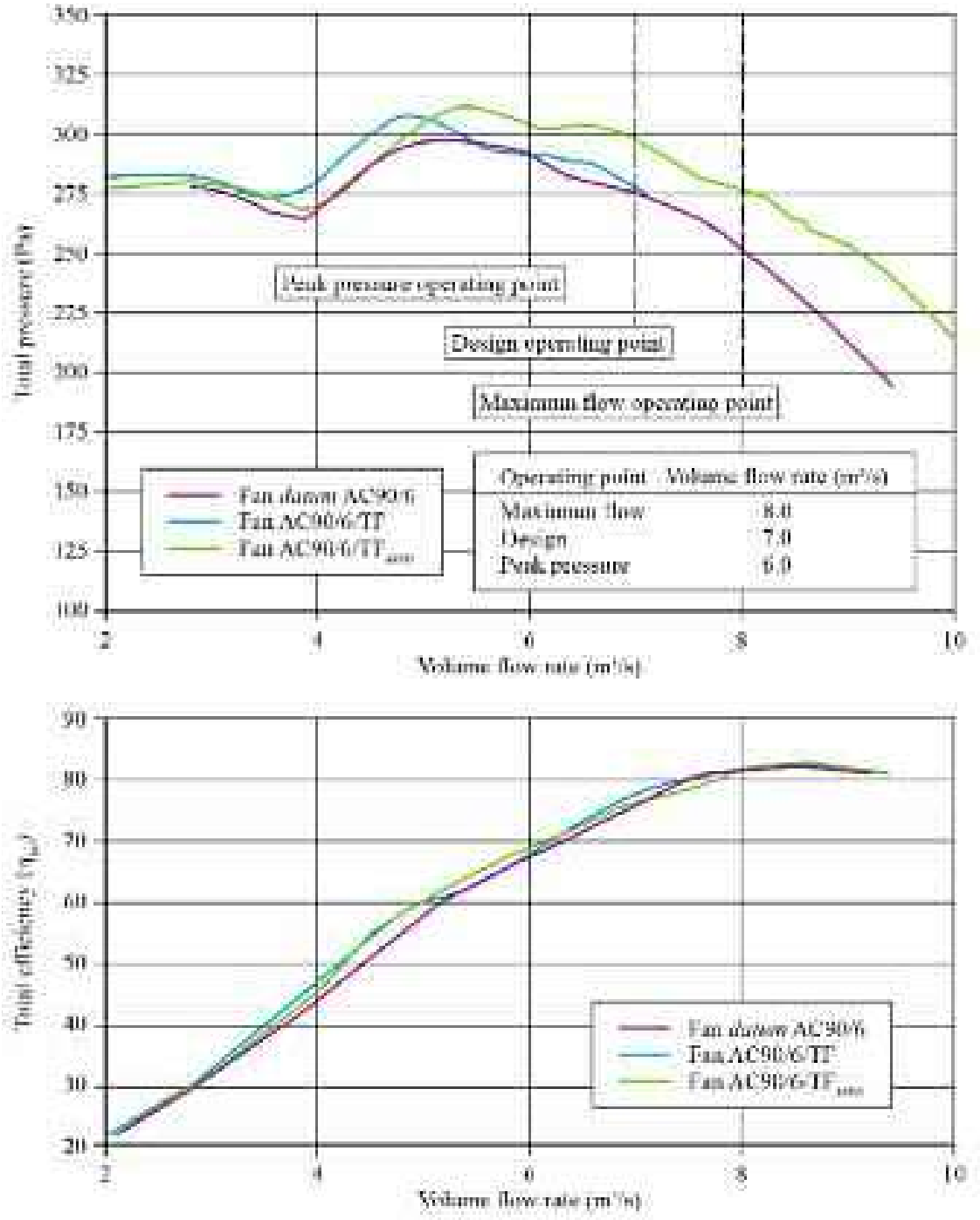

FIGURE 12.3. The performance characteristics of the studied fan *datum* AC90/6 without a fitted blade-tip end-plate, with a constant thickness blade-tip end-plate, AC90/6/TF and with a multiple vortex break-down blade-tip end-plate, AC/6/TF$_{MVB}$. The authors measured performance characteristics with the blade tip pitch angle set to 28 degrees in a Type C standardised airway (ducted inlet, free outlet) in accordance with ISO 5801:2007 requirements (2007).

Acoustic Performance

We began our assessment of the relative performance of the fan AC90/6/TF$_{MVB}$ with an analysis of outlet far-field A-filtered one-third octave sound power level (L_W) spectrum. We provide measured sound power level spectrum data for the fan *datum* AC90/6, AC90/6/TF and AC90/6/TF$_{MVB}$, Figure 12.4.

Consider the sound power level spectrum for the fan *datum* AC90/6, AC90/6/TF and AC90/6/TF$_{MVB}$. Both the fan AC90/6/TF and AC90/6/TF$_{MVB}$ exhibit significantly lower broadband noise than the fan *datum* AC90/6. Additionally, the fan AC90/6/TF$_{MVB}$ exhibits consistently lower sound power levels across the spectrum. At the second harmonic of blade passing frequency the fan AC90/6/TF$_{MVB}$ sound power level was approximately 3.5 dB lower than the fan *datum* AC90/6. Bianchi *et al.* (2009b) considered the significance of the second harmonic of blade passing frequency. Bianchi *et al.* (2009b) observed that Magliozzi *et al.* (1973) and Cumpsty (1974, 1977) had characterised the second harmonic of blade passing frequency. These scholars concluded that the tone occurring with the second harmonic of blade passing frequency may occur with a disturbance of the inflow into the fan. This inflow disturbance affects the end-wall boundary layer and its interaction with the blade's wake.

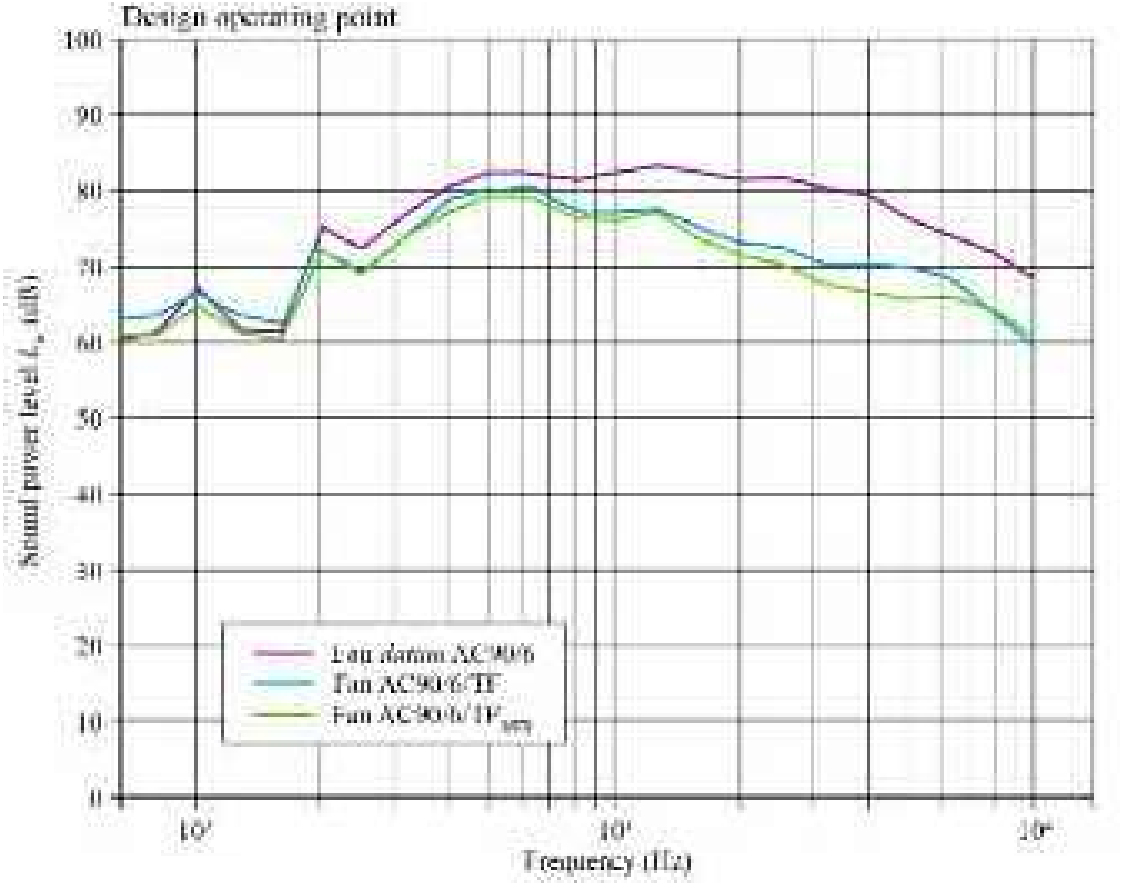

FIGURE 12.4. Outlet far-field A-filtered one-third octave sound power level (L_W) spectrum measured at the fan design operating point. Measured sound power level spectrum data is for the fan *datum* AC90/6, AC90/6/TF and AC90/6/TF$_{MVB}$.

The largest reduction in fan AC90/6/TF$_{MVB}$ sound power level relative to the fan *datum* AC90/6 was over a frequency range from 1.5 kHz to 10 kHz. Bianchi *et al.* (2011) studied the impact of blade-tip end-plates on fan far-field noise. They concluded that the reduction in far-field noise occurred as a consequence of the blade-tip end-plate's impact on the blade tip-to-casing gap flow-field. Specifically, the presence of a blade-tip end-plate disrupts and mixes turbulence into the tip-to-casing leakage vortex that form through the blade tip-to-casing gap. The result is both lower tonal peaks and broadband noise. Khourrami and Choudari (2001) studied blade-tip generated noise. They concluded that the convection of the blade tip-to-casing leakage vortex is primarily responsible for tonal noise. In contrast, they concluded that vortex instability is primarily responsible for broadband noise. Therefore, we may conclude that blade-tip end-plates impact both leakage vortex convection and stability.

We may gain an additional insight into the acoustic characteristics of the studied fan configurations by considering measured overall fan far-field sound power level L_W, Table 12.3. We calculated the A-weighted overall sound power level as we are most concerned with an observer's perception of the impact of blade-tip end-plates. A-weighting is applied to measured sound levels to account for the relative loudness perceived by the human ear, as the ear is less sensitive to low audio frequencies. It is employed by arithmetically adding a table of values, listed by third-octave bands, to the measured sound pressure levels in dB. We logarithmically added the resulting third-octave band measurements to provide a single A-weighted value describing the sound in dB(A).

Consider the A-weighted sound power level of the fan AC90/6/TF$_{MVB}$ and fan *datum* AC90/6. It is evident that a lower A-weighted sound power level at the maximum flow, design and peak pressure operating points characterises the fan AC90/6/TF$_{MVB}$. At the maximum flow operating point the fan AC90/6/TF$_{MVB}$ is 4.4 dB(A) quieter. At the design operating point the fan AC90/6/TF$_{MVB}$ is 5.8 dB(A) quieter. At the peak pressure operating point the fan AC90/6/TF$_{MVB}$ is 8.2 dB(A) quieter. From this we may conclude that as the fan AC90/6/TF$_{MVB}$ blade loading increases, the multiple vortex breakdown blade-tip end-plate becomes more effective.

Far-field Directivity Analyses

Our directivity analysis starts with a review of the azimuthal distribution of outlet sound pressure level (L_P) cross-spectra between the near- and far-field, Figure 12.5. We generated the azimuthal distributions at the studied fans' design operating point. The azimuthal distributions illustrates that the highest sound pressure levels for the fan *datum* AC90/6 and AC90/6/TF are at zero degrees, on the fan axis. The maximum levels are 81 dB and 82 dB respectively. This result is self-consistent with Leggat and Siddon's (1978) results and indicates that the fan *datum* AC90/6 and AC90/6/TF are behaving like dipolar noise sources. Within this context a monopole noise source is a source which radiates sound equally well in all directions. A dipole noise source consists of two monopole sources of equal strength, but opposite phase and separated by a small distance compared with the wavelength of sound.

Table 12.3. *Experimentally measured overall sound power level,* L_W *for the three studied fan configurations at their maximum flow, design and peak pressure operating points. The authors made acoustic measurements in accordance with ISO 10302:2011 requirements (2011).*

	datum AC90/6		AC90/6/TF		AC90/6/TF$_{MVB}$	
Operating point	Unweighted Overall L_W dB	A-weighted Overall L_W dB(A)	Unweighted Overall L_W dB	A-weighted Overall L_W dB(A)	Unweighted Overall L_W dB	A-weighted Overall L_W dB(A)
Maximum flow	100.1	92.5	96.7	89.3	98.6	88.1
Design	96.8	92.5	96.6	87.9	94.7	86.7
Peak pressure	95.4	93.2	922	87.1	89.9	85.0

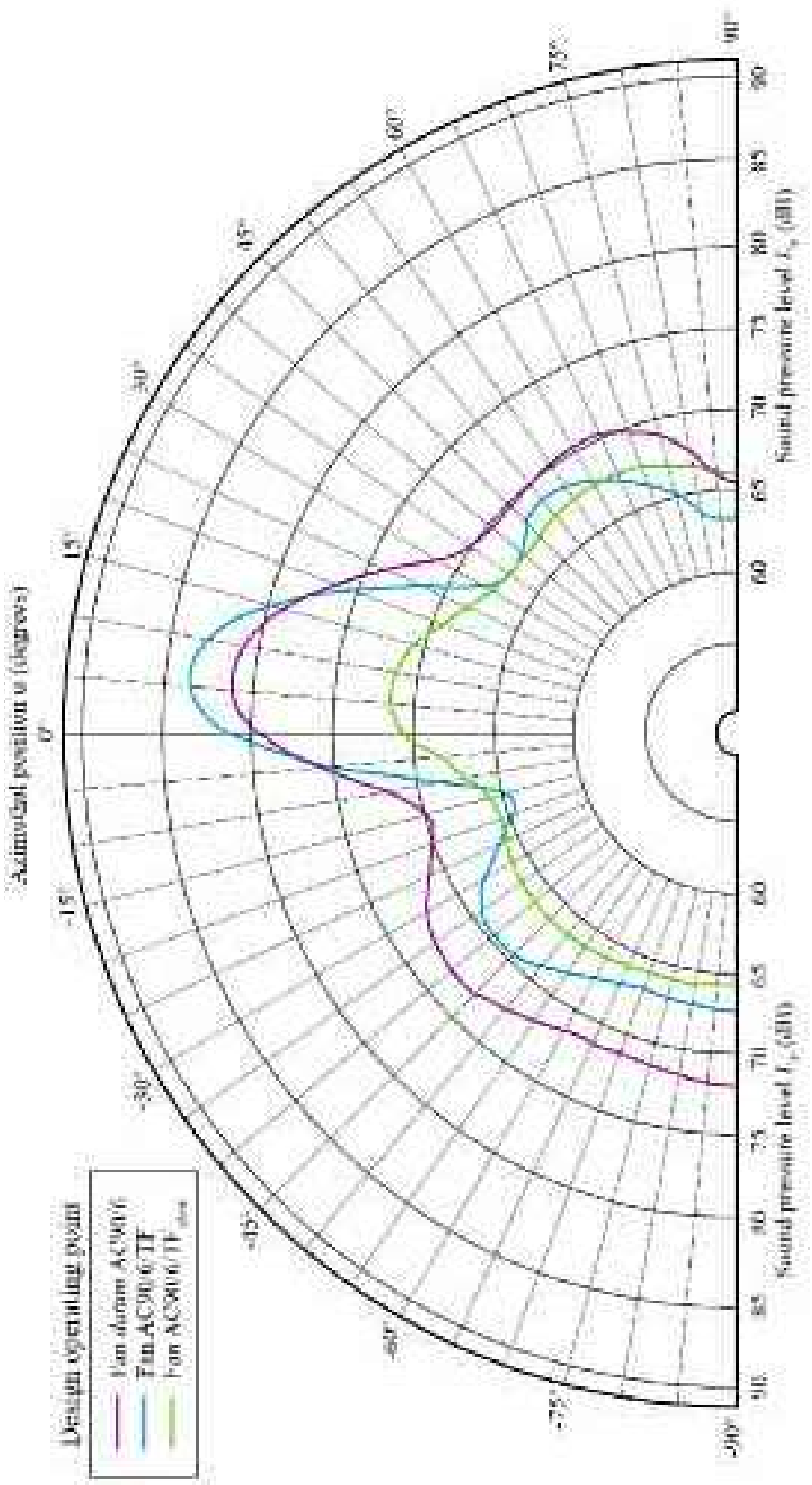

FIGURE 12.5. Far-field directivity of measured fan integrated sound pressure level (L_P) at the fan design operating point. The authors made measurements with the studied fans installed in a type A (free inlet, free outlet) fan installation. Directivity for fan AC90/6/TF$_{MVB}$ was both attenuated and isotropic in comparison with fan *datum* AC90/6 or AC90/6/TF.

In contrast to the fans *datum* AC90/6 and AC90/6/TF, the fan AC90/6/TF$_{MVB}$ exhibited peak sound pressure levels of 71 dB at zero degrees, on the fan axis. This is respectively 10 dB and 11 dB lower than the fan *datum* AC90/6 and AC90/6/TF. Most surprising was the near isotropic radiation pattern of the fan AC90/6/TF$_{MVB}$. Within this context, we define an isotropic noise source as one that has the same value when measured in different directions. We may attribute this isotropic behaviour to the multiple vortex breakdown blade-tip end-plate inducing a shift in acoustic emissions from higher to lower frequency. Bianchi *et al.* (2011) studied the azimuthal distribution of fan outlet sound pressure level cross-spectra between the near- and far-field. They concluded that the attenuation of sound pressure level on the fan axis correlated with the presence of vortical structures in the exhaust flow.

The beneficial effect of the multiple vortex breakdown blade-tip end-plate is less evident off the fan axis. The fan AC90/6/TF and AC90/6/TF$_{MVB}$ exhibit similar azimuthal sound pressure level distributions off the fan axis. Both are consistently lower than the fan *datum* AC90/6 when at more than 20 degrees off the fan axis. However, there is a difference between the off fan axis sound pressure levels of the fan AC90/6/TF and AC90/6/TF$_{MVB}$. The fan AC90/6/TF$_{MVB}$ off fan axis sound pressure level is more isotropic than that of fan AC90/6/TF.

The fan AC90/6/TF$_{MVB}$ isotropic azimuthal distribution of sound pressure level indicates that the multiple vortex breakdown blade-tip end-plate has affected blade-tip noise sources. Low frequency noise sources classically radiate axially. High frequency noise sources classically radiate radially. The primary difference between the azimuthal distributions of sound pressure level for the fan AC90/6/TF and AC90/6/TF$_{MVB}$ is a reduction in the sound pressure level on the fan axis. As low frequency noise classically radiates axially, this change implies that the multiple vortex breakdown blade-tip end-plate has induced a change in near-field noise sources. The intensity of low frequency near-field noise sources has been reduced. Enhanced control of the blade tip-to-casing leakage vortex may be responsible for this reduction.

The isotropic radiation pattern of fan AC90/6/TF$_{MVB}$ may indicate that the dipole characteristic of both the fan *datum* AC90/6 and AC90/6/TF has changed to a quadrupole characteristic. Just as two opposite phase monopoles comprise a dipole, two opposite dipoles comprise a quadrupole noise source. Shah *et al.* (2010) have studied swirling-flow noise. They concluded that we may attribute a quadrupole source's acoustic signature in a low Mach number flow to the turbulent mixing of swirling flow-field features. This mixing reduces the intensity of low frequency near-field noise sources and scatters dipolar noise sources. It is this scattering that results in a change from a dipole to quadrupole characteristic.

We may gain a further insight into the directivity of fan far-field noise by studying far-field directivity 'maps' of the sound pressure level spectrum. Figures 12.6, 12.7 and 12.8 present these maps for the fan *datum* AC90/6, AC90/6/TF and AC90/6/TF$_{MVB}$.

Consider the directivity map for the fan *datum* AC90/6, Figure 12.6. The directivity map indicates that both tonal and broadband noise is . We recorded the highest sound pressure levels from zero to 30 degrees. This observation is self-consistent with Wright (1976) and Leggat and Siddon's (1978) conclusions. It indicates that the

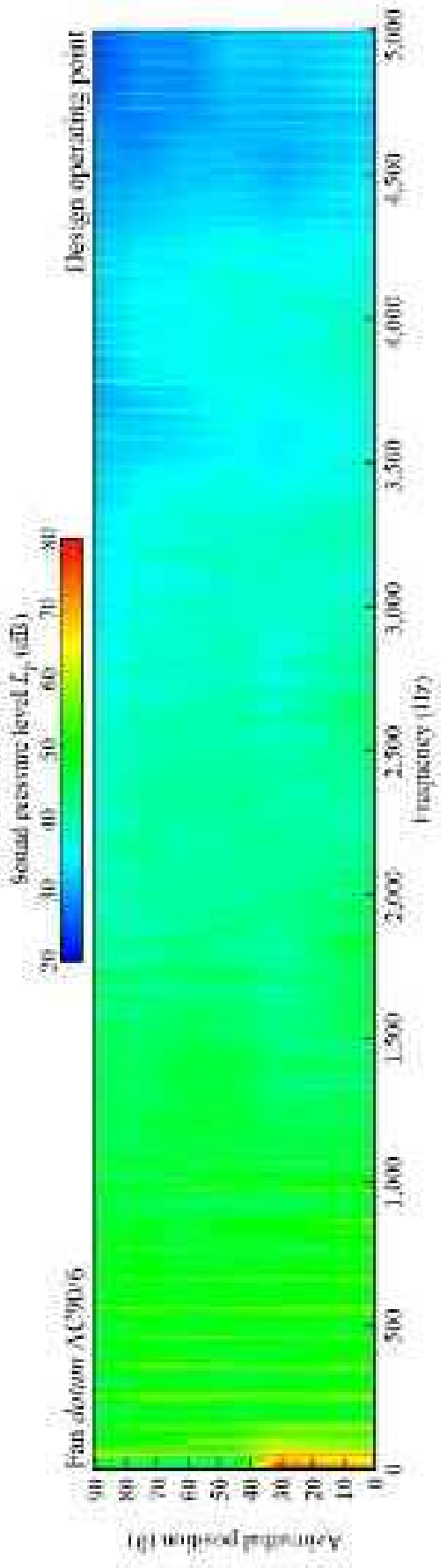

FIGURE 12.6. Measured far-field directivity of the sound pressure level (L_p) spectrum for the fan *datum* AC90/6 measured at the fan design operating point. The measured data illustrates that the sound pressure level spectrum is anisotropic with azimuthal position.

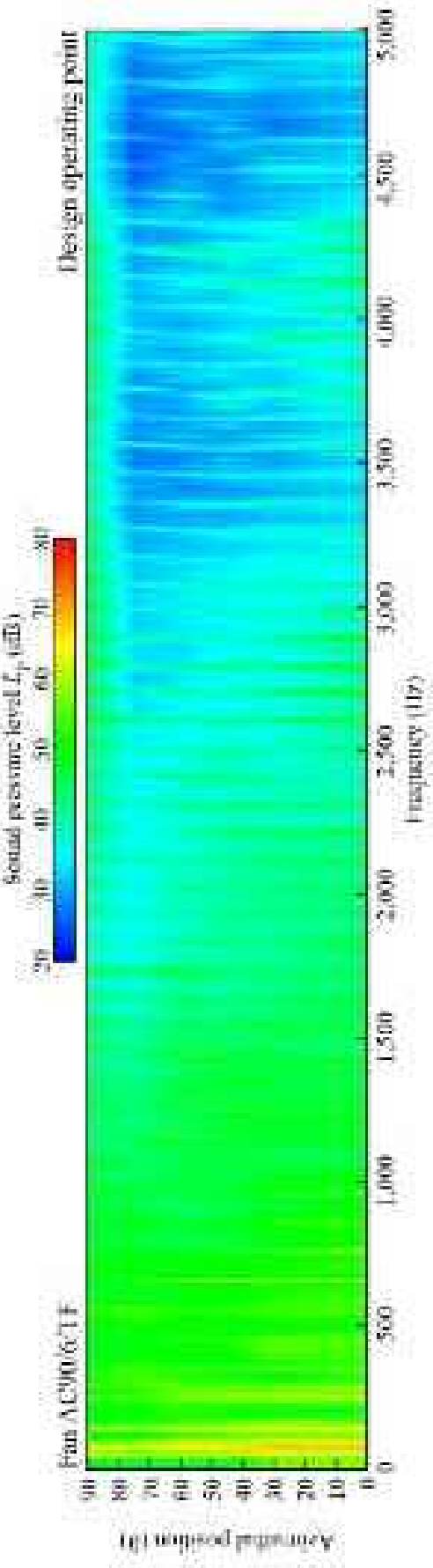

FIGURE 12.7. Measured far-field directivity of the sound pressure level (L_p) spectrum for the fan AC90/6/TF measured at the fan design operating point. The measured data illustrates that the sound pressure level spectrum is anisotropic with azimuthal position.

fan *datum* AC90/6 is behaving like a dipolar noise source. Bianchi *et al.* (2011) studied fan *datum* AC90/6's directivity and concluded that there are identifiable map features. The first of these features occurred with the blade passing frequency. The second to sixth occurred with the blade passing frequencies second, third, four, fifth and sixth harmonic. The directivity map indicates that the blade passing frequency and its second harmonic are isotropic. In contrast, the third to sixth harmonics exhibit reducing sound pressure level with increasing azimuthal angle.

The directivity map for the fan *datum* AC90/6 characterises the broadband noise between tonal peaks that occur with the blade passing frequency and its harmonics. For frequencies up to approximately 1.2 kHz, the broadband noise is typically between 50 and 60 dB. As frequency increases, the broadband noise decreases. Above 2 kHz, the broadband noise falls as low as 30 dB, with peak values on the fan axis and minimum values at 90 degrees to the fan axis. The very low broadband noise levels at frequencies above approximately 3.5 kHz result in the emergence of higher order harmonics of blade passing frequency. These harmonics first emerge over a frequency range of 3.5 to 3.7 kHz over an azimuthal range from 45 to 90 degrees. These harmonics are evident up to a frequency of 4.2 kHz over an azimuthal range from 60 to 90 degrees. Above 4.2 kHz the harmonics merge with the broadband noise.

Consider the directivity map for the fan AC90/6/TF, Figure 12.7. The directivity map indicates that the acoustic characteristics of the fan AC90/6/TF are essentially similar to the fan *datum* AC90/6 up to the fourth harmonic of blade passing frequency. Above the fourth harmonic of blade passing frequency there is a reduced sound pressure level at zero degrees, on the fan axis. There is also a slight increase in the sound pressure level at 90 degrees for all tonal features.

The directivity map for the fan AC90/6/TF characterises the broadband noise between tonal peaks that occur with the blade passing frequency and its harmonics. For frequencies up to approximately 1.4 kHz, the broadband noise is typically between 50 and 60 dB. Above 1.4 kHz the broadband noise level reduces as it did for the fan *datum* AC90/6, but more rapidly. Partly as a consequence of the lower broadband noise, higher order harmonics of the blade passing frequency remain evident up to 4.3 kHz. After 4.3 kHz, these harmonics merge with the broadband. Broadband noise falls as low as 25 dB over an azimuthal range from 45 to 90 degrees. Broadband noise is typically 40 dB on the fan axis. A primary difference between the fan *datum* AC90/6 and fan AC90/6/TF is the sound pressure level at an azimuthal position of 90 degrees. Over a frequency range from 2.5 to 5.0 kHz, the fan AC90/6/TF exhibits consistently higher sound pressure levels than the fan *datum* AC90/6.

Consider the directivity map for the fan AC90/6/TF$_{MVB}$, Figure 12.8. The map indicates that both broadband and tonal sound pressure levels are different to those of both fan *datum* AC90/6 and AC90/6/TF at frequencies above the blade passing frequency. The blade passing frequency exhibits a peak in sound pressure level at an azimuthal position of 30 degrees. After the fifth harmonic of blade passing frequency at approximately 500 Hz, the higher harmonics of blade passing frequency are evident over the full azimuthal range from 0 to 90 degrees. Between 500 Hz and 1.2 kHz, we may characterise the fan AC90/6/TF$_{MVB}$ directivity map by a reduction in the on-axis

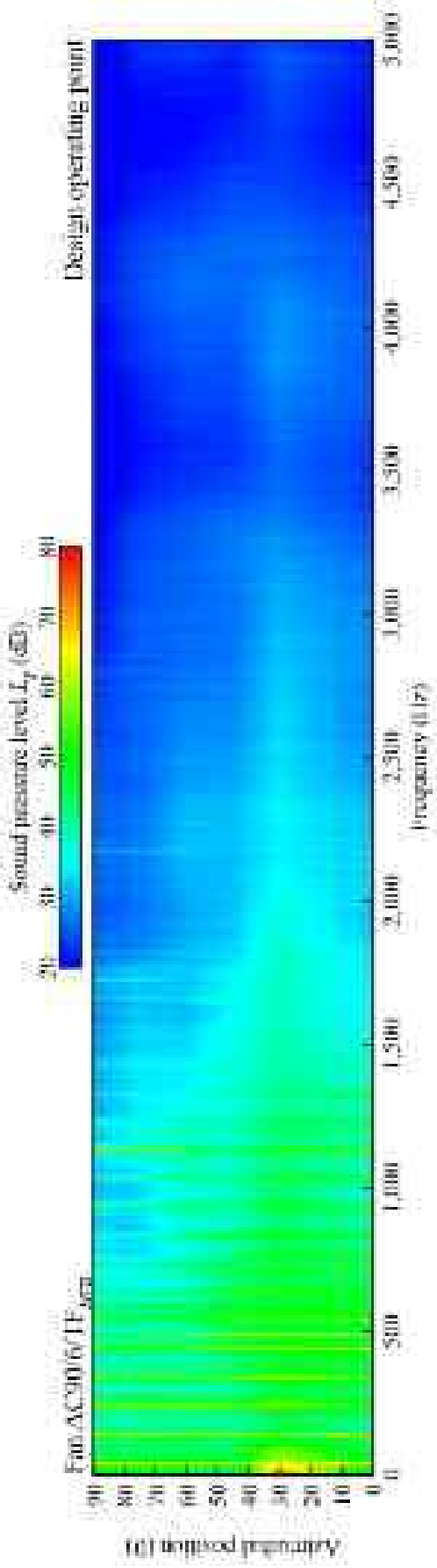

FIGURE 12.8. Measured far-field directivity of the sound pressure level (L_p) spectrum for the fan AC90/6/TF$_{MVB}$ measured at the fan design operating point. The measured data illustrates that the sound pressure level spectrum is more isotropic with azimuthal position than either the fan *datum* AC90/6 or AC90/6/TF.

broadband noise. As broadband noise reduces, the harmonics of blade passing frequency become more evident over an azimuthal range from 45 to 90 degrees.

At frequencies above 1.5 kHz, the fan AC90/6/TF$_{MVB}$ directivity map exhibits a rapid reduction in broadband and tonal noise over an azimuthal range from 30 to 90 degrees. At frequencies above 2 kHz, harmonics of the blade passing frequency have merged with the broadband noise. At frequencies above 2 kHz, the azimuthal distribution of sound pressure level is essentially isotropic, with one exception. At an azimuthal position of 30 degrees there is a directivity map feature. This feature exhibits a near constant 30 dB sound pressure level, and is evident from 2 kHz to 5 kHz. This feature is unique to fan AC90/6/TF$_{MVB}$'s directivity map. A review of the three directivity maps indicates that despite the feature, above 2 kHz the fan AC90/6/TF$_{MVB}$ broadband noise was consistently lower than both the fan *datum* AC90/6 and AC90/6/TF.

CONCLUSIONS

In this chapter we present an experimental investigation of the fan *datum* AC90/6, the fan AC90/6/TF and the fan AC90/6/TF$_{MVB}$. We used a near- and far-field correlation technique in combination with a span-wise analysis of coherence values and a directivity analysis. The fan AC90/6/TF$_{MVB}$ measured pressure developing capability improved in comparison to the fan *datum* AC90/6 and fan AC90/6/TF. We achieved the improvement in pressure developing capability without an efficiency penalty. Efficiency of the fan AC90/6/TF$_{MVB}$ remained similar to that of the studied fan with no fitted end-plate or with any of the other studied end-plate configurations despite an increase in blade loading.

Studying directivity patterns and using a coherence analysis characterises the impact of blade-tip end-plate design. We were able to establish that the fan AC90/6/TF$_{MVB}$ incorporating the newly conceived end-plate results in both a reduced tonal and overall fan far-field noise. We found that the fan far-field A-weighted sound power level for the fan AC90/6/TF$_{MVB}$ was lower than the fan *datum* AC90/6 over its entire operating range. At the maximum flow operating point it was 4.4 dB(A) quieter. At the design operating point it was 5.8 dB(A) quieter. At the peak pressure operating point it was 8.2 dB(A) quieter. We also found that the highest sound pressure levels for the fan *datum* AC90/6, AC90/6/TF and AC90/6/TF$_{MVB}$ at the design operating point were on the fan axis. They were respectively 81, 82 and 71 dB. This indicates that the fan AC90/6/TF$_{MVB}$ on-axis sound pressure level is 10 dB lower than fan *datum* AC90/6 and 11 dB lower than fan AC90/6/TF. This reduction of near-axis noise correlates with the presence of coherent swirling structures which the blade-tip end-plate induced.

The reported research verifies the technical merit of the fan AC90/6/TF$_{MVB}$ incorporating the newly conceived end-plate, providing insight into the flow-field physics underpinning the reduced fan far-field noise. The newly conceived end-plate effectively minimises blade-tip leakage vortex intensity, avoids vortex breakdown and additionally induces a blade-tip flow-field feature that reduces far-field near-axis

fan noise. It is this combination that is responsible for the low noise of the fan AC90/6/TF$_{MVB}$.

REFERENCES

ISO 5801:2007 (2007), *Industrial Fans: Performance Testing Using Standardised Airways.*

ISO 10302:2011 (2011), *Acoustics: Measurement of Airborne Noise Emitted and Structure-borne Vibration Induced by Small Air-moving Devices Part 1: Airborne Noise Measurement.*

Bianchi, S., Corsini, A., Rispoli, F. and Sheard, A.G. (2009a), 'Detection of Aerodynamic Noise Sources in Low-speed Axial Fans with Tip End-plates', *Proceedings of the IMechE Part C, Journal of Mechanical Engineering Science*, vol. 223, pp. 1379–1392.

Bianchi, S., Corsini, A., Rispoli, F. and Sheard, A.G. (2009b), 'Experimental Aeroacoustic Studies on Improved Tip Configurations for Passive Control of Noise-signature in Low-speed Axial Fan', *Transactions of the ASME, Journal of Vibration & Acoustics*, vol. 131, paper no. 061007, pp. 1–10.

Bianchi, S., Corsini, A., Rispoli, F. and Sheard, A.G. (2011), 'Far-field Radiation of Tip Aerodynamic Sound Sources in Axial Fans Fitted with Passive Noise Control Features', *Transactions of the ASME, Journal of Vibration & Acoustics*, vol. 133, paper no. 051001, pp. 1–11.

Corsini, A. and Rispoli, F. (2004), 'Using Sweep to Extend the Stall-free Operational Range in Axial Fan Rotors,' *Proceedings of the Institution of Mechanical Engineers Part A, Journal of Power and Energy*, vol. 218, pp. 129–139.

Corsini, A. and Sheard, A.G. (2007), 'Tip End-plate Concept Based on Leakage Vortex Rotation Number Control', *Journal of Computational and Applied Mechanics*, vol. 8, pp. 21–37.

Corsini, A. and Sheard, A.G. (2013), 'End-plate for Noise-by-flow Control in Axial Fans', *Periodica Polytechnique, Mechanical Engineering*, vol. 57(2), pp. 3–16.

Corsini, A., Rispoli, F. and Sheard, A.G. (2007), 'Development of Improved Blade-tip End-plate Concepts for Low-noise Operation in Industrial Fans', *Proceedings of the IMechE Part A, Journal of Power and Energy*, vol. 221, pp. 669–681.

Corsini, A., Rispoli, F. and Sheard, A.G. (2009), 'Aerodynamic Performance of Blade-tip End-plates Designed for Low-noise Operation in Axial-flow Fans', *Transactions of the ASME, Journal of Fluids Engineering*, vol. 131, paper no. 081101, pp. 1–13.

Corsini, A., Rispoli, F. and Sheard, A.G. (2010), 'Shaping of Tip End-plate to Control Leakage-vortex Swirl in Axial-flow Fans', *Transactions of the ASME, Journal of Turbomachinery*, vol. 132, paper no. 031005, pp. 1–9.

Cumpsty, N.A. (1974), 'Sum and Difference Tones from Turbomachines', *Journal of Sound and Vibration*, vol. 32, pp. 383–386.

Cumpsty, N.A. (1977), 'Review: A Critical Review of Turbomachinery Noise', *Transaction of the ASME, Journal of Fluids Engineering*, vol. 99, pp. 278– 293.

Fukano, T. and Jang, C.M. (2004), 'Tip Clearance Noise of Axial Flow Fans Operating at Design and Off-design Condition', *Journal of Sound and Vibration*, vol. 275, pp. 1027–1050.

Fukano, T., Takamatsu, Y. and Kodama, Y. (1986), 'The Effects of Tip Clearance on the Noise of Low Pressure Axial and Mixed Flow Fans', *Journal of Sound and Vibration*, vol. 105, pp. 291– 308.

Holste, F. and Neise, W. (1997), 'Noise Source Identification in a Propfan Model by Means of Acoustical Near-field Measurements', *Journal of Sound and Vibration*, vol. 203, pp. 641–665.

Inoue, M., Kuroumaru, M. and Fukuhara, M. (1986), 'Behavior of Tip Leakage Flow Behind an Axial Compressor Rotor', *Transactions of the ASME, Journal of Engineering for Gas Turbines and Power*, vol. 108, pp. 7– 14.

Jensen, C.E. (1986), 'Axial-flow Fan', Patent No. US 4,630,993, 23 December.

Kameier, F. and Neise, W. (1977), 'Rotating Blade Flow Instability as a Source of Noise in Axial Turbomachines', *Journal of Sound and Vibration*, vol. 203, pp. 833–853.

Khourrami, M.R. and Choudari, M. (2001), 'A Novel Approach for Reducing Rotor Tip-clearance Induced Noise in Turbofan Engines', *Proceedings of the 7th AIAA/CEAS Aeroacoustics Conference*, Maastricht, The Netherlands, 28–30 May.

Leggat, L.J. and Siddon, T.E. (1978), 'Experimental Study of Aeroacoustic Mechanism of Rotor-vortex Interactions', *Journal of the Acoustical Society of America*, vol. 64, pp. 1070–1077.

Longet, C.M.L. (2003), 'Axial Flow Fan with Noise Reducing Means', Patent No. US 2003/0123987 A1, 3 July.

Longhouse, R.E. (1978), 'Control Tip-vortex Noise of Axial Flow Fans by Rotating Shrouds', *Journal of Sound and Vibration*, vol. 58, pp. 201–214.

Magliozzi, B., Johnson, B.V., Hanson, D.B. and Metzger, F.B. (1973), 'Noise and Wake Structure Measurements in a Subsonic Tip Speed Fan – Tabulation and Plots of Test Data', NASA Technical Report CR-132259, 23 July.

Marcinowski, H. (1953), 'Einfluss des Laufradspalts und der Luftfuehrung bei einem Kuehlgeblaese axialer Bauart', *Motortechnische Zeitschrift*, vol. 14, pp. 259–262.

Mimura, M. (2003), 'Axial Flow Fan', US Patent No. 6,648,598 B2, 18 November.

Mugridge, B.D. and Morfey, C.L. (1972), 'Sources of Noise in Axial Flow Fan', *Journal of the Acoustical Society of America*, vol. 51, pp. 1411–1426.

Quinlan, D.A. and Bent, P.H. (1998), 'High Frequency Noise Generation in Small Axial Flow Fans', *Journal of Sound and Vibration*, vol. 218, pp. 177–204.

Shah, P.D., Mobed, D., Spakovszky, Z., Brooks, T.F. and Humphreys, W.M. (2010), 'Aero-acoustics of Drag Generating Swirling Exhaust Flows', *AIAA Journal*, vol. 48(4), pp. 719-727.

Sheard, A.G., Corsini, A. and Rispoli, F. (2009), 'A Meridional Fan', Patent No. GB 2,452,104 B, 22 July.

Uselton, R.B., Cook, L.J. and Wright, T. (2008), 'Fan with Reduced Noise Generation', Patent No. US 7,351,041 B2, 1 April.

Wright, S.E. (1976), 'The Acoustic Spectrum of Axial Flow Machines', *Journal of Sound and Vibration*, vol. 45(2), pp. 165–223.

Chapter 13

Installed Acoustic Performance of Cooling Axial Fans Fitted with End-plates

S. Bianchi, A. Corsini and A.G. Sheard

ABSTRACT

The chapter presents an investigation of the far-field noise emissions of a fan with blade-tip end-plates designed to control the blade tip-to-casing leakage vortex swirl level when installed in a compact cooling unit. We tested a fan AC90/6 without blade-tip end-plates that we named fan *datum* AC90/6, and three variants of the fan with different end-plate geometries. The fan AC90/6/TF incorporated a constant thickness end-plate. The fan AC90/6/TF$_{VTE}$ incorporated a variable thickness end-plate. The fan AC90/6/TF$_{MVB}$ incorporated an end-plate designed to control the blade tip-to-casing leakage vortex's swirl level. When fitted in a compact cooling unit, fan inlet flow draws through the unit, passing over a tube bank. As a consequence, the fan inlet flow is both distorted and more turbulent than when installed in a standardised airway. The fan inlet flow's distortion and increase in turbulence level had little impact on the acoustic performance of fan *datum* AC90/6, but did reduce the effectiveness of all fans with end-plates. The fan AC90/6/TF$_{MVB}$ has an overall noise level 5.8 dB(A) lower than the fan *datum* AC90/6 when we measured the performance at the fan design operating point in a standardised airway. When installed in a compact cooling unit, the AC90/6/TF$_{MVB}$ has an overall noise level 2.5 dB(A) lower than the fan *datum* AC90/6. The reported research illustrates the importance of installation effects on fan acoustic performance. The newly conceived blade-tip end-plate design was less effective when installed in a compact cooling unit then when installed in a standardised airway. Nevertheless, the achieved 2.5 dB(A) reduction results in the fan AC90/6/TF$_{MVB}$ being the lowest noise fan in its class and therefore, we concluded that the blade-tip end-plate incorporated into the fan AC90/6/TF$_{MVB}$ was a success.

This chapter is a revised and extended version of Bianchi, S., Corsini, A. and Sheard, A.G. (2012), 'Installed Aeroacoustic Performance of Cooling Axial Fans Fitted with End-plates', *Noise Control Engineering Journal*, vol. 60, pp. 519–527.

NOMENCLATURE

Latin letters

BPF	blade-passing frequency [Hz]
D_h	hub diameter
D_c	casing diameter
K_s	specific noise level
ℓ	blade chord
p_t	total pressure
r_v	radial distance from the vortex axis
Ro	Rossby number
SPL	sound pressure level [dB]
SWL(A)	'A' weighted sound power level [dB(A)]
T	blade pitch
V_a	axial velocity at r
V	volume flow rate

Greek letters

τ	rotor tip clearance
Ω	tip leakage vortex rotation rate scale

INTRODUCTION

The use of compact cooling units, fitted with induced draft fans is widespread within both the air conditioning industry and in air-cooled condenser and cooling tower applications (Wilber and Zammit, 2005; Van de Spuy *et al.*, 2009; Owen and Kroger, 2011). Common to these applications is the importance of ensuring adequate condenser cooling and overall acoustic performance of the compact cooling unit. Consequently, there is interest within the air movement and control community in establishing installed, as opposed to laboratory fan aerodynamic and acoustic performance. Installed performance is invariably reduced when compared to the laboratory performance as a consequence of the distorted flow-field and elevated turbulence the installation generates (Bolton, 1990). Distortion and turbulence reduce the effectiveness of passive noise control techniques, contributing to reduced installed acoustic performance.

The air movement and control community has historically favoured the use of passive noise control techniques when attempting to minimise fan noise. The intent of these passive techniques is to influence positively dominant noise generation mechanisms. The passive noise control technique most widely adopted within the air movement and control community are blade-tip appendages. Researchers have studied extensively the design of fan blade-tip appendages (Quinlan and Bent, 1998; Longet, 2003; Mimura, 2003; Uselton *et al.*, 2005). These blade-tip appendages constitute anti-vortex devices, with those scholars who have studied their application reaching a consensus that they influence the blade tip-to-casing flow. A consequence of this influence is that it reduced the intensity of blade-tip noise generation mechanisms.

Reduction in the intensity of noise generation mechanisms occurs as a consequence of the role that organised structures play within turbulent flow in the noise generation process. The control of organised structures constitutes a way to reduce fan noise (Ffowcs Williams, 1977). Akturk and Camci (2010) reported a novel tip platform extension experimental study that successfully controlled blade tip-to-casing flow-field structures. The result was a more efficient fan with improved acoustic performance. Akturk and Camci (2010) successfully applied their developed flow control methodology to blade tip-to-casing leakage flow control in ducted lift fans for vertical take-off and landing applications (Akturk and Camci, 2011a, 2011b).

The research reported in this chapter presents an experimental programme of work that establishes a fan's installed performance when fitted with Corsini and Sheard's (2013) blade-tip end-plate. Corsini and Sheard (2013) developed a novel blade-tip end-plate design to control the blade tip-to-casing leakage vortex. The design exploited a linkage between the end-plate's chord-wise profile and augmentation and diminution of blade tip-to-casing leakage vortex near-axis swirl (Jones *et al.*, 2001; Herrada and Shtern, 2003). The objective of exploiting this linkage is to influence the momentum transfer from the blade tip-to-casing leakage flow and thus force some 'waviness' into the leakage vortex trajectory. Srigrarom and Kurosaka (2000) successfully utilised this approach when optimising a delta-wing platform. Sheard *et al.* (2009) defined Corsini and Sheard's (2013) design methodology, maintaining the blade tip-to-casing leakage vortex rotation number above a critical threshold value. By maintaining the leakage vortex rotation number above a critical threshold value, one avoids vortex bursting with an associated reduction in fan acoustic emissions.

FAMILY OF FANS UNDER INVESTIGATION

We conducted the reported research on a family of commercially available cooling fans. The studied fan configuration, coded AC90/6, incorporates a six-blade un-swept rotor, with modified ARA-D profile aerofoil blades, Table 13.1. One may set the blade-pitch angle during final assembly to customise the fan to a desired duty point. We used a direct coupled-induction 400-volt (AC), 3-phase motor to drive the rotor at a constant speed of 950 rpm, resulting in a 44.7 m/s blade tip speed and a 95 Hz blade-passing frequency (BPF). In its original embodiment, the studied fan did not include a blade-tip end-plate. We used it as a *datum* against which to assess the performance of fan variants with blade-tip end-plates. Therefore, in the reported research we refer to the fan without blade-tip end-plates as the fan *datum* AC90/6.

Blade-tip End-plates for Noise Control

Bianchi *et al.* (2009) studied the aerodynamic and acoustic benefit that occurs with adding a constant thickness blade-tip end-plate. The designs developed for tip-vortex control and drag reduction in aircraft wings and catamaran hulls inspired the constant thickness blade-tip end-plate design. The constant thickness blade-tip end-plate ran along the blade pressure surface, ending at the blade trailing edge with a

Table 13.1. *The fan* datum *AC90/6 blade geometry and rotor specification.*

	Fan *datum* AC90/6		
Blade geometry	Hub	Mid-span	Tip
Pitch angle (°)	36	58.8	28
Camber angle (°)	46	44	41
Solidity	1.24	0.86	0.30
Fan rotor			
Blade number		6	
Blade tip pitch angle (°)		16–28	
Blade tip stagger angle (°)		74–62	
Hub-to-casing diameter ratio σ		0.22	
Tip diameter (mm)		900.0	
Rotor tip clearance τ (% span)		1.0	
Rated rotational frequency (r/min)		935–950	

square tail. When fitted with a constant thickness blade-tip end-plate, we named the fan AC90/6/TF.

Following Ito *et al.*'s method (1985), Corsini and Sheard (2007) concluded that there is a threshold value of the Rossby number below which vortex rotation cannot reduce if the vortex is to remain stable. Corsini and Sheard (2007) concluded that for the fan *datum* AC90/6, the blade tip-to-casing leakage vortex Rossby number remained above the threshold value and did not burst. However, the fan AC90/6/TF leakage vortex Rossby number fell below the threshold value at approximately 90 per cent chord and did burst. Vortex bursting is acoustically productive, with Corsini and Sheard (2007) proposing a variable thickness blade-tip end-plate that maintained a leakage vortex Rossby number above the required threshold value and therefore did not burst. When fitted with the variable thickness blade-tip end-plate, we named the studied fan AC90/6/TF$_{VTE}$.

Corsini *et al.* (2007) studied the aerodynamic performance of fan AC90/6/TF$_{VTE.}$ They concluded that the variable thickness blade-tip end-plate design successfully avoided blade tip-to-casing leakage vortex bursting. An assessment of aerodynamic performance demonstrated an improved pressure developing capability and fan efficiency that one may attribute to the leakage vortex not bursting. However, noise measurements made by Corsini and Sheard (2013) indicated that the variable thickness blade-tip end-plate resulted in a broadband noise level approximately 0.5 dB higher than that occurring with the constant thickness end-plate. Corsini *et al.* (2007) concluded that the variable thickness blade-tip end-plate induced the creation of multiple organised vortical structures. These vortical structures did burst, with the breakdown acoustically productive enough to result in the observed increase in overall fan far-field broadband noise.

The work of Corsini *et al.* (2007) was continued by Corsini *et al.* (2009, 2010) who concluded that the multiple organised vortical structures induced in the blade tip region by the variable thickness blade-tip end-plate were disproportionately

acoustically productive. Therefore, they concluded that the blade-tip end-plate required redesign to minimise the swirling intensity and size of vortices in the blade tip region. Whilst minimising intensity and size of vortical structures, the end-plate design must also ensure that neither the blade tip-to-casing leakage vortex nor those organised vortical structures that are created burst. Corsini and Sheard (2013) developed a design process to control the blade-tip leakage flow. They used the design process to design a new blade-tip end-plate, named the Multiple Vortex Breakdown (MVB) end-plate. When they fitted the studied fan with the MVB blade-tip end-plate, they named it fan AC90/6/TF$_{MVB}$, Figure 13.1.

Fan Aerodynamic Performance

We measured the performance characteristics of the studied fan using a Type B standardised airway (free inlet, ducted outlet) in accordance with ISO 5801:2007 requirements (2007). The performance characteristics of the studied fan illustrate the impact on pressure rise of blade-tip end-plate geometry, Figure 13.2. Therefore, the addition of the constant thickness, variable thickness and multiple vortex breakdown blade-tip end-plates results in an increase in blade loading. We would expect blade-tip noise sources to become more acoustically productive with increasing blade loading. An increase in blade loading will offset partially any reduction in fan far-field noise attributed to adding a blade-tip end-plate. Consequentially we conservatively assess the reduction in fan far-field noise if one neglects an increase in blade loading. Therefore, we chose to neglect the change in pressure rise with the change in blade-tip treatment.

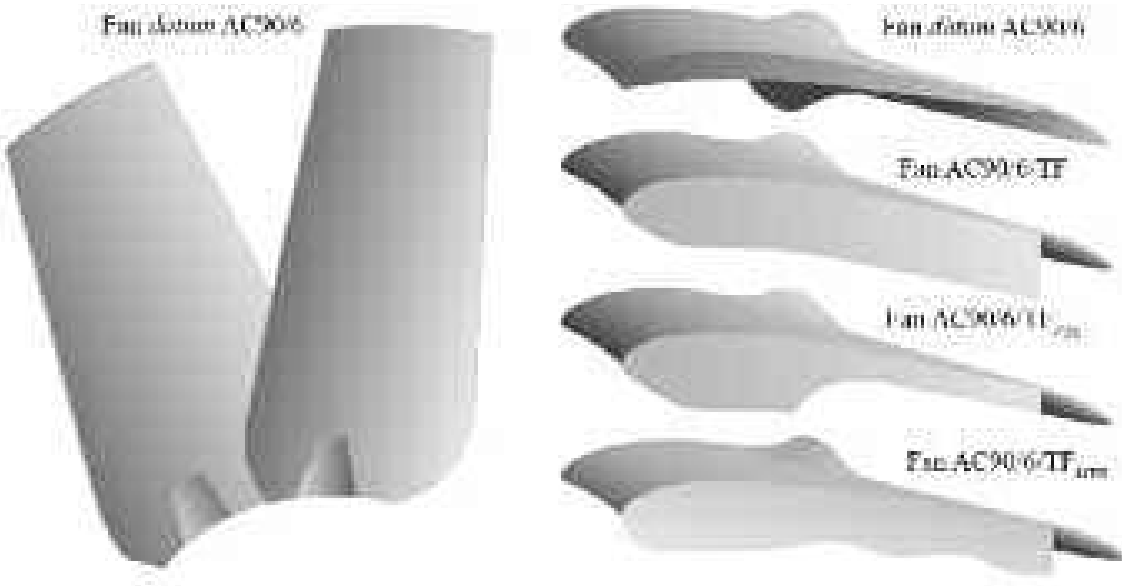

FIGURE 13.1. The studied fan *datum* AC90/6 without a fitted blade-tip end-plate, the fan AC90/6/TF with a constant thickness blade-tip end-plate, the fan AC90/6/TF$_{VTE}$ with a variable thickness blade-tip end-plate and the fan AC90/6/TF$_{MVB}$ incorporating a blade-tip end-plate designed using Corsini and Sheard's (2013) noise-by-flow control design procedure.

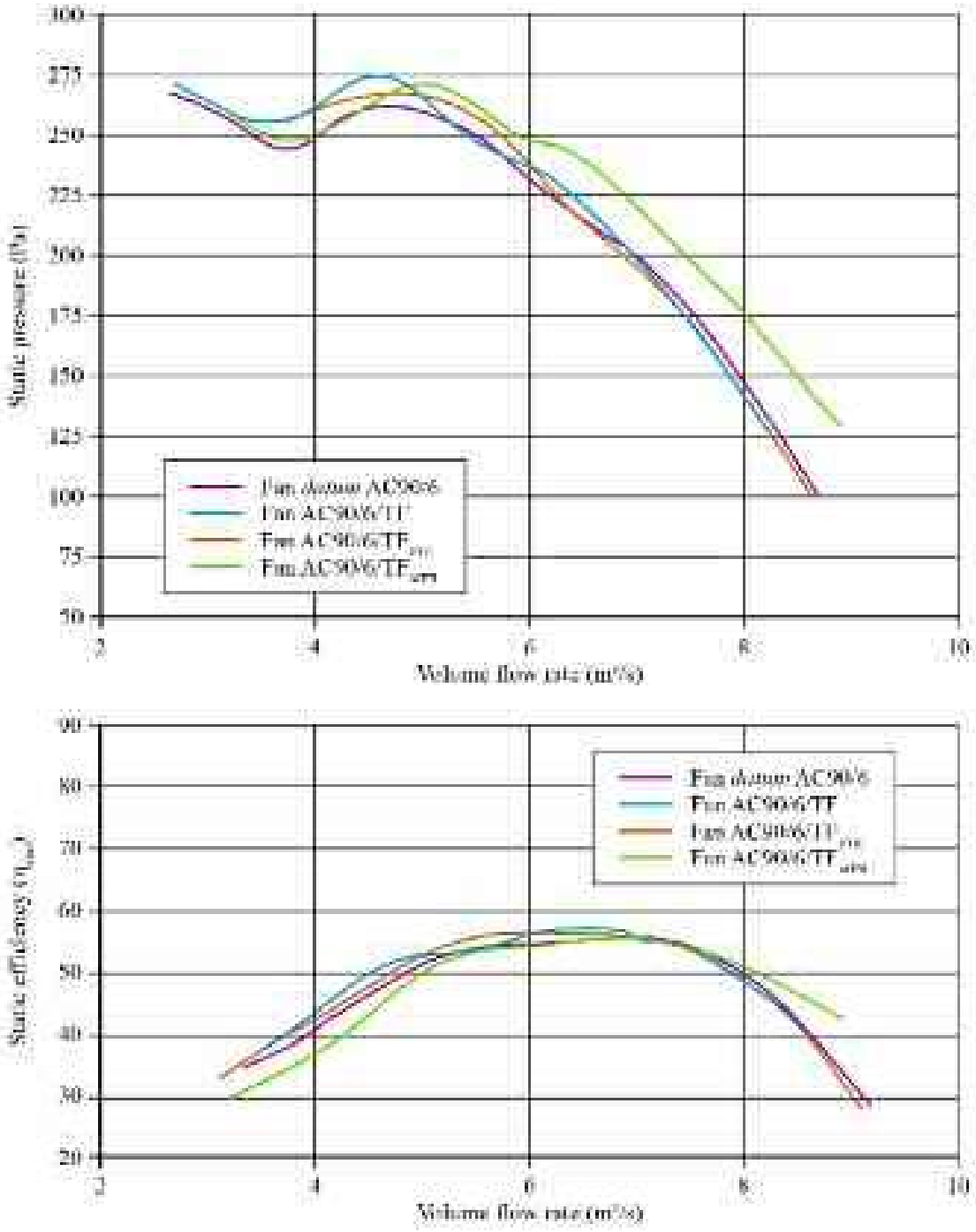

FIGURE 13.2. The performance characteristics of the studied fan *datum* AC90/6 without a fitted blade-tip end-plate, with a constant thickness blade-tip end-plate, AC90/6/TF with a variable thickness blade-tip end-plate, AC/6/TF$_{VTE}$ and with the multiple vortex breakdown blade-tip end-plate, AC/6/TF$_{MVB}$. The authors measured performance characteristics with the blade tip pitch angle set to 28 degrees in a Type B standardised airway (free inlet, ducted outlet) in accordance with ISO 5801:2007 requirements (2007).

ACOUSTIC METHODOLOGY

In the programme of work reported in this chapter, we measured fan far-field noise in both a standardised airway and installed over a compact cooling unit's tube bank. We performed the standardised airway acoustic measurements to determine the azimuthal distribution of fan far-field noise. Blade-tip end-plates are a passive noise control device, and are sensitive to inlet turbulence level. Therefore, we may reasonably expect the installed performance of the studied fan configurations to be lower than the performance when fitted in a standardised airway. Our objective in making both installed and standardised airway acoustic measurements was to establish the difference between the two. This difference is a measure of the resilience of each blade-tip end-plate design to installation effects.

For both the installed and standardised airway, we made fan far-field acoustic measurements using Bianchi *et al.*'s (2011) methodology. We made measurements of far-field noise on the fan centre line and plus and minus 30, 45, 60, 75 and 90 degrees off the fan centre line. We used a data acquisition system to log the far-field microphone signal, Table 13.2. For each of the studied fans, and at each azimuthal position, we logged the far-field microphone signal for 30 seconds and repeated each measurement three times. We calibrated the far-field microphone in accordance with ISO IEC61672-1 requirements (2002). We estimated its accuracy to be 0.1 to 0.2 dB at 1 kHz. Prior to making acoustic measurements, we removed the impeller from the studied fan and measured only the motor's far-field noise spectra. We then post processed all subsequent acoustic measurements to eliminate the motor's contribution to both the measured overall noise level and spectra.

Acoustic Measurements in a Standardised Airway

We made acoustic measurements in accordance with ISO 10302:2011 requirements (2011). The test-rig was a Type A standardised airway, Figure 13.3, with the fan downstream from a plenum chamber with a free outlet. The rotor centre line was two metres from the floor. The fan inlet bell-mouth was aerodynamically optimised to provide uniform and unseparated flow into the fan. We acoustically treated the downstream and upstream plena to minimise noise transmissions from the air stream into the fan and the outside environment. The fan's inlet airflow passed through an aerofoil louver in the top of the facility, enabling pressure across the fan to be varied.

Table 13.2. *Far-field microphone and data acquisition system specification.*

Far-field microphone	Brüel&Kjær 4954 (2006)
Frequency range	0 Hz: 20 kHz
Sapling frequency	50 kHz
Dynamic range	Up to 165 dB
Sound analyser	01dB-Metravib dBFA Suite

FIGURE 13.3. The standardised airway test rig set-up in a semi-anechoic chamber with a Type A (fan downstream from a plenum chamber with a free outlet) fan installation.

Installed Acoustic Measurements

We made acoustic measurements in accordance with ISO 10302:2011 requirements (2011). The test-rig was a compact cooling unit's tube bank, Figure 13.4. We installed the fan on the compact cooling unit's top plate over the tube bank. In operation, the fan induces a reduced pressure over the top of the tube bank relative to atmosphere that draws air through the tube bank. This compact cooling unit tube bank is typical of the installations into which the studied fan is fitted. This type of compact cooling unit finds widespread application in oil refineries and petrochemical plants.

The compact cooling unit coils are manufactured from seamless copper tubing that is kept in place with corrugated aluminium plate-type cooling fins. There are three vertical rows of coils on the compact cooling unit's front face and another three on the back face at an angle of approximately 60 degrees. In each case, the three rows are staggered to maximise heat transfer from the tubes to the air passing over them. In this application, the fan induces a velocity of between 4.0 and 4.3 metres per second over the coils, with an associated pressure drop across the coils of typically 200 Pa.

FIGURE 13.4. The studied fan installed over a compact cooling unit's tube bank that is located in a semi-anechoic chamber to facilitate fan performance and noise measurement. When installed over the compact cooling unit's tube bank, the fan inlet flow draws through the unit, passing over a tube bank.

STANDARDISED AIRWAY FAR-FIELD ACOUSTIC RESULTS

The purpose of the research presented in this chapter is to investigate fan far-field noise when fitted with blade-tip end-plates. Specifically, we aimed to establish the effectiveness of the multiple vortex breakdown blade-tip end-plate. We commenced our investigation with an analysis of:

- far-field sound pressure level, L_P directivity; and,
- far-field sound power level, L_W spectrum.

We made our measurements of sound pressure level directivity and sound power level spectrum with the studied fan configurations installed in a standardised airway. We made all acoustic measurements with the fan running at 950 rpm and with a blade angle of 28 degrees resulting in the fan operating at its nominal design operating point. We defined the design operating point as a flow rate of 7 m^3/s. Each of the four studied fan configurations produced a slightly different pressure rise at the design flow rate, Figure 13.2. This was a consequence of the blade-tip end-plates affecting both fan aerodynamic and acoustic performance.

Far-field Directivity

Our analysis starts with a review of the azimuthal distribution of far-field sound pressure level (L_P), Figure 13.5. The azimuthal distribution illustrates that the highest sound pressure levels are at zero degrees, on the fan axis. The maximum levels for the fan *datum* AC90/6, AC90/6/TF and AC90/6/TF$_{VTE}$ are 79 dB, 82 dB and 78 dB respectively. This result is self-consistent with Leggat and Siddon's (1978) results and indicates that the three studied fan configurations are behaving like dipolar noise sources. Within this context, a monopole noise source is a source which radiates sound equally well in all directions. A dipole noise source consists of two monopole sources of equal strength but opposite phase and separated by a small distance compared with the wavelength of sound.

In contrast to the fans *datum* AC90/6, AC90/6/TF and AC90/6/TF$_{VTE}$, the fan AC90/6/TF$_{MVB}$ exhibited a peak sound pressure level of 71 dB at zero degrees, on the fan axis. This is respectively 8 dB, 11 dB and 7 dB lower than the fan *datum* AC90/6, AC90/6/TF and AC90/6/TF$_{VTE}$. Most surprising was the near isotropic radiation pattern of the fan AC90/6/TF$_{MVB}$. Within this context, we define an isotropic noise source as a noise source that has the same value when measured in different directions. We may attribute this isotropic behaviour to the multiple vortex breakdown blade-tip end-plate inducing a shift in acoustic emissions from higher to lower frequency. Bianchi *et al.* (2011) studied the azimuthal distribution of fan outlet sound pressure level cross-spectra between the near- and far-field. They concluded that the attenuation of sound pressure level on the fan axis correlated with the presence of vortical structures in the exhaust flow.

The beneficial effect of the multiple vortex breakdown blade-tip end-plate is less evident off the fan axis. The fan AC90/6/TF, AC90/6/TF$_{VTE}$ and AC90/6/TF$_{MVB}$ exhibit similar azimuthal sound pressure level distributions off the fan axis. All three are consistently lower than the fan *datum* AC90/6 when at more than 20 degrees off the fan axis. However, there is a difference between the off fan axis sound pressure levels of the fan AC90/6/TF and AC90/6/TF$_{VTE}$ than fan AC90/6/TF$_{MVB}$. The fan AC90/6/TF$_{MVB}$ off fan axis sound pressure level is more isotropic than that of either fan AC90/6/TF or AC90/6/TF$_{VTE}$.

The fan AC90/6/TF$_{MVB}$ isotropic azimuthal distribution of sound pressure level indicates that the multiple vortex breakdown blade-tip end-plate has affected blade-tip noise sources. Low frequency noise sources classically radiate axially. High frequency noise sources classically radiate radially. The primary difference between the azimuthal distributions of sound pressure level for the fan AC90/6/TF and AC90/6/TF$_{VTE}$ and the fan AC90/6/TF$_{MVB}$ is a reduction in the sound pressure level on the fan axis. As low frequency noise classically radiates axially, this change implies that the multiple vortex breakdown blade-tip end-plate has induced a change in near-field noise sources. The intensity of low frequency near-field noise sources has been reduced. Enhanced control of the blade tip-to-casing leakage vortex may be responsible for this reduction.

The isotropic radiation pattern of fan AC90/6/TF$_{MVB}$ may indicate that the dipole characteristic of the fans *datum* AC90/6, AC90/6/TF and AC90/6/TF$_{VTE}$ has

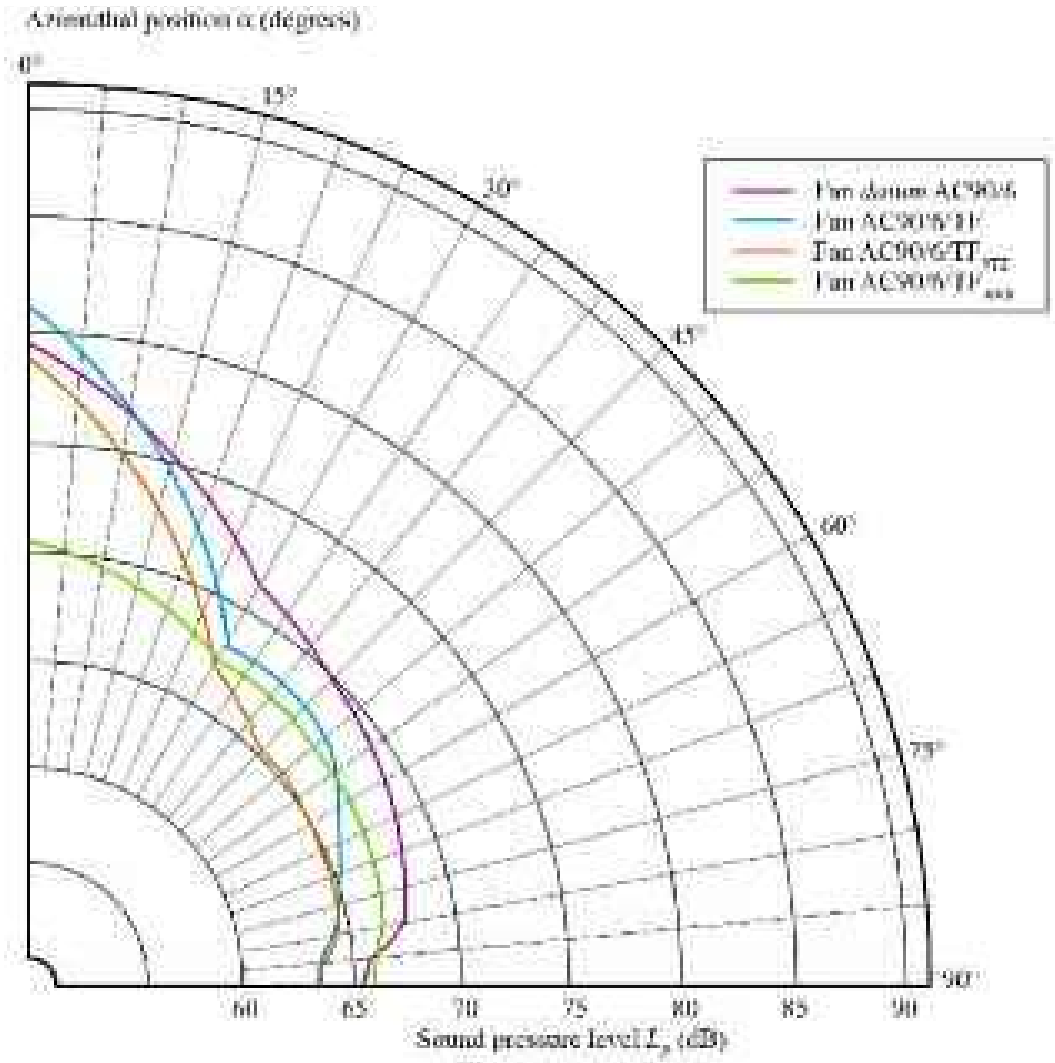

FIGURE 13.5. Far-field directivity of measured fan integrated sound pressure level (L_P) at the fan design operating point. The authors made measurements over the studied fans' operating range in a semi-anechoic chamber in a Type A (fan downstream from a plenum chamber with a free outlet) installation. Directivity for fan AC90/6/TF$_{MVB}$ was both attenuated and isotropic in comparison with fan *datum* AC90/6, AC90/6/TF or AC90/6/TF$_{VTE}$.

changed to a quadrupole characteristic. Just as two opposite phase monopoles make up a dipole, two opposite dipoles make up a quadrupole noise source. Shah *et al.* (2010) have studied swirling-flow noise. They concluded that we may attribute a quadrupole source's acoustic signature, in a low Mach number flow, to the turbulent mixing of swirling flow-field features. This mixing reduces the intensity of low frequency near-field noise sources and thus scatters dipolar noise sources. It is this scattering that results in a change from a dipole to quadrupole characteristic.

We may complement our directivity analysis with a consideration of both fan far-field overall A-weighted overall sound power level, L_WA and specific noise level, K_S. We apply A-weighting to measured sound levels in an effort to account for the relative perceived by the human ear, as the ear is less sensitive to low audio frequencies. Specific noise level is a metric that provides a measure of the net fan noise

emission. It provides a measure of acoustic efficiency at a fan's actual operating point. By plotting A-weighted overall sound power level against specific noise level, we are able to gain an insight into the change in fan acoustic performance with changing operating point, Figure 13.6. The design operating point for each of the studied fans corresponds to the mid-point of data. The maximum flow operating point corresponds to the left hand end of the data. The peak pressure operating point corresponds to the right hand end of the data.

Plotting A-weighted overall sound power level against specific noise level illustrates the effectiveness of the multiple vortex breakdown blade-tip end-plate. The fan AC90/6/TF$_{MVB}$ exhibits consistently lower A-weighted sound power levels and specific noise levels than the other three studied fan configurations. The fan AC90/6/TF, AC90/6/TF$_{VTE}$ and AC90/6/TF$_{MVB}$ exhibit the same trend of increasing A-weighted sound power level with increasing specific noise level. This trend is in contrast to the fan *datum* AC90/6 that exhibits a reducing A-weighted sound power level with increasing specific noise level. A reducing A-weighted sound power level with increasing specific noise level indicates that the frequency distribution of sound energy changes favourably. The result of this favourable change is a lower A-weighted

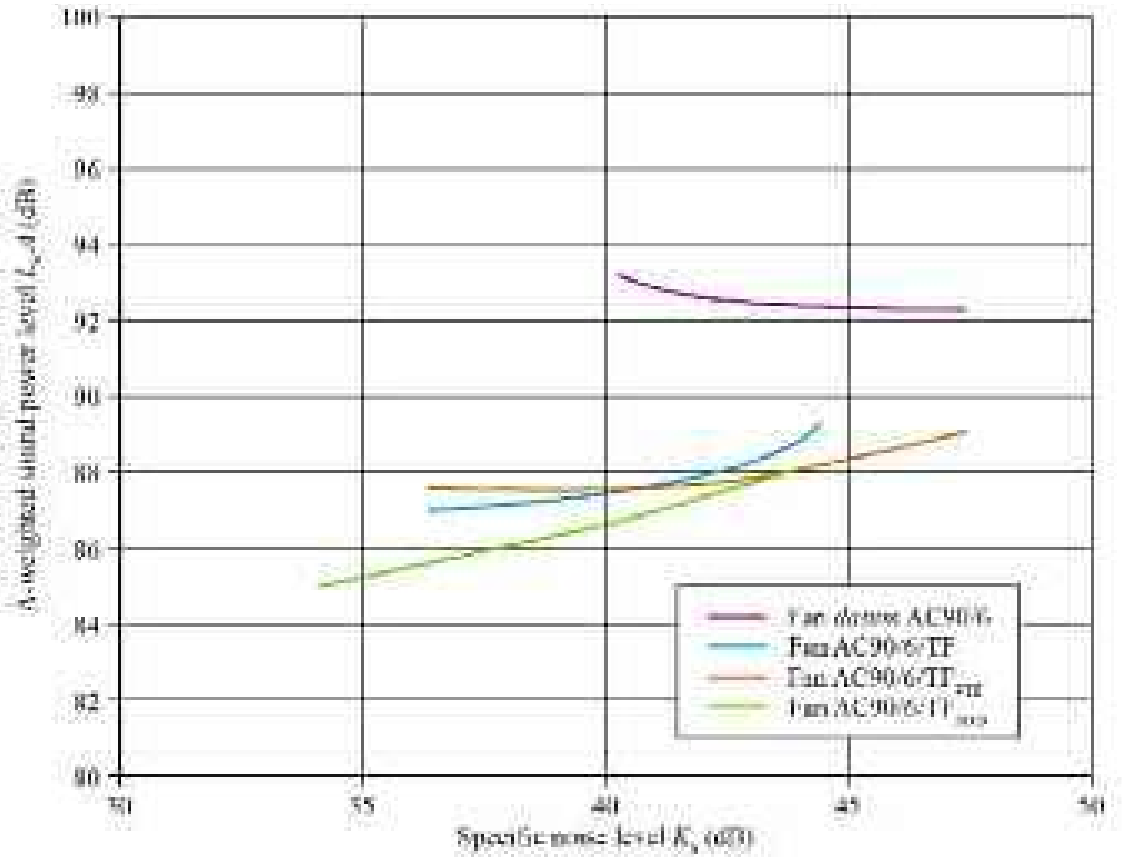

FIGURE 13.6. The change in specific noise level (K_s) with changing A-weighted sound power level (L_WA). The authors made measurements over the studied fans' operating range in a semi-anechoic chamber in a Type A (fan downstream from a plenum chamber with a free outlet) instalation. The fan AC90/6/TF$_{MVB}$ exhibits lower noise levels than the fan *datum* AC90/6, AC90/6/TF or AC90/6/TF$_{VTE}$ over the entire fan operating range.

sound power level despite increasing specific noise level. The fan AC90/6/TF$_{MVB}$ A-weighted sound power level does increase with increasing specific noise level. Despite this caveat, as we have previously noted, fan AC90/6/TF$_{MVB}$ outperforms the other three studied fan configurations. Both A-weighted sound power levels and specific noise levels are lower across the entire fan operating range.

Spectral Analysis

Our directivity analysis and A-weighted overall sound power level against specific noise level analysis provide an insight into the fan AC90/6/TF$_{MVB}$'s acoustic performance. We may complement this analysis with an analysis of far-field narrowband sound power level (L_W) spectrum, Figure 13.7. The sound power level spectrum is integrated over a hemisphere to provide an overall assessment of each fan configuration.

Consider the integrated sound power level spectrum for the four studied fan configurations, Figure 13.7. At frequencies below approximately 1 kHz, the integrated

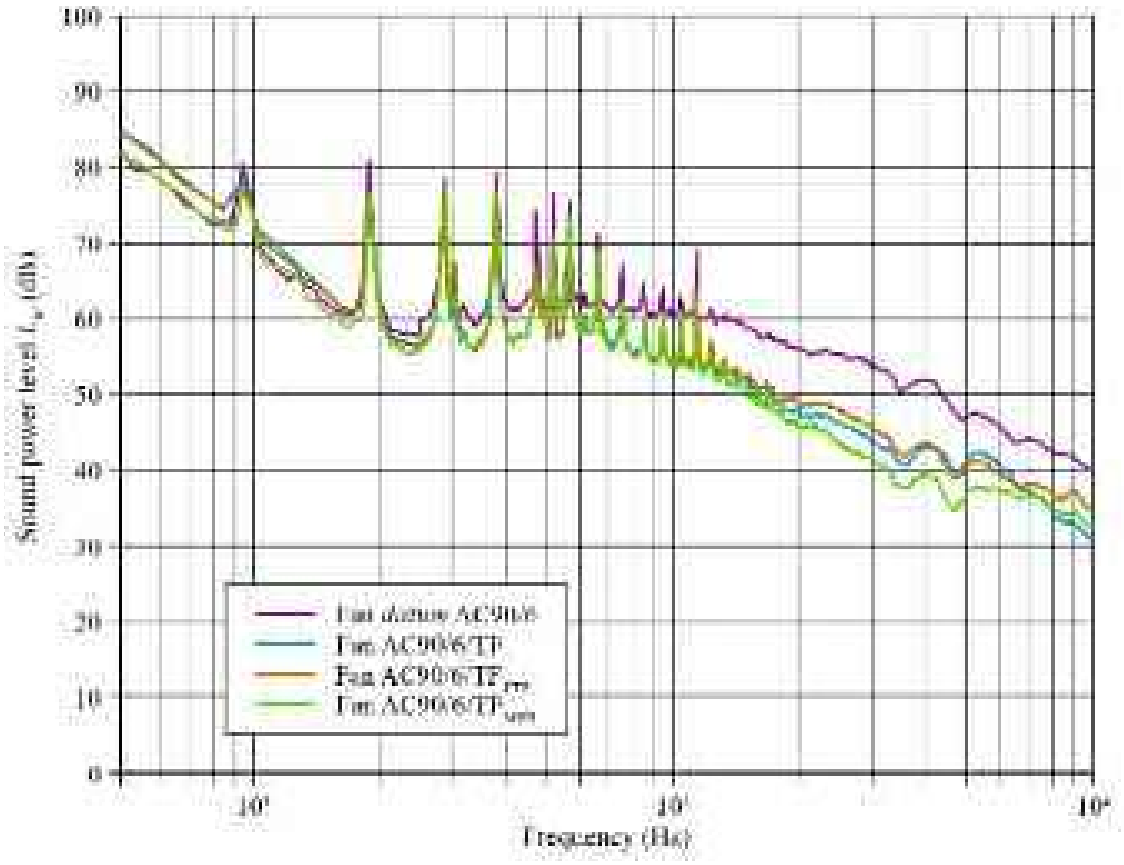

FIGURE 13.7. Outlet far-field narrowband sound power level (L_W) spectrum measured at the fan design operating point. The author made measurements over the studied fans' operating range in a semi-anechoic chamber in a Type A (fan downstream from a plenum chamber with a free outlet) installation. The authors provide measured sound power level spectrum data for the fan *datum* AC90/6, AC90/6/TF, AC90/6/TF$_{VTE}$ and AC90/6/TF$_{MVB}$.

sound power level spectrum for the four studied fan configurations is similar. There is one notable exception to the similarity. The three studied fan configurations with fitted blade-tip end-plates exhibit lower tonal peaks than the fan *datum* AC90/6 up to the tenth harmonic of blade passing frequency. The difference between the studied fans' broadband noise is apparent at frequencies above 1 kHz. The three studied fan configurations with fitted blade-tip end-plates exhibit broadband noise that is typically 10 dB lower than the fan *datum* AC90/6. At frequencies above 13 kHz, the fan AC90/6/TF$_{MVB}$'s broadband noise is typically 4 dB lower than fan AC90/6/TF or AC90/6/TF$_{VTE}$ and 14 dB lower than fan *datum* AC90/6. Therefore, we may conclude that all blade-tip end-plates reduce tonal noise. However, the multiple vortex breakdown blade-tip end-plate is more effective at reducing the broadband noise.

INSTALLED FAR-FIELD ACOUSTIC RESULTS

We complemented our standardised airway measurements with acoustic measurements that we made with the studied fan configurations installed over a compact cooling unit's tube bank. When installed over a compact cooling unit's tube bank, each fan configuration operated at a slightly different operating point, Table 13.3. The installed operating point varies as a consequence of the blade-tip end-plates affecting the fan aerodynamic, as well as acoustic performance. Despite the variation, the studied fan configurations operated relatively close to their nominal design operating flow rate of 7 m^3/s.

We considered varying the blade angle from fan to fan in an attempt to match the installed operating point more closely. In practice matching, we simply change one configuration for another, and measure the resultant far-field noise level. We concluded that a constant fan speed and blade angle and changing installed operating point was the appropriate approach to assessing installed acoustic performance. Our investigation of the installed performance of the four studied fan configurations comprised an analysis of:

- far-field sound power level, L_W spectrum; and,
- overall sound power level, L_W and A-weighted overall sound power level, L_WA.

Table 13.3. *The measured operating points for the four studied fan configurations. In each case, the authors installed the fan over a compact cooling unit's tube bank where the fan was rotating at 950 rpm with a blade angle of 28 degrees.*

Installed operating points	Volume flow rate (m^3/s)	Static pressure rise (Pa)
datum AC90/6	7.6	176.5
AC90/6/TF	7.5	174.0
AC90/6/TF$_{VTE}$	7.5	174.6
AC90/6/TF$_{MVB}$	7.7	189.5

Spectral Analysis

We undertook our analysis of installed far-field narrowband sound power level (L_W) spectrum using the same method that one uses for the standardised airway analysis. Once again, the sound power level spectrum was integrated over a hemisphere to provide an overall assessment of each fan configuration.

Consider the integrated sound power level spectrum for the four studied fan configurations, Figure 13.8. The integrated sound power level spectrum is noticeably different to that measured with the sour studied fan configurations in a standardised airway, Figure 13.7. When installed, the four studied fan configurations are all subjected to an increase in the inflow turbulence level as a consequence of passing though the tube bank. This has a significant impact on the magnitude of the 95 Hz blade passing frequency tonal peak. The blade passing frequency tonal peak is equally affected for all four studied fan configurations.

Consider the tonal peak that occurs with the 190 Hz first harmonic of blade passing frequency for the fan *datum* AC90/6 and AC90/6/TF. It is lower than the tonal peak that occurs with the blade passing frequency. This is in contrast to the standardised airway result, where the first harmonic tone amplitude is similar to the

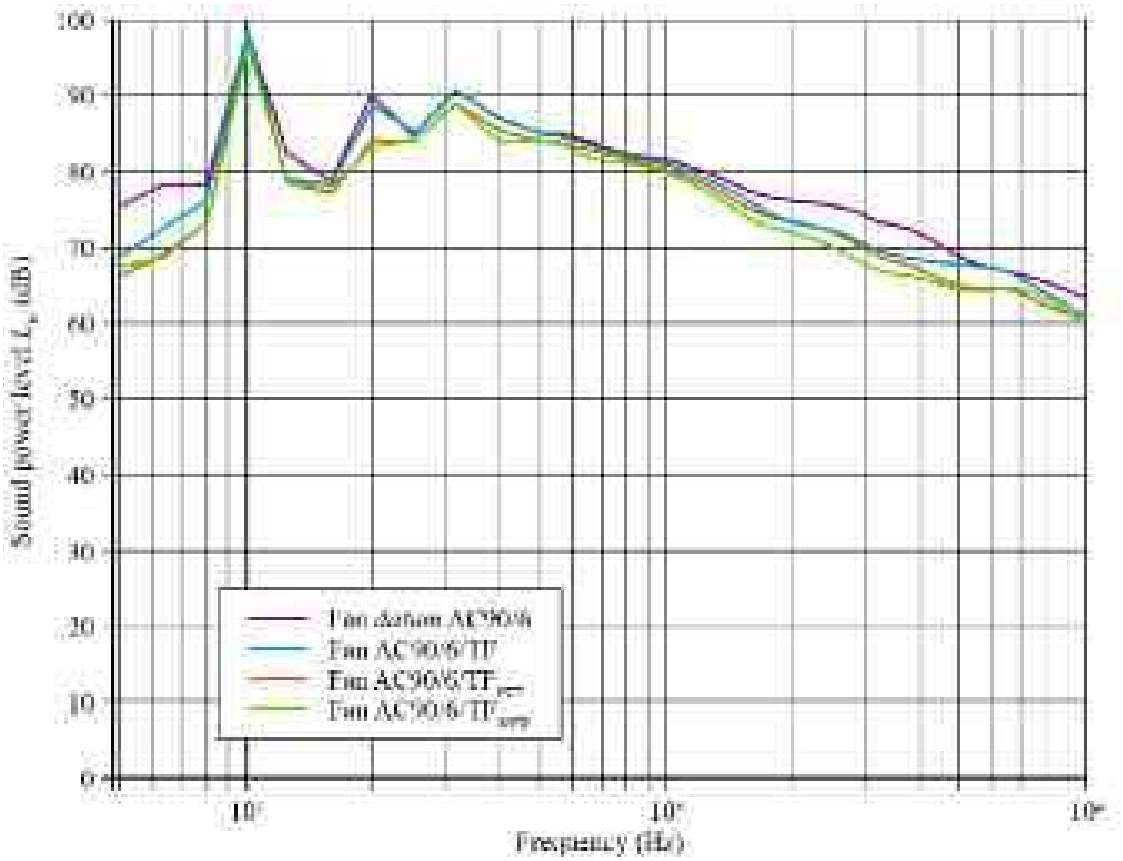

FIGURE 13.8. Outlet far-field A-filtered one-third octave sound power level (L_W) spectrum measured at the fan design operating point when installed over the compact cooling unit's tube bank. The authors provide measured sound power level spectrum data for the fan *datum* AC90/6, AC90/6/TF, AC90/6/TF$_{VTE}$ and AC90/6/TF$_{MVB}$.

blade passing frequency tone amplitude. Additionally, the fan AC90/6/TF$_{VTE}$ and AC90/6/TF$_{MVB}$ first harmonic tonal peak is barely greater than the broadband noise. Engineers classically associate the first harmonic with disturbances of the inflow. Therefore, we would have expected the tonal peak that occurred with the first harmonic of blade passing frequency to increase in amplitude.

Consider the tonal peak that occurs with the 285 Hz second harmonic of blade passing frequency for the four studied fan configurations. The peak amplitudes are similar to those of fan *datum* AC90/6 and AC90/6/TF at the first harmonic of blade passing frequency. Once again, this is in contrast to the standardised airway results. The standardised airway results feature tonal amplitude of the second harmonic that is similar to the blade passing frequency and its first harmonic. At frequencies above the second harmonic of blade passing frequency fan AC90/6/TF$_{MVB}$ exhibits generally lower broadband noise then the other studied fan configurations.

Overall Noise

We may gain an insight into the acoustic performance of the multiple vortex breakdown blade-tip end-plate by considering both fan far-field overall sound power level, L_W and A-weighted overall sound power level, L_WA. Sound power level is a measure of sound energy. We also calculated the A-weighted overall sound power level as we are most concerned with an observer's perception of the impact of blade-tip end-plates. We applied A-weighting to measured sound levels in an effort to account for the relative loudness perceived by the human ear, as the ear is less sensitive to low audio frequencies. It is employed by arithmetically adding a table of values, listed by third-octave bands, to the measured sound pressure levels in dB. The resulting third-octave band measurements are logarithmically added to provide a single A-weighted value describing the sound in dB(A).

We present a comparison of sound power level plotted against the A-weighted sound power level, Figure 13.9. We made all measurements at the fan design operating point. We compared the acoustic performance of the four studied fans when measured in both a Type A (fan downstream from a plenum chamber with a free outlet) standardised airway and when installed over the compact cooling unit's tube bank. Consider the standardised airway and installed acoustic data for the fan *datum* AC90/6. It is apparent that the fan datum AC90/6 acoustic performance is relatively insensitive to installation effects. Both the sound power and A-weighted sound power levels change by less than one decibel. Surprisingly, the installed sound power and A-weighted sound power levels are lower than when tested in a standardised airway.

Consider the standardised airway and installed acoustic data for the fan AC90/6/TF. When tested in a standardised airway, the fan AC90/6/TF has a similar sound power level to the fan *datum* AC90/6, but an A-weighted sound power level that is approximately 5 dB(A) lower. Therefore, adding a constant thickness blade-tip end-plate does not significantly reduce the generated sound energy. However, it does shift the frequency at which that energy is radiated to the far-field and thus

makes the fan far-field noise more acceptable to a human observer. In sharp contrast, fan AC90/6/TF's installed sound power and A-weighted sound power level is essentially identical to that of the fan *datum* AC90/6. The above illustrates an inconvenient truth. The fan AC90/6/TF sounds quieter to a human observer when witnessed in a back-to-back test with the fan *datum* AC90/6 in a standardised airway. There is then an implicit assumption that installed acoustic performance will also be similarly improved. The inconvenient truth is that when installed, there is no benefit associated with fitting the constant thickness blade-tip end-plate.

Consider the standardised airway and installed acoustic data for the fan AC90/6/TF$_{VTE}$. When tested in a standardised airway, the fan AC90/6/TF$_{VTE}$ is essentially similar to that of the fan AC90/6/TF. Sound power level remains essentially the same as fan *datum* AC90/6, but the A-weighted sound power level is approximately 5 dB(A) lower. In contrast to the fan AC90/6/TF, the fan AC90/6/TF$_{VTE}$'s installed A-weighted sound power level is approximately 2 dB(A) lower than the fan *datum* AC90/6. The above illustrates a second inconvenient truth. The fan AC90/6/TF$_{VTE}$ was never put into service. Its performance in a standardised airway indicated there was only a marginal improvement compared to the fan AC90/6/TF. In actuality, the fan AC90/6/TF$_{VTE}$ would have resulted in a 2 dB(A) reduction in A-weighted sound power level if it had been put into service.

Consider the standardised airway and installed acoustic data for the fan AC90/6/TF$_{MVB}$. When tested in a standardised airway, the fan AC90/6/TF$_{MVB}$ is unique in that there is a significant reduction in both sound power and A-weighted sound power level. Unlike either the constant or variable thickness blade-tip end-plates, the multiple vortex breakdown blade-tip end-plate has reduced the sound power radiated to the far-field. Therefore, we may conclude that the multiple vortex breakdown blade-tip end-plate is a more effective passive noise control device than either the constant or variable thickness end-plates.

In a standardised airway, the fan AC90/6/TF$_{MVB}$'s A-weighted sound power level is 5.8 dB(A) lower than the fan *datum* AC90/6. The reduction in A-weighted sound power level is reduced by installation effects from 5.8 dB(A) to 2.5 dB(A). This reduction is a consequence of inflow turbulence reducing the effectiveness of the multiple vortex breakdown blade-tip end-plate. Despite this caveat, both the fan AC90/6/TF$_{MVB}$'s sound power and A-weighted sound power levels were lower than the other studied fan configurations.

We may complement our analysis of sound power and A-weighted sound power level with a consideration of specific noise level, K_S. As we have previously mentioned, specific noise level is a metric that provides a measure of the net fan noise emission. We compute it by subtracting the overall noise emission from the sound equivalent of the aerodynamic power delivered to the air at the fan's operating point. This provides a measure of acoustic efficiency at a fan's actual operating point, which is slightly different for each studied fan configuration as the blade-tip end-plates affect the fan characteristics, Figure 13.2. Therefore, specific noise level provides us with a metric that we may compare directly irrespective of changing operating point.

Consider the specific noise levels for the studied fan configurations, Table 13.4. It is apparent that the fan AC90/6/TF$_{MVB}$'s specific noise level is lower than the other

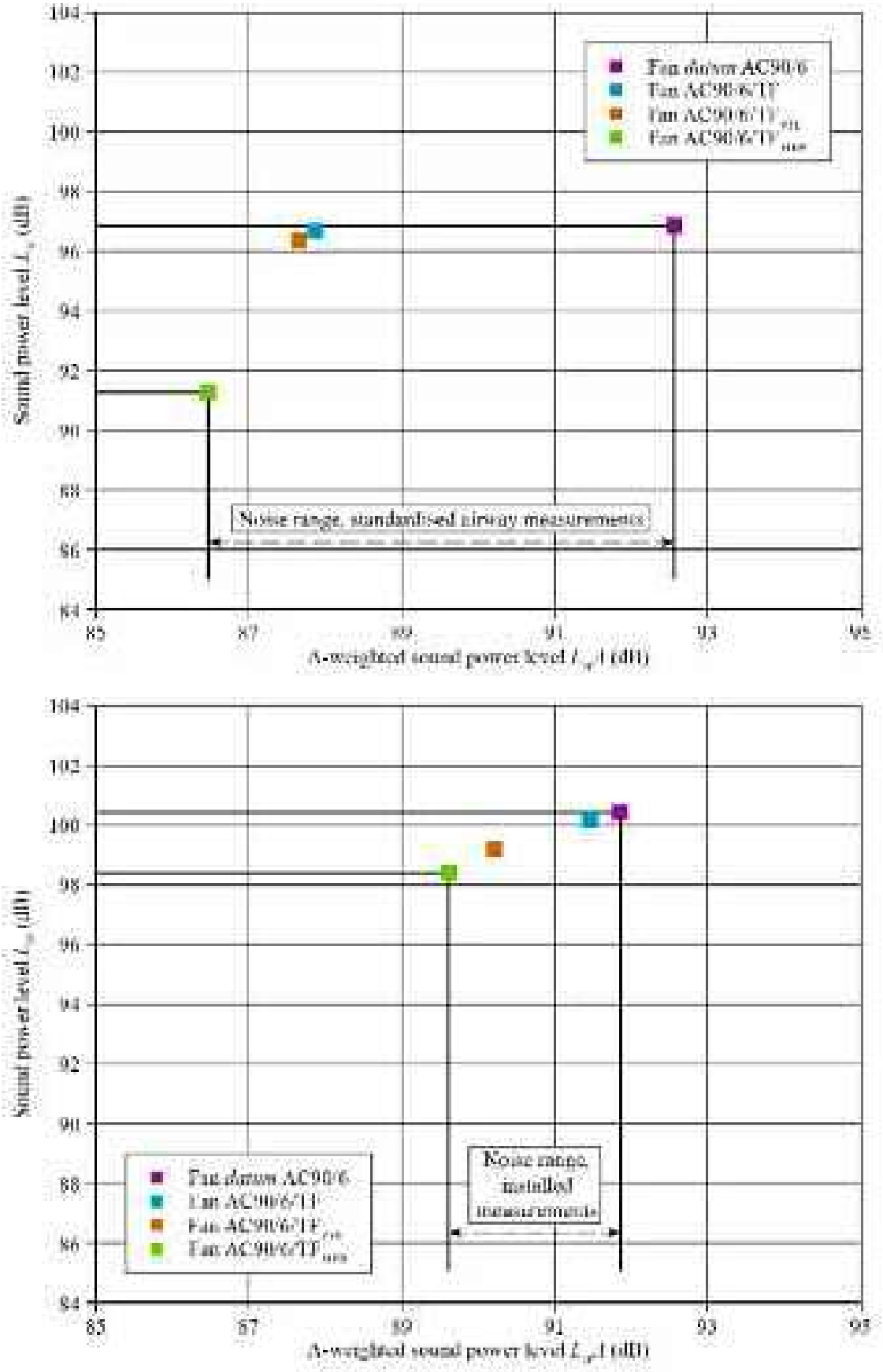

FIGURE 13.9. A comparison of sound power level (L_W) plotted against the A-weighted sound power level (L_WA) with all measurements made at the fan design operating point. The acoustic performance of the four studied fans is compared when measured in both a Type A (fan downstream from a plenum chamber with a free outlet) installation and when installed over a compact cooling unit's tube bank.

Table 13.4. *Overall specific noise levels,* K_S *for each of the four studied fan configurations when installed, rotating at 950 rpm and with a blade angle of 28 degrees.*

	K_S (dB)	ΔK_S to fan *datum* AC90/6 (dB)
datum AC90/6	43.0	0.00
AC90/6/TF	43.0	–0.02
AC90/6/TF$_{VTE}$	41.8	–1.20
AC90/6/TF$_{MVB}$	40.5	–2.50

studied fan configurations. The fan AC90/6/TF$_{MVB}$'s specific noise level is 2.5 dB lower than the fan *datum* AC90/6. Therefore, we may conclude that when operating in-service the multiple vortex breakdown blade-tip end-plate is an effective passive noise control device.

CONCLUSIONS

In this chapter we present an assessment of the installed aerodynamic and acoustic performance of four fan variants, three of which incorporated blade-tip end-plates. We tested a fan AC90/6 without blade-tip end-plates that we named fan *datum* AC90/6, and three fan variants with different end-plate geometries. The fan AC90/6/TF incorporated a constant thickness end-plate. The fan AC90/6/TF$_{VTE}$ incorporated a variable thickness end-plate. The fan AC90/6/TF$_{MVB}$ incorporated a multiple vortex breakdown (MVB) end-plate designed to control the blade tip-to-casing leakage vortex's swirl level.

In a standardised airway at its design operating point, the fan AC90/6/TF$_{MVB}$'s far-field a-weighted sound power level was 5.8 dB(A) lower than that of the fan *datum* AC90/6 without a fitted blade-tip end-plate. When tested installed over a cooling unit's tube bank, that 5.8 dB(A) reduction was degraded to a 2.5 dB(A) reduction. Although a 2.5 dB(A) reduction is an apparently modest improvement, in combination with the reduced tonal noise peaks, the resultant compact cooling unit acoustic performance when fitted with the fan AC90/6/TF$_{MVB}$ was the best in its class. We achieved this improvement without increasing the fan's manufacturing cost, or changing any of the mechanical or electrical interfaces within the compact cooling unit.

The research reported in this chapter illustrates the importance of installation effects on fan performance. Although installation effects degraded the performance of the fan AC90/6/TF$_{MVB}$, it still out performs the fan AC90/6/TF with the constant thickness blade-tip end-plate. We associated the fan AC90/6/TF with lower A-weighted sound power levels than fan *datum* AC90/6 when tested in a standardised airway. However, fan far-field A-weighted sound power level was almost identical when installed. In contrast, the fan AC90/6/TF$_{MVB}$ was able to deliver a 'real world' noise reduction when installed.

REFERENCES

ISO 5801:2007 (2007), *Industrial Fans: Performance Testing Using Standardised Airways.*

ISO 10302:2011 (2011), *Acoustics: Measurement of Airborne Noise Emitted and Structure-borne Vibration Induced by Small Air-moving Devices Part 1: Airborne Noise Measurement.*

ISO IEC61672-1 (2002), *Electroacoustics: Sound Level Meters: Specifications.*

Akturk, A. and Camci, C. (2010), 'Axial Flow Fan Tip Leakage Flow Control using Tip Platform Extensions', *Transactions of the ASME, Journal of Fluids Engineering*, vol. 132, pp. 101–110.

Akturk, A. and Camci, C. (2011a), 'Tip Clearance Investigation of a Ducted Fan used in VTOL UAVS. Part 1: Baseline Experiments and Computational Validation', *Proceedings of the 56th American Society of Mechanical Engineers Turbine and Aeroengine Congress*, Vancouver, Canada, 6–10 June, paper no. GT2011-46356.

Akturk, A. and Camci, C. (2011b), 'Tip Clearance Investigation of a Ducted Fan used in VTOL UAVS. Part 2: Novel Treatments via Computational Design and their Experimental Verification', *Proceedings of the 56th American Society of Mechanical Engineers Turbine and Aeroengine Congress*, Vancouver, Canada, 6–10 June, paper no.GT2011-46359.

Bianchi, S., Sheard, A.G., Kinghorn, I.R., Corsini, A. and Rispoli, F. (2009), 'Experimental Development of a Measurement Technique to Resolve the Radial Distribution of Fan Aeroacoustic Emissions', *Noise Control Engineering Journal*, vol. 57, pp. 360–369.

Bianchi, S., Corsini, A., Rispoli, F. and Sheard, A.G. (2011), 'Far-field Radiation of Tip Aerodynamic Sound Sources in Axial Fans Fitted with Passive Noise Control Features', *Transactions of the ASME, Journal of Vibration & Acoustics*, vol. 133, paper 051001, pp. 1–11.

Bolton, A.N. (1990), 'Installation Effects in Fan Systems', *Proceedings of the IMechE, Part A: Journal of Power and Energy*, vol. 204, pp. 201–215.

Brüel & Kjær (2006), *4954 ¼-inch Prepolarized Free-field Microphone Manual.*

Corsini, A. and Sheard, A.G. (2007), 'Tip End-plate Concept Based on Leakage Vortex Rotation Number Control', *Journal of Computational and Applied Mechanics*, vol. 8, pp. 21–37.

Corsini, A. and Sheard, A.G (2013), 'End-plate for Noise-by-flow Control in Axial Fans', *Periodica Polytechnique, Mechanical Engineering*, vol. 57(2), pp. 3–16.

Corsini, A., Rispoli, F. and Sheard, A.G. (2007), 'Development of Improved Blade-tip End-plate Concepts for Low-noise Operation in Industrial Fans', *Proceedings of the IMechE Part A, Journal of Power and Energy*, vol. 221(5), pp. 669–681.

Corsini, A., Rispoli, F. and Sheard, A.G. (2009), 'Aerodynamic Performance of Blade-tip End-plates Designed for Low-noise Operation in Axial Flow Fans', *Transactions of the ASME, Journal of Fluids Engineering*, vol. 131, paper no. 081101, pp. 1–13.

Corsini, A., Rispoli, F. and Sheard, A.G. (2010), 'Shaping of Tip End-plate to Control Leakage Vortex Swirl in Axial Flow Fans', *Transactions of the ASME, Journal of Turbomachinery*, vol. 132, paper no. 031005, pp. 1–9.

Ffowcs Williams, J.E. (1977), 'Aeroacoustics', *Annual Review of Fluid Mechanics*, vol. 9, pp. 447–468.

Herrada, M.A. and Shtern, V. (2003), 'Vortex Breakdown Control by Adding Near-axis Swirl and Temperature Gradients', *Physical Review E, Statistics, Nonlinear, and Soft Matter Physics*, vol. 68, paper no. 041202, pp. 1–8.

Ito, T., Suematsu, Y. and Hayase, T. (1985), 'On the Vortex Breakdown Phenomena in a Swirling Pipe-flow', *Memoirs of the Faculty of Engineering, Nagoya University*, vol. 37, pp. 117–172.

Jones, M.C., Hourigan, K. and Thompson, M.C. (2001), 'The Generation and Suppression of Vortex Breakdown by Upstream Swirl Perturbations', *Proceedings of 14th Australian Fluid Mechanics Conference*, Adelaide, Australia, 10–14 December.

Leggat, L.J. and Siddon, T.E. (1978), 'Experimental Study of Aeroacoustic Mechanism of Rotor-vortex Interactions', *Journal of the Acoustical Society of America*, vol. 64, pp. 1070–1077.

Longet, C.M.L. (2003), 'Axial Flow Fan with Noise Reducing Means', Patent No. US 2003/0123987 A1, 3 July.

Mimura, M. (2003), 'Axial Flow Fan', US Patent No. 6,648,598 B2, 18 November.

Owen, M.T.F. and Kroger, D.G. (2011), 'An Investigation of Air-cooled Steam Condenser Performance Under Windy Conditions Using Computational Fluid Dynamics', *Transactions of the ASME, Journal of Engineering for Gas Turbines and Power*, vol. 133, paper no. 064502, pp. 1–4.

Quinlan, D.A. and Bent, P.H. (1998), 'High Frequency Noise Generation in Small Axial Flow Fans', *Journal of Sound and Vibration*, vol. 218, pp. 177–204.

Shah, P.D., Mobed, D., Spakovszky, Z.S., Brooks, T.F. and Humphreys, W.M. (2010), 'Aeroacoustics of Drag-Generating Swirling Exhaust Flows', *AIAA Journal*, vol. 48(4), pp. 719-727.

Sheard, A.G., Corsini, A. and Rispoli, F. (2009), 'A Meridional Fan', Patent No. GB 2,452,104 B, 22 July.

Srigrarom, S. and Kurosaka, M. (2000), 'Shaping of Delta-wing Platform to Suppress Vortex Breakdown', *AIAA Journal*, vol. 38, pp. 183–186.

Uselton, R.B., Cook, L.J. and Wright, T. (2005), 'Fan with Reduced Noise Generation', US Patent No. 6,872,048 B2, 29 March.

Van der Spuy, S.J., von Backström, T.W. and Kröger, D.G. (2009), 'Performance of Low Noise Fans in Power Plant Air-cooled Steam Condensers', *Noise Control Engineering Journal*, vol. 57, pp. 341–347.

Wilber, K.R. and Zammit, K. (2005), 'Development of Procurement Guidelines for Air-cooled Condensers', *Proceedings of the Advanced Cooling Strategies/Technologies Conference,* Sacramento, CA, USA, 1–2 June.

Appendix 1

A Meridional Fan

A.G Sheard, A. Corsini and F. Rispoli

ABSTRACT

This appendix is adapted from the patent 'A meridional fan'. The adaption aims to present the invention in a more accessible way to the reader, without significantly altering the patent's content.

A need to minimise fan far-field noise inspired the research that resulted in the intellectual property that forms the basis of the patent. The described passive noise control technique involves varying the geometry of blade-tip end-plates, fitted to each blade of an axial or mixed flow fan. The objective when optimising end-plate geometry is to vary the resistance of flow over the end-plate. Varying the resistance is critical as a consequence of the primary flow-field feature associated with the leakage flow, the blade tip-to-casing leakage vortex. The leakage vortex constitutes a dominant noise source that increases fan far-field noise if its intensity falls below a critical threshold allowing it to burst. The invention that is the subject of this appendix incorporates variations in the blade-tip end-plate geometry that enable one to manage the intensity of the leakage vortex. By optimising the geometry, we may both minimise leakage flow rate, maximising fan efficiency and also ensure the leakage vortex does not burst, thus minimising fan far-field noise.

INTRODUCTION

The present invention relates to meridional fans, particularly, but not exclusively, to axial flow fans designed for large scale air movement applications. Typical applications include drawing air over commercial air conditioning unit tube banks, ventilating commercial buildings, underground railway and metro tunnel systems. The largest are used as forced and induced draft fans in steam power plant

This chapter is a revised and extended version of Sheard, A.G., Corsini, A. and Rispoli, F. (2009), 'A Meridional Fan'. Patent No. GB 2 452 104 B, 22 July.

boiler systems and as process-critical components in steel and cement manufacturing facilities.

Typically located in a duct system, the fan blades are manufactured with a minimal clearance between the blade-tip and the casing within which they rotate. Fan efficiency is inversely proportional to this blade tip-to-casing clearance, and therefore the fan blades' outer surface is contoured in the form of an arc. The contouring ensures that the blade tip-to-casing clearance is minimised over the entire blade chord from leading to trailing edge, maximising fan efficiency.

When operating the fan, blades rotate, and this rotation induces a higher pressure downstream of the fan than upstream. The aerodynamic forces at play within the fan's blade-to-blade passages induce this differential pressure. These forces manifest themselves as a higher pressure on the blades' pressure surface and a lower pressure on the blades' suction surface. A result of this differential pressure across each blade is that air is driven though the blade tip-to-casing clearance from the high to low pressure blade surface. This leakage flow reduces the fan's efficiency and also results in creating aerodynamic flow-features that are acoustically productive and generate both broadband noise and tones that collectively increase the fan's far-field noise level.

Known methods for reducing the blade tip-to-casing leakage flow are first, to reduce the clearance between the blade tip and casing to a minimum and second, to extend the clearance length. Incorporating a blade-tip end-plate on each blade may extend the clearance length. This end-plate increases the clearance's length in the direction of the leakage flow and thereby increases the resistance the flow must overcome as it passes though the clearance. For any given differential pressure from blade pressure to suction surface, this increase in resistance results in reducing the leakage flow velocity and therefore reducing the leakage mass flow rate.

The invention presented in this appendix seeks to provide improved blade-tip end-plate geometry. The improved geometry both increases fan efficiency and simultaneously reduces the fan's far-field noise. This improvement is achieved by managing the intensity of the flow-field features associated with the blade tip-to-casing leakage flow. The primary flow-field feature associated with the leakage flow is a leakage vortex, which constitutes both an aerodynamic loss mechanism that reduces fan efficiency and a noise source that increases fan far-field noise.

Engineers within the air movement and control community have known of the benefits of fitting blade-tip end-plates since the 1950s. The increase in fan efficiency was modest in comparison with the increase in manufacturing cost and therefore they have not traditionally been fitted to improve fan efficiency. However, in some applications minimising noise is more important than minimising cost, and in these application blade-tip end-plates are a standard feature. These early blade-tip end-plates were typically of a constant thickness from the blade leading to trailing edge. The engineers designing them simply made them as large as the available manufacturing technology would permit.

It is intuitively logical to make a blade-tip end-plate as large as possible, as it maximises the resistance to flow through the blade tip-to-casing clearance and therefore minimises the leakage flow rate. However, we discovered that a non-uniform

end-plate profile can result in both an increase in fan efficiency and reduction in fan far-field noise. The non-uniform end-plate profile still maximises the resistance to flow through the blade tip-to-casing clearance, but also facilitates leak flow management. It is this ability to manage the leakage flow that facilitates minimising fan far-field noise.

BLADE-TIP END-PLATES

An axial flow fan comprises a hub to which blades are attached that rotates within a casing, Figure A.1. The fan casing comprises a cylindrical ring that forms one part of the duct system within which the fan is installed. The hub and blades sweep an area such that the blade tips are close to the fan casing with the minimum possible gap size for each application. It is each fan blade's tip, close to the casing, to which blade-tip end-plates are fitted.

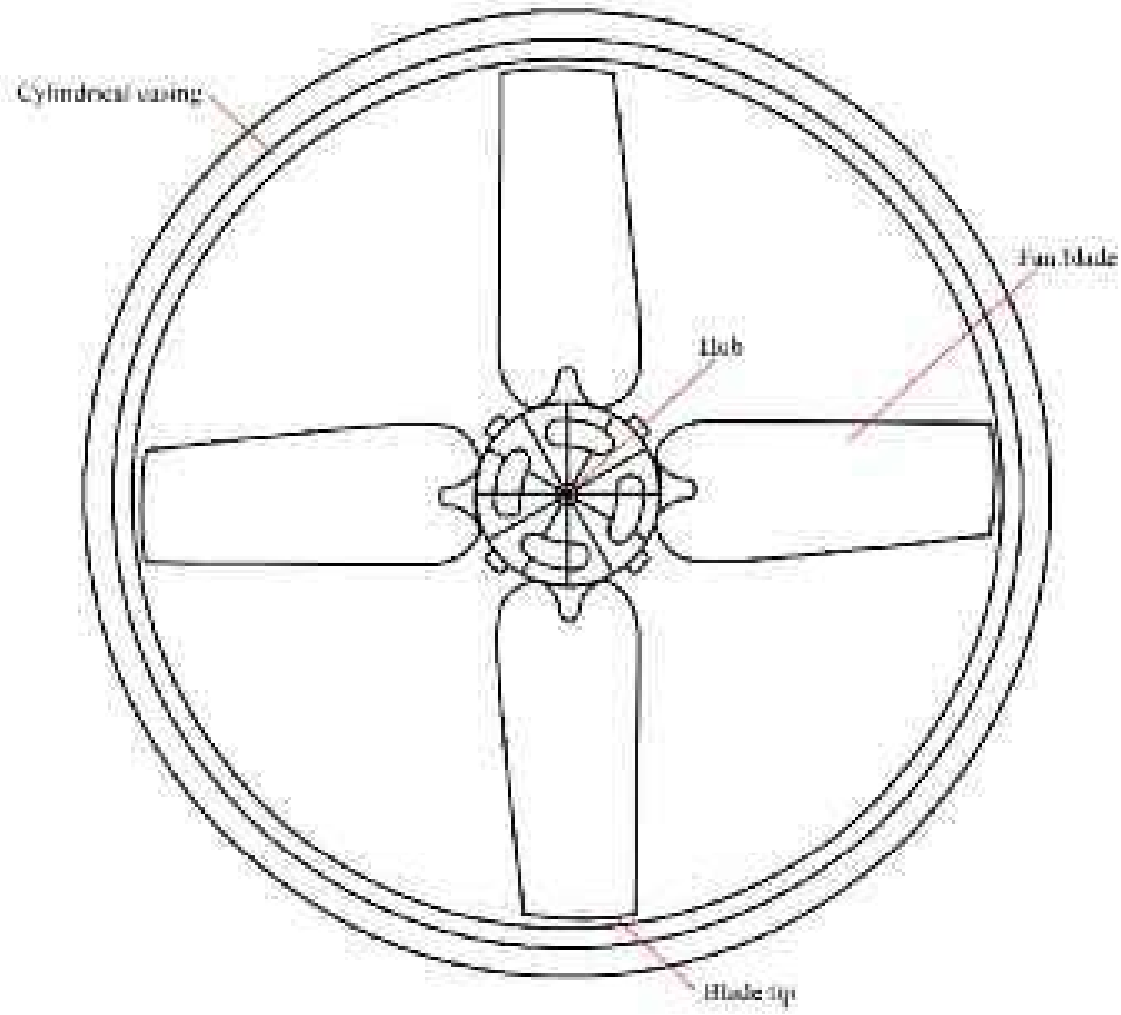

FIGURE A1. An axial flow fan with four blades mounted on a hub located within a cylindrical casing.

The invention presented in this appendix has novelty as a consequence of the variable thickness of the blade-tip end-plate concept, Figure A.2. The end-plate thickness varies in both the axial and the radial direction. In the axial direction the end-plate thickness increases and decreases from the blade leading to trailing edge. In the radial direction the end-plate thickness increases, thus decreasing the blade tip-to-casing gap size. In this example the radial increase in end-plate thickness varies in the circumferential direction, providing an additional variable when optimising end-plate geometry.

The objective when optimising end-plate geometry is to vary the flow resistance over the end-plate. Varying the resistance is critical as a consequence of the primary flow-field feature associated with the leakage flow, the blade tip-to-casing leakage vortex. This leakage vortex originates at the point along the blade-chord of maximum differential pressure across the blade. It constitutes a dominant noise source that increases fan far-field noise. We discovered that traditional constant thickness blade-tip end-plates reduce the leakage vortex's intensity below a critical threshold value. As the leakage vortex reaches this threshold value the vortex bursts. Vortex bursting is acoustically productive, resulting in an increase in broadband noise and a tone at the vortex rotational frequency that together increase fan far-field noise.

The acoustic productivity of a leakage vortex increases further if its axial velocity is reduced so far that the blade-to-blade static pressure field drives it across the blade passage. If the leakage vortex is driven across the blade passage it bursts on impact with the adjacent blade. Therefore, the more effective a constant thickness blade-tip end-plate is at reducing the leakage flow rate, the further it reduces the intensity of the leakage vortex. Consequently, the probability that the leakage vortex will either burst, or burst and be driven across the blade passage increases, with a resultant increase in fan far-field noise. The invention that is the subject of this appendix incorporates variations in the blade-tip end-plate geometry. These variations enable one to manage the leakage vortex's intensity such that it remains above its

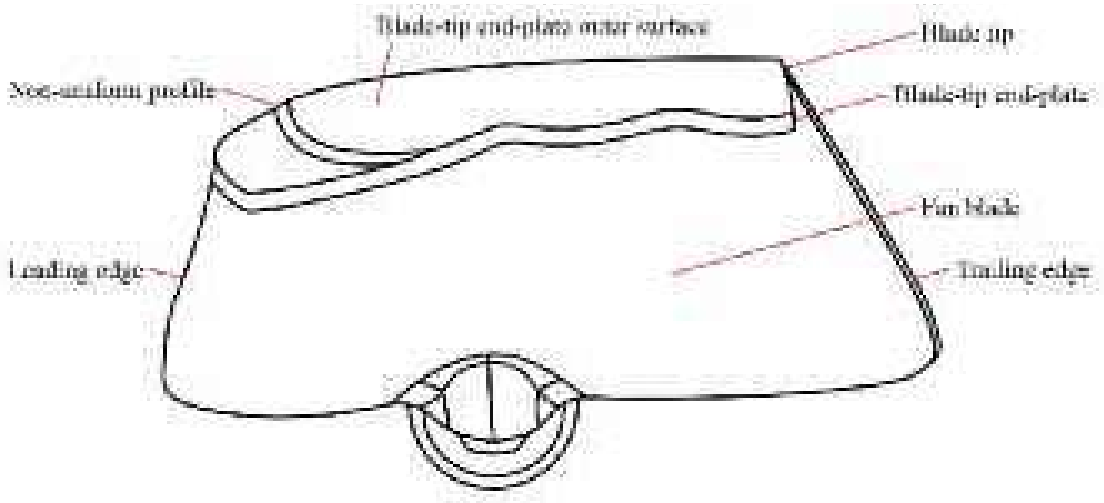

FIGURE A.2. A view looking down onto the tip of an axial fan blade, illustrating the blade-tip end-plate design.

critical value and does not burst. By optimising the geometry, we may both minimise the leakage flow rate and also maintain the leakage vortex's intensity above its critical value. This optimisation both maximises fan efficiency whilst minimising fan far-field noise.

We may clarify the form of the blade-tip end-plate by considering an axial cross section though the blade, Figure A.3. The fan blades are driven from left to right in Figure A.3, and it is this motion that results in the higher pressure on the blade pressure surface than the blade suction surface. Consequently, air spills over the blade tip through the blade tip-to-casing clearance from the pressure to the suction surface. The gap forms a leakage flow path for air from the pressure surface to the blade's suction surface. Changing the end-plate's thickness may vary the resistance to the leakage flow. Minimising the mass flow rate from the pressure surface to the suction surface may maximise fan efficiency. Ensuring that the blade tip-to-casing leakage vortex intensity is maintained above a critical threshold value and does not burst may minimise the fan's far-field noise. Varying end-plate thickness provides a fan

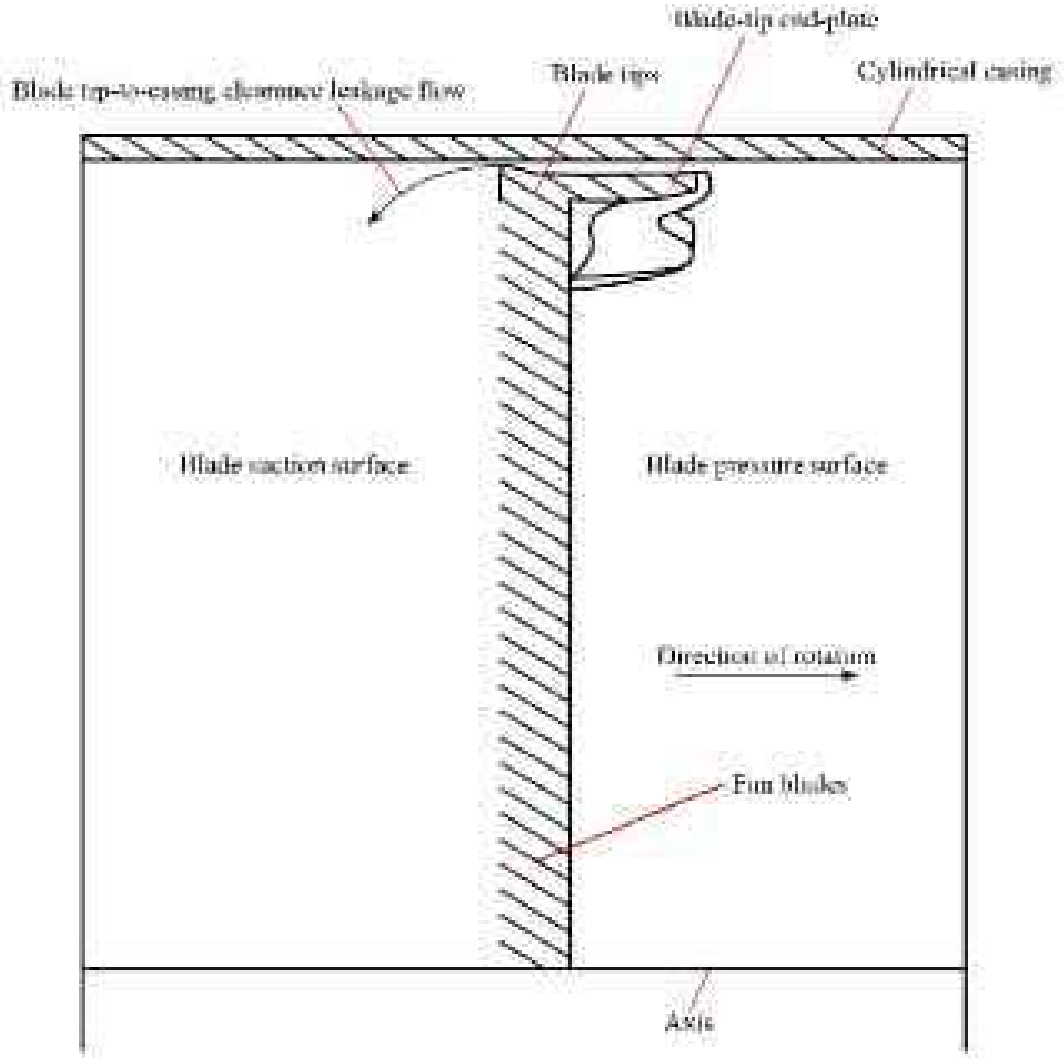

FIGURE A.3. An axial section through a fan blade within the cylindrical casing, illustrating the blade-tip end-plate design.

designer with a way to minimise mass flow rate whilst maintaining leakage vortex intensity above the critical value.

We may augment the end-plate geometry with a continuous stepped shoulder between the blade suction surface and the end-plate that extends from the blade leading to trailing edge, Figure A.4. Alternatively, the stepped shoulder may consist of many stepped recesses spaced between the blades' leading to trailing edge, Figure A.5. These stepped recesses are typically regularly spaced, but may be irregularly spaced. The end-plate's outer surface has a non-uniform profile in the circumferential direction. The non-uniformity is comprised of undulations or grooves, or a mixture of both, to form the blade-tip end-plate outer profile. The undulations or groves may extend partially or completely along the end-plate in the axial direction. A further embodiment of the end-plate incorporates recesses or grooves in its outer surface, Figure A.6. These recesses or grooves do not need to extend to the blade leading or trailing edge, but may be concentrated in the end-plate's outer surface.

A fan designer may use the different methods of providing a non-uniform blade-tip end-plate in any combination. The optimum combination depends on fan diameter, speed and blade number. In this appendix we have shown a fan with four blades. However, the number of blades may vary depending on the particular application. Although we show the described end-plate embodiment fitted to an axial flow fan, the invention is also applicable to mixed flow fans. In these instances, the fan casing is not necessarily cylindrical, but may be conical. A change in casing diameter from blade leading to trailing edge does not adversely affect the invention's ability to vary the resistance to flow through the blade tip-to-casing clearance. Therefore, the invention is applicable to both axial and mixed flow fans.

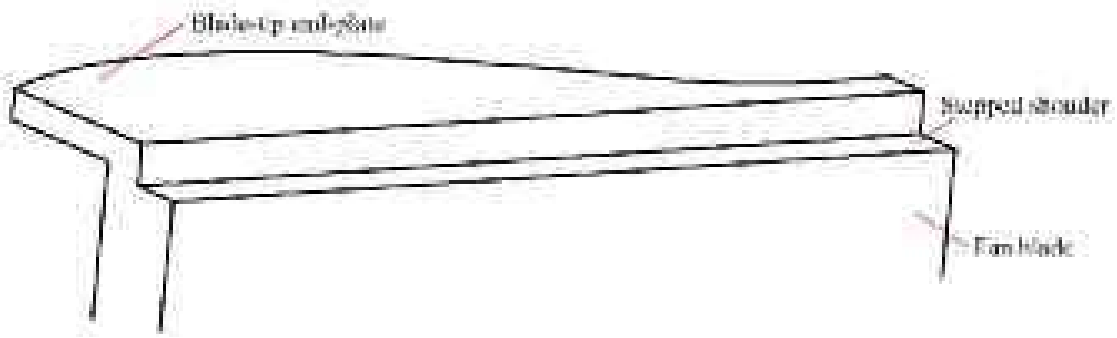

FIGURE A.4. The blade-tip end-plate incorporating a continuous stepped shoulder from blade leading to trailing edge that serves to decelerate abruptly the airflow as it exits the blade tip-to-casing gap.

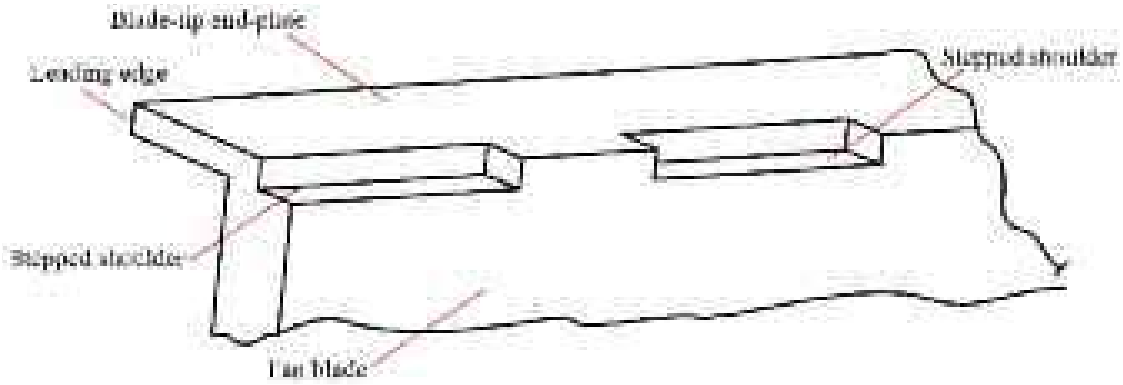

FIGURE A.5. A further embodiment of the blade-tip end-plate incorporating series of cutaway stepped shoulders.

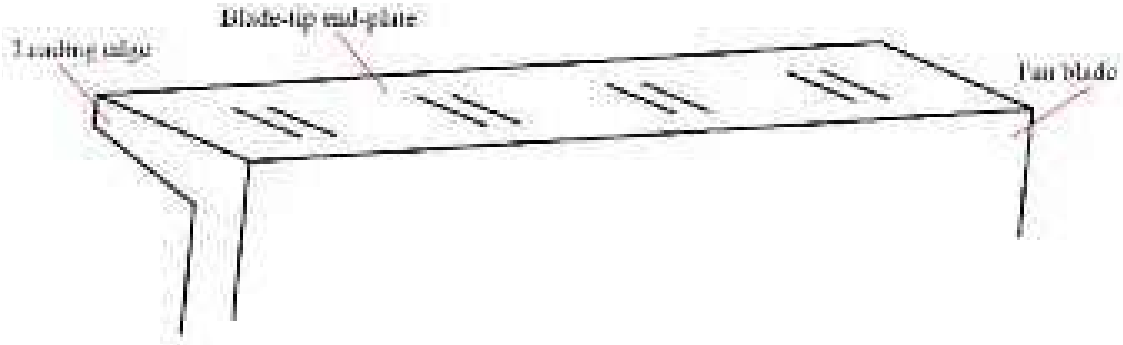

FIGURE A6. A further embodiment of the blade-tip end-plate in which the end-plate outer surface has many spaced recesses or grooves which may or may not extend through to the leading edge or the outer surface's trailing edge.

CLAIMS

1. The invention is applicable to axial and mixed flow fans where the fan blades rotate within a casing, driving air through a duct system. When rotating, a plurality of fan blades describes an arc that follows a circular path adjacent to the fan casing. The blade tips each have a leading edge, a trailing edge and an outer surface. There is a leakage path from the blade pressure to suction surface through the blade tip-to-casing clearance. There is varying resistance to flow through this tip-to-casing clearance as the blade-tip end-plate geometry alters. This blade-tip end-plate geometry changes the resistance to flow through the blade tip-to-casing clearance by altering the leakage flow path's length and thickness.
2. A fan, according to Claim 1, wherein the circumferential axial extent of the blade-tip end-plate varies from blade leading to trailing edge.
3. A fan, according to Claim 1 or 2, wherein the intersection of the blade-tip end-plate and the blade includes a stepped shoulder that extends at least partially from the blade leading to trailing edge.

4. A fan, according to Claim 3, wherein the stepped shoulder comprises many stepped recesses at the blade-tip end-plate's intersection and blade from the blade leading to trailing edge.
5. A fan, according to Claim 4, wherein the stepped recesses are regularly spaced from the blade leading to trailing edge.
6. A fan, according to any of the preceding claims, wherein the blade-tip end-plate's outer surface has a non-uniform profile in the circumferential direction.
7. A fan, according to any of the preceding claims, wherein the blade-tip end-plate's outer surface has a non-uniform profile in the axial direction.
8. A fan, according to Claim 6 or 7, wherein undulations, grooves or a mixture of both, form the blade-tip end-plates' non-uniform profile.
9. A fan, according to Claim 8, wherein the undulations and grooves extend partially or completely along the axial extent of the blade-tip end-plate outer surface.

Bibliography

Page numbers in italics refer to figures or tables

Akaike, S., Kuoki, S. and Katagiri, M., 'Noise Reduction of Radiator Cooling Fan for Automobile. Three-dimensional Analysis of the Flow between the Blades of the Fan,' *Japan Society of Automotive Engineers,* vol. 22(3), pp. 79-84, 1991, 305

Akturk, A. and Camci, C., 'Axial Flow Fan Tip Leakage Flow Control using Tip Platform Extensions,' *Transactions of the ASME, Journal of Fluids Engineering,* vol. 132(5), pp. 1-10, 2010, 307, 357

Akturk, A. and Camci, C., 'Tip Clearance Investigation of a Ducted Fan used in VTOL UAVS. Part 1: Baseline Experiments and Computational Validation,' *Proceedings of the 56th American Society of Mechanical Engineers Turbine and Aeroengine Congress,* Vancouver, Canada, 6-10 June, paper no. GT2011-46356, 2011., 307, 357

Akturk, A. and Camci, C., 'Tip Clearance Investigation of a Ducted Fan used in VTOL UAVS. Part 2: Novel Treatments via Computational Design and their Experimental Verification,' *Proceedings of the 56th American Society of Mechanical Engineers Turbine and Aeroengine Congress,* Vancouver, Canada, 6-10 June, paper no. GT2011-46359, 2011., 307, 357

Amiet, R. K., 'Noise Due to Turbulent Flow Past a Trailing Edge', *Journal of Sound and Vibration,* vol. 47(3), pp. 387-393, 1976., 9, 160

Arakawa, C., Fleig, O., Makoto, I. and Masakazu, S., 'Numerical Approach for Noise Reduction of Wind Turbine Blade Tip with Earth Simulator', *Journal of the Earth Simulator,* vol. 2, pp. 11-23, 2005., 294

Ashforth-Frost, S. and Jambunathan, K., 'Effect of Nozzle Geometry and Semi-confinement on the Potential Core of a Turbulent Axi-symmetric Free Jet,' *International Communications in Heat and Mass Transfer,* vol. 23(2), pp. 155-162, 1996., 163, 164

Baad, P.K., 'Effects of Acoustic Loading on Axial Flow Fan Noise Generation,' *Noise Control Engineering,* vol. 8, pp. 5-15, 1977, 305

Bae, J.W., Breuer, K.S. and Tan, C.S., 'Active Control of Tip Clearance Flow in Axial Compressors,' *Transactions of the ASME, Journal of Turbomachinery,* vol. 127, pp. 352-362, 2005., 217

Bechert, D.W., 'Sound Absorption Caused by Vorticity Shedding, Demonstrated with a Jet Flow', *Journal of Sound and Vibration,* vol. 70(3), pp. 389-405, 1980, 182, 185

Belady, C.L., 'Winglet-Enhanced Fan,' Patent No. US 6,776,578 B2, 17 August, 2004, 196, 218

Bender, E.E., Anderson, B.H. and Yagle, P.J., 'Vortex Generator Modeling for Navier-Stokes Codes,' *Proceedings of the 3rd ASME/JSME Joint Fluids Engineering Conference,* New York, NY, USA, 15 July, paper no. FEDSM99-5919, 1999, 19

Benjamin, T.B., 'The Theory of Vortex Breakdown,' *Journal of Fluid Mechanics,* vol. 14, pp. 583-629, 1962, 201, 250

Bhat, T. R. S., 'Experimental Study of Acoustic Characteristics of Jets from Dual Flow Nozzles,' *Proceedings of the 7th AIAA/CEAS Aeroacoustics Conference,* Maastricht, The Netherlands, 28-30 May, Paper No. AIAA-2001-2183, 2001, 9

Bianchi, S., Corsini, A., and Sheard, A.G., 'Experimental Characterisation of the Far-field Noise in Axial Fans Fitted with Shaped Tip End-plates,' *International Scholarly Research Network, Mechanical Engineering,* vol. 2012, paper no. 212358, pp. 1-9, 2012, *13*

Bianchi, S., Corsini, A., Rispoli, F. and Sheard, A.G., 'A Critical Review of Passive Noise Control Techniques in Industrial Fans,' *Transactions of the ASME, Journal of Engineering for Gas Turbines & Power,* vol. 136(4), paper no. 044001, pp. 1-10, 2014, 217, 271

Bianchi, S., Corsini, A., Rispoli, F. and Sheard, A.G., 'Detection of Aerodynamic Noise Sources in Low-speed Axial Fans with Tip End-plates,' *Proceedings of the IMechE Part C, Journal of Mechanical Engineering Science,* vol. 223, pp, 1379-1392, 2009, 12, 89, 95, 96, *97, 98,* 99, 100, 103, 137, 307, 337

Bianchi, S., Corsini, A., Rispoli, F. and Sheard, A.G., 'Experimental Aeroacoustic Studies on Improved Tip Configurations for Passive Control of Noise-Signature in Low-speed Axial Fan,' *Transactions of the ASME, Journal of Vibration & Acoustics,* vol. 131, paper no. 061007, pp. 1-10, 2009, 158, 168, 169, 176, 185, 307, 344

Bianchi, S., Corsini, A., Rispoli, F. and Sheard, A.G., 'Experimental Investigation of the Near-field Aero-acoustic Noise Sources of a Low-speed Axial Fan,' *Proceedings of the XIX Biannual Symposium on Measuring Techniques in Turbomachinery,* Saint Genesius Rode, Belgium, 7-8 April, 2008, 161, 166, 167

Bianchi, S., Corsini, A., Rispoli, F. and Sheard, A.G., 'Far-field Radiation of Tip Aerodynamic Sound Sources in Axial Fans Fitted with Passive Noise Control Features,' *Transactions of the ASME, Journal of Vibration & Acoustics,* vol. 133, paper no. 051001, pp. 1-11, 2011, 224, 228, 342, 347, 350, 361, 364

Bianchi, S., Corsini, A., Rispoli, F. and Sheard, A.G., 'Near-field Aeroacoustic Experimental Investigation in Low Speed Axial Fans,' *Proceedings of the American Society of Mechanical Engineers Noise Control and Acoustics Division NoiseCon2008,* Dearborn, MI, USA, 28-30 July, 2008, 166, 167

Bianchi, S., Sheard, A.G., Kinghorn, I. R., Corsini, A. and Rispoli, F., 'Experimental Development of a Measurement Technique to Resolve the Radial Distribution of Fan Aeroacoustic Emissions,' *Noise Control Engineering Journal,* vol. 57, pp. 360-369, 2009, 12, 53, 57, 59, 60, *61,* 64, 65, 85, 93, 94, 128, 129, *130,* 133, *209,* 223, 224, 276, 325, 357

Blake, W. K. and Gershfeld, J.L., 'The Aeroacoustics of Trailing Edges,' in Gad-el-Hak, M. (Ed.), *Frontiers in Experimental Fluid Mechanics,* Springer-Verlag, Berlin, pp. 457-532, 1989, 159, 160

Blake, W. K., *Mechanics of Flow-induced Sound and Vibrations, Vols I & II,* Academic Press, Orlando, FL, USA, 1986, 2, 134

Bogey, C and Bailly, C., 'Investigation of Sound Sources in Subsonic Jets using Causality Methods on LES Data,' *Proceedings of the 11th AIAA/CEAS Aeroacoustics Conference (26th AIAA Aeronautics Conference),* Monterey, CA, USA, 23-25 May 2005, paper no. AIAA 2005-2885, 2005, 171

Bolton, A.N., 'Installation Effects in Fan Systems,' *Proceedings of the IMechE, Part A: Journal of Power and Energy,* vol.204, pp. 201-215, 1990, 356

Booth, T.C., Hepworth, H.K. and Dodge, P.R., 'Rotor-tip Leakage: Part I-Basic Methodology,' *Transactions of the ASME, Journal of Engineering for Gas Turbines and Power,* vol. 104(1), pp.154-161, 1982, 218

Borello, D., Borelli, P., Quagliata, E. and Rispoli, F., 'A Multi-grid Additive and Distributive Parallel Algorithm for FEM Turbomachinery CFD, *Proceedings of the European Congress on Computational Methods in Applied Sciences (ECCOMAS CFD 2001),* Swansea, UK, 4-7 September, 2001, 221, 247, 277

Borello, D., Corsini, A. and Rispoli, F., 'A Finite Element Overlapping Scheme for Turbomachinery Flows on Parallel Platforms,' *Computers and Fluids,* vol. 3, pp. 1017-1047, 2003, 199, 221, 247, 277

Brinckerhoff, P., *Electricity Generation Cost Model - 2011 Update, Revision 1,* Department for Energy and Climate Change, London, UK, August, 2011, 4

Brookfield, J.M. and Waitz, I.A., 'Trailing Edge Blowing for Reduction of Turbomachinery Fan Noise,' *AIAA Journal of Propulsion and Power,* vol. 16, pp. 57-64, 2000, 18, 306

Brooks, T.F. and Marcolini, M.A., 'Airfoil Tip Vortex Formation Noise,' *AIAA Journal,* vol. 24(2), pp. 246-252, 1986, 160, 166, 167

Brooks, T.F., Pope, D.S. and Marcolini, M.A., 'Airfoil Self-noise and Prediction,' NASA Reference Publication 1218, 1989, 17, 159, 160, 166

Brown, E.H. and Clifford, S.F., 'On the Attenuation of Sound by Turbulence,' *Journal of the Acoustical Society of America,* vol. 60(4), pp. 788-794, 1976, 179

Brüel & Kjær, *4954 1/4 inch Prepolarized Free-field Microphone Manual,* 2006, 132

Bryanston-Cross, P., 'Particle Image Velocimetry (PVI) Principle of Operation,' *Remote Sensing and Global Modelling Lecture Series,* University of Warwick, Warwickshire, UK, 2010, 7, *9*

Burdsall, E.A. and Urban, R.H., *Fan-Compressor Noise: Prediction, Research and Reduction Studies,* Pratt and Whitney Aircraft, Defence Technical Information centre, East Hartford, CT, USA, 1971, 292

Bushnell, D.M., 'NASA Research on Viscous Drag Reduction II', in *Laminar-Turbulent Boundary Layers, Vol. 11,* E.M. Uram and H.E. Weber (Eds), ASME, New York, NY, pp. 93-98, 1984, 17

Carpenter, P.W. and Morris, P.J., 'Growth of 3-D Instabilities in Flow over Compliant Walls,' *Proceedings of the 4th Asian Congress of Fluid Mechanics,* Hong Kong, China, 21-25 August 1989, 17

Carpenter, P.W., 'The Optimization of Multiple-panel Compliant Walls for Delay of Laminar-turbulent Transition', *AIAA Journal,* vol. 31, p. 1187, 1993, 12, 17

Coleman, W. S., 'Roughness Due to Insects,' in *Boundary Layer and Flow Control, Vol. 2,* G. V.Lachmann (Ed.), Pergamon Press, Oxford UK, pp. 682-747, 1961, 4

Coles, D., 'The Law of the Wake in the Turbulent Boundary Layer,' *Journal of Fluid Mechanics,* vol. 1, pp. 191-226, 1956, 164

Cornaro, C.C., Fleischer, A.S. and Goldstein, R.J., 'Flow Visualization of a Round Jet Impinging on Cylindrical Surfaces,' *Experimental Thermal and Fluid Science,* vol. 20(2), pp. 66-78, 1999, 163, 164

Corsini, A. and Rispoli, F., 'Flow Analyses in a High-pressure Axial Ventilation Fan with a Non-linear Eddy Viscosity Closure,' *International Journal of Heat and Fluid Flow,* vol. 26, pp. 349-361, 2005, 221, 278, 318

Corsini, A. and Rispoli, F., 'Using Sweep to Extend Stall-free Operational Range in Sub-sonic Axial Fan Rotors,' *Proceedings of the IMechE Part A, Journal of Power and Energy,* vol. 218, pp. 129-139, 2004, 7, 199, 217, 221, 223, 247, 248, 271, 278, 279, 320, 324, 340

Corsini, A. and Sheard, A.G., 'End-plate for Noise-by-Flow Control in Axial Fans', *Periodica Polytechnique, Mechanical Engineering,* vol. 57(2) pp. 3-16, 2013, 12, 13, 16, 337, *338,* 341, 357, 358

Corsini, A. and Sheard, A.G., 'Tip End-plate Concept Based on Leakage Vortex Rotation Number Control', *Journal of Computational and Applied Mechanics,* vol. 8, pp. 21-37, 2007, 12, 13, 31, 33, 56, 89, 127, 128, 161, 165, 218, 220, 221, 224, 225, 246, 247, 248, 249, 250, 251, 252, 253, 255, 271, 273, 274, 277, 307, 310, *311,* 312, 314, 320, 322, 340, 358

Corsini, A., Delibra, G. and Sheard, A. G., 'On the Role of Leading-edge Bumps in the Control of Stall Onset in Axial Fan Blades,' *Transactions of the ASME, Journal of Fluids Engineering,* vol. 135, paper no. 081104, pp. 1-9, 2013, 10, *11,* 12

Corsini, A., Perugini, B., Rispoli, F., Sheard, A.G. and Kinghorn, I.R., 'Aerodynamic Workings of Blade-tip End-plates Designed for Low-noise Operation in Axial-flow Fans,' *Proceedings of the 52nd American Society of Engineers Gas Turbine and Aeroengine Congress,* Montreal, Canada, 14-17 May, paper no. GT2007-27465, 2007, 13

Corsini, A., Rispoli, F. and Santoriello, A., 'A New Stabilized Finite Element Method for Advection-Diffusion-Reaction Equations using Quadratic Elements,' in Vad, J., Lajos, T. and Schilling, R. (Eds), *Modelling Fluid Flow: The State of the Art,* Springer Verlag, Berlin, Germany, 2004, 221, 247, 277

Corsini, A., Rispoli, F. and Sheard, A.G., 'Aerodynamic Performance of Blade Tip End-plates Designed for Low-noise Operation in Axial Flow Fans', *Transactions of the ASME, Journal of Fluids Engineering,* vol. 131, paper no. 081101, pp. 1-13, 2009, 312, 341, 358

Corsini, A., Rispoli, F. and Sheard, A.G., 'Development of Improved Blade Tip End-plate Concepts for Low-noise Operation in Industrial Fans', *Proceedings of the IMechE Part A, Journal of Power and Energy,* vol. 221(5), pp.669-681, 2007, 13, 247, 249, 250, 253, 255, 265, 266, 272, 274, 277, 286, 289, 307, 312, 324, 340, 341, 358

Corsini, A., Rispoli, F. and Sheard, A.G., 'Shaping of Tip End-plate to Control Leakage Vortex Swirl in Axial Flow Fans', *Transactions of the ASME, Journal of Turbomachinery,* vol. 132, paper no.. 031005, pp. 1-9, 2010, 12, 13, 272, 274, 307, *311,* 312, 320, 341, 358

Corsini, A., Rispoli, F., Santoriello, A. and Tezduyar, T, 'Improved Discontinuity-capturing Finite Element Techniques for Reaction Effects in Turbulence Computation,' *Computational Mechanics,* vol. 38, pp. 356-364, 2006, 318

Corsini, A., Rispoli, F., Sheard, A.G. and Kinghorn, I.R., 'Investigation of Improved Blade-tip Concept for Axial Flow Fan,' *Proceedings of the 51st American Society of Mechanical Engineers Gas Turbine and Aeroengine Congress,* Barcelona, Spain, 8-11 May, paper no. GT2006-90592, 2006, 33, 56, 128, 198, 199, 220, 247

Corsini, A., Rispoli, F., Sheard, A.G. and Kinghorn, I.R., 'The Aerodynamic Interaction of Tip Leakage and Mainstream Flows in a Fully Ducted Axial Fan,' *Proceedings of the 49th American Society of Mechanical Engineers Gas Turbine and Aeroengine Congress,* Vienna, Austria, 14-17 June, paper no. GT2004-53408, 2004, 217, 221, 248, 279

Craft, T.J., Launder, B.E. and Suga, K., 'Development and Application of a Cubic Eddy-viscosity Model of Turbulence,' *International Journal of Heat and Fluid Flow',* vol. 17, pp. 108-155, 1996, 199, 221, 246, 247, 277, 318

Cumpsty, N. A., 'A Critical Review of Turbomachinery Noise,' *Transactions of the ASME, Journal of Fluids Engineering,* vol. 99, pp. 278-293, 1977, 2, 28, 29, 39, 41, 53, 65, 84, 85, 96, 124, 125, 271, 292, 336, 344

Cumpsty, N. A., 'Sum and Difference Tones from Turbomachines,' *Journal of Sound and Vibration,* vol. 32, pp. 383-386, 1974, 41, 43, 47, 65, 96, 344

Curle, N., 'The Influence of Solid Boundaries upon Aerodynamic Sound,' *Proceedings of the Royal Society,* vol. A20, pp. 505-514, 1955, 159

De Rosier, B., Normand, M.D. and Peleg, M., 'Effect of Lag on the Symmetrised Dot Pattern (SDP) Displays of the Mechanical Signatures of Crunchy Cereal Foods,' *Journal of the Science of Food and Agriculture,* vol. 75, pp. 173-178, 1997, 63

Envia, E. and Nallasamy, M., 'Design Selection and Analysis of a Swept and Leaned Stator Concept,' *Journal of Sound and Vibration,* vol. 228, pp. 793- 836, 1999, 7

Escudier, M. and Zehnder, N., 'Vortex Flow Regimes,' *Journal of Fluid Mechanics,* vol. 115, pp. 105-121, 1982, 199–200, 249

Escudier, M., 'Confined Vortices in Flow Machinery,' *Annual Review of Fluid Mechanics,* vol.19, pp. 27-52, 1987, 196, 243, 307, 310

Fedala, D., Kouidri, S., Rey, R., Carolus, T. and Schneider, M., 'Incident Turbulence Interaction Noise from an Axial Fan,' *Proceedings of the 12th AIAA/CEAS Aeroacoustics Conference (27th AIAA Aeroacoustics Conference),* Cambridge, MA, USA, 8-10 May, paper no. AIAA 2006-2477, 2006, 159

Ffowcs Williams, J. E. and Hall, L. H., 'Aerodynamic Sound Generation by Turbulent Flow in the Vicinity of a Scattering Half Plane,' *Journal of Fluid Mechanics,* vol. 40(4), pp. 657-670, 1970, 7, 12

Ffowcs Williams, J. E. and Hawkings, D.L., 'Sound Generated by Turbulence and Surfaces in Arbitrary Motion, *Philosophical Transactions of the Royal Society,* vol. A264, pp. 321-342, 1969, 159

Ffowcs Williams, J. E., 'Aeroacoustics,' *Annual Review of Fluid Mechanics,* vol.9, pp. 447-468, 1977, 307, 357

Fiedler, H. E. and Fernholz, H. H., 'On Management and Control of Turbulent Boundary Layers,' *Progress in Aerospace Sciences,* vol. 27, pp. 305-387, 1990, 5

Fleeter, S., 'Discrete Frequency Noise Reduction Modeling for Application to Fanjet Engines, *Journal of the Acoustical Society of America,* vol. 68(3), pp. 957-965, 1980, 5

Fukano, T and Takamatsu, Y., 'The Effects of Tip Clearance on the Noise of Low-pressure Axial and Mixed Flow Fans,' *Journal of Sound and Vibration,* vol. 105, pp. 291-308, 1986, 148, 195, 217, 284

Fukano, T. and Jang, C., 'Tip Clearance Noise of Axial Flow Fans Operating at Design of Off-design Condition', *Journal of Sound and Vibration,* vol. 275, pp. 1027-1050, 2004, 3, 29, 30, 53, 85, 160, 217, 271, 337

Fukano, T. and Takamatsu, Y., 'The Effects of Tip Clearance on the Noise of Low-pressure Axial and Mixed Flow Fans,' *Journal of Sound and Vibration,* vol. 105, pp. 291-308, 1986, 148

Fukano, T., Kodama, Y. and Takamatsu, Y., 'Noise Generated by Low Pressure Axial Flow Fans. I - Modeling of the Turbulent Noise', *Journal of Sound and Vibration,* vol. 50, pp. 63-74, 1977, 29, 85, 160, 188

Fukano, T., Kodama, Y. and Takamatsu, Y., 'Noise Generated by Low Pressure Axial Flow Fans. II - Effects of Number of Blades, Chord Length and Camber of Blade', *Journal of Sound and Vibration,* vol. 50, pp. 75-88, 1977, 29, 160

Fukano, T., Kodama, Y. and Takamatsu, Y., 'Noise Generated by Low Pressure Axial Flow Fans. II - Effects of Number of Blades, Chord Length, and Camber of Blade', *Journal of Sound and Vibration,* vol. 50, pp. 75-88, 1977, 85

Fukano, T., Takamatsu, Y. and Kodama, Y., 'The Effects of Tip Clearance on the Noise of Low-pressure Axial and Mixed Flow Fans', *Journal of Sound and Vibration,* vol. 105, pp. 291-308, 1986, 2, 93, 129, 224, 243, 271, 305, 306, 336

Furukawa, M., Inoue, M., Saiki, K. and Yamada, K., 'The Role of Tip Leakage Vortex Breakdown in Compressor Rotor Aerodynamics,' *Transactions of the ASME, Journal of Turbomachinery,* vol.121, pp. 469-480, 1999, 217, 225, 243, 249, 271, 286, 320

Gad-el-Hak, M., *Flow Control: Passive, Active, and Reactive Flow Management,* Cambridge University Press, London, UK, 2000, 306

Gad-el-Hak, M., Pollard, A. and Bonnet, J-P. (Eds), *Flow Control: Fundamentals and Practices,* Springer-Verlag, Paris, France, 1998, 5

Ganz, U.W.., Joppa, P.D. and Scharpf, D.F., *Boeing 18-inch Fan Rig Broadband Noise Test,* Report NASA CR-1998-208704, 1998, 53, 85, 124, 160, 195, 243

Garg, A.K. and Leibovich, S., 'Spectral Characteristics of Vortex Breakdown Flow-fields', *Physics of Fluids,* vol. 22(11), pp. 2053-2064, 1979, 31–3, 56, 89, 128, 202, 220, 251, 273–4, 307, 310

Gbadebo, S.A., Cumpsty, N.A. and Hynes, T.P., 'Interaction of Tip Clearance Flow and Three-dimensional Separations in Axial Compressors,' *Proceedings of the 51st American Society of Mechanical Engineers Gas Turbine and Aeroengine Congress',* Barcelona, Spain, 8-11 May, paper no. GT2006-90071, 2006, 223

George, A.R. and Kim, Y.N., 'High-frequency Broadband Rotor Noise,' *AIAA Journal,* vol. 15(4), pp. 538-545, 1977, 160

Gerard, A., 'Bruit de Raie des Ventilateurs Axiaux: Estimation des Sources par Modèles Aéroacoustiques Inverses et Nouvelles Méthodes de Controle,' Thèse de doctorat, Université de Sherbrooke, 2006, 14

Gerard, A., Berry, M., Masson, P. and Gervais, Y., 'Passive Adaptive Control of Tonal Noise from Subsonic Axial Fans using Flow Control Obstructions,' *Proceedings of the 3rd International Symposium of Fan Noise,* Lyon, France, 17-19 September, 2007, 14

Glick, P. A., 'The Distribution of Insects, Spiders, and Mites in the Air', Technical Bulletin No. 673, US Department of Agriculture, 1939, 4

Gorny, L.J. and Koopmann, G.H., 'Axial Fan Blade Tone Cancellation using Optimally Tuned Quarter Wavelength Resonators,' *Transactions of the ASME, Journal of Vibration and Acoustics,* vol. 131(2), paper no. 021002, pp. 1-13, 2009, 14

Gorny, L.J., Koopmann, G.H., Neise, W. and Lemke, O., 'Attenuation of Ducted Axial Propulsors' Blade Tone Noise using Adaptively Tunable Resonators', *Proceedings of the 13th AIAA/CEAS Aeroacoustics Conference (28th AIAA Aeroacoustics Conference),* Rome, Italy, 21-23 May, paper no. AIAA 2007-3529, 2007, 14

Goth, Y., Besombes, M., Chassaignon, C. and Gerard, A., 'Fan Tonal Noise Reduction using Calibrated Obstructions in the Flow: an Experimental Approach,' *Proceedings of the Fan 2012 Conference,* Senlis, France, 18-20 April, 2012, 14

Gray, J., 'Studies in Animal Locomotion: the Propulsive Power of the Dolphin,' *Journal of Experimental Biology,* vol. 13, pp. 192-199, 1936, 17

Grilliat, J. and Jacob, M.C., 'Tip Leakage Experiment - Part One: Aerodynamic and Acoustic Measurements', *Proceedings of the 13th AIAA/CEAS Aeroacoustic Conference (28th AIAA Aeroacoustics Conference),* Rome, Italy, 21-23 May, paper no. AIAA 2007-3684, 2007, 160

Guedel, A., 'Scattering of an Acoustic Field by a Free-jet Sheer Layer,' *Journal of Sound and Vibration,* vol. 100, pp. 285-304, 1985, 323

Guedel, A., *Acoustique des Ventilateurs Génération du Bruit et Moyens de Reduction,* Editions PYC Livres, 1999, 16

Guitton, A., Jordan, P., Laurendeau, E. and Delville, J., 'Velocity Dependence of the Near Pressure Field of Subsonic Jets: Understanding the Associated Source Mechanisms,' *Proceedings of the 13th AIAA/CEAS Aeroacoustic Conference (28th AIAA Aeroacoustics Conference),* Rome, Italy, 21-23 May, paper no. AIAA 2007-3661, 2007, 170

Heidelberg, L.J., Sutliff, D.L. and Nallasamy, M., 'Azimuthal Directivity of Fan Tones Containing Multiple Mode,' *Proceedings of the 3rd AIAA/CEAS Aeroacoustics Conference,* Atlanta, GA, USA, 12-14 May, paper no. AIAA-97-1587, 1997, 125

Herrada, M.A. and Shtern, V., 'Vortex Breakdown Control by Adding Near-axis Swirl and Temperature Gradients,' *Physical Review E, Non-linear Sofy Matter Physics,* vol. 68(1), paper no. 041202, pp. 1-8, 2003, 196, 204, 244, 252, 307, 310, 357

Holste, F. and Neise, W., 'Noise Source a`Identification in a Prop Fan Model by Means of Acoustical Near Field Measurements', *Journal of Sound and Vibration,* vol. 203, pp. 641-665, 1997, 2, 28, 33, 36, 56, 85, 90, 93, 128, 133, 166, 198, 220, 245, 275, 308, 336, 339

Howe, M. S., 'On the Absorption of Sound by Turbulence, *Journal of Applied Mathematics,* vol. 32(1-3), pp. 187-209, 1984, 9, 14, 323, 324

Ingard, U., 'On the Theory and Design of Acoustic Resonators,' *Journal of the Acoustical Society of America,* vol. 25(6), pp. 1037-1061, 1953, 14

Inoue, M. and Furukawa, M., 'Physics of Tip Clearance Flow in Turbomachinery,' *Proceedings of the ASME2002 Joint US - European Fluids Engineering Division Conference,* Montreal, Quebec, Canada, 14-18 July, paper no. FEDSM2002-31184, pp. 777-789, 2002, 200, 221, 225, 247, 249, 277, 286, 305

Inoue, M., Kuroumaru, M. and Furukawa, M., 'Behavior of Tip Leakage Flow Behind and Axial Compressor Rotor,' *Transaction of the ASME, Journal of Gas Turbine and Power,* vol. 108, pp. 7-14, 1986, 31, 89, 127, 340

ISO 10302:1996, 34, 59, 93, 129, 279, 284, *312, 330, 346*

ISO 10302:2011, 361, 362

ISO 5801:2007, 34, 35, 57, *58,* 90, *91,* 128, *129, 130,* 198, 207, *210,* 223, 246, *275, 309, 310, 312, 327, 339,* 342, *343,* 358, *359*

ISO IEC61672-1 (2002), 361

Ito, T., Suematsu, Y. and Hayase, T., 'On the Vortex Breakdown Phenomena in a Swirling Pipe-flow,' *Memoirs of the Faculty of Engineering, Nagoya University,* vol. 37, pp. 117-172, 1985, 31, 56, 89, 128, 201, 202, 250, 251, 273, 310, 358

Jacob, M.C., Boudet, J., Casalino, D. and Michard, M., 'A Rod-airfoil Experiment as Benchmark for Broadband Noise Modelling,' *Theoretical and Computational Fluid Dynamics,* vol. 19, pp. 171-196, 2005, 174

Jang, C.M., Fukano, T. and Furukawa, M., 'Effects of the Tip Clearance on Vortical Flow and its Relation to Noise in an Axial Flow Fan,' *JSME Transactions Series B,* vol. 46(3), pp. 356-365, 2003, 217, 271

Jensen, C. E., 'Axial Flow Fan,' Patent No. US 4,630,993, 23 December 1986, 12, 196, 218, 243, 271, 337

Jones, M.C., Hourigan, K. and Thompson, M.C., 'The Generation and Suppression of Vortex Breakdown by Upstream Swirl Perturbations,' *Proceedings of the 14th Australian Fluid Mechanics Conference,* Adelaide, Australia, 10-14 December, pp. 347-350, 2001, 196, 204, 244, 252, 307, 310, 357

Jordan, P and Gervais, Y., 'Subsonic Jet Aeroacoustics: Associating Experiments, Modelling and Simulations', *Experiments in Fluids,* vol. 44, pp. 1-21, 2008, 125, 144

Joslin, R. D. and Morris, P. J., 'The Effect of Compliant Walls on Secondary Instabilities in Boundary-layer Transition', *AIAA Journal,* vol. 30(2), pp. 332-339, 1992, 17

Joslin, R. D., Morris, P. J. and Carpenter, P. W., 'The Role of Three-dimensional Instabilities in Compliant Wall Boundary-layer Transition', *AIAA Journal,* vol. 29(10), pp. 1603-1610, 1991, 5, 17

Joslin, R. D., Russell, H.T. and Choudhari, M.M., 'Synergism of Flow and Noise Control Technologies', *Progress in Aerospace Science,* vol.41, pp. 363-417, 2005, 306

Julliard, J., Antoine, H., Lozachmeur, C and Roure, A., 'Active Control of the Directivity of Fan Tones Noise,' *Proceedings of the RTO AVT Symposium on Active Control Technology for Enhanced Performance Operational Capabilities of Military Aircraft, Land Vehicles and Sea Vehicles,* Braunschweig, Germany, 8-11 May, 2000, 125

Kameier, F. and Neise, W., 'Rotating Blade Flow Instability as a Source of Noise in Axial Turbomachines,' *Journal of Sound and Vibration,* vol. 203, pp. 833-853, 1997, 3, 29, 30, 53, 54, 85, 86, 306, 337

Kandula, M. and Vu, B., 'On the Scaling Laws for Jet Noise in Subsonic and Supersonic Flow,' *Proceedings of the 9th AIAA/CEAS Aeroacoustics Conference and Exhibition,* Hilton Head, SC, USA, 12-14 May, paper no. AIAA 2003-3288, 2003, 171

Karlsson, S. and Holmkvist, T., 'Guide Vane Ring For a Return Flow Passage in Axial Fans and a Method of Protecting It,' US Patent No. 4,602,410, 29 July, 1986, 243, 306, 307

Kendall, J.M., 'Measurements of Noise Produced by Flow Past Lifting Surfaces,' *Proceedings of the 16th AIAA Aerospace Meeting,* Huntsville, AL, 16-18 January, paper no.78-239, 1978, 160

Khourrami, M.R. and Choudari, M., 'A Novel Approach for Reducing Rotor Tip-clearance Induced Noise in Turbofan Engines,' *Proceedings of the 7th AIAA/CEAS Aeroacoustics Conference,* Maastricht, The Netherlands, 28-30 May, paper no. AIAA 2001-2148, 2001, 160, 235, 282, 345

Kirk, B.S., Peterson, J.W., Stogner, R.H. and Carey, G.F., 'lobMesh: A C++ Library for Parallel Adaptive Mesh Refinement/Coarsening Simulations,' *Engineering with Computers,* vol. 22, pp. 237-254, 2006, 318

Kramer, M.O., 'Boundary Layer Stabilization by Distributed Damping,' *Journal of the Aeronautical Sciences,* vol. 24(6), pp. 459-460, 1957, 17

Lakshminarayana, B., Zaccaria, M and Marathe, B., 'The Structure of Tip Clearance Flow in Axial Flow Compressors', *Transactions of the ASME, Journal of Turbomachinery,* vol. 117, pp. 336-347, 1995, 305–6, 313

Laurendeau, E., Jordan, P., Delville, J. and Bonnet., 'Nearfield-farfield Correlations in Subsonic Jets: What Can They Tell Us?', *Proceedings of the 13th AIAA/CEAS Aeroacoustics Conference (28th AIAA Aeroacoustics Conference),* Rome, Italy, 21-23 May, paper no. AIAA 2007-3614, 2007, 36, 62, 72, 75, 86, 93, 125, 133, 168, 170, 177, 179, 183

Laurendeau, E., Jordan, P., Delville, J. and Bonnet., 'Source Mechanism Identification by Near Field-far Field Pressure Correlations in Subsonic Jets', *International Journal of Aeroacoustics,* vol. 7, pp. 41-68, 2008, 170

Leggat, L. J. and Siddon, T. E., 'Experimental Study of Aeroacoustic Mechanism of Rotor-vortex Interactions,' *Journal of the Acoustical Society of America,* vol. 64, pp.1070-1077, 1978, 3, 30, 37, 39, 53, 54, 61, 85, 86, 87, 94, 132, 135, 136, 161, 168, 276–7, 326, 348, 364

Leibovich, S., 'The Structure of a Vortex Breakdown,' *Annual Review of Fluid Mechanics,* vol. 10, pp. 221-246, 1978, 199, 201, 248–9, 250

Lighthill, M. J., 'On Sound Generated Aerodynamically. I. General Theory,' *Proceedings of the Royal Society of London A,* vol. 211, pp. 564-587, 1952, 125, 294

Lighthill, M. J., 'On Sound Generated Aerodynamically. II: Turbulence as a Source of Sound,' *Proceedings of the Royal Society of London A,* vol. 222, pp. 1-32, 1954, 2, 125, 144, 158, 168, 294

Lin, J.C., 'Control of Turbulent Boundary-layer Separation using Micro-vortex Generators,' *Proceedings of the 30th AIAA Fluid Dynamics Conference,* Norfolk, VA, USA, 28 June- 1 July, paper no. AIAA 99-3404, 1999, 19

Liu, C. K., Kline, S. J. and Johnston, J. P., 'An Experimental Study of Turbulent Boundary Layer on Rough Walls,' Report MD-15, Stanford University, 1966, 6

Longet, C.M.L., 'Axial Flow Fan with Noise Reducing Means,' Patent No. US 2003/0123987 A1, 3 July 2003, 12, 196, 243, 271, 307, 337, 356

Longhouse, R. E., 'Control Tip-vortex Noise of Axial Flow Fans by Rotating Shrouds,' *Journal of Sound and Vibration,* vol. 58, pp. 201-214, 1978, 3, 29, 30, 53, 85, 149, 305, 306, 337

Lowson, M.V., 'Some Experiments on Fan Noise and their Implication', *Journal of the Acoustical Society of America,* vol.52(1A), p 165, 1972, 159

Lucca-Negro, O and O'Doherty, T., 'Vortex Breakdown: A Review,, *Progress in Energy and Combustion Science,* vol. 27, pp. 431-481, 2001, 199, 248

Magliozzi, B., Johnson, B.V., Hanson, D.B. and Metzger, F.B., 'Noise and Wake Structure Measurements in a Subsonic Tip Speed Fan - Tabulation and Plots of Test Data', NASA Technical Report CR-132259, 23 July, 1973, 41, 65, 95, 159, 344

Mankbadi, R. and Liu, J.T.C., 'Sound Generated Aerodynamically Revisited: Large-scale Structures in a Turbulent Jet as a Source of Sound', *Philosophical Transactions of the Royal Society of London A,* vol.311, pp. 183-217, 1984, 125, 144

Marcinowski, H., 'Einfluss des Laufradspalts und der Luftfuehrung bei einem Kuehlgeblaese axialer Bauart,' *Motortechnische Zeitschrift,* vol. 14, pp. 259-262, 1953, 3, 29, 53, 85, 125, 159, 337

Massey, S. J., Thomas, R. H., Abdol-Hamid, K. S. and Elmilgui, A. A., 'Computational and Experimental Flow Field Analysis of Separate Flow Chevron Nozzles and Pylon Interaction,' *Proceedings of the 9th AIAA/CEAS Aeroacoustics Conference and Exhibit,* Hilton Head, SC, USA, 12-14 May, paper no. AIAA 2003-3212, 2003, 9

Miles, J. H., 'Core Noise Diagnostics of the Turbofan Engine Noise Using Correlation and Coherence Functions,' *Journal of Propulsion and Power,* vol. 26(2), pp. 303-316, 2010, 179

Miles, J. H., 'Procedure for Separating Noise Sources in Measurements of Turbofan Engine Core Noise,' *Proceedings of the 12th AIAA/CEAS Aeroacoustics Conference (27th AIAA Aeroacoustics Conference),* Cambridge, MA, USA, 8-10 May, paper no. AIAA2006-2580, 2006, 3, 30, 36, 53, 54, 62, 85, 86, 93, 133, 168, 179

Mimura, M., 'Axial Flow Fan,' US Patent No. 6,648,598 B2, 18 November 2003, 12, 196, 218, 243, 271, 307, 337, 356

Möhring, W., Muller, E. and Obermeier, F., 'Problems in Flow Acoustics,' *Review of Modern Physics,* vol. 55, pp. 707-724, 1983, 151

Mongeau, L., Thompson, D. E. and McLaughlin, D. K., 'A Method for Characterizing Aerodynamic Sound Sources in Turbomachines,' *Journal of Sound and Vibration,* vol.181, pp. 369-389, 1995, 3, 30, 53, 54, 85, 86

Mugridge, B. D. and Morfey, C.L., 'Sources of Noise in Axial Flow Fan', *Journal of the Acoustical Society of America,* vol. 51, pp. 1411-1426, 1972, 3, 29, 36, 53, 85, 93, 133, 337

Narasimha, R., Narayan, K.Y. and Parthassarathi, S.P., 'Parametric Analysis of Turbulent Wall Jets in Still Air,' *Aeronautical Journal,* vol. 77, pp. 355-359, 1973, 164

Nash, E.C., Lowson, M.V. and McAlpine, A., 'Boundary-layer Instability Noise on Aerofoils,' *Journal of Fluid Mechanics,* vol. 382, pp. 27-61, 1999, 150

Neise, W. and Koopmann, G.H., 'Reduction of Centrifugal Fan Noise by Use of Resonators,' *Journal of Sound and Vibration,* vol. 73(2), pp. 297-308, 1980, 14

Nelson, D.A. and Cooper, B.A., 'A "Reduced-Noise Gas Flow Design Guide" for NASA Glenn Research Center,' *Proceedings of INTERNOISE 99, the International Congress on Noise Control Engineering,* Fort Lauderdale, FL, USA, 6-8 December, vol. 1, pp. 77-82, 1999, 53, 85, 125

Owen, M.T.F. and Kröger, D.G., 'An Investigation of Air-cooled Steam Condenser Performance Under Windy Conditions Using Computational Fluid Dynamics'', *Transactions of the ASME, Journal of Engineering for Gas Turbines and Power,* vol. 133, paper no. 064502, pp. 1-4, 2011, 356

Pickover, C.A., 'On the Use of Symmetrized Dot Patterns for the Visual Characterization of Speech Waveforms and Other Sampled Data,' *Journal of the Acoustical Society of America,* vol. 80, pp. 955-960, 1986, 63, 79

Powell, A., 'Mechanisms of Aerodynamic Sound Production,' AGARD Report No. 466, 1963, 272, 286, 294

Powell, A., 'The Theory of Vortex Sound,' *Journal of the Acoustical Society of America,* vol. 33, pp. 177-195, 1964, 272, 286, 294, *295*

Quinlan, D. A. and Bent, P. H., 'High Frequency Noise Generation in Small Axial Flow Fans, *Journal of Sound and Vibration,* vol. 218, pp. 177-204, 1998, 12, 69, 196, 217, 218, 243, 271, 306, 337, 356

Rains, D.A., 'Tip Clearance Flows in Axial Flow Compressors and Pumps', PhD Thesis, California Institute of Technology, http://resolver.caltech.edu/CaltechETD:etd-04152003-112816, 1954, 313, 314

Reischman, M.M., 'A Review of Compliant Coating Drag Reduction Research at ONR,' in *Laminar-Turbulent Boundary Layers, vol. 11,* E.M. Uram and H.E. Weber (Eds), ASME, New York, NY, pp. 99-105, 1984, 17

Ribner, H., 'Quadrupole Correlations Governing the Pattern of Jet Noise,' *Journal of Fluid Mechanics,* vol. 38, pp. 1-24, 1969, 62

Ribner, H., 'The Generation of Sound by Turbulent Jets,' *Advances in Applied Mechanics,* vol. 8, pp. 103-182, 1964, 168

Roger, M. and Moreau, S., 'Broadband Self-noise from Loaded Fan Blades,' *AIAA Journal,* vol. 42(3), pp. 536-544, 2004, 160

Ross, T., 'Sound Scattering from Oceanic Turbulence', PhD thesis, University of Victoria, Australia, 1998, 16

Roy, B., Chouhan, M. and Kaundinya, K.V., 'Experimental Study of Boundary Layer Control Through Tip Injection on Straight and Swept Compressor Blades,' *Proceedings of the 50th American Society of Mechanical Engineers Gas Turbine and Aeroengine Congress,* Reno, NV, USA, 6-9 June, paper no. GT2005-68304, 2005, 217

Saiyed, N.H., Bridges, J.E. and Mikkelsen, K.L., 'Acoustics and Thrust of Separate-flow Exhaust Nozzles with Mixing Devices for High-bypass-ratio Engines,' *Proceedings of the 6th Aeroengine Conference and Exhibit,* Lahaina, HI, 12-14 June, paper no. AIAA-200-1961, 2000, 306

Sawyer, S. and Fleeter, S., 'Passive Control of Turbomachine Noise,' *Proceedings of the International Compressor Engineering Conference,* West Lafayette, IN, USA, 14-17 July, pp. 779-784, 1998, 6

Schulten, J., 'Sound Generated by Rotor Wakes Interacting with a Leaned Vane Stator', *AIAA Journal,* vol.20, pp. 1352-1358, 1982, 7

Schulten, J., 'Vane Sweep Effects on Rotor/stator Interaction Noise', *AIAA Journal,* vol.35, pp. 945-951, 1997, 7

Schultz, T.J., 'Synthesis of Social Surveys on Noise Annoyance', *Journal of the Acoustical Society of America,* vol. 64, pp. 377-405, 1978, 63

Shah, P.D., Mobed, D., Spakovszky, Z. and Brooks, T.F., 'A Novel Turbomachinery Air-brake Concept for Quiet Aircraft,' *Proceedings of the 52nd American Society of Mechanical Engineers Gas Turbine and Aeroengine Congress,* Montreal, Canada, 14-17 May, paper no. GT2007-27635, 2007, 125, 144

Shah, P.D., Mobed, D., Spakovszky, Z. and Brooks, T.F., 'Aeroacoustics of Drag Generating Swirling Exhaust Flows,' *Proceedings of the 13th AIAA/CEAS Aeroacoustics Conference (28th AIAA Aeroacoustics Conference),* Rome, Italy, 21-23 May, paper no. AIAA-2007-3714, 2007, 125, 144

Shah, P.D., Mobed, D., Spakovszky, Z.S., Brooks, T.F. and Humphreys, W.M., 'Aeroacoustics of Drag-Generating Swirling Exhaust Flows,' *AIAA Journal,* vol. 48(4), pp. 719-727, 2010, 365

Sharland, I.J., 'Sources of Noise in Axial Flow Fans', *Journal of Sound and Vibration,* vol., pp. 302-322, 1964, 29, 85

Sheard, A.G., Corsini, A. and Bianchi, S., 'A Method of Detecting Stall in an Axial Fan,' Patent No. GB 2,468,571, 24 December, 2010, 63

Sheard, A.G., Corsini, A. and Rispoli, F., 'A Meridional Fan,' Patent No. GB 2,452,104 B, 22 July 2009, 12, 243, 307, 313, 341, 357

Smith, G.D.G. and Cumpsty, N.A., 'Flow Phenomena in Compressor Casing Treatment,' *Transactions of the ASME, Journal of Engineering for Gas Turbines and Power,* vol.106, pp. 532-541, 1984, 195, 217, 243, 271, 306

Sottek, R. and Genuit, K., 'Sound Quality Evaluation of Fan Noise Based on Hearing-related Parameters', *Proceedings of the 3rd International Symposium of Fan Noise',* Lyon, France, 17-19 September, 2007, 63

Spall, R.E., Gatski, T.B. and Grosch, C.E., 'A Criterion for Vortex Breakdown,' *Physics of Fluids,* vol. 30, pp.3434-3440, 1987, 31, 89, 127–8, 196, 200, 202, 220, 243, 249, 251, 273, 307, 310, 313

Srigrarom, S. and Kurosaka, M., 'Shaping of Delta-wing Platform to Suppress Vortex Breakdown', *AIAA Journal,* vol. 38, pp. 183-186, 2000, 12, 196, 204, 244, 252, 307, 357

Storer, J.A. and Cumpsty, N.A., 'Tip Leakage Flow in Axial Compressors, *Transactions of the ASME, Journal of Turbomachinery,* vol. 113, pp. 252-259, 1991, 195, 217, 243, 271, 305, 324

Subaschandar, N., Kumar, R. and Sundaram, S., 'Drag Reduction due to Riblets on a GAW(2) Aerofoil, *Journal of Aircraft,* vol. 36(5), pp. 890-892, 1999, 7

Sujudi, D. and Haimes, R., 'Identification of Swirling Flow in 3-D Vector Fields,' *Proceedings of the 12th AIAA Computational Fluid Dynamics Conference,* San Diego, CA, USA, 19-22 June, paper no. AIAA-95-1715-CP, 1995, 289

Sutliff, D.L., Tweedt, D.L., Fite, E.B. and Envia, E., 'Low-speed Fan Noise Reduction with Trailing Edge Blowing,' *International Journal of Aeroacoustics,* vol. 1(3), pp. 275-305, 2002, *18*

Takata, H. and Tsukuda, Y., 'Stall Margin Improvement by Casing Treatment - Its Mechanism and Effectiveness', *Transactions of the ASME, Journal of Engineering for Power,* vol. 99, pp. 121-133, 1977, 195, 217, 243, 271, 306

Tam, C.K.W., Golebiowski, M and Seiner, J.M., 'On the Two Components of Turbulent Mixing Noise from Supersonic Jets,' *Proceedings of the 2nd AIAA/CEAS Aeroacoustics Conference,* State College, PA, USA, 6-8 May, paper no. AIAA 96-1716, 1996, 125

Tester, B.J. and De Mercato, L., 'Far-field Directivity of Rotor-alone Tones Radiated from Fan Intakes with Spliced Liners for Different Intake Shapes, with Flow,' *Proceedings of the 12th AIAA/CEAS Aeroacoustics Conference (27th AIAA Aeroacoustics Conference),* Cambridge, MA, USA, 8-10 May, paper no. AIAA 2006-2456, 2006, 125

Thomas, R.H., Choudhari, M.M. and Joslin, R.D., 'Flow and Noise Control: Review and Assessment of Future Directions,' NASA TM-2002-211631, 1 April, 2002, 306

Thompson, D.W., King, P.I. and Rabe, D.C., 'Experimental and Computational Investigation on Stepped Tip Gap Effects on the Flowfield of a Transonic Axial-flow Compressor Rotor,' *Transactions of the ASME, Journal of Turbomachinery,* vol. 120, pp. 477-486, 1998, 195, 217, 243, 271, 306

Tinney, C.E. and Jordan, P., 'The Near Pressure Field of Co-axial Subsonic Jets', *Journal of Fluid Mechanics,* vol. 611, pp. 175-204, 2008, 183

Tsai, C-Y., and Widnall, S.E., 'Examination of Group-velocity Criterion for Breakdown of Vortex Flow in a Divergent Duct,' *Physics of Fluids,* vol. 23, pp. 864-870, 1980, 201, 250

Tyler, J. and Sofrin, T., 'Axial Flow Compressor Noise Studies,' *SAE Transactions,* vol. 70, pp. 309-332, 1962, 5

Uchida, S., Nakamura, Y. and Ohsawa, M., 'Experiments on the Axisymmetric Vortex Breakdown in a Swirling Air Flow,' *Transactions of the Japan Society for Aeronautical Space Sciences,* vol. 27, pp. 206-216, 1985, 31, 56, 89, 128, 202, 220, 251, 273, 307, 310

Uselton, R.B., Cook, L.J. and Wright, T., 'Fan with Reduced Noise Generation,' US Patent No. 6,872,048 B2, 29 March 2005, 12, 218, 307, 356

Uselton, R.B., Cook, L.J. and Wright, T., 'Fan with Reduced Noise Generation,' US Patent No. 7,351,041 B2, 1 April 2008, 196, 271

Uselton, R.B., Cook, L.J. and Wright, T., 'Fan with Reduced Noise Generation,' US Patent No. 7,351,041 B2, 1 April, 2008, 243

Vad, J., Kosco, G., Gutermuth, M., Kasza, Z., Tabi, T. and Csorgo, T., 'Study of the Aeroacoustic and Aerodynamic Effects of Soft Coating upon Airfoil', *JSME International Journal Series C Mechanical Systems, Machine Elements and Manufacturing,* vol. 49(3), pp. 648-656, 2006, 217

Van der Spuy, S.J., von Backström, T.W. and Kröger, D.G., 'Performance of Low Noise Fans in Power Plant Air-cooled Steam Condensers,' *Noise Control Engineering Journal,* vol.57, pp. 341-347, 2009, 356

Wadia, A.R. and Booth, T.C., 'Rotor-tip Leakage: Part II-Design Optimization Through Viscous Analysis and Experiment,' *Transactions of the ASME, Journal of Engineering for Gas Turbines and Power,* vol.104(1), pp. 162-169, 1982, 218, 315

Wadia, A.R., Szucs, P.N. and Crall, D.W., 'Inner Workings of Aerodynamic Sweep,' *Transactions of the ASME, Journal of Turbomachinery,* vol. 120(4), pp. 671-682, 1998, 217, 271

Walsh, M. J., 'Drag Characteristics of V-groove and Transverse Curvature Riblets,' in *Viscous Flow Drag Reduction, Progress in Astronautics and Aeronautics, Vol. 72,* G. R. Hough (Ed.), AIAA, Reston, VA, USA, pp. 169-184, 1980, 6

Wang, M., Moreau, S., Iaccarino, G. and Roger, M., 'LES Prediction of Wall-pressure Fluctuations and Noise of a Low-speed Airfoil,' *Aeroacoustics,* vol. 8(3), pp. 177-198, 2009, 174

Welch, P.D.,'The use of the Fast Fourier Transform for the Estimation of Power Spectra: a Method Based on Time Averaging Over Short, Modified Periodograms', *IEEE Transactions on Audio and Electroacoustics,* vol. 15(2), pp. 70-73, 1967, 62

Wen-Shiang, C., Lauchle, G.C. and Thompson, D.F., 'Subsonic Axial Flow Fan Noise and Unsteady Rotor Force', *Journal of the Acoustical Society of America,* vol. 85(2), pp. 641-647, 1989, 305

Wennerstrom, A. J., 'Vane Configuration for Fluid Wake Re-energization,' US Patent No. 4,318,669, 9 March, 1982, 10

Widnall, S.E., 'The Acoustic Spectrum of Axial Flow Machines,' *Journal of Sound and Vibration,* vol. 45, pp. 165-223, 1976, 142

Wilber, K.R. and Zammit, K., 'Development of Procurement Guidelines for Air-cooled Condensers,' *Proceedings of the Advanced Cooling Strategies/Technologies Conference,* Sacramento, CA, USA, 1-2 June, 2005, 356

Winkler, J., Temel, F.Z. and Carolus, T., 'Concepts, Design and Characterization of a Small Aeroacoustic Wind Tunnel Facility with Application to Fan Blade Measurements,' *Proceedings of the 3rd International Symposium of Fan Noise,* Lyon, France, 17-19 September, 2007, 160, 161

Woodward, R. P., Elliott, D. M., Hughes, C. E. and Berton, J. J., 'Benefits of Swept-and-leaned Stators for Fan Noise Reduction,' *Journal of Aircraft,* vol. 38(6), pp. 1130-1138, 2001, 6, *8*

Wright, S. E., 'The Acoustic Spectrum of Axial Flow Machines', *Journal of Sound and Vibration,* vol. 45(2), pp. 165-223, 1976, 28, 29, 47, 271, 282, 336, 348

Wright, S.E.'The Acoustic Spectrum of Axial Flow Machines', *Journal of Sound and Vibration,* vol. 45(2), pp. 165-223, 1976, 2, 53, 84, 85, 124, 136, 142

Wu, J.D. and Chuang, C.Q., 'Fault Diagnosis of Internal Combustion Engines using Visual Dot Patterns of Acoustic and Vibration Signals,' *Independent Non-destructive Testing and Evaluation (NDT&E) International,* vol. 38, pp. 605-614, 2005, 63

Author Index

Subject Index

Page numbers in italics refer to figures or tables